

JTCG/MD WP #12 /
AIR FORCE
ARMY NAVY

VOLUME 1 OF 2

12
II

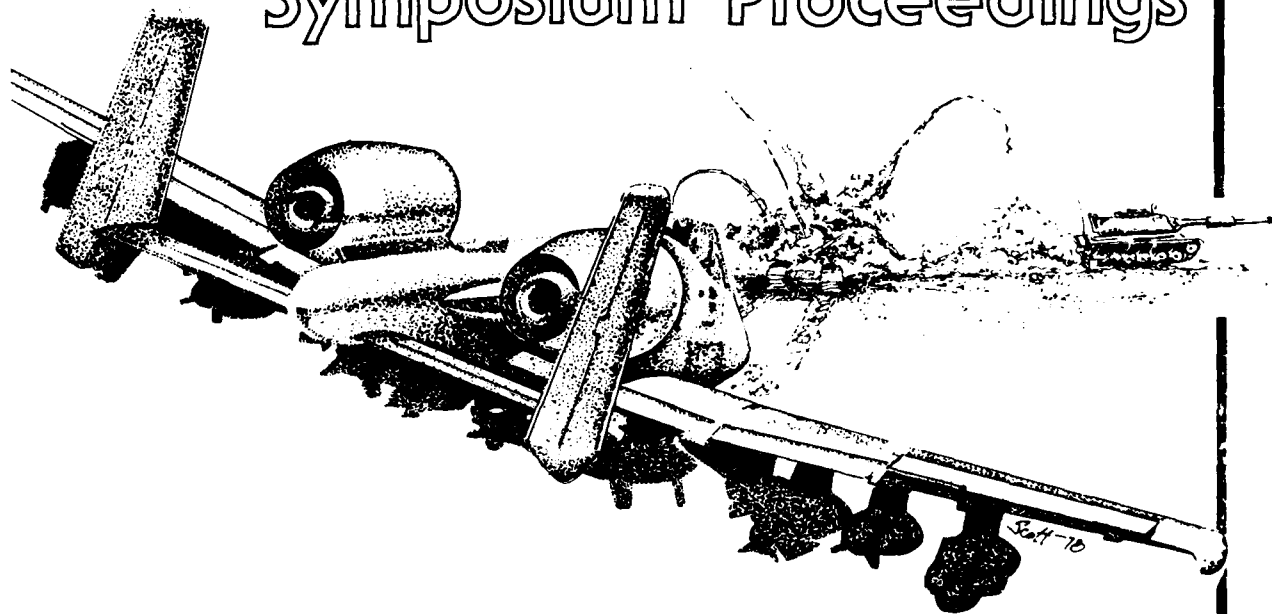
LEVEL

SDTIC
ELECTE
APR 9 1980
D

ADA 082875

Fourth

Aircraft/Stores Compatibility Symposium Proceedings



SPONSORED BY:
JOINT TECHNICAL COORDINATING
GROUP FOR MUNITIONS DEVELOPMENT

HELD AT:
CIVIC AUDITORIUM
FORT WALTON BEACH, FLORIDA
12-14 OCTOBER 1977

FILE COPY

APPROVED FOR PUBLIC RELEASE, DISTRIBUTION UNLIMITED

8049002

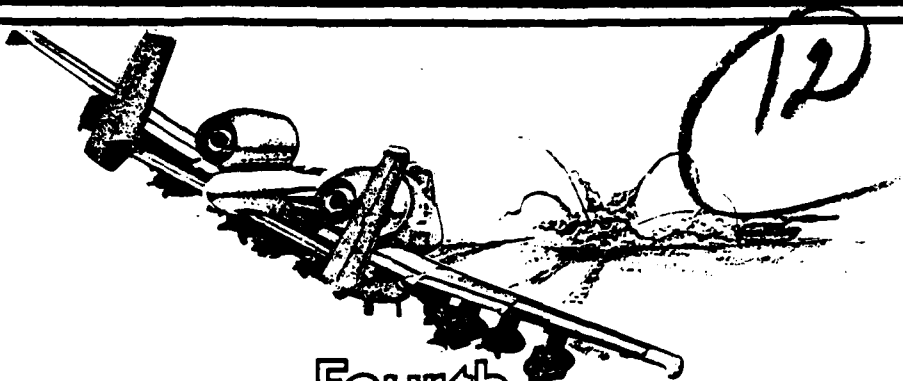
DDC

NOTICE

When Government drawings, specifications, or other data are used for any purpose other than in connection with a definitely related Government procurement operation, the United States Government thereby incurs no responsibility nor any obligation whatsoever; and the fact that the Government may have formulated, furnished, or in any way supplied the said drawings, specifications, or other data, is not to be regarded by implication or otherwise as in any manner licensing the holder or any other person or corporation, or conveying any rights or permission to manufacture, use, or sell any patented invention that may in any way be related thereto.

DISTRIBUTION. All papers have been approved for public release, with unlimited distribution, and are so marked on their title pages. The widest dissemination of this document is encouraged.

All papers were reviewed for release in accordance with AFR 190-12 and AFR 190-17 or appropriate USA or USN documents. Distribution statements were made in accordance with AFR 80-45 or appropriate USA or USN documents which implemented DOD Directive 5200.20, 24 Sep 70. Initial distribution of this document, to the List of Attendees, accomplished by the Air Force Armament Laboratory (DLJC), Eglin AFB, FL 32542, USA. Other requests for this document must be referred to the Defense Documentation Center (DDC), Cameron Station, Alexandria, VA 22314, USA (Attn: TCA).



Fourth
Aircraft/Stores Compatibility
Symposium Proceedings

12-14 OCTOBER 1977

VOLUME I

DTIC
SELECTED
APR 9 1980
C

SPONSORED BY
JOINT TECHNICAL COORDINATING GROUP
FOR
MUNITIONS DEVELOPMENT
(JTCG/MD)

PROCEEDINGS COMPILED BY
AIR FORCE ARMAMENT LABORATORY
ARMAMENT DEVELOPMENT AND TEST CENTER
AIR FORCE SYSTEMS COMMAND

UNCLASSIFIED

SECURITY CLASSIFICATION OF THIS PAGE (When Data Entered)

REPORT DOCUMENTATION PAGE		READ INSTRUCTIONS BEFORE COMPLETING FORM	
1. REPORT NUMBER	2. GOVT ACCESSION NO.	3. RECIPIENT'S CATALOG NUMBER	
4. TITLE (and Subtitle) Aircraft/Stores Compatibility Symposium Proceedings (with) H. H. et Fort Walton Beach, Florida on 12-14 October 1977, Volume I		5. TYPE OF REPORT & PERIOD COVERED Final - 12-14 Oct 77	
7. AUTHOR(s) Various, described in text.		6. PERFORMING ORG. REPORT NUMBER JTCG/MD WP12	
9. PERFORMING ORGANIZATION NAME AND ADDRESS Various, described in text.		8. CONTRACT OR GRANT NUMBER(s)	
11. CONTROLLING OFFICE NAME AND ADDRESS Aircraft Compatibility Branch Munitions Division Air Force Armament Laboratory		10. PROGRAM ELEMENT, PROJECT, TASK AREA & WORK UNIT NUMBERS	
14. MONITORING AGENCY NAME & ADDRESS (if different from Controlling Office) Air Force Armament Laboratory Armament Development and Test Center Eglin AFB FL 32542		12. REPORT DATE 12 - 14 October 1977	
		13. NUMBER OF PAGES 508	
		15. SECURITY CLASS. (of this report) UNCLASSIFIED	
16. DISTRIBUTION STATEMENT (of this Report) Approved for public release: distribution unlimited. JTCG/MD-WP-12-Vol-1		15a. DECLASSIFICATION/DOWNGRADING SCHEDULE	
17. DISTRIBUTION STATEMENT (of the abstract entered in Block 20, if different from Report) Clifford L. Bore Edward M. Schmidt Edmund J. Gier			
18. SUPPLEMENTARY NOTES Volumes 1 and 2 Available in DDC			
19. KEY WORDS (Continue on reverse side if necessary and identify by block number)			
Aircraft	Aeroelastic	Aeroheating	Scaling
Store	Wind Tunnel	Electromagnetic	A-10
Compatibility	Flight Test	Jettison	F-16
Aerodynamics	Cost Effectiveness	Separation	Airloads
Structures	Muzzle Blast	Flowfield	Ejector Racks
			Bomb Racks
			Lugs
			MIL-A-8591
20. ABSTRACT (Continue on reverse side if necessary and identify by block number) These proceedings contain the technical papers presented at the Fourth Aircraft/ Stores Compatibility Symposium held at the Civic Auditorium, Fort Walton Beach, Florida, USA on 12-14 October 1977 which was sponsored by the Joint Technical Coordinating Group for Munitions Development (JTCG/MD). Purpose of the symposium was to bring together world-wide technical expertise to review and discuss air- craft/store compatibility developments and experiences. Technical papers were presented in five different sessions: General, Store Separation, Aero/Structures, Bomb Racks/Interface, and Experimental. Each of the 35 papers (Cont'd on reverse)			

DD FORM 1 JAN 73 1473 EDITION OF 1 NOV 65 IS OBSOLETE

UNCLASSIFIED

SECURITY CLASSIFICATION OF THIS PAGE (When Data Entered)

440X01

discuss

UNCLASSIFIED

SECURITY CLASSIFICATION OF THIS PAGE(When Data Entered)

in the proceedings has its own abstract, and contains sections including presentation of data, discussion of findings, and recommendations/conclusions. The compilation of these papers, each focusing on the compatibility problem, should prove extremely valuable to aircraft and store designers by making each aware of the others' technical problems and possible solutions.

UNCLASSIFIED

SECURITY CLASSIFICATION OF THIS PAGE(When Data Entered)

FOREWORD

This publication contains the proceedings of and technical papers presented at the Fourth JTCG/MD Aircraft/Stores Compatibility Symposium, held at the Civic Auditorium, Fort Walton Beach, Florida, USA on 12-14 October 1977.

The purpose of the symposium was to bring together the technical expertise within Government and industry throughout the world to review and discuss compatibility developments and experiences. Exchanging methods and ideas is essential in present and future systems development. No one organization holds all the answers to aircraft/stores compatibility problems. Solutions to these problems depend upon coordinated efforts by both aircraft and store designers who are aware of the other's requirements.

The symposium committee wishes to express its appreciation to those persons responding to the call for papers, the authors and the presenters, the session chairmen, and the attendees for their contributions in making the symposium highly successful. Special appreciation is extended to Major General Howard M. Lane, USAF, Commander, Armament Development and Test Center, Air Force Systems Command, for his welcoming remarks in opening the symposium.

Accession For	
NTIS <input type="checkbox"/>	<input checked="" type="checkbox"/>
DDC TAB <input type="checkbox"/>	<input type="checkbox"/>
Unannounced <input type="checkbox"/>	<input type="checkbox"/>
Justification <input type="checkbox"/>	<input type="checkbox"/>
By _____	
Distribution/ _____	
Availability _____	
Dist	Avail and/or special
A	

Acknowledgement is made to all those people from Eglin AFB who worked long hours so diligently, cheerfully and efficiently to give us such a pleasant, professional success.

Suggestions are welcomed for making our next conference (late 1979) even more productive. Comments may be forwarded to Mr. C. S. Epstein, Air Force Armament Laboratory (DLJCE), Eglin AFB, FL, USA, 32542.

Publication of this report does not constitute Air Force approval of the technical papers' findings or conclusions. It is published only for the exchange and stimulation of ideas.



CHARLES S. EPSTEIN
Chairman, Working Party 12
JTCG/MD

SYMPOSIUM COMMITTEE

Mr. C. S. Epstein	USAF/AFSC
Mr. W. P. Steeper	USN/NAVAIR
Mr. Frank Shifrar	USAF/AFLC
Mr. Larry Doyle	US Army/AVRADCOM

PAPER SELECTION

Mr. W. P. Steeper	USN/NAVAIR
Mr. C. S. Epstein	USAF/AFSC

SESSION CHAIRMEN

GENERAL	Mr. R. V. Frank, Army AVRADCOM
STORE SEPARATION	Mr. B. R. Bowers, USAF AFATL
AERO/STRUCTURES	Mr. W. P. Steeper, USN NAVAIR
BOMB/RACKS INTERFACE	Mr. T. E. Milhous, USN NADC
EXPERIMENTAL	Mr. C. S. Epstein, USAF AFATL

PROCEEDINGS

Mr. C. S. Epstein	USAF/AFSC
-------------------	-----------

HOST ORGANIZATION

The Armament Development and Test Center
Air Force Systems Command

TABLE OF CONTENTS

VOLUME 1

PAPERS

PAGE

GENERAL SESSION

1. THE INFLUENCE OF AERODYNAMIC DESIGN OF EXTERNAL STORES ON EFFECTIVENESS/COST RATIO OF AN AIRFORCE
C. L. Bore
Hawker-Siddeley Aviation, Ltd. 1
2. INVESTIGATION OF MUZZLE BLAST FROM AAH, 30MM, AREA WEAPON SUBSYSTEM.
E. M. Schmidt and E. J. Gion
US Army Ballistic Research Laboratory 11
3. KINETIC HEATING OF AIRCRAFT CONVENTIONAL ARMAMENTS AND EQUIPMENT
K. G. Smith
Hunting Engineering Ltd 33
4. ELECTROMAGNETIC CHARACTERISTICS OF ARMAMENT EQUIPMENT
E. Dankievitch
Dayton T. Brown, Inc.
D. Ballard
Naval Air Systems Command 107
5. ON THE PERTURBED MOTION OF AN AIRCRAFT FOLLOWING THE JETTISONING OF A STORE
S. M. Ramachandra
Hindustan Aeronautics Ltd 125

STORE SEPARATION SESSION

6. A RAPID PREDICTIVE METHOD FOR THREE-DIMENSIONAL TRANSONIC FLOW FIELDS ABOUT PARENT AIRCRAFT WITH APPLICATION TO EXTERNAL STORES
S. S. Stahara, M. J. Hensch, S. C. Perkins
and J. R. Spreiter
Nielsen Engineering and Research, Inc. 155

PAPERS

PAGE

7. ANALYTICAL EVALUATION OF THE LIMITATIONS OF THE
VARIOUS SCALING LAWS FOR FREEDROP STORE SEPARATION
TESTING 197
J. C. Marshall
Sverdrup/ARO, Inc.
8. APPLICATION OF A GENERAL PURPOSE DYNAMIC ANALYSIS
PACKAGE TO THE PROBLEMS OF STORE SEPARATION 235
B. H. Welch and B. J. Richter
Lockheed Missiles and Space Co, Inc.
9. A BROAD BASED TECHNIQUE FOR THE PREDICTION OF STORE
SEPARATION 255
D. Gardner and A. L. Guest
British Aircraft Corp Ltd
10. SIX-DEGREES-OF-FREEDOM SYSTEM FOR STORE SEPARATION 293
STUDIES IN ONERA WIND TUNNELS
Jacques Coste
Office National Dietudes et de Recherches Aerospatiales
(O.N.E.R.A.)
11. A-10 AIRCRAFT STORE CERTIFICATION PROGRAM REVIEW 305
Capt S. C. Korn
USAF Aeronautical Systems Division
R. J. Arnold
Air Force Armament Laboratory

AERO/STRUCTURES SESSION

12. EVALUATION OF PREDICTION METHODS FOR AIRCRAFT/EXTERNAL
STORE FLUTTER CLEARANCE 333
S. J. Pollock and D. E. Cooley
Air Force Flight Dynamics Laboratory
13. INVESTIGATION OF THE UNSTEADY AIRLOADS ON WING-STORE
CONFIGURATIONS IN SUBSONIC FLOW 367
J. W. G. Van Nunen, R. Roos, and J. J. Meijer
National Aerospace Laboratory (NLR)
14. PARAMETRIC APPROACH TO FLUTTER CERTIFICATION OF AIRCRAFT
CONFIGURED WITH EXTERNAL STORES 401
A. Clelland
Aeronautical Systems Division
15. PREDICTION OF THE UNSTEADY AIRLOADS ON HARMONICALLY
OSCILLATING SPHEROIDS BASED ON AN ANALYTICAL SOLUTION
OF THE GOVERNING WAVE EQUATION 429
K-L Chao and Dr. H. Forsching
Deutsche Forschungs-und versuchsanstalt for Luft-und
Raumfahrt (DFVLR)

PAPERS

PAGE

- | | | |
|-----|--|-----|
| 16. | FLUTTER MODEL STUDIES OF THE F-16 WING WITH STORES
J. T. Foughner, Jr.
NASA Langley Research Center
C. T. Bensinger
General Dynamics Corp | 455 |
| 17. | THE ONERA POSITION ON THE USE OF FEEDBACK CONTROL
AGAINST FLUTTER DUE TO EXTERNAL WING-MOUNTED STORES
R. Dat, R. Destuynder, and J. J. Angelini
Office National D'Etudes et de Recherches
Aerospaciales (O.N.E.R.A.) | 473 |

TABLE OF CONTENTS

VOLUME 2

<u>PAPERS</u>	<u>PAGE</u>
18. AERODYNAMIC INTERACTIONS OF STORES AND AIRFRAMES D. H. Peckham Royal Aircraft Establishment Paper presented by N. Gregory	495
19. THE AFATL LOADS PROGRAM; MACLIP (MAXIMUM AIRCRAFT CARRIAGE LOADS AT INSTALLED POSITIONS), A DISCUSSION OF THE TECHNIQUE C. W. Ingram and W. W. Dyess, Jr. Air Force Armament Laboratory	533
20. THE PROPER USE OF MILITARY SPECIFICATION MIL-A-8591E FOR DESIGN OF STORES TO BE USED BY THE USAF W. W. Dyess, Jr. Air Force Armament Laboratory	559
<u>BOMB-RACKS/INTERFACE SESSION</u>	
21. THE PREDICTION OF EJECTION RELEASE UNIT (ERU) PERFORMANCE M. J. Twigger, Royal Aircraft Establishment	581
22. TEST COMPARISON OF THE SADDLE LUG AND BAIL LUG STORE SUSPENSION AND RELEASE SYSTEMS D. R. McGivern Dayton T. Brown, Inc. T. E. Milhous Naval Air Development Center R. V. Frank Army Aviation Systems Command	613
23. IMPULSE CARTRIDGES AS THE POWER SOURCE FOR STORES SEPARATION EQUIPMENT W. P. Peck Naval Ordnance Station	639
24. MEASUREMENT OF SUSPENSION LOADS AND DETERMINATION OF SUSPENSION RELIABILITY FOR A STORE IN THE F-111 WEAPONS BAY T. L. Paez and S. D. Meyer Sandia Laboratories	653

PAPERS

PAGE

25. AN INVESTIGATION OF THE EFFECTS OF EXTERNAL STORES ON THE DYNAMIC STABILITY OF AIRCRAFT 703
Lt T. E. Speer
Air Force Armament Laboratory

EXPERIMENTAL SESSION

26. SIMULATION OF SWAY BRACES AND MOUNTING GAPS ON SMALL-SCALE MODELS FOR WIND TUNNEL TESTS 731
R. E. Dix
Sverdrup/ARO Inc
27. INFLIGHT MEASUREMENT OF AERODYNAMIC LOADS ON CAPTIVE STORES. DESCRIPTION OF THE MEASUREMENT EQUIPMENT AND COMPARISON OF RESULTS WITH DATA FROM OTHER SOURCES 755
G. J. Alders
National Aerospace Laboratory (NLR)
28. GENERATION OF AERODYNAMIC INFLUENCE COEFFICIENTS FROM AIRCRAFT-STORE SEPARATION KINEMATICS 787
G. F. Cooper and Jon Gnagy
Pacific Missile Test Center
29. A COMPARISON OF FLIGHT TEST RESULTS AND 6 DOF CALCULATIONS USING THE INCREMENTAL COEFFICIENT METHOD FOR RELEASES FROM THE F-111 WEAPONS BAY 813
R. N. EVERETT
Sandia Laboratories
30. EFFECTS OF EXTERNAL STORES ON THE AIR COMBAT CAPABILITY OF A DELTA WING FIGHTER 841
L. Spearman
NASA Langley Research Center
31. PRESSURE AND HEAT-TRANSFER MEASUREMENTS ON SEVERAL PYLON-MOUNTED STORE CONFIGURATIONS 861
R. K. Matthews and G.D. Spencer
Sverdrup/ARO Inc
Major J. C. Key, Jr.
Air Force Armament Laboratory
32. THE EFFECTS OF WEAPONS BAY TURBULENCE SUPPRESSION DEVICES ON WEAPONS CARRIAGE AND SEPARATION 895
R. L. Clark
Air Force Flight Dynamics Laboratory
J. W. Doran
Air Force Weapons Laboratory

<u>PAPERS</u>	<u>PAGE</u>
33. A SIMPLIFIED TECHNIQUE FOR THE SOLUTION OF SUBSONIC FLOWS USING SURFACE SINGULARITIES F. W. Martin and J. E. Burkhalter Auburn University	945
34. GRUMMAN STORE SEPARATION PHOTOGRAMMETRY TECHNIQUES T. J. Reilly Grumman Aerospace Corp	989
35. AIM-9E & J MISSILES - STATIC AND DYNAMIC STRUCTURAL CHARACTERISTICS AND CAPABILITIES DETERMINATION AND IMPROVEMENT PROGRAM FOR WARNER ROBINS AIR LOGISTIC CENTER (Alternate Paper - not presented) R. C. Fusco Dayton T. Brown, Inc.	1029
LIST OF ATTENDEES	1093

THE JOINT TECHNICAL COORDINATING GROUP (JTTCG) ITS MISSION, ORGANIZATION, AND PRODUCTS

THE MISSION

The JTTCG was formed in 1964 as an attempt to better coordinate the identification and solution of various technical problems known to be common among the three major service organizations. It is a mechanism to exchange information and jointly study identified common problems. Solutions are thus provided that are acceptable to the three services, reduce duplication of effort, and enhance interservice operability.

THE ORGANIZATION

The JTTCG (Fig 1) is chartered by the office of the Secretary of Defense and operates under the direction of the Joint Logistics Commanders (JLC). The JLC, which consists of the commanders of AFSC, AFLC, NMC and DARCOM, meet quarterly and agree on the fundamental courses of action to be jointly pursued.

Subordinate to the JLC are various working groups and panels. It is in these groups and panels where specific technical matters are actually resolved using the broader guidelines provided by the JLC. There are currently nine Technical Coordinating Groups (Fig 2) of which the relevant one to this technical area is the second one - Munitions Development (MD). Under this Coordinating Group there are fifteen Working Parties (Fig 3). This symposium is sponsored by Working Party 12, Aircraft/Stores Compatibility. The structure of Working Party 12 is shown in Figure 4.

THE PRODUCTS

The only practical way that a tri-service committee such as WP12 (and its predecessor organizations) can exert any lasting influence is to generate useful, timely, relevant documents addressing various aspects of their broad problem area. Achievement of this goal is manifest in the following sampling of WP12 efforts:

MIL-HDBK-244, Guide to Aircraft/Stores Compatibility. Addresses broad compatibility considerations and provides specific guidance on selection of design and qualification standards, specifications and criteria. (Published)

MIL-STD-1289, Ground Fit and Compatibility Tests of Airborne Stores. Provides procedures and criteria for evaluating the physical compatibility of stores with aircraft in a ground environment. (Published)

Aircraft/Stores Interface Manual (ASIM). Provides authoritative physical information on aircraft and suspension equipment needed to make preliminary evaluations of physical aircraft/store compatibility (Published). A second volume of this document is currently in preparation which will provide store mass properties and scaled drawings to be used with Volume I for aircraft/store compatibility studies.

MIL-STD-XXX, Aircraft/Stores Certification Procedures. Provides recommended procedures and criteria for conducting aircraft/stores compatibility ground and flight tests. Addresses preliminary tests such as wind tunnel and structural tests as well as final flight tests. (To be published about 3rd Quarter CY78)

MIL-STD-YYY, Bomb Rack Design. Provides geometric and structural design criteria, similar to that provided in MIL-A-8591E, for bomb racks. (In work, publication schedule not established)

Aircraft/Stores Compatibility Symposium. Held every other year since 1969 to exchange problems and ideas throughout the international military, industrial and academic community. Proceedings are published after each symposium.

Joint Development Plans. JDP's are drafted for various products to be developed for joint service use. These plans, when finalized, provide the basic guidance for design and qualification of the hardware desired. A recent example of this is the Multiple Stores Ejector Rack (MSER).

JOINT TECHNICAL COORDINATING GROUPS

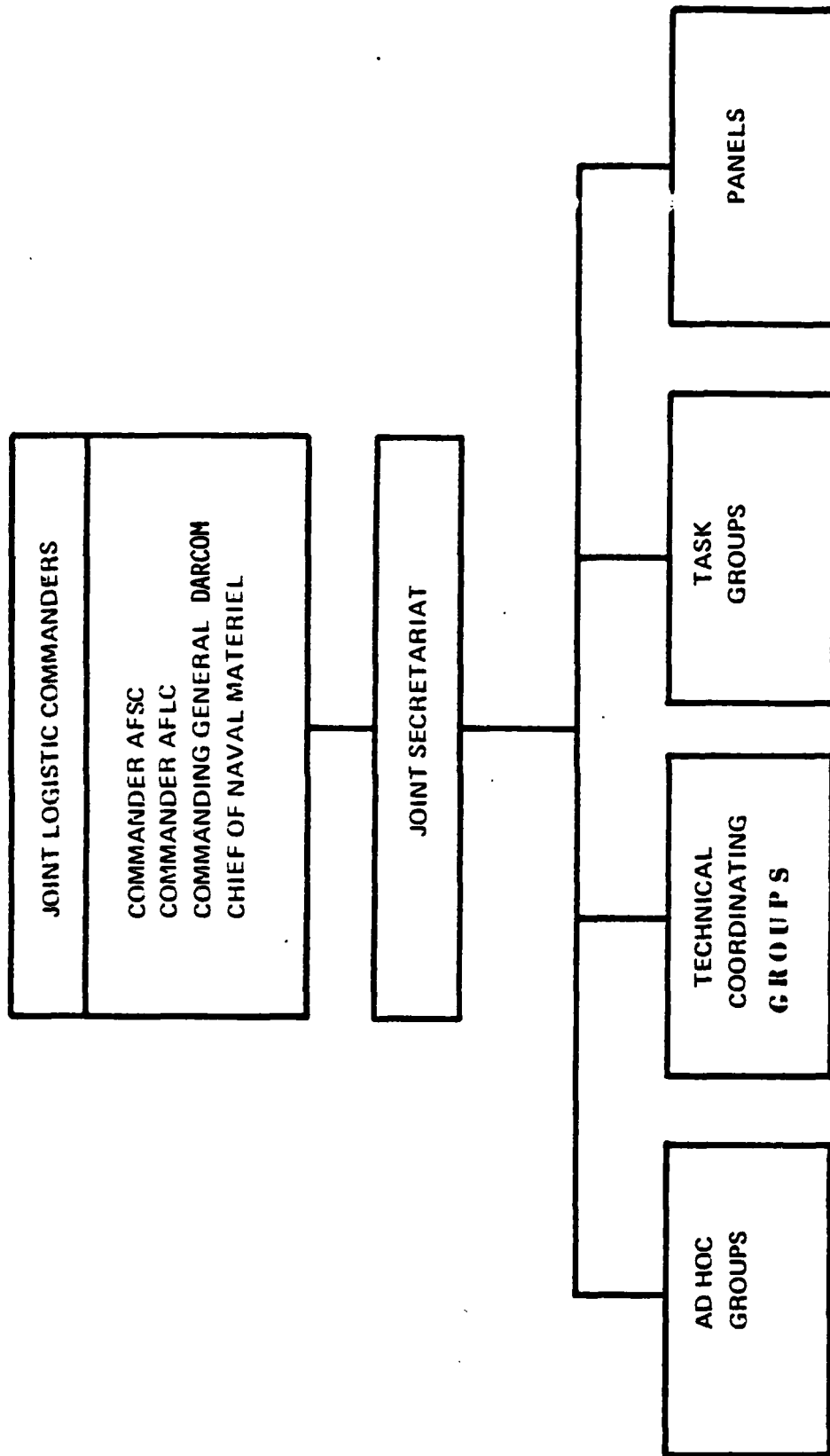


FIGURE 1

JOINT TECHNICAL COORDINATING GROUPS

- ME - MUNITIONS EFFECTIVENESS
- MD - MUNITIONS DEVELOPMENT
- MC - METEOROLOGY AND CALIBRATION
- ADMIT - AERONAUTICAL DEPOT MAINTENANCE
INDUSTRIAL TECHNOLOGY
- TIS - THERMAL IMAGING SYSTEMS
- AD - AERIAL DELIVERY
- AS - AIRCRAFT SURVIVAL
- RPV - REMOTELY PILOTED VEHICLES
- FF - FOSSIL FUELS STANDARDIZATION AND
UTILIZATION

JOINT TECHNICAL COORDINATING GROUPS

JTCG/MD

- WP NO. 1 - EXPLOSIVES
- WP NO. 2 - MISSILES AND ROCKETS
- WP NO. 3 - FIRE CONTROL
- WP NO. 4 - GUNS
- WP NO. 5 - PYROTECHNICS
- WP NO. 6 - SHIPPING/STORAGE CONTAINERS
- WP NO. 7 - FLAME AND INCENDIARY DEVICES
- WP NO. 8 - WARHEADS
- WP NO. 9 - FUZES
- WP NO. 10 - BOMBS, CLUSTERS, DISPENSERS AND MINES
- WP NO. 11 - RACKS, EJECTION CARTRIDGES
- WP NO. 12 - AIRCRAFT/STORES COMPATIBILITY
- WP NO. 13 - FUEL-AIR EXPLOSIVES
- WP NO. 14 - MUNITIONS HANDLING AND LOADING EQUIP
- WP NO. 15 - LASER ORDNANCE APPLICATIONS

AX

FIGURE 3

JOINT TECHNICAL COORDINATING GROUPS

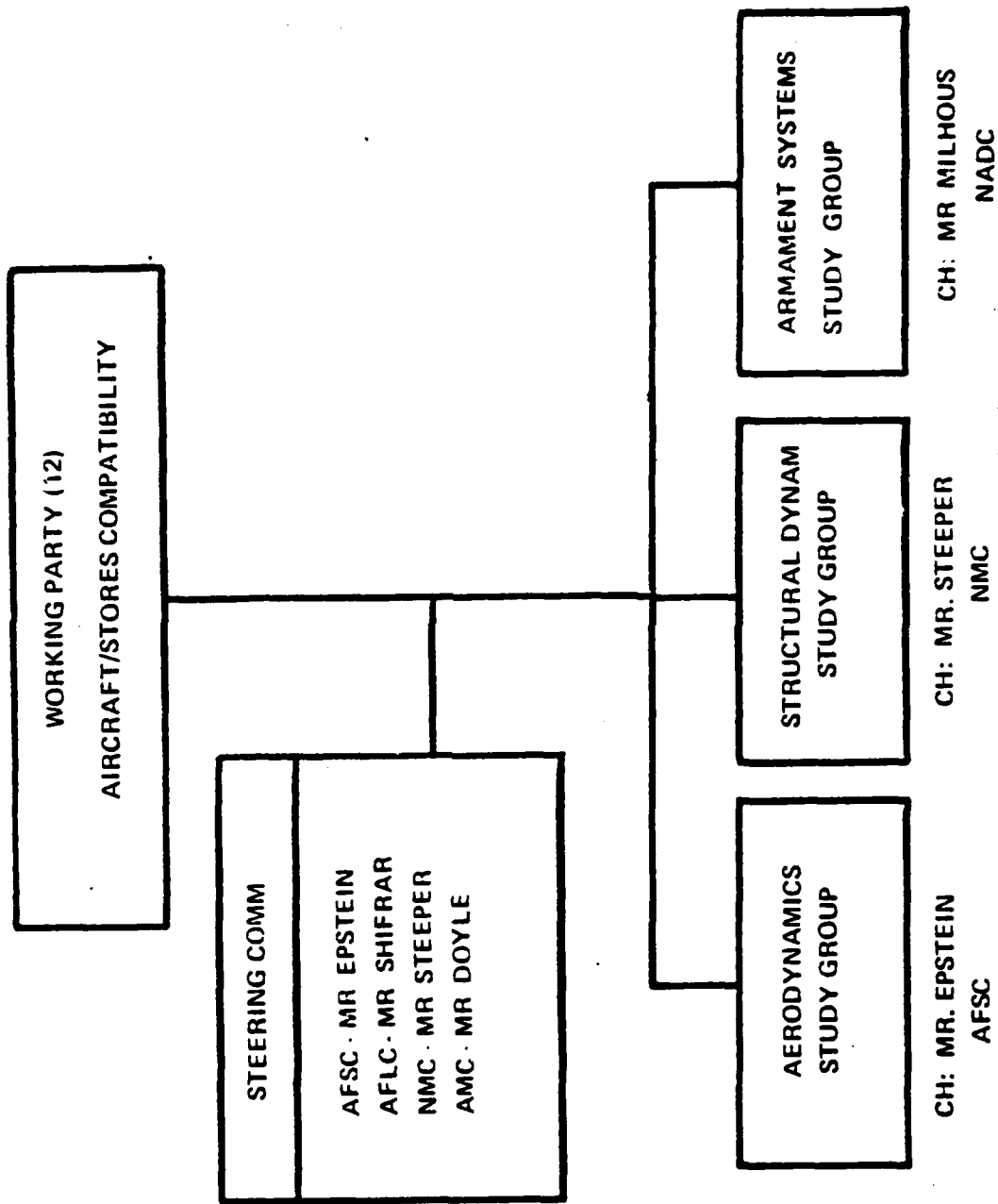


FIGURE 4

THE INFLUENCE OF AERODYNAMIC DESIGN OF
EXTERNAL STORES ON
EFFECTIVENESS/COST RATIO OF AN AIR FORCE

(U)

(Article UNCLASSIFIED)

by

Clifford L. Bore

Hawker Siddeley Aviation, Kingston, Surrey, U.K.

ABSTRACT (U) The aerodynamic effects of external stores are manifest by various changes to the performance, flying qualities, manoeuvrability and integrity of the aircraft that has to deliver those stores, as well as the accuracy of delivery of the stores. The extent and means of practical improvements in aerodynamic design and techniques have been studied, and it has been concluded that by introducing the recommended improvements, together with interchangeability, the effectiveness/cost ratio of air force should be doubled or better. This paper outlines briefly the nature of the improvements and discusses the effectiveness/cost concepts.

Approved for public release; distribution unlimited

THE INFLUENCE OF AERODYNAMIC DESIGN OF
EXTERNAL STORES ON
EFFECTIVENESS/COST RATIO OF AN AIR FORCE

by

Clifford L. Bore

INTRODUCTION

Over the past ten years or so, aircraft designers have been coming to the conclusion that the drag of external stores is commonly so excessive that the loaded aircraft are seriously degraded, in terms of effectiveness per unit cost, as a result.

Consequently research has been in progress in the U.K. for some years, which has demonstrated that the drag penalties of external stores can be cut drastically. Arising from a U.K. initiative, an AGARD Working Group was set up under my chairmanship (ref. 1) to study the drag and other aerodynamic effects of external stores, and this has now concluded.

The detailed recommendations (on how to improve the aerodynamics of stores) will not be discussed here but the broadest conclusions will be discussed in the light of an attempt to put different improvements into perspective by means of elementary effectiveness/cost assessments.

EFFECTIVENESS PER UNIT COST OF AIR FORCE

The aim of the assessments

The first question that arose in the course of the study was "Why should the standards of aerodynamic design change so radically halfway down the store pylons"(fig. 1) ?

In trying to answer that, one immediately comes up against arguments about the relative costs of aircraft and of the stores. So one needs some way of assessing the value of aerodynamic qualities in terms of money, to find which improvements will be the most valuable. It was clear that in the absence of such assessments we might be faced with responses from store purchasers that might be paraphrased something like this.

" O.K., so you believe you can reduce aerodynamic drag, and release disturbances, by redesigning stores and their carriers. You may well be right - but do you realise how much all those stores on the shelves cost ? It was A LOT OF MONEY, and we will not spend a lot more without a compelling reason ! How much are those improvements worth, in money ?"

Leading conclusions of assessments

That response contains good questions that merit unequivocal answers. It is not claimed that the answers outlined here are "correct", for there can be no single well-defined scenario in which our air forces will need to

operate, but they do illuminate which features contribute most sensitively to the effectiveness per unit cost. Furthermore, it is felt that these broad-brush assessments are sufficiently conservative to justify these conclusions that will be supported by the ensuing discussion:-

- 1) There is good reason to suppose that implementation of the improvements recommended will at least double the effectiveness per unit cost of air forces.
- 2) It seems that the necessary cost of investment in research, redesign and earlier re-equipment will be in the order of one per cent of the benefit flowing from this.

Assessing the value of an air force

The "value" is defined as proportional to its capability of killing targets in a short intensive war, in which the majority of the stock of aircraft are lost by the last day. The constant of proportionality is taken as the cost of a datum air force with present-day capabilities and costs, for the same scenario. Thus if modifications were incorporated which would multiply the target-kill probability by a factor of 1.50 (say) while the life cycle cost of the air force was factored by 1.10, it could be said that the value of the air force was 1.50 times the datum value, and the cost was 1.10 times the datum cost, so the modified effectiveness/cost ratio would be $(1.50)/(1.10)$, that is 1.36 - or a 36% improvement.

Drag

Fig. 2 shows an example of the significance of store drag on a fighter/ground attack aircraft. It can be seen that with the original pylons and twin-store carriers, the store drag when installed was one-and-a-half times the entire drag of the clean aircraft, so that a mere 13% reduction in store drag was equivalent to the entire drag of the wing. Improvements to the twin-store carrier and the bottom of the pylons brought the drag to the level that has been in service (second block). Using more recent work in the U.K., it should be possible to cut the installed drag down to the magnitude indicated by the dotted rectangle - a further improvement equivalent to eliminating the drag of the fuselage and tail of the clean aircraft ! It is not conceivable that improvements approaching this magnitude can be made on the clean aircraft, whatever forms of advanced aerodynamics may be devised.

In order to assess the value of the benefits stemming from drag improvements, a number of mission calculations have been made, based on typical drag reductions demonstrated in wind-tunnel tests for pylon-mounted stores on both AS and CAS aircraft. These reductions of drag were assumed to be split equally between the dropable stores and the pylons/racks. Greater benefits could be achieved in many cases, notably when using conformal carriage.

As one would expect, the various forms of benefit differ greatly.

- 1) The saving in fuel for the mission is less than might be guessed, because of the fixed allowances at base and for full-throttle flight. For existing aircraft the lifetime fuel is reduced by about 9% (and the lifetime fuel costs about as much as the aircraft). So this is not the big deal.

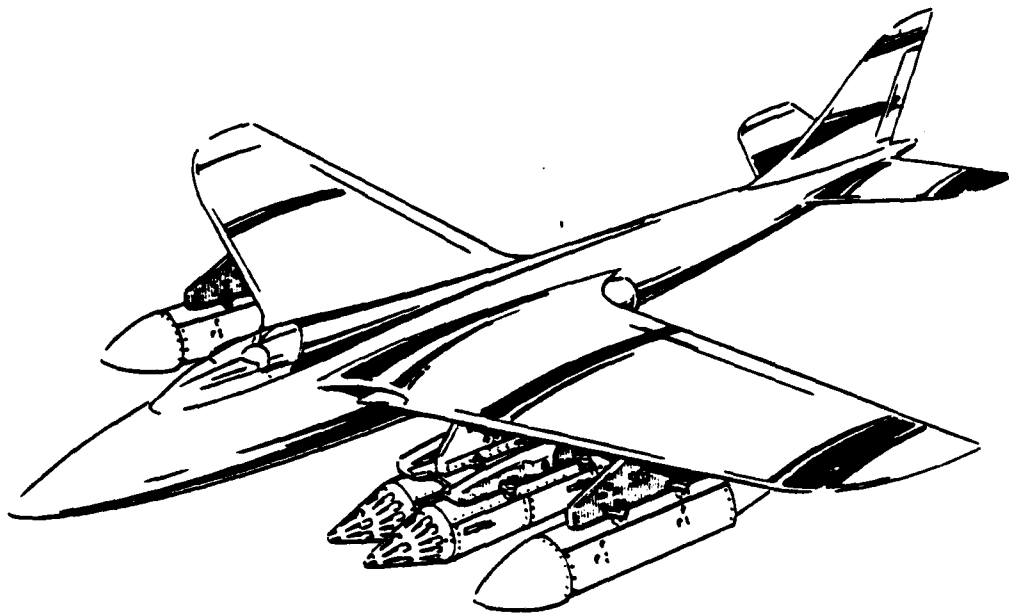


Fig.1 WHY SHOULD THE AERODYNAMIC CLEANLINESS CHANGE AT THE PYLON?

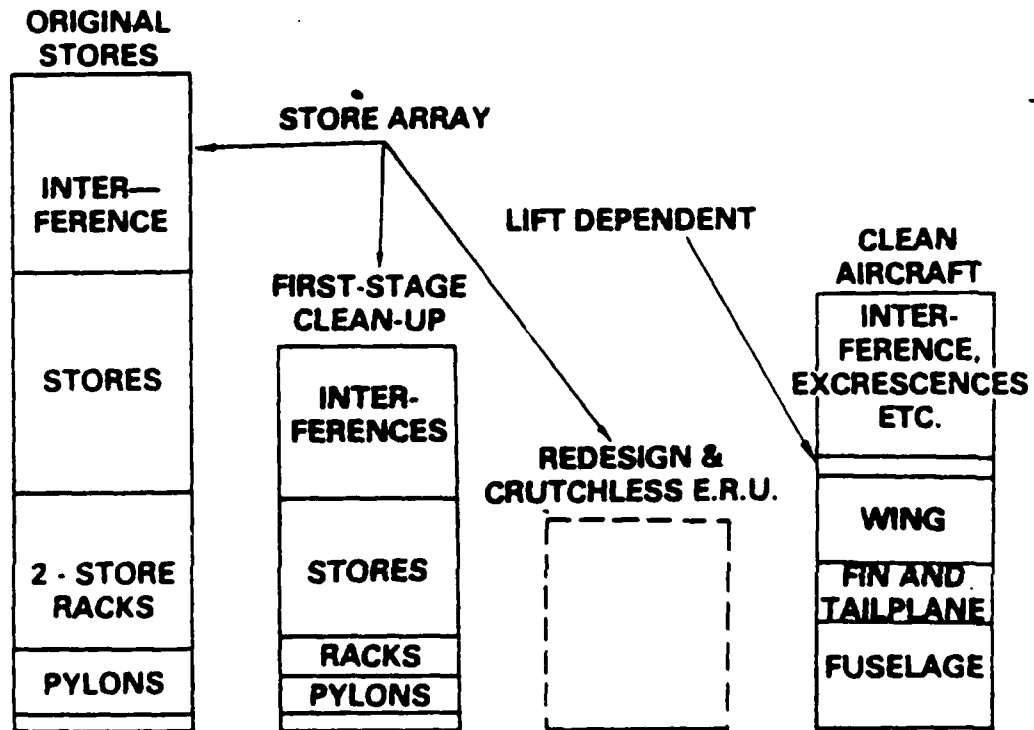


Fig.2 SIGNIFICANCE OF STORE DRAG AND DRAG REDUCTIONS

For new designs, the size and cost of the new aircraft could be reduced by about 3%, and the total saving of fuel would be around 12%

- 2) Area coverage over enemy territory, and target opportunities, would be increased about 33% if the aircraft were based at half its initial radius of action behind the front line, and about 48% if based back at two-thirds of its initial radius.
- 3) Penetration speed may be increased by perhaps 0.05 to 0.10 in Mach number. Typically this may reduce attrition and consequently the number of aircraft and crews needed by about 7% to 15%.
- 4) Performance and manoeuvrability is radically improved, particularly the SEP and turning rates. In air combat scenarios these benefits are enormous, as can be seen by reflecting that an improvement in turning rate of 5 degrees per second may halve the attrition rate and would therefore halve the number of aircraft and crews needed for a given war. For air combat scenarios, the typical drag reductions could lead to improvements of over 100% in effectiveness.
- 5) The average benefit due to drag reduction would depend on the particular mixture of modes pressed into use, but it seems reasonable to suppose that a typical average benefit stemming from drag reductions alone would be around 30% of the value of the datum air force.

Store Release

The effectiveness of an air force is proportional to the probability of destroying the target, so that a programme which halves the average area of weapon scatter doubles the value. To take another example arbitrarily, improvements in store jettison techniques which reduce the dimensions of the average scatter pattern by a mere 15% (both laterally and longitudinally) would increase the effectiveness of the air force by 30% on this score alone. It should be possible to do better than this quite readily.

Interchangeability and Standardisation

It has been agreed widely that NATO loses 30% to 50% of its potential effectiveness through lack of inter-operability (refs. 2 - 5). Furthermore, there have been authoritative complaints of corrosion, fretting and fatigue of ageing racks, and too many different types of racks (ref. 6). In effect, the only qualities shared by all existing racks are excessive drag and high release disturbances. If we accept the assurances given by high-ranking NATO officers, it follows that re-equipment with interchangeable racks and stores would multiply the datum effectiveness by 1.4 to 2.0 on this score alone. To err on the conservative side, it seems safe to suppose that the benefits of interchangeability (with all the improvements in logistics efficiency that follow) would be equivalent to at least a factor of 1.20 on effectiveness/cost ratio.

Overall Benefits

The overall benefits will be multiplied by each of the independent factors of improvement. The factors discussed here have been assessed (rather arbitrarily, erring on the side of caution) as around 1.3 for the performance benefits due to drag reduction, another 1.3 or more for improved accuracy of delivery, and 1.2 for benefits stemming from inter-operability. In addition, there should be benefits stemming from improvements in flying qualities, structural integrity and lower-cost store

certification programmes. These benefits will be significant (particularly the latter) but will not be allowed for here. Combining these, it appears that the effectiveness of NATO air forces could be better than doubled by incorporating the improvements recommended.

Costs

Designs to improved standards would not be more expensive than current designs, especially as standardisation would be improved. Re-equipment earlier than envisaged would be the main expense. Fig. 3 shows an assessment of life-cycle costs (based in part on ref.7) which suggests that purchase costs for stores to last the lifetime of an aircraft are around 10% of the life-cycle cost of the air force. It follows that even a massive programme of re-equipment equivalent to replacing 10% of all the stores would cost only about 1% of the datum cost of the air force. It should be borne in mind that a great deal of the research that should be put to use has already been done: it is the decision to use that investment in knowledge that will be crucial.

MANAGEMENT OF DESIGN

It has been argued that very large benefits can be reaped by investing a relatively small sum (the order of 1% of the benefit) in redesign of the aerodynamics of external stores and their carriers. At first sight it seems incredible that such inefficient weapon delivery systems (in terms of effectiveness for money) have resulted from such highly developed technologies as those at the heart of aircraft design and weapon design, especially to any engineer working assiduously on his assigned task in one field or the other. How can it happen that such meticulous design in each field may lead to such inefficiency when combined ?

The answer is, of course, rooted in history, but it can be seen now that the trouble has been that the aircraft and the stores have been designed as separate entities - not as intimately interacting components of a system.

The aircraft designer has been told (in effect) "Design a machine that will carry those stores a given distance at given speed, for minimum cost". Meanwhile the weapon designer has been told to "Design a missile that delivers so much punch, at minimum cost". This simple splitting of the task has often resulted in excessively costly aircraft because trivial cost savings on the store have led to grossly excessive drag on the combination. Keeping the stores "cheap" has made the air force expensive: a classical case of "the tail wagging the dog" !

In case plain language is not impressive enough, it is possible to state this conclusion more academically. Weapon delivery systems in the form of aircraft with external stores constitute an outstanding example of the fact that, in general, a system is not optimised by adopting the parameters that would optimise isolated parts of the system.

It can be concluded that aircraft and their stores should be designed and purchased in conjunction, to optimise the weapon system. The results of this recommendation will be manifest by elimination of excrescences, better aerodynamic shapes of stores including carriers, revised positioning of stores, improved crutchless (i.e. no sway braces), twin-ram ERU's and much wider interchangeability of stores onto different aircraft. Consequently fewer, smaller aircraft with smoother stores will provide more defence at less cost.

**LIFE CYCLE COST:
AIRCRAFT**

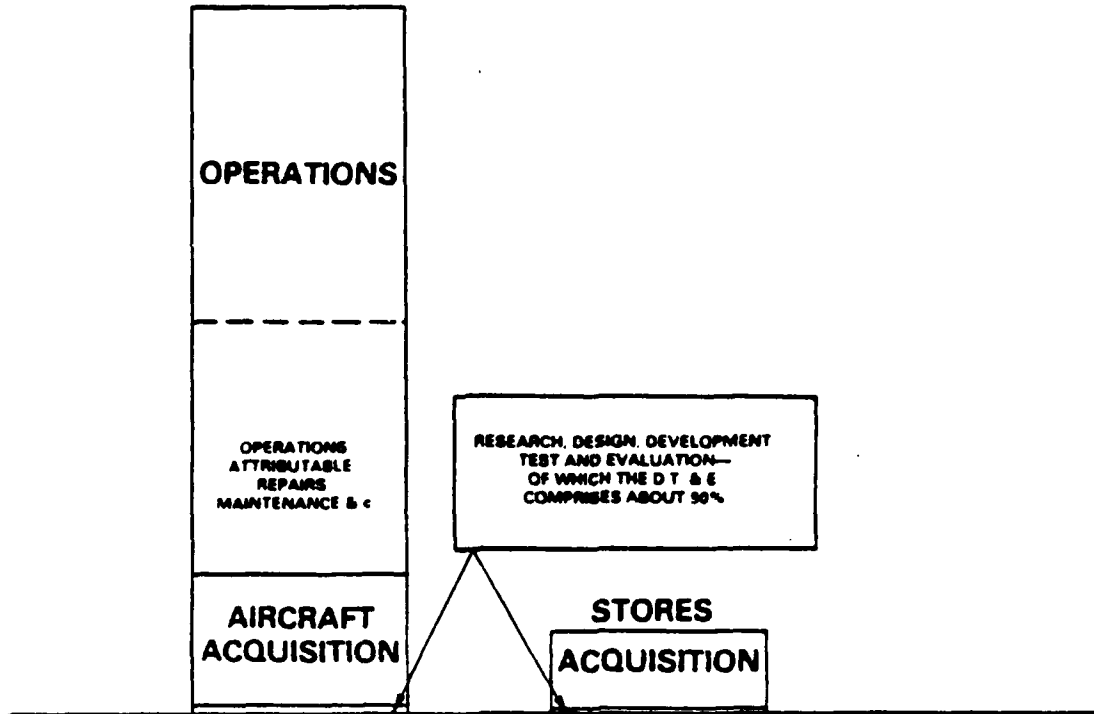


Fig.3 WHERE THE COSTS GO

The great danger of compartmented management is that one man's "lot of money" may be another man's "relatively small sum", so that the "relatively small" investment needed to secure much greater savings (say 100 times the investment) may be beyond the budget of the department that should make the investment. As Lamar said (ref. 7), this is a defect of management not only for purchasing (as in our topic) but also when research and the thinking stage of design is a very small, and separately funded, part of the entire air force procurement process. The overall sums of money are so large that the wastages flowing from compartmented management should not be perpetuated.

REFERENCES

- 1) C.L. Bore Objectives of the AGARD FDP Working Group on drag and other aerodynamic effects of external stores. Proc. 3rd Aircraft/Stores Compatibility Symposium, Arlington Va, Sept. 1975.
- 2) — NATO equipment standardisation - the German view. pp. 562-6 International Defense Review, Aug. 1976.
- 3) J.L. Fareham Strike aircraft and bombs - the West's compatibility problem. pp. 80-85 RUSI, Sept. 1976.
- 4) BBC TV "The Price of Peace". Transcript of transmission of 16th June, 1975. Panorama, BBC TV.
- 5) R.H. Ellis Air Defence of the West - a view from NATO'S central (Genl.) region. 15th Anglo-American Aero. Confce. May/June 1977.
- 6) T.E. Milhouse Future navy weapons suspension requirements. Paper 10, Vol. 1, Proc. 3rd. Aircraft/Stores Compatibility Symposium, Arlington Va, Sept. 1975.
- 7) W.E. Lamar The role of preliminary design in reducing development, production and operational costs of aircraft systems. Paper 1, AGARD-CP-147, Vol. 1. Oct. 1973.

AUTOBIOGRAPHY

Clifford L. Bore

Clifford L. Bore served an apprenticeship before going on to study aeronautical engineering at Queen Mary College (London University) - graduating B.Sc. (Eng) in 1951. Joined the R&D Department of Hawker Aircraft (Now Hawker Siddeley Aviation, Kingston) and became responsible for various topics in materials, structures and aerodynamic load prediction. Awarded the degree of M.Sc. (Eng) for a thesis of the prediction of fatigue life in 1959. In 1957 placed in charge of aspects of project aerodynamics such as air intake design, kinetic heating and wave drag. Became responsible also for wing design, on designs such as the P.1154 and the "Harrier." Now Head of Research. Represents the UK aircraft industry on the AGARD Fluid Dynamics Panel. Was chairman of the AGARD Working Group on "Drag and Other Aerodynamic Effects of External Stores," which has just completed its report.

INVESTIGATION OF MUZZLE BLAST FROM THE AAH, 30mm,
AREA WEAPON SUBSYSTEM

(Article UNCLASSIFIED)

by

EDWARD M. SCHMIDT AND EDMUND J. GION
Ballistic Research Laboratory
US Army Armament Research and Development Command
Aberdeen Proving Ground, MD 21005

ABSTRACT: (U) An experimental program has been conducted to investigate the nature of the muzzle blast generated from the 30mm gun to be installed on the Advanced Attack Helicopter (AAH). Both the free field and reflected blast overpressure levels are measured in order to compare with existing scaling laws. The data show the blast generation process to be more complicated than previously anticipated. In addition to the initial blast pulse, a succession of strong shocks are seen to emanate from the supersonic shear layer of the propellant gas jet. In some cases, the secondary pressure peaks are greater than the initial pulse. When compared with scaling laws, the agreement with the data is poor. Not only do these laws fail to predict correct pressure levels, they also lack sensitivity to changes in the weapon configuration.

"Approved for public release; distribution unlimited."

I. INTRODUCTION

The installation of medium caliber weapons on helicopters gives rise to interface problems between the gun and the aircraft. Both the recoil and blast impulses must be absorbed or reduced to acceptable levels. The Advanced Attack Helicopter (AAH) will incorporate a 30mm automatic cannon as a secondary armament system. Under the condition of maximum gun elevation, the weapon muzzle is placed in close proximity to the aircraft surface, Fig. 1. Since the resulting muzzle blast may damage structural and electrical components located in the helicopter nose, it is of interest to examine the detailed firing signature of the 30mm cannon.

Both experimental^{1,2} and theoretical^{3,4} investigations of the free field muzzle blast are available; however, since surface reflection is a fully three-dimensional, unsteady process, there is only a limited body of data available describing this process⁵⁻⁷. Mabey and Capps⁵ test a small caliber rifle in a wind tunnel and present data on the overpressure pulse at an adjacent surface. This type study is applicable to fixed wing aircraft which fire while in high-speed forward flight. For helicopters, firing may be accomplished from a hover or while in relatively low speed forward flight. Yagla⁶ has developed a technique to estimate the reflected blast overpressures on the surface of naval ships. The technique is based on a complete set of data describing the free field blast structure which is then used to develop the velocity at which the blast wave propagates across the surface of interest. By assuming that a Mach stem forms at the point of reflection, the overpressure level may be computed from the Rankine-Hugoniot relations. The agreement between the estimated and measured pressures is very good. The data on the free field blast structure are currently being generated from experimental measurements, which limits the use of the technique to those weapons whose properties are known. Additionally, the method does not give information on the detailed pressure-time history; rather, it only permits determination of the initial pressure behind the lead wave of the blast field.

One of the more accessible sources of information of both free field and reflected blast overpressures is contained in a set of scaling laws developed by Westine^{7,8}. Using measurements taken in the blast about a wide variety of guns, he develops a set of scaling parameters to describe the complete pressure pulse, i.e., peak pressure, impulse, and time of arrival. The parameters are based upon classical bare charge scaling parameters, but include modifications to account for energy imparted to the projectile, gun tube caliber and length.

The present paper is an investigation into the nature of muzzle blast from 30mm cannon. The study is directed at measuring the pressure pulses at selected locations, observing the blast development and reflection process, and comparison of measured data with the

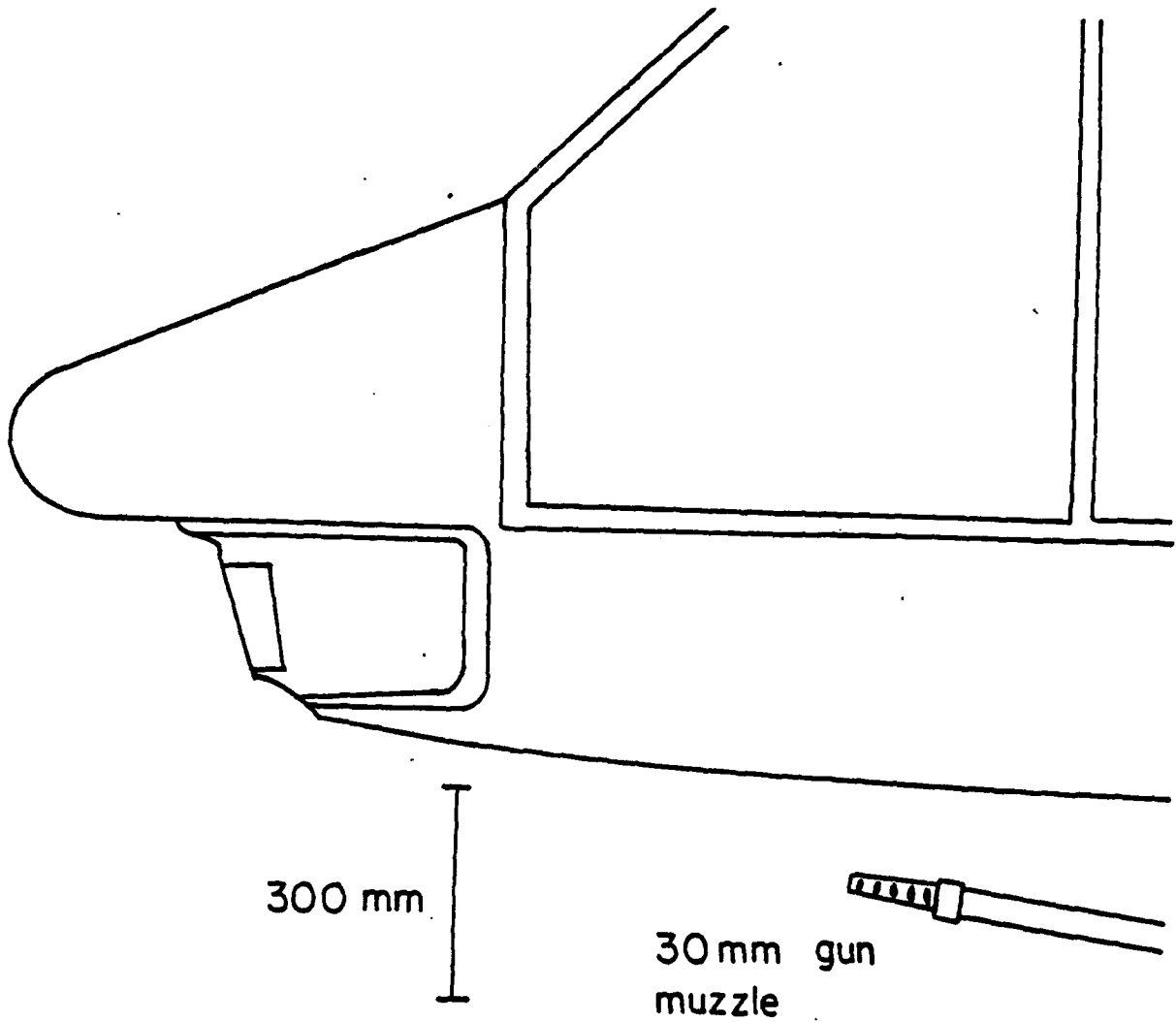


Figure 1. Schematic of 30mm Gun at Maximum Elevation Relative to AAH

Westine scaling relationships. Based on the results of this initial survey, the need for further research will be discussed.

II. EXPERIMENT

Tests are conducted in the BRL Aeroballistics Range⁹. Launch velocity is determined from the spark shadowgraph station data. The blast field is measured using the test set-up shown in Figures 2a and 2b. The 30mm cannon is located 300mm (10 calibers) above a flat plate having dimensions of 0.9m x 0.9m x 0.02m. The plate is parallel to the weapon boreline. Three pressure gauges are used to measure both free field and reflected blast overpressures. The free field gauge, FF1, is a static pressure probe of a "miniaturized" design manufactured by Southwest Research Institute¹⁰. The gauge is aligned with gun muzzle, 300mm (10 calibers) above it. On the plate surface, two Kistler, Model 201B2, piezoelectric transducers are installed. One gauge, P1, is directly below the muzzle while the second gauge, P2, is located 300mm forward of this station. In addition to pressure measurements, spark shadowgraphs of the muzzle blast are taken. Only one photograph is taken of each firing; therefore, multiple firings are required to describe the muzzle blast reflection process.

At the time these experiments were being considered, the AAH cannons were undergoing a reconfiguration to convert them from the WECOM-30 round to the ADEN/DEFA family of 30mm ammunition. This change was mandated in order to insure NATO commonality and interoperability. Therefore, an attempt was made to include representative samples of both types of ammunition in the current testing. Additionally, to cover the range of potential gun tube designs which were AAH candidates, two barrel lengths were included in the testing. The first is an aircraft cannon chambered for the WECOM-30 round and has a tube length of 1.07m (42 inches). The second is a Mann barrel chambered for the T206 round (a round similar to, but approximately 25mm longer than the WECOM-30) and has a tube length of 1.27m (50 inches).

In each weapon, two different rounds are fired: the WECOM-30 and a simulated ADEN-30, Figure 3. The WECOM-30 is the 30mm Cartridge, Training, XM639. Since actual ADEN ammunition was not available, a simulated cartridge was fabricated from the XM639 cartridge by pulling the projectile, inserting 5 grams more propellant, and reloading with a 30mm, HEIT 306 E10 projectile. A comparison of the physical properties of these rounds and an actual ADEN round is given in Table 1.

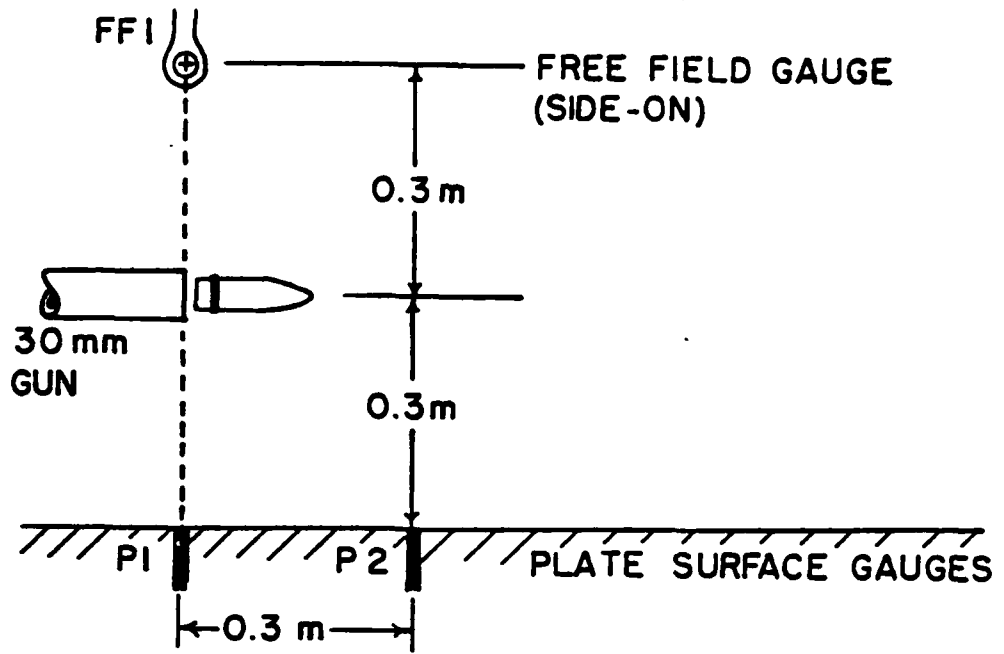


Figure 2a. Schematic of Test Set-Up

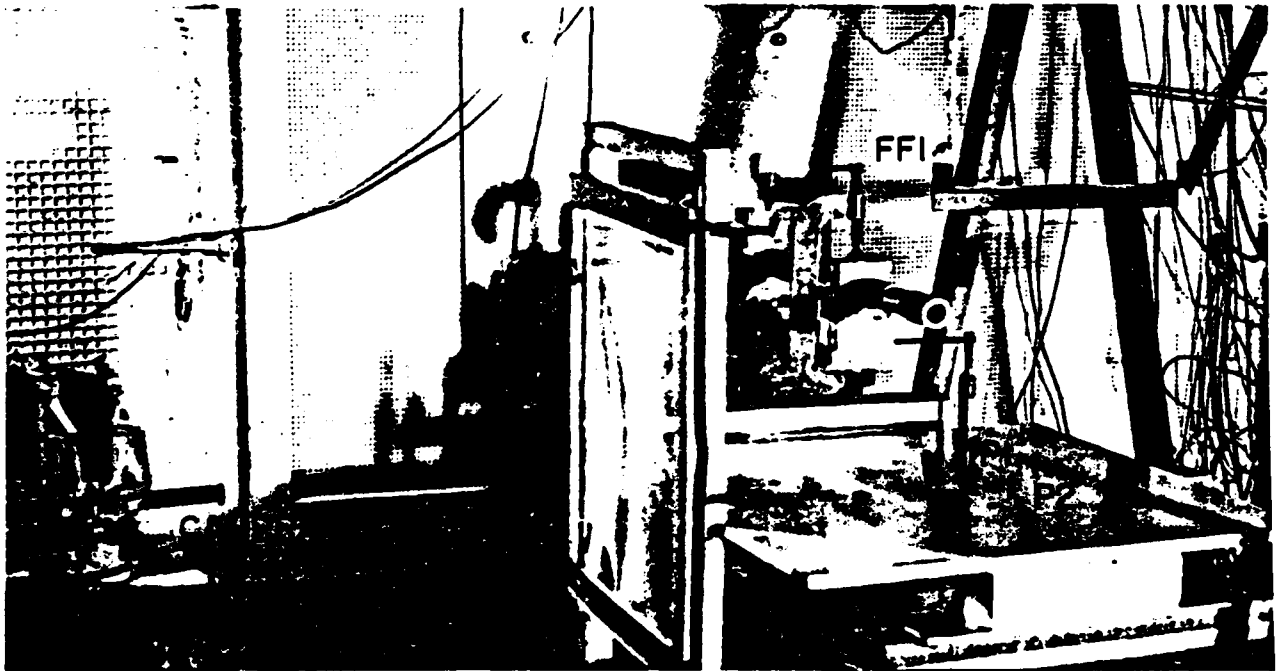


Figure 2b. Photograph of Test Equipment

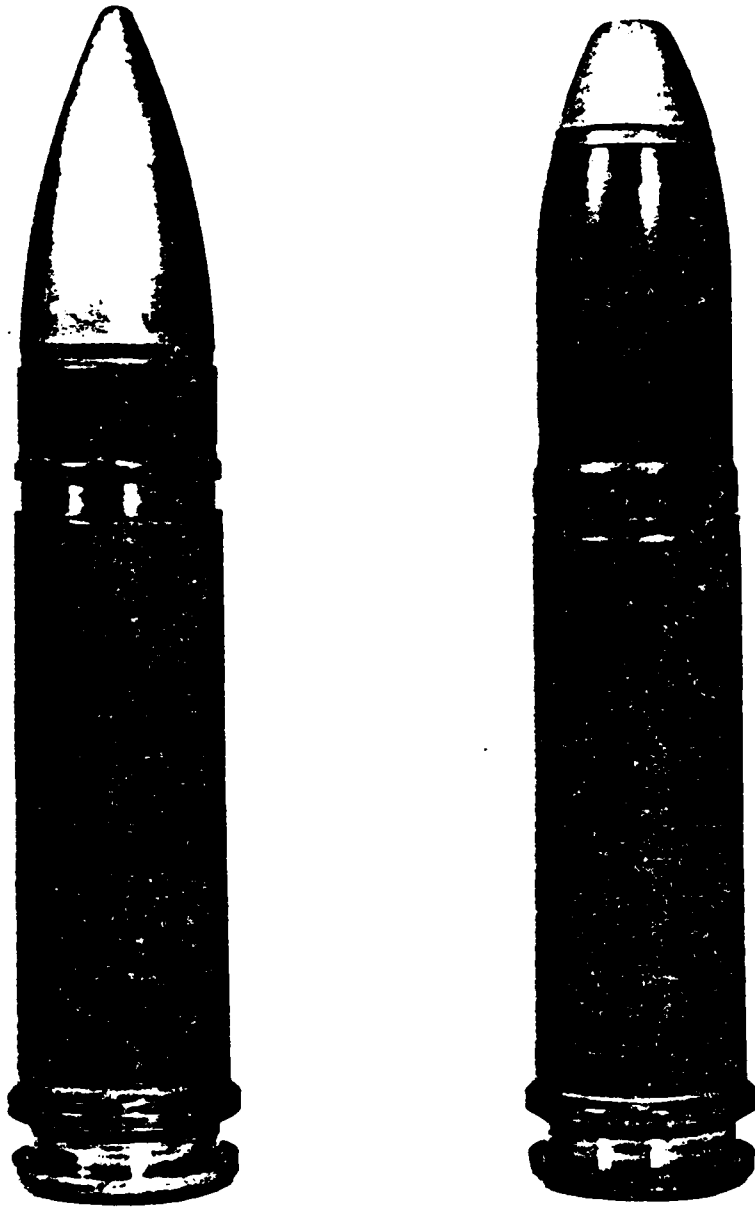


Figure 3. Photograph of Test Cartridges

TABLE 1: COMPARATIVE CARTRIDGE PROPERTIES

	PROJECTILE DESIGNATION	PROJECTILE WEIGHT (g)	PROPELLANT WEIGHT (g)	GUN TUBE LENGTH (mm)	MUZZLE VELOCITY (m/s)
WECOM-30	XM639,TP	193	40	1067	682
				1270	666
SIMULATED ADEN-30	T306E10,TP	256	45	1067	703
				1270	662
ADEN-30	MK4z	220	46.5	1516	792

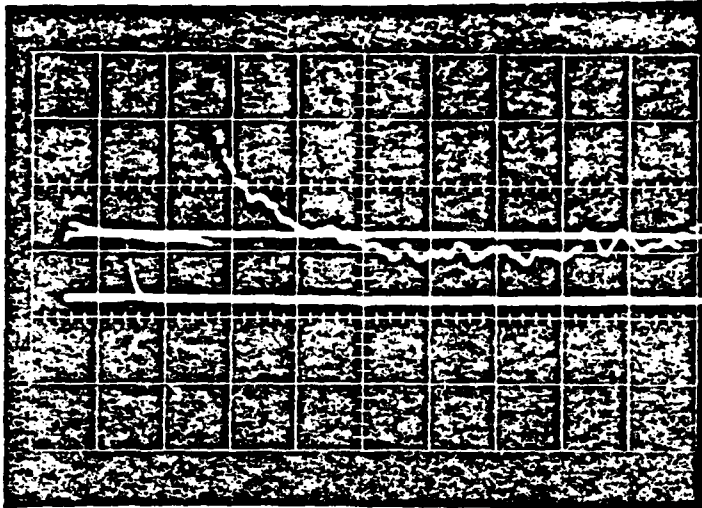
The simulated ADEN-30 is seen to be a reasonable approximation as a member of this family of ammunition. Examination of the muzzle velocity variation between the short and long tubes produces an apparent anomaly; namely, a velocity decrease as the gun tube is lengthened. This is due to the chambering of the longer tube. This weapon was chambered for a cartridge which is approximately 12.5mm longer than the present rounds. As such, the initial obturation and combustion are not optimal resulting in decreased ballistic efficiency.

III. RESULTS

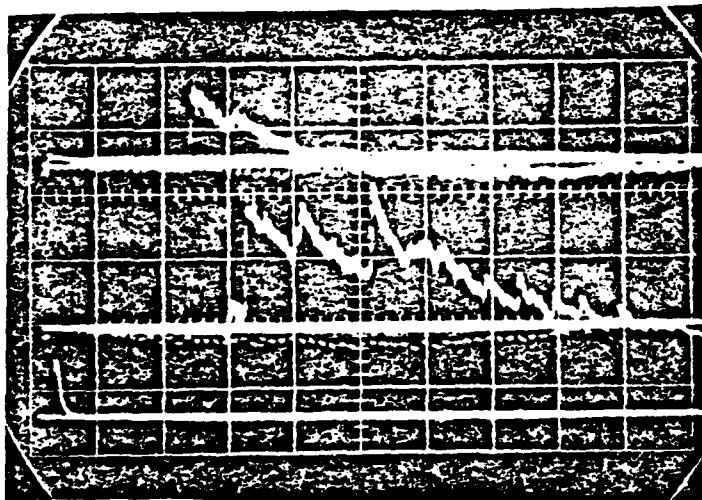
A sample set of pressure gauge outputs is shown in Figure 4. The data are for a single WECOM-30 round fired from the short tube; however, the significant features of these traces are common to all gun/cartridge combinations tested. The oscilloscopes are triggered simultaneously by the arrival of the precursor blast* at the first surface gauge, P1. The main blast arrives at both the free field, FF1, and plate, P1, gauges simultaneously. Since these are both 10 calibers from the muzzle, this indicates the symmetric nature of the muzzle blast prior to reflection from the plate. The pressure decay for these two gauges is also similar. Sixty-five μ s after arrival of the main blast both FF1 and P1 show the passage of a weak compression, and after 200 μ s, the pressure at both stations decays through ambient.

The trace obtained from the second plate gauge, P2, is quite interesting. This gauge is located on the plate surface ten calibers (0.3m) forward of the muzzle. The gauge output, Figure 4, shows the arrival of a series of pressure pulses in rapid succession. The low

*The precursor blast is generated by the column of air forced out of the gun tube ahead of the projectile.



FF1, FREE FIELD GAUGE



PI, PLATE SURFACE GAUGE

P2, " " "

Figure 4. Oscilloscope Traces of Transducer Outputs; Short Gun Firing WECOM-30 (Sweep = 100 microseconds/div.)

amplitude pulse of 20 μ s duration prior to the main blast is the precursor blast. The short duration of this pulse relative to that sensed at P1 indicates that the main blast is rapidly overtaking the precursor blast. After the main blast, a series of strong secondary compressions pass gauge P2 at roughly 100 μ s intervals. The second of these compressions shows a peak overpressure greater than that behind the main blast. The generation of these pressure pulses is clearly observed in the spark shadowgraphs, Figure 5.

The time base is referenced to a time zero when the projectile base clears the muzzle. Figure 5 shows the muzzle flow 86 μ s after arrival of the precursor blast and 130 μ s prior to arrival of the main blast. In addition to the precursor and main blasts, two sets of compression waves are readily apparent and are identified in Figure 5. The first set, termed lip-compressions, originates close to the muzzle lip within the shear layer of the propellant gas jet. This shear layer is a region where the high velocity propellant gases are accommodated to the nearly stationary outside air through the action of viscosity. The layer is either initially turbulent or rapidly undergoes transition to turbulent flow. Such a high velocity turbulent layer generates strong acoustic signals as it propagates. These signals are observed throughout the photographic sequence. The second set of compression waves, termed outer-layer compressions, seem to originate in the outer edge of the propellant gas jet. This region is thought to contain the vortex or "smoke" ring associated with weapon firing. The waves are seen to coalesce in the downrange direction as the flow field develops. This behavior explains why the secondary compressions are sensed at pressure gauge P2 but not at P1. Because the optical data are from a series of firings, it is not possible to develop a one-to-one correlation between the observed waves and measured pressure pulses.

The overpressures measured for both rounds fired from the short gun are presented in Figure 6. To permit comparison of the two sets of data, the time scale is referenced to the arrival of the main blast at gauge P1. The maximum pressure is measured at gauge P2, 45° forward of the muzzle. For the WECOM-30, the peak overpressure is 3.1 atmospheres (45 psi) and occurs after a secondary compression. Unfortunately, insufficient data was acquired to fully define the ADEN-30 pressure profile at the station. For the gauges located in line with the muzzle, the reflected pressure at gauge P1 shows similar behavior to the free field pressure at gauge FF1; however, the amplitude of the reflected pressure is roughly 2.4 times that of the free field value.

Similar data acquired from firings of the long gun are shown in Figure 7. In this case, the peak pressures again occur at gauge station P2; however, while strong secondary compressions are observed, their amplitude diminishes with respect to that of the main blast.

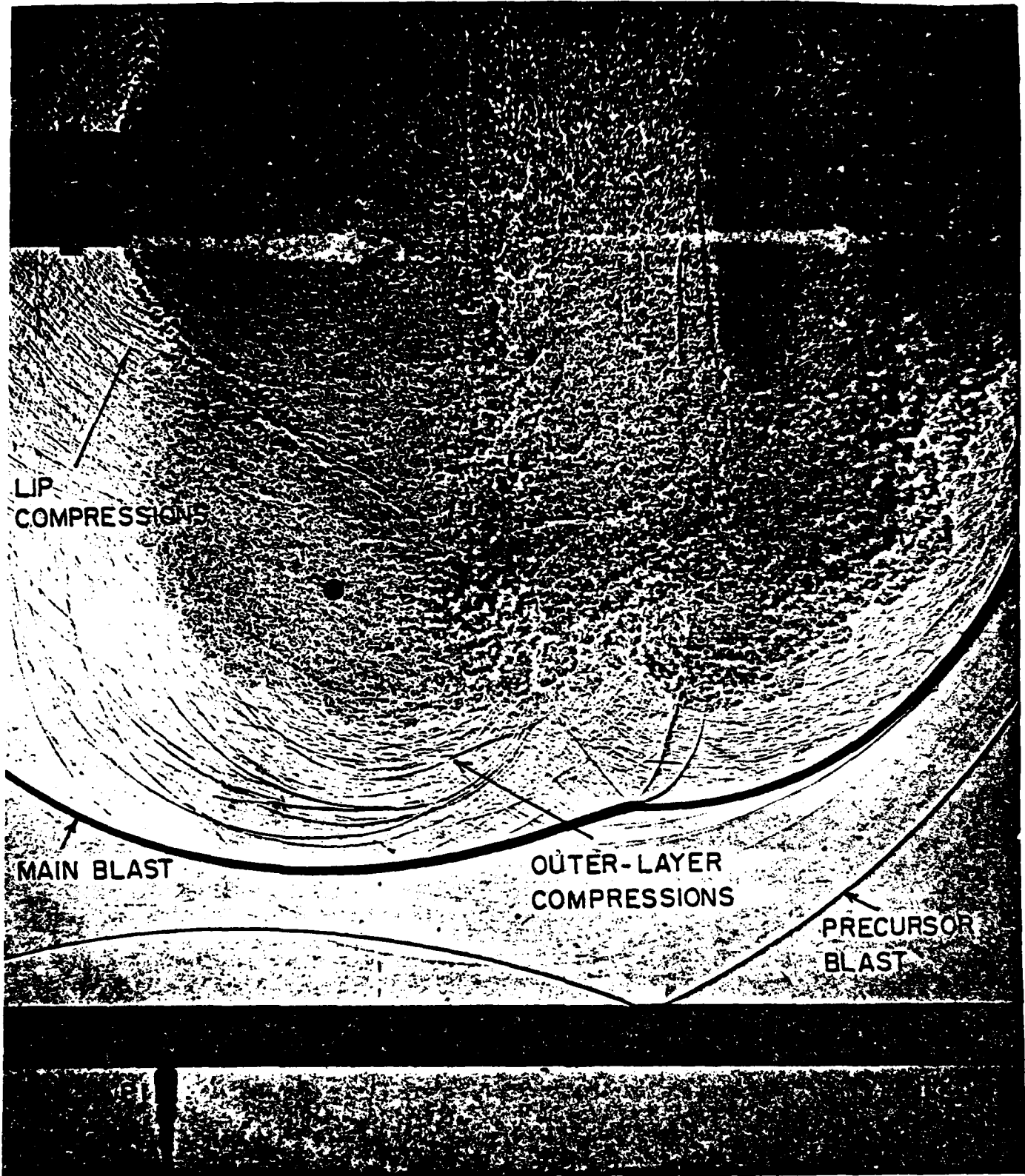


Figure 5. Spark Shadowgraph of Muzzle Blast from Short Gun
Firing WECOM-30, $t = 387$ microseconds after Shot
Ejection

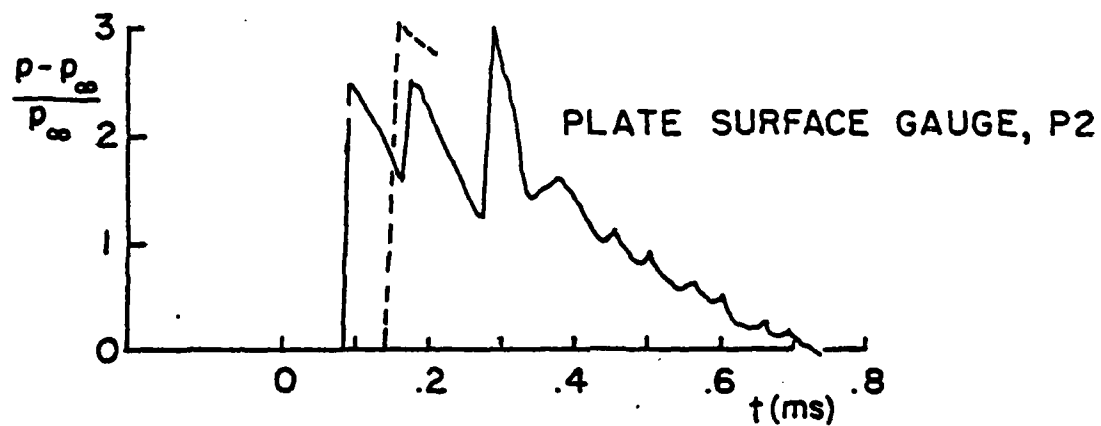
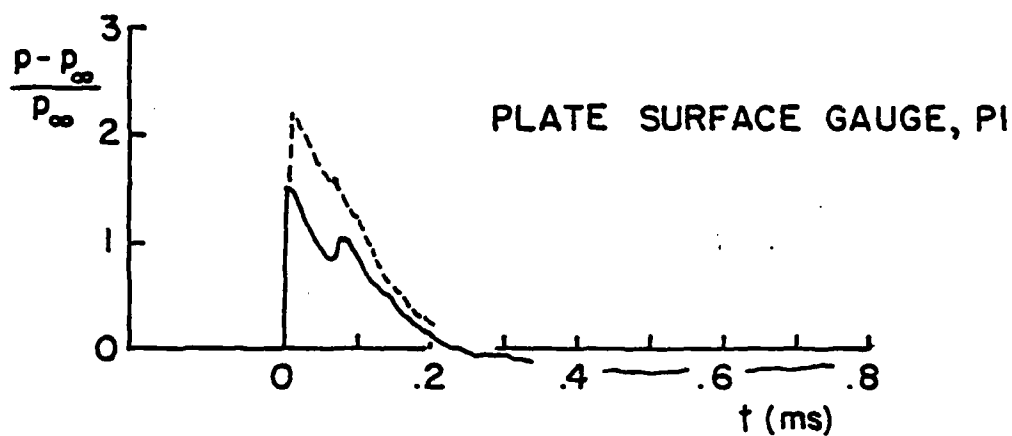
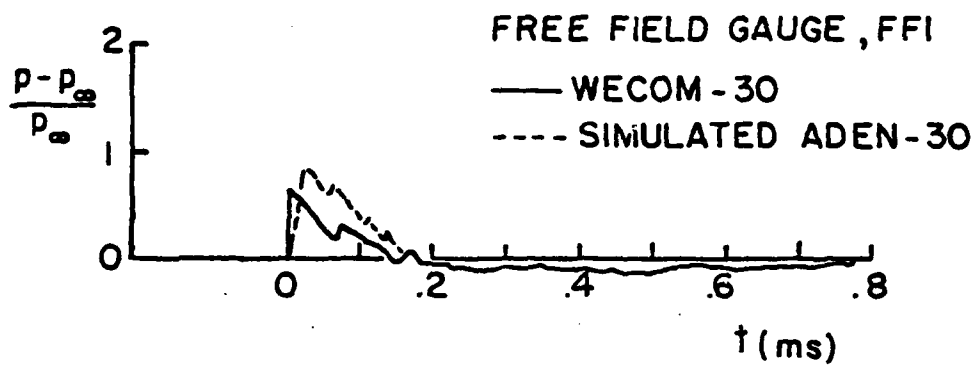


Figure 6. Measured Blast Overpressures from Short Gun,
 L = 1.07 m (42 inches)

FREE FIELD GAUGE, FFI

— WECOM-30

--- SIMULATED ADEN-30

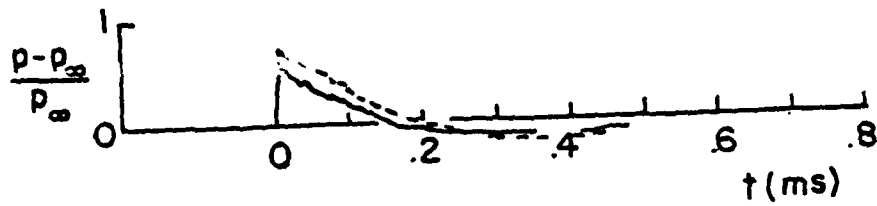


PLATE SURFACE GAUGE, P1

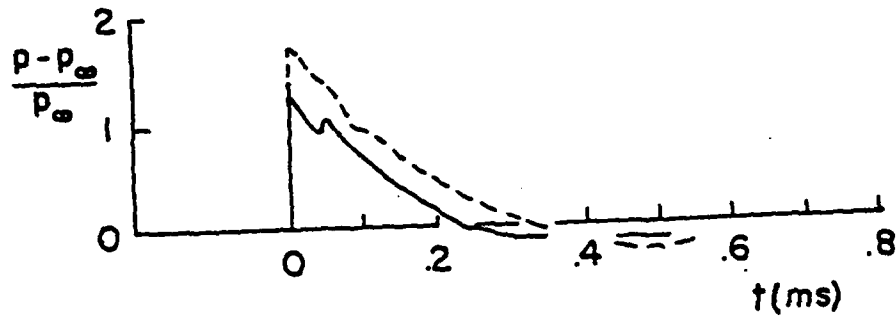


PLATE SURFACE GAUGE, P2

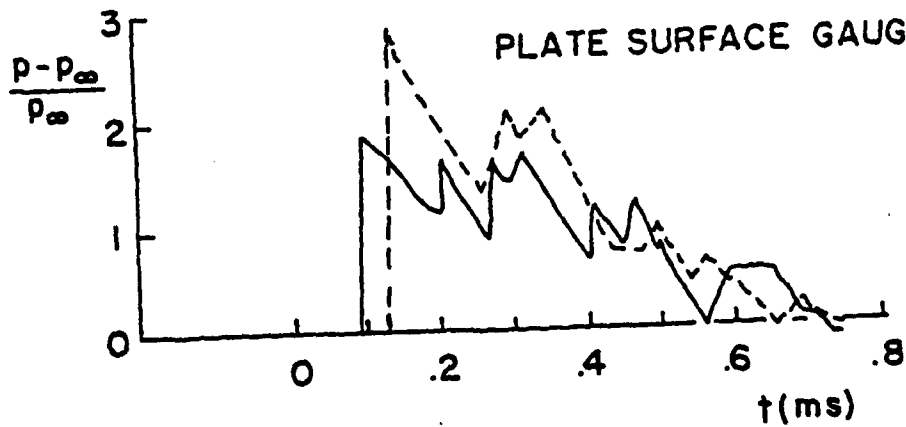


Figure 7. Measured Blast Overpressures from Long Gun,
L = 1.27 m (50 inches)

Comparison of Figures 6 and 7 demonstrates that the blast from the long gun is less intense than that from the short gun. It is of interest to examine the accuracy with which blast scaling laws model these results.

IV. COMPARISON WITH SCALING LAWS

Westine⁷ presents a scaling analysis which describes the muzzle blast from closed breech guns. The results are universal in the sense that any caliber or velocity weapon may be treated. Both free field and reflected blast properties are dealt with. By assuming that the blast has a smooth pressure decay (Friedlander equation), Westine's scaled peak pressure and impulse contours may be used to construct the positive phase of the blast overpressure pulse.

In describing the free field blast overpressure and impulse, Westine presents two types of scaling plots. In one case, he presents contours of scaling parameters based on a series of 20mm tests, Figure 8. In the other, he gives cross plots of these parameters along a line perpendicular to the gun muzzle, Figure 9. These are based on measurements taken from a wide variety of weapons ranging from a 0.22 caliber rifle through to a 105mm howitzer. A difficulty arises in comparing the two sets of data. Near the weapon muzzle, his contour plots and crossplots disagree by a factor of three or more. For this reason, both possible pressure pulses from his plots are computed and compared to the measured data, Figure 10.

The agreement between the results of the Westine scaling analysis and the present experiments is not good. Not only does the scaling law fail to predict the pressure levels and duration which agree with a given set of test data, it also does not show sensitivity to changes in the weapon firing configuration. For example, one of the peak overpressures predicted with the short gun firing WECOM-30 ammunition is close to the measured value; however, when the ADEN ammunition is fired, the prediction shows very low sensitivity to this change whereas the data records a 40% growth in overpressure.

Westine also presents a set of scaling contours which describe the reflected blast overpressure levels on a surface located beneath, but parallel to, the gun bore. These contours were developed from firings of two different small caliber weapons and cover a standoff of from 16 through 50 calibers between the plate and the muzzle centerline. The present data were acquired at a standoff of 10 calibers; therefore it is necessary to extrapolate Westine's results to this distance. The comparison between the scaling law and the present results is shown in Figure 11. It is seen that the agreement is extremely poor. While the measured overpressure levels show an increase of more than a factor of two over the free field values, Westine's reflected overpressure predictions are approximately equal to his free field values. This

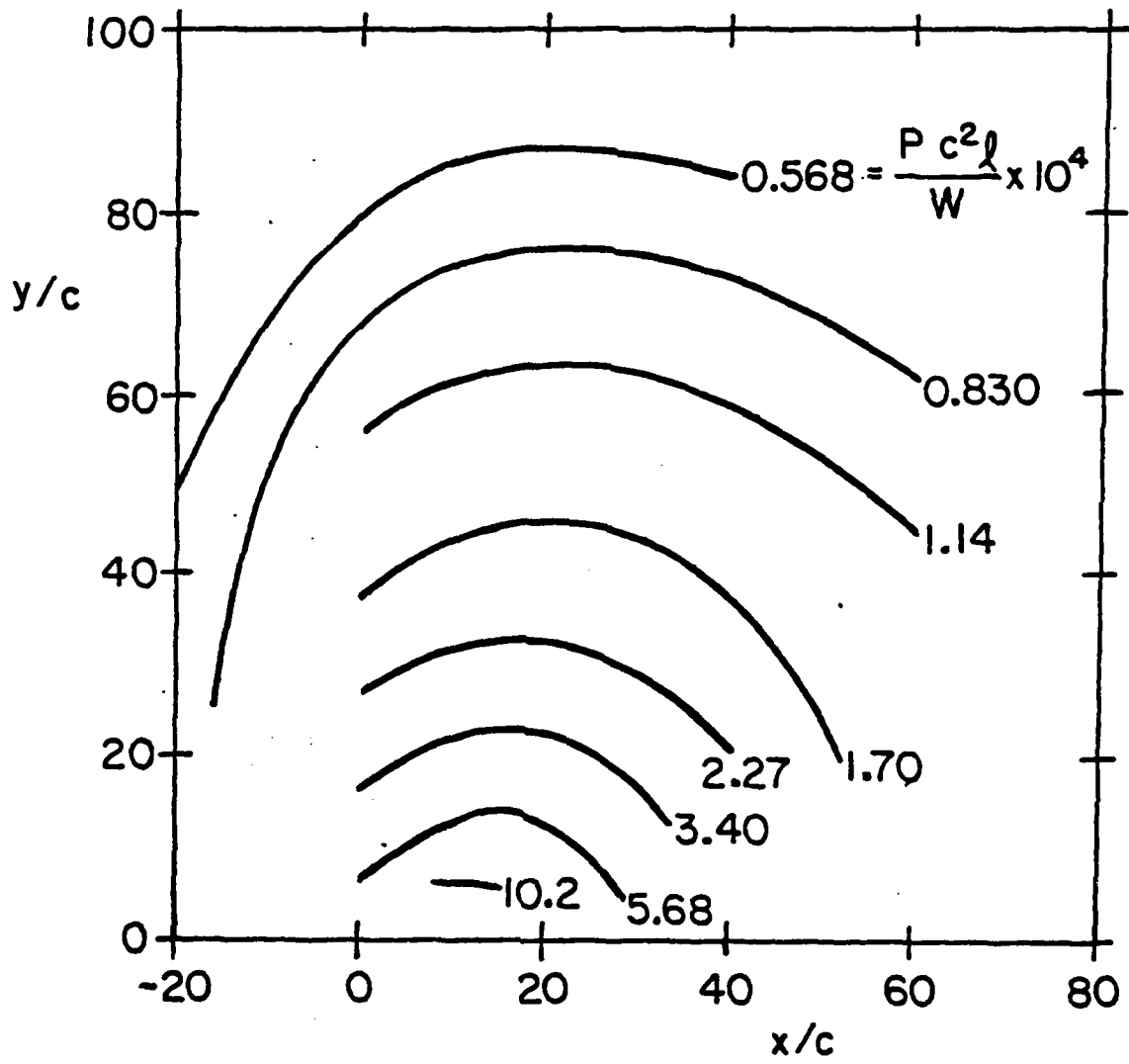
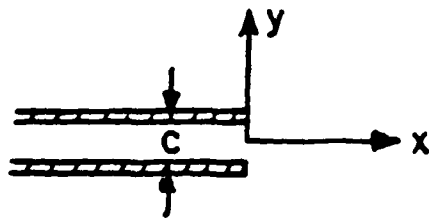


Figure 8. Westine's Contours of the Scaled, Side-on Overpressure Parameter for Free Field Blast

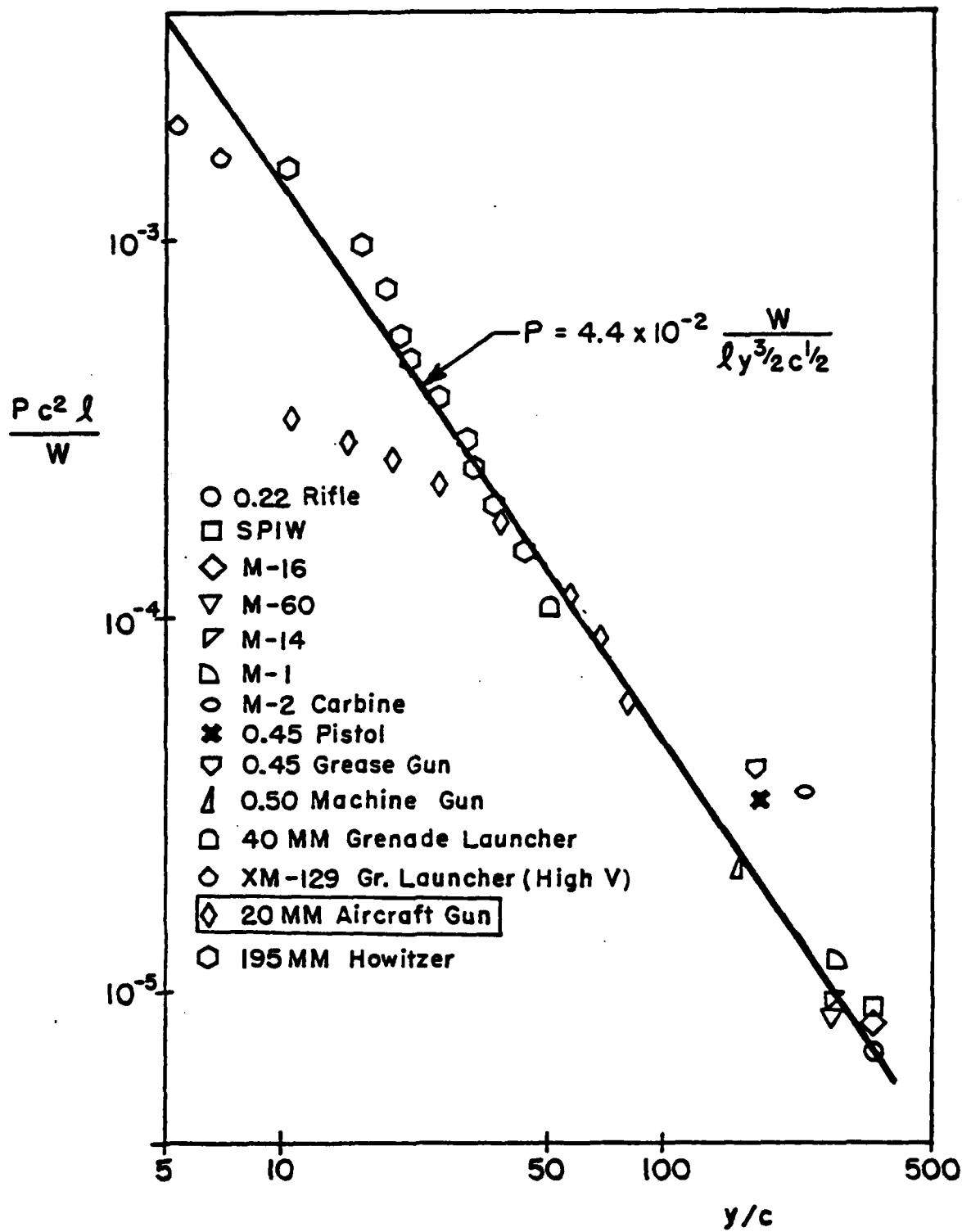
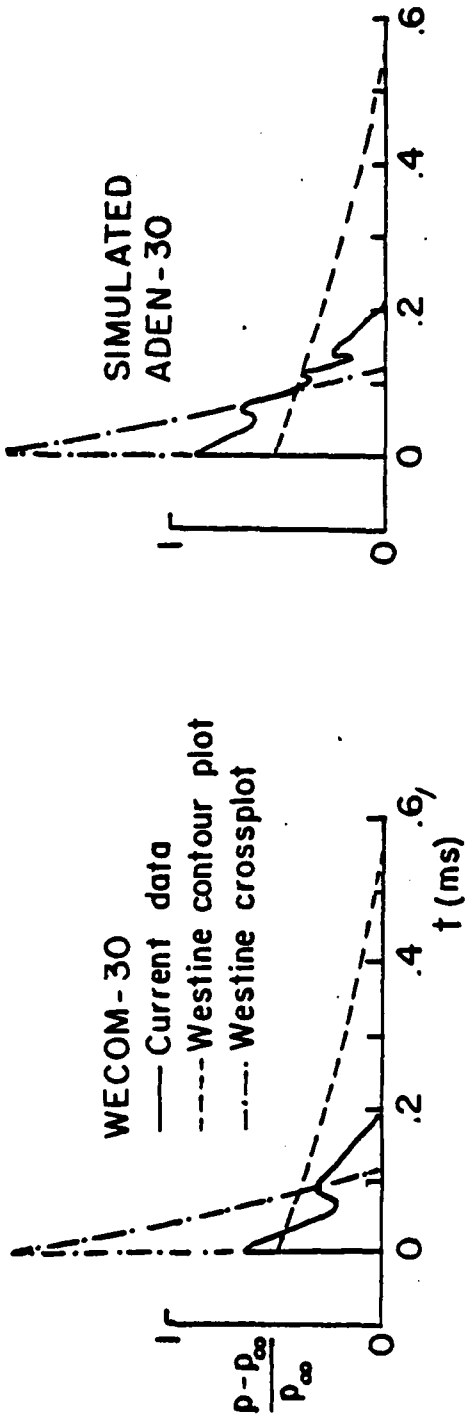


Figure 9. Westine's Crossplot of the Scaled, Side-on Overpressure Parameter for Free Field Blast

SHORT GUN, L = 1.07 m



LONG GUN, L = 1.27 m

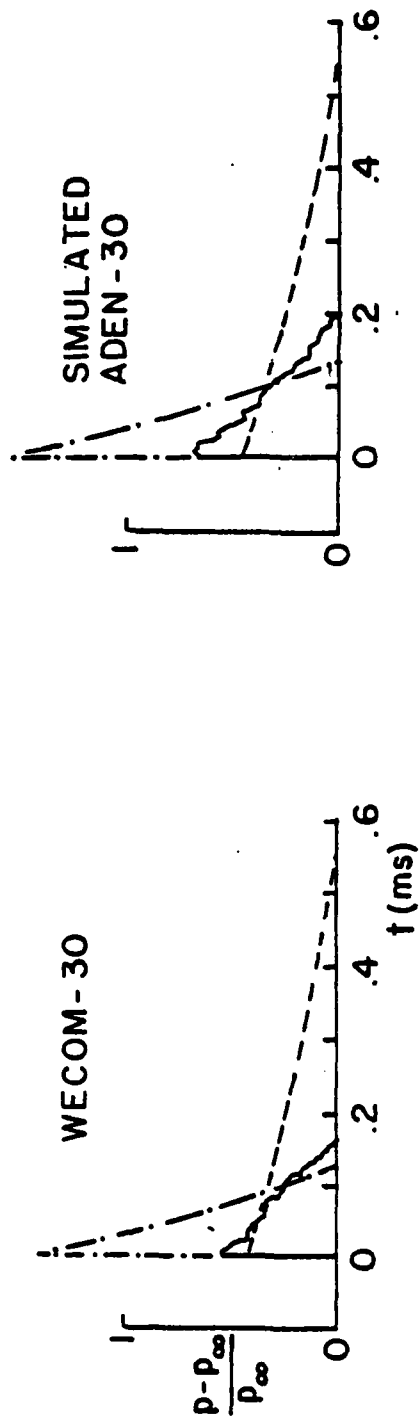


Figure 10. Comparison of Present Measurements of Free Field Blast with Predictions of Westine's Scaling Law

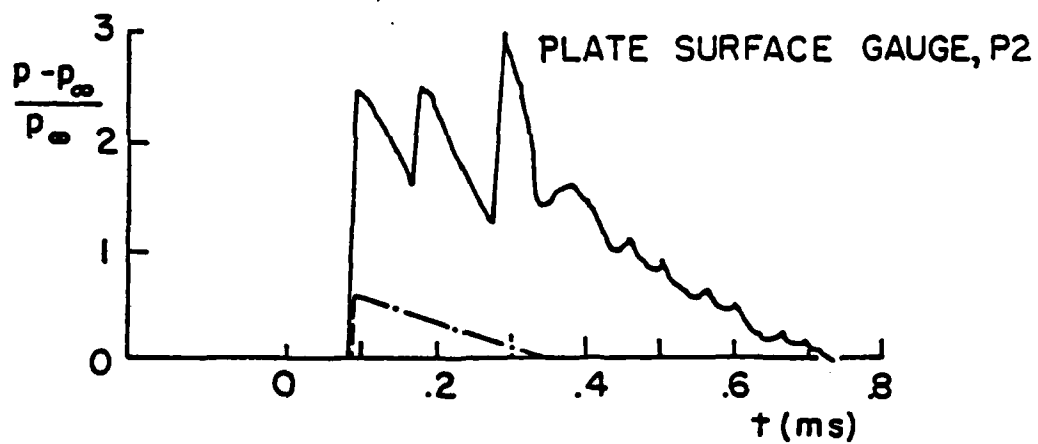
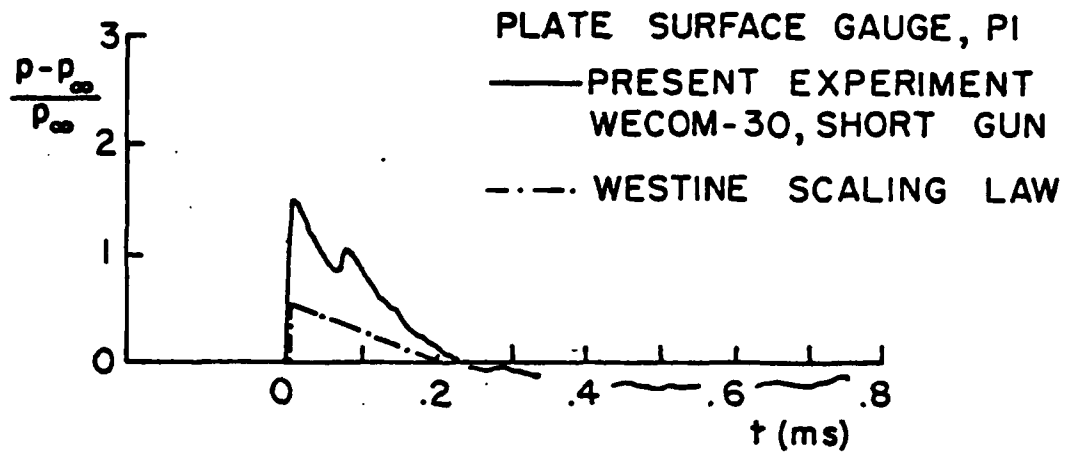


Figure 11. Comparison of Present Measurements of Reflected Blast with Predictions of Westine's Scaling Law

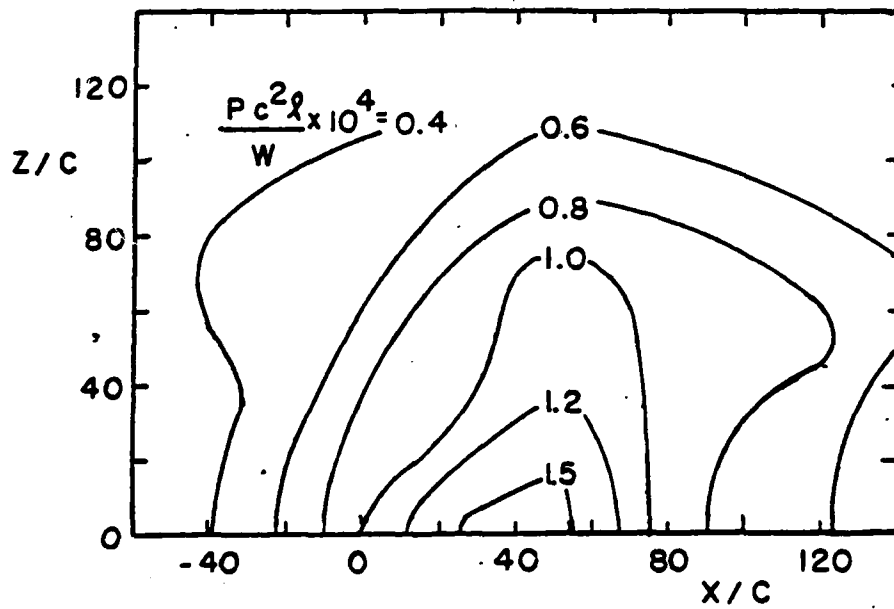
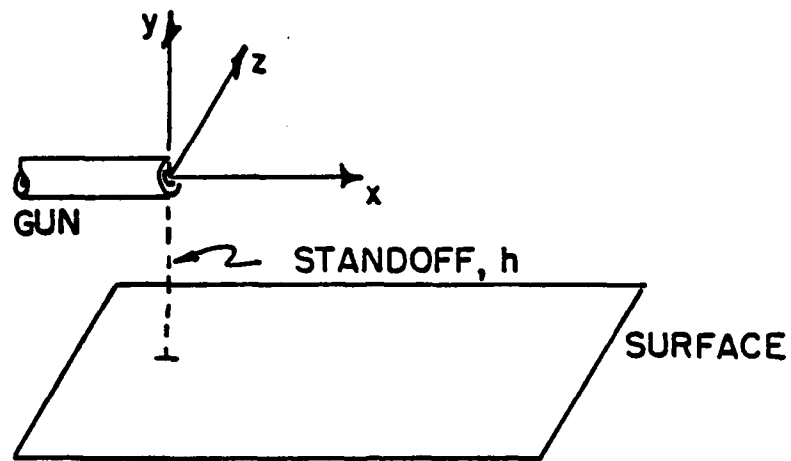


Figure 12. Westine's Contours of Reflected Blast Overpressure Parameter for $h/c = 50$.

behavior is not physically reasonable. Reflection of a blast wave at a surface aligned roughly perpendicular to its direction of propagation should result in a significant increase in pressure over the free field static or side-on level. Even linear theory predicts an increase in pressure by a factor of two (as observed in the current data when comparing the pressures measured at gauges FF1 and P1). This inconsistency in the scaling law is not due to the extrapolation from 16 to 10 caliber standoff. Identical results are obtained in comparing his reflected isobar contours with his free field contours at similar geometric locations, e.g., compare the reflected pressure isobars for a standoff of 50 calibers, Figure 12, with the free field overpressure isobars at $y/c = 50$, Figure 8.

A further difficulty in comparing the measurements with scaling laws or theoretical treatments is the lack of information regarding secondary compressions. The data show that these secondary pulses are a significant portion of the overall blast loading signature. In some instances, these pulses reach absolute pressures greater in magnitude than the initial shock. Additionally, they are seen to possess a fairly regular, high frequency structure which may excite structural vibrations of the aircraft.

V. CONCLUSIONS AND RECOMMENDATIONS

An experimental program has been conducted to investigate the blast field from 30mm aircraft cannon typical of those considered for the AAH. The free field and reflected blast is examined both with pressure transducers and optical techniques. The results of this preliminary investigation show:

- a. There are strong secondary compression pulses generated in the viscous, shear layers of the propellant gas jet;
- b. These secondary compressions show peak pressure levels greater than those behind the main blast;
- c. Comparison between the present measurements and existing scaling laws show poor agreement both as to actual pressure pulses and to changes in the firing configuration.

Based on these preliminary results, it is advisable to conduct further research into the muzzle blast generation and reflection process. More detailed data on the free field and plate surface pressure would be obtained. The plate orientation with respect to the weapon would be varied to examine the effects of separation distance and obliquity. Simultaneous, sequential spark shadowgraphs of the muzzle blast would be acquired to define the origin of secondary compression pulses and relate these to measured pressure data. The

effect of muzzle devices in altering the flow phenomena should also be investigated. Finally, it would be worthwhile to obtain data on an actual aircraft (AAH) or components of it in order to relate laboratory results and analyses to actual hardware.

REFERENCES

1. E. M. Schmidt and D. D. Shear, "Optical Measurements of Muzzle Blast," AIAA Journal, Vol. 13, No. 8, August 1975. pp. 1086-1091.
2. G. Klingenberg, "Investigation of Combustion Phenomena Associated with the Flow of Hot Propellant Gases - III: Experimental Survey of the Formation and Decay of Muzzle Flow Fields and of Pressure Measurements," to be published in Combustion and Flame.
3. F. Maillie, "Projectile Environment During Intermediate Ballistics," ADPA 1st International Symposium on Ballistics, Orlando, FL, 13-15 November 1974.
4. J. Erdos and P. DelGuidice, "Gas Dynamics of Muzzle Blast," AIAA Journal, Vol. 13, No. 8, August 1975. pp. 1048-1055.
5. D. G. Mabey and D. S. Capps, "Blasts from Aircraft Guns at Subsonic and Supersonic Speeds," Proceedings of 3d International Symposium on Ballistics, ADPA, Kahlruhe, Germany, 23-25 March 1977.
6. J. J. Yagla, "Analysis of Gun Blast Phenomena for Naval Architecture, Equipment, and Propellant Charge Design," ADPA 3d International Symposium on Ballistics, Kahlruhe, Germany, 23-25 March 1977.
7. P. S. Westine, "Structural Response of Helicopters to Muzzle and Breech Blast. Vol. I: Blast Field About Weapons," SWRI FTR-02-2029, Southwest Research Institute, San Antonio, Texas, November 1968. AD 844287L.
8. P. S. Westine, "The Blast Field About the Muzzle of Guns," The Shock and Vibration Bulletin, Vol 39, Part 6, March 1969, pp. 139-149.
9. W. H. Braun, "The Free Flight Aerodynamics Range," BRL Report 1048 U. S. Army Ballistic Research Laboratory, Aberdeen Proving Ground, MD, July 1958. AD 20249.
10. P. S. Westine and F. Hoese, "Blast Gauge for Measuring Shocks with Short Wave Lengths," SWRI IR-02-2643-01, Southwest Research Institute, San Antonio, Texas, May 1970. AD 907402L.

Biographical Sketch:

Dr. Edward M. Schmidt is an Aerospace Engineer with the Fluid Physics Branch, Launch and Flight Division, U. S. Army Ballistic Research Laboratory, Aberdeen Proving Ground, MD. He holds B.S. (1964), M.S. (1965), and Ph.D. (1969) degrees in Aeronautical Engineering from the Polytechnic Institute of Brooklyn. Following award of his Ph.D., Dr. Schmidt spent two years on active duty in the Army assigned to the Office of the Project Manager, Utility Tactical Transport Aircraft System (UTTAS), in St. Louis, MO. From 1971 to the present, he has been with BRL. His main area of interest is experimental gasdynamics. He has performed research on the interior, transitional, and exterior ballistics of guns. His most recent works deal with gun muzzle blast signatures and sabot separation.

Dr. Edmund J. Gion is a Research Physicist with the Fluid Physics Branch, Launch and Flight Division, U. S. Army Ballistic Research Laboratory, Aberdeen Proving Ground, MD. He has a B.S. degree (1959) from Reed College, M.S. degree (1961) and Ph.D. degree (1965) from Lehigh University, all in Physics. His work with BRL began immediately following his Ph.D. studies. He has been engaged principally in experimental measurements and techniques in high-speed flows from gun muzzles as well as shock tubes.

KINETIC HEATING
OF
AIRCRAFT CONVENTIONAL ARMAMENT AND EQUIPMENT
(UNCLASSIFIED)

by
KEITH G. SMITH

HUNTING ENGINEERING LIMITED, AMPHILL, ENGLAND

ABSTRACT. This paper reviews the work to establish the temperatures likely to be reached by conventional armament and equipment when carried on representative operational sorties. Results of extensive mathematical modelling are presented and for model validation purposes compared with flight test results. The validated models are then used to compute flight limitations, in terms of cruise/dash Mach. No. and flight duration to prevent overheating during sorties flown in varying sea level ambient temperature. Various methods of presenting flight limitations for operational sorties are presented and compared.

"Approved for public release; distribution unlimited"

LIST OF FIGURES

1. MAXIMUM ATMOSPHERIC TEMPERATURES
2. DIURNAL CYCLES OF MAXIMUM GROUND LEVEL ATMOSPHERIC TEMPERATURE OVER LAND
3. DIURNAL CYCLES OF MAXIMUM GROUND LEVEL ATMOSPHERIC TEMPERATURE OVER SEA AREAS
4. DIAGRAMMATIC REPRESENTATION OF BODY FOR COMPUTATION OF HEAT CONDUCTION INTO STRUCTURE
5. RETARDED 1,000lb HE BOMB - TEMPERATURE RECORDING POSITIONS
6. SOLAR RADIATION TRIAL - COMPARISON OF RECORDED AND SIMULATED TEMPERATURES OF SKIN AND THERMOCOUPLE NUMBER 3)
7. ASSUMED DIURNAL RANGES OF TEMPERATURE AND SOLAR RADIATION INTENSITY IN A 35°C SEA LEVEL MAXIMUM AMBIENT TEMPERATURE
8. PREDICTED TEMPERATURES OF EXTERNAL SKIN AND THERMOCOUPLE NUMBER 3) WHEN WEAPON IS EXPOSED TO SOLAR RADIATION IN A 35°C SEA LEVEL MAXIMUM AMBIENT TEMPERATURE
9. "OVEN TRIAL" - COMPARISON OF RECORDED AND SIMULATED TEMPERATURE OF THERMOCOUPLE NUMBER 3)
10. COMPARISON BETWEEN MEASURED AND CALCULATED TEMPERATURES FOR RETARDED 1,000lb HE BOMB
11. HYPOTHETICAL LOW-LOW FLIGHT PROFILE
12. HYPOTHETICAL HIGH-LOW-HIGH FLIGHT PROFILE
13. BL755 - TEMPERATURE-TIME HISTORIES FOR COMPONENTS (LOW-LOW SORTIE)
14. BL755 - TEMPERATURE-TIME HISTORIES FOR COMPONENTS (HIGH-LOW-HIGH SORTIE)
15. VARIATION OF AMBIENT TEMPERATURE AND INTENSITY OF SOLAR RADIATION WITH TIME
16. BL755 - VARIATION OF NOSE CONE AND CARTRIDGE/FUZE ASSEMBLY TEMPERATURES DUE TO EXPOSURE TO SOLAR RADIATION

17. BL755 - VARIATION OF BOMBLET SURFACE OF EXPLOSIVE FILLING TEMPERATURE WITH TIME DUE TO EXPOSURE TO SOLAR RADIATION (REMOTE FROM STRONGBACK)
18. COMPARISON OF MEASURED AND SIMULATED TEMPERATURES OF 30mm ADEN GUN AMMUNITION DURING A SORTIE OF THE LIGHTNING AIRCRAFT
19. HYPOTHETICAL LOW AND HIGH LEVEL SORTIE PROFILES
20. TEMPERATURE-TIME VARIATION OF 30mm ADEN GUN AMMUNITION DURING LOW-LEVEL ATTACKS - 45°C S.L. AMBIENT TEMPERATURE
21. TEMPERATURE-TIME VARIATION OF 30mm ADEN GUN AMMUNITION DURING HIGH LEVEL ATTACKS - 45°C S.L. AMBIENT TEMPERATURE
22. EFFECT OF FIRING THE GUNS ON THE MAXIMUM GUN/AMMUNITION TEMPERATURES DURING LOW-LEVEL ATTACKS (MACH 1.0 DASH)
23. EFFECT OF FIRING THE GUNS ON THE END OF SORTIE GUN/AMMUNITION TEMPERATURES DURING LOW-LEVEL ATTACKS (MACH 1.0 DASH)
24. EFFECT OF FIRING THE GUNS ON THE MAXIMUM GUN/AMMUNITION TEMPERATURES DURING HIGH-LEVEL ATTACKS (MACH 1.8 DASH)
25. EFFECT OF FIRING THE GUNS ON THE END OF SORTIE GUN/AMMUNITION TEMPERATURES DURING HIGH-LEVEL ATTACKS (MACH 1.8 DASH)
26. HYPOTHETICAL HIGH-LOW-LOW-HIGH (HLLH) SORTIE PROFILE
27. TEMPERATURE-TIME HISTORY FOR FUZE V.T.907 CARRIED EXTERNALLY ON HLLH SORTIE
28. TEMPERATURE-TIME HISTORY FOR FUZE V.T.907 CARRIED INTERNALLY ON HLLH SORTIE
29. TEMPERATURE-TIME HISTORY FOR E.R.U. NO.2 MK.1 CARRIED EXTERNALLY ON HLLH SORTIE
30. TEMPERATURE-TIME HISTORY FOR E.R.U. NO.2 MK.1 DURING INTERNAL CARRIAGE ON HLLH SORTIE
31. FLIGHT LIMITATIONS FOR E.R.U. NO.2 MK.1 DURING INTERNAL CARRIAGE ON HLLH SORTIE
32. FLIGHT LIMITATIONS FOR FUZE V.T.907 DURING INTERNAL CARRIAGE ON HLLH SORTIE

33. FLIGHT LIMITATION CHART FOR FUZE V.T.907
34. FLIGHT LIMITATION CHART FOR E.R.U. CARTRIDGE NO.2 MK.2
35. FLIGHT LIMITATION CHART FOR E.R.U. NO.2 MK.1 AND FUZING UNIT NO.3 MK.2
36. FLIGHT LIMITATION CHART FOR IGNITER FRANGIBLE PILLAR NO.1A MK.1
37. FLIGHT LIMITATION CHART FOR 1,000lb BOMBS N1, MK 10 AND MK 83 MOD.3 USN AND 500lb BOMBS MK21 AND MK.82 MOD.1
38. FLIGHT LIMITATION CHART FOR 2" ROCKET A/C NO.2 AND NO.3 IN LAUNCHER NO.7 MK.1 (MATRA)
39. FLIGHT LIMITATION CHART FOR 1,000lb BOMB M.C.HE. MKS.6-12 AND 540lb BOMB MK.2 (TORPEX FILLED)
40. FLIGHT LIMITATION CHART FOR EXPLOSIVE BOLT (PYLON JETTISON)

INTRODUCTION

The carriage and functioning environment of weapons and associated equipment carried on modern day strike aircraft is very severe, particularly with respect to the temperatures resulting from kinetic heating. Most conventional weapons and equipment contain explosive fillings and other components which have relatively low temperature limitations. For example, the explosive filling of most conventional weapons has an upper temperature limitation of 76°C; for other weapons such as air delivered rockets the maximum operating temperature is only 70°C.

As a result of these relatively low temperature limitations the performance of the aircraft delivering/carrying such weapons/equipment must be limited to avoid a hazardous situation arising which could endanger the delivery aircraft. To avoid such situations arising it is necessary to apply the following limitations to the aircraft's performance:

1. Limit the maximum likely ambient temperature in which the sortie takes place.
2. Limit the Mach. No. during the sortie.
3. Limit the duration of the sortie.

Obviously, under operational conditions these limitations are often combined, it is not satisfactory to apply a single limitation.

To compute the maximum temperatures reached by weapon systems and associated equipment it is essential to obtain data relating to world wide sea level ambient temperatures likely to be experienced by aircraft flying operational sorties. With this data available it is then necessary to produce mathematical models which adequately predict the temperatures of weapon systems and equipment flown on these sorties. These models must be capable of dealing with a wide range of methods of heat transfer, i.e. forced convection, natural convection, radiation etc., and simple/complex weapon structures and installations. With the ambient temperature known and the flight sortie characteristics defined, the mathematical models can then be used to compute the maximum temperatures likely to be reached. However, with these temperatures computed, the problem of limiting the aircraft's performance to ensure overheating does not occur must be addressed. Defining performance limitations is particularly difficult because "on the day" the pilot may wish to fly a sortie profile which is different to that used in the mathematical modelling exercise, thus limitations of ambient air temperature, Mach. No. or duration are not strictly applicable.

In this paper work conducted in UK on the overall problem of kinetic heating of aircraft carried/delivered weapons and associated equipment is reviewed. Results of our studies into the likely sea level ambient temperatures, development of mathematical models and their validation, and the problem of applying flight limitation are presented.

Our studies have been in progress for some 13 years and Hunting Engineering are the sole contractor to the UK Ministry of Defence, Directorate of Air Armament for this work. To monitor the studies which are undertaken, MoD formed a Thermal Effects on Aircraft Conventional Armament, Stores and Equipment (TEACASE) Working Group. The types of armaments/equipment considered include bombs (high explosive, practice and fire bombs), cluster weapons, flares, rockets, fuzes, ejection release units and their cartridges, fuzing units, ejection seat systems and many other specialised cartridges and pyrotechnics. Aircraft considered include Buccaneer, Phantom, Harrier, Jaguar, Lightning, Tornado and F111.

The studies we have completed have also addressed the problem of minimum temperatures experienced by weapons and equipment; the mathematical models developed being sufficiently general to cope adequately with both the low and high temperature environment. However, this paper considers only the high temperature environment.

SEA LEVEL AMBIENT TEMPERATURES

In order to assess the maximum temperature likely to be experienced by weapons, their components and associated equipment it is necessary to first define realistic maximum/minimum sea level ambient temperatures in which operational sorties are likely to be flown. The ambient temperature can affect the temperatures reached by weapons/equipment etc. in two ways:

- (1) The initial temperatures of components are dependent upon the ambient temperature and their possible exposure to solar radiation, particularly for aircraft which may be on stand-by for periods of up to 30 days.
- (2) The stabilisation/recovery temperatures associated with given flight conditions are dependent on ambient temperature.

In addition to the maximum ambient temperatures, consideration must also be given to diurnal temperature cycles particularly when very long repeat sorties are to be considered. The maximum temperature on any day will only be maintained for a limited period of time and to assess component temperatures during repeated sorties on the basis of a constant maximum ambient temperature would give pessimistic results.

MAXIMUM GROUND LEVEL TEMPERATURES

The occurrence of high ambient temperatures has been studied and the results are presented in Appendix 1. Neglecting temperatures with less than 1% probability of occurring, the following conclusions can be made:

- (1) In overseas areas, with the exception of the Red Sea and the Persian Gulf, the maximum temperature likely to occur with a greater than 1% probability is 35°C. When the Red Sea and Persian Gulf are considered this temperature increases to 40°C.
- (2) The maximum temperature likely to occur over land with a greater than 1% probability is 45°C. This temperature occurs with more than 1% probability only in the eastern part of the Sahara desert.

LAPSE RATES

For our studies in the UK MoD, two definitions of maximum tropical ambient temperatures are available and are presented in Figure 1. The Royal Aeronautical Society (R.Ae.S.) Data Sheet specifies a linear lapse rate from 45°C at sea level to -40°C at 48,000 ft., the corresponding Av.P.970 lapse rate is from 50°C at sea level to 28°C at 3,000 ft. and then to -40°C at 40,000 ft. The R.Ae.S. data is based on conditions regarded as extreme being exceeded on average only on one day per year; the Av.P.970 data however is based on extreme temperatures occurring on ten days per year. The two specifications are inconsistent for altitudes below 1,000 ft., however, at altitudes above 3,000 ft. the two are consistent with the basis on which they were compiled; the Av.P.970 temperatures being some 12°C to 14°C lower than those of the R.Ae.S. for the same altitude.

The R.Ae.S. data provides the most severe environment but is possibly unrealistic for the following reasons:

- (1) The temperatures at each altitude are experienced on average in only one location once a year.
- (2) The maximum temperatures are unlikely to occur at all altitudes at the same time.

Thus, the specified Av.P.970 temperatures are thought to be the most realistic, and in the UK is the recommended data to use in kinetic heating studies.

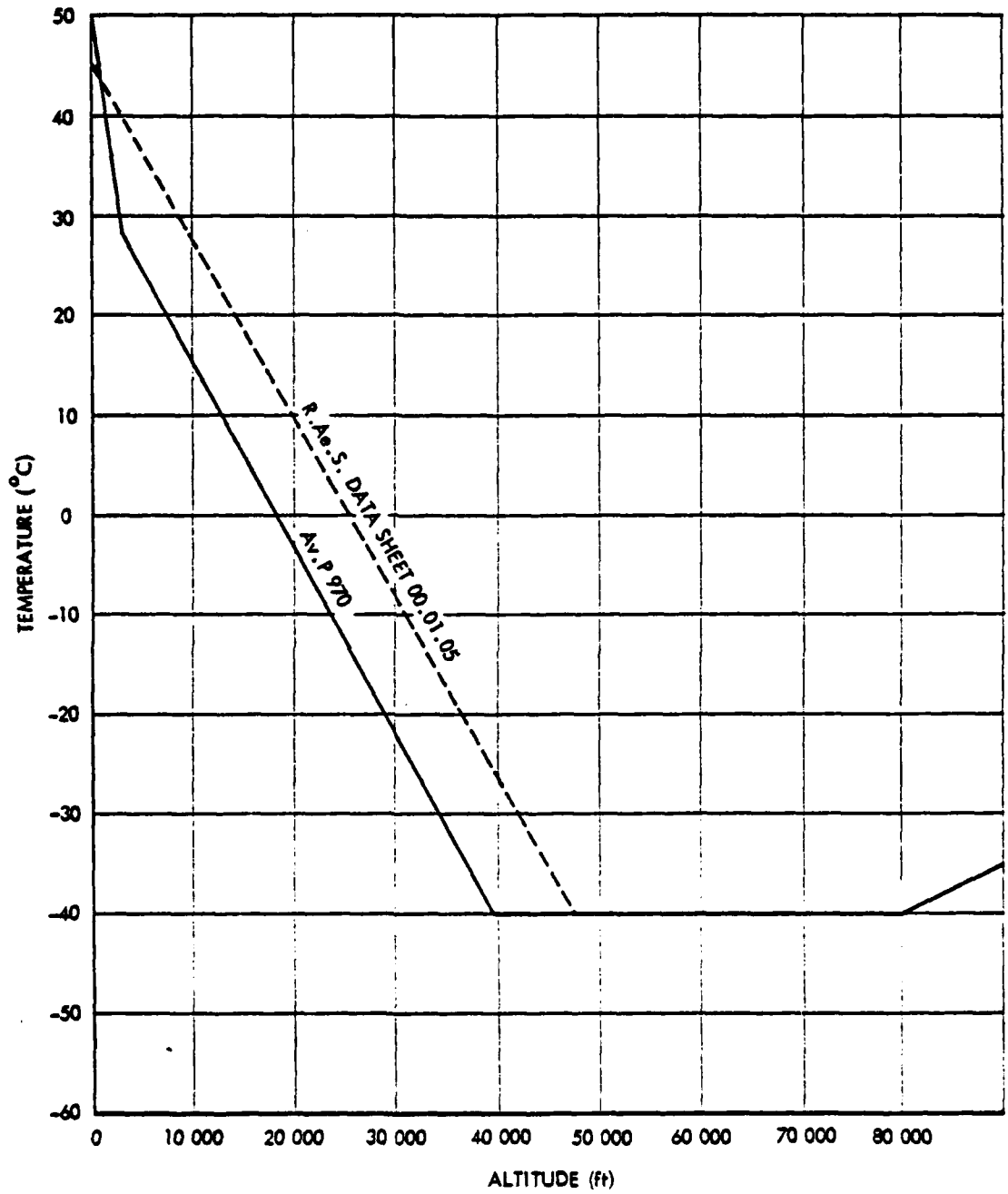


Fig. 1 Maximum Atmospheric Temperatures

DIURNAL CYCLES

To assess the temperatures reached by weapons/equipment during repeated sorties the variation of ambient temperature with time must be specified. Figures 2 and 3 show the estimated diurnal cycle of maximum temperatures over land and sea respectively. Both are based on an assumed sinusoidal cycle between maximum and minimum daily temperatures.

The highest mean daily minimum temperature during any one month for any recording station quoted in Reference 1 is 31.6°C. Since this is an average value, the minimum daily temperature can be higher; but is unlikely to exceed 35°C. Thus, the diurnal cycle of the maximum temperature over land has been assumed to be sinusoidal between 45°C and 35°C.

Less data is available for daily minimum temperatures over sea. However, for the purpose of kinetic heating studies the variation between maximum and minimum daily temperatures has been assumed to be the same as over land, i.e. 10°C.

SOLAR RADIATION

The initial temperatures of weapons at take-off may be affected by periods of exposure to solar radiation. For internally carried (i.e. bomb bay) components the effect of solar radiation is small, however, externally carried systems can experience an increase in temperature of up to 25°C relative to the shade temperature.

The effect of solar radiation varies considerably with the type of weapon/component, particularly on its colour and composition of its outside surface. Hence, the effect of solar radiation must be considered separately for each type of weapon, detailed consideration being given to probable storage and standby conditions likely to be encountered.

RECOMMENDATIONS

From our investigations of maximum world wide ambient air temperatures at sea level for use in kinetic heating studies it is recommended that maximum temperatures of 45°C and 35°C are used for overland and over-sea environments respectively. It is also recommended that these temperatures represent daily maxima of sinusoidal diurnal cycles about means of 40°C and 30°C respectively.

It is recommended that the diurnal cycles of Figures 2 and 3 be used for assessing kinetic heating effects during flight for altitudes below 1,000 ft. and that the maximum temperature atmosphere specified in Av.P.970 (Figure 1) should be used at altitudes above 1,000 ft. irrespective of the time of day.

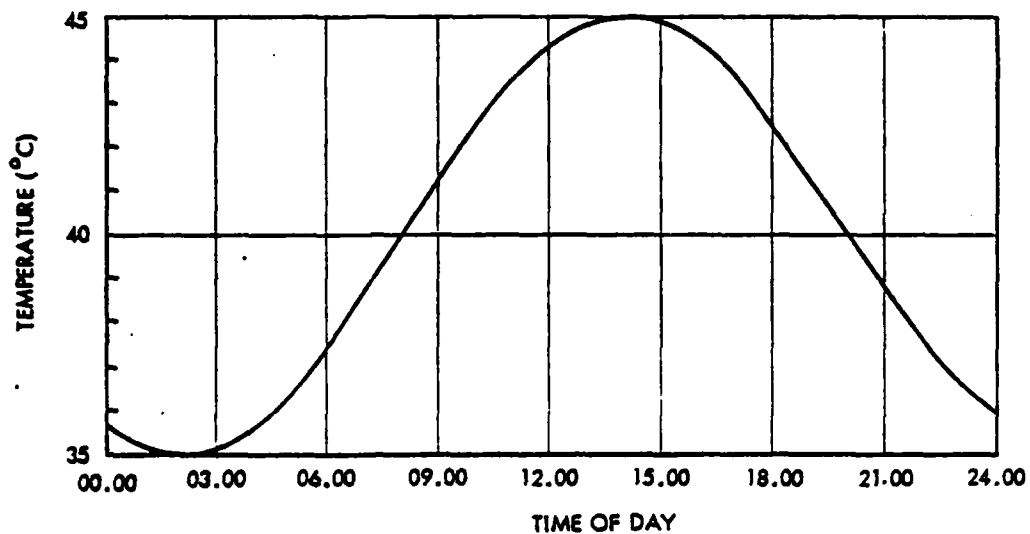


Fig.2 Diurnal Cycle of Maximum Ground Level Atmospheric Temperatures over Land

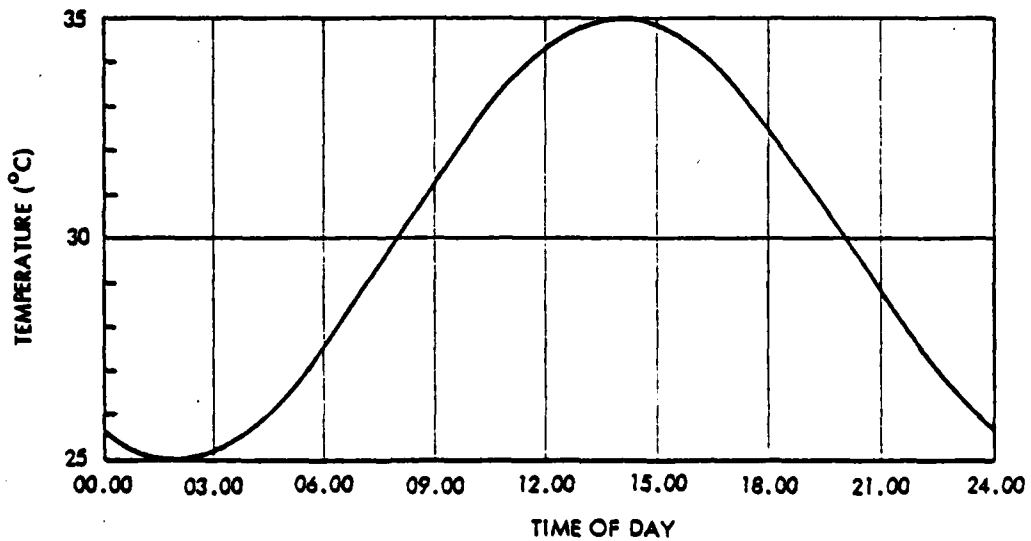


Fig.3 Diurnal Cycle of Maximum Sea Level Atmospheric Temperatures in Tropical Sea Areas

It is further recommended that the effects of solar radiation on equipment prior to take-off be taken into consideration.

MATHEMATICAL MODELLING

GENERAL INTRODUCTION AND DEFINITIONS

When a body travels through the air at high speed, the air in contact with the body will have the same speed as the body. At a small distance from the surface of the body the air will be at rest and therefore a large velocity gradient will exist across a thin layer of air adjacent to the body; the boundary layer. As large shear forces exist across the boundary layer the work done by these forces is converted into heat. At some position on the body (the stagnation point) it is possible that the kinetic energy of the air flow is converted entirely into pressure and heat energy. The temperature associated with these conditions is termed the stagnation temperature (T_s). On other surfaces, where the air is brought to rest by the shear forces, and if the body was perfectly insulated the temperature experienced by the surface of the body is termed the recovery temperature (T_r). Apart from small areas which could experience stagnation temperatures, the recovery temperature is generally the highest temperature the body will experience. It should be noted that in installations where entry/exit holes exist on conical surfaces, vortex heating can occur and temperatures well in excess of the stagnation temperature can be experienced.

If the temperature of the body is T , the rate of heat flow into the body (q) will be proportional to $(T_r - T)$

$$q = h(T_r - T)$$

where 'h' is the heat transfer coefficient. The heat transfer coefficient is a complex quantity and depends upon the physical properties of the air, the surface temperature of the body and the flight conditions. A large discontinuity in the value of 'h' also occurs when the flow changes from laminar to turbulent; much higher values being associated with the turbulent flows.

TYPICAL METHOD OF CALCULATION

To calculate the temperature distribution within the body it is necessary to compute the recovery temperature and heat transfer coefficient. A typical method of computing these parameters, for a forced convection heat transfer environment is presented below. A method of computing the temperature distribution in the body under these conditions is also presented.

Stagnation Temperature

From energy considerations $Jc_p T_s = Jc_p T_a + \frac{1}{2} V^2$ where

- J - Mechanical Equivalent of Heat
- T_a - Ambient air temperature (°K)
- T_s - Stagnation temperature (°K)
- V - Velocity of air (ft/sec)
- C_p - Specific heat of air at constant pressure (assumed constant between temperatures T_a and T_s)

From the above equation:

$T_s = T_a \left(1 + \frac{(\gamma-1)M^2}{2} \right)$ where γ is the ratio of specific heats
M is the flow Mach. No.

Recovery Temperature

The equation above for the stagnation temperature assumes all of the energy of the air is converted into heat. This is generally not so, and the recovery temperature is a temperature allowing for such losses, such that

$$T_r = T_a \left(1 + r \frac{(\gamma-1)M^2}{2} \right)$$

where T_r is the recovery temperature (°K)
'r' is the recovery factor

The recovery factor is a function of Prantl and Reynolds Nos. and has the following values:

- 'r' = 0.85 - Laminar Flow
- 'r' = 0.90 - Turbulent Flow

Thus, for turbulent air flows the recovery temperature is given by:

$$T_r = T_a (1 + 0.18M^2)$$

Heat Transfer Coefficient

For forced convection in a fluid $\frac{(Nu)^*}{(St)} = Pr^* Re^*$

- where
- Nu - Nusselt No.
 - St - Stanton No.
 - Pr - Prantl No.
 - Re - Reynolds No.

It has been shown that for a wide range of Mach. Nos. and temperatures a close approximation for the heat transfer in both laminar and turbulent flow is obtained if the physical properties of fluid (air) appearing in the incompressible flow equations are evaluated at a temperature corresponding to an intermediate temperature. The parameters dependent on this intermediate temperature are indicated by the asterisk (*).

The Nusselt No. (Nu) is given by:

$$Nu = \frac{hx}{k}$$

where h - Heat transfer coefficient
 x - Suitable body dimension (ft)
 k - Thermal conductivity of the fluid

The Prandl No. (Pr) is given by:

$$Pr = \frac{\gamma C_p}{k}$$

where γ = Viscosity of the fluid
 C_p = Specific heat at constant pressure

The Reynolds No. (Re) is given by:

$$Re = \frac{V\rho x}{\gamma}$$

where V = Velocity of fluid (ft/sec)
 ρ = Density of fluid (slugs/ft³)

Thus,

$$\left(\frac{hx}{kSt}\right)^* = \left(\frac{\gamma C_p}{k}\right)^* \left(\frac{V\rho x}{\gamma}\right)^* \text{ or } \left(\frac{h}{St}\right)^* = C_p V \rho^*$$

Using Reynolds Analogy

$$St = \frac{1}{2} A \cdot Cf$$

where A is a constant and is derived experimentally. The value used is 1.22.

Cf is the skin friction coefficient and for a turbulent boundary layer is given by

$$Cf = B Re^{-1/5}$$

where B is another constant which is determined experimentally and found to be 0.0825.

$$\begin{aligned} \text{Therefore } St^* &= 0.0504 Re^{*-1/5} \\ \text{and hence } h &= 0.0504 C_p \cdot Re^{*-1/5} V \cdot \rho^* \\ &= 0.0504 C_p \left(\frac{V \rho^* x}{\mu^*} \right)^{-0.2} V \cdot \rho^* \end{aligned}$$

μ^* is given by

$$\mu^* = 31 \times 10^{-9} \left(\frac{T^* 3/2}{T^* + 117} \right)$$

where T^* is the intermediate temperature.

$$\text{Therefore } h = 0.0504 C_p \left(\frac{V^{0.8}}{x^{0.2}} \right) \left[\frac{31 \times 10^{-9} T^{*3/2}}{\rho^* (T^* + 117)} \right]^{0.2} \rho^*$$

Since $\rho^* = \frac{\rho T_a}{T^*}$ where T_a is the ambient air temperature ($^{\circ}K$)

$$h = 0.00159 C_p \left(\frac{V^{0.8}}{x^{0.2}} \right) \frac{\rho^{0.8} T_a^{0.8}}{T^{*0.5} (T^* + 117)^{0.2}}$$

Using a value of 7.72 for C_p (CHU/slug/ $^{\circ}C$)

$$h = \frac{0.0125 V^{0.8} \rho^{0.8} T_a^{0.8}}{x^{0.2} T^{*0.5} (T^* + 117)^{0.2}} \text{ CHU/ft}^2/\text{sec/}^{\circ}C.$$

The intermediate temperature T^* can be calculated from

$$T^* = 0.58T + 0.42T_a + 0.032M^2 T_a$$

where T is the surface temperature of the body ($^{\circ}K$).

It can therefore be seen that the value of the heat transfer coefficient 'h' is a function of body surface temperature and is therefore a continuously varying parameter. Thus it is generally necessary to adopt an iterative solution for the values of 'h' and T. Alternatively providing small computing time steps are used, and the value of T is not changing rapidly, the value of T calculated at the previous time interval can be used without significant loss in accuracy.

Calculation of Heat Conducted into Body

The following paragraphs outline the equations for computing the heat conducted into an axisymmetric body at a general longitudinal station (x).

Surface Equation

Referring to Fig.4a consider the section of the body bounded by the radii R_1 and R_3 .

This segment is then subdivided at radius R_2 into segments of equal thickness ΔR , each segment having the same thermal properties.

Let the temperatures at R_1 (surface), R_2 and R_3 be T_1 , T_2 and T_3 respectively.

Then in a small time interval Δt for the segment between radii R_1 & R_2

Heat transferred into segment - Heat transferred out of segment
= Heat stored in segment.

i.e.

$$h \Delta t R_1 \left[T_R - \left(\frac{T_1 + T_1'}{2} \right) \right] - K_1 \frac{\Delta t}{\Delta R} \left(R_1 - \frac{\Delta R}{2} \right) \left[\left(\frac{T_1 + T_1'}{2} \right) - \left(\frac{T_2 + T_2'}{2} \right) \right]$$

$$= R_1 \frac{\Delta R}{2} \rho_1 C_1 (T_1' - T_1)$$

where T_1' , T_2' and T_3' are the temperatures reached after time Δt

h = heat transfer coefficient

K_1 = thermal conductivity of material

ρ_1 = density of material

C_1 = specific heat of material .

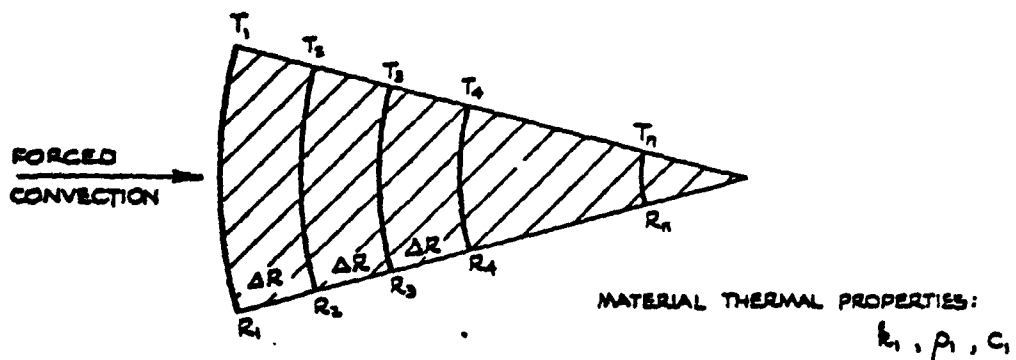


FIG.4A DIAGRAM FOR SURFACE EQUATION

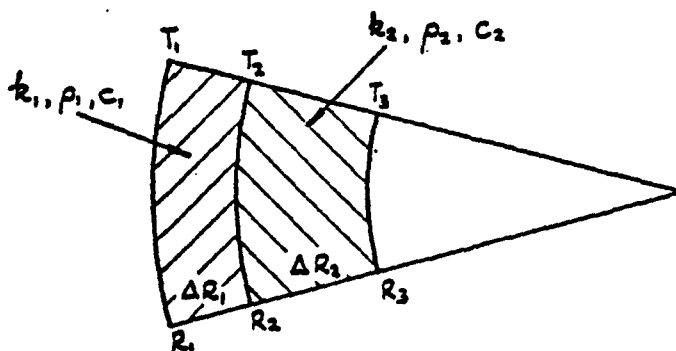


FIG.4B DIAGRAM FOR INTERNAL POINT WITH ADJACENT MATERIALS DIFFERENT

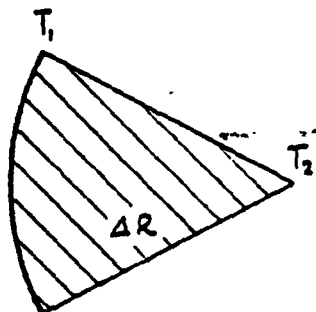


FIG.4C DIAGRAM FOR POINT AT CENTRE

FIG.4 - DIAGRAMMATIC REPRESENTATION OF BODY FOR COMPUTATION OF HEAT CONDUCTION INTO STRUCTURE

General Internal Point

At a point within the body where the adjacent materials have the same properties, then from Fig. 4a

$$\begin{aligned} & \frac{K_1 \Delta t}{\Delta R} \left[R_2 + \frac{\Delta R}{2} \right] \left[\left(\frac{T_1 + T_1'}{2} \right) - \left(\frac{T_2 + T_2'}{2} \right) \right] - \frac{K_1 \Delta t}{\Delta R} \left[R_2 - \frac{\Delta R}{2} \right] \left[\left(\frac{T_2 + T_2'}{2} \right) - \left(\frac{T_3 + T_3'}{2} \right) \right] \\ & = \left[\frac{\Delta R}{2} \rho_1 C_1 + \frac{\Delta R}{2} \rho_2 C_2 \right] R_2 [T_2' - T_2] \end{aligned}$$

At a point within the store where the adjacent materials are different, then from Fig. 4b

$$\begin{aligned} & \frac{K_1 \Delta t}{\Delta R} \left[R_2 + \frac{\Delta R}{2} \right] \left[\left(\frac{T_1 + T_1'}{2} \right) - \left(\frac{T_2 + T_2'}{2} \right) \right] - \frac{K_2 \Delta t}{\Delta R} \left[R_2 - \frac{\Delta R}{2} \right] \left[\left(\frac{T_2 + T_2'}{2} \right) - \left(\frac{T_3 + T_3'}{2} \right) \right] \\ & = \left[\frac{\Delta R}{2} \rho_1 C_1 + \frac{\Delta R}{2} \rho_2 C_2 \right] R_2 [T_2' - T_2] \end{aligned}$$

where $K_2 \rho_2 C_2$ are the thermal properties of the adjacent material.

Equation for Centre of Store

From Fig. 4c

$$K_1 \frac{\Delta t}{\Delta R} \left(\frac{\Delta R}{2} \right) \left[\left(\frac{T_1 + T_1'}{2} \right) - \left(\frac{T_2 + T_2'}{2} \right) \right] = \rho C \left(\frac{\Delta R}{2} \right)^2 (T_2' - T_2)$$

Solution of the above equations

By substitution of the initial values of temperature into the above equations a set of simultaneous equations will be formed in each case from which the values of T_1^1 T_2^1 T_3^1 etc. can be obtained after the time interval Δt . These new temperatures are then used as initial temperatures in the above equations and the new set of equations solved to obtain the temperatures after a further time interval Δt . This process is then continued as long as required.

Using the basic method of computation outlined a suite of computer programs has been compiled capable of dealing with a complete range of kinetic heating problems associated with a variety of different structures. The basic equations for computing the heat conducted into the body have been suitably modified to cater for non-homogenous bodies in which the heat transfer can be by a variety of different modes. The equations are of a very general form and have been extended to cope with heating sources such as solar radiation, natural convection as well as the forced convection outlined.

THEORETICAL RESULTS

EFFECTS OF SOLAR RADIATION

It has been explained in the earlier paragraphs how the ambient air temperature and exposure to solar radiation has a significant effect on the initial temperatures of weapons and equipment. Using the basic mathematical models outlined the temperatures of weapon components and associated equipment have been computed prior to being 'flown' on operational sorties.

To illustrate the effect of solar radiation and compare the theoretical estimates with trials results, a conventional retarded HE bomb will be considered. The general outline of the weapon together with the location of the component under consideration, (the timer) is presented in Figure 5. In the trial, the weapon was placed in the open for a period of 24 hours with the nose pointing south. The solar radiation intensity was measured by a solarimeter and the temperature at the various positions inside and outside the weapon monitored by thermocouples.

The measured and predicted temperatures experienced by the skin of the weapon and the timer (i.e. thermocouple position 3) are compared in Figure 6. This figure shows excellent agreement between the trial and computed temperatures over the 24 hour period.

Many such trials have been conducted on a complete range of weapons and equipment at different sites throughout the world and in all cases the simulations of the trials results have been very good. We are therefore of the opinion that the models we have generated for computing the temperatures of components etc. exposed to solar radiation have been validated and they can confidently be used in kinetic heating studies.

For the retarded HE bomb the effect of the weapon's external paint colour (absorption coefficient) on the temperatures reached by the external skin and internal timer when exposed to solar radiation have been computed using the model. The diurnal cycles of ambient temperature and solar radiation used in these computations are presented in Figure 7 and refer to a 35°C sea level maximum

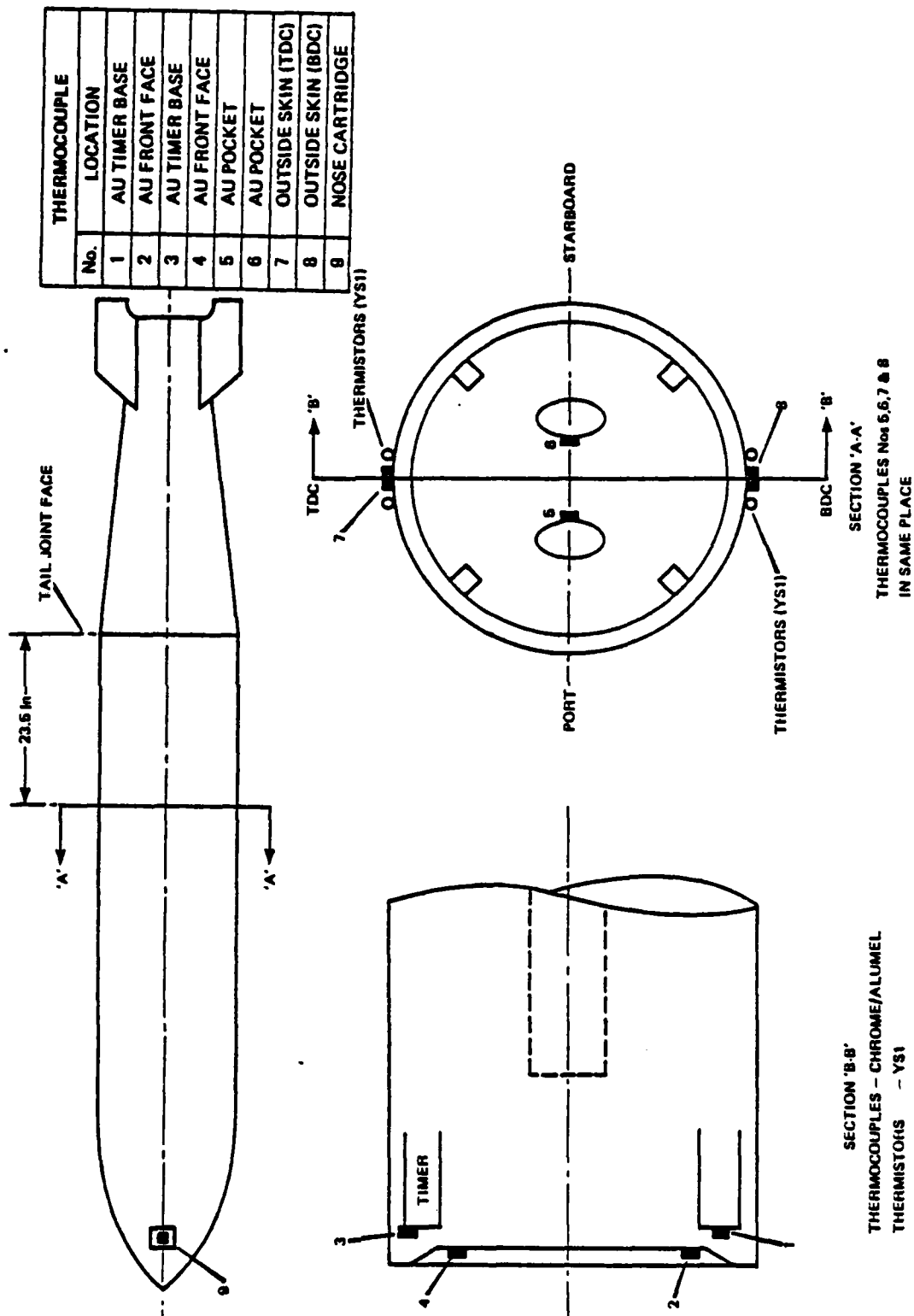


FIG. 5 RETARDED 10001b HE BOMB - TEMPERATURE RECORDING POSITIONS

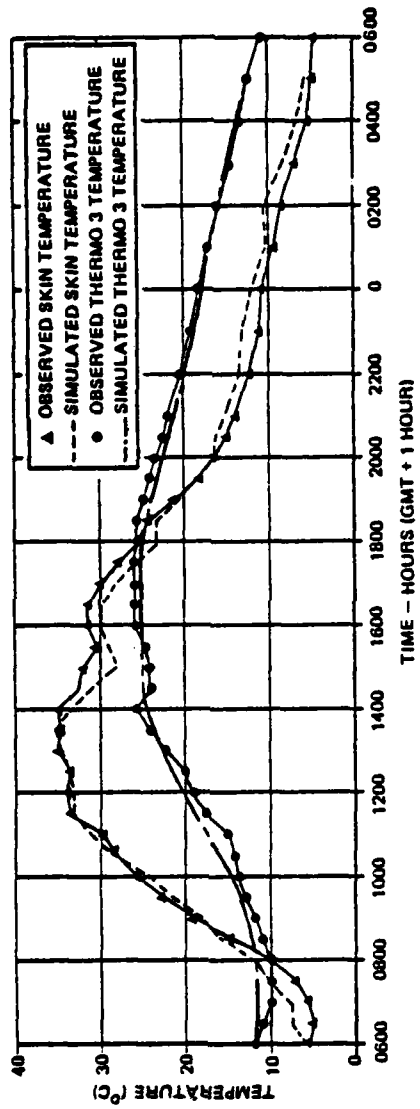


FIG. 6 SOLAR RADIATION TRIAL - COMPARISON OF RECORDED AND SIMULATED TEMPERATURES OF SKIN AND THERMO 3 (THERMOCOUPLE NO. 3)

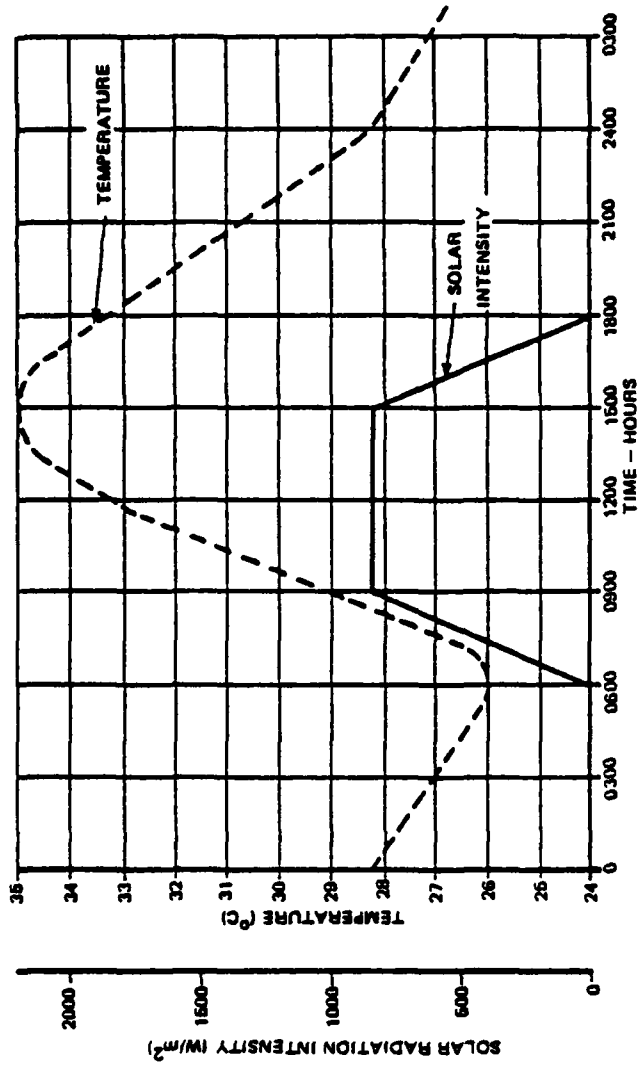


FIG. 7 Assumed Diurnal Ranges of Temperature and Solar Radiation Intensity in a 350C Sea Level Maximum Ambient Temperature

temperature. The variation of skin and timer temperatures with time when exposed to these conditions are presented in Figure 8 for absorption coefficients ranging from 0.2 (white paint) to 1.0 (matt black paint).

The Figure 8a shows that a maximum difference of approximately 27°C occurs at the skin surface between the black and white paint schemes (absorption coefficients of 1 and 0.2). The corresponding difference for the timer can be seen (from Figure 8b) to be approximately 12°C.

The same weapon was used in a radiant heating trial using a simulated heating rig. The skin temperature of the weapon was continuously monitored and the heat input so adjusted to simulate the temperature-time history likely to be experienced by the weapon during an operational sortie. The results of this trial are presented in Figure 9 which again shows good agreement between the measured and simulated temperatures of the weapons timer. The results of this trial give confidence in the models ability to predict the heat conduction into the weapon structure.

PREDICTION OF IN-FLIGHT TEMPERATURES

Flight trials using the weapon configuration previously shown have been conducted in relatively high ambient air temperatures (i.e. 30°C). During the flight trials the temperatures of the skin, surface of explosive filling and 3 cms deep into the filling of the weapon were measured at various longitudinal stations relative to the nose. The pertinent flight conditions for one of the flights are presented below:

TIME (Mins.)	0	5	10	40
SPEED (ft/sec)	300	832	925	925
AMB. AIR TEMP. °C	30	30	30	30
AIR DENSITY SLUGS/FT ²	0.0022	0.0022	0.0022	0.0022

The relevant weapon details at a position 3ft. from the nose are as follows:

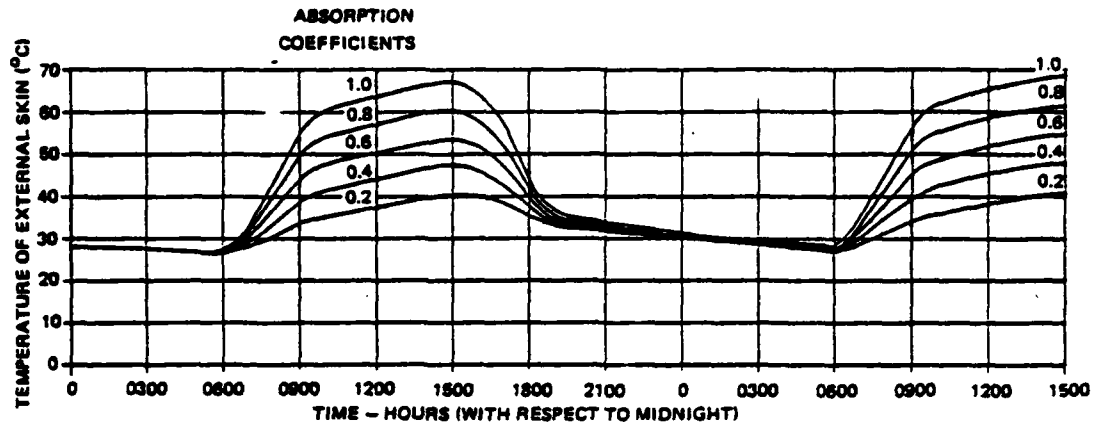


FIG. 8a. Predicted Temperatures of the External Skin when the Store is Exposed to Solar Radiation in a 35°C Sea Level Maximum Ambient Temperature

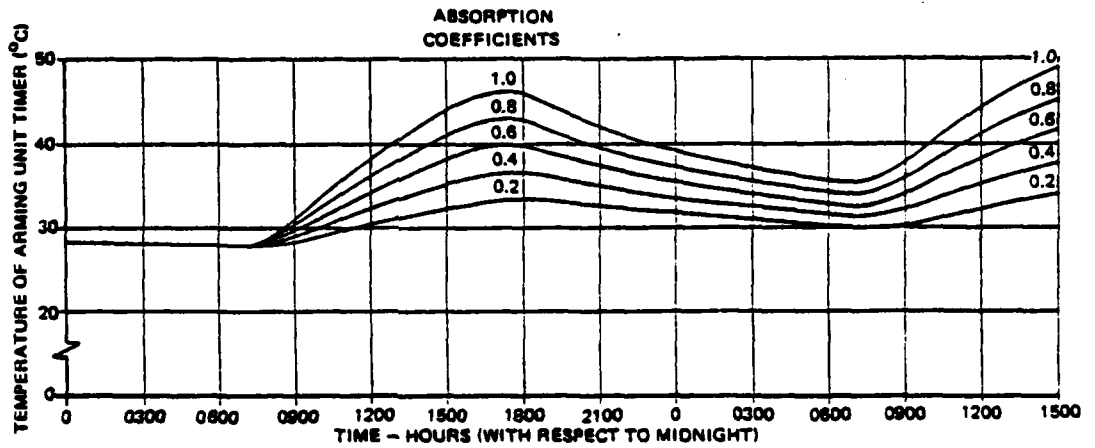


FIG. 8b. Predicted Temperatures of the Arming Unit Timer when the Store is Exposed to Solar Radiation in a 35°C Sea Level Maximum Ambient Temperature

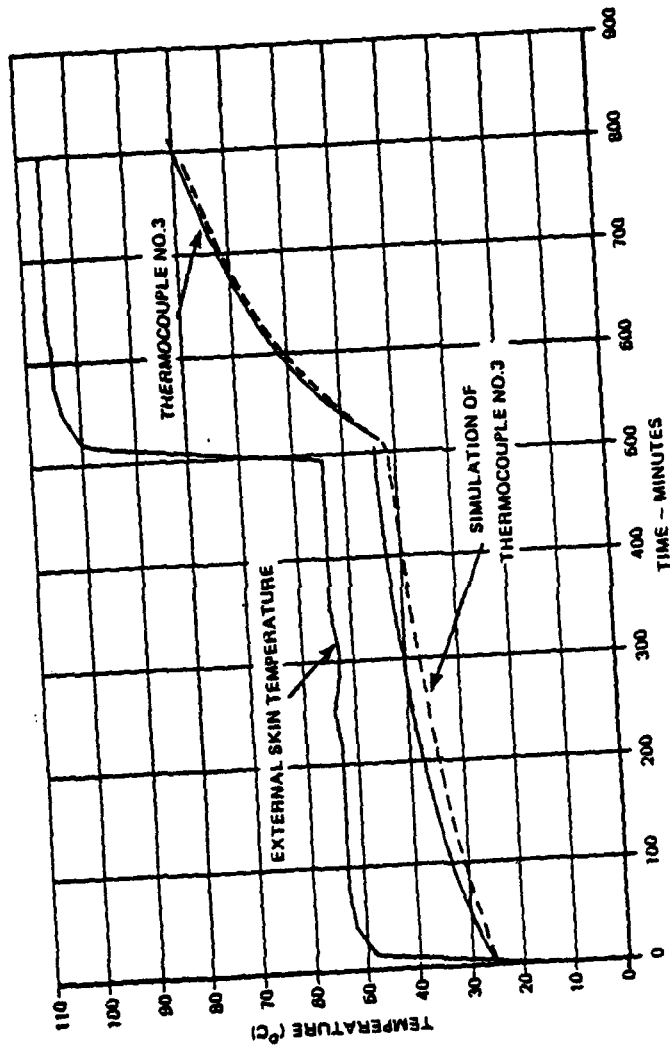


FIG. 9 "OVEN" TRIAL - COMPARISON OF RECORDED AND SIMULATED TEMPERATURES OF TIMER

PARAMETER	OUTER CASE	BITUMEN LINER	H.E. FILLING
RADIUS (INS)	8.2	7.6	7.59
CONDUCTIVITY (CHU/in. min. °C)	0.0401	0.000068	0.000359
THERMAL DIFFUSIVITY* (ins ² /min)	1.286	-	0.0179

* Thermal Diffusivity = $\frac{k\rho}{c}$

Using this data in the mathematical model the variation of temperature with time for the weapon's skin surface of filling and 3 cms deep into the H.E. filling is presented in Figure 10. Also shown in the figure are the measured temperatures for these components.

Considering the difficulties in measuring the ambient air temperature accurately during the flight trials, good agreement is shown for the skin temperatures and for the temperatures measured 3 cms deep into the HE filling. If the ambient air temperature was changed by 3°C excellent agreement between predicted and measured skin temperatures would be achieved, and the temperature 3 cms deep into the H.E. filling would be within 1°C of that measured.

The surface of H.E. filling temperature however shows considerable difference from that predicted. This difference can be attributed to:

- (1) The mathematical model assumes perfect thermal contact between adjacent materials.
- (2) Difficulties of accurately measuring the surface temperature, i.e. the mounting and location of the thermocouples.
- (3) The method of mounting the skin thermocouples on the instrumented weapon could result in heat being conducted into the centre of the weapon.

It is however, considered that the theoretical calculations give a sufficiently accurate assessment of the temperatures of the

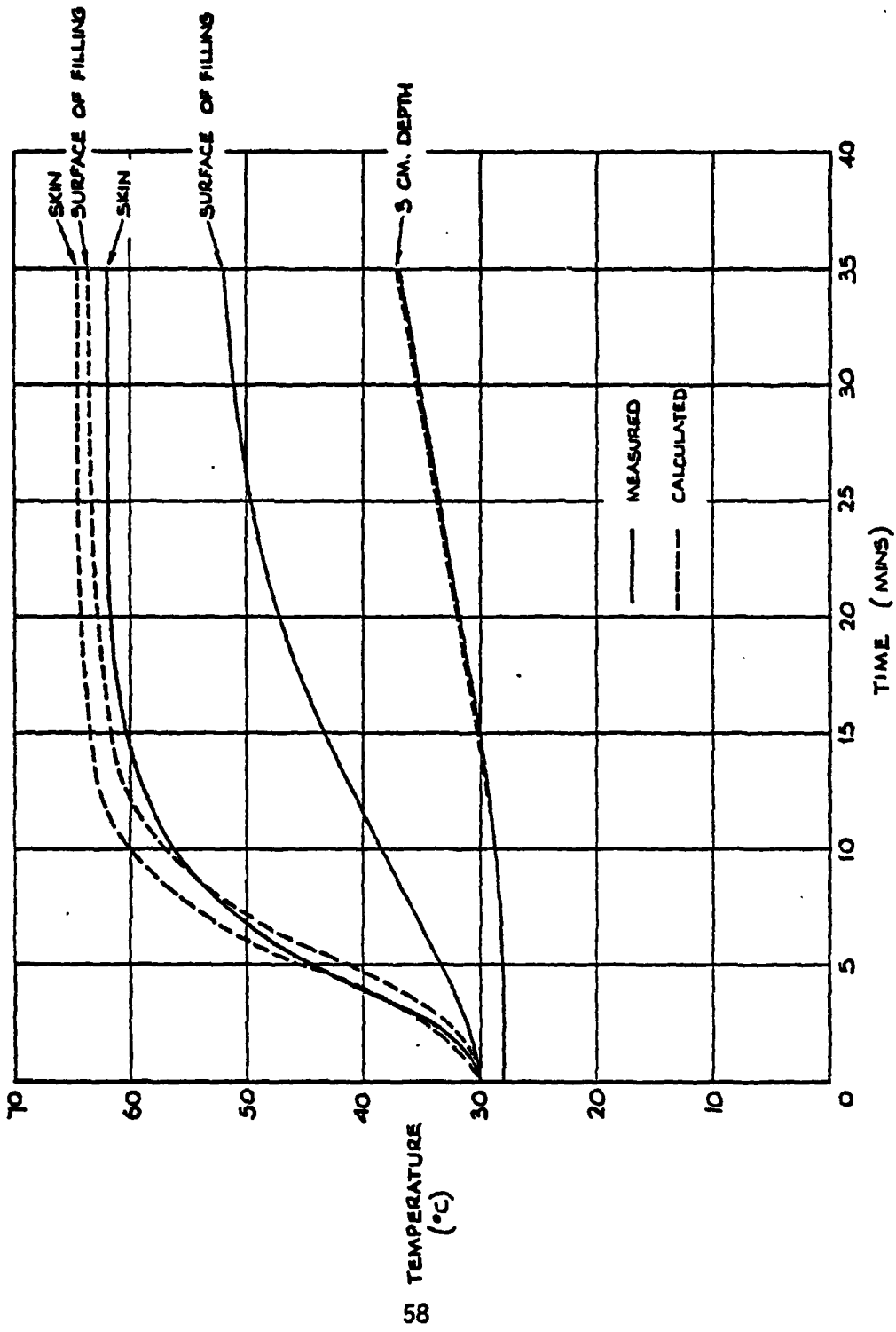


FIG. 10 COMPARISON BETWEEN MEASURED AND CALCULATED TEMPERATURES
(RETARDED 1000lb HE BOMB)

components within the weapon.

Many trials have been undertaken with a large variety of weapons/equipment flown on many UK, European and USA aircraft; the results obtained have been simulated using the suite of mathematical models developed and generally good agreement has been achieved. Kinetic heating studies of this type have been in progress in the UK for approximately 13 years, and we are of the opinion that our mathematical models have been validated and can be used in kinetic heating studies with confidence.

Considerable mathematical modelling of the temperatures likely to be experienced by the BL755 Cluster Weapon have been completed. In fact from the theoretical studies completed a decision to use the relatively cheap "low temperature" rather than the expensive "high temperature" bomblet explosive filling was made. The limiting temperature of the cheaper filling is 76°C and our modelling exercises predicted a maximum temperature under the most severe conditions of 74°C.

Some computed results for the BL755 Cluster Weapon when flown on the hypothetical LOW-LOW and HIGH-LOW-HIGH sorties shown in Figures 11 and 12 are presented in Figures 13 and 14 respectively. The components considered were:

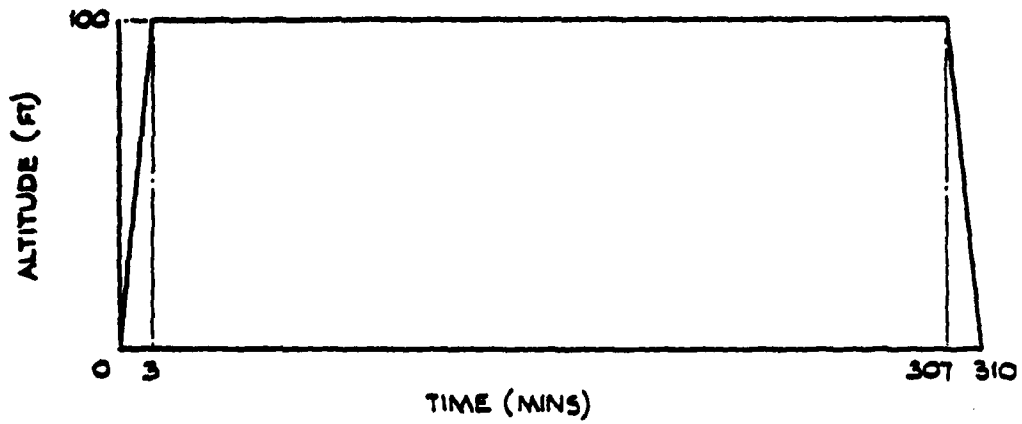
- Nose cone
- Cartridge/fuze assembly
- Bomblet surface of filling

For completeness the variation of temperature with time for these components when exposed to the ambient temperature and solar radiation diurnal cycles of Figure 15 are presented in Figures 16 and 17. Again these Figures clearly show the effect on maximum temperature of the external paint colour (surface absorptivity).

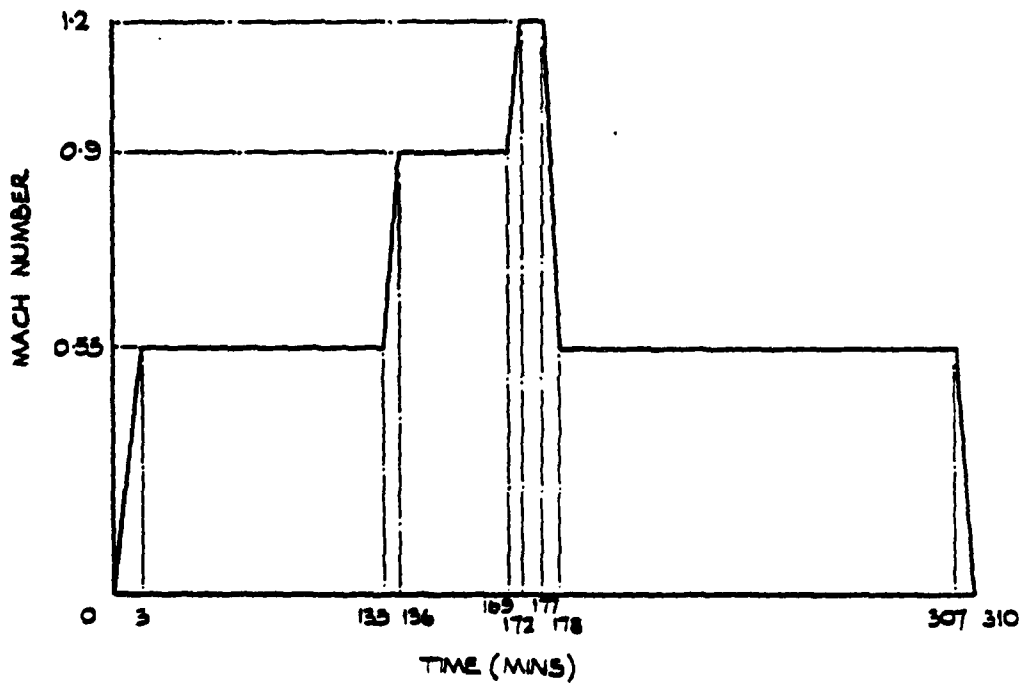
The basic mathematical models have been applied to a complete range of weapon systems including Gun installations. Figure 18 presents the measured and simulated temperatures of the inlet air, breech and feed-chute rounds of 30mm Aden gun ammunition carried during a sortie of the UK Lightning Aircraft. The Figure shows good correlation between the trial and predicted temperatures results for all three components.

Again the results obtained confirm the validity of the mathematical models and demonstrate their flexibility.

Another heating source which must be considered when studying gun installations, particularly the Aden Gun installations, is that which occurs when the gun fires. Obviously, the increase in the



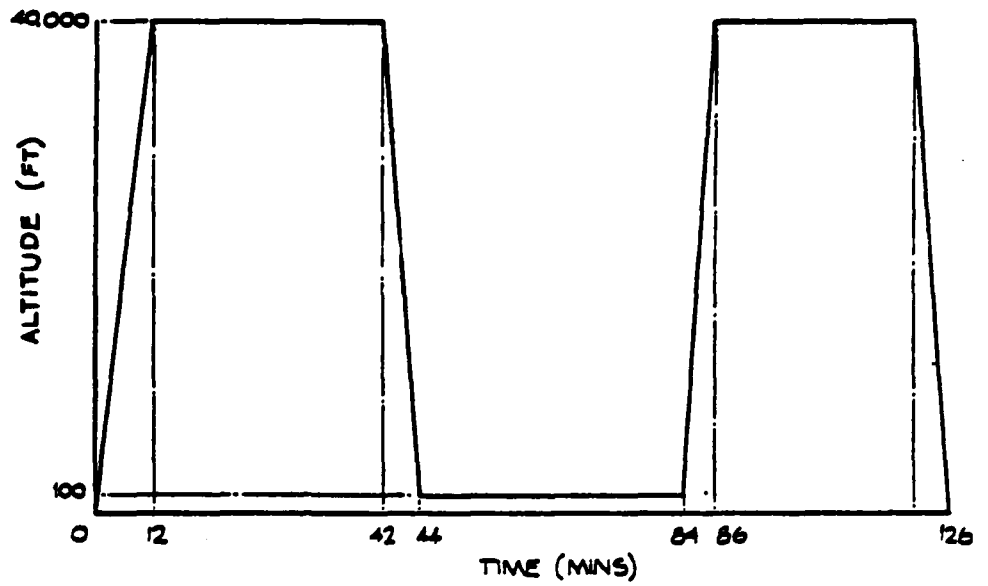
LOW-LOW SORTIE ~ ALTITUDE v TIME (DIAGRAMMATIC)



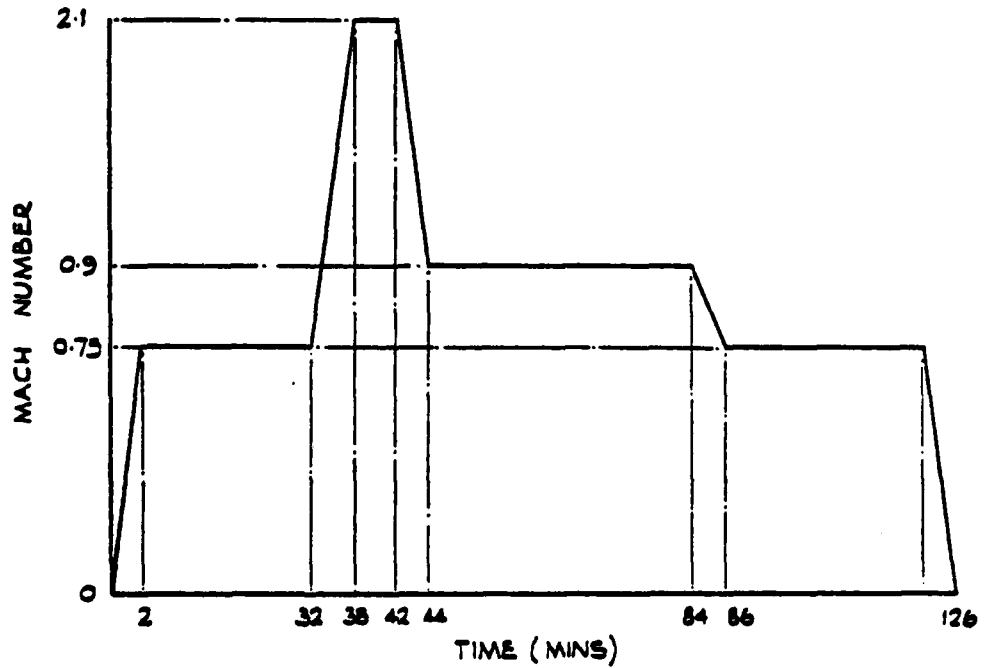
LOW-LOW SORTIE ~ MACH NO. v TIME (DIAGRAMMATIC)

FIG. 11.

LOW-LOW FLIGHT PROFILE



HIGH-LOW-HIGH SORTIE — ALTITUDE v TIME
(DIAGRAMMATIC)



HIGH-LOW-HIGH SORTIE — MACH NO v TIME
(DIAGRAMMATIC)

FIG. 12.

HIGH-LOW-HIGH FLIGHT PROFILE

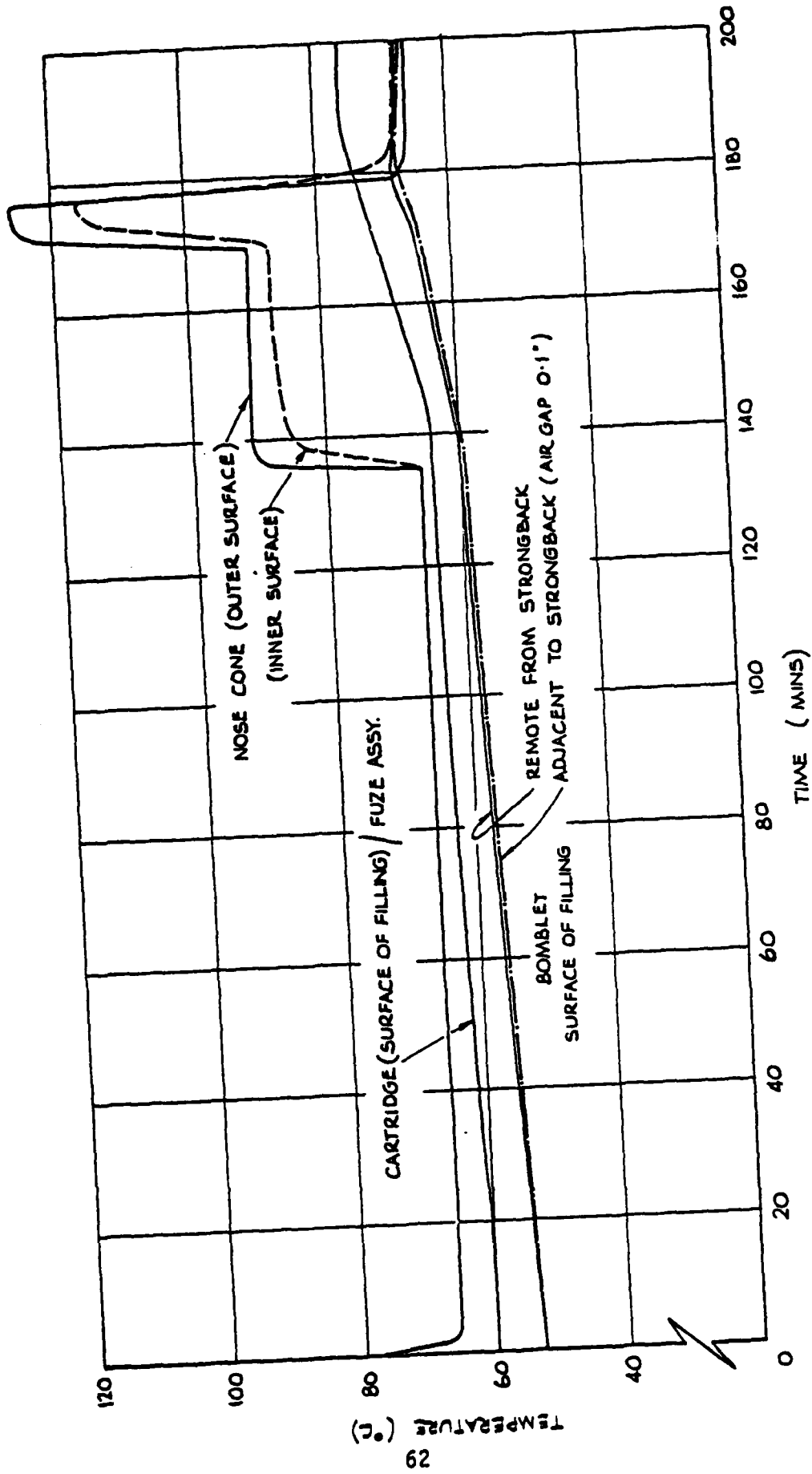


FIG. 13 TEMPERATURE-TIME HISTORIES FOR COMPONENTS ~ LOW-LOW SORTIE

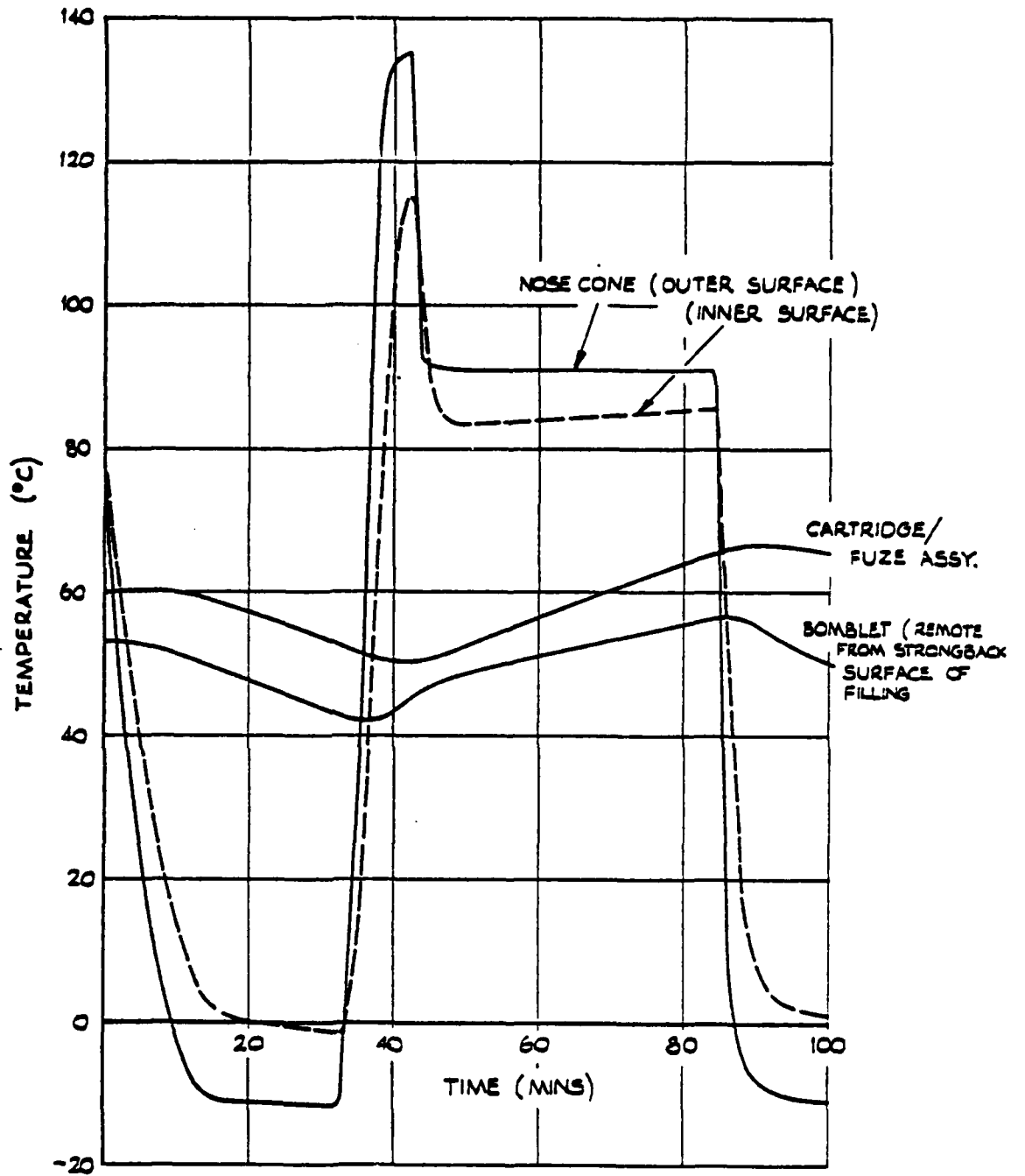


FIG. 14 TEMPERATURE-TIME HISTORIES FOR COMPONENTS
HIGH-LOW-HIGH SORTIE

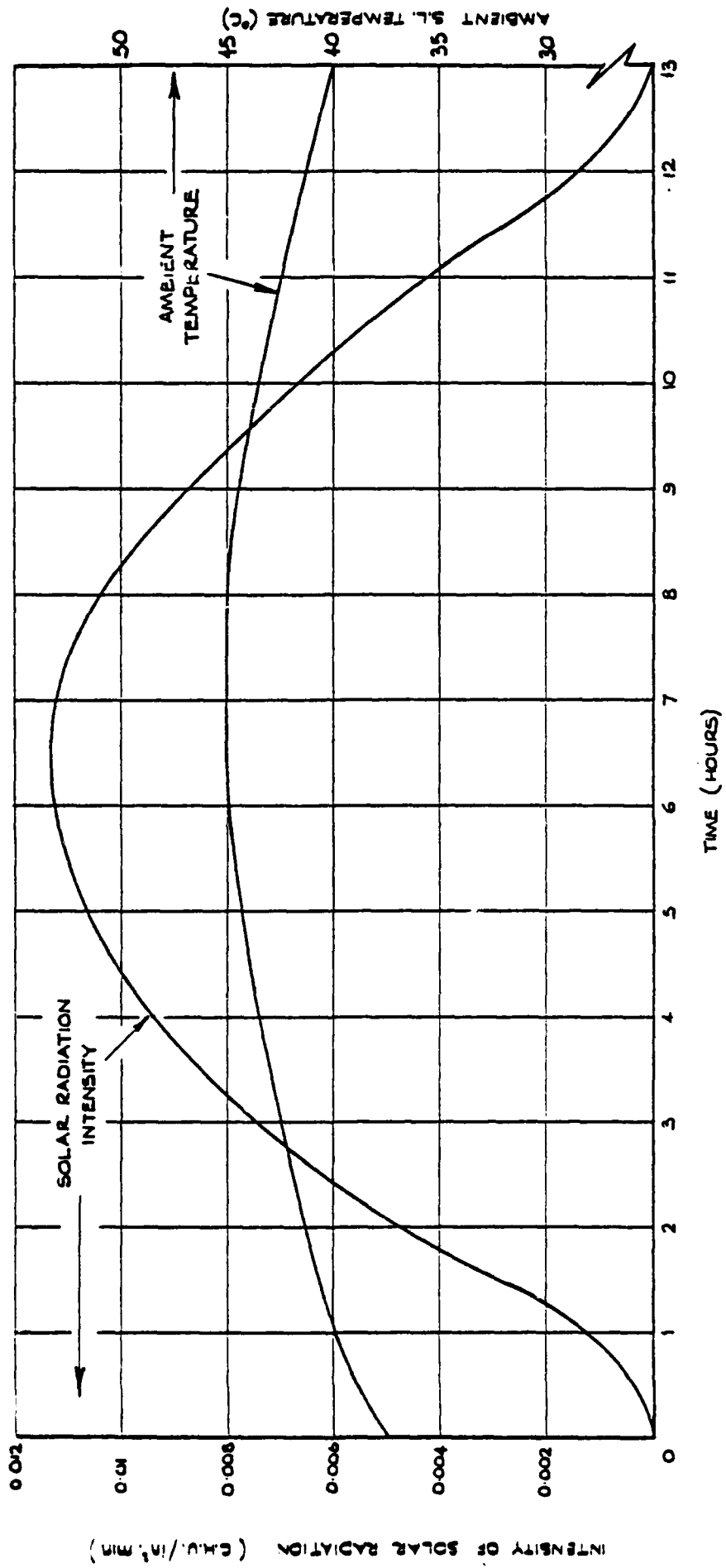


FIG 15 VARIATION OF AMBIENT TEMPERATURE & INTENSITY OF SOLAR RADIATION WITH TIME.

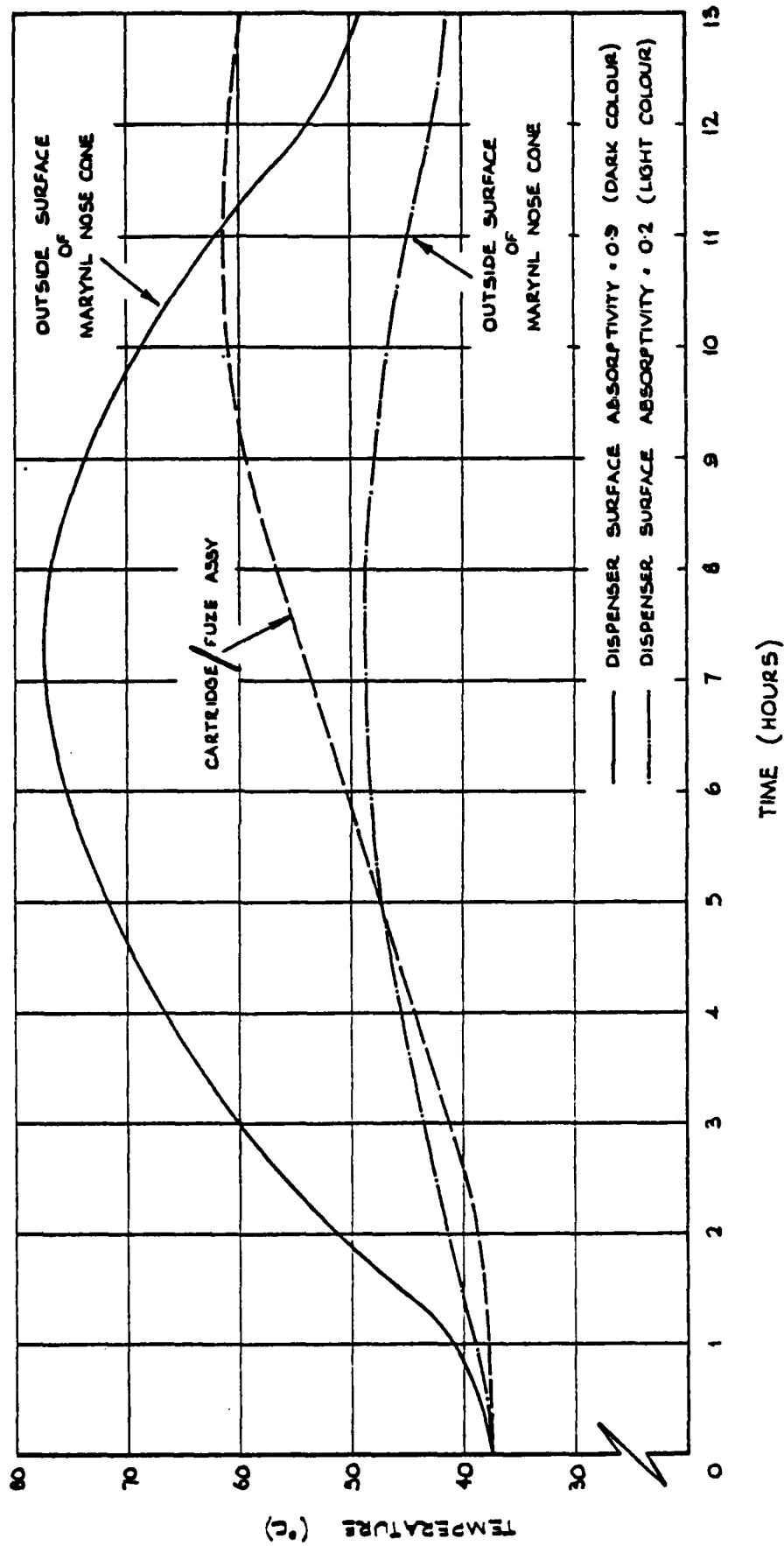


FIG. 16 BL755 VARIATION OF NOSE CONE & CARTRIDGE/FUZE ASSEMBLY TEMPERATURE DUE TO EXPOSURE TO SOLAR RADIATION

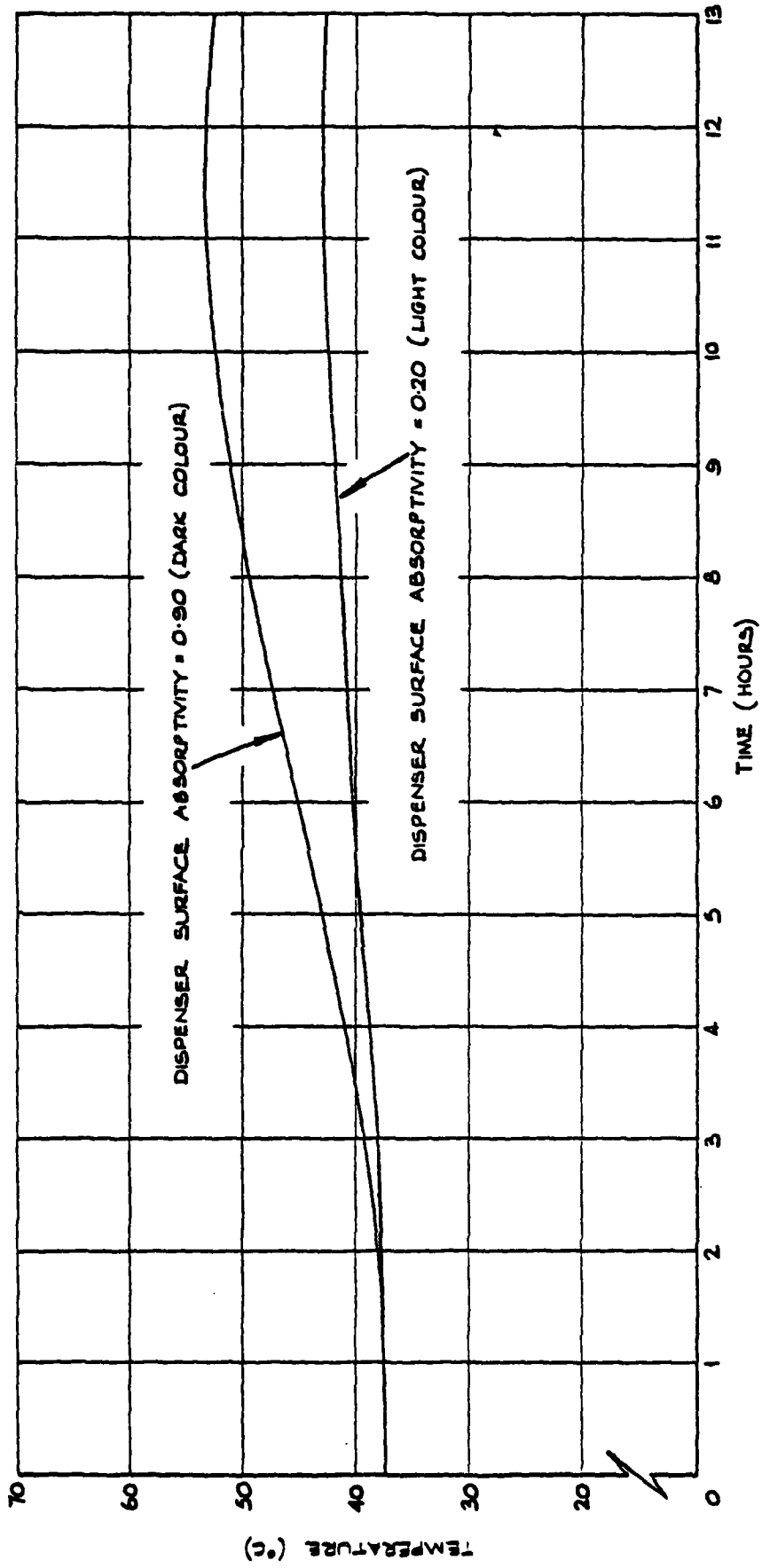


FIG.17 BL755 VARIATION OF BOMBLET SURFACE OF EXPLOSIVE FILLING TEMPERATURE WITH TIME DUE TO EXPOSURE TO SOLAR RADIATION (REMOTE FROM STRONGBACK)

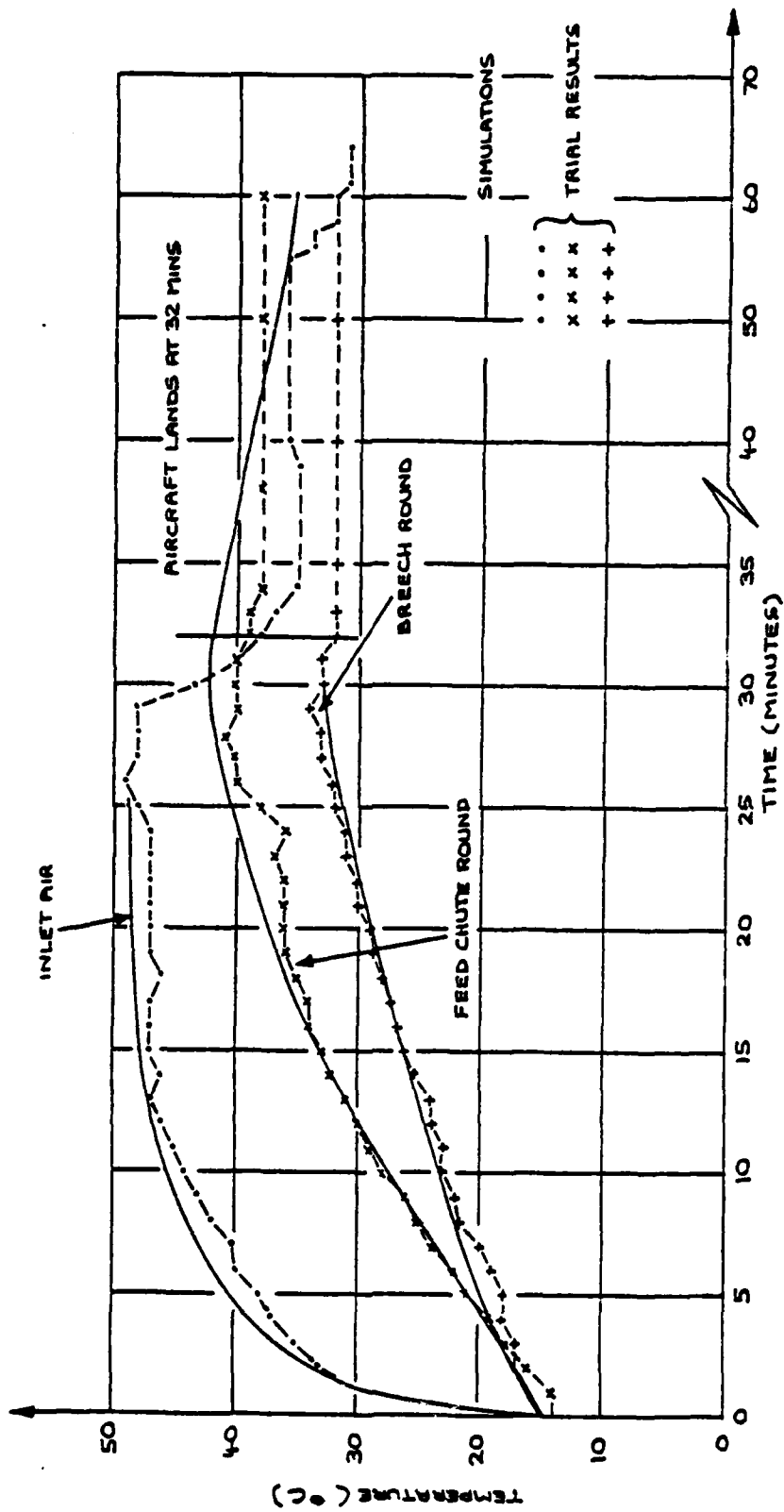


FIG. 18. COMPARISON OF MEASURED AND SIMULATED TEMPERATURES OF 30MM ADEN GUN AMMUNITION DURING A SORTIE OF THE LIGHTNING AIRCRAFT

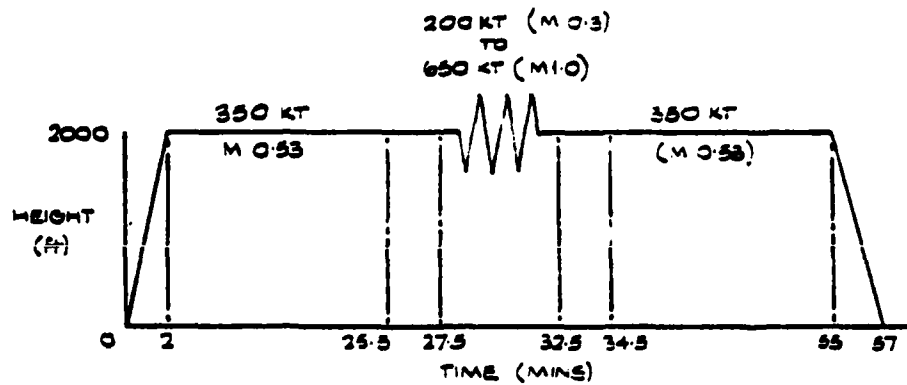
breech temperatures which occur after gun firing, is a function of the number of rounds of ammunition fired. From gun firing trials empirical relationships for the increase in breech temperature as a function of the number of rounds of ammunition fired have been derived for use in kinetic heating studies.

For the hypothetical Low Level and High Level sorties shown in Figure 19, the temperatures of the 30mm Aden Gun ammunition have been computed and are presented in Figures 20 and 21. The effect of firing 100 rounds of ammunition at the end of the dash phase, at Mach Nos. of 1.0 and 1.8 for the Low and High Level sorties respectively is clearly shown. Also computed were the maximum gun/ammunition temperatures and end of sortie gun/ammunition temperatures as a function of number of rounds fired for sorties flown in varying sea level ambient temperatures. These temperatures are presented in Figures 22 and 23 and Figures 24 and 25 for the Low and High Level sorties respectively.

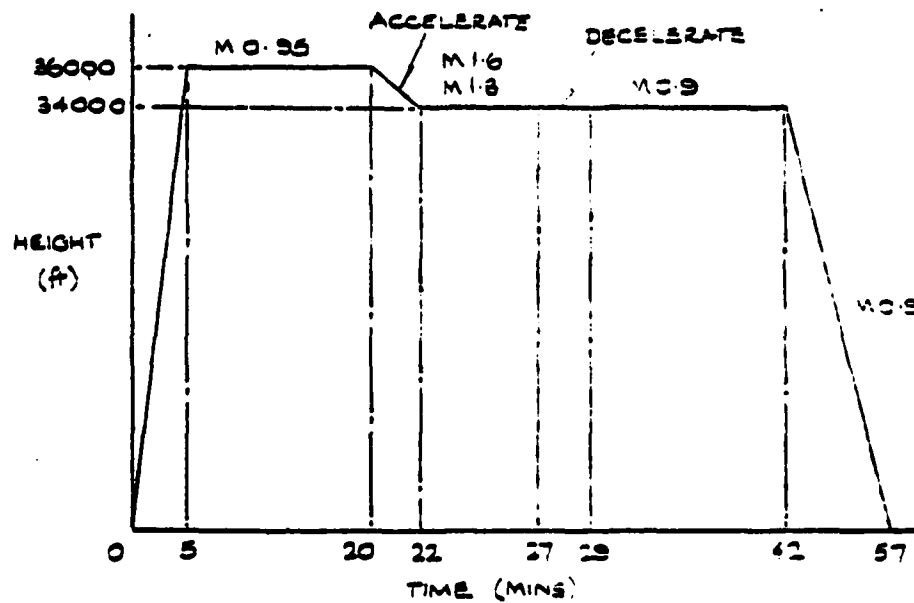
Another environment to which considerable attention has been given is that of the bomb bay of the UK Buccaneer Aircraft. The engine jet pipes pass through the bomb bay and the stabilisation temperatures obtained are considerably in excess of the recovery temperature compatible with ambient flight conditions. From flight trials results it has been found that during aircraft manoeuvres the bomb bay temperature could be related to engine r.p.m., and this empirical relationship had to be incorporated in the mathematical models. For a straight and level flight at 200 ft. AGL and a Mach No. of 0.825 in a sea level ambient temperature of 45°C , the recovery temperature is 85°C . However, for the same conditions, the stabilisation temperature within the bomb bay is 105°C , i.e. an increase of 20°C due to jet pipe heating.

For the hypothetical High-Low-Low-High sortie presented in Figure 26, the variation of temperature with time for the VT907 Fuze for external and internal carriage environments in a sea level ambient temperature of 45°C are presented in Figures 27 and 28. Although the heat transfer rates for the external carriage environment are considerably higher than for the internal environment, the maximum temperature recorded during internal carriage on this sortie is 90°C which is 8°C higher than for internal carriage. Corresponding temperature-time histories for the Ejection Release Unit No.2 Mk.1 for the external and internal environments are presented in Figures 29 and 30.

The maximum temperature limitations of both the VT907 Fuze and Ejection Release Unit is 70°C , and this is exceeded during carriage on the specified sortie when flown in a sea level ambient temperature of 45°C .



a) LOW LEVEL ATTACK



b) HIGH LEVEL ATTACK

FIG19 - HYPOTHETICAL LOW AND HIGH LEVEL SORTIES

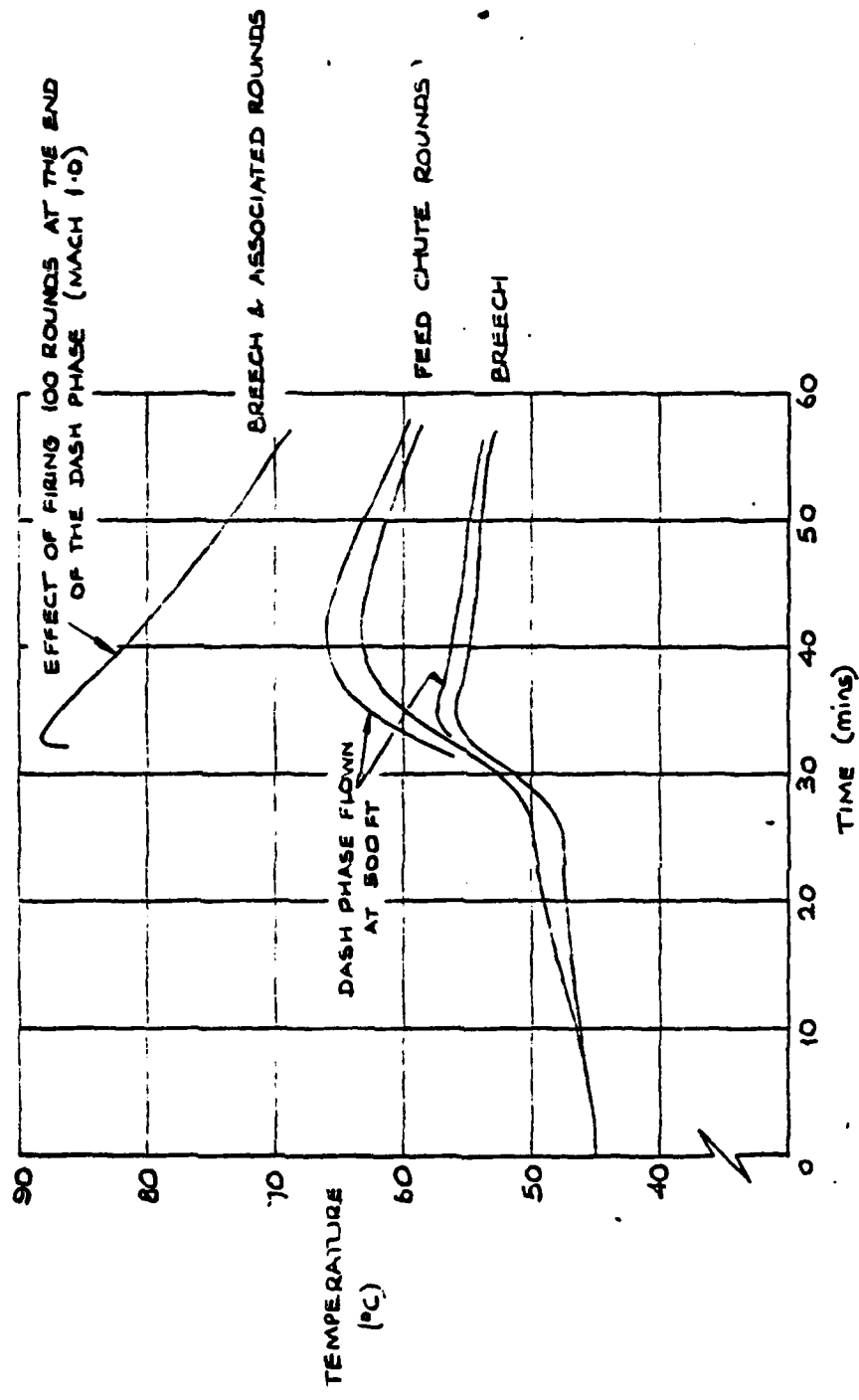


FIG. 20 TEMP-TIME FOR 30mm ADEN GUN & AMMUNITION
 LOW LEVEL ATTACK — 45°C S.L. AMBIENT

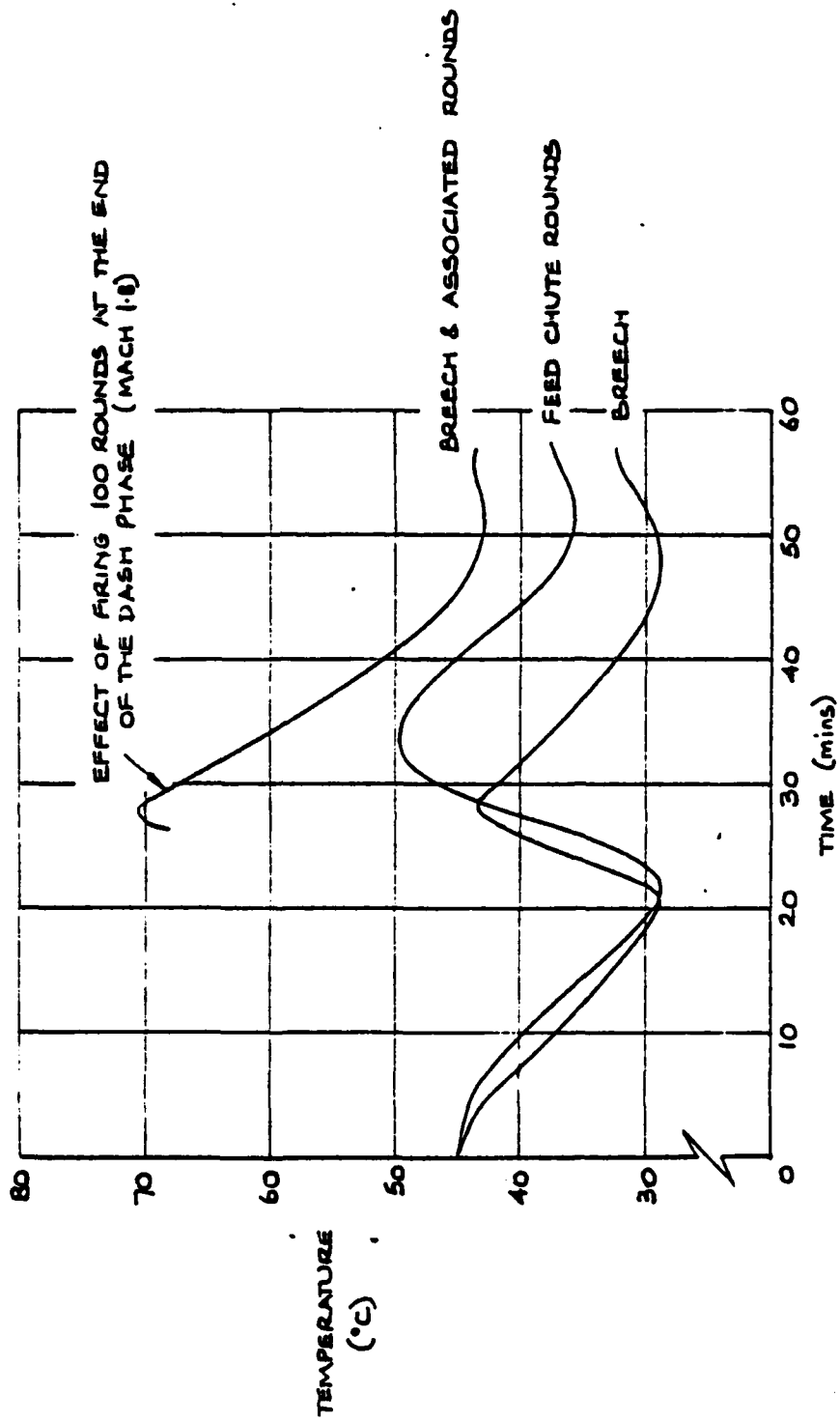


FIG. 21 TEMP - TIME FOR 30mm ADEN GUN & AMMUNITION
HIGH LEVEL ATTACK ~ 45°C S.L. AMBIENT

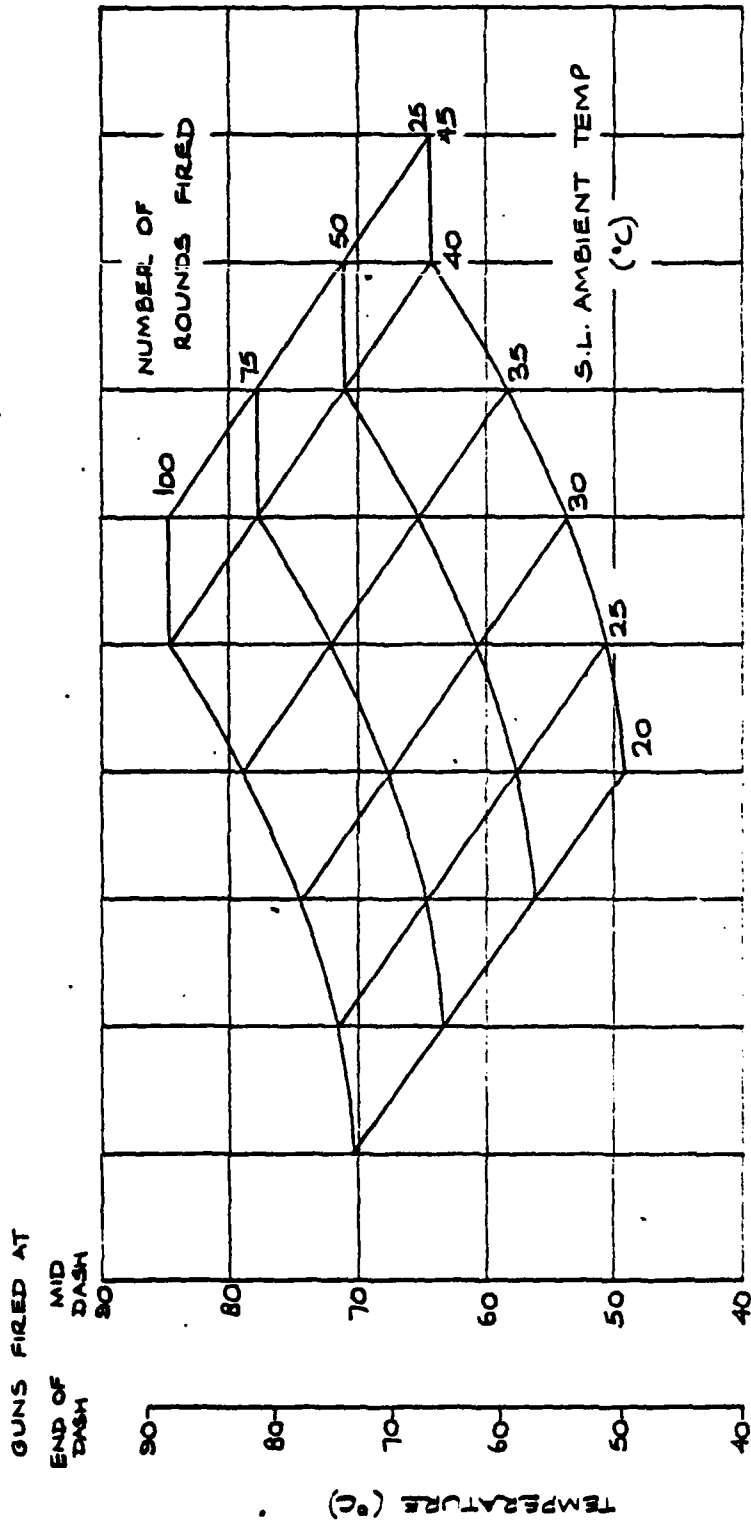


FIG. 22 EFFECT OF FIRING ON THE MAXIMUM GUN/AMMUNITION TEMPERATURE

LOW LEVEL ATTACK — MACH 1.0 DASH

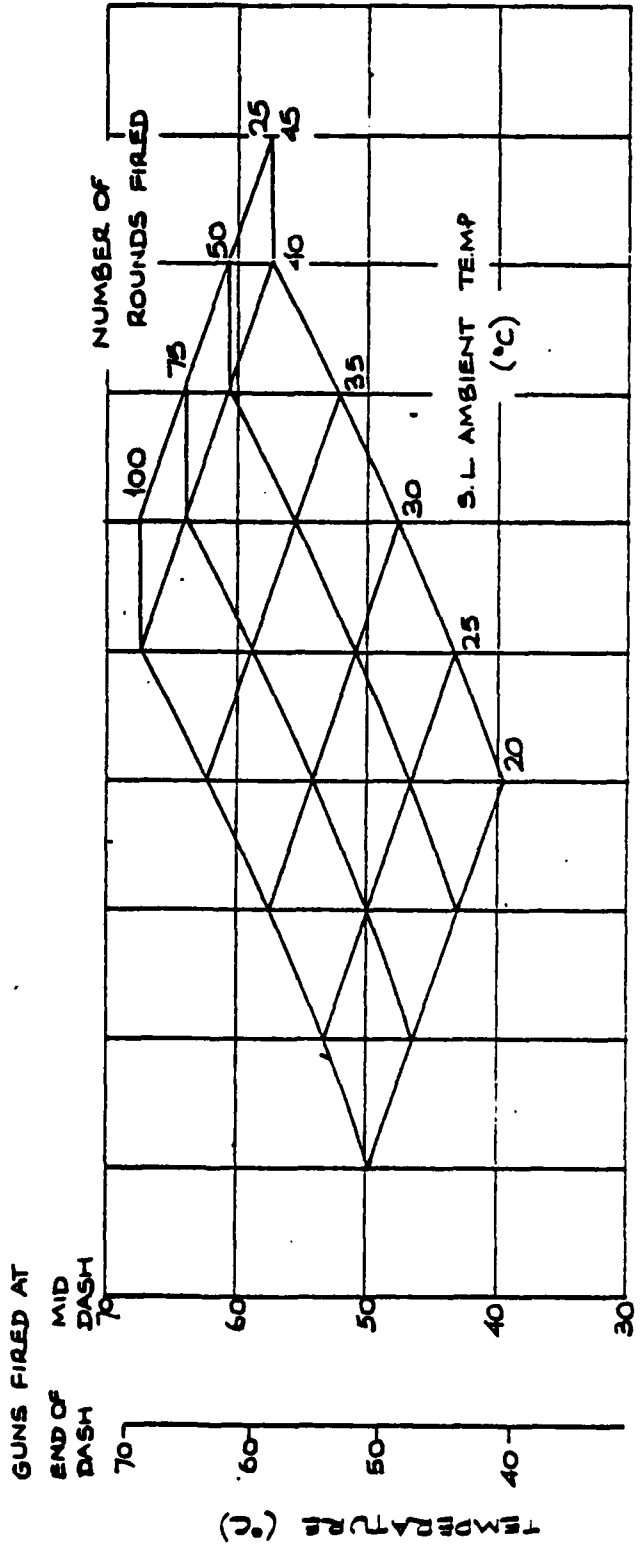


FIG. 23 EFFECT OF FIRING THE GUNS ON END-OF-SORTIE GUN/AMMUNITION TEMPERATURE — LOW LEVEL ATTACK — MACH 1.0 DASH

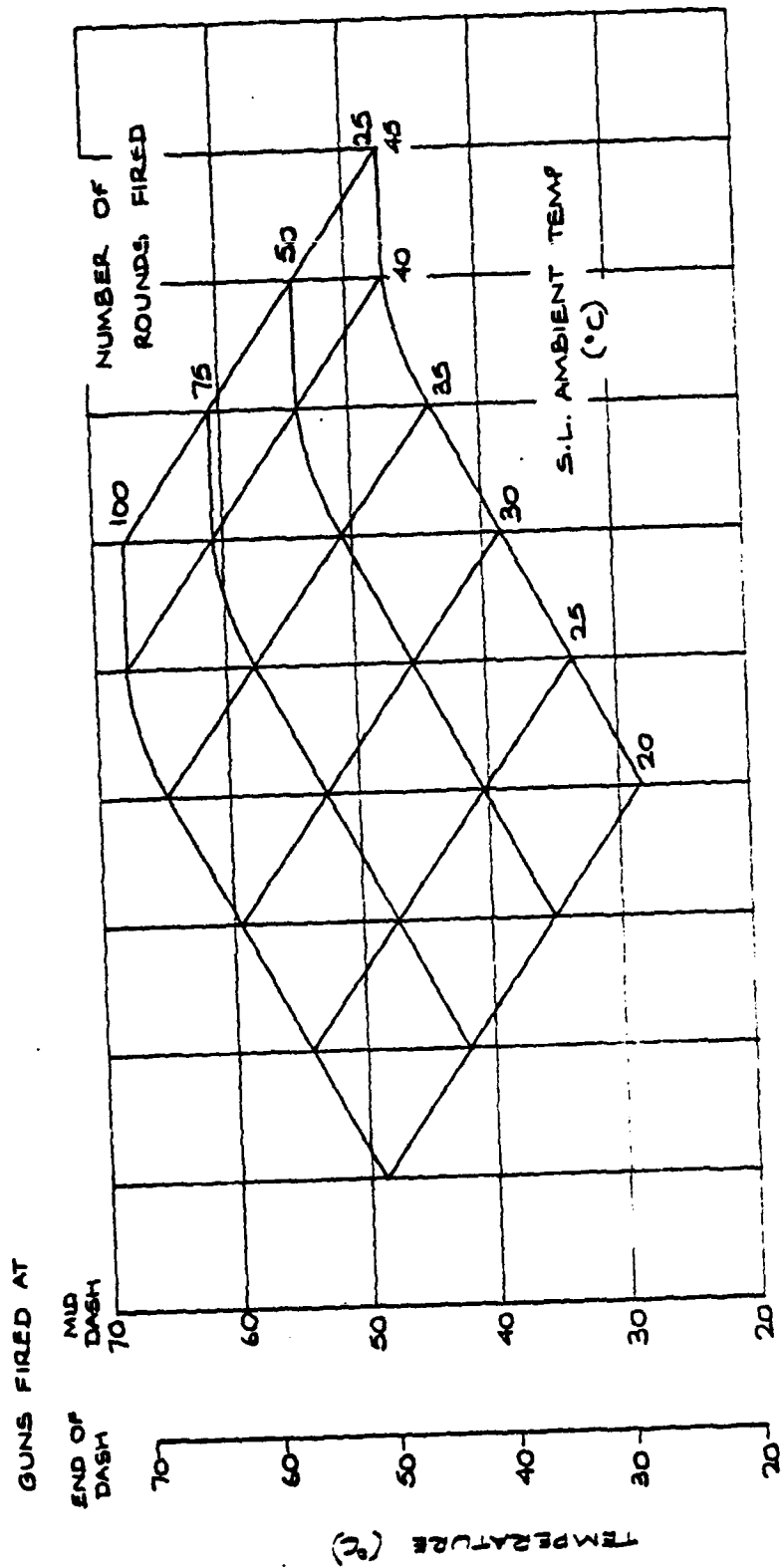


FIG. 24 EFFECT OF FIRING ON THE MAXIMUM GUN / AMMUNITION TEMPERATURE
HIGH LEVEL ATTACK - MACH 1.8 DASH

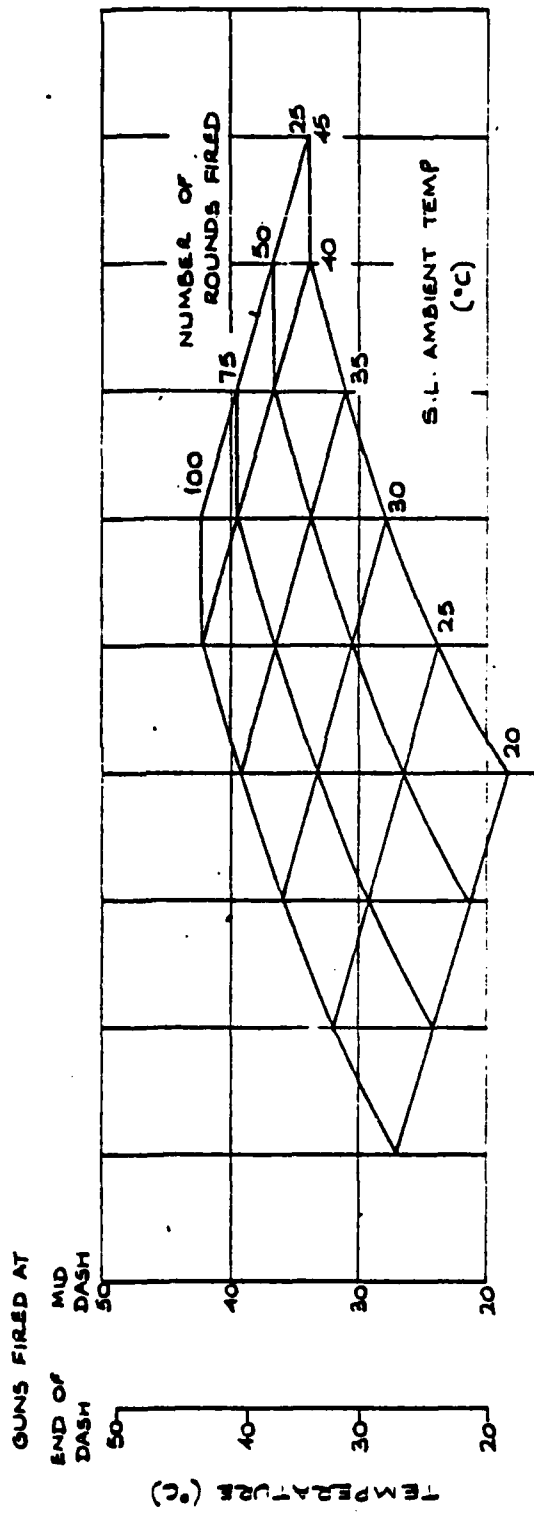
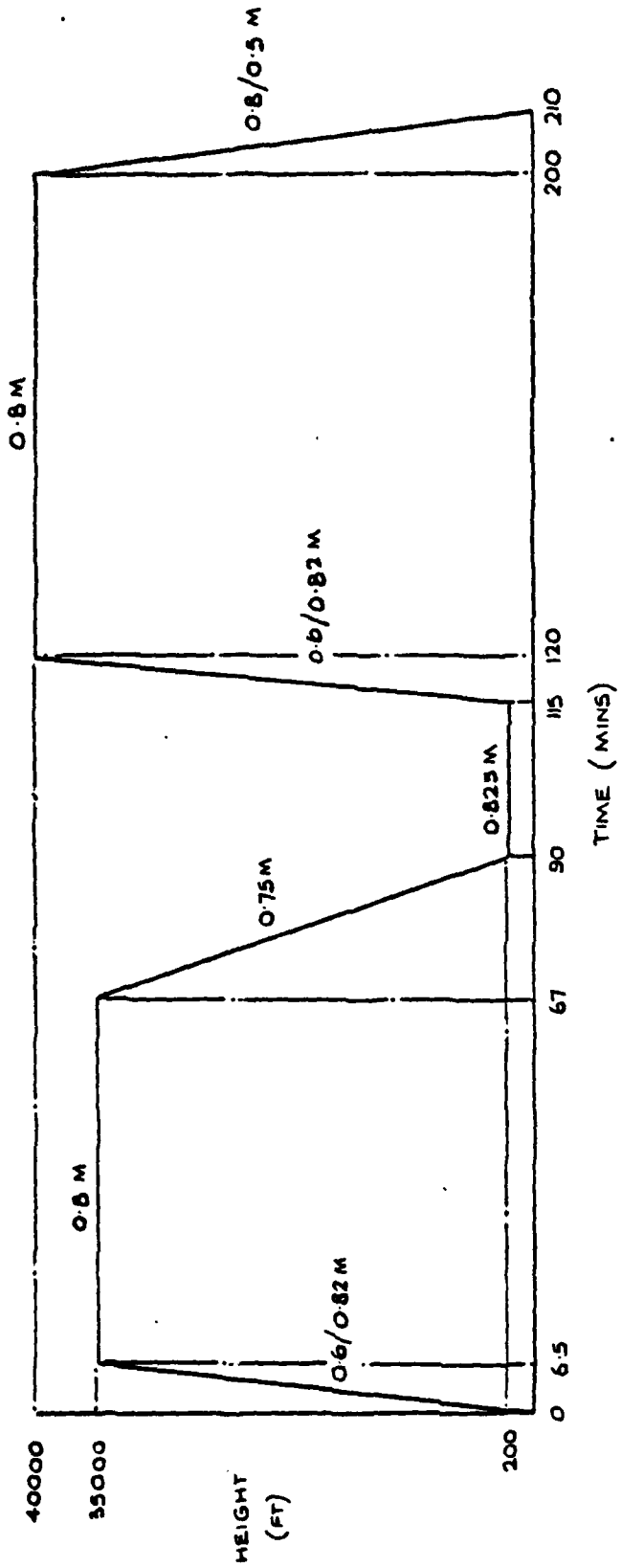


FIG 25 EFFECT OF FIRING THE GUNS ON END-OF-SORTIE GUN/AMMUNITION TEMPERATURE — HIGH LEVEL ATTACK — MACH 1.8 DASH



FLIGHT PROFILE - H.L.L.H. SORTIE

FIG. 26

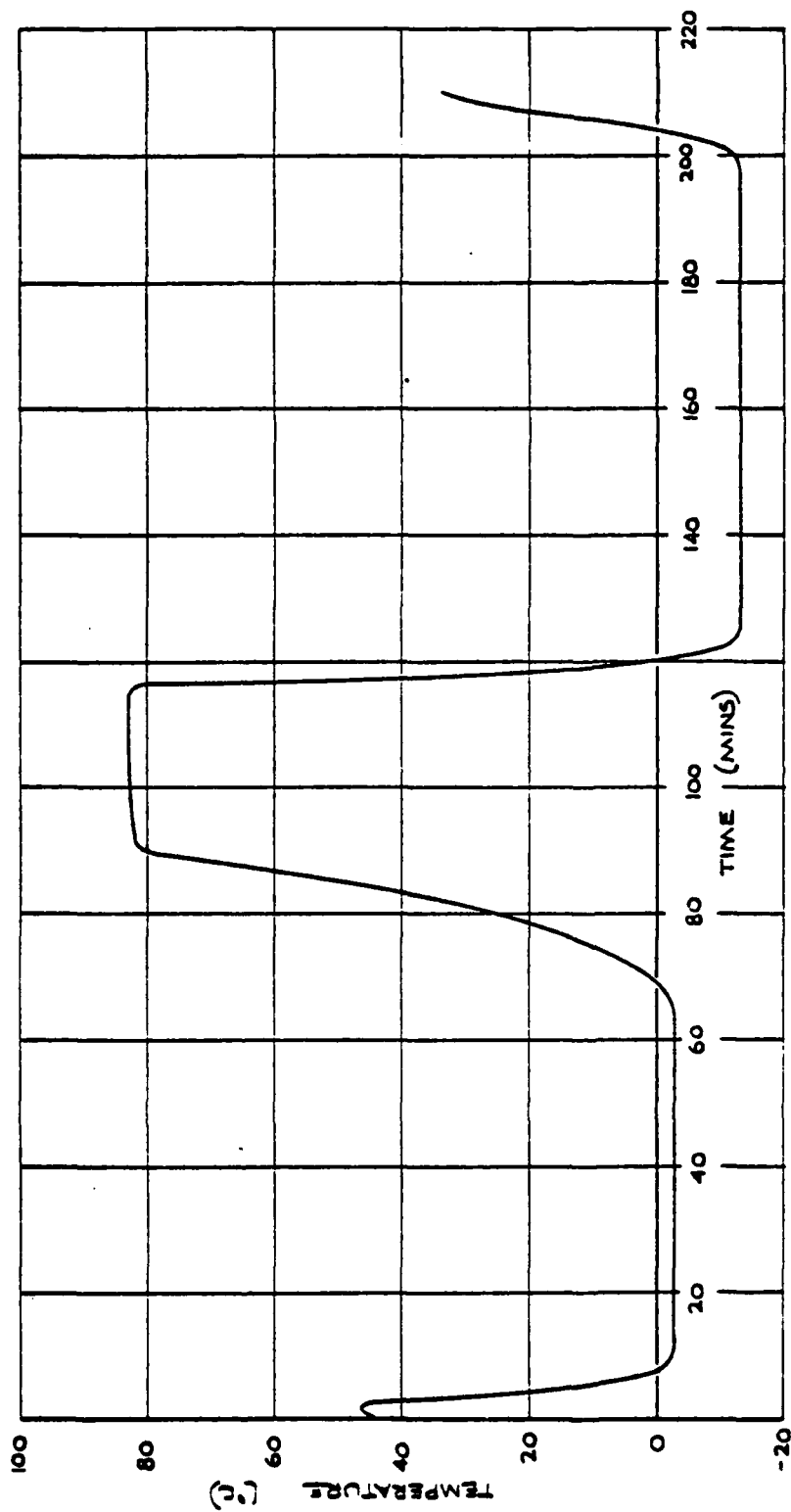


FIG. 27 TEMP - TIME FOR FUZE V.T. 507 (EXTERNAL) — H.L.L.H SORTIE

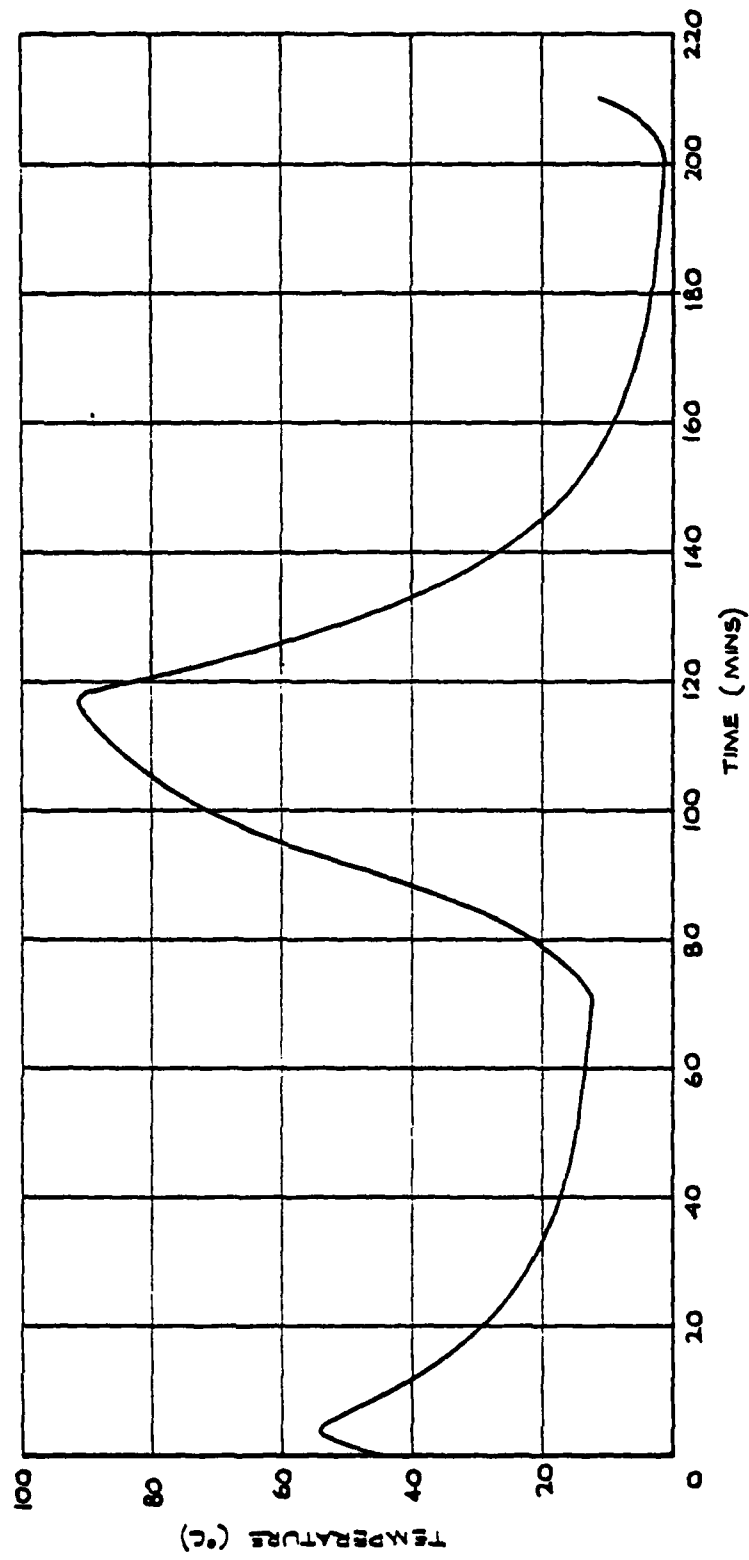


FIG. 28 TEMP - TIME FOR FUZE V.T. 807 (INTERNAL) — H.L.L.H. SORTIE

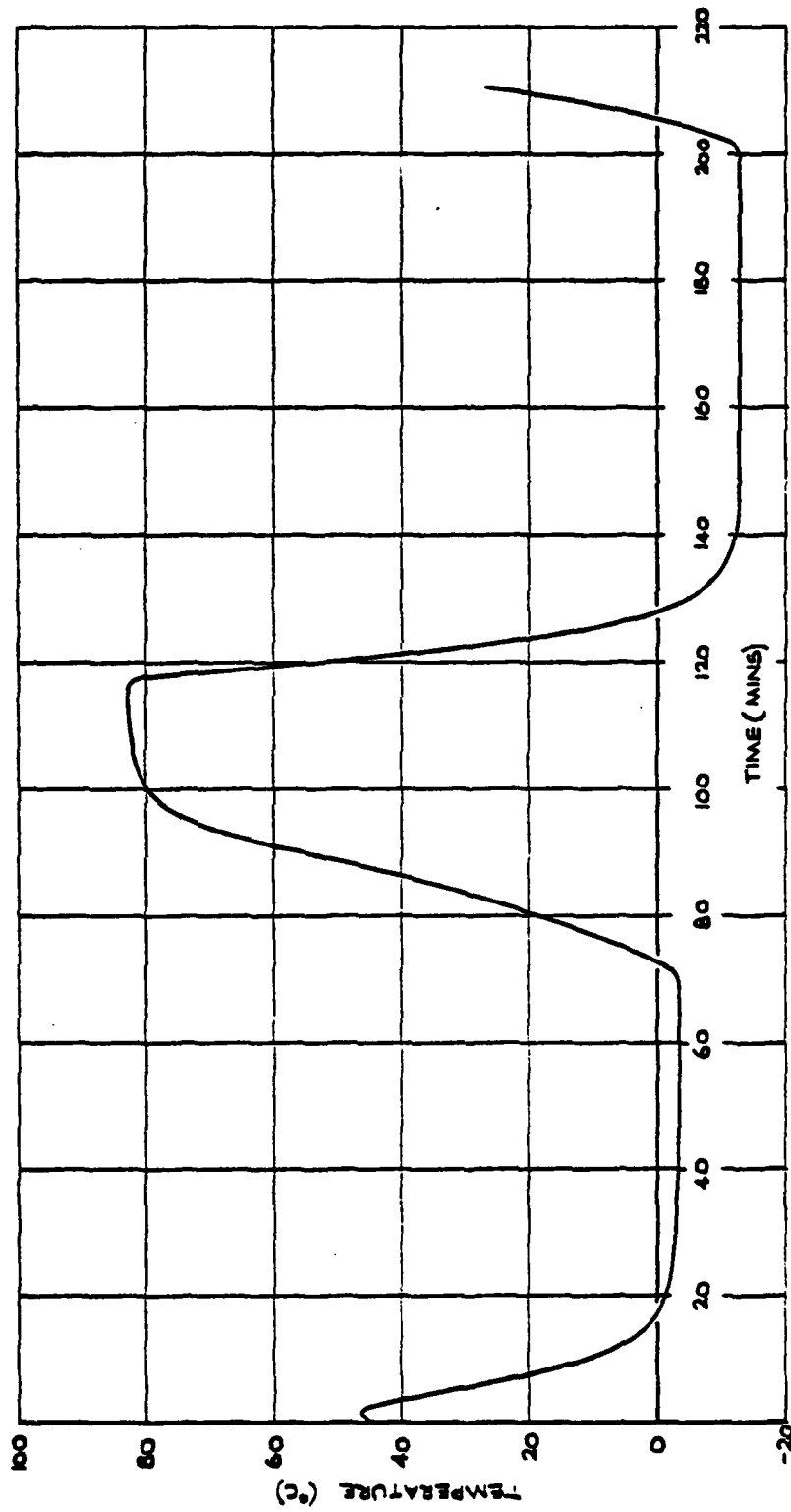


FIG. 20 TEMP-TIME FOR E.R.U. NO.2 MK.1 (EXTERNAL) ~ H.L.L.H. BORTÉ

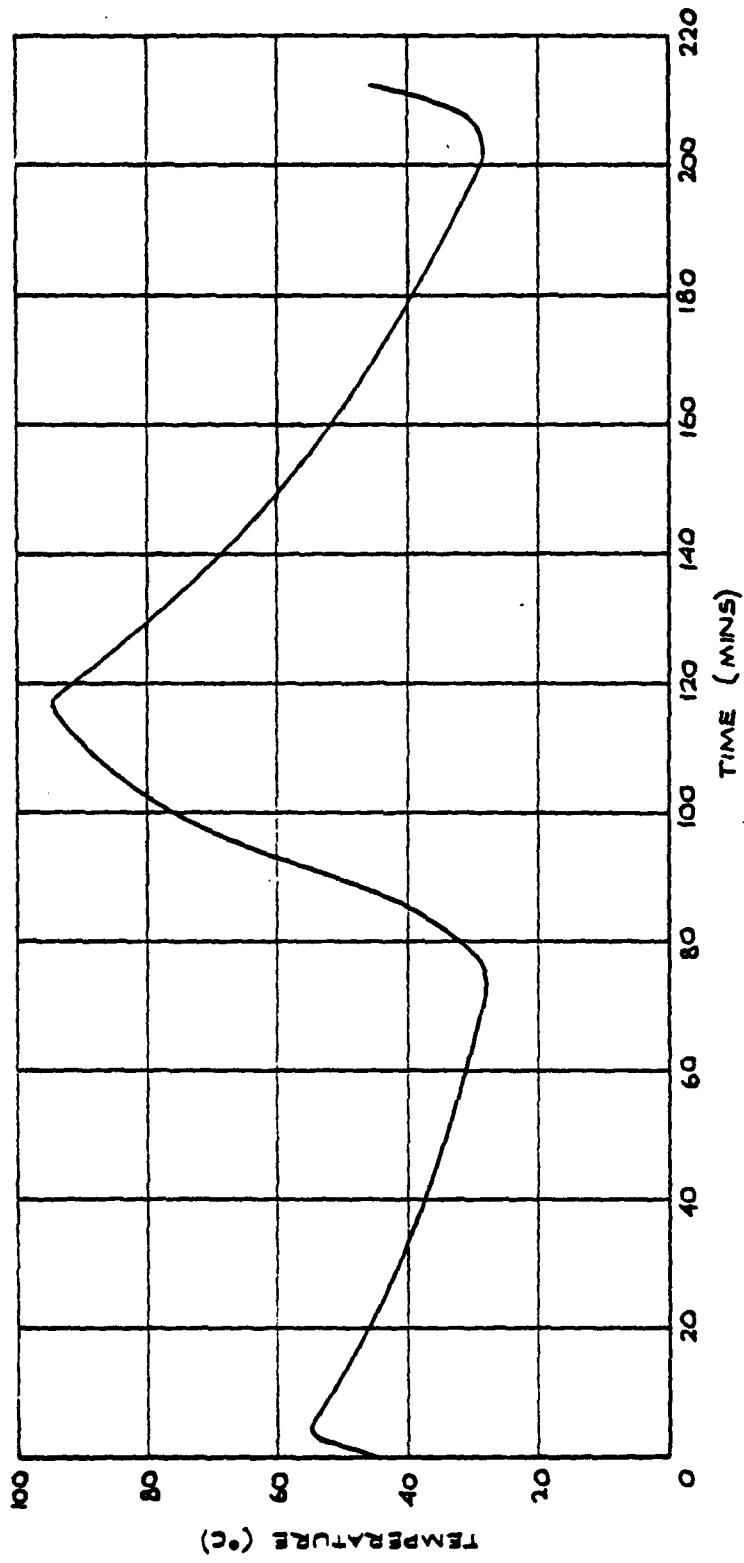


FIG. 30 TEMP-TIME FOR E.R.U. NO.2 MK.1 (INTERNAL) — H.L.L.H. SORTIE

FLIGHT LIMITATIONS

To prevent the overheating of temperature sensitive components of weapons and associated equipment, during carriage on operational sorties, it is necessary to somehow limit the performance of the delivery aircraft. These limitations could take the form of limiting the sea level ambient temperature in which the sortie is to be flown or alternatively limiting the flight Mach No. or flight duration.

Typical flight limitations for the internal carriage of the Ejection Release Unit and VT907 Fuze when carried during the hypothetical High-Low-Low-High sortie (Figure 26) are presented in Figures 31 and 32. These limitations apply to the dash phase of the sortie and combinations of sea level ambient temperature, dash Mach No. and dash duration presented ensure that the 70°C limiting temperature of the components is not exceeded. Implicit in these flight limitations is that the pre and post dash phases of the sortie are flown at the specified Mach Nos. and heights. To implement these limitations in operational use could prove difficult and inflexible because of the need to fly the specified pre and post dash phase of sorties.

To overcome this an alternative method of presentation has been derived which enables the entire sortie; cruise and dash phases to be planned so that the limiting temperature of a component will not be exceeded. These so called Flight Limitation Charts are applicable to sorties having no more than two phases with one phase being flown at low level.

Flight Limitation Charts for external carriage are presented in Figures 33 to 40 for the following components.

- Figure 33 - VT907 Fuze (70°C)
- Figure 34 - Ejection Release Unit Cartridge No.2 Mk.2 (70°C)
- Figure 35 - Ejection Release Unit No.2 Mk.1 (70°C)
- Figure 36 - Igniter Frangible Pillar No.1A Mk.1 (70°C)
- Figure 37 - 1,000lb Bombs N1, Mk.10, Mk.83 and 500lb Bombs Mk.21 and Mk.82, Mod 1 (76°C)
- Figure 38 - 2" Rockets A/C No.2 and No.3 in Launcher No.7 Mk (MATRA) (60°C)
- Figure 39 - 1,000lb Bomb M.C. H.E. Mks 6 to 12 and 540lb Bomb Mk.2 (Torpex filled) (76°C)
- Figure 40 - Explosive Bolt (pylon jettison) (70°C)

() indicates maximum temperature limitation.

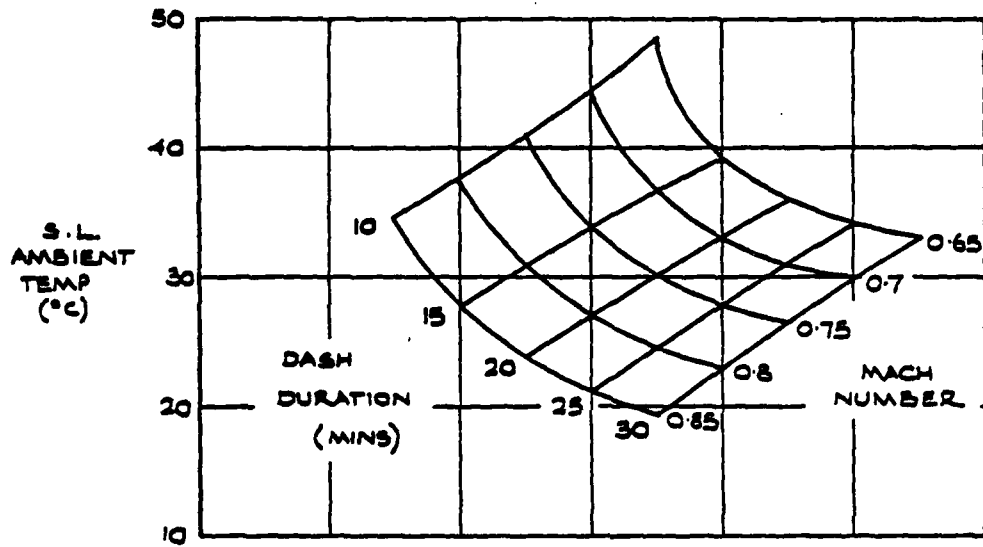


FIG. 31 FLIGHT LIMITATIONS FOR E.R.U. NO.2 MK.1 (INTERNAL)
H.L.L.H. SORTIE

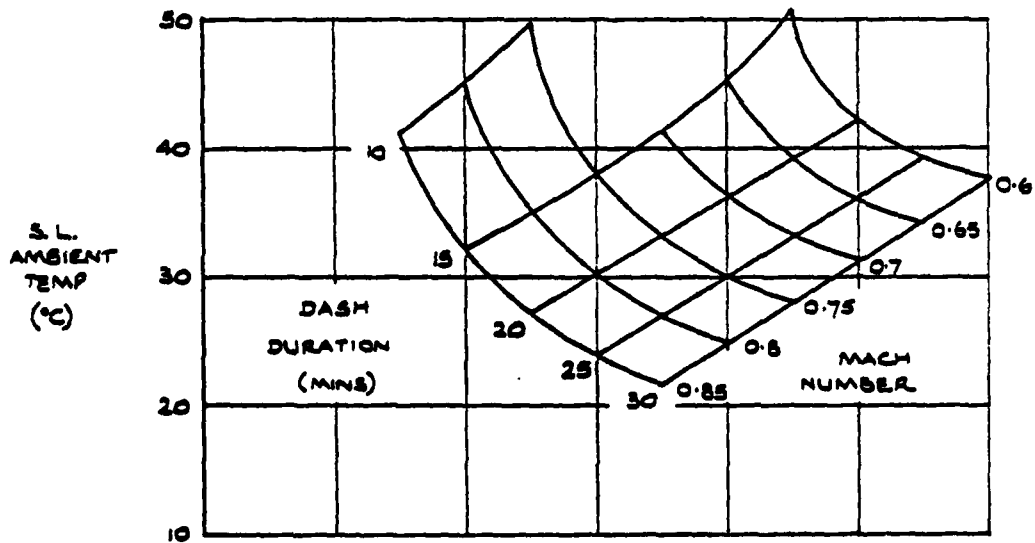
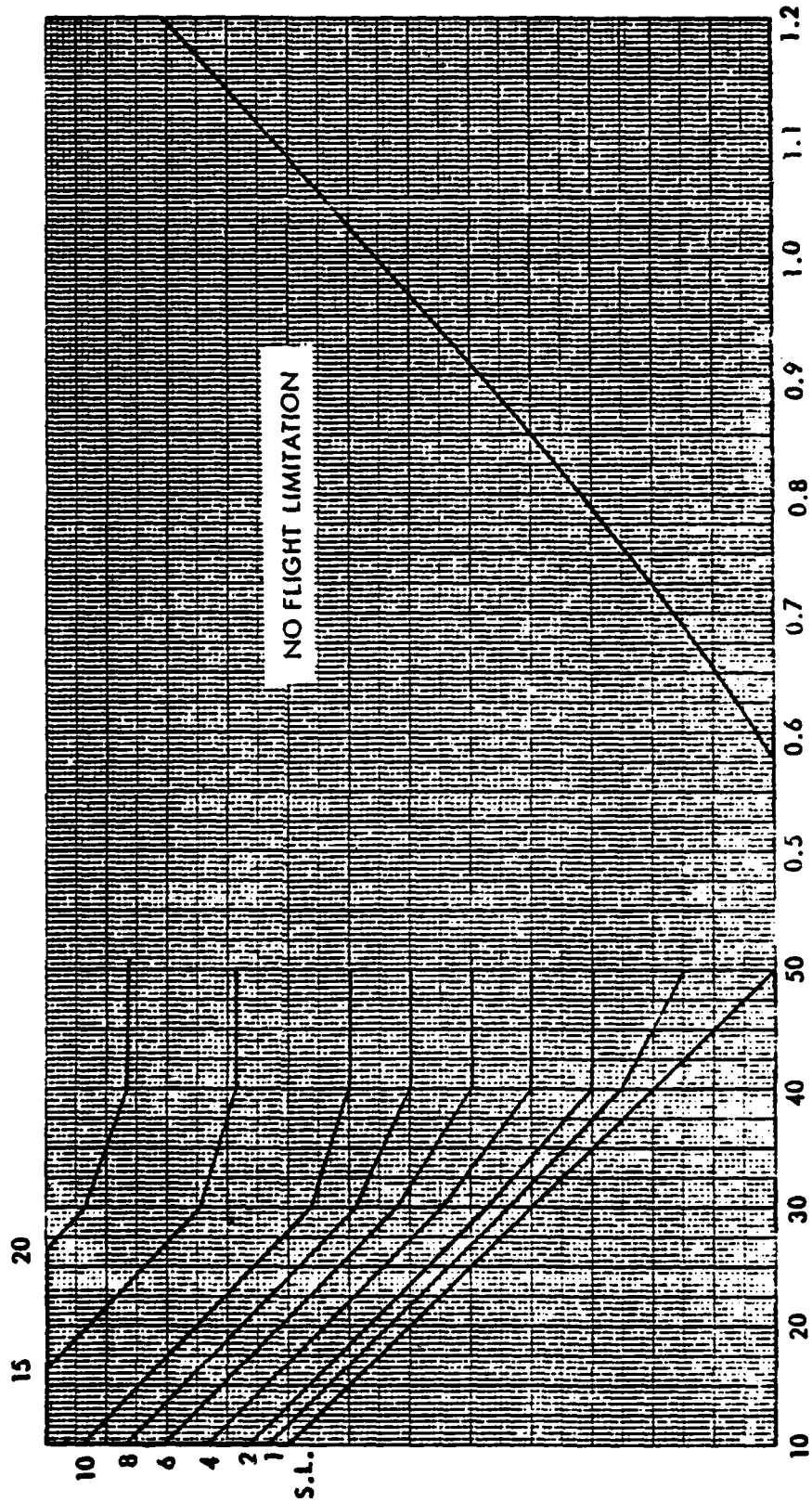


FIG. 32 FLIGHT LIMITATIONS FOR FUZE V.T. 907 (INTERNAL)
H.L.L.H. SORTIE

MINIMUM HEIGHT FLOWN (KILO FT)



SEA LEVEL AMBIENT TEMP (°C)

MAXIMUM MACH No. WHICH MAY BE FLOWN

FIG. 33 FLIGHT LIMITATION CHART FOR VT FUZE 907 EXTERNAL CARRIAGE

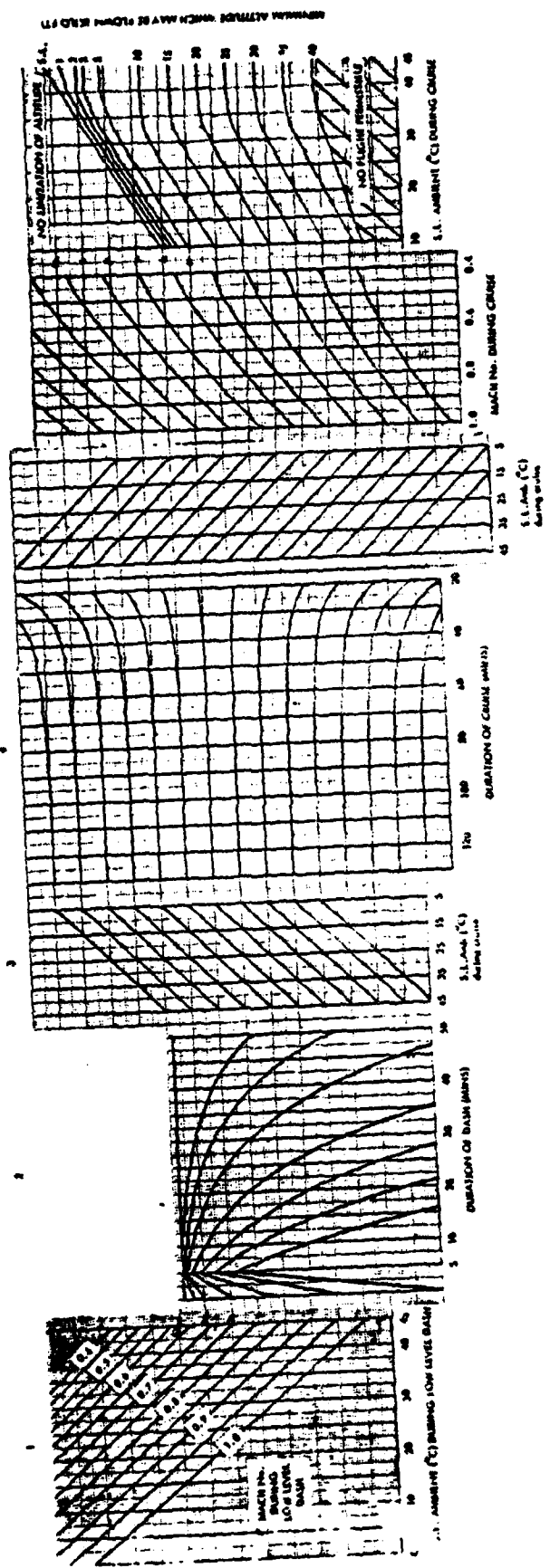


FIG. 24 FLIGHT LIMITATION CHART FOR P. U. CARTRIDGE No. 2 Mk. 3 Pylon Insulation

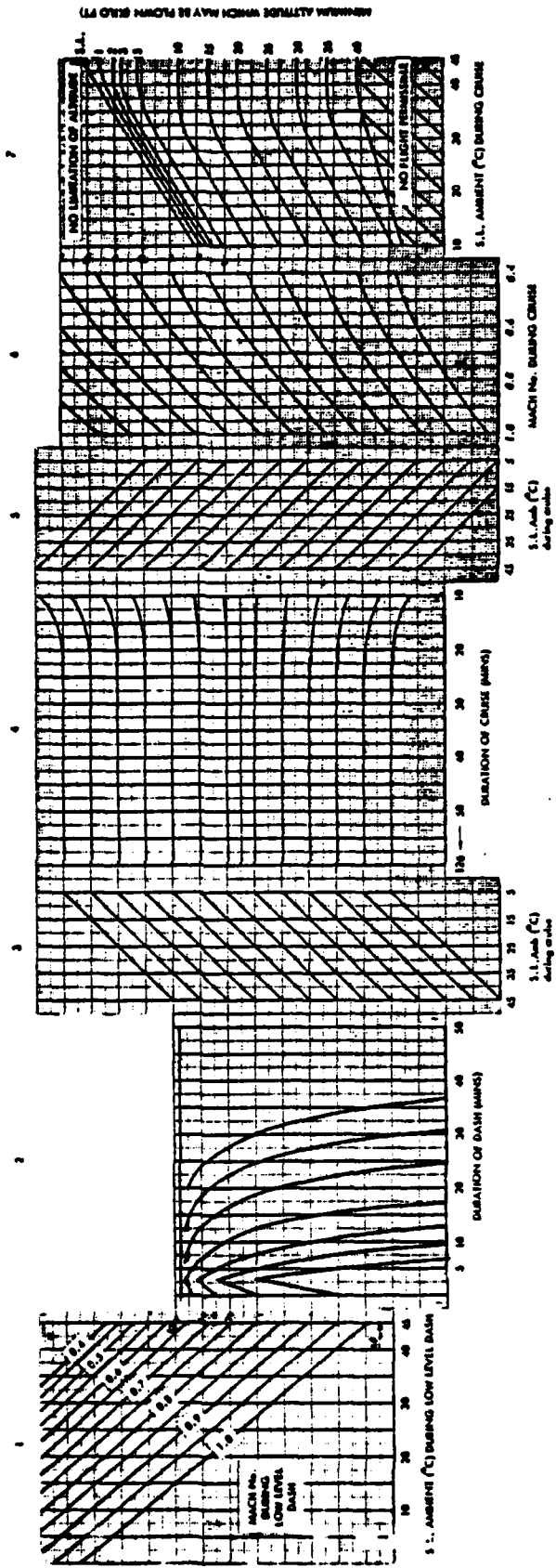


FIG. 26 FLIGHT LIMITATION CHART FOR E.U. No. 2, 1 & 3 FLYING UNIT No. 3 M. 3 FROM INSTALLATION

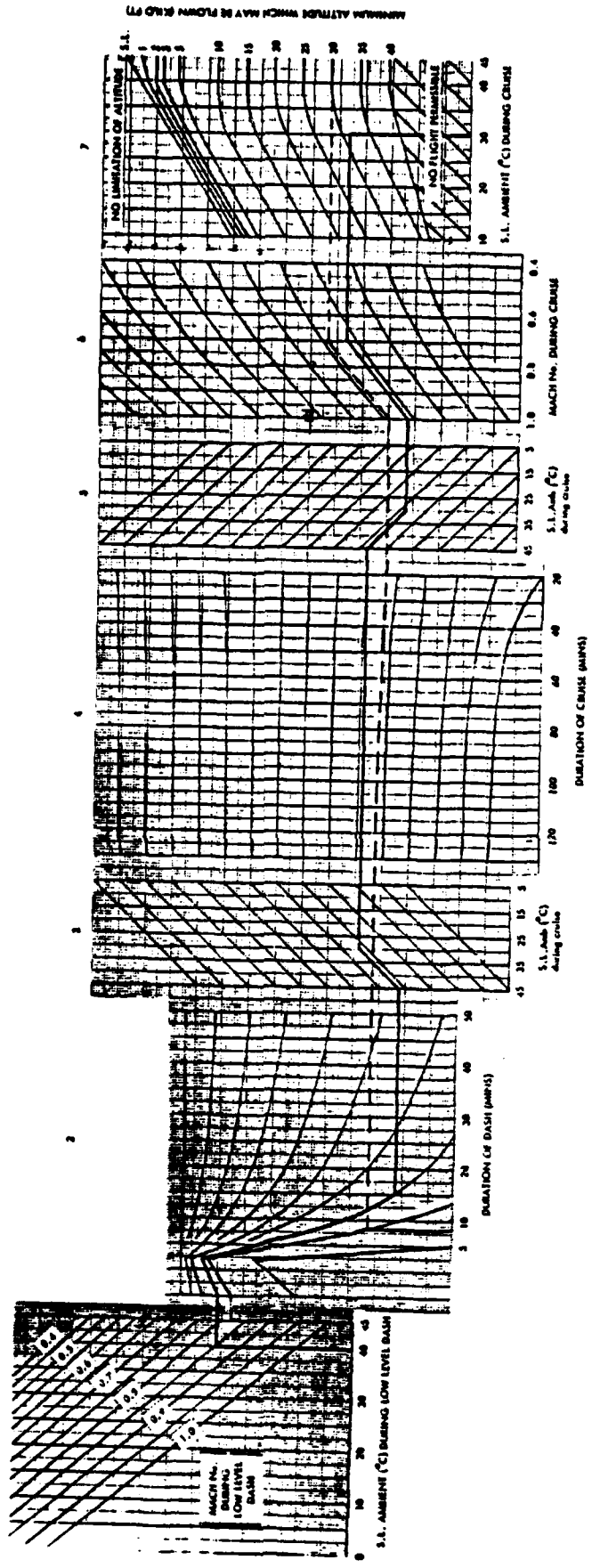


FIG. 37
 FLIGHT LIMITATION CHART FOR 108B BOMBS N.1. M6 18 8 46 80 Mod. 3 USM and
 108B BOMBS M6.21 & M6.22 Mod. 1 EXTERNAL CARRIAGE

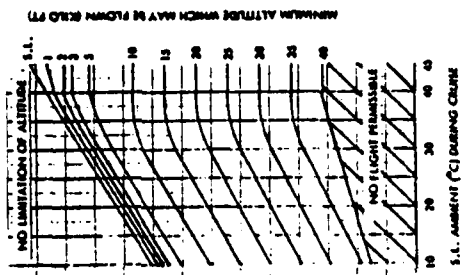
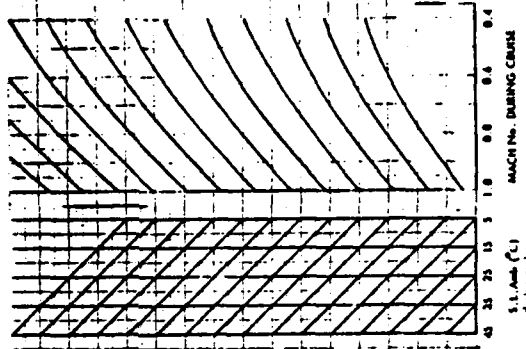
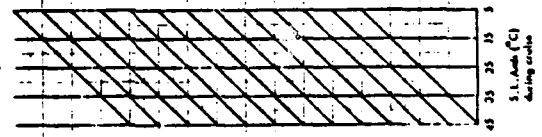
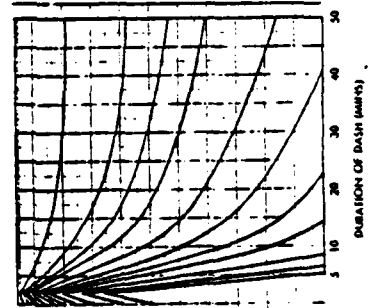
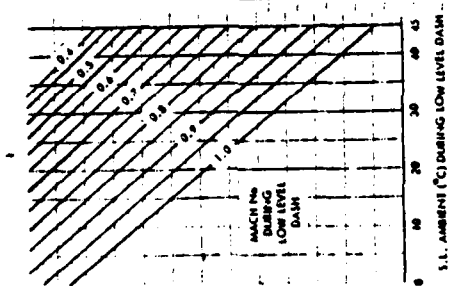


FIG. 28 FLIGHT LIMITATION CHART FOR 1000 LB BOMB M.C. N.E. AM. 4-12 AND 540 LB BOMB M. 2 (TOPPER FILLER)

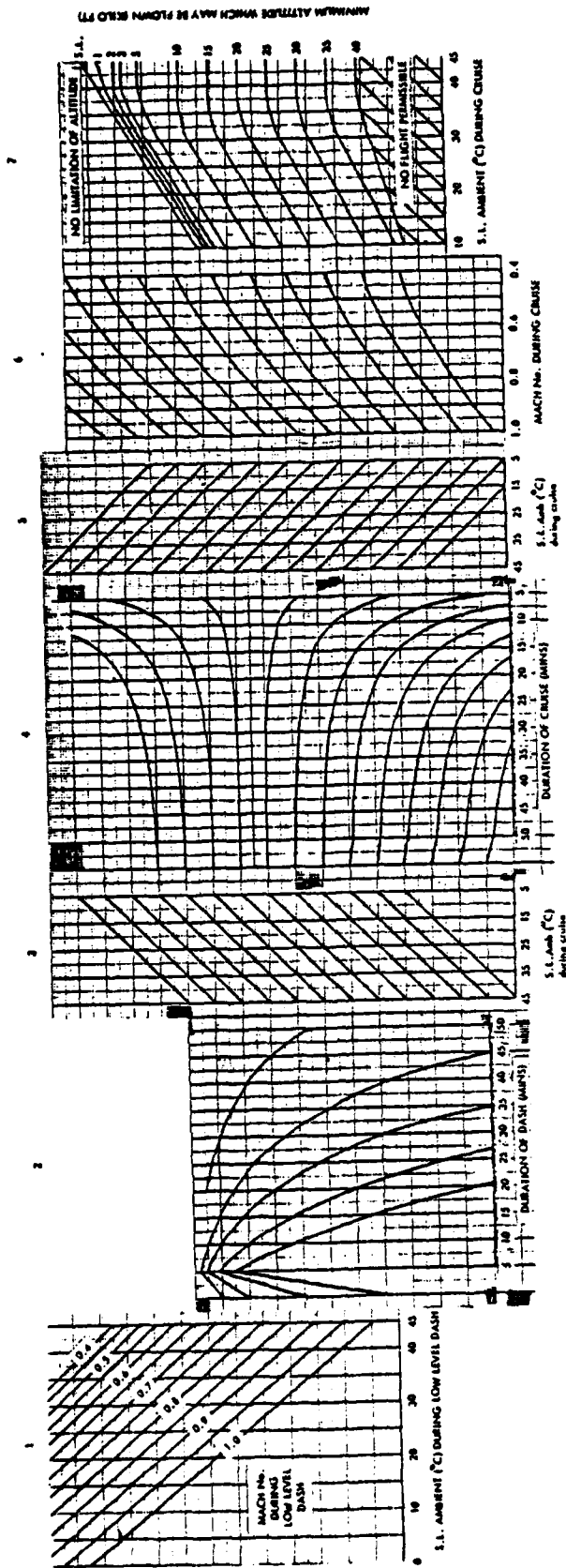


FIG. 40 FLIGHT LIMITATION CHART FOR EXPLOSIVE BOLT PYLON (EBP)

Method of Use of Flight Limitation Charts

The following examples are presented to illustrate the method of use of the charts, and for illustrative purposes the chart for the 1,000lb Bombs N1, Mk.10 and Mk.83 having a maximum temperature limitation of 76°C has been selected (Figure 37).

Examples

1. A sortie is required to be flown with a low level dash over land in a sea level ambient temperature of 40°C ; the Mach No. and duration of the dash phase being 0.85 and 15 minutes respectively. The cruise phase of the sortie is required to be flown over sea, the ambient temperature being 30°C and it is required to fly at a Mach No. of 0.70 for 80 minutes. What is the minimum altitude at which the cruise phase must be flown to prevent over-heating?

Starting at graph 1, the Mach No. is set on the appropriate sea level ambient temperature line, and a horizontal line drawn from this point onto the left hand side of graph 2. From this point on graph 2, the shape of the curves is, then followed, until an intersection is made with the vertical line through the required low level dash duration. A horizontal line is then drawn from this point onto the left hand side of graph 3. This procedure is then followed until the point on the left hand side of graph 7 is reached. On graph 7, the line is drawn horizontally across the graph, the point where this line intersects the vertical line through the required ambient temperature then gives the minimum altitude required. For this example, the minimum altitude is 31,000 ft.

2. A sortie is required to be flown entirely over land in a sea level ambient temperature of 45°C . A cruise phase of 20 minutes flown at a Mach No. of 0.70 at 30,000 ft. is required. What is the maximum duration of the low level dash which can be flown at $M = 0.82$? Starting with graph 7 and working from right to left the duration is found to be 8 minutes.

CONCLUSIONS

This paper has outlined some of the work undertaken by Hunting Engineering Limited on the problem of kinetic heating of conventional armament and equipment when carried on sorties of modern day aircraft.

Temperatures reached by sensitive weapon system components and associated equipment have been shown to be dependent upon:

Sea Level ambient temperature.

Exposure to solar radiation.

Flight Mach. No.

Flight duration.

Mathematical models used to compute the temperature-time histories of components have been outlined and generally validated by comparison with experimental results for a complete range of different heating environments and weapon systems/installations.

The results of mathematical modelling exercises have been presented and used to compile Flight Limitation "Carpets". These "carpets" presenting combinations of:

Sea level ambient temperature.

Flight Mach. No.

Flight duration.

which ensure overheating of temperature sensitive components does not occur.

An alternative, and more flexible method of limiting an aircraft's performance to prevent overheating of components, the Flight Limitation Chart, has been outlined and its use demonstrated. Using the Flight Limitation Charts a typical two phase flight sortie can be planned "on the day" to ensure overheating does not occur.

The type of work presented in this paper has been in progress in the UK for approximately 13 years and we are confident that we have the necessary experience, mathematical models etc. to cater for today's and tomorrow's flight environments.

APPENDIX 1

THE PROBABILITY OF THE OCCURRENCE
OF HIGH AMBIENT AIR TEMPERATURES

APPENDIX 1

THE PROBABILITY OF THE OCCURRENCE OF HIGH AMBIENT AIR TEMPERATURES

LIST OF CONTENTS

Para.

- 1 AMBIENT TEMPERATURE
- 2 TABLE OF REGIONAL TEMPERATURE PROBABILITIES

LIST OF ILLUSTRATIONS

Fig.

- 1 Absolute Maximum Temperatures
- 2 Average Annual Maximum Temperatures
- 3 Average Daily Maximum Temperatures - Hottest Month

Charts of 'Iso-Probability' for Occurrence of Temperatures of:

- 4 30°C
- 5 35°C
- 6 40°C
- 7 45°C
- 8 50°C

APPENDIX 1

THE PROBABILITY OF THE OCCURRENCE OF HIGH AMBIENT AIR TEMPERATURES

I AMBIENT TEMPERATURE

Since the temperature achieved by an object in the shade is a function of the ambient air temperature, it is important that the frequency of occurrence of high air temperatures be examined. Fig.1 shows a map on which are marked isotherms of the highest ever recorded temperatures (absolute maximum temperature), Fig.2 shows isotherms of the average of the highest temperature recorded each year (average annual maximum temperatures), and Fig.3 shows isotherms of the average of the daily maximum temperatures recorded in the hottest month of the year.

Accurate prediction of the probability of particular ranges of temperatures occurring cannot be made without detailed examination of the records of the 1800 meteorological stations from which the temperature charts have been compiled. On the basis of the data available, and the following simplifying assumptions, estimates have been made of the probability of specified temperatures being reached.

Assumptions

In order to provide a simple method of numerical comparison, the following assumptions have been made:

- (i) That the meteorological data used relates to a mean period of 25 years.
- (ii) That the maximum temperature recorded in the last 25 years is reached or exceeded at least once in any 25 year period.
- (iii) That maximum temperatures fail to reach the average maximum as often as they exceed it.
- (iv) That, if the probability that the maximum temperature occurring on any day will exceed an average maximum is $\frac{1}{x}$, the probability of the temperatures being at or above the average maximum at any time (overall probability) is $\frac{1}{4x}$; i.e. it is assumed that the maximum temperature in any 24 hours is maintained for six hours. However, the absolute maximum temperature is unlikely to be reached or exceeded for more than 1 hour giving an overall probability of $\frac{1}{24x}$.

On the basis of these assumptions it can be stated that:

- (1) At any point on an isotherm of absolute maximum temperature (see Fig. 1) the temperature will reach or exceed the temperature of that isotherm for more than 1 hour on one day in 25 years, giving an overall probability of $\frac{1}{25 \times 365 \times 24} = \frac{1}{219000}$.

- (2) At any point on an isotherm of average annual maximum temperature (see Fig.2) the temperature will reach or exceed the temperature of that isotherm on one day in two years, giving an overall probability of $\frac{1}{2 \times 365 \times 4} = \frac{1}{2920}$.
- (3) At any point on an isotherm of average daily maximum for the hottest month (see Fig.3) during that month the temperature will exceed that of the isotherm on 15 days of the 30. During the year the temperature will exceed that of the isotherm on more than 15 days since it may do so in months other than the hottest. Hence the overall probability is greater than $\frac{15}{365 \times 4} = \frac{1}{96}$.

In areas bounded by an isotherm the probability of the occurrence of the temperature of that isotherm is greater than at points on that isotherm.

Figs. 4 - 8 inclusive, show maps on which the three types of isotherm considered are combined as lines of 'iso-probability' for fixed temperatures of 30, 35, 40, 45 and 50°C respectively.

Table 1 shows the regions of the world in which temperatures of 40, 45, 50 and 55°C can occur and shows the probabilities of these temperatures occurring.

NOTE: All the information on meteorological conditions has been obtained from "Tables of Temperature, Relative Humidity and Precipitation for the World" published by H.M.S.O ref. M.O.617 a-f.

2 TABLE OF REGIONAL TEMPERATURE PROBABILITIES

TABLE 1

PROBABILITY			
During Year	$\frac{1}{219,000}$	$\frac{1}{2,920}$	$\frac{1}{96}$
During Hottest Month	$\frac{1}{18,250}$	$\frac{1}{243}$	$\frac{1}{8}$

TEMPERATURE	REGION		
55°C*	Small area of Sahara Desert	Nil	Nil
50°C	Area of Sahara in Algeria, Tunisia & Libya. Small area of Sudan, Persia, Iraq, Pakistan, Australia & U.S.A.	2 small areas of Sahara Desert	
45°C	North Africa, Mediterranean, Middle East, Persia, Pakistan, India, Australia and small areas in U.S.A. and South America.	Sahara Desert, Arabian Desert, Afghanistan & Pakistan. Small area in Australia.	Small area of Sahara Desert
40°C	African Continent, Southern Europe, Southern Asia, Australia, U.S.A. and areas of South America.	North Africa, Arabia, Persia, Iraq, Syria, Afghanistan, Pakistan, Turkmen S.S.R., Kazak S.S.R., Uzbek S.S.R., India, Australia & areas in U.S.A., South America & China	North Africa (Inland), Arabia, Iraq, Pakistan & India.

* The absolute maximum world temperature recorded is 57°C.

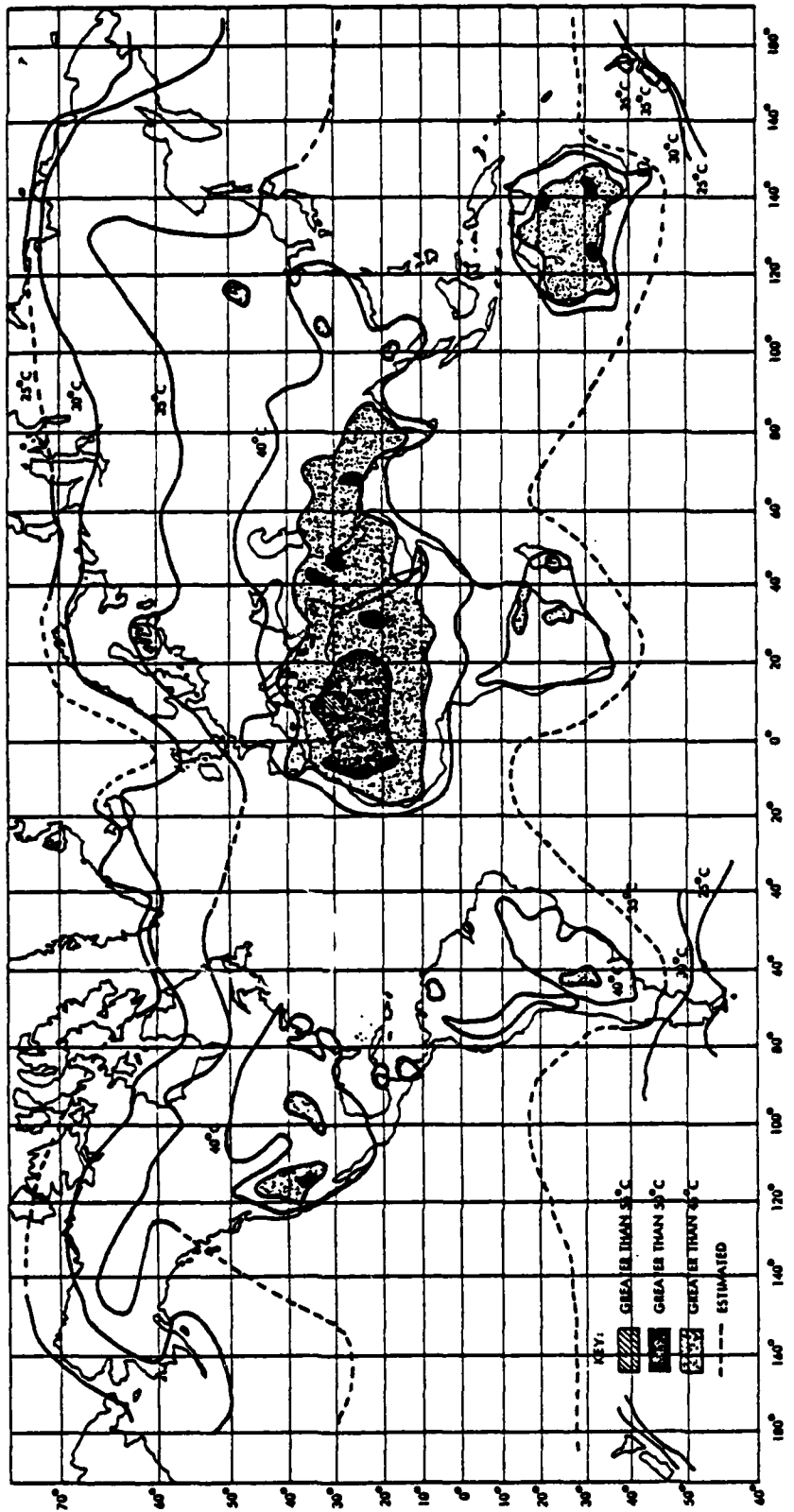


Fig. 1 Absolute Minimum Temperatures (°C)

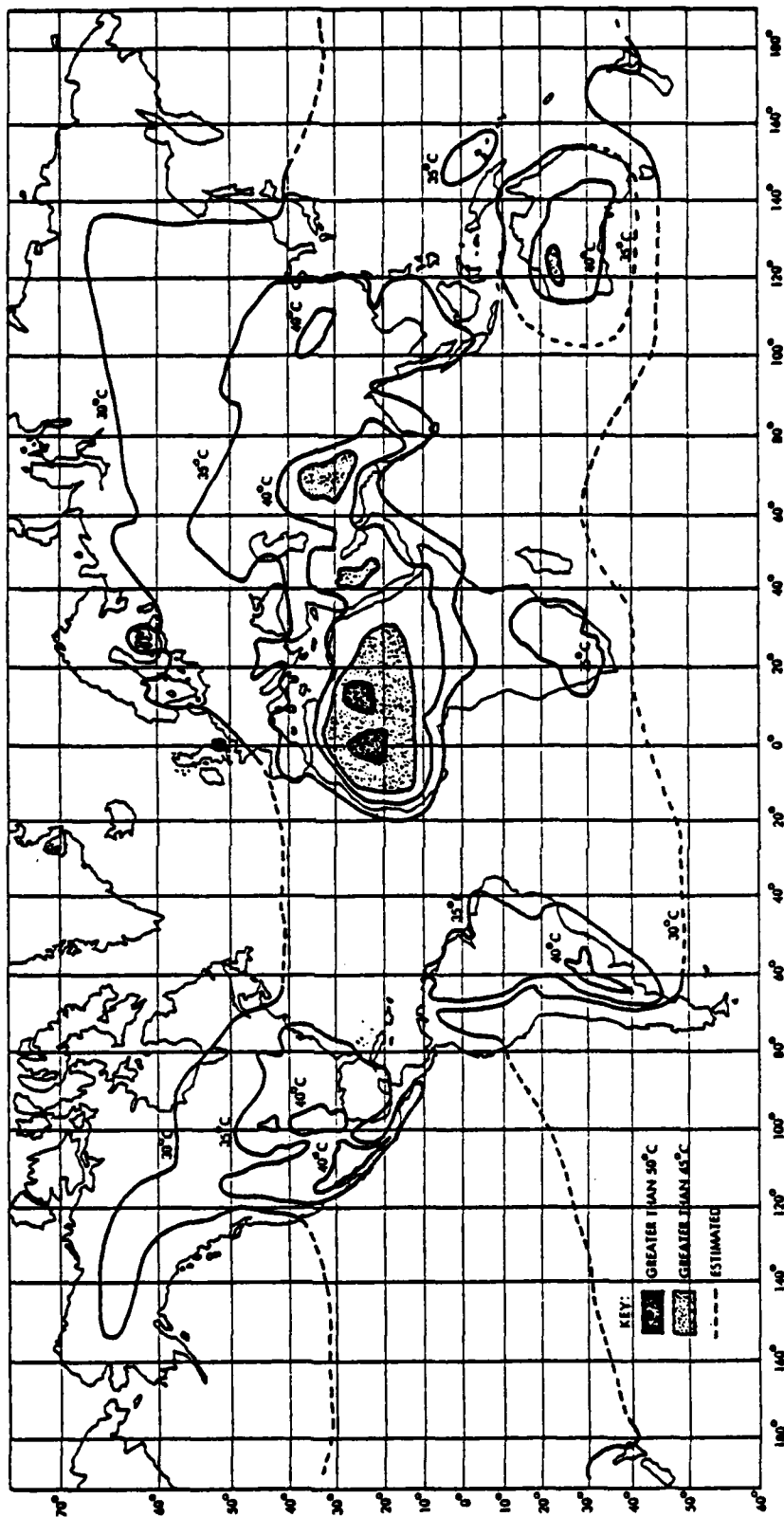


Fig. 2 Average Annual Maximum Temperature (°C)

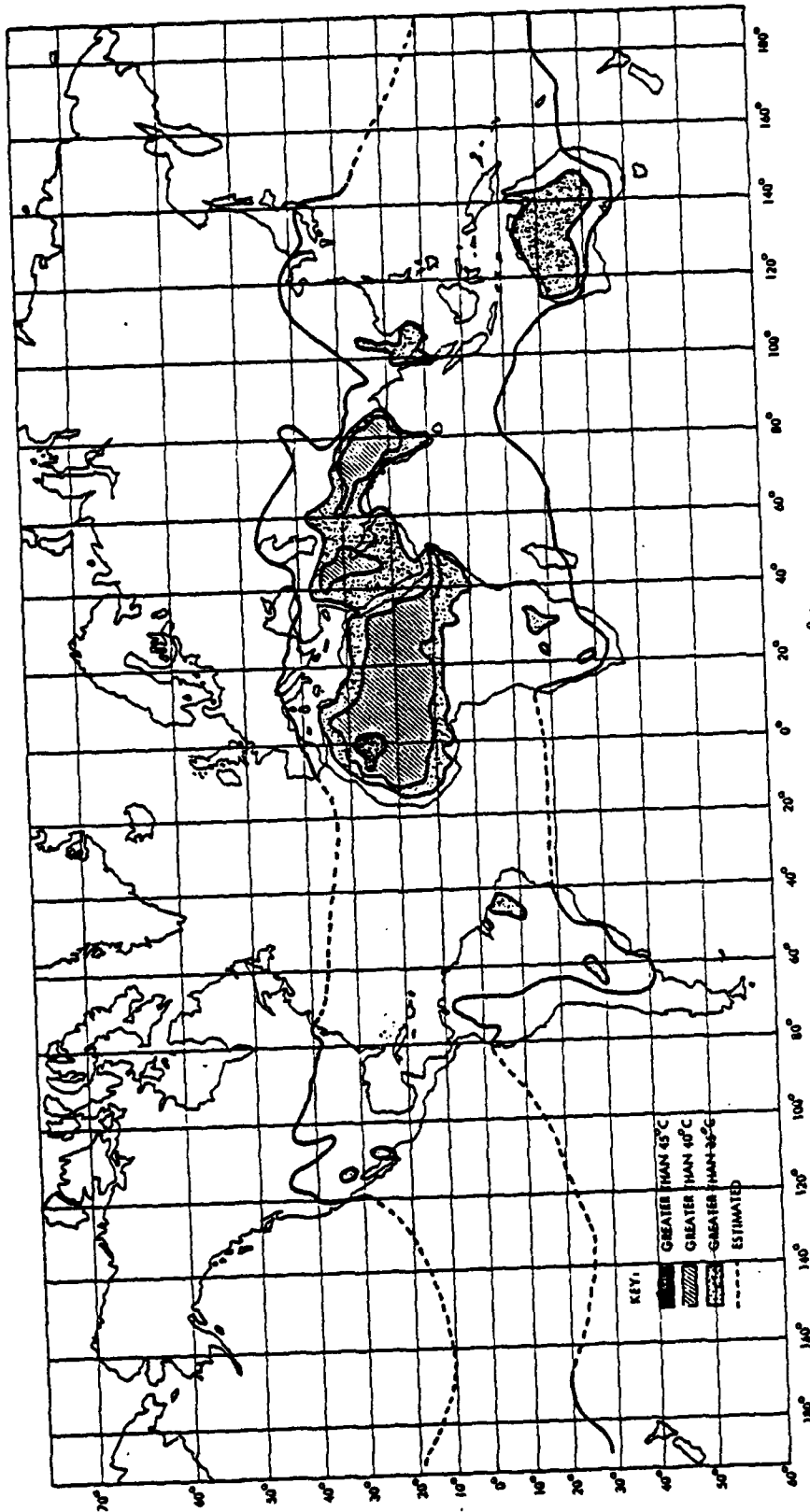


Fig. 3 Average Daily Maximum Temperatures - Hottest Month (°C)

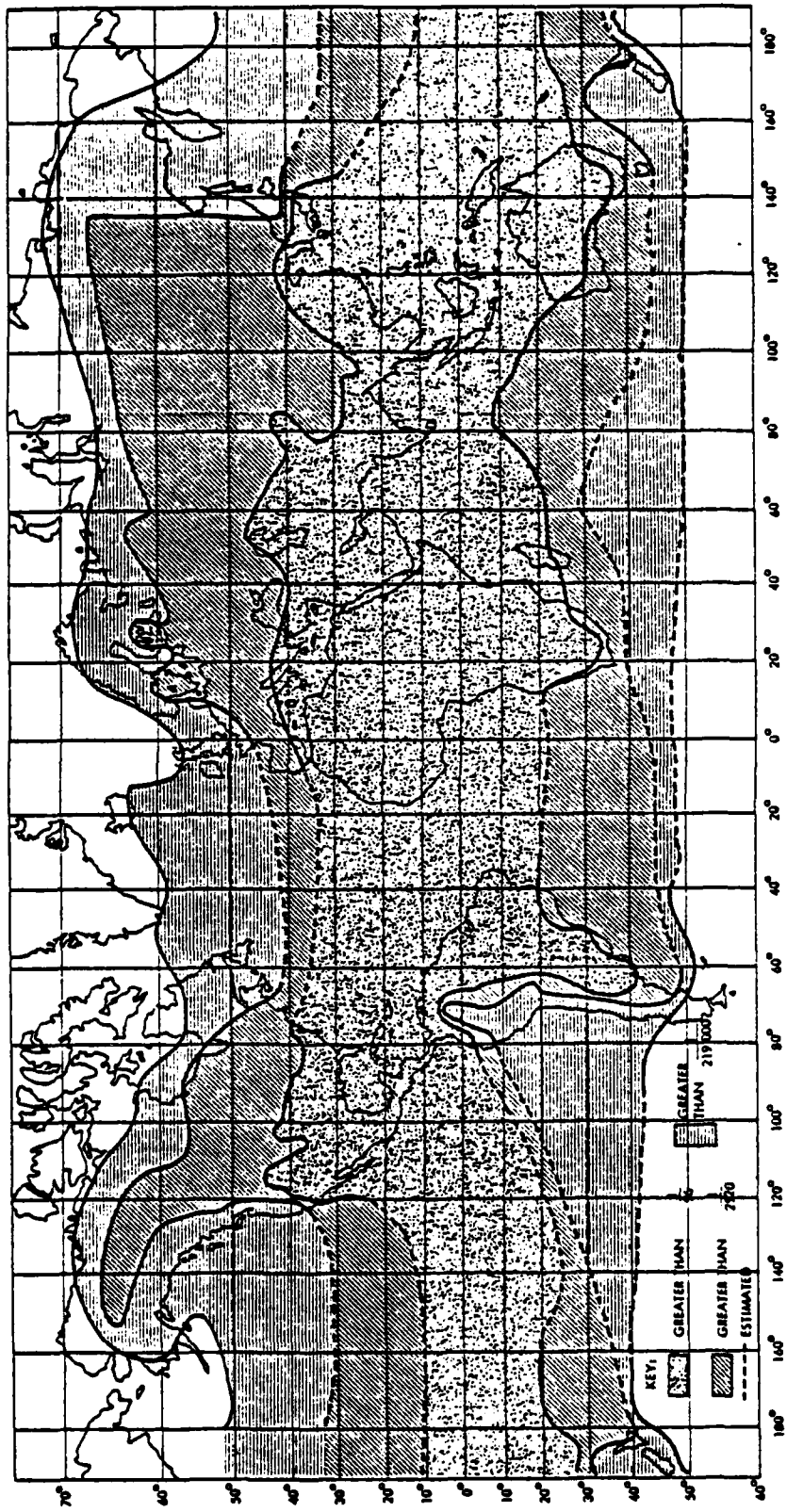


Fig. 4 Chart of "the-Probability" for Occurrence of Temperatures of 30° C

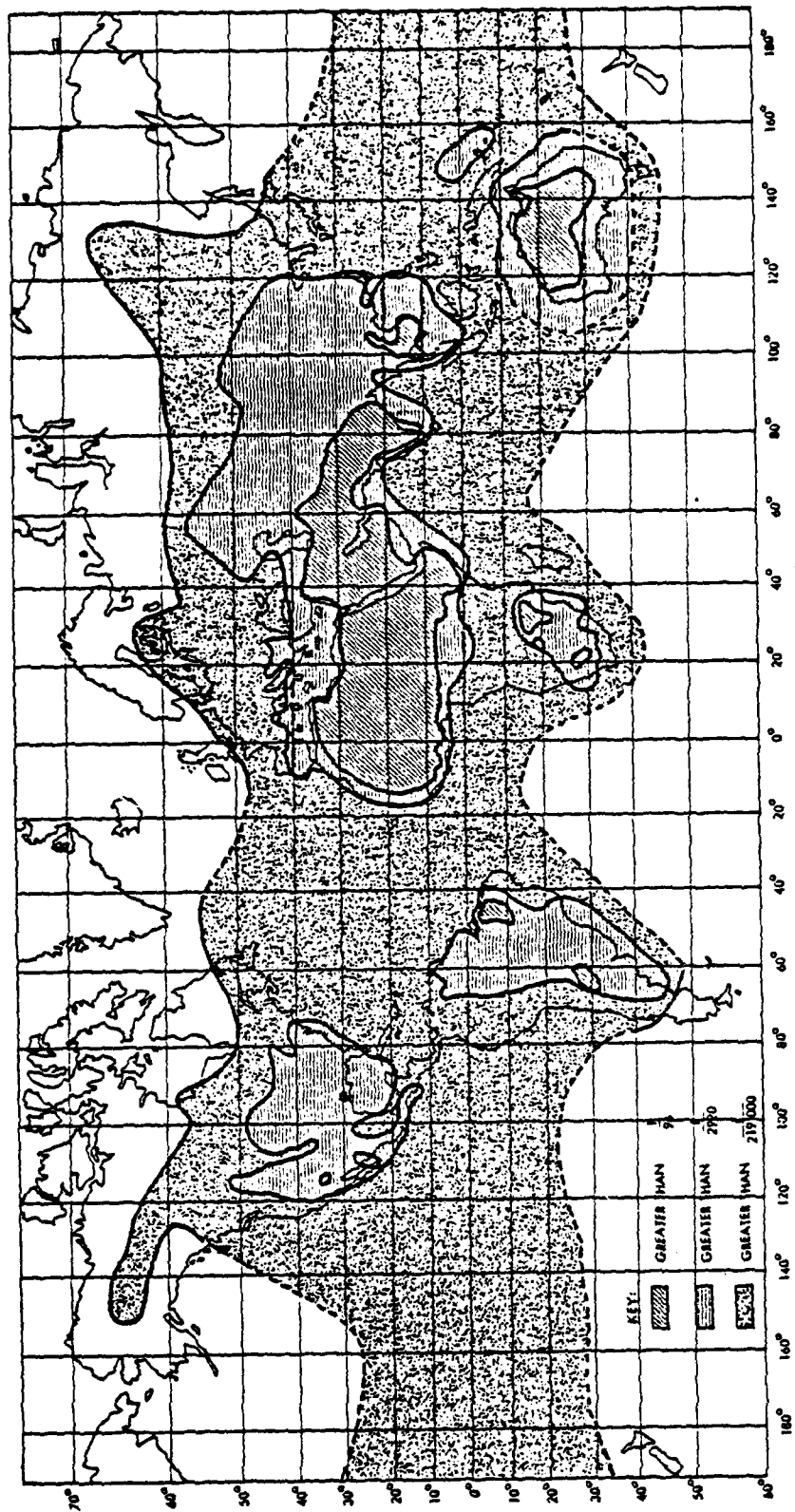


Fig. 5 Chart of "No-Probability" for Occurrence of Temperatures of 35° C.

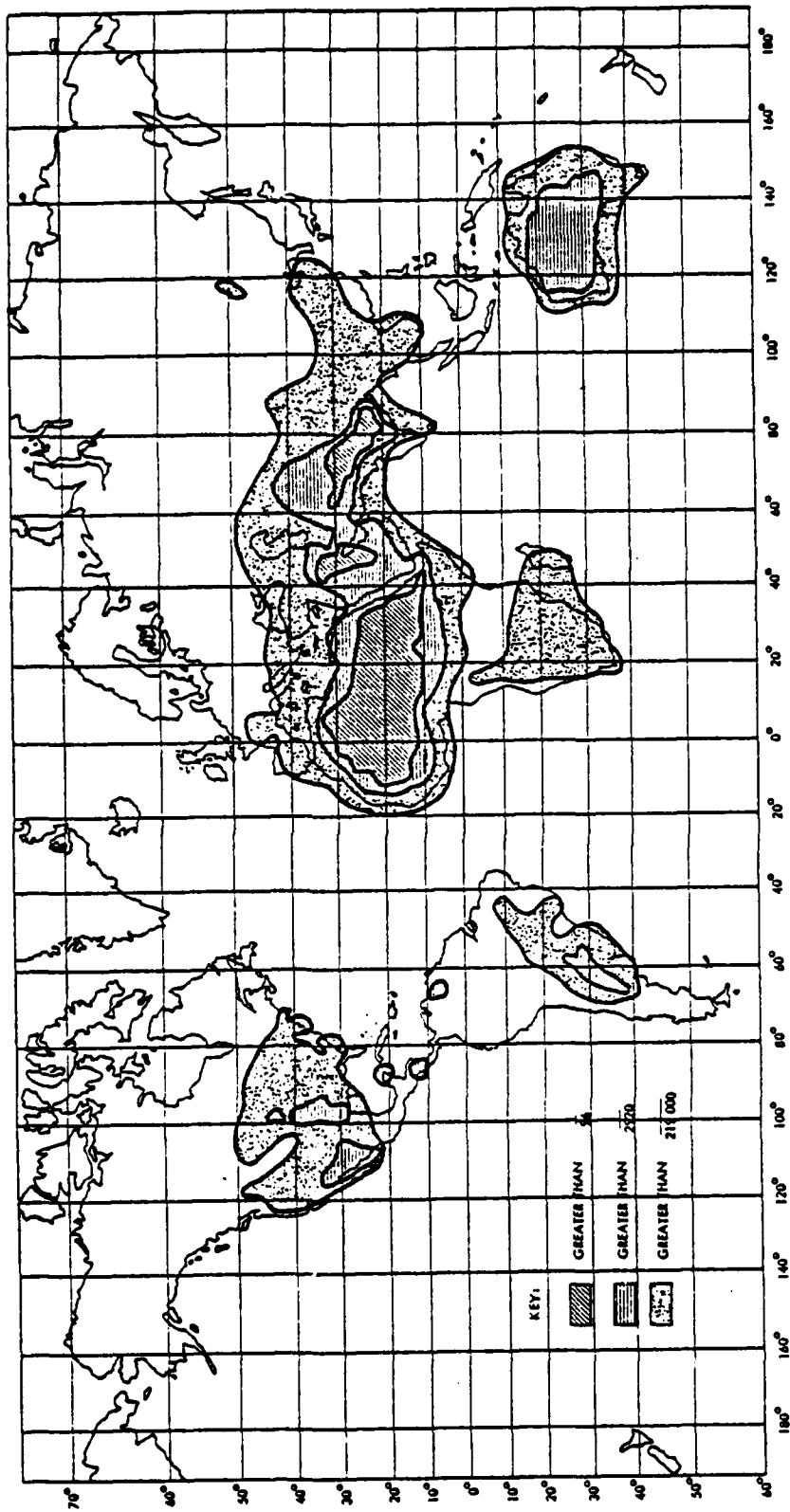


Fig. 6 Chart of "No-Probability" for Occurrences of Temperatures of 40°C

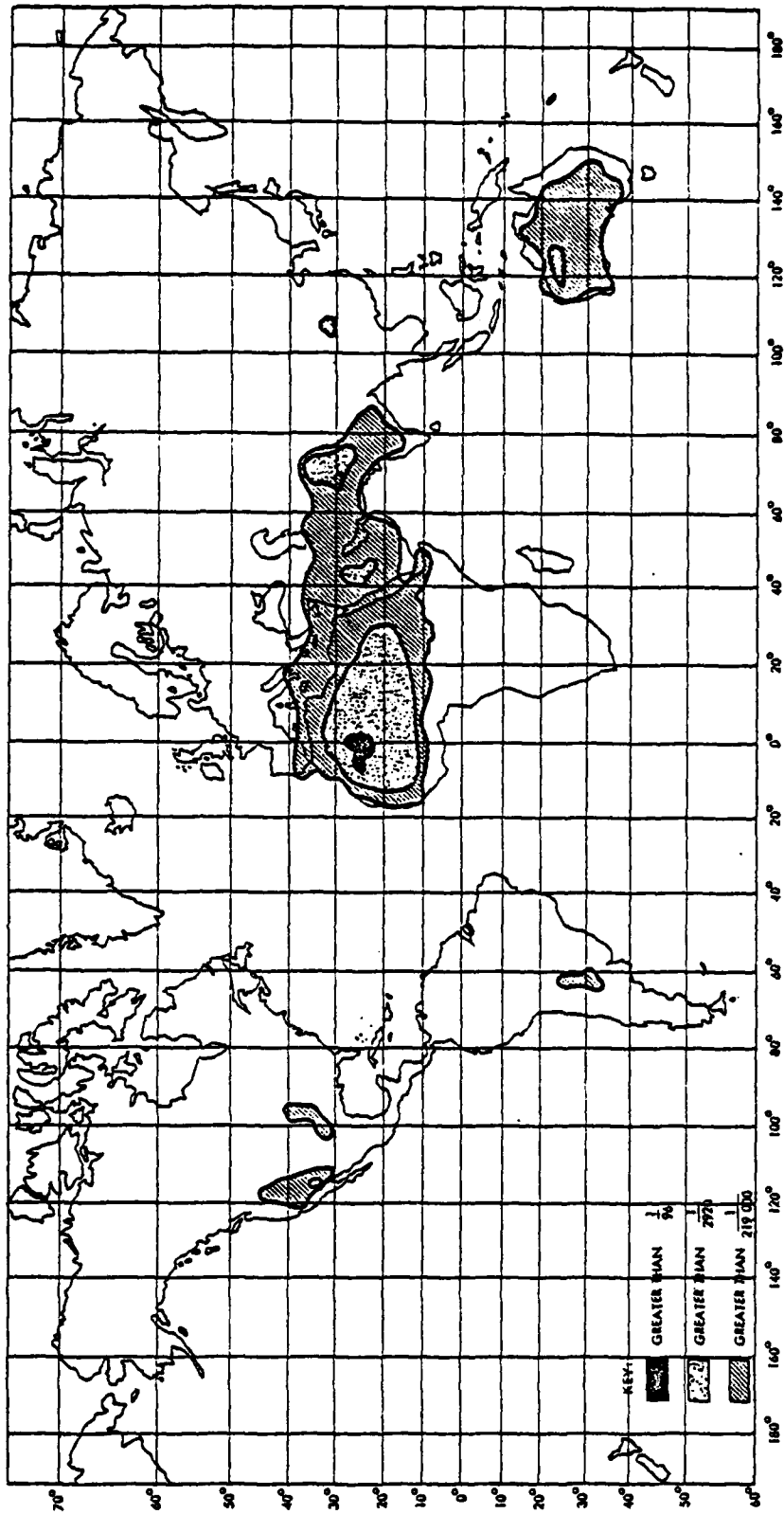


Fig.7 Chart of "In-Probability" for Occurrence of Temperatures of 45°C

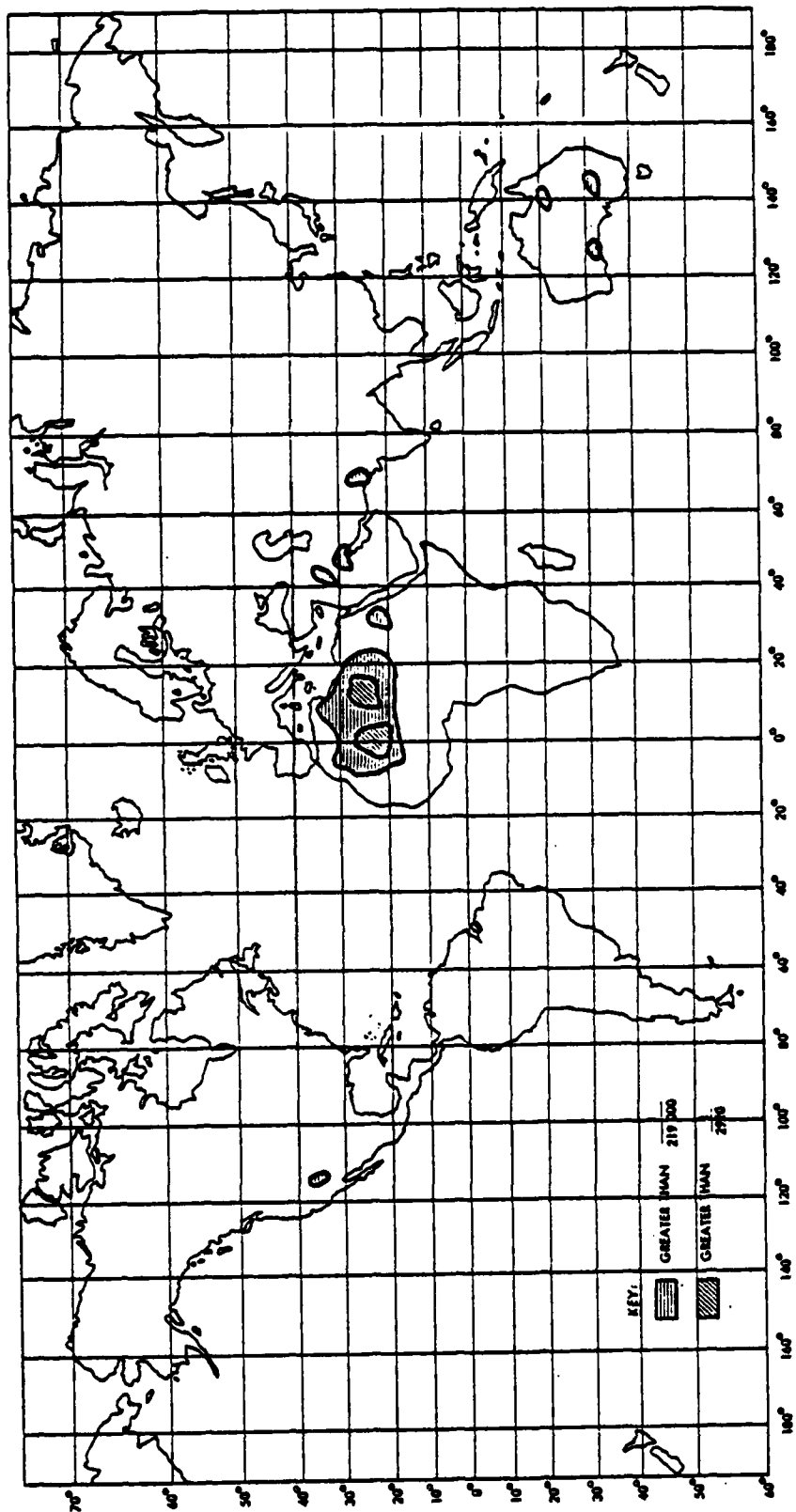


Fig. 8 Chart of "iso-probability" for Occurrence of Temperatures of 30°C

AUTOBIOGRAPHY

KEITH G. SMITH

Mr Smith was born in England on September 7th 1938, graduated from London University in 1961 with an honours degree in Aeronautical Engineering, specialising in aerodynamics and flight dynamics and gained an M.Sc. in Aerodynamics at the College of Aeronautics, Cranfield in 1962.

He joined English Electric Aviation (G.W. Division) in 1962 to undertake missile aerodynamic studies. In 1969 he joined Hunting Engineering Limited as an aerodynamicist, appointed Chief Aerodynamicist in 1970.

Experience gained at Hunting Engineering not only covers weapon aerodynamics but also operational analysis of current and future weapon systems. He is currently Manager, Systems Group with the responsibility of generating future Air, Land and Naval weapon system concepts.

Mr Smith is an Associate Fellow of the Royal Aeronautical Society and a member of the American Institute of Aeronautics and Astronautics.

ELECTROMAGNETIC CHARACTERISTICS OF ARMAMENT EQUIPMENT

Article Unclassified

(U)

By

Edward Dankievitch

Dayton T. Brown, Inc.

&

(D. Ballard, AIR 53211)

Naval Air System Command

Abstract. (U) Aircraft armament systems initially were thought of as electromagnetic hooks that dropped bombs. The technical advancements in aircraft electronics and the increased level of the radiated environment has exposed the armament system as both victim and foe in the electromagnetic compatibility war. It is the purpose of the laboratory to verify if the test item meets the parameters of its design specification. However, much of the armament equipment used today has been designed to old specifications, the obvious result being the equipment "meets spec." but is a potential problem in actual use. The purpose of this paper is to describe the results of testing armament equipment in a realistic electromagnetic environment. The goal is not to call for a redesign of all armament systems but to expose the hazardous area to the aircraft designer so that steps can be taken to ensure mission success.

"Approved for public release; distribution unlimited."

FIGURES

- Figure 1 Wing Ground Plane
- Figure 2 Conducted Emission, CE03/04 Triple Ejection Rack
- Figure 3 Radiated Emission, RE02, Rocket Launcher Pod
- Figure 4 Conducted Emission, CE03/04 Rocket Launcher Pod
- Figure 5 Conducted Emission, CE03/04 Multiple Ejection Rack
- Figure 6 Radiated Emission, RE02, Multiple Ejection Rack
- Figure 7 Radiated Emission, RE02, Frequency Coded Firing Switch
- Figure 8 Conducted Emission, CE03/04, Frequency Coded Firing Switch
- Figure 9 Conducted Emission, CE03/04, Linear Electromechanical Actuator
- Figure 10 Conducted Emission, CE03/04, In Flight Operational Bomb Rack Latch
- Figure 11 Conducted Emission, MIL-I-6181D, In Flight Operational Bomb Rack Latch

Not too long ago, the armament systems were thought of as electro-mechanical hooks that dropped bombs. The concerns of the armament designer were in the areas of mechanical loading, lag time, and that the system functioned during cold temperatures and altitude. Far down on the designer's list of concerns, if at all, was radio frequency interference. This placement was justified by the fact that the specifications allowed "no limitations" on the amplitude of manual operated switch transient noise, not exceeding a maximum occurrence of twice per normal operational period. The general interpretation of "operational period" was, in the case of aircraft, one flight or mission. The result of all this was the broadband transients generated during the activation of the armament system was exempt from measurement and thus control. The susceptibility requirements of the old specifications also failed to test the equipment to realistic requirements. It was reasoned that a system composed of electromechanical devices could not be malfunctioned by the electrical field created by applying 100,000 μ v to the terminals of antenna.

Laboratory testing of armament systems under this type of specification interpretation produced few failures and thus created a sense of security among the manufacturers and the users.

The technical advancements witnessed during the early 1960's caused some people to stop limiting their thinking to terms of Radio Frequency Interference and consider the electromagnetic compatibility of the entire system. For example, the possible activation of electro-explosive devices accelerated the study and implementation of Hazardous Electromagnetic Radiation effects on Ordnance precautions. As good as the HERO precautions were, they were concerned with only part of the problem. As the aircraft became more technically advanced, it also became more susceptible to voltage transients in addition to creating vast amounts of conducted and radiated RF energy itself. The problem and its potential for disaster was recognized as one of compatibility among all systems, whether located on the aircraft, land-based, or shipboard. In short, the system must survive the RF environment; it must function within and it matters not if this environment is intentional, inadvertent, friendly or foe.

As the interest in the EMC parameters of the armament equipment increased, the testing techniques and procedures were then scrutinized. When an older RFI specification was called out in a drawing package, it asked for nothing more than a test on a black box. Little consideration was taken as to what the item was, how it operated, how it was grounded and what it was expected to do. The point most often overlooked was what were the needs and requirements of the aircraft manufacturer, and could compatibility between armament and aircraft be possible? In an attempt to test the equipment in a configuration most nearly simulating the aircraft installation, some basic changes to the test specification setups were proposed. The first was to design a fixture that would provide a typical ground scheme for the equipment. The specifications in general would have the equipment setup on a ground plane and bonded to ground via a copper strap. These ground straps connected to the cleaned surfaces of

the test item and soldered to the ground plane would provide the best possible ground.

However, in the real world, as in the case of a MER or TER, the ground would be through only a single long wire. The mounting lugs and swaybraces would in most cases be anodized and painted, and could not be relied upon for any type of ground path. It is this, the real world not the ideal, that the equipment must be tested in. The proposed fixture took the form of a wing ground plane. It was 10 feet long, 4 feet above the screen room floor with one end bonded to the screen room ground. On the outboard end, provisions were made to mount the armament to be tested. Non-conductive supports were provided to handle the weight of the various pylons, ejector pods, and bomb racks. The power and signal/control cables could now be routed down the 10-foot wing ground plane to an auxiliary screen room entering through a filter panel. Control circuits were designed for each test item to provide power, control and to monitor its operation. The use of the anteroom provided RF isolation for the test equipment. Thus the emission and susceptibility parameters of the test item could be measured without chance of test equipment upset.

The providing of a realistic test bed for armament testing was paralleled by the interest of the aircraft manufacturer to know exactly the RF parameters of government - furnished equipment. Interest in this area reached a peak when the difficulty in suppressing the EMI failures of the AMAC system became known. It was stated that perhaps the AMAC wasn't such a large problem when it was known that other equipments had demonstrated EMC failures equal to, if not greater than, the equipment in question. It was at this point that the manufacturer of the S3A requested the electromagnetic emission profile of all GFE armament equipment it would carry.

A test program was undertaken that would provide an EMI data base for all GFE armament equipment. The equipment was tested to the same specification that it was designed to, with the exception that all transients were to be measured and recorded. In addition, testing was also performed to the requirements of MIL-STD-461A.

Prior to the preparation of the data bank of EMI data on armament equipment, a search through our files was performed to determine the magnitude of the problem. This search exposed excessive emission levels emanating, both conducted and radiated, from MER racks of 100 dB above the MIL-STD-461A limits. The collections of EMC data yielded the following results:

<u>Item</u>	<u>Specification</u>	<u>Max Above Spec. Conducted</u>	<u>Max Above Spec. Radiated</u>
TER	MIL-STD-461A	72 dB	-
LAU-68/TER	MIL-STD-461A	40 dB	60 dB
MER	MIL-STD-461A	100 dB	68 dB
FCFS	MIL-STD-461A	75 dB	35 dB
BRU-14 (LEMA)	MIL-STD-461A	75 dB	-
IFOBRL	MIL-STD-461A	68 dB	-
IFOBRL	MIL-I-6181D	42 dB	-

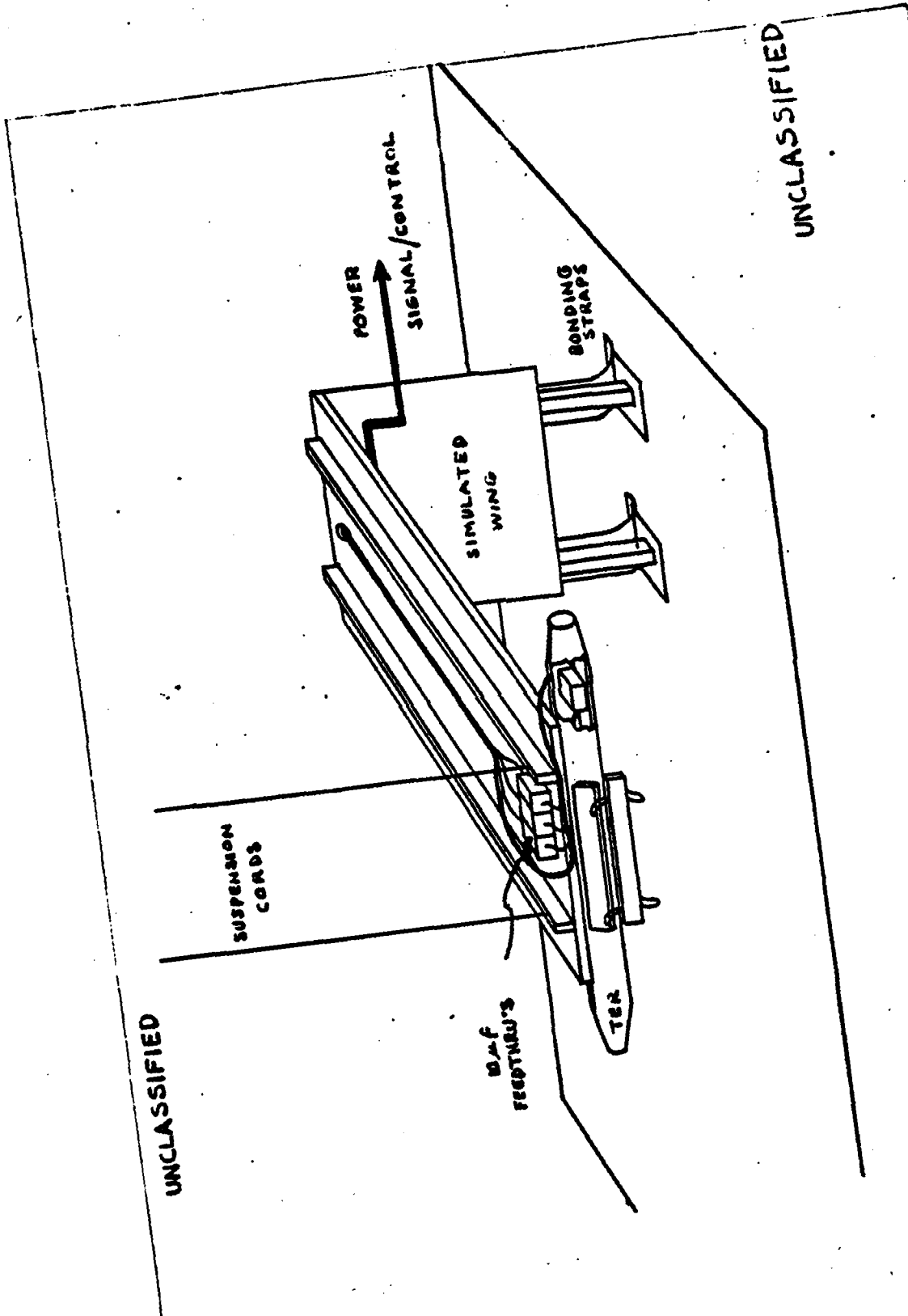
This is a brief summary of the work that was performed. It is intended to demonstrate that the armament equipments are capable of producing high levels of broadband transient noise.

It should be noted that not only are the electromagnetic components a source for this RF energy, but also the initiation of the impulse cartridges. When this data was presented to the Navy, the question was asked what problems are caused by EMI in the fleet. Are not these equipments in current use with little adverse effects? The response to these questions was that the high level EMI possesses greater threats to the newer aircraft utilizing solid-state components and low level logic. The result was obvious; all the equipment in present use could not be suppressed and the new aircraft using this equipment would have to protect itself against it. In the case of the S3A a study of its EMI vulnerability was concentrated in three areas. The first was to determine what level of broadband emissions it could tolerate. The second was to perform on-board compatibility tests with those equipments judged to be potentially hazardous. The third and most unlikely to implement was the suppression of the actual offending component. The reason for this was only on new contracts could the newer specification be imposed. The three-step program worked quite well. Components on the BRU-14 selected for suppression were the IFOBRL and LEMA. An in-cable filter was designed for the TER but was not needed when the compatibility tests indicated the TER acceptable.

Up to this point the discussion has been focused upon the RF noise generated by the armament equipment and the vulnerability of the new aircraft. The next topic is then the susceptibility of the armament equipment. The Electro Explosive Devices were protected by the efforts of the HERO community and relays and stepper switches were not likely to be affected by EMI. The cause then for concern came about for two reasons: the new specification introduced a variety of susceptibility tests and the use of low level solid-state circuits. Two items found to malfunction in the presence of RF energy were the Electronic Stepper Switch and the Frequency Coded Firing Switch. Another problem was the RF transient caused by the cartridge ejecting a sonobuoy, suscepting the firing circuits and thereby ejected several other sonobuoys.

Do EMI problems exist in armament systems? Yes indeed. They create it, are themselves affected by it and possess the ability to upset other equipments. We have seen a time when EMI was of very little concern. In the 1960's this began to change to a concern for what amount of RF energy it emitted. The technological advancements in it and its control circuitry has made the armament system a potential victim to EMI. The present has exposed yet another problem. New aircraft will be tested in field strengths of 200 v/m, and in carrier-based operation could experience field strengths in excess of several hundreds of volts per meter. The concern then, in addition to its vulnerability, is in the armament itself acting as an antenna and coupling this high level RF energy into the aircraft systems.

The purpose here is not to discourage the use of solid-state, digital composite materials, or any of the other advancing technologies, but to expose the possible hazardous areas to the designers of aircraft and armament systems, so that steps can be taken to ensure that all systems are compatible and the aircraft can function successfully in its real environment.



UNCLASSIFIED

UNCLASSIFIED

FIGURE 1 TYPICAL SET-UP

CE03-TER

UNCLASSIFIED



UNCLASSIFIED

FIGURE 2

UNCLASSIFIED

REO2 - LAU 68 B/A RIPPLE FIRE

--- FORWARD
--- AFT

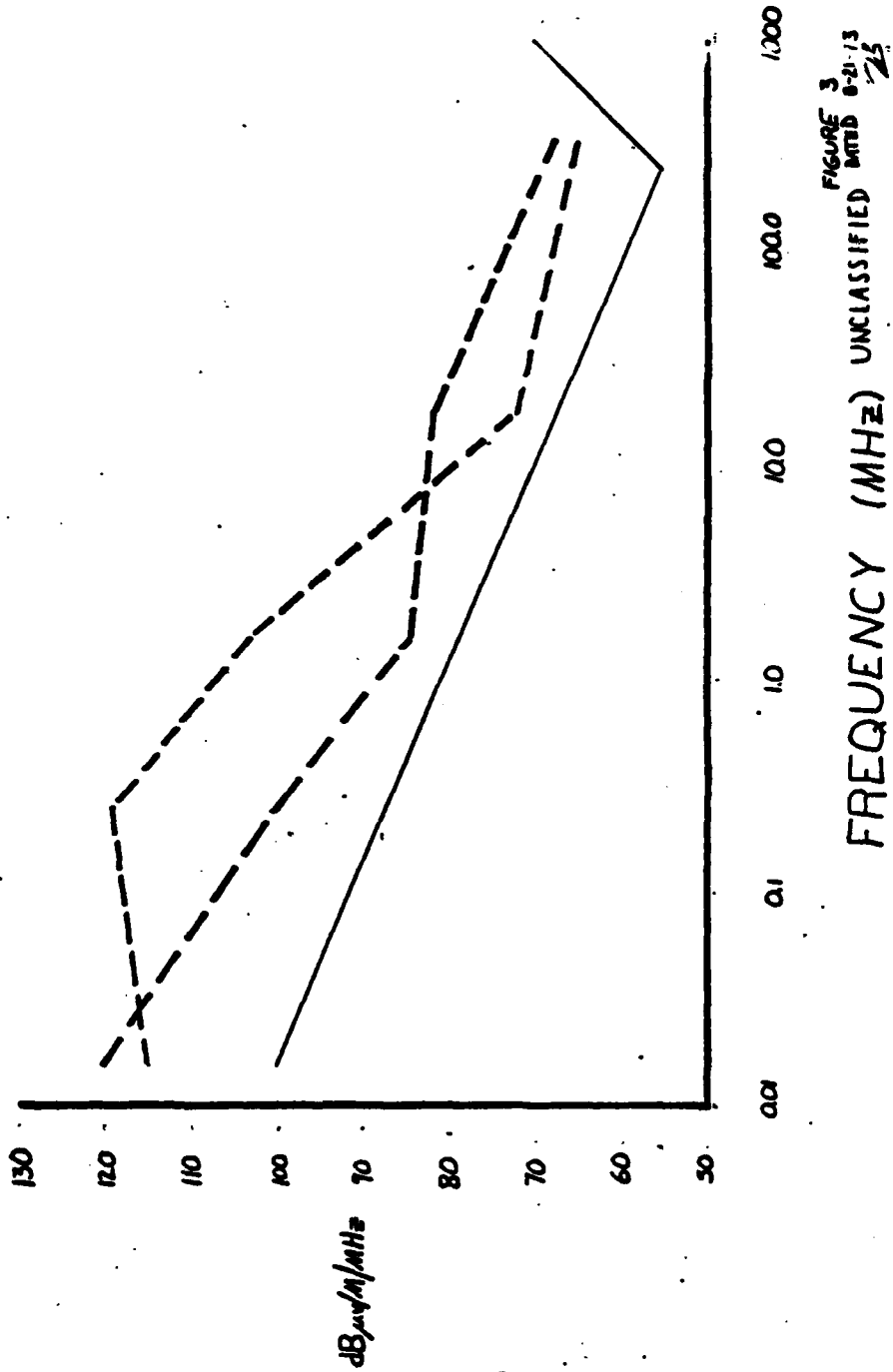


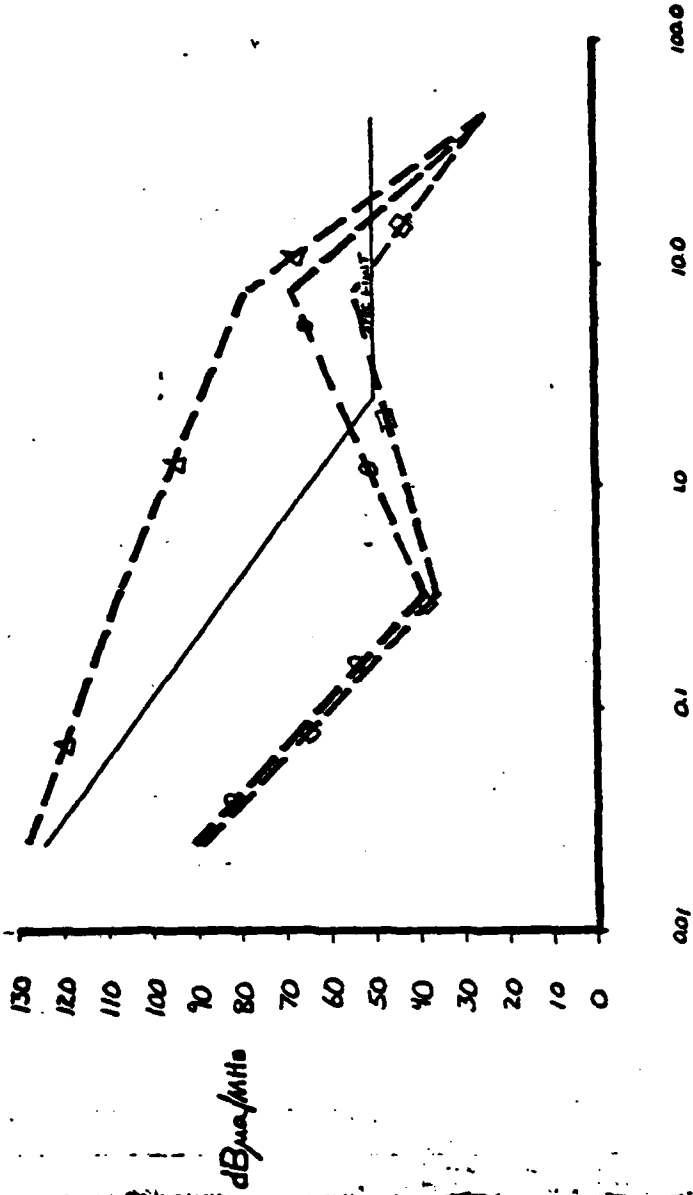
FIGURE 3
UNCLASSIFIED
DATE 8-21-13
25

UNCLASSIFIED

CEO3 - LAU68 B/A

RIPPLE FIRE

- ☆---☆ PIN 8
- ⊖---⊖ PIN 6
- ⊕---⊕ PIN 4



UNCLASSIFIED

FIGURE 4

FREQUENCY (MHZ)

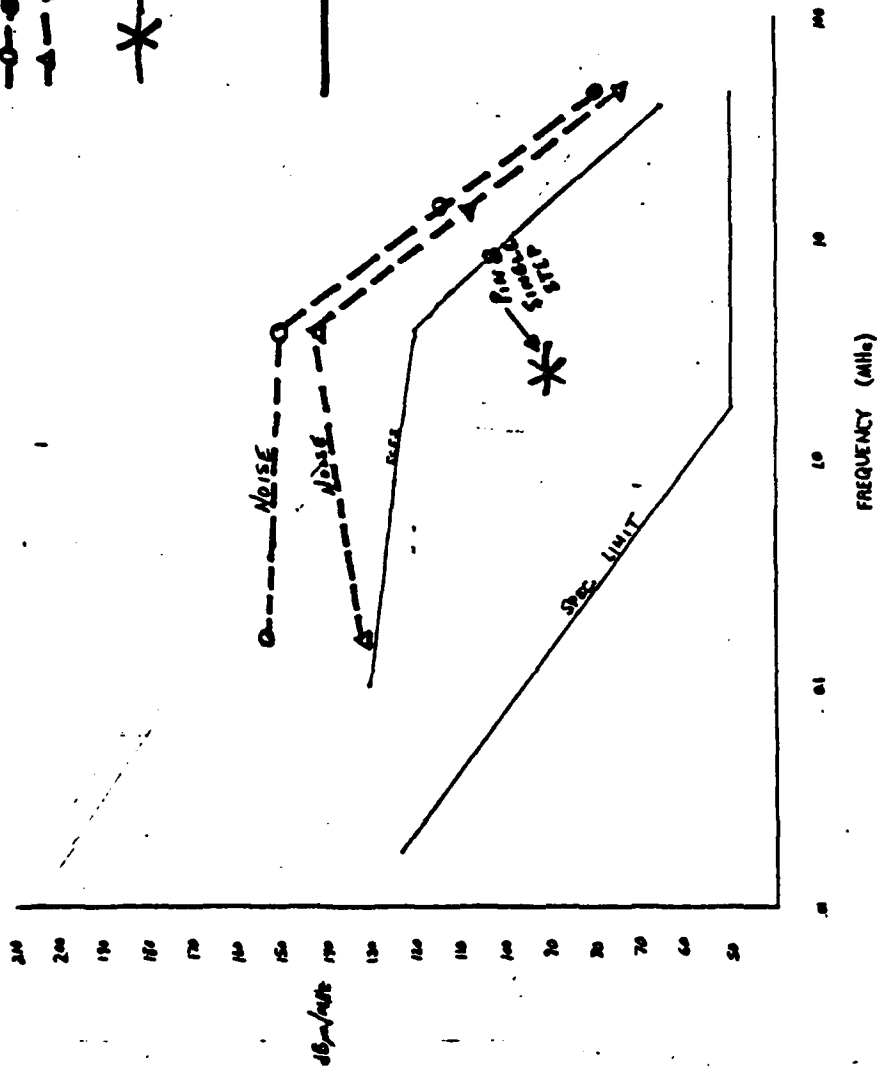
LIMITS FOR CE03 + CE04
BROADBAND EMISSIONS

UNCLASSIFIED

- LEGEND
- MULTIPLE EJECTA RACK
 - NOISE
 - △— NOISE
 - STATION TRANSMISSION - PMS

NOISE
INACTIVE

FCFS



UNCLASSIFIED

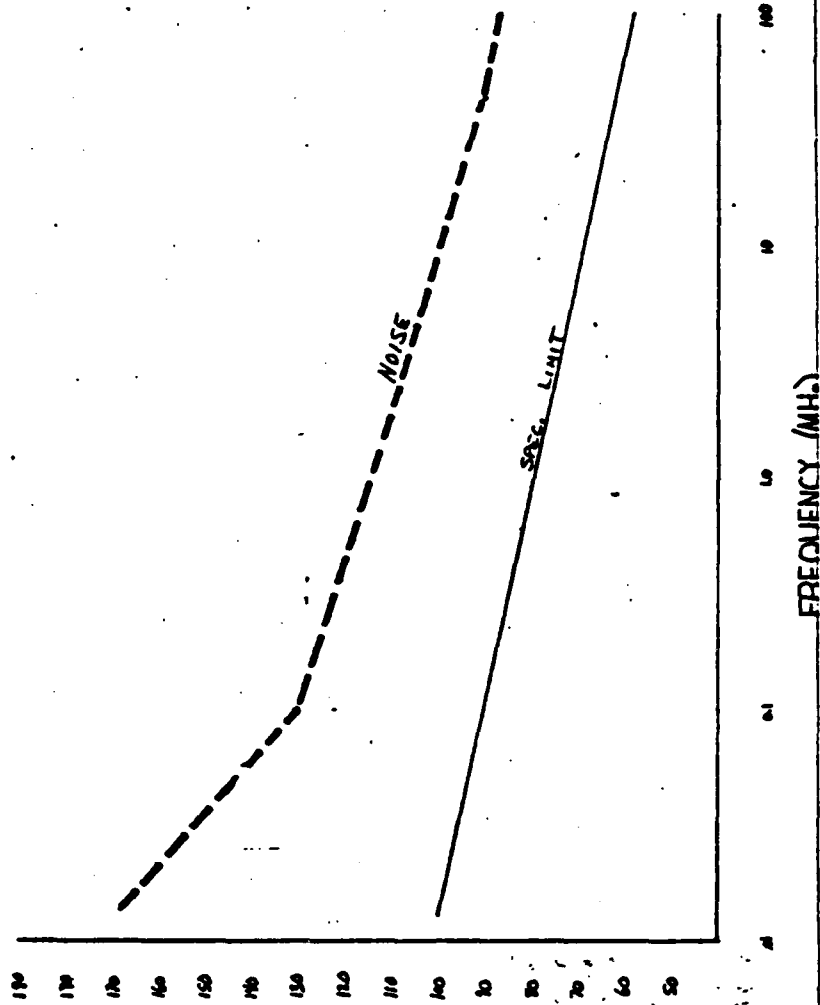
FIGURE 15

July 1970

LIMITS FOR REO2
BROADBAND EMISSION

UNCLASSIFIED

MULTIPLE EJECTOR RACK
RIPPLE MODE
— SPEC. LIMIT
- - - INTERFERENCE

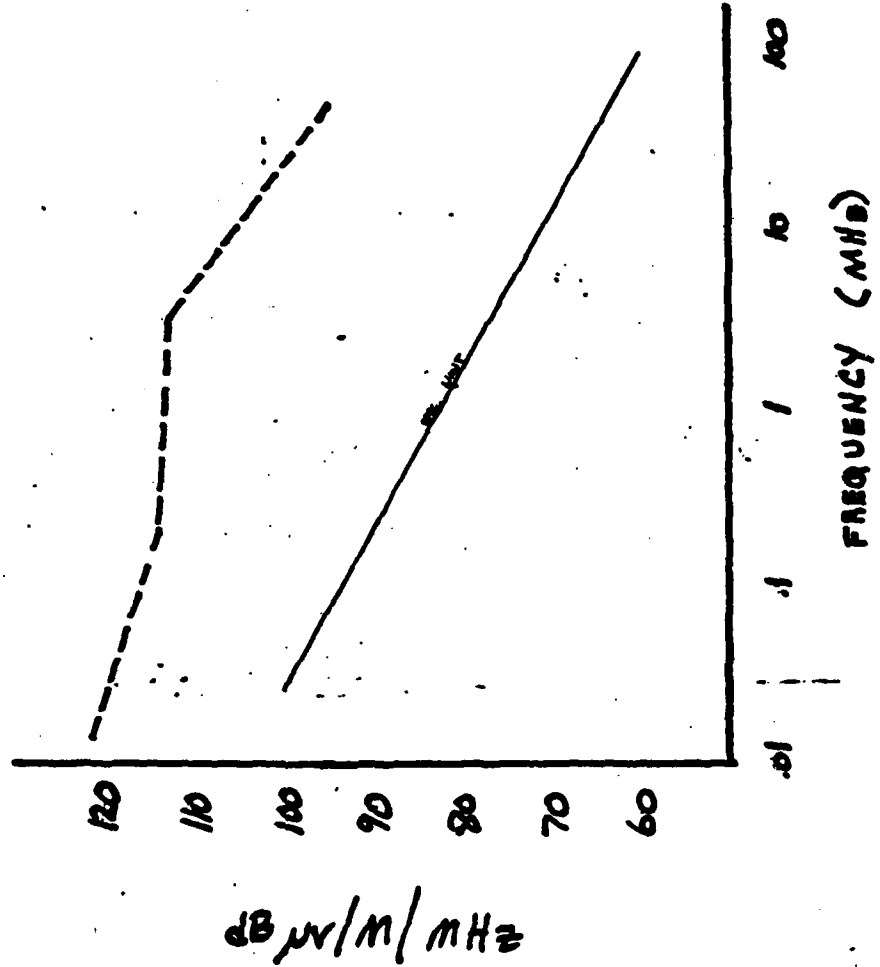


UNCLASSIFIED

FIGURE 6

REO2 FCFS
RIPPLE, STORES ACTIVE

UNCLASSIFIED

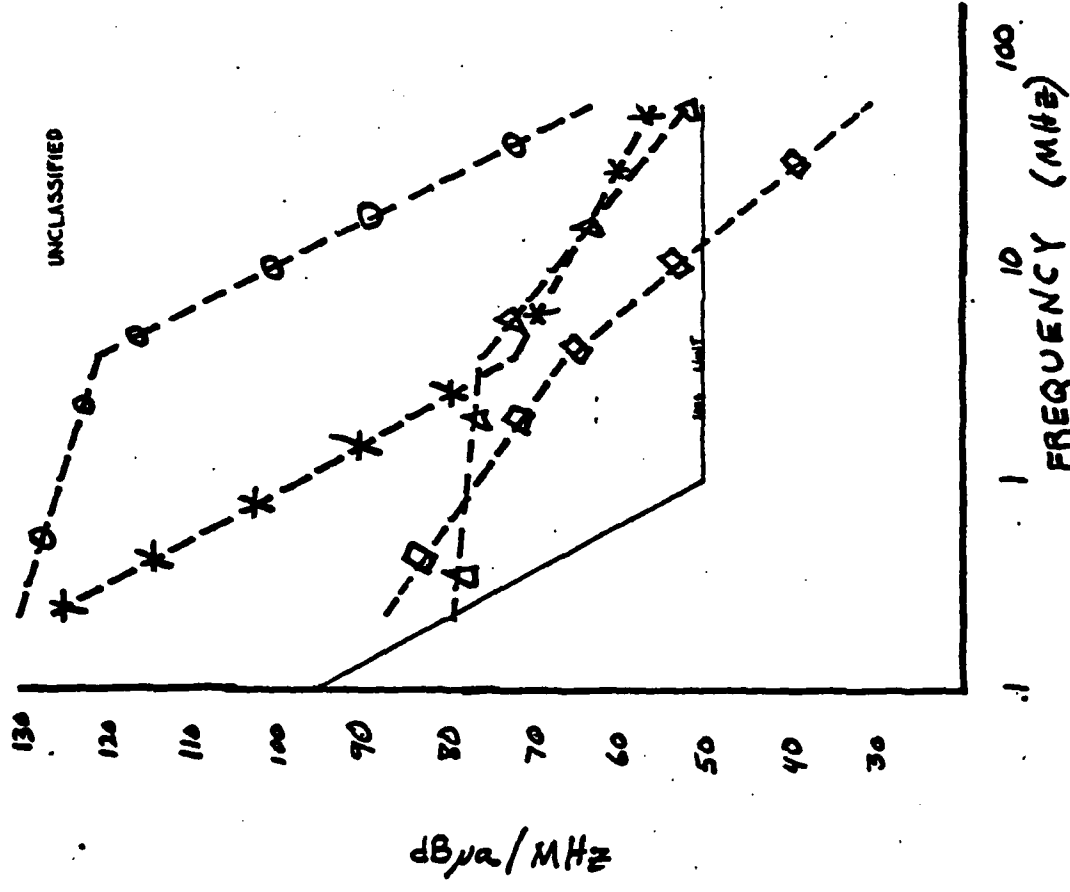


UNCLASSIFIED

Figure 7
Rev. 11/20/78

CE03 FCFS

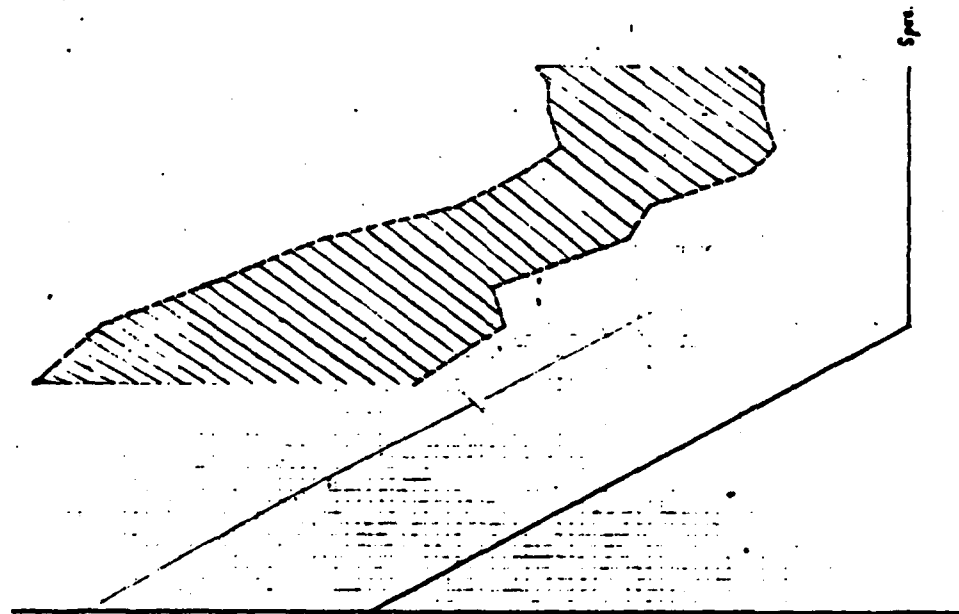
- — ○ LAUNCHER D.C. BUS
- * — * DECODER +2.8 VDC
- △ — △ ENCODER -2.8 VDC
- — □ ENCODER -2.8 VDC



UNCLASSIFIED

FIGURE 8

LIMITS FOR CE03 & CE04
 BROADBAND EMISSIONS
 MIL - STD - 461



ITEM --- IFOBRL (LINEAR ACTIVITY)

Z/N --- 300110-00-088

DATE --- AUGUST 1974

S/N NO --- D 1251

P 1275

P 1289

E 0137

E 0150

E 0403

E 0505

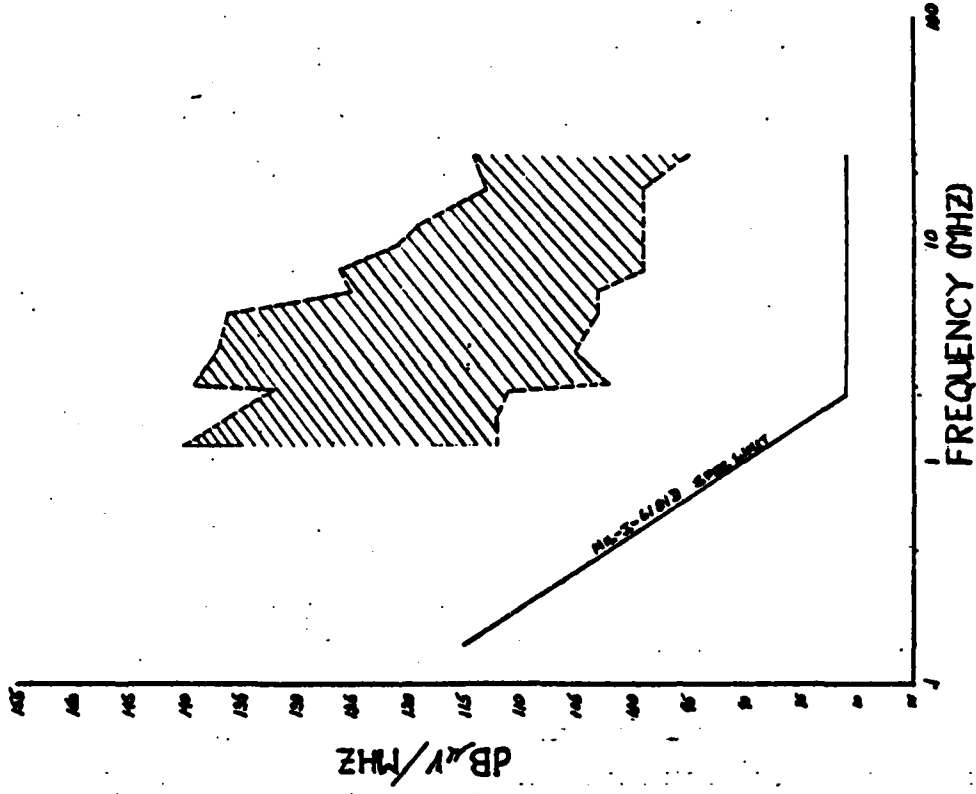
UNCLASSIFIED

FIGURE 10

dB RE/MHz

CONDUCTED INT. BROADBAND
MIL-I-6181D

UNCLASSIFIED



UNCLASSIFIED

FIGURE 11

ITEM----- 2 FORN. (SIMILAR ACTUAL)
 J/N----- 30010-00-000
 DATE----- AUGUST 1974
 S/N N8-- D 1281
 D 1267
 D 1275
 D 1289
 E 0137
 E 0150
 E 0103
 E 0506

EDWARD DANKIEVITCH

EMC PROJECT ENGINEER

Mr. Dankievitch has been employed by Dayton T. Brown, Inc. since 1964. During this period, he has been associated with the EMC Group, where he is presently responsible for the technical aspects of EMC services. These include: interference source studies and suppression, filter design, EMI related transient pulse phenomena effects and the preparation of control plans, procedures and reports.

Education:

Dowling College
B.S. in Physics - 1973

New York State University
A.A.S. Electrical Technology - 1964

Employment:

1964 to Present - Dayton T. Brown, Inc., Project Engineer

Since joining Dayton T. Brown, Inc., Mr. Dankievitch has had the following duties:

- Provided consultation services to NASC on related EMP programs.
- Provide unique cost effective filtering techniques for Aircraft Avionic Systems (Navy Weapons Racks).
- Automate techniques for interference measurements (Fairchild FSS-250 Spectrum and Surveillance System uses and techniques).
- Integrate automatic techniques into mobile test facilities for on-site surveys of power transmission lines.
- Design, implement and evaluate EMI suppression devices for aircraft, and ground support equipment.
- TEMPEST consultant and testing.

He is presently serving as a Consultant Member to the SAE AE-4 Committee tasked on shipboard EMC problems (i.e. vulnerability, EMP, EMI, and others).

Publication:

Laboratory Testing Advancements in High Level Radiation - IEEE International Symposium on EMC, 1977

ON THE PERTURBED MOTION OF AN AIRCRAFT
FOLLOWING THE JETTISONING OF A STORE

(U)

(Article UNCLASSIFIED)

by

Sridhar M. Ramachandra
Design Bureau, Hindustan Aeronautics Limited
Bangalore-560017, India

ABSTRACT. (U) Military aircraft carry stores like bombs, rockets and fuel tanks which have to be jettisoned as required by the particular flight mission. The weight and inertia contribution of these stores forms a significant fraction of the corresponding parameters of the basic aircraft. Further, in the case of externally carried stores the aerodynamic characteristics of the basic aircraft are also modified significantly by these stores. Jettisoning of the stores imparts an impulsive change to the inertial and aerodynamic parameters of an otherwise trimmed flight thereby producing both linear and angular accelerations to the aircraft system. The paper studies the perturbed motion of an aircraft in the short interval before the vehicle is trimmed again by the Pilot after the stores are jettisoned. Beginning with a set of four coupled differential equations of motion, analytical solutions have been obtained for the symmetrical gravity jettisoning of the stores, giving the trim changes and vertical accelerations encountered by the aircraft. An expression is also given for calculating the installed drag and lift coefficient of stores in the presence of the aircraft flow field from a measurement of the aircraft accelerations immediately after release. Examples of typical flight path perturbations for a hypothetical aircraft configuration have been calculated.

"Approved for public release; distribution unlimited"

LIST OF FIGURES

- Fig. 1. Aircraft and its coordinate system.
- Fig. 2. Description of store location geometry.
- Fig. 3. Variation of longitudinal velocity \mathcal{U} vs. t.
- Fig. 4. Heaving velocity \mathcal{W} vs. t.
- Fig. 5. Variation of pitch velocity $\dot{\theta}$ vs. t.
- Fig. 6. Variation of pitch angle θ vs. t.
- Fig. 7. Variation of yawing velocity $\dot{\psi}$ vs. t.
- Fig. 8. Variation of ψ vs. t.
- Fig. 9. Variation of ζ vs. t.
- Fig. 10. Variation of ξ vs. t.
- Fig. 11. Perturbed trajectory (wind axes system)

LIST OF APPENDICES

- Appendix-1 Aerodynamic data of aircraft
- Appendix-2 Aircraft-engine-store data
- Appendix-3 Assumed store installation location
- Appendix-4 Table of integral
- Appendix-5 Aircraft response to store jettison

LIST OF SYMBOLS

- m_0 = mass of the basic aircraft after jettison
 m_s = mass of the store
 I_{yy}, I_{zz} = moments of inertia of basic aircraft about y and z axes
 I_{sy}, I_{sz} = moments of inertia of stores about their c.g. - w.r.t. y and z axes
 u_0 = initial cruise velocity of aircraft before jettison along x-axis
 u', w' = perturbation velocity components along x and z axes
 u, w = velocity components of aircraft along x and z axes
 $\dot{\phi}, \dot{\psi}$ = angular velocities of aircraft about y and z axes
 Ω_e = engine r.p.m.
 T = engine thrust
 h_0 = cruising altitude of aircraft before jettison
 k_{yy}, k_{zz} = radii of gyration of basic aircraft about the basic aircraft c.g.
 k_{sy}, k_{sz} = radii of gyration of stores about their body c.g.
 $H(t)$ = Heaviside unit step function
 k_e = radius of gyration of engine about the axis of rotation
 ξ = dimensionless longitudinal displacement of aircraft in the wind axis system (positive to right)
 ζ = dimensionless vertical displacement of aircraft in the wind axes system (positive downward)
 τ = mean aerodynamic time
 θ = angle of pitch (positive nose up)
 ψ = angle of yaw
 σ = density ratio
 $M_0 = m_0 / \rho_0 S c$ = airplane relative based on m.a.c.
 $C_{D_0}, C_{L_0}, C_{m_0}$ = drag, lift and pitching moment coefficient of the basic aircraft
 $C_{D_{\delta_z}}, C_{L_{\delta_z}}, C_{m_{\delta_z}}$ = drag, lift and moment coefficient derivatives due to stabilizer deflection
 $\delta_z, \delta_r, \delta_a$ = stabilizer, rudder and aileron deflection
 $C_{D_s}, C_{L_s}, C_{m_s}$ = drag, lift and moment coefficient due to the external store
 $C_{m_{\delta_r}}, C_{m_{\delta_a}}$ = yawing moment derivative due to rudder and aileron deflection
 C_{m_0} = yawing moment coefficient of basic aircraft

INTRODUCTION

Military aircraft carry stores like bombs, rockets and fuel tanks which have to be jettisoned as required by the particular flight mission. The weight and moment of inertia contribution of these stores forms a significant fraction of the corresponding parameters of the basic aircraft. Further, in the case of externally carried stores under the wings and/or the fuselage the aerodynamic characteristics of the basic aircraft are also modified significantly. Jettisoning of the stores imparts an impulsive change to the inertial and aerodynamic parameters of an otherwise trimmed flight thereby producing both linear and angular accelerations to the aircraft system. However, the developments leading to the conformal carriage of stores to alleviate the problem somewhat. These accelerations are made very much more severe with the use of power ejection for the release of stores as with ERU on single store pylons or TER or MER systems which generate upward reactions comparable to the aircraft weight. It may be expected that the release of the store disturbs the equilibrium of the aircraft for only a short duration duration after which the Pilot applies corrective action to restore it back to equilibrium. The perturbations will be seen to consist of a longitudinal acceleration of the aircraft along the flight path due to a sudden reduction in mass and aerodynamic drag due to release of the stores. Again the moment equilibrium about the airplane center of gravity is upset due to the sudden removal of the gravity moment, the moment of inertia and the aerodynamic contributions to these moments of the stores. This causes aircraft pitching which when coupled with the gyroscopic inertia of the engines also generates a small yawing motion. The yawing motion is aggravated in the case of unsymmetrical store jettison when a rolling motion is a natural consequence.

MATHEMATICAL FORMULATION

Consider the motion of an aircraft (Fig.1) carrying external stores like drop tanks, bombs or missiles carried either externally or internally as the case may be. In case the stores are carried internally either within the fuselage or the wing, the aircraft experiences finite perturbations to its mass and inertia characteristics because of jettisoning of the stores.

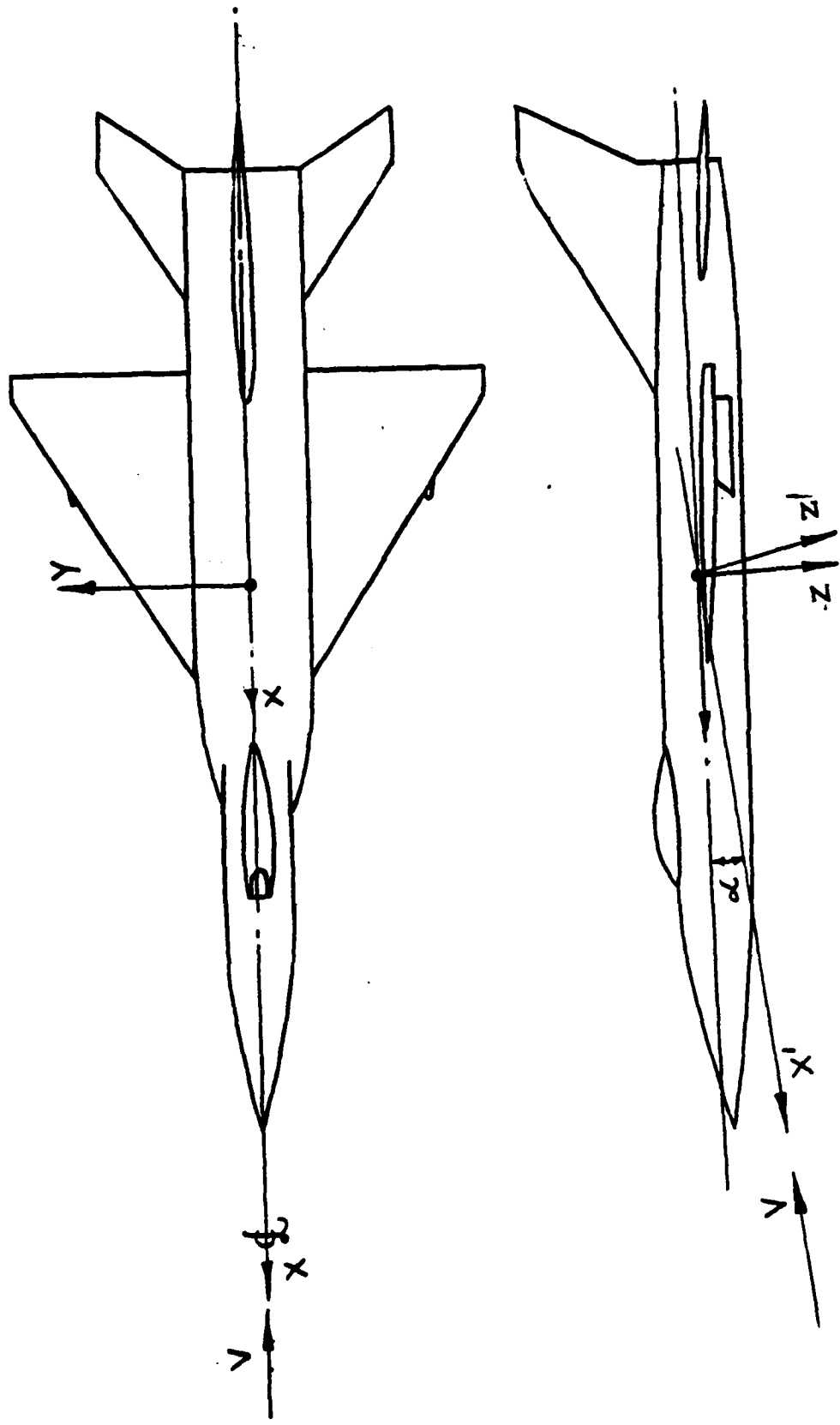


FIG. 1. AIRCRAFT CO-ORDINATE SYSTEM

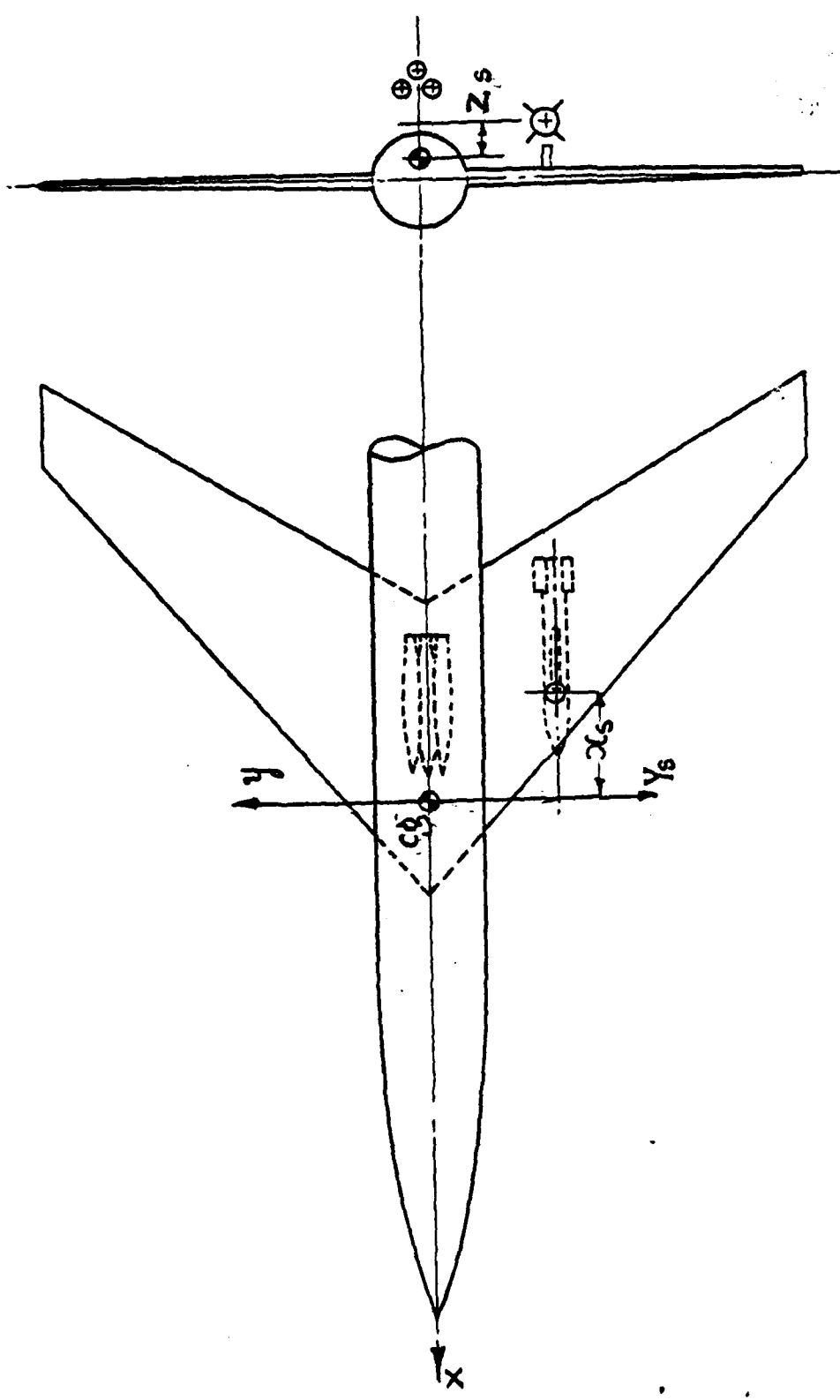


FIG. 2. DESCRIPTION OF STORE LOCATION

If the stores are carried externally on pylons, jettisoning the stores causes finite perturbations to both the inertial and the aerodynamic characteristics of the aircraft. These perturbations cause momentary variations to the trimmed recti-linear flight path of the aircraft at the time of jettison. We shall be interested in studying the perturbed flight path of the aircraft in the few moments after jettison before the human pilot or autopilot system applies the necessary controls to restore the aircraft to recti-linear motion.

To begin with, we shall consider the case of gravity jettisoning of the stores symmetrically with respect to the longitudinal axis of the aircraft. The general equations of motion relevant to this problem are

$$\left. \begin{aligned} m\dot{u} &= F_x - m(\dot{\psi} + \omega \eta) \\ m\dot{w} &= F_z + m(\dot{\alpha} \eta - \dot{\psi} \rho) \\ I_{yy} \dot{\beta} &= M_y + (I_{xz} - I_{xz}) \dot{\beta} \eta + I_{xz} (\dot{\alpha}^2 - \dot{\beta}^2) - I_e \Omega_e \dot{\alpha} \\ I_{xz} \dot{\alpha} &= M_x + (I_{xz} - I_{yy}) \dot{\beta} \eta + I_{xz} (\dot{\beta} - \dot{\alpha} \eta) + I_e \Omega_e \dot{\beta} \end{aligned} \right\} \quad (1)$$

Assuming that the stores are jettisoned symmetrically with the aircraft trimmed for straight and level flight and that the engine thrust line passes through the longitudinal axis of the aircraft we get

$$\dot{\psi} = \dot{\beta} = \dot{\alpha} = \dot{\phi} = \dot{\delta}_a = \dot{\delta}_r = 0 \quad (2)$$

Further assuming that the aircraft inertia distribution is nearly symmetric so that $I_{xz} \approx 0$, we may write eqns. (1) as

$$\left. \begin{aligned} m\dot{u} &= F_x - m\omega \eta \\ m\dot{w} &= F_z + m\alpha \eta \\ I_{yy} \dot{\beta} &= M_y \\ I_{xz} \dot{\alpha} &= M_x + I_e \Omega_e \dot{\beta} \end{aligned} \right\} \quad (3)$$

where F_x , F_y , M_y , M_x are defined by and

$$\left. \begin{aligned} F_x &= T - \frac{1}{2} \rho V^2 S (C_x + C_{m\dot{\alpha}} \dot{\alpha}) \\ F_z &= mg - \frac{1}{2} \rho V^2 S (C_z + C_{z\dot{\alpha}} \dot{\alpha} + \frac{c}{2V} C_{z\dot{\beta}} \dot{\beta}) \\ M_y &= \frac{1}{2} \rho V^2 S c [C_m + C_{m\dot{\alpha}} \dot{\alpha} + \frac{c}{2V} (C_{m\dot{\beta}} \dot{\beta} + C_{m\dot{\alpha}} \dot{\alpha})] \\ M_x &= \frac{1}{2} \rho V^2 S b C_n \end{aligned} \right\} \quad (4)$$

The axes of coordinates (x, y, z) are shown in Fig.1, space fixed coordinates being used with the origin coinciding with the center of gravity of the aircraft at $t = t_0$ and the flight path assumed parallel to the x-axis. At time $t = t_0$, jettisoning of the stores causes discontinuous changes in the inertial and aerodynamic characteristics of the aircraft. The mass and inertia of the aircraft at any time t may be written in general, as

$$\left. \begin{aligned} m &= m_0 + m_s H(t_0 - t) \\ I_{yy} &= I_{oyy} + (I_{sy} + m_s y_0^2) H(t_0 - t) \\ I_{zz} &= I_{ozz} + (I_{sz} + m_s z_0^2) H(t_0 - t) \end{aligned} \right\} \quad (5)$$

and the aerodynamic coefficients C_x , C_z and C_m may be written

$$\left. \begin{aligned} C_x &= C_{x_0} + C_{x_s} H(t_0 - t) + 4\mu_L^2 K (1 + m)^2 / \sigma^2 \\ C_z &= C_{z_0} + C_{z_s} H(t_0 - t) \\ C_m &= C_{m_0} + (C_{m_s} - (z_s/c) C_{z_s}) H(t_0 - t) \end{aligned} \right\} \quad (6)$$

where $H(t)$ is the Heaviside unit function defined by

$$\left. \begin{aligned} H(t) &= 0 & t &\leq 0 \\ H(t) &= 1 & t &> 0 \end{aligned} \right\} \quad (7)$$

and assuming the nose up pitching moment to be positive. When dealing with problem of multiple store jettisoning eqn. (5) may be written as

$$\left. \begin{aligned} m &= m_0 + \left(\sum_i m_{si} \right) H(t_0 - t) \\ I_{yy} &= I_{oyy} + \sum_i (I_{s_{yi}} + m_{si} y_{si}^2) H(t_0 - t) \\ I_{zz} &= I_{ozz} + \sum_i (I_{s_{zi}} + m_{si} z_{si}^2) H(t_0 - t) \end{aligned} \right\} \quad (8)$$

where m_{si} , y_{si} , z_{si} refer to the mass, y and z coordinates of the i-th store and the summation extends over all the stores jettisoned at one instant t_0 . Further the aerodynamic coefficients in eq. (6) may be

written as

$$\left. \begin{aligned} C_x &= C_{x_0} + 4\mu_L^2 K (1 + \sum_i m_{si})^2 / \sigma^2 + \sum_i C_{x_{si}} H(t_0 - t) \\ C_z &= C_{z_0} + \sum_i C_{z_{si}} H(t_0 - t) \\ C_m &= C_{m_0} + \sum_i (C_{m_{si}} - (z_{si}/c) C_{z_{si}}) H(t_0 - t) \end{aligned} \right\} \quad (9)$$

Again, $C_{x_{si}}$, $C_{z_{si}}$, $C_{m_{si}}$ are the drag, lift and pitching moment contributions of the i-th store and the summation extends over all the stores jettisoned at the instant $t = t_0$.

Release of the store alters the flow field around the aircraft as a function of time as the relative distance between them increases. Because of the complexity of the store motion and the even more complex interference field between the aircraft and the store, the coefficients of drag, lift and pitching moment, C_{x_0} , C_{z_0} and C_{m_0} , respectively become complicated functions of time t . To make the problem tractable we shall assume them to be constant during the small period of time of interest in this problem. Further, the induced drag factor K will be assumed to be the same with or without the presence of the external stores. Whereas, this may not be fully satisfied with the usual large sized external stores, like fuel tanks, it may be more valid in the case of high density stores like bombs. If u_0 be the velocity of the aircraft at $t = t_0$ and u' , ω' , δ' , η' the perturbations in the linear and angular velocities after jettison and assuming

$$(u'/u_0), (\omega'/u_0) \ll 1 \quad (10)$$

we may write the velocity components of the aircraft as

$$u = u_0 + u', \quad \omega = \omega' \quad (11)$$

and the resultant velocity of the aircraft as

$$V = (u^2 + \omega^2)^{1/2} \approx u_0 + u' \quad (12)$$

We shall assume the angle of attack α to be nearly constant during the perturbed motion so that $\dot{\alpha} = 0$. Further, the engine is assumed to be operating at a constant rotational speed Ω_e at nearly constant altitude h_0 so that the thrust $T \approx$ constant. The equations of motion (3) may be written in linearised dimensionless form as

$$\left. \begin{aligned} (1+m'H)\ddot{u} &= \mu_2 C_T - \frac{1}{2}\sigma [C_{x_0} + 4\mu_2^2 K(1+m')^2/\sigma^2 (1-4\beta) + C_{x_0}\delta_2 + C_{x_0}H] \\ (1+m'H)\ddot{\omega} &= (1+m'H)(\mu_2 + \mu_2\delta_2) - \frac{1}{2}\sigma (C_{z_0} + C_{z_0}\delta_2 + \frac{1}{2}C_{z_0}\eta_2 + C_{z_0}H) \\ (1+m_y'H)\ddot{\delta} &= (\sigma/2K_{yy})[(M_1 + M_2H)(1+2\beta) + \frac{1}{2}C_{m_y}\eta_2] \\ (1+m_z'H)\ddot{\eta} &= (A\sigma/2K_{zz})N(1+2\beta) + \omega_e \Omega_e K_e \mu_e \eta_2 \end{aligned} \right\} \quad (13)$$

where we have defined

$$\left. \begin{aligned} u &= u'/u_0 & \omega &= \omega'/u_0 & \delta &= \delta'/\omega & \eta &= \eta'/\omega & \omega &= u_0/c \\ \eta_2 &= \eta_2/c & \delta_2 &= \delta_2/c & \sigma &= P/P_0 & \omega_e &= \Omega_e/m_0 & m' &= m_0/m_0 \\ m_y' &= m_y'K_y & m_z' &= m_z'K_z & A &= b/c & C_T &= T/W_0 & \Omega_e &= \Omega_e/\omega \\ \xi &= \alpha/c & \eta &= \eta/c & K_{yy} &= K_{yy}/c & K_{zz} &= K_{zz}/c & K_{\delta\eta} &= K_{\delta\eta}/c \end{aligned} \right\} \quad (14a)$$

$$\left. \begin{aligned}
 K_{xz} &= k_{xz}/c & K_e &= (K_e/K_{ozz})^2 & t' &= (t_0 - t)/\tau_0 & \tau_0 &= m_0/\rho_0 S u_0 \\
 K_y &= (K_{zy}^2 + \eta_z^2)/K_{ozz} & K_z &= (K_{xz}^2 + \zeta_x^2)/K_{ozz} & \mu_c &= m_c/\rho_0 S c & \mu_L &= W_0/\rho_0 u_0^2 S \\
 I_{yy} &= m_0 k_{oyy}^2 & I_{ozz} &= m_0 k_{ozz}^2 & I_{zy} &= m_0 k_{zy}^2 & I_{xz} &= m_0 k_{xz}^2 \\
 \dot{u} &= \partial \underline{u}/\partial t' & \dot{w} &= \partial \underline{w}/\partial t' & \dot{q} &= \partial \underline{q}/\partial t' & \dot{r} &= \partial \underline{r}/\partial t'
 \end{aligned} \right\} (14b)$$

and assuming further that the products

$$\omega \underline{q} \approx 0, \quad \underline{q} \underline{q} \approx 0 \quad (15)$$

and representing $H(t')$ by H for the sake of conciseness.

SOLUTION OF THE GOVERNING EQUATIONS

Eqs. (13) represent a set of four coupled, autonomous, linear, first order differential equations for the state variables $\underline{u}, \underline{w}, \underline{q}, \underline{r}$ of the aircraft together with the initial conditions

$$\underline{u} = \underline{w} = \underline{q} = \underline{r} = 0 \text{ at } t' = 0 \quad (16)$$

An examination of equations (13) shows that the strategy of solution should be to solve eq. (13a) for \underline{u} and use it to solve the remaining equations of (13) in sequence. Thus, the solution for the longitudinal velocity perturbation \underline{u} may be written from eqn. (13a) as

$$\underline{u} = \underline{u}_{max} f_0 \quad (17)$$

where

$$\left. \begin{aligned}
 \underline{u}_{max} &= \pi_{x_0} \mu_L \bar{c} & f_0 &= (1 - e^{-t'/\bar{c}}) \\
 \pi_{x_0} &= (C_x \sigma X - \mu_L C_T) / \mu_L (1 + m') \\
 X &= C_{x_0} + C_{x_{\delta_0}} \delta_0 + C_{x_{\dot{\delta}_0}} + C_{x_{\ddot{\delta}_0}} \\
 \bar{c} &= \sigma C_{x_0} / 2(1 + m') = 2K \mu_L^2 (1 + m') / \sigma
 \end{aligned} \right\} (18)$$

The \underline{u} perturbation is seen to be an exponentially damped function in time t' with a time constant \bar{c} defined above and attaining a maximum value given in eq. (18) asymptotically. Further, from eq. (18) it is also seen that for a given aircraft, the relaxation time increases with altitude and the relative store mass parameter m' . The longitudinal acceleration along the flight path after jettison is larger for high drag and light weight stores than for low drag and heavier ones. Using \underline{u} we may write the solution of \underline{q} in eq. (13c) with the initial condition (16) as

$$\underline{q} = [A_1 / (1 - \beta \bar{c})] [2\beta \bar{c} \underline{u} + (1 - \beta \bar{c} + 2\underline{u}_{max}) f_1] \quad (19)$$

where $\beta = \sigma C_{m\dot{\gamma}} / 4K_{\dot{\gamma}} (1+m')$ $h_1 = 2M/Cm\dot{\gamma}$

$$M = M_1 + M_2 \quad M_1 = C_{m\delta_s} + C_{m\delta_a} \delta_s \quad M_2 = C_{m\delta_s} - \zeta_{\delta_s} C_{m\delta_s} \quad (20)$$

$$f_1 = e^{\beta t'} - 1$$

with $\dot{\gamma}$ assumed positive nose-up. Since $\dot{\gamma} = -(\partial\theta/\partial t')/\mu_c$, integrating $\dot{\gamma}$ with respect to t' we obtain an expression for the angle of pitch θ as

$$\theta = \frac{h_1 \mu_c}{1-\beta \bar{\tau}} \left\{ t' (1-\beta \bar{\tau}) (1+2\mathcal{Z}_{max}) + 2\beta \bar{\tau}^2 \mathcal{Z} - \frac{(1-\beta \bar{\tau} + 2\mathcal{Z}_{max})}{\beta} f_1 \right\} \quad (21)$$

Again, the solution of the heaving velocity perturbation \dot{w} may be obtained from eq. (13b) and after some simplification can be written as

$$\dot{w} = [h_2 + h_0 h_1 (1+2\mathcal{Z}_{max})] t' + 2h_1 \frac{(h_0 - \beta \bar{\tau}^2 h_2)}{1-\beta \bar{\tau}} \mathcal{Z} - \frac{h_0 \dot{\gamma}}{\beta} \quad (22)$$

where

$$h_0 = \frac{\sigma C_{z\dot{\gamma}}}{4(1+m')} - \mu_c \quad h_2 = \frac{\sigma C_{z\dot{\gamma}}}{4(1+m')} + \mu_c \quad h_3 = \mu_c - \frac{\sigma \bar{z}}{2(1+m')} \quad (23)$$

Similarly, the solution for the yawing velocity perturbation $\dot{\chi}$ may be obtained from eq. 13(d) which may be written after simplification as

$$\dot{\chi} = h_4 [(1+2\mathcal{Z}_{max}) t' + 2\bar{\tau} \mathcal{Z}] + h_5 \dot{\gamma} \quad (24)$$

where

$$\left. \begin{aligned} h_4 &= \left[\frac{\sigma AN}{2K_{max}^2} - m_c \bar{z}_c K_c \mu_c h_1 \right] / (1+m') \\ h_5 &= m_c \bar{z}_c K_c \mu_c / \beta (1+m') \\ N &= C_{n\dot{\gamma}_r} + C_{n\dot{\gamma}_a} \delta_r + C_{n\dot{\gamma}_a} \delta_a \end{aligned} \right\} \quad (25)$$

The vertical acceleration n_{z_0} of the aircraft, normal to the flight path, at the instant $t = 0$ due to the store release can be written

$$n_{z_0} = (\dot{w}/g)_{t=0} = -\dot{w}_0/\mu_c = \frac{\sigma \bar{z}}{2\mu_c (1+m')} - \frac{4\beta \bar{\tau} \mathcal{Z}_{max} h_1 \bar{F}_0}{1-\beta \bar{\tau}} - 1 \quad (26)$$

where \dot{w}_0 is obtained from eq. (24a) by differentiating with respect to t' and setting $t' = 0$

$$\begin{aligned} \bar{z} &= C_{z_0} + C_{z\delta_s} \delta_s + C_{z\delta_a} \\ \bar{F}_0 &= \mathcal{Z}_0^2 / g c \end{aligned} \quad (27)$$

and \bar{F}_0 is the Froude's number of the aircraft.

The longitudinal acceleration n_x of the aircraft along the flight path due to the store release is given by

$$n_x = n_{x_0} e^{t'/\bar{\tau}} \quad (28)$$

where n_{x_0} is the maximum flight path acceleration attained at the instant $t' = 0$ and is given by eq. (18). It is also seen from eq. (28) that n_{x_0} decays exponentially with time with a time constant \bar{T} . This expression can be used to estimate the installed drag coefficient C_{x_s} of one or a cluster of stores from flight tests by measuring the longitudinal acceleration n_{x_0} of the aircraft with a sensitive accelerometer, since the airplane zero-lift drag coefficient C_{x_0} , the induced drag coefficient C_{x_i} and the trim drag coefficient $C_{x_0} \delta_s$ will be known for a given aircraft.

If the accelerometers are placed in the plane of symmetry of the aircraft at its center of gravity with their axes parallel and perpendicular to the longitudinal axis x' of the aircraft, the measured accelerations $(n_{x'}, n_{z'})$ in the body axes system are related to the accelerations (n_x, n_z) of eqns. (25) and (28) in the wind axes system by the equations

$$\left. \begin{aligned} n_x &= n_{x'} \cos \alpha - n_{z'} \sin \alpha \\ n_z &= n_{x'} \sin \alpha + n_{z'} \cos \alpha \end{aligned} \right\} \quad (29)$$

which are reduced to

$$n_x = n_{x'} - n_{z'} \alpha \quad n_z = n_{x'} + n_{z'} \alpha \quad (30)$$

for small angles of attack α of interest.

The store drag coefficient C_{x_s} may be expressed from eq. (18) as

$$C_{x_s} = \frac{2\mu_L}{\sigma} [C_T + (1+m')n_{x_0}] - (C_{x_0} + C_{x_{i_s}} \delta_s + C_{x_{t_s}}) \quad (31)$$

This expression may be compared with that given by Pinsky [1] and King [2]. Pinsky's expression for the installed drag coefficient of a store may be written in terms of the present symbolism as

$$C_{x_s} = 2C_{x_0} - (2m'/\mu_L/\sigma)n_{x_0} \quad (32)$$

Similarly, eq. (26) may be used to obtain the installed lift coefficient C_{z_s} which, even though of relatively secondary importance, is nevertheless of interest in the study of aerodynamic interference problems. Thus, we write C_{z_s} as

$$C_{z_s} = \frac{2\mu_L(1+m')}{\sigma} \left[1 + n_{z_0} + \frac{4\beta \bar{T} \mathcal{U}_{\max} h_1 \mathcal{F}_0}{1-\beta \bar{T}} \right] - (C_{z_0} + C_{z_{i_s}} \delta_s) \quad (33)$$

It is interesting to study the trajectory of the aircraft in the wind axes system after releasing the store. The trajectory parameters (ξ, ζ, ψ)

are obtained by integrating eqns. \mathcal{U} , \mathcal{W} and \mathcal{I} with respect to t' and may be written as

$$\xi = -\mu_c \mathcal{U}_{max} (t' + \tau f_0) \quad (34)$$

$$\zeta = -\mu_c \left\{ [h_3 + h_0 h_1 (1 + 2\mathcal{U}_{max})] \frac{t'^2}{2} + \frac{2h_1 (h_0 - \beta \tau^2 h_2)}{1 - \beta \tau} (t' + \tau f_0) + \frac{h_0 h_1}{\beta(1 - \beta \tau)} \left[t'(1 - \beta \tau)(1 + 2\mathcal{U}_{max}) - 2\beta \tau^2 \mathcal{U} - \frac{1 - \beta \tau + 2\mathcal{U}_{max}}{\beta} f_1 \right] \right\} \quad (35)$$

$$\psi = -\mu_c h_0 \left[(1 + 2\mathcal{U}_{max}) \frac{t'^2}{2} + 2\tau \mathcal{U}_{max} (t' + \tau f_0) \right] - \frac{\mu_c h_0}{1 - \beta \tau} \left[(1 - \beta \tau)(1 + 2\mathcal{U}_{max}) t' - 2\beta \tau^2 \mathcal{U} + \frac{1 - \beta \tau + 2\mathcal{U}_{max}}{\beta} f_1 \right] \quad (36)$$

In this ψ is the angle of yaw of the aircraft at time t' with respect to the initially trimmed flight path direction.

Appendix 3 contains a list of typical integrals used in obtaining the above solutions.

DISCUSSION OF RESULTS

Figs. 3-8 show the variation of the perturbation parameters \mathcal{U} , \mathcal{W} , \mathcal{I} , \mathcal{J} , θ , ψ with the dimensionless time in the interval $0 < t' < 1$ for the Phantom F-4 aircraft with assumed engine data for a typical case of symmetrical jettison of 2 x 1000 lb. bombs for two flight altitudes 0 and 15000 ft. and three Mach numbers 0.6, 0.8 and 1.2. Cases of simultaneous release of 4 x 1000 lb. bombs are shown for the trajectory parameters ξ and ζ . The variation of the perturbation trajectory parameters ξ , ζ of the aircraft for a given altitude and Mach number are shown in Figs. 9 and 10 as a function in time in $0 < t' < 1$ in the wind axes system while the perturbed flight path itself is shown in Fig. 11. The aerodynamic characteristics of the aircraft required for these example calculations have been taken from Ref. 3 and are listed in Appendices 1 and 2 while the store inertia properties and their assumed installation locations are listed in Appendix-3 for a particular type of 1000 lb. bomb in use.

It is seen from these figures that, in general, all the parameters \mathcal{U} , \mathcal{W} , \mathcal{I} , \mathcal{J} show a reversal of trend between $M = 0.8$ and 1.2 for both $h = 0$ and $h = 14$ Kft which may be explained by the differences in the aircraft aerodynamic characteristics in the subsonic and supersonic speed regimes. The relaxation time τ increases with altitude and decreases with Mach number as may be expected.

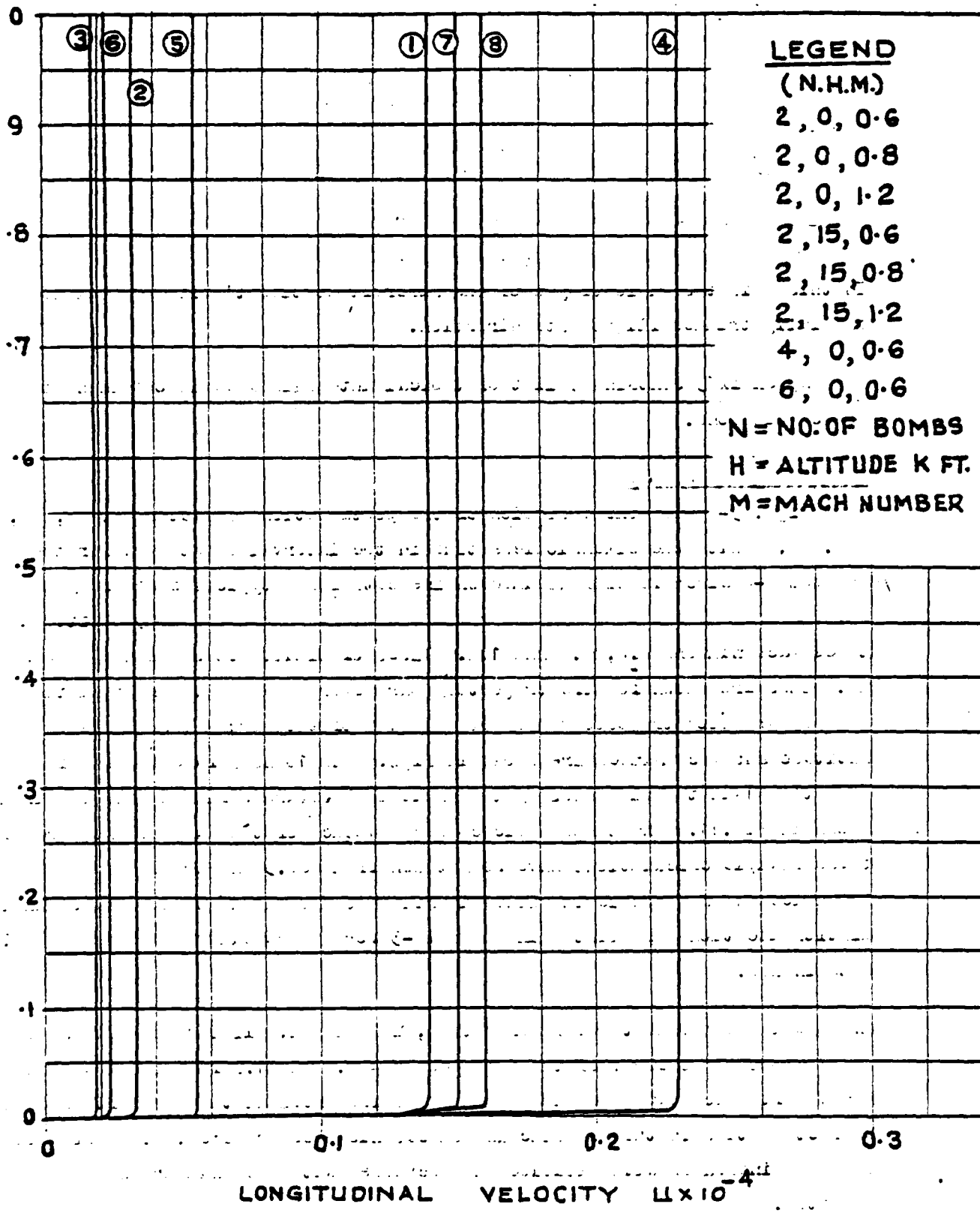


FIG. 3 VARIATION OF u WITH t

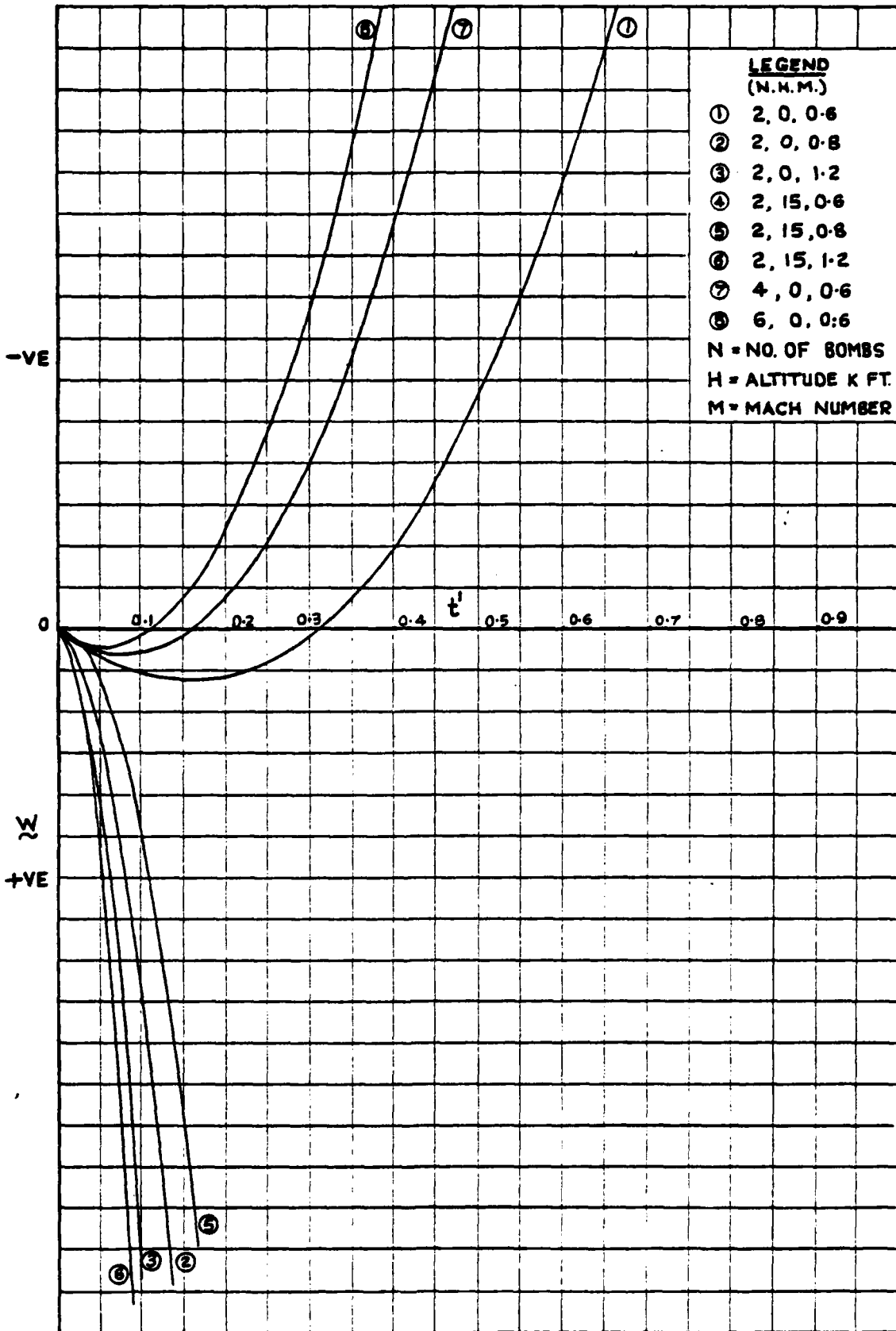


FIG. 4 HEAVING VELOCITY w VS t

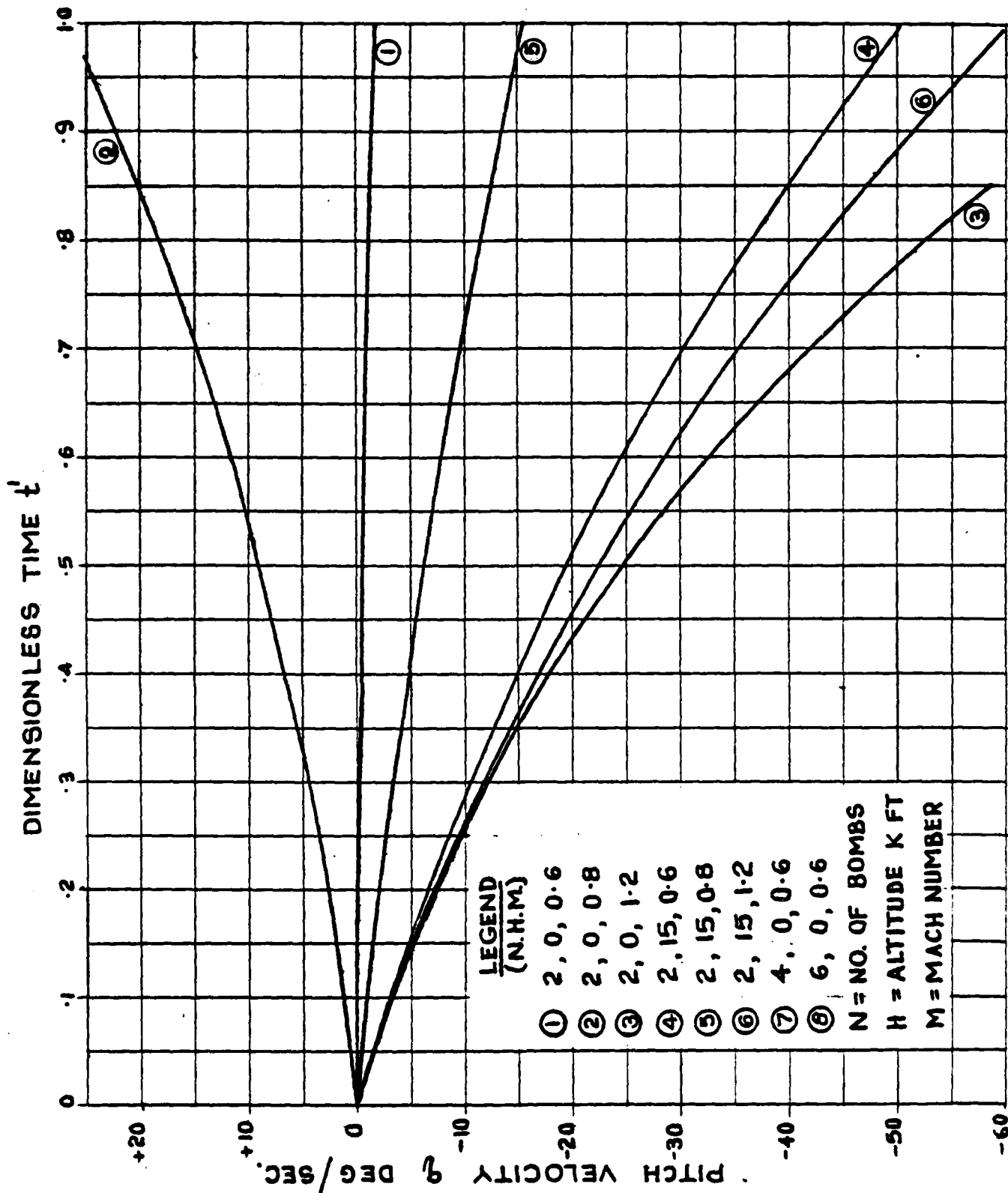


FIG. 5 VARIATION OF q WITH t'

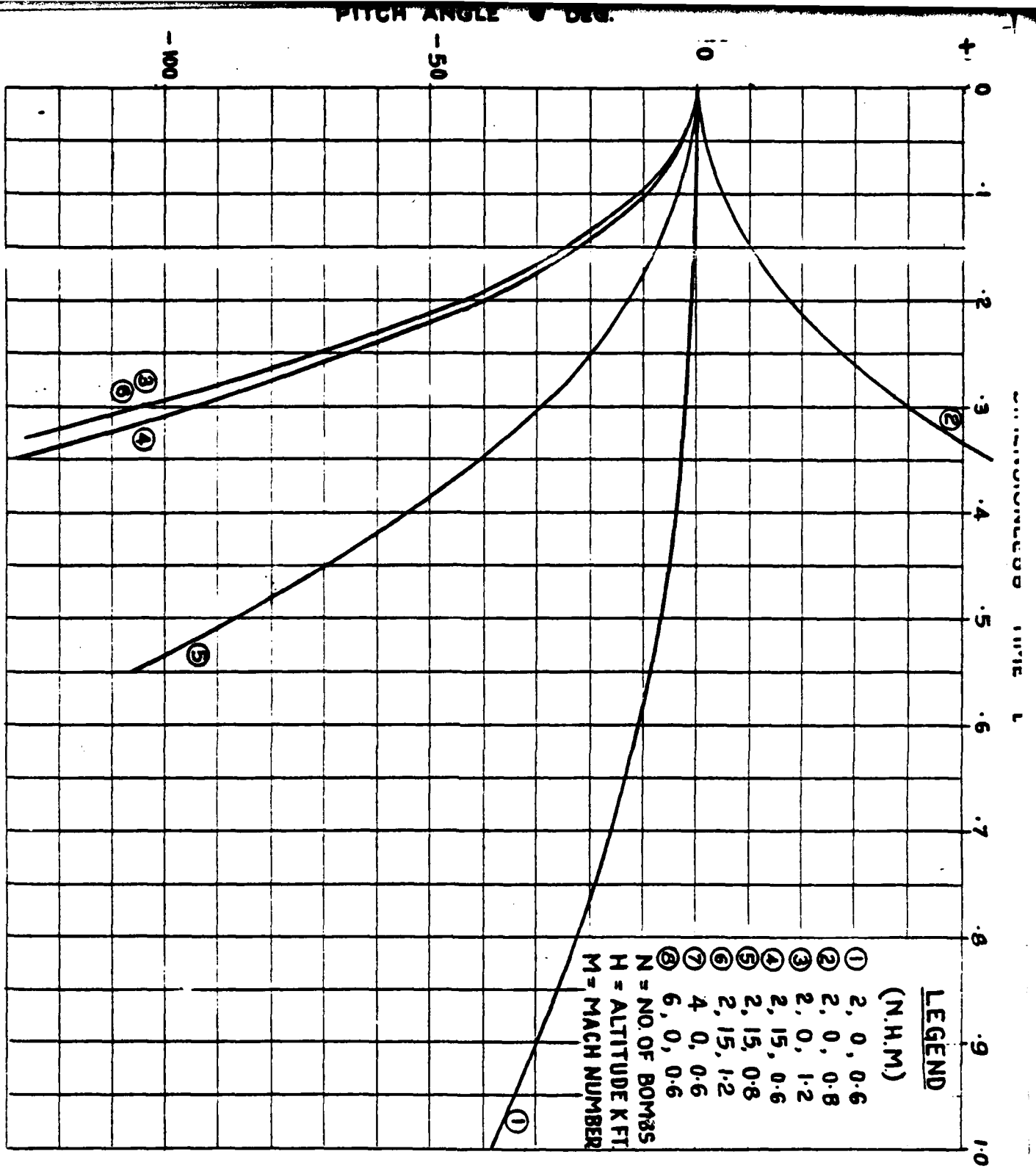


FIG. 6. VARIATION OF θ WITH t

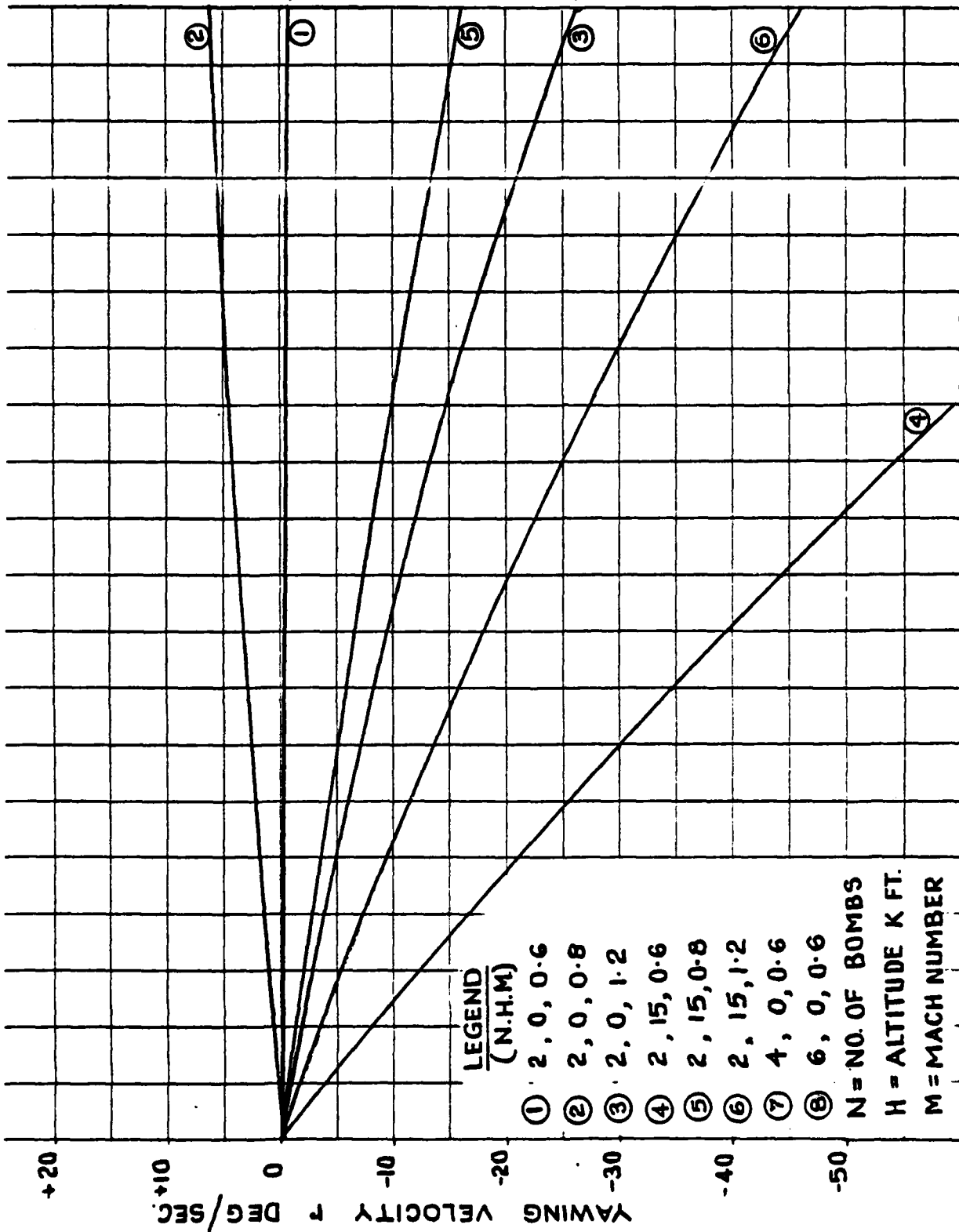


FIG.7 VARIATION OF r WITH t

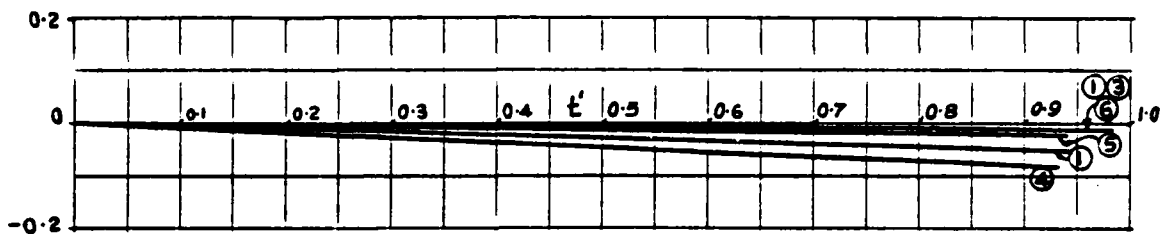


FIG. 8 VARIATION OF ψ vs t

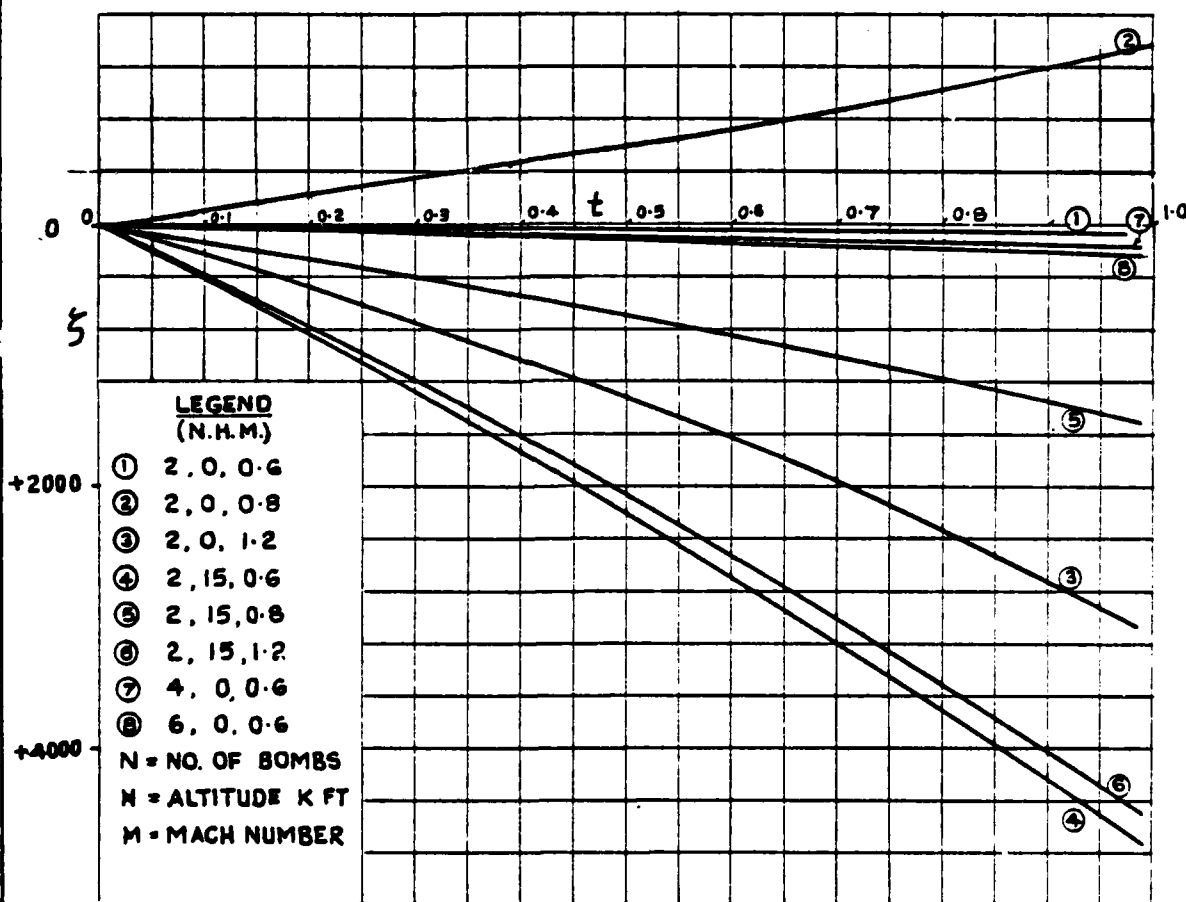


FIG. 9 VARIATION OF ζ vs t

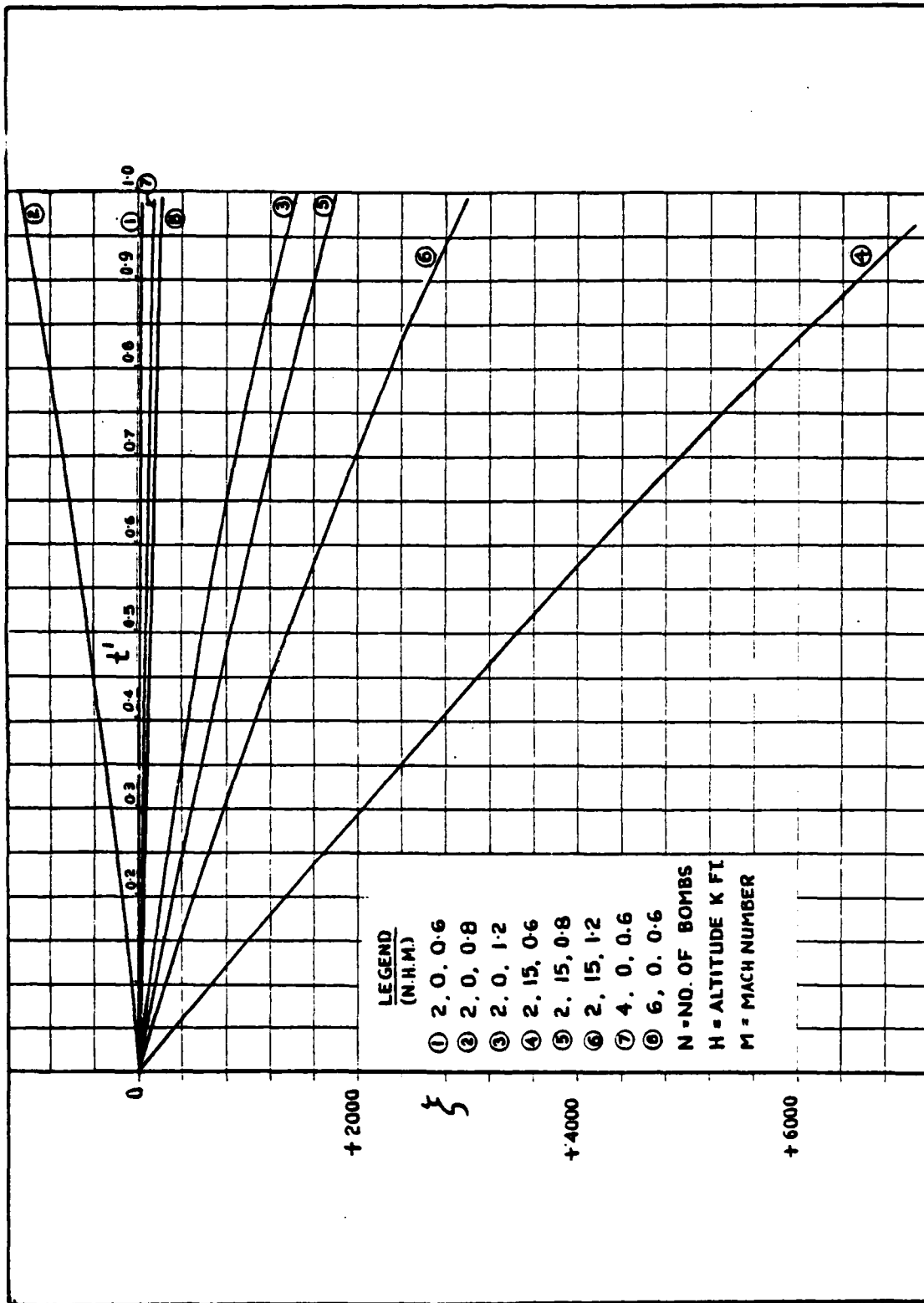


FIG. 10 VARIATION OF t' VS. t

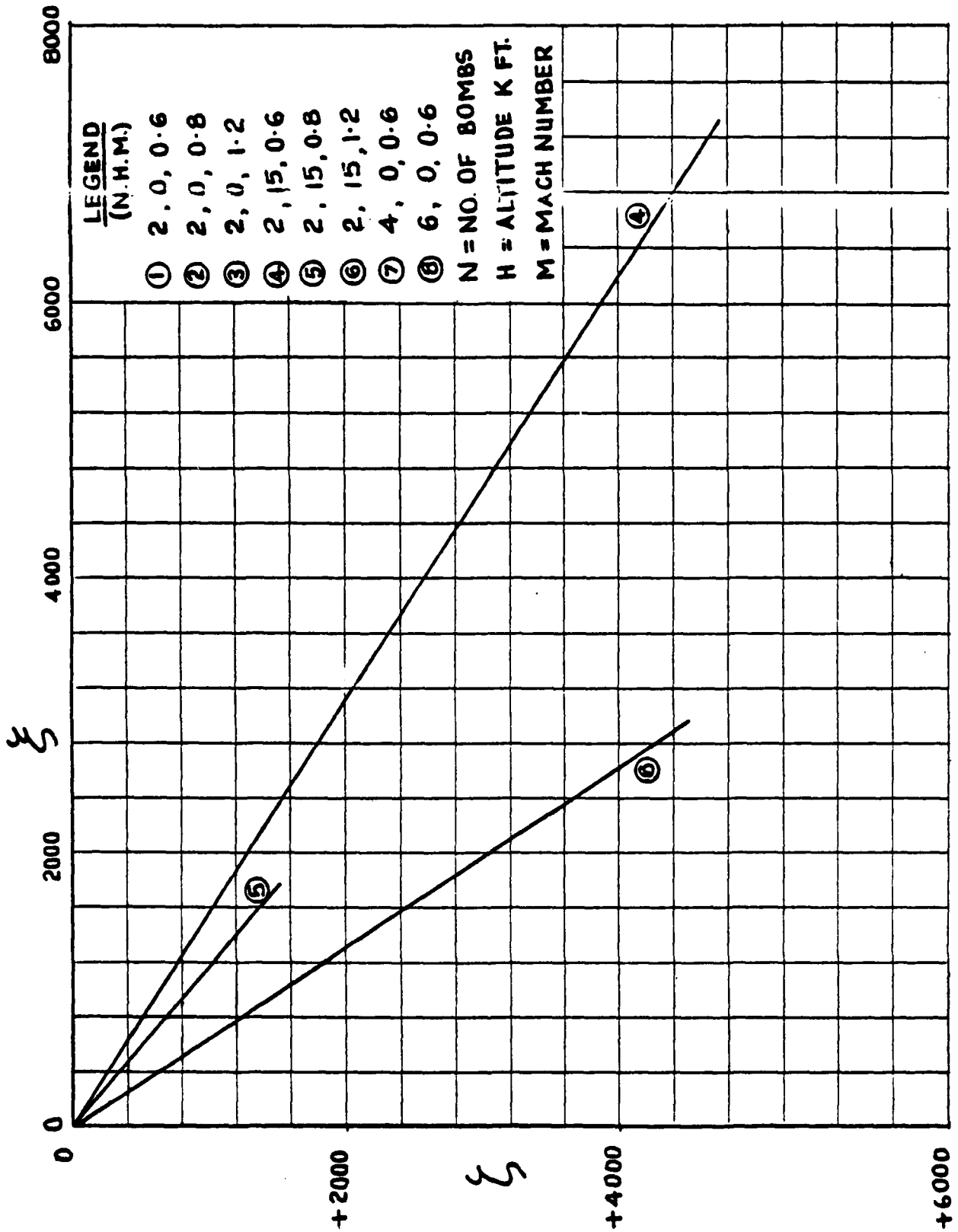


FIG. II PERTURBED TRAJECTORY ζ VS. ζ

The variation of the longitudinal velocity perturbation y is shown in Fig.3. The perturbation velocity y exhibits a nearly step jump over a short time period, the magnitude of the jump decreasing as the flight Mach number increases from $M = 0.6$ to 1.2 . The increment U_{\max} in the longitudinal velocity increases from 14% at $M = 0.6$ to just 2% at $M = 0.6$, the increments increasing with the flight altitude. Increasing the number of stores jettisoned also increases U_{\max} although not appreciably.

The interesting behaviour of the heaving velocity perturbation w for $h = 0$ and $M = 0.6$ is shown in Fig.4 for the case of simultaneous jettison of 2, 4 and 6 x 1000 lb. bombs where it is seen that $w < 0$ (upward) at first attaining a maximum negative value and soon changes into a positive (downward) velocity, increasing monotonically and rapidly. It is seen that the time interval over which this trend reversal of w occurs decreases rapidly as the jettisoned weight (the number of 1000 lb. bombs) increases, the magnitude of the maximum negative value of w also following a similar behaviour.

The perturbation pitching velocity q and the pitch angle θ are increasingly nose up between $M = 0.6$ and 0.8 and become nose down for $M = 1.2$. The pitching velocity q (Fig.5) caused by store dropping is also seen to be significant and larger at higher altitudes than at sea level due to the higher density and the aerodynamic damping prevailing at the lower altitudes.

The yawing angular velocity perturbation r (Fig.7) due to the coupling between q and engine gyroscopic torque changes sign in the same Mach number range as above, although nevertheless, the heading change caused is negligible (Fig.8).

Figs. 9 and 10 for the variation of ξ and ζ with t' show the nearly linear behaviour of all the curves. The actual perturbed trajectory of the aircraft in the wind axes reference frame appears to be nearly linear (Fig.11), the flight path becoming steeper as M increases from 0.6 to 1.2 . However, the sign of the flight path slope reverses as M increases from 0.6 to 1.2 . The sign of the flight path slope also reverses as M increases from 0.8 to 1.2 for both sea level and 15000 ft.

Appendix 5 contains a table of the overall aircraft response to stores release as a function of altitude, Mach number and the weight of stores released. The longitudinal acceleration n_{x0} due to store jettison is seen to be higher at sea level than at 15000 ft. due to the greater store drag relief obtained at sea level compared to that at the higher altitude. The normal acceleration is lower at a higher altitude than at sea level increasing from $M = 0.6$ to 0.8 and decreasing between $M = 0.8$ to 1.2 .

In the case of unsymmetrical store jettison, the analysis requires consideration of the roll mode of the aircraft and side slipping motion in addition to the four degrees of freedom considered above. This will be discussed in a later paper.

The aircraft undergoes a longitudinal trim change due to the release of the store and the subsequent motion so as to bring the airplane back to the initial trim speed U_0 prior to store drop and in addition to equilibrate the longitudinal moment unbalance.

The above analysis of the aircraft motion can also be used in the case of stores ejected from TER or MER or single store pylons in which the stores are given an initial impulse, essentially in the form of a downward velocity. The aircraft experiences a reaction comprising of an upward force and a corresponding moment about the center of gravity of the aircraft which may be modelled for mathematical analysis in the same manner as above in the case of gravity release.

SUMMARY

A method for calculating the disturbed motion of an aircraft subsequent to release of external stores has been described. A method for the flight determination of the installed drag and lift coefficients of single or multiple stores using these results is also indicated.

ACKNOWLEDGEMENT

The author gratefully appreciates the assistance of Dr.M.Krishnamurthy for programming the equations for numerical computation.

APPENDIX - 1
AERODYNAMIC DATA OF AIRCRAFT

H	0 ft. $\delta = 1$			15000 ft. $\delta = .565$		
M	0.6	0.8	1.2	0.6	0.8	1.2
α_0°	1.3	0.5	0.4	3.4	1.2	-0.3
δ_s	0	0.4	-1.0	-1.25	-0.4	-1.5
C_L	0.15	0.08	0.03	0.21	0.15	0.05
C_D	.0205	.015	0.04	.028	.0205	0.04
C_{x_0}	-.0171	-.0143	-.0402	-.0155	-.0174	-.0399
$C_{x_{\delta s}}$.0082	.0030	-.0021	.0228	.0078	.0006
C_{z_0}	-.1504	-.0801	-.0297	-.2113	-.1504	-.0501
C_{m_0}	.0095	.0128	.0016	-.0027	.0058	-.0039
C_{n_0}	.00	.0054	-.0071	-.0022	-.0011	-.0014
$C_{m_{\delta s}}$.000	.0034	-.0078	-.0122	-.0037	-.0134
$C_{m_{\delta z}}$.0095	.0095	.0095	.0095	.0095	.0095
$C_{x_{\delta z}}$.0082	.0030	-.0021	.0228	.0078	.0006
$C_{z_{\delta s}}$	-.3599	-.345	-.3000	-.3843	-.3699	-.35
$C_{z_{\delta z}}$	-1.5871	-1.5669	-1.837	-1.6547	-1.6209	-1.9586
$C_{L_{\delta s}}$.36	.345	.3	.385	.37	.35
$C_{L_{\delta z}}$	-.53	-.48	-.45	-.56	-.53	-.51
$C_{D_{\delta s}}$	-2.35	-2.32	-2.72	-2.45	-2.4	-2.9
$C_{D_{\delta z}}$	-.068	-.058	-.025	-.0725	-.063	-.035
$C_{m_{\delta s}}$.008	.01	.005	.005	.009	.0065
$C_{m_{\delta z}}$.0025	.004	.001	.0024	.0035	.0100
$C_{n_{\delta s}}$.035	.028	.004	.04	.035	.015
T (lbs)	5796	7539	45235	4472	5821	25558
T_{δ} (lbs)	537	955	2148	302	539	1214
T (lbs)	6333	8493	47383	4775	6360	26772

APPENDIX - 2
AIRCRAFT-ENGINE STORE DATA

S	=	530 ft ²
J	=	16.04 ft.
b	=	38.67 ft.
I_{oyy}	=	122186 slug - ft ²
I_{ozz}	=	139759 slug - ft ²
W_e	=	3672 lb. (J79GES)
K_{ee}	=	1.1 ft.
X_s	=	9.67 ft.
Z_s	=	8.0 ft.
H_s	=	1000 lb.
I_{sy}	=	8.872 slug ft ² per bomb
I_{sz}	=	8.872 slug ft ² per bomb
W_0	=	38924 lb.

Rotor weight = 40% Engine weight

Rotor mass = 0.4 x Engine mass = 45.652 slugs (assumed)

Engine max. R.P.M. = 10000, idling r.p.m. = 0.4 x Max.
r.p.m. (assumed)

Engine idling angular momentum = 23200 slug - ft²/sec.

radius of gyration of rotor = K_e = 1.1 ft.

C_{xz} = -.0019 per bomb.

APPENDIX - 3

ASSUMED STORE INSTALLATION LOCATION

0.5 (b/2) spanwise

0.2 c streamwise on chord (local chord unit)

0.35 c below the wing

$$y_s = 0.5 \times \frac{38.67}{2} = 9.67 \text{ ft.}$$

$$z_s = 8 \text{ ft. assumed}$$

$$C_{M_s} = C_{D_s} \frac{S_{ref}}{S_M} = \frac{0.00167 \times 28}{530 \times (0.3048)^2} = 0.00095$$

$$K_{yy} = K_{xx} = 0.3207 \times 0.508 \text{ m.}$$

$$= \frac{0.3207 \times 0.508}{0.3048} \text{ ft.} = 0.5345 \text{ ft.}$$

$$I_{yy} = I_{zz} = \frac{1000}{32.2} \times (.5345)^2 = 8.872 \text{ slug ft}^2$$

APPENDIX - 4

TABLE OF INTEGRALS

$$1. \int (1 + \alpha H)^{-1} dx = x / (1 + \alpha)$$

$$2. \int H (1 + \alpha H)^{-1} dx = x / (1 + \alpha)$$

$$3. \int e^{\beta x} H(x) dx = (e^{\beta x} - 1) / \beta$$

$$4. \int x (1 + \alpha H)^{-1} dx = x^2 / 2(1 + \alpha)$$

$$5. \int x H (1 + \alpha H)^{-1} dx = x^2 / 2(1 + \alpha)$$

$$6. \int e^{\beta x} (1 + \alpha H)^{-1} dx = (e^{\beta x} + \alpha) / \beta(1 + \alpha)$$

$$7. \int e^{\beta x} H (1 + \alpha H)^{-1} dx = (e^{\beta x} - 1) / \beta(1 + \alpha)$$

$$8. \int e^{\beta x} (1 + \alpha H)^{-1} x dx = (x - \frac{1}{\beta}) e^{\beta x} / \beta(1 + \alpha)$$

$$9. \int e^{\beta x} H (1 + \alpha H)^{-1} x dx = (x - \frac{1}{\beta}) e^{\beta x} / \beta(1 + \alpha)$$

APPENDIX - 5

AIRCRAFT RESPONSE TO STORE JETTISON

Bomb	H Kft	M	$M \times 10^4$ max	n_{z_0}	n_{z_0}	\bar{z}	τ_0 (sec)
2 x 1000	0	.6	-.14	-.1548	-1.0709	.001275	1.4796
2 x 1000	0	.8	.03	-.2075	-1.1082	.000403	1.1097
2 x 1000	0	1.2	.02	-1.1578	-.8573	.000090	.7398
2 x 1000	15	.6	.23	-.1167	-.8808	.002521	1.5625
2 x 1000	15	.8	.06	-.1554	-.9956	.000798	1.1719
2 x 1000	15	1.2	.02	-.6542	-.8412	.000177	.7813
4 x 1000	0	.6	-.15	-.1600	-1.0669	.001338	1.4796
6 x 1000	0	.6	-.16	-.1649	-1.0632	.00140	1.4796

REFERENCES

1. W.J.G. Pinskar : Theoretical consideration of possible techniques for the measurement of store drag in flight. RAE TR 68249, Oct. 1968.
2. A.P.King : Flight investigation of a technique for the measurement of the total and interference drag of external stores. AGARD-CP-71-71, Aerodynamic Interference, Agard Conference Proc. No.71, Fluid Dynamics Panel Specialists Meeting, Silver Springs, Maryland, U.S.A., Sept. 28-30, 1970..
3. Robert K.Heffley & Wayne F.Jewell : Aircraft Handling qualities data - NASA CR-2144, Dec. 1972.

AUTOBIOGRAPHY

SRIDHAR M. RAMACHANDRA

B.E. (Electrical Engineering), University of Mysore, India, 1950. D.I.I.Sc. (Aeronautical Engineering), Indian Institute of Science, Bangalore, India, 1952. Ph.D. (Aeronautical & Astronautical Engineering), University of Illinois, Urbana, Illinois, 1962. After graduating from the Indian Institute of Science, Mr. Ramachandra was appointed as a Lecturer in 1953 in the Department of Aeronautics. Apart from graduate teaching and research, he was involved in the design of a 9 ft. x 14 ft. open circuit wind tunnel and a 15 ft. diameter free spinning tunnel. Besides he was connected with several hundred hours of wind tunnel testing on aircraft models. In 1959 he went to the University of Illinois for his Doctoral work which he completed in 1962 with a thesis on the structure of shock waves in monatomic gases. He returned to the Indian Institute of Science in 1962 and continued graduate teaching and research in rarefield gas dynamics, conical flow theory. He was made an Assistant Professor in 1962. In 1965 he was invited to be the first head of the Department of Aeronautics at the American aided Indian Institute of Technology, Kanpur, where he continued undergraduate and graduate teaching and research in rarefield gas dynamics, wing theory, V/STOL studies, air transportation studies and flight laboratory work. In December 1971, he joined Hindustan Aeronautics Limited as Chief of Aerodynamics & Flight Testing and was elevated as Deputy Chief Designer in May 1974 and is Incharge of Technology and Analysis at present. Research interests include transonic flows, parameter identification, computer aided design, flight dynamics rarefield gas flows and traffic equilibrium problems.

A RAPID PREDICTIVE METHOD FOR THREE-DIMENSIONAL
TRANSONIC FLOW FIELDS ABOUT PARENT AIRCRAFT
WITH APPLICATION TO EXTERNAL STORES

(U)

(Article UNCLASSIFIED)

by

Stephen S. Stahara
Michael J. Hensch
Stanley C. Perkins, Jr.
John R. Spreiter

Nielsen Engineering & Research, Inc.
510 Clyde Avenue, Mountain View, CA 94043

ABSTRACT. (U) The initial development of an engineering predictive method for external store trajectory applications at transonic speeds is described. The work represents the first phase in the systematic development of a capability for determining six-degree-of-freedom store trajectories from realistic fighter aircraft configurations at speeds throughout the transonic regime. The emphasis of the initial work has been the development and verification of a theoretical method for the rapid computation of three-dimensional characteristic of modern fighter-bombers. The first objective of this paper is to describe the method and its initial application to a class of simplified wing-body configurations. The second objective is to present highlights of experimental results from a parallel wind tunnel test program designed to test the theory and isolate important features through detailed systematic measurements of flow fields, surface pressures, and forces and moments. A description of the extension of the method to include multiple store and pylon combinations, which is currently underway, is also provided.

"Approved for public release; distribution-unlimited."

LIST OF FIGURES

- Figure 1. Schematic representation of transonic equivalence rule for slender wings and bodies.
- Figure 2. Summary of transonic equivalence rule parameters for several fighter/bomber aircraft.
- Figure 3. Solution procedures developed for model midwing/circular body combination - inner problem.
- Figure 4. Solution procedures developed for outer problem-thickness dominated flow.
- Figure 5. Comparison of theoretical results using outer flow solution procedures with data at $M = 0.975$ for a parabolic-arc body of revolution with a bumpy midsection; $D/l = 1/14$ and $\Delta R/D = 1/5$.
- Figure 6. Details of model wing-body combination.
- Figure 7. Flow-field survey locations for model wing/body test in AEDC 4T tunnel.
- Figure 8. Size of supersonic pockets on pressure and suction side of wing at the spanwise location $y = 2$ inches.
- Figure 9. Size of subsonic pockets on pressure and suction side of wing at the spanwise location $y = 2$ inches for various angles of attack at $M_\infty = 1.025$.
- Figure 10. Side-to-side symmetry comparisons of the 4T data for the scaled F-16 wing/body combination at $z = -1.0$ in., $\alpha = 0^\circ$, $M_\infty = 0.925$.
- Figure 11. Comparison of body surface pressure coefficients from 4T and 16T tests for scaled F-16 wing/body combination.
- Figure 12. Comparisons of theoretical and experimental results for the local upwash angle for flow past the scaled F-16 wing/body combination at $M_\infty = 0.925$ and $\alpha = 0^\circ$.
- Figure 13. Comparisons of theoretical and experimental results for the local sidewash angle for flow past the scaled F-16 wing/body combination at $M_\infty = 0.925$ and $\alpha = 0^\circ$.
- Figure 14. Comparisons of theoretical and experimental results for the local upwash angle for flow past the scaled F-16 wing/body combination at $M_\infty = 0.925$ and $\alpha = 0^\circ$.

LIST OF FIGURES (concluded)

- Figure 15. Comparisons of theoretical and experimental results for the local sidewash angle for flow past the scaled F-16 wing/body combination at $M_\infty = 0.925$ and $\alpha = 0^\circ$.
- Figure 16. Comparisons of theoretical and experimental results for the local upwash angle for flow past the scaled F-16 wing/body combination at $M_\infty = 0.925$ and $\alpha = 5^\circ$.
- Figure 17. Comparisons of theoretical and experimental results for the local sidewash angle for flow past the scaled F-16 wing/body combination at $M_\infty = 0.925$ and $\alpha = 5^\circ$.
- Figure 18. Comparisons of theoretical and experimental results for the local sidewash and upwash angles for flow past the scaled F-16 wing/body combination at $M_\infty = 0.975$ and $\alpha = 0^\circ$.
- Figure 19. Comparisons of theoretical and experimental results for the local sidewash and upwash angles for flow past the scaled F-16 wing/body combination at $M_\infty = 0.975$ and $\alpha = 5^\circ$.
- Figure 20. Illustration of wing-body/pylon/stores model configuration.

INTRODUCTION

The purpose of this paper is to present a progress report on a combined theoretical/experimental investigation directed toward developing a rational predictive method for determining external store trajectories at transonic speeds. The study, jointly sponsored by the Air Force Office of Scientific Research, the Air Force Armament Laboratory, and the Air Force Flight Dynamics Laboratory, is directed principally toward fighter/bomber aircraft operating at transonic conditions. The primary objective of this first phase of the investigation is the development of an accurate and rapid predictive method for the computation of the three-dimensional transonic flow field due to the parent aircraft. During a subsequent phase of the study, which is currently underway, the extension of that method to include pylon-mounted single stores located under the fuselage and/or under the wings is being carried out.

In view of the successful external store trajectory methods recently developed for purely subsonic (ref. 1) and purely supersonic (ref. 2) flow, noting in particular the favorable applications of the subsonic method (refs. 3-5), there is no doubt of the utility of such predictive techniques for establishing weapon system design criteria. These methods are capable not only of enhancing the performance and safety of weapons delivery, but they also provide a means for reducing the time required for both wind-tunnel and full-scale flight tests relating to store certification programs.

For applications at transonic speeds, the development of such techniques becomes significantly more complicated, and a more intensive development of the basic theoretical solution method is required due to the essential nonlinear character of the flow. The linear methods previously developed for the subsonic and supersonic problems (refs. 1,2) do not apply and finite difference solutions are necessary. However, for the complex geometries typical of realistic external store/fighter-bomber configurations, together with the large number of separate cases usually required for a trajectory analysis, the exclusive use of three-dimensional finite-difference methods is not practical. These facts identify the primary constraints on any transonic external store predictive method, i.e., it must be capable of predicting at an engineering level the essential nonlinear features of transonic flow, while remaining computationally economical so as not to severely limit its use as a design tool. Additionally, the method must possess the capability of treating the complex geometries characteristic of the multiple pylon/store combinations employed with modern fighter/bombers. The only method currently capable of accomplishing this, on a

$$(1 - M_\infty^2) (\phi_B)_{xx} + (\phi_B)_{yy} + (\phi_B)_{zz} = \frac{M_\infty^2}{U_\infty} \left[\left(1 + \frac{\gamma-1}{2} M_\infty^2 \right) \phi_{Bx}^2 + \phi_{By}^2 + \phi_{Bz}^2 \right] x$$

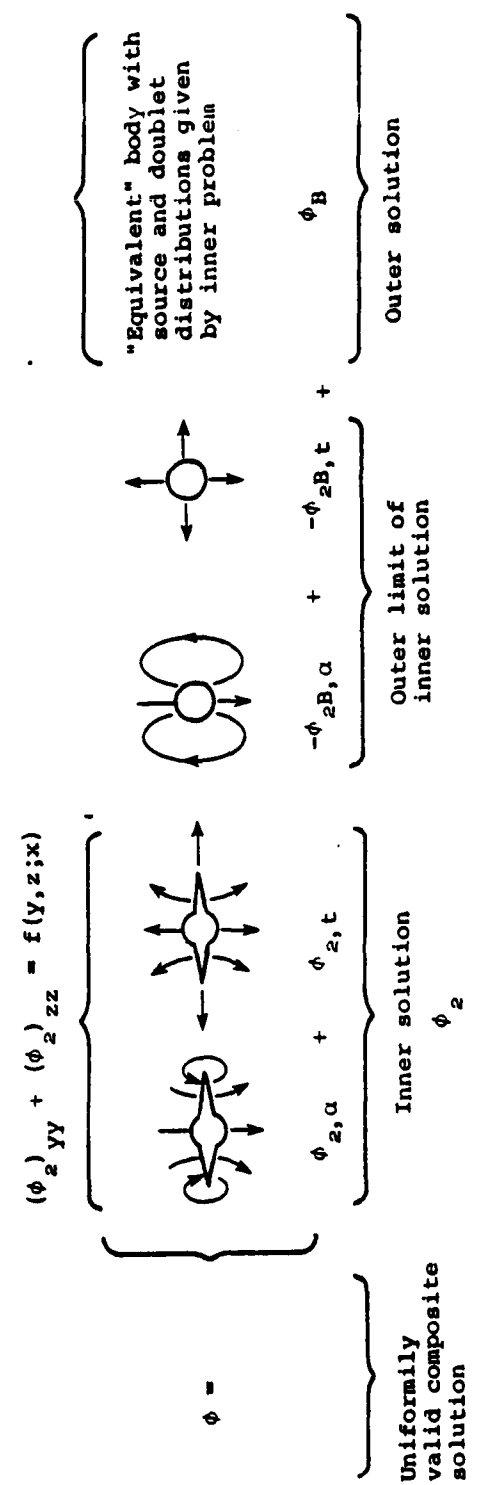
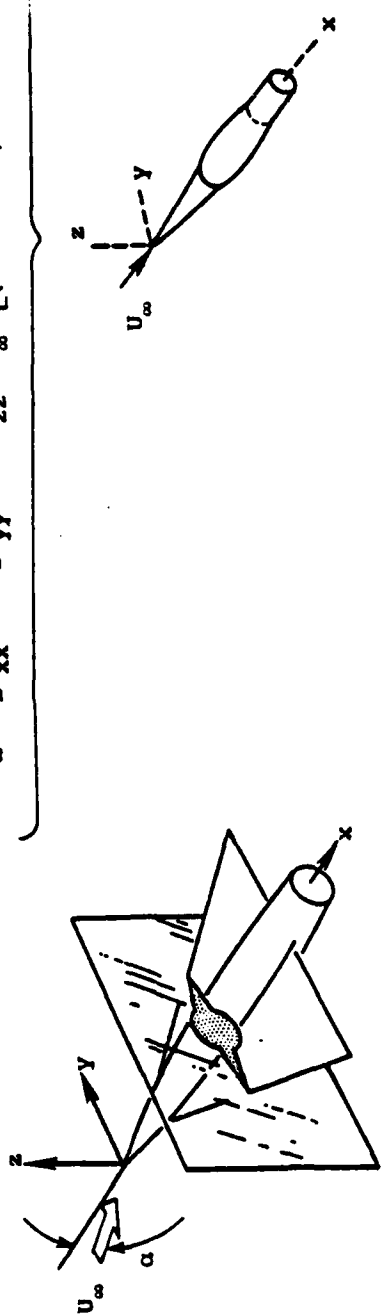


Figure 1.- Schematic representation of transonic equivalence rule for slender wings and bodies.

AIRCRAFT	WING SPAN (ft.)	LENGTH (ft.)	EST. WGT. (lb.)	λ	α	τ	σ	ϵ	σ^*
F-4B	38.5	58.3	50,000	0.33	0.052	0.046	0.046	0.063	0.20
F-15	42.8	63.9	40,000	0.33	0.033	0.088	0.021	0.087	0.21
YF-16	30.0	47.0	17,500	0.32	0.029	0.057	0.022	0.067	0.17

$$\lambda = b/l$$

$$\alpha = F_{\max}^* / q_{\infty} V_{\infty}^2 b^2$$

$$\tau = S_{\max} / bl$$

where

b = semispan

F^* = integrated lateral force

l = body length

M_{∞} = free stream Mach number

S = cross-sectional area

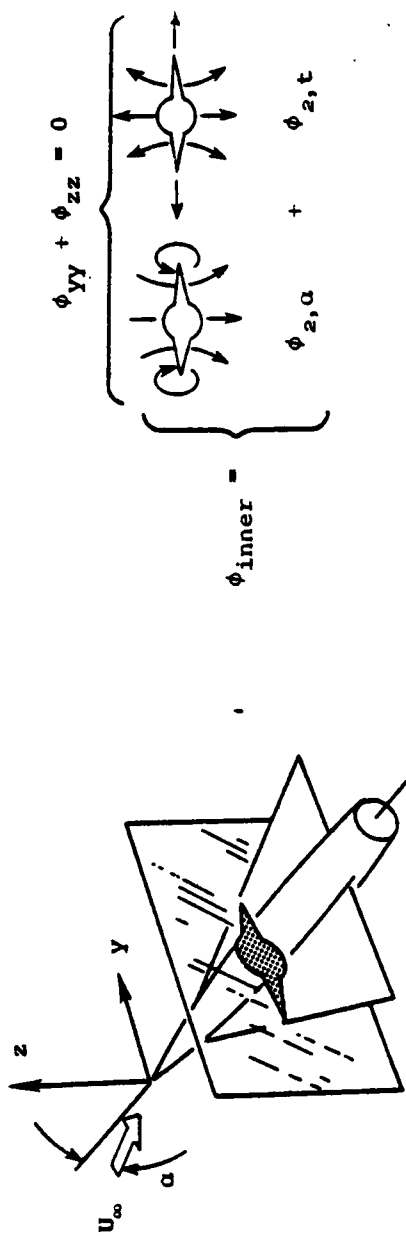
V_{∞} = free-stream velocity

$$\sigma = \alpha \lambda^2 / 2 \tau^{1/2}$$

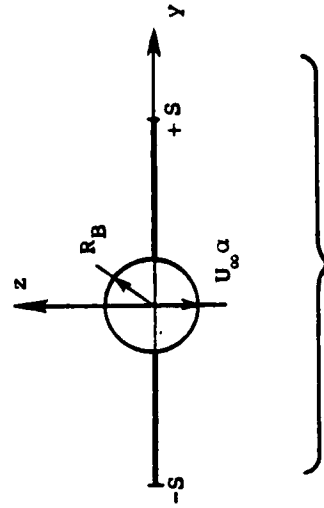
$$\epsilon = [M_{\infty}^2 (\gamma + 1) \tau \lambda^2]^{1/2}$$

$$\sigma^* = M_{\infty} (\gamma + 1)^{1/2} \epsilon \tau^{1/2}$$

Figure 2.- Summary of transonic equivalence rule parameters for several fighter/bomber aircraft.

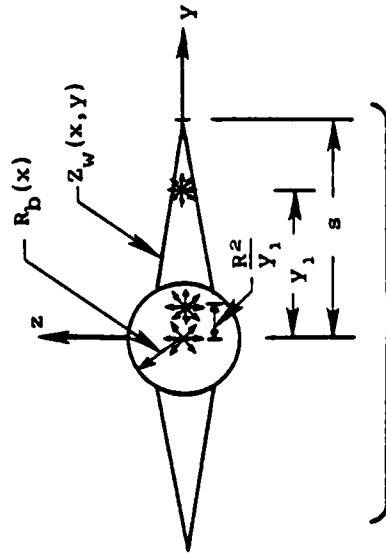


Lifting problem - $\phi_{2,\alpha}$



Spreiter's analytic solution for circular body and zero-thickness wings

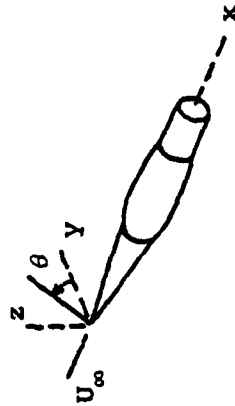
Thickness problem - $\phi_{2,t}$



Stocker's method of distributed singularities

Figure 3.- Solution procedures developed for model midwing/circular body combination - inner problem.

$$(1 - M_\infty^2) \phi_{xx} + \phi_{yy} + \phi_{zz} + \frac{M_\infty^2}{U_\infty} \left[\left(1 + \frac{\gamma - 1}{2} M_\infty^2 \right) \phi_x^2 + \phi_y^2 + \phi_z^2 \right] x$$



Expansion for $\sigma_* < 1$

$$\phi_{\text{outer}} = \phi_0(x, r) + \sigma_* \psi_1(x, r) \sin \theta + O(\sigma_*^2, \sigma_*^2 \ln \sigma_*)$$

Solution Method

PDE for ϕ_0 is usual nonlinear transonic small-disturbance axisymmetric equation

PDE for ψ_1 is linear with nonconstant coefficients dependent on ϕ_0

(ϕ_0, ψ_1) both solved by finite-difference SLOR using Murman-Cole type-dependent difference operators

Figure 4.- Solution procedures developed for outer problem-thickness dominated flow.

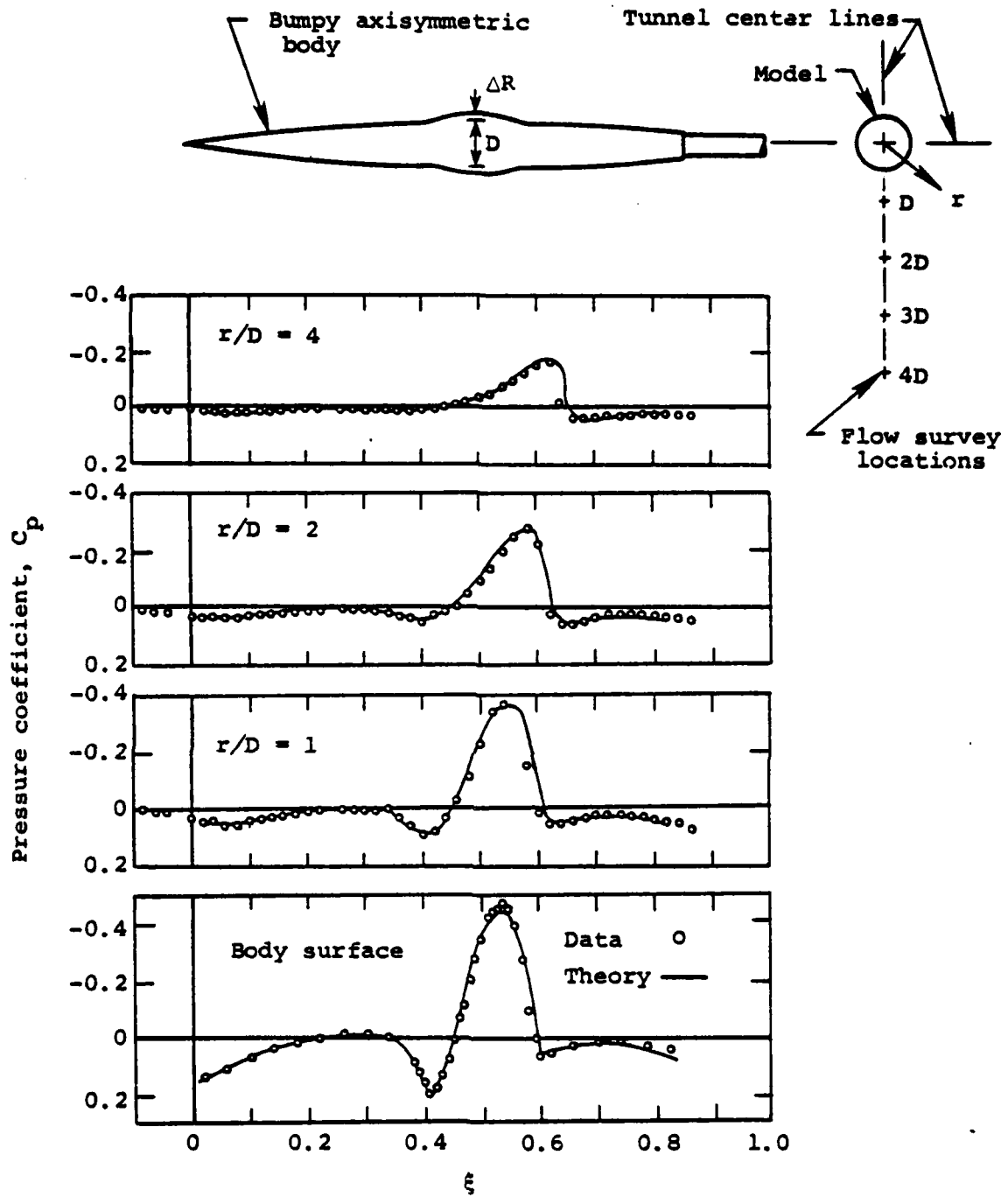


Figure 5.- Comparison of theoretical results using outer flow solution procedures with data at $M_\infty = 0.975$ for a parabolic-arc body of revolution with a bumpy midsection; $D/l = 1/14$ and $\Delta R/D = 1/5$.

rational basis, is the transonic equivalence rule technique, and that method is discussed in the following section.

The overall plan of the present investigation is to develop the predictive capability in a framework similar to that used in the successful subsonic and supersonic programs (refs. 1,2). This involves the development of the theory in a systematic, step-by-step fashion, aided by specifically-designed, parallel wind-tunnel tests to check and verify the predictive method at significant points. The tasks accomplished during the completed initial phase are discussed in detail below and include the preliminary development of the theoretical model, the design and construction of the wing-body models, separate wind-tunnel tests in the AEDC 4t and 16T tunnels, verification of the quality of the data and choice of test parameters, and the initial comparisons of the data and theory.

THEORETICAL PREDICTIVE METHOD

TRANSONIC EQUIVALENCE RULE

Although the theoretical essentials of the transonic equivalence rule have been known for some time (refs. 6,7), it has been only recently that a fundamental mathematical study and extension of the technique (refs. 8-10) removed some of the previous limitations and resulted in a method capable of general three-dimensional transonic flow field prediction. The major contribution of the work in references 8-10 is the discovery that the transonic flow about lifting, three-dimensional configurations possesses, under reasonably mild restrictions satisfied by most modern transonic fighter or transport aircraft, a particularly simple structure and symmetry. The flow field has two distinct regions: an inner, linear region similar to that in slender-body theory; and an outer, nonlinear region governed by a transonic, small-disturbance equation. The behavior of the flow in the outer, nonlinear region is "equivalent to" that produced by a line distribution along the body axis of a combination of sources related to the total cross-sectional area, axial lift distribution, and spanwise wing loading, and doublets related to the axial lift distribution.

The theoretical essentials of the equivalence rule are summarized schematically in figure 1, which exhibits the breakdown of the total solution into the various component problems. The total solution is shown as decomposed into three categories: the inner solution ϕ_2 , indicated by the translating and expanding cross sections in the y,z plane; the outer or far field behavior of the inner solution, indicated by the translating and expanding circles; and the

Nose Coordinates		6-percent Airfoil		6-percent Airfoil		Surface Pressure Locations	
X, in.	Y, in.	Percent Chord	Y/c, percent	Percent Chord	Y/c, percent	Orifice	X, in.
0.0	0.0	0.0	0.0	0.0	0.0	1	3.00
0.5	0.162	2.5	0.650	0.5	0.928	2	4.00
1.0	0.313	5.0	1.096	0.75	1.126	3	5.00
1.5	0.453	7.5	1.472	1.25	1.436	4	6.00
2.0	0.583	10.0	1.800	2.50	1.962	5	7.00
2.5	0.703	15.0	2.350	5.0	2.626	6	8.00
3.0	0.813	20.0	2.798	7.5	3.182	7	8.75
3.5	0.912	30.0	3.452	10.0	3.648	8	9.50
4.0	1.000	40.0	3.842	15.0	4.388	9	10.25
4.5	1.078	50.0	3.996	20.0	4.948	10	11.00
5.0	1.146	60.0	3.910	25.0	5.374	11	11.75
5.5	1.203	65.0	3.770	30.0	5.684	12	12.50
6.0	1.250	70.0	3.554	35.0	5.890	13	13.25
6.5	1.287	80.0	2.812	40.0	5.992	14	14.00
7.0	1.313	85.0	2.170	45.0	5.984	15	14.75
7.5	1.328	90.0	1.476	50.0	5.850	16	15.50
8.0	1.333	95.0	0.738	55.0	5.586	17	16.25
		100.0	0.0	60.0	5.204	18	17.00
				65.0	4.728	19	17.75
				70.0	4.174	20	18.50
				75.0	3.550	21	19.25
				80.0	2.874	22	20.00
				85.0	2.166	23	21.00
				90.0	1.454	24	22.00
				95.0	0.740	25	23.00
				100.0	0.0		

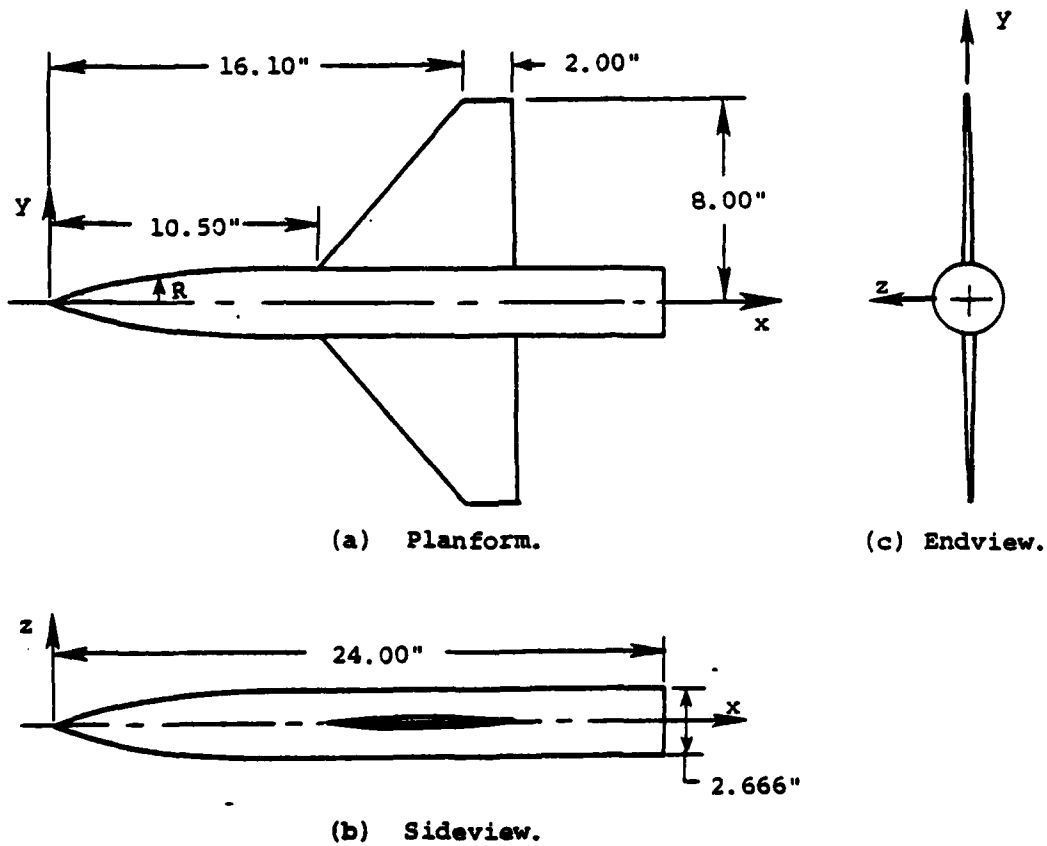


Figure 6.- Details of model wing-body combination.

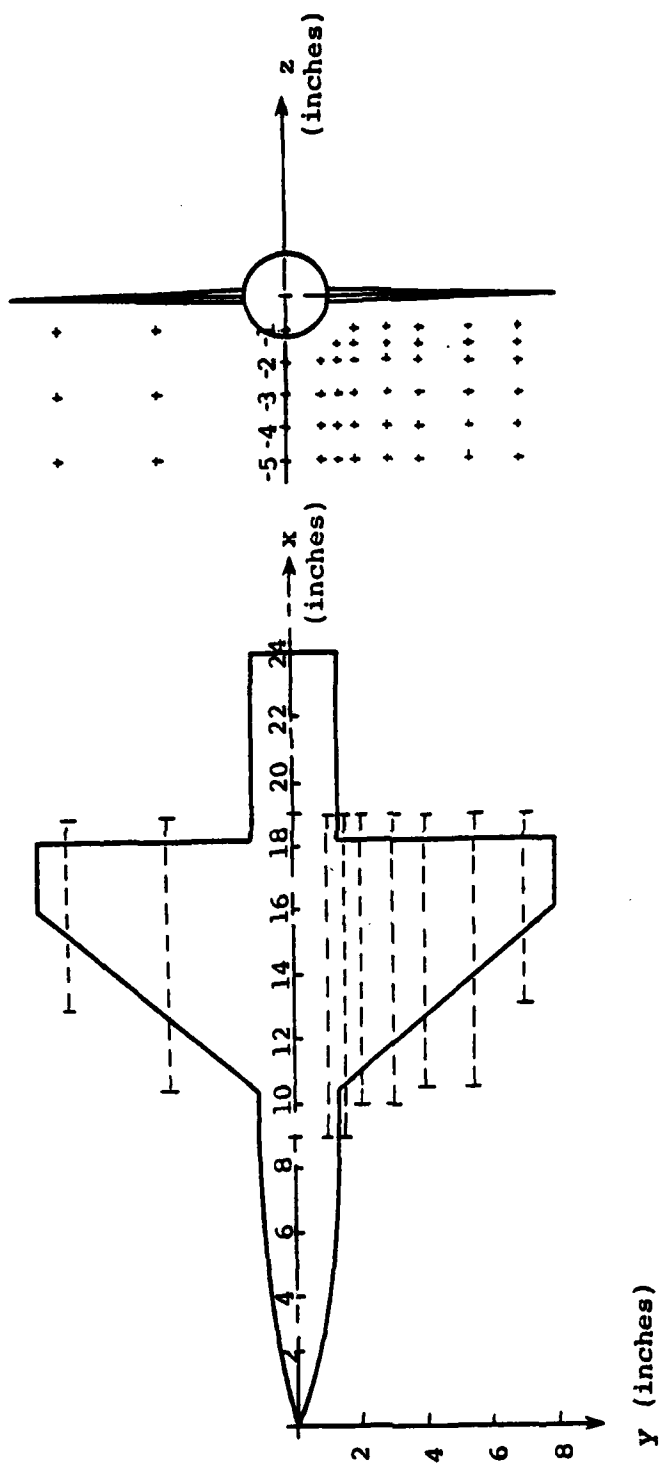


Figure 7.- Flow-field survey locations for model wing/body test in AEDC 4T tunnel.

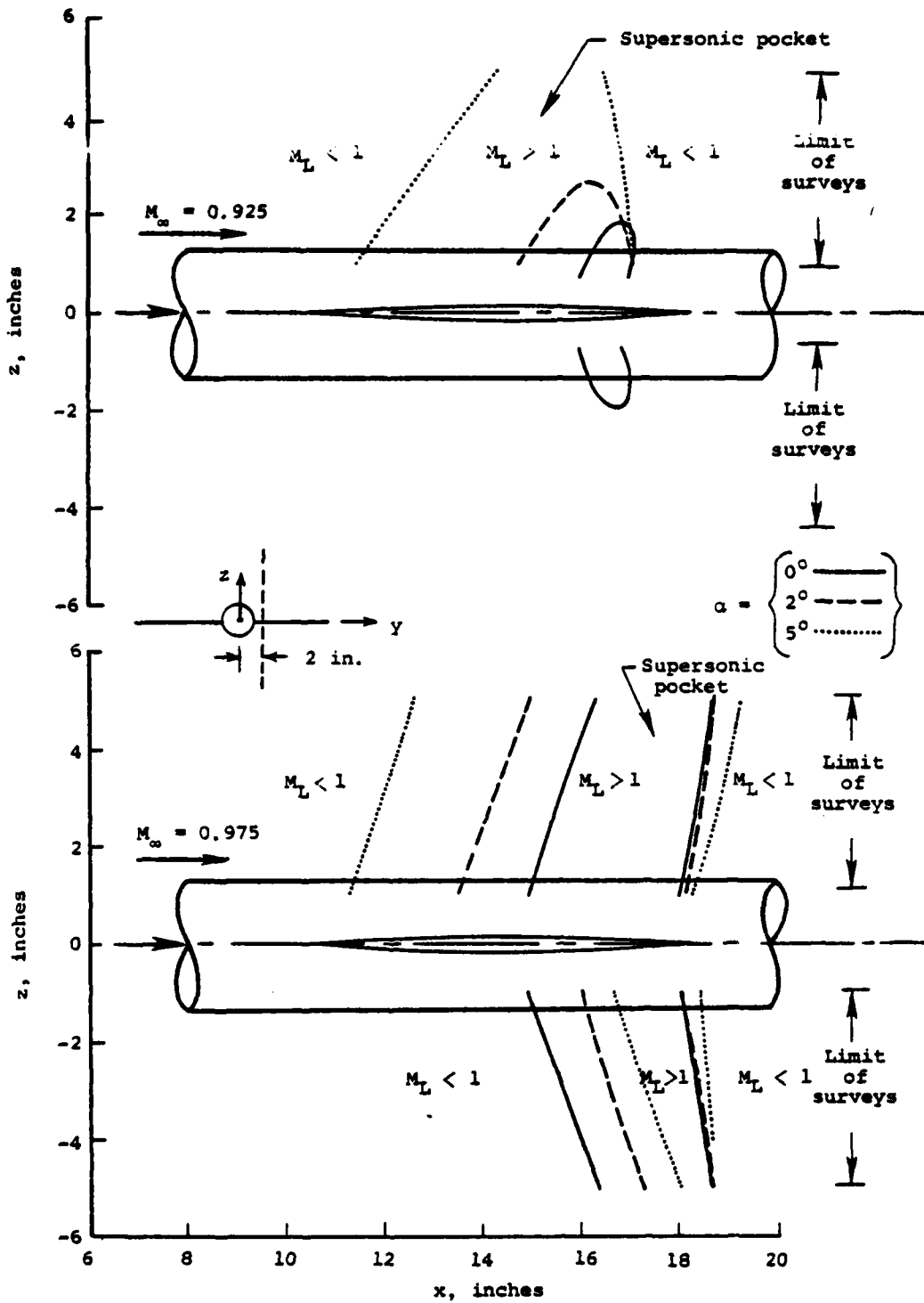


Figure 8.- Size of supersonic pockets on pressure and suction side of wing at the spanwise location $y = 2$ inches.

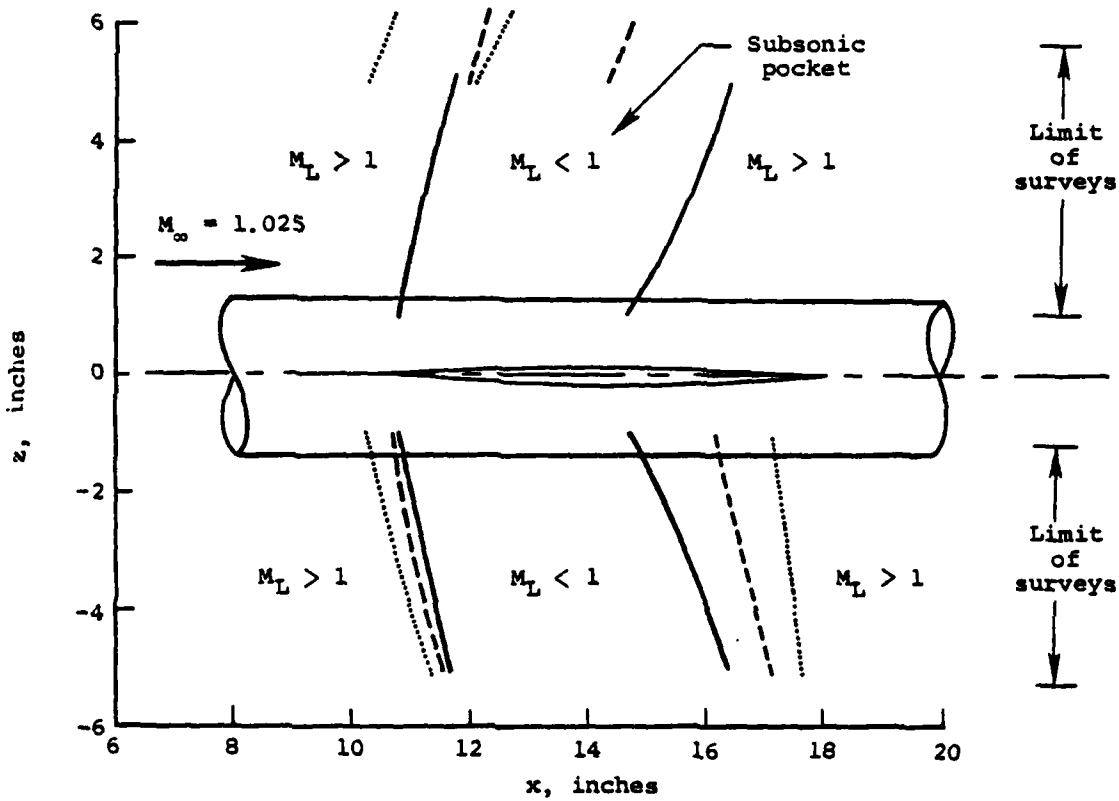
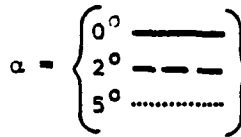
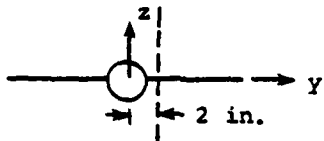
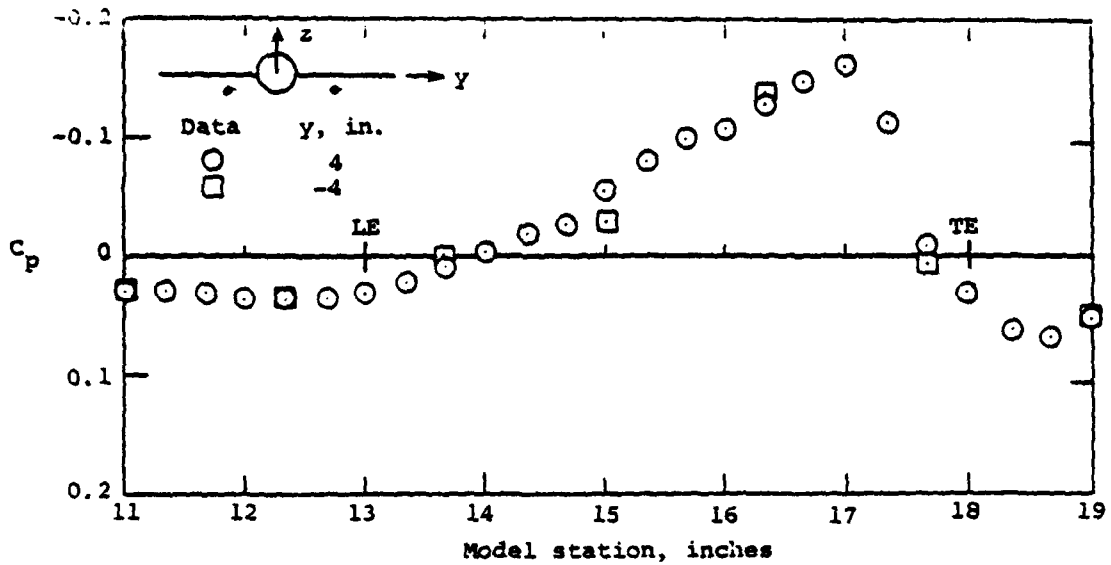
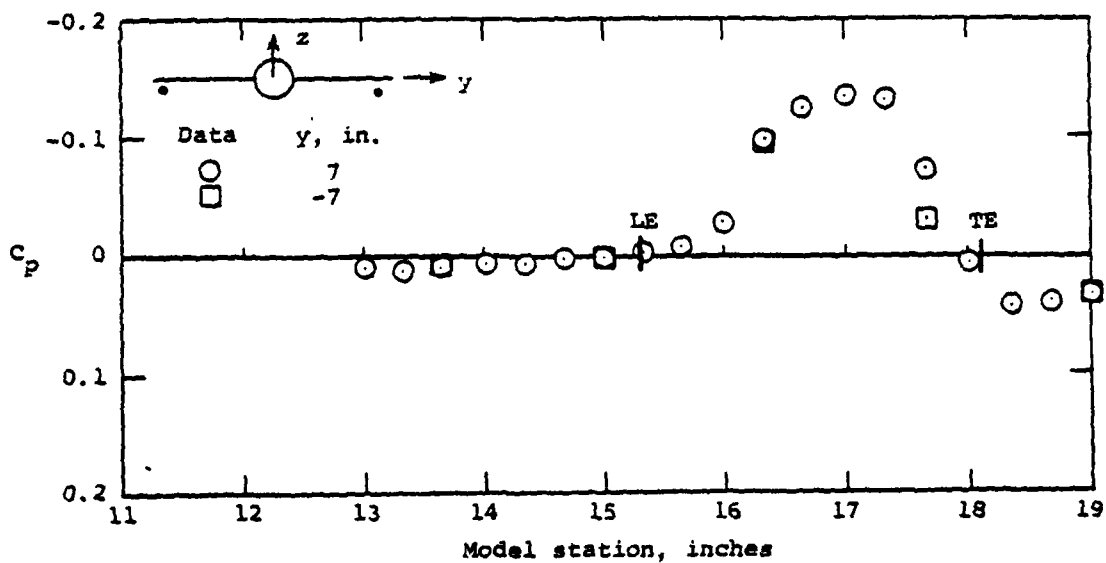


Figure 9.- Size of subsonic pockets on pressure and suction side of wing at the spanwise location $y = 2$ inches for various angles of attack at $M_\infty = 1.025$.

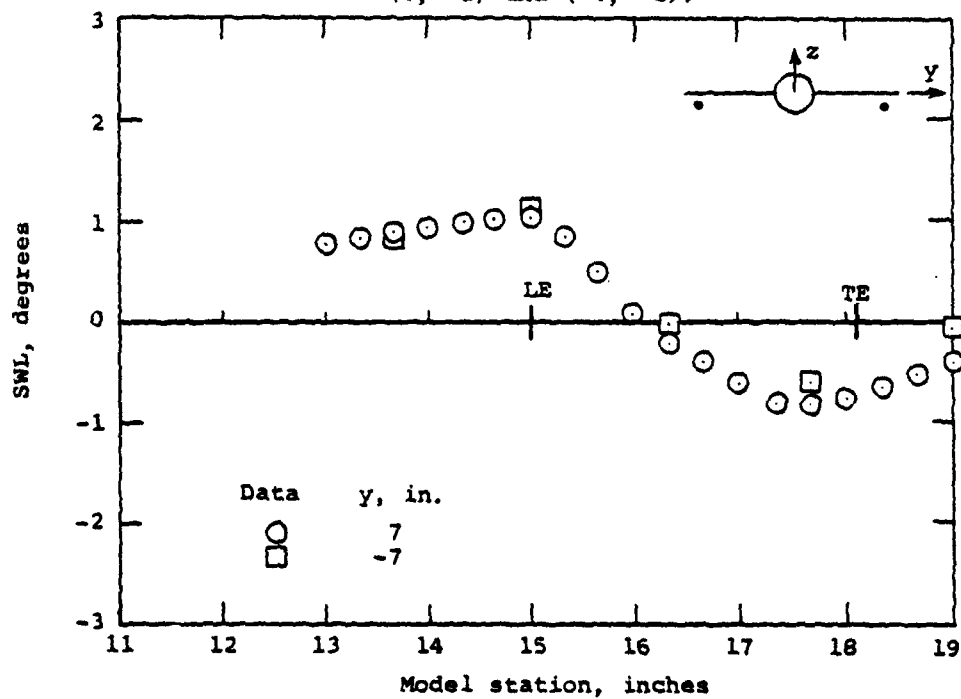
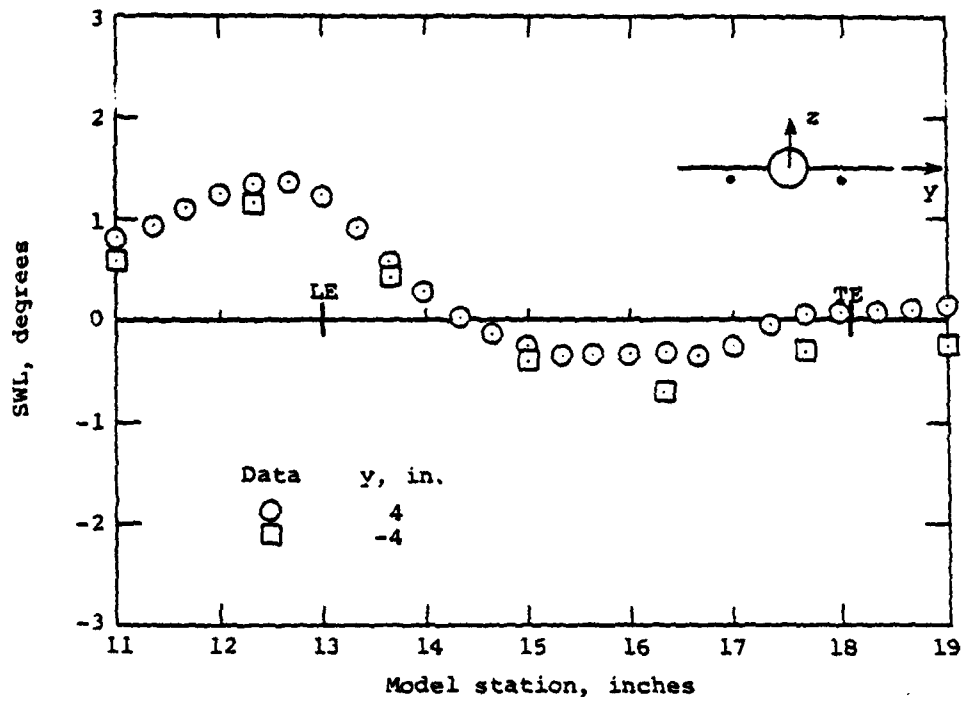


(a) Pressure coefficient comparison for (y,z) equal to $(4, -1)$ and $(-4, -1)$.



(b) Pressure coefficient comparison for (y,z) equal to $(7, -1)$ and $(-7, -1)$.

Figure 10.- Side-to-side symmetry comparisons of the 4T data for the scaled F-16 wing/body combination at $z = -1.0$ in., $\alpha = 0^\circ$, $M_\infty = 0.925$.



(d) Sidewash comparison for (7, -1) and (-7, -1).

Figure 10.- Continued.

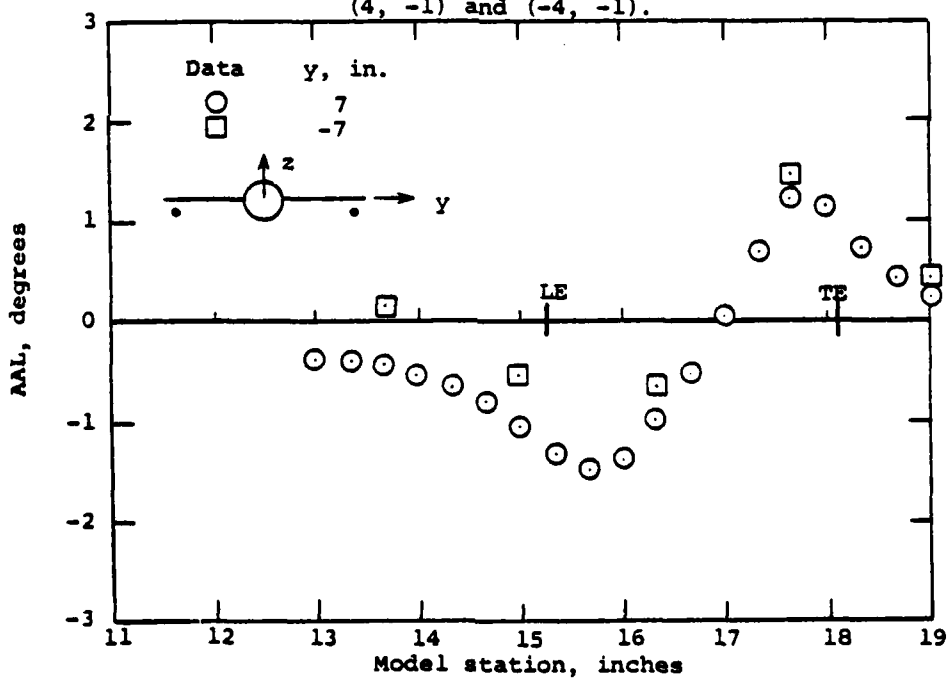
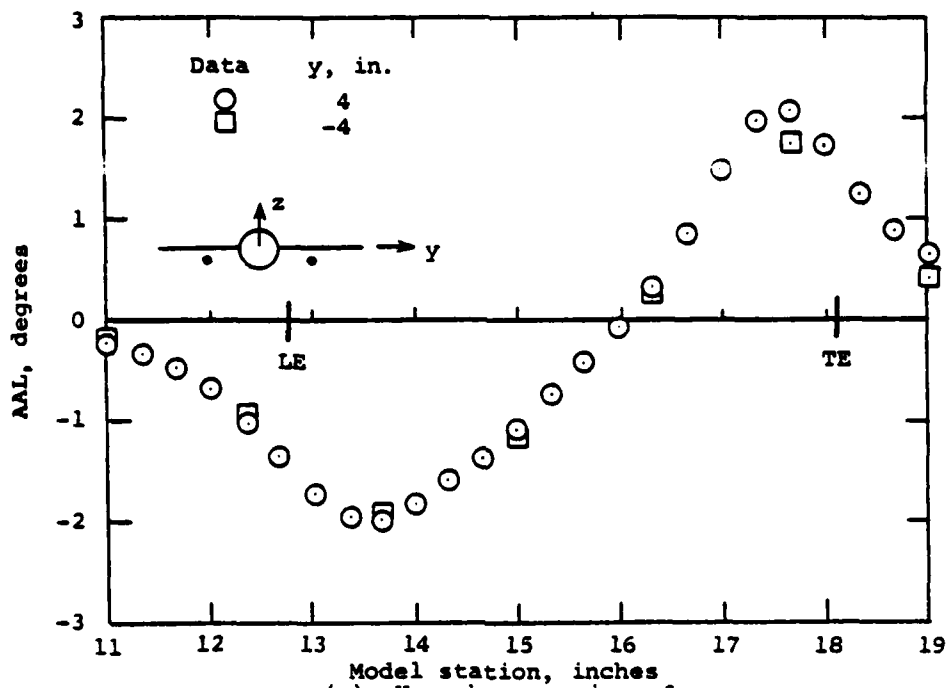


Figure 10.- Concluded.

outer solution ϕ_B , indicated by the axisymmetric flow over an "equivalent" body whose singularity (source, doublet, etc.) distributions match those determined by the outer behavior of the inner solution.

The inner solution accounts for the geometrically complicated details of the aircraft and satisfies the surface flow tangency condition in the crossflow (y,z) plane at each x -station. The governing equation, as indicated in figure 1, is linear so that superposition is possible. Consequently, the thickness $\phi_{2,t}$ and lift $\phi_{2,\alpha}$ effects can be treated separately.

The structure of the equivalence rule is governed principally by a parameter σ_* (refs. 8,9) involving a combination of the configuration thickness ratio, lift-force parameter, and leading-edge sweep, and represents essentially the ratio of lift/thickness effects. Depending on the magnitude of σ_* , the nonlinear, outer problem classifies into three distinct domains:

- 1) $\sigma_* \ll 1$, thickness dominated;
- 2) $\sigma_* = O(1) \neq 0$, intermediate; and
- 3) $\sigma_* \gg 1$, lift dominated.

In the thickness-dominated domain, the basic, nonlinear outer flow is axisymmetric; that is, determined principally by a line source distribution, and the lift and other asymmetric effects can be determined by a linearized analysis. In the lift-dominated domain, the nonlinear outer flow is no longer axisymmetric, but rather has a structure determined by both a line source and line doublet distribution. Consequently, its solution must simultaneously satisfy the source and doublet inner boundary condition. The intermediate domain possesses essentially the same structure as the lift-dominated case and must be solved using the same techniques.

In order to investigate both the typical cruise flight conditions and ranges of the transonic similarity parameters for transonic store separation from current fighter-bombers, calculations of these quantities were made for a number of aircraft at transonic cruise conditions. The results of the calculations for the F-4B, F-15, and YF-16 are of interest and have been included in figure 2. Most noteworthy is the fact that the transonic similarity parameter σ_* is small, indicating that the most important calculations for this study lie in the thickness-dominated ($\sigma_* \ll 1$) rather than lift-dominated ($1/\delta_* \ll 1$) regime. This is quite significant, since in this regime, it is sufficient to consider the first-order thickness and lift solutions in the inner flow.

Moreover, the lift (and other asymmetric properties) can be treated linearly in the outer flow.

SOLUTION PROCEDURES DEVELOPED

Because of the different character of the inner and outer regions, separate solution procedures are required for each. As indicated in figure 3, for the inner region Laplace equation solutions are needed for the thickness problem $\phi_{2,t}$ and the lift problem $\phi_{2,\alpha}$. For the simplified wing-body configurations considered in this study, the method of distributed singularities developed by Stocker (ref. 11) is directly applicable and convenient for determining the thickness problem. As shown in the sketch in the lower left of figure 3, it models wing thickness by placing a continuous distribution of two-dimensional sources along the wing chordal plane together with their appropriate images within the body. For the lift problem, the analytic conformal mapping solution determined by Spreiter (ref. 12) for a circular body with mid-mounted zero-thickness wings is employed.

Determination of the outer problem requires solution of the three-dimensional nonlinear transonic differential equation shown in figure 4. For the thickness-dominated regime characteristic of the flows considered in this study, the outer solution can be expanded in terms of the two dependent quantities (ϕ_0, ψ_1) as shown in figure 4. Here ϕ_0 represents the primary axisymmetric flow component and ψ_1 the correction due to lift. The governing partial differential equation for ϕ_0 is the usual nonlinear axisymmetric transonic small-disturbance equation, while that for ψ_1 is linear but with non-constant coefficients dependent on ϕ_0 . The solution procedure employed for both of these components is a finite-difference successive line over-relaxation (SLOR) procedure using Murman-Cole type-dependent difference operators. To verify the nonlinear solution procedures, a number of cases were run for a variety of equivalent body profiles. One of the most severe tests of the outer flow solution procedures, and which relates directly to the bumpy equivalent bodies expected from the present study, is illustrated in figure 5 and displays the typically good results obtained. The case shown is for the axisymmetric flow at $M_\infty = 0.975$ past a bumpy body composed of a basic parabolic-arc profile with thickness ratio $D/l = 1/14$ together with a sinusoidal bump centered about the midpoint with $\Delta R/D = 1/5$. Comparisons with the data of reference 13 display excellent agreement.

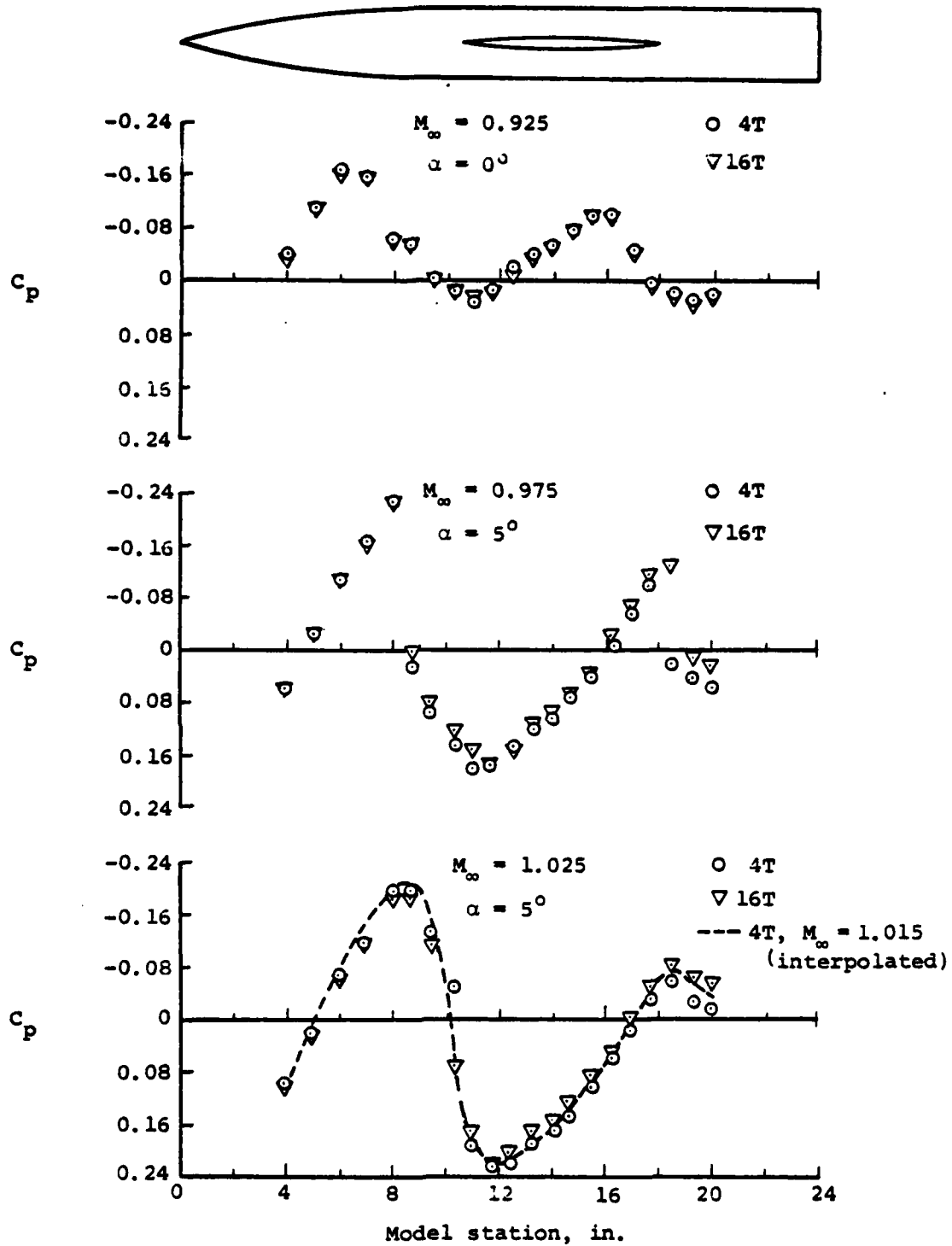


Figure 11.- Comparison of body surface pressure coefficients from 4T and 16T tests for scaled F-16 wing/body combination.

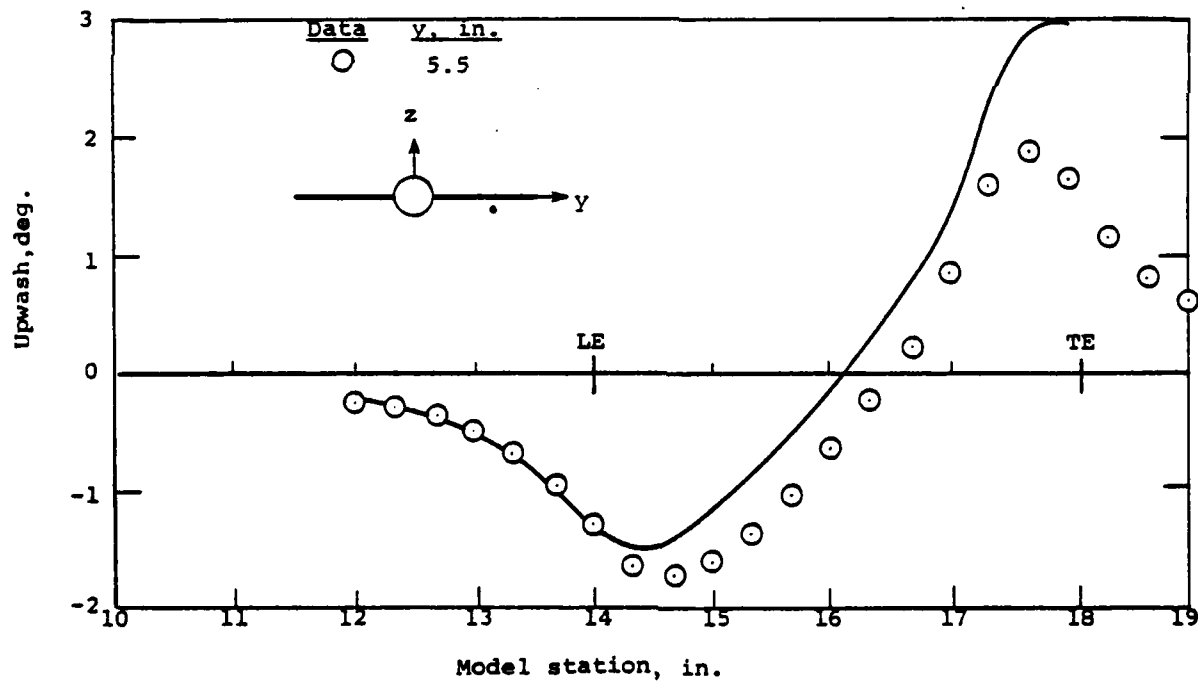
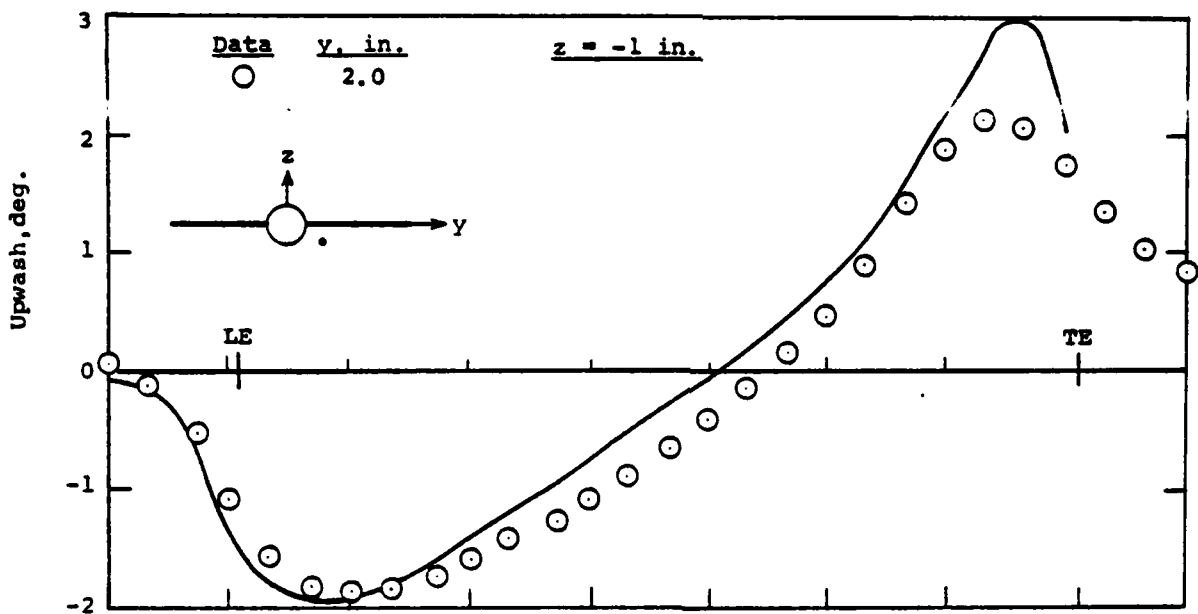


Figure 12.- Comparisons of theoretical and experimental results for the local upwash angle for flow past the scaled F-16 wing/body combination at $M_\infty = 0.925$ and $\alpha = 0^\circ$.

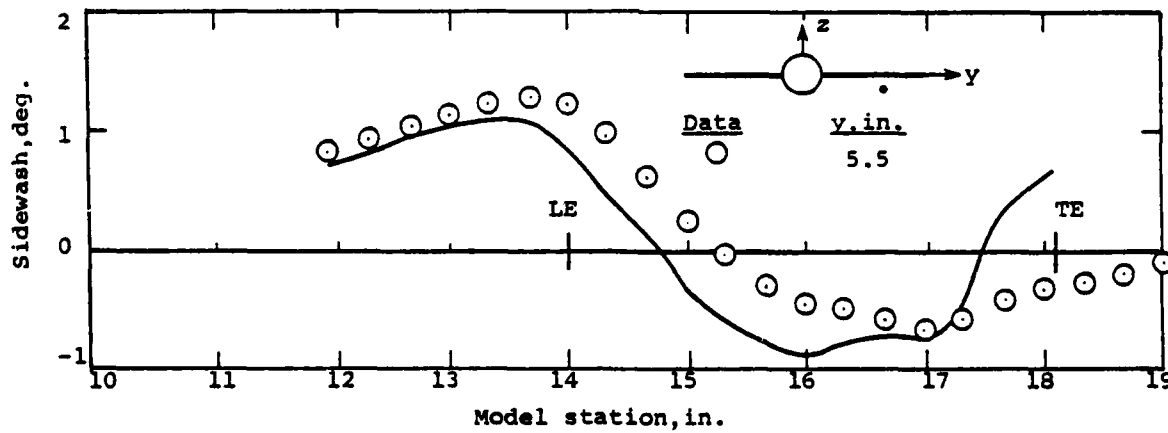
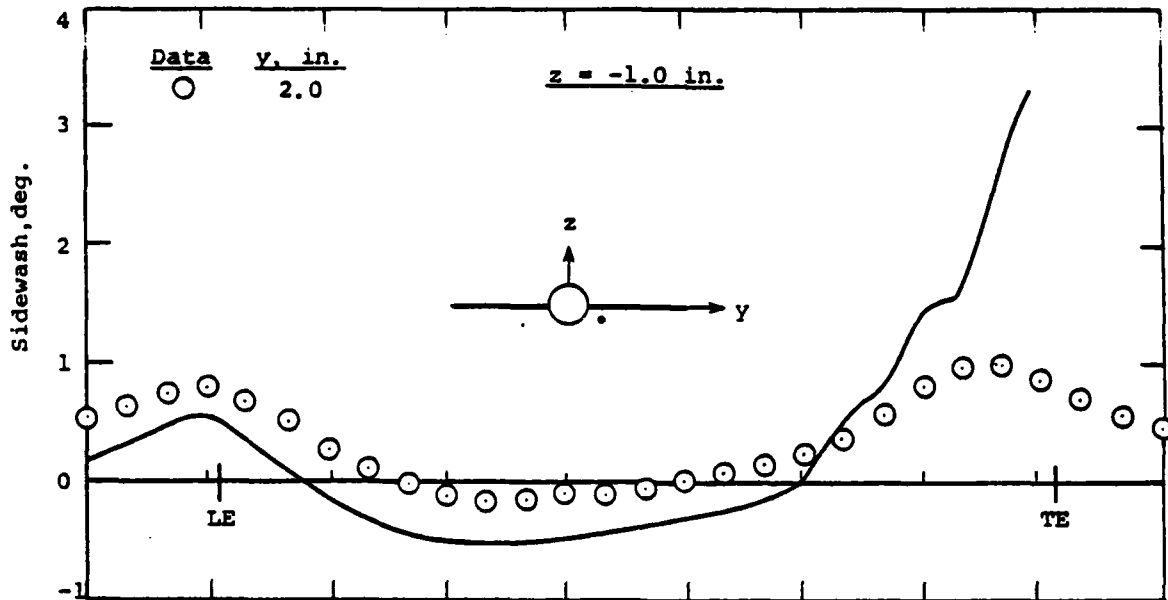


Figure 13.-Comparisons of theoretical and experimental results for the local sidewash angle for flow past the scaled F-16 wing/body combination at $M_\infty = 0.925$ and $\alpha = 0^\circ$.

EXPERIMENTAL PROGRAM

MODEL DESIGN

The design of the test model was constrained by the dual objectives of (1) testing a simplified but geometrically-related configuration characteristic of modern fighter-bombers, and (2) obtaining as wide a range as possible of the transonic similarity parameters. The model size was established by the conflicting requirements of minimizing wind-tunnel interference and maximizing pressure probe accuracy measurements. To provide a critical check of the equivalence rule theory, two different sets of wings having identical planforms are needed. This provides two different equivalent bodies to test the outer expansion procedure as well as two values of the lift/thickness (σ_*) parameter for each angle of attack.

The model chosen is illustrated in figure 6 and is an idealized 22.5:1 scale model of the F-16. The body is circular with a three-caliber parabolic-arc nose profile followed by a straight cylinder. The two sets of identical planform wings are mid-mounted, cropped delta wings having thickness only (zero camber and twist) profiles whose ordinates are based on (1) a scaled F-16 wing (4% thick), and (2) a NACA 65A006 airfoil. Thickness-only profile wings are necessary since the zero lift situation ($\sigma_* = 0$) provides a critical check of the theory. Because of the significant dependence of the theory on lift, a force balance is included in the model. Twenty-five surface pressure taps are provided on the body surface primarily to check wind-tunnel interference.

TEST PROGRAM DESCRIPTION

Two separate tunnel tests were performed and are reported in detail in reference 14. The initial entry was in the AEDC 4T transonic tunnel where the primary data were obtained. A subsequent entry in the AEDC 16T transonic tunnel was made to obtain a limited amount of repeat data for assessing both wind-tunnel interference as well as tunnel flow quality effects. To obtain all of the important flow conditions of interest in transonic flight - from subcritical to slightly supercritical, to strongly supercritical, to mildly supersonic - testing was done in the 4T tunnel at three Mach numbers ($M_\infty = 0.925, 0.975, 1.025$) and three angles of attack ($\alpha = 0^\circ, 2^\circ, 5^\circ$). The principal flow field data were taken using the Captive Trajectory System (CTS) at typical store locations on the pressure side of the wing. Secondary data were taken on the suction side of the wing in order to obtain additional diagnostic information for evaluating the analytical model. Figure 7 displays the flow field survey

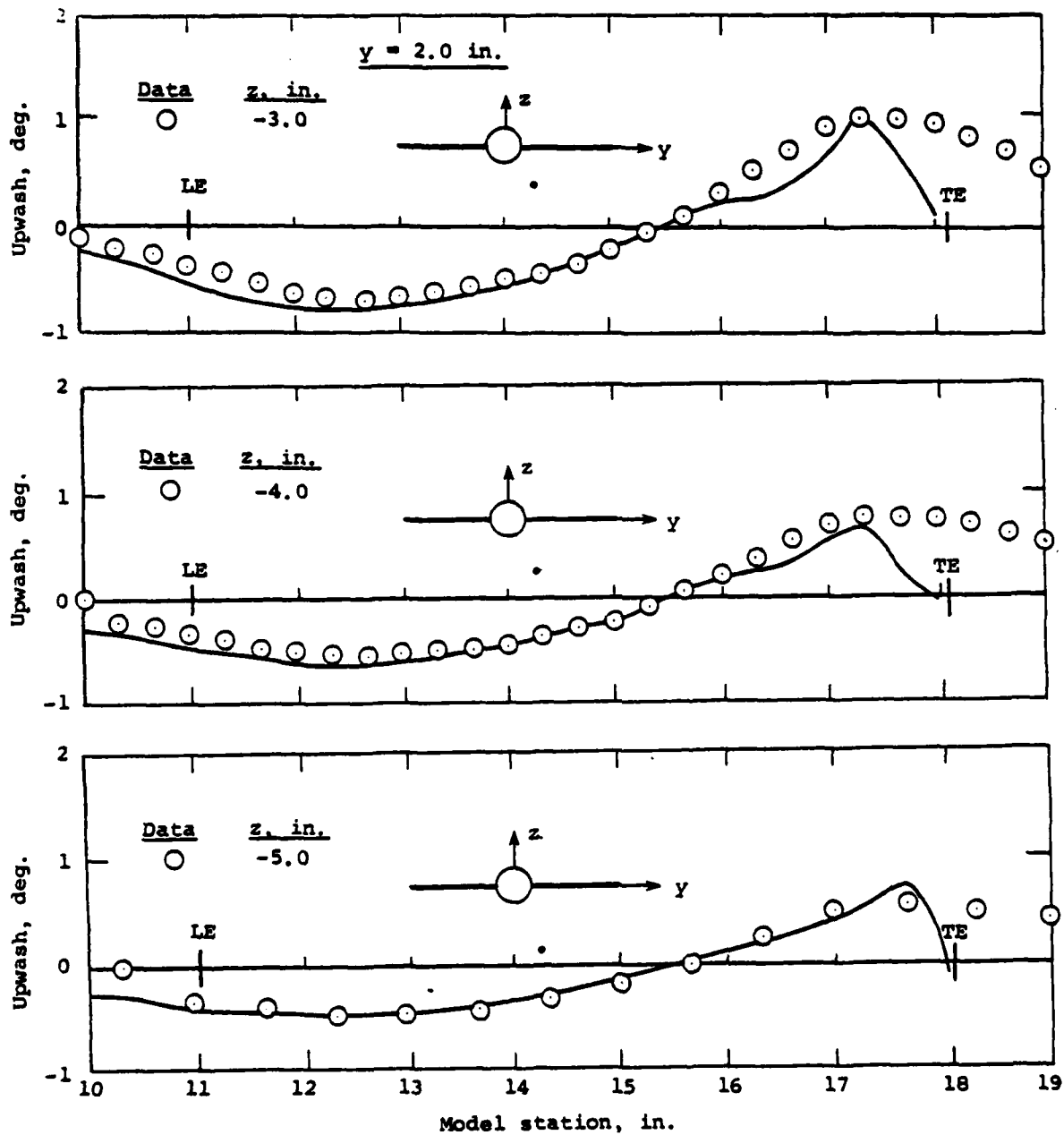


Figure 14.- Comparisons of theoretical and experimental results for the local upwash angle for flow past the scaled F-16 wing/body combination at $M_\infty = 0.925$ and $\alpha = 0^\circ$.

locations for the inner flow field. Symmetric side-to-side surveys were made to assess flow quality and repeatability. Outer flow field surveys were also taken on a cylindrical surface as far from the model centerline as the CTS would allow ($R = 14.14$ inches) to provide measured outer boundary conditions as input to the theoretical model to evaluate wind-tunnel wall interference.

TEST RESULTS

A thorough survey of the 4T experimental results has verified that the test parameters were exceptionally well selected in view of providing as wide a range of transonic phenomena as possible. The data display flow conditions from subcritical to slightly supercritical, to strongly supercritical, to mildly supersonic, as were desired. For the two subsonic free stream Mach numbers, figure 8 illustrates this fact and displays the growth of the supersonic pockets on the pressure and suction sides of the wing. The results are for an (x,z) plane located at the spanwise location $y = 2$ inches (25% semispan) and are for the model with the scaled F-16 wing. The figure on the top indicates the extent of the supersonic zone at $M_\infty = 0.925$ for the three angles of attack, while corresponding results for $M_\infty = 0.975$ are shown in the bottom plot. The symbol M_L denotes the local Mach number. Since the vertical limits of the inner flow surveys was $1 \leq |z| \leq 5$ inches, the maximum lateral locations of the larger supersonic pockets on the suction side were beyond the last inner survey location at $z = 5$ inches. However, only for the $M_\infty = 0.975$, $\alpha = 5^\circ$ case did the pocket extend out to the outer flow survey location at $z = 14$ inches. These results indicate the extreme sensitivity of the flow at supercritical conditions. Analogous results for $M_\infty = 1.025$ are shown in figure 9 which displays the variation and growth of the embedded subsonic pocket. Of particular note in both figures 8 and 9 is that, at modest angles of attack, flow conditions on the pressure side of the wing remain primarily subsonic for a wide range of conditions.

An indication of the quality of the data obtained in the 4T tunnel is indicated in figure 10 which displays side-to-side symmetry comparisons for flow surveys of pressure, side-wash, and upwash at $M_\infty = 0.925$ and $\alpha = 0^\circ$ at a vertical location just under the wing ($z = 1$ inch) and at the two spanwise locations $z = \pm 4$, ± 7 inches which are 50% and 88%, respectively, of the semispan. In these surveys, the x location of the local leading and trailing edges of the wing are denoted by LE and TE. The comparisons indicate extremely good flow field symmetry and are typical of the 4T data. The slight discrepancy of one-quarter of a degree observed

in the upwash at the extreme spanwise location $z = \pm 7$ inches can actually be traced to tunnel flow quality, but is already at the limits of the accuracy attainable (ref. 14) for these tests.

In order to achieve the range of flow conditions desired for the aerodynamically clean model configurations tested, the necessity of selecting two of the test Mach numbers so close to one ($M_\infty = 0.975, 1.025$) was unavoidable. Consequently, the question of whether significant wall interference effects were present in the data is quite pertinent. In addition, since subsequent tunnel entries are planned, establishment of the band of free-stream Mach numbers about $M_\infty = 1$ outside of which tunnel effects are small is essential.

An indication of the presence of wind-tunnel effects in the 4T data is provided by figure 11 which displays the comparison of body surface pressures obtained on the scaled F-16 wing/body combination from tests in the AEDC 4T and 16T tunnels. Indicated in the upper plot are the nonlifting results for $M_\infty = 0.925, \alpha = 0^\circ$, while corresponding lifting, pressure side results for $M_\infty = 0.975, \alpha = 5^\circ$ and $M_\infty = 1.025, \alpha = 5^\circ$ are displayed in the two lower plots. The results shown for the nonlifting $M_\infty = 0.925$ flow exhibit essentially no interference effects and are typical at this Mach number for lifting conditions as well. Those shown in the middle plot for the pressure side for $M_\infty = 0.975, \alpha = 5^\circ$ indicate some slight discrepancies, while similar pressure side results for $M_\infty = 1.025, \alpha = 5^\circ$ indicate somewhat larger discrepancies. As a direct indication of tunnel interference effects, however, these discrepancies are clouded by two additional factors present in the 16T data. These are (1) the model/sting support strut from the tunnel floor, and (2) flow quality effects. The 16T model support strut is known to be capable of causing a Mach number decrement of up to $M_\infty = 0.01$ in the test section (ref. 14). Compensation for that decrement has been attempted in the comparisons for the $M_\infty = 1.025$ results shown in the bottom figure. Here the 4T tunnel results for $M_\infty = 1.025$, shown as the circular symbol (\odot), have been extended to $M_\infty = 1.015$ (---) to compare with the 16T data by interpolating between the 4T results for $M_\infty = 0.975$ and 1.025. Some improvement is indicated but the discrepancies are not eliminated.

Our conclusions from the comparative tunnel tests are that (1) essentially no interference exists at $M_\infty = 0.925$, (2) at $M_\infty = 0.975$ and 1.025 minor interference exists on the pressure side of the wing/body, (3) the outer flow field measurements obtained afford a means of accounting for tunnel

effects in the theoretical model, and (4) the 4T data is adequate for testing the theoretical model.

COMPARISONS OF DATA WITH PRESENT THEORY

Some comparisons of flow field properties at locations typical of external store placement have been obtained with the present theory and 4T data for the scaled (4% thick) F-16 wing/body and are exhibited in figures 12 through 19. Figure 12 displays results at $M_\infty = 0.925$ and $\alpha = 0^\circ$ for the local upwash angle in degrees at the same vertical location in the crossflow plane but two different spanwise stations. Corresponding results for the local sidewash angle are presented in figure 13. Figures 14 and 15 display analogous results at a fixed spanwise location and for three vertical locations in the crossflow plane. With the exception of some discrepancies near the trailing edge, which are associated with discontinuities in the axial area distribution derivatives not yet accounted for in the theory, the agreement is quite good. These results provide an important nonlifting check case ($\sigma_* = 0$) essential to verifying the theoretical method.

Similar results for a lifting flow are provided in figures 16 and 17 for $M_\infty = 0.925$ and $\alpha = 5^\circ$. Aside from the discrepancies near the trailing edge, agreement is again satisfactory. The final comparisons shown in figures 18 and 19 are for a strongly supercritical flow. Figure 18 displays results for the local upwash and sidewash angles for a survey close to the wing at the 50% semispan location for the nonlifting flow at $M_\infty = 0.975$, while figure 19 shows the analogous lifting result at $\alpha = 5^\circ$. Once again, the comparisons are quite favorable.

CURRENT EXTENSIONS OF PREDICTIVE METHOD

With the successful preliminary development and verification of the predictive technique accomplished, the secondary development directed toward achievement of a practical engineering predictive tool is currently underway. The tasks involve improvements in the current theoretical model as well as extensions of the basic capability of the method and subdivide into three categories. The first consists of refinement of the wing/body alone predictive model observed as necessary from comparisons with data. This includes treatment, not yet accounted for in the theory, of the discontinuities in the axial area distribution derivatives that occur at breaks in the wing leading edge and at the trailing edge, and also development of the capability for imposing a measured outer flow boundary condition. The second major task consists of carrying out a systematic experimental program involving the model wing-body previously used together with multiple

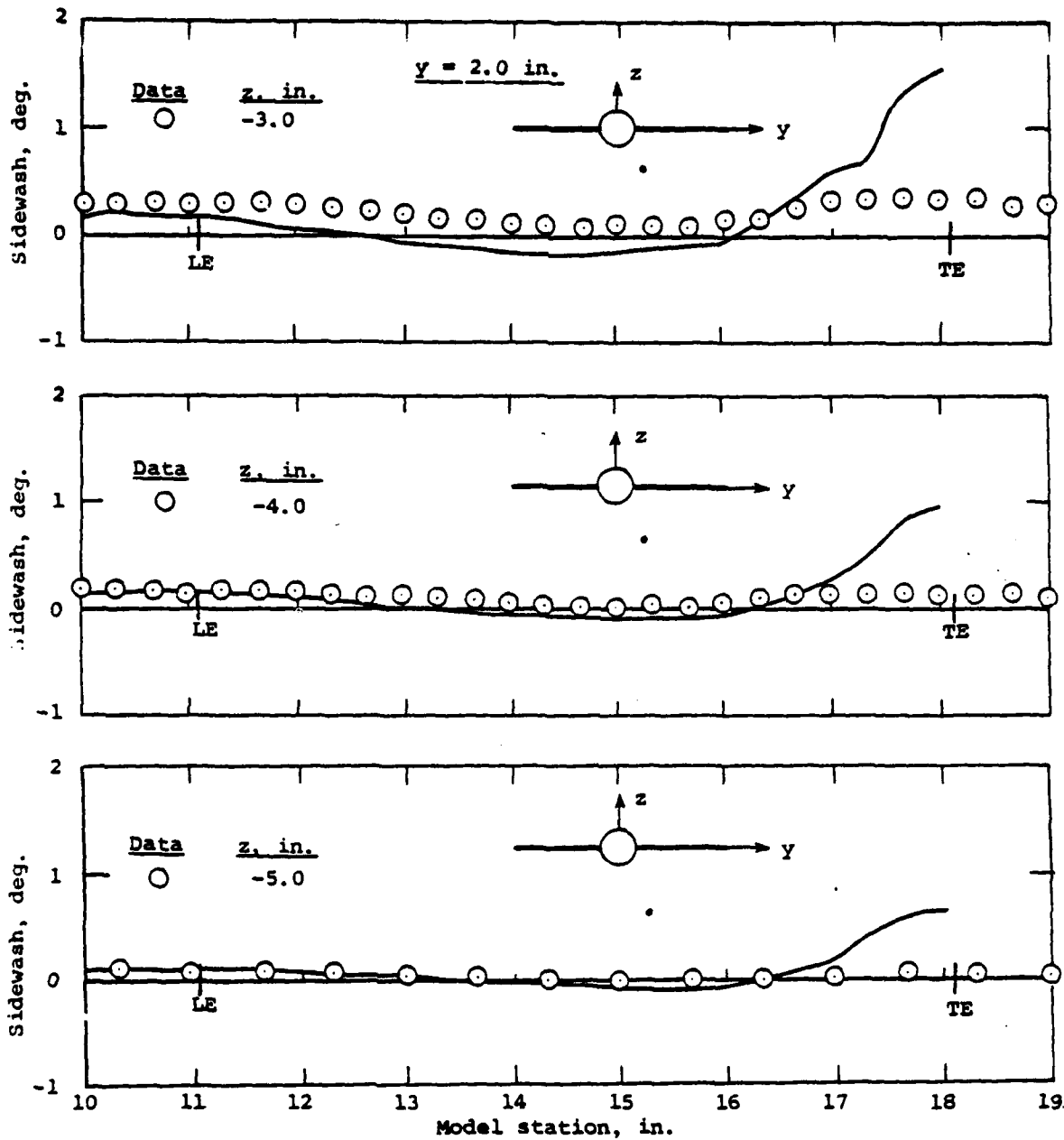


Figure 15.- Comparisons of theoretical and experimental results for the local sidewash angle for flow past the scaled F-16 wing/body combination at $M_\infty = 0.925$ and $\alpha = 0^\circ$.

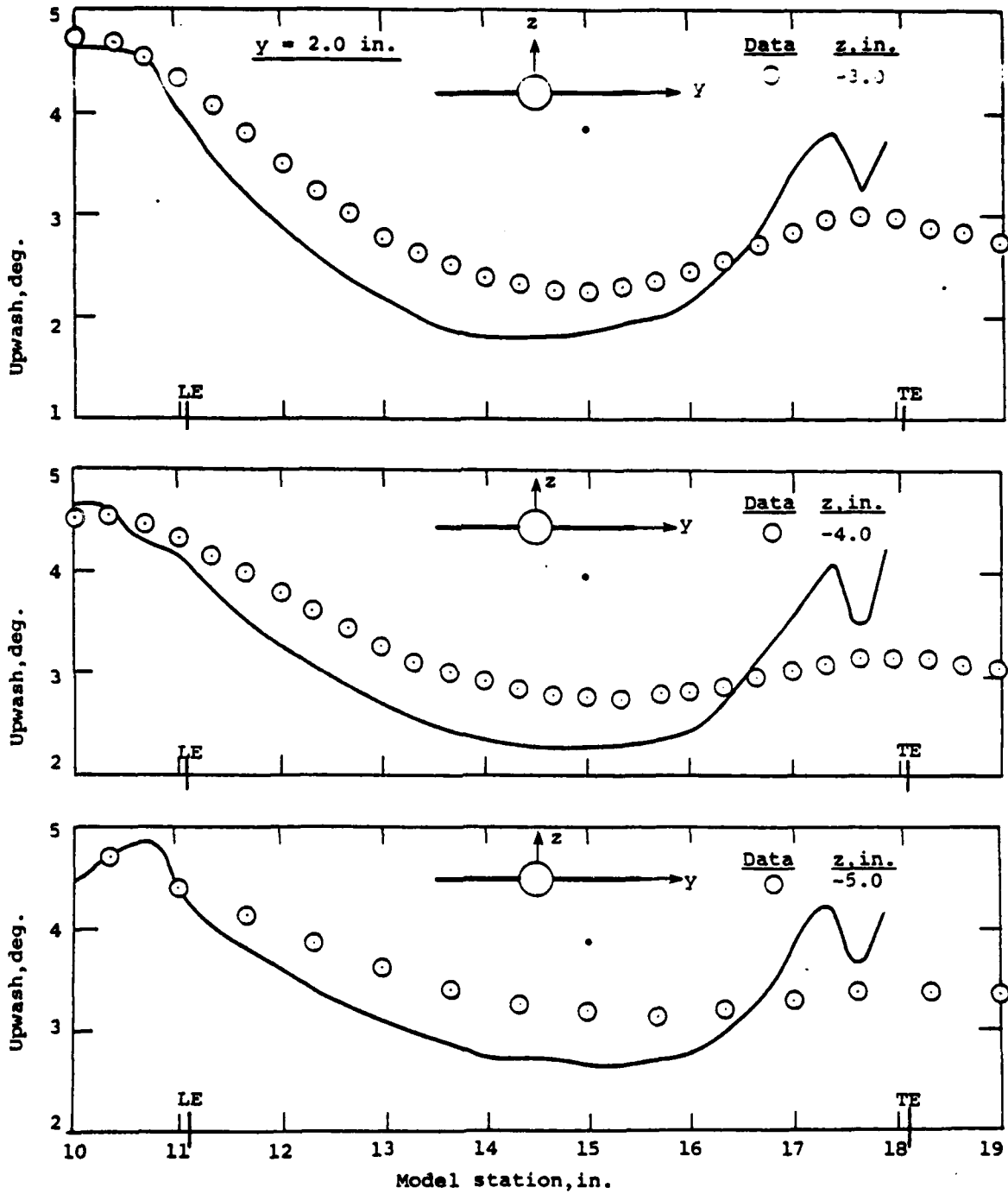


Figure 16.- Comparisons of theoretical and experimental results for the local upwash angle for flow past the scaled F-16 wing/body combination at $M_\infty = 0.925$ and $\alpha = 5^\circ$.

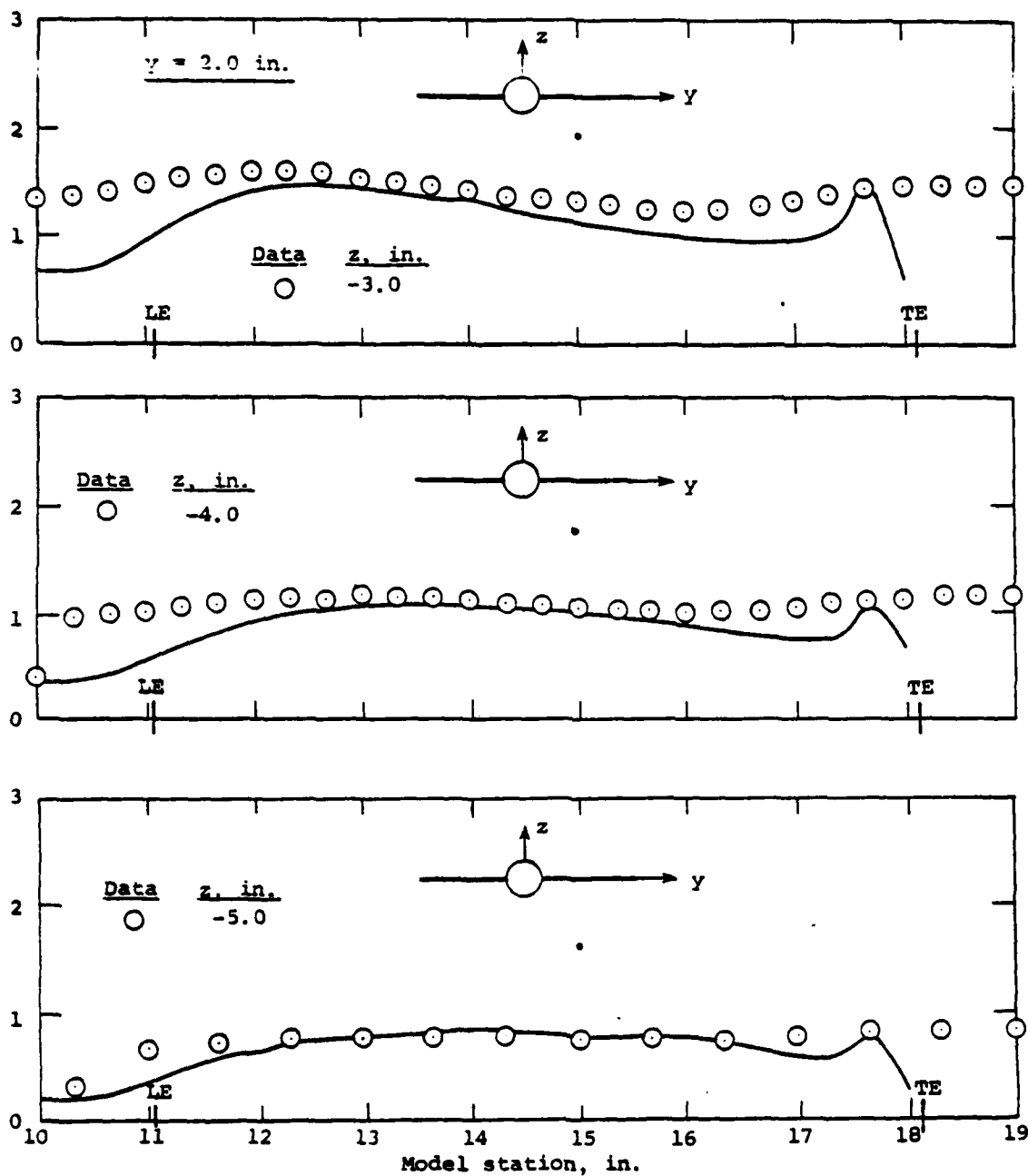


Figure 17.- Comparisons of theoretical and experimental results for the local sidewash angle for flow past the scaled F-16 wing/body combination at $M_\infty = 0.925$ and $\alpha = 5^\circ$.

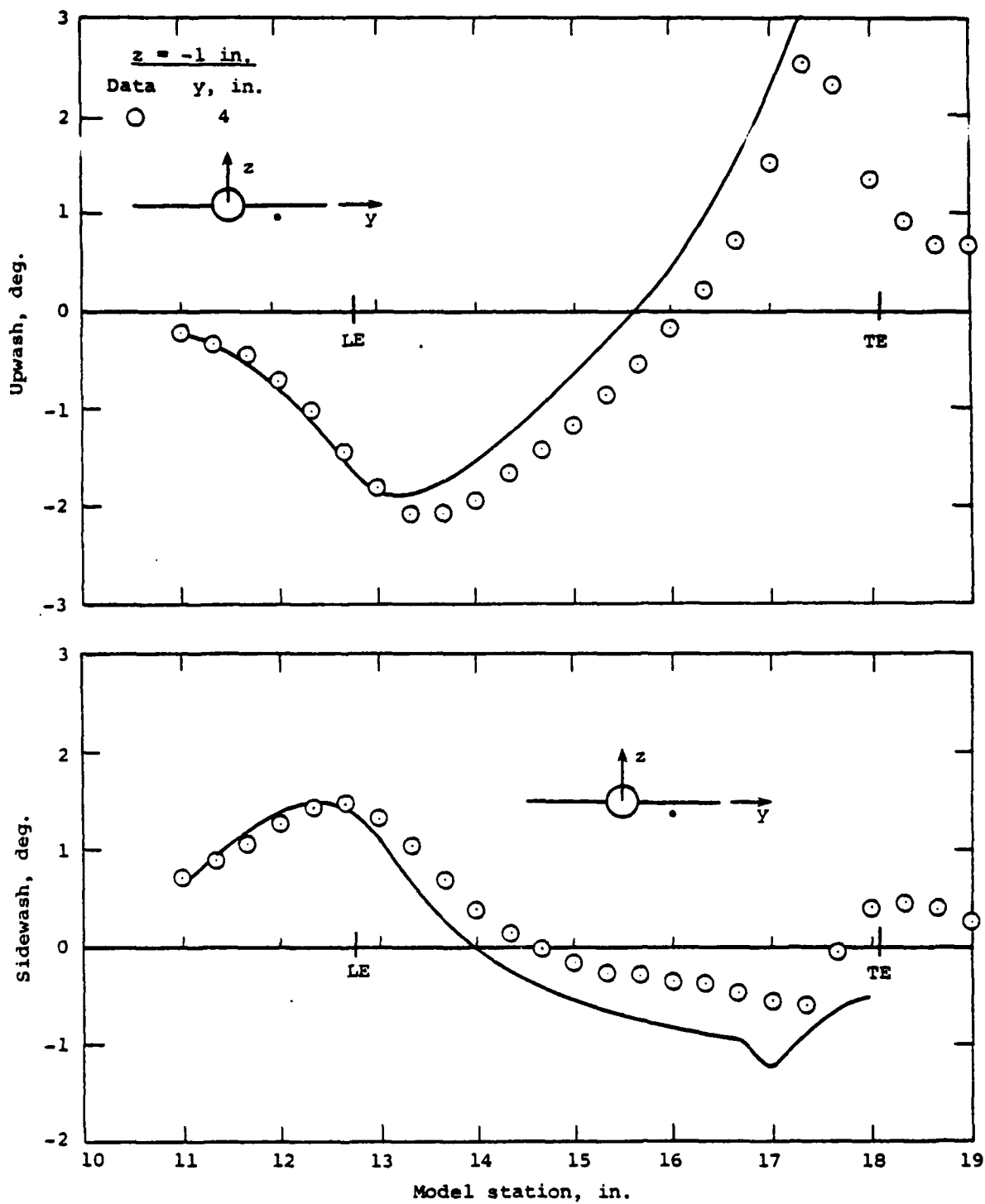


Figure 18.- Comparisons of theoretical and experimental results for the local sidewash and upwash angles for flow past the scaled F-16 wing/body combination at $M_\infty = 0.975$ and $\alpha = 0^\circ$.

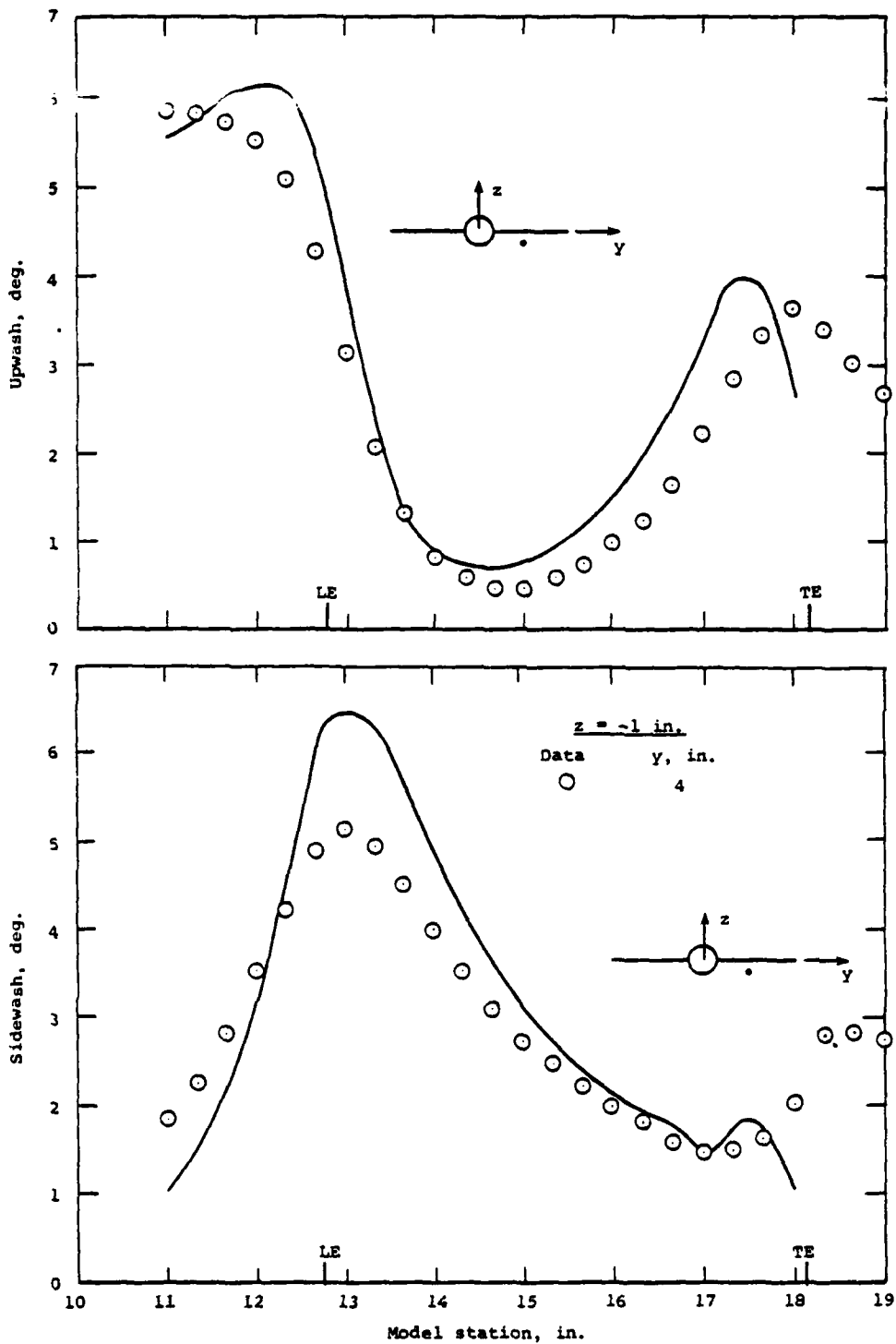


Figure 19.- Comparisons of theoretical and experimental results for the local sidewash and upwash angles for flow past the scaled F-16 wing/body combination at $M_\infty = 0.975$ and $\alpha = 5^\circ$.

pylon/store combinations. This will provide the necessary comparison data for the third task which is the extension of the theoretical model to include multiple pylons and stores.

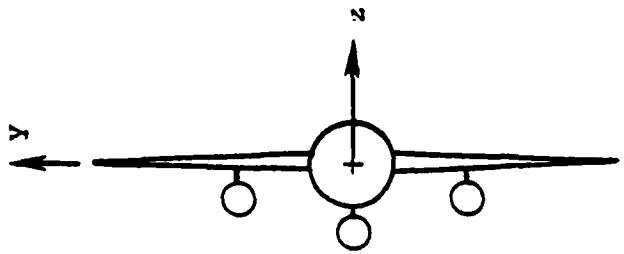
The wing-body/pylon/stores model combination envisioned is illustrated in figure 20, and consists of two wing-mounted single store/swept pylon combinations plus a fuselage-mounted single store/straight pylon combination. We note that the scaled size of the stores approximately represent a 350 gallon external fuel tank and will provide a severe test of the theoretical model. A systematic model buildup is planned in order to isolate important individual effects contributing to the complex flow phenomena present under the wing. The measurements will consist of (1) the flow field under the model aircraft in and near the region normally occupied by the store, and (2) store surface pressures and loadings at various locations in the flow field. These measurements provide a test of the theory's ability to predict both the flow field seen by the store, as well as to compute the loading experienced by the store.

Finally, the extension of the theoretical model to include multiple pylon/store combinations will involve work on both the inner and outer region solution techniques. For the inner region, a generalized finite-element solver is necessary to treat the more complicated multi-body geometry. For the outer region, a modification of the outer flow solution procedure is needed to include a simplified two-line equivalent body scheme to account properly for the store separating from the parent aircraft.

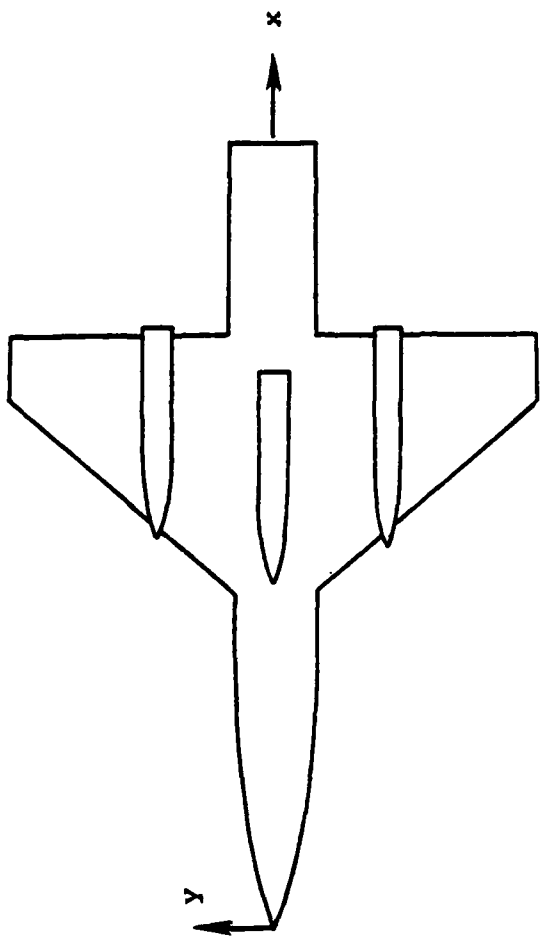
CONCLUDING REMARKS

The initial development of a theoretical predictive method for external store trajectory applications to configurations characteristic of modern fighter-bombers at transonic speeds has been carried out. The emphasis of the initial work has been the development and verification of the theoretical method for computing the three-dimensional transonic flow field due to the parent aircraft alone. A parallel wind-tunnel test program specifically designed to test the theory and isolate important features through detailed systematic measurements of flow fields, surface pressures, and forces and moments was carried out for a simplified wing-body combination modeled on the F-16. The extensive data obtained provide an adequate base for testing both the present analytical model as well as other theoretical methods.

The initial comparisons between experimental and the present predictive method indicate generally good agreement. Several modest improvements needed in the theoretical model



(c) Rear view.



(a) Bottom view.



(b) Side view.

Figure 20.- Illustration of wing-body/pylon/stores model configuration.

have been identified and are currently being carried out. Extension of the method to include multiple pylon-single store combinations is the next major task and will be pursued in the next phase. A parallel wind-tunnel program to provide the needed verification of the theory is also planned.

REFERENCES

1. Dillenius, M. F. E., Goodwin, F. K., and Nielsen, J. N.: Extension of the Method of Predicting Six-Degree-of-Freedom Store Separation Trajectories at Speeds Up to the Critical Speed to Include a Fuselage with Noncircular Cross Section, Vol. I - Theoretical Method and Comparisons with Experiment. AFFDL-TR-74-130, March 1974.
2. Dillenius, M. F. E., Goodwin, F. K., and Nielsen, J. N.: Prediction of Supersonic Store Separation Characteristics. Vol. I - Theoretical Methods and Comparisons with Experiment. Technical Report AFFDL-TR-76-41, Vol. I, May 1976.
3. Spahr, H. R.: Theoretical Store Separation Analyses of a Prototype Store. J. of Aircraft, vol. 12, no. 10, pp. 807-811, October 1975.
4. Spahr, H. R.: Theoretical Store Separation Analyses of a Prototype Store and Comparison with a Flight Drop Test. AIAA Paper No. 74-776 presented at AIAA Mechanics and Control of Flight Conference, Anaheim, CA, August 5-9, 1974.
5. Spahr, H. R., Everett, R. N., and Kryvoruka, J. K.: A Multifaceted Store Separation Analysis. Proceedings of the AIAA 9th Aerodynamic Testing Conference, Arlington, TX, pp. 292-300, June 7-9, 1976.
6. Oswatitsch, K. and Keune, F.: The Flow Around Bodies of Revolution at Mach Number 1. Proc. Conf. on High-Speed-Aeronautics, Polytechnic Institute of Brooklyn, NY, pp. 113-131, 1955.
7. Heaslet, M. A. and Spreiter, J. R.: Three-Dimensional Transonic Flow Theory Applied to Slender Wings and Bodies. NACA Rept. 1318, 1957.
8. Cheng, H. K. and Hafez, M. M.: Equivalence Rule and Transonic Flow Involving Lift. Aero. Eng. Dept. Univ. of So. CA., Los Angeles, CA, Rept. USCAE 124, April 1973.
9. Cheng, H. K. and Hafez, M. M.: Transonic Equivalence Rule: A Nonlinear Problem Involving Lift. J. Fluid Mech., vol. 72, part 1, pp. 161-187, November 1975.
10. Barnwell, R. W.: Transonic Flow About Lifting Wing-Body Combinations. AIAA Paper No. 74-185, 1974.

11. Stocker, P. M.: Supersonic Flow Past Bodies of Revolution with Thin Wings of Small Aspect Ratio. Aero. Quart. Vol. III, pp. 61-79, May 1951.
12. Spreiter, J. R.: The Aerodynamic Forces on Slender Plane and Cruciform-Wing and Body Combinations. NACA Rept. 962, 1950.
13. Taylor, R. A.: Pressure Distributions at Transonic Speeds for Bumpy and Indented Midsections of a Basic Parabolic-Arc Body. NASA Memo. 1-22-59A, February 1959.
14. Perkins, S. C., Jr., Stahara, S. S., and Hensch, M. J.: Data Report for a Test Program to Study Transonic Flow Fields About Aircraft with Application to External Stores. Vols. I to VI, NEAR TR 138, July 1977.

AUTOBIOGRAPHY

Stephen S. Stahara

Dr. Stephen S. Stahara received his B.S. in Engineering Science from Case Institute of Technology in 1964, and his Master's and Ph.D. in Aeronautics and Astronautics in 1965 and 1969, respectively, from Stanford University.

Dr. Stahara joined Nielsen Engineering and Research, Inc. early in 1969 and has engaged in a variety of theoretical and experimental investigations relating to aerodynamic configurations. These have included development of a nonplanar lifting surface theory for all-flexible parawings, theoretical and experimental investigation of sail rotors for high altitude platforms, and development of analytical and finite-difference methods for both steady and unsteady transonic flows.

As Senior Scientist, he presently has responsibility for directing research and development of a number of computational fluid dynamics activities. These include investigations of fighter/bomber external store trajectories at transonic speeds, nonaxisymmetric transonic projectile design, unsteady supercritical flows about airfoils and slender bodies, and transonic compressor studies.

AUTOBIOGRAPHY

Michael J. Hensch

Dr. Michael J. Hensch received his B.S. degree in Mechanical Engineering from the University of Santa Clara in 1962. From 1962 to 1966, he worked for United Technology Center. His duties involved heat transfer and fluid mechanics analyses applied to solid and hybrid rocket engines. In 1971 he received his Ph.D. in Mechanical Engineering from Stanford University. He has been employed at Nielsen Engineering and Research, Inc. since 1973. His primary areas of interest have been missile aerodynamics and transonics.

AUTOBIOGRAPHY

Stanley C. Perkins, Jr.

Stanley C. Perkins, Jr. received his B.S. degree in Mechanical Engineering from the University of Rochester in 1973. In 1974 he received his M.S. degree in Applied Mechanics from Stanford University. He has been employed at Nielsen Engineering and Research, Inc., Mountain View, California, from 1974 to present, where he has participated in the development of prediction methods to determine aerodynamic characteristics of wing-body-tail and upper-surface-blown flap STOL configurations and in the development of a data base for the prediction of airframe/propulsion system interference effects. He has also worked in the areas of missile aerodynamics, transonics, and store separation.

AUTOBIOGRAPHY

John R. Spreiter

Dr. John R. Spreiter received his B.S. in Aeronautical Engineering from University of Minnesota in 1943, and his M.S. and Ph.D. from Stanford University in 1947 and 1954, respectively. He was employed at NASA/Ames Research Center from 1943 to 1968, where he performed theoretical investigations in aerodynamics, with emphasis on transonic studies, and also in space science. In 1968, he left his position as Chief of the Theoretical Studies Branch, Space Sciences, to become Professor of Applied Mechanics at Stanford University. Dr. Spreiter is internationally recognized as a transonic flow expert and is a major contribution to modern transonic theory.

Dr. Spreiter has acted as consultant for Nielsen Engineering and Research, Inc. since 1969.

ANALYTICAL EVALUATION OF THE LIMITATIONS OF
THE VARIOUS SCALING LAWS FOR FREEDROP
STORE SEPARATION TESTING

(U)

(Article UNCLASSIFIED)

by

JOHN C. MARSHALL

ARO, Inc.

AEDC Division

A Sverdrup Corporation Company
Arnold Air Force Station, Tennessee

ABSTRACT. (U) Several techniques have been established for defining the dynamic simulation requirements of wind tunnel models used in freedrop store separation tests. A three-degree-of-freedom set of motion equations and a linearized model of the store aerodynamic characteristics are used to define the model simulation parameters for Froude Scaling, Heavy Mach Scaling, and Light Mach Scaling. Trajectory calculations for both a stable store and an unstable store are presented using each of the three scaling techniques, and comments are made regarding the merits and practical limitations of each.

"Approved for public release; distribution unlimited."

LIST OF FIGURES

Figure Number

- 1 Coordinate Notation
- 2 Stable Store Aerodynamics
- 3 Aircraft Flow Field for Stable Store
- 4 Unstable Store Aerodynamics
- 5 Aircraft Flow Field for Unstable Store
- 6 Froude Scaling with Stable Store
- 7 Heavy Mach Scaling with Stable Store
- 8 Light Mach Scaling with Stable Store
- 9 Froude Scaling with Unstable Store
- 10 Heavy Mach Scaling with Unstable Store
- 11 Light Mach Scaling with Unstable Store

NOMENCLATURE

C_A	Store axial-force coefficient, (axial force/ $q_\infty S$)
C_m	Store pitching-moment coefficient, (pitching moment/ $q_\infty Sd$)
$C_{m\dot{q}}$	Store pitch damping derivative, 1/rad
$C_{m\alpha}$	Derivative of pitching-moment coefficient with angle of attack, 1/rad
ΔC_m	Incremental pitching-moment coefficient on the store resulting from flow field streamline curvature
C_N	Store normal-force coefficient, (normal force/ $q_\infty S$)
$C_{N\alpha}$	Derivative of normal-force coefficient with angle of attack, 1/rad
d	Store reference dimension, ft
F_{EJ}	Ejector force acting on the store perpendicular to the body longitudinal axis, positive downward, lbf
$\Delta F'$	Model ejector force augmentation to compensate for gravity deficiency, lbf
F_X	Total force acting on the store parallel to the body longitudinal axis, positive forward, lbf
F_Z	Total force acting on the store perpendicular to the body longitudinal axis, positive downward, lbf
g	Acceleration due to gravity, ft/sec ²
$\Delta g'$	Model gravitational deficiency, ft/sec ²
I	Store moment of inertia in the pitch plane, slug.ft ²
m	Store mass, slugs
M	Total moment acting about the store center of gravity in the pitch plane, ft.lbf

q_{∞}	Airstream dynamic pressure, $\frac{1}{2}\rho_{\infty}V_{\infty}^2$, psf
S	Store reference area, ft ²
t	Trajectory time from instant of store release from the aircraft, sec
t_e'	Time of action of the model ejector, sec
T_{∞}	Airstream static temperature, °R
V_{∞}	Store velocity relative to the free stream, ft/sec
W	Store weight, lbm
X	Store center of gravity coordinate from the carriage position on the aircraft, measured parallel to the earth horizontal, positive in the forward direction, ft
X_{EJ}	Distance from the store center of gravity to the line of action of the ejector force, positive if the ejector acts forward of the center of gravity, ft
Z	Store center of gravity coordinate from the carriage position on the aircraft, measured perpendicular to the earth horizontal, positive in the downward direction, ft
$\Delta Z'$	Calculated adjustment to the observed store-model vertical displacement to correct for gravity deficiency and ejector-force augmentation effects, ft
α	Store aerodynamic angle of attack, deg
$\Delta\alpha$	Incremental angle of attack on the store resulting from net flow-field streamline inclination, deg (Figs. 3 and 5) or radian (Equations 7-13)
θ	Store geometric pitch attitude with respect to the earth horizontal, positive if the store nose is raised, radian or deg (Figs. 6 through 11)
ρ_{∞}	Airstream density, slugs/ft ³

- ()' Primed quantities refer to model-scale dimensions or properties defined by the scaling laws or the wind tunnel operating parameters
- ($\dot{}$) A single dot denotes a first derivative of the parameter with respect to time
- ($\ddot{}$) A double dot denotes a second derivative of the parameter with respect to time

I. INTRODUCTION

Wind tunnel testing is generally carried out using reduced-size, but geometrically scaled, models of the vehicle being studied. Thus, the experiments are simulations rather than duplications of the actual flight environment. By definition, a simulation is not a true representation, but gives an "appearance of reality" while being, in fact, a counterfeit. The value of scale-model testing lies in the assumption that certain non-dimensional factors can be defined and measured which relate data obtained on the small models to performance of the full sized vehicle. Application of this philosophy has been the substance of experimental development of aircraft and related aerodynamic systems for many years.

Dimensional analysis has shown that the static, or steady state, aerodynamic forces on a body can be reasonably simulated on a scale model if the model is geometrically reproduced and if the airstream compressibility and viscous characteristics (Mach number and Reynolds number) are reproduced. In the case of dynamic, or non-steady state flight, it is necessary to simulate not only the applied forces but also the inertial response of the body to these forces. Such is the situation in the case of freedrop, or dynamic drop, store separation testing.

The techniques for defining the required parameters for dynamic similitude are not new, and have appeared in the literature (e.g., Refs. 1 and 2) on many occasions. The intent of this paper is primarily to demonstrate the effects of the compromises one must always make in applying the scaling laws to practical wind tunnel situations. This demonstration will be carried out through sample calculations of store motion through typical assumed aircraft flow fields. Simplified (three degree of freedom) equations of motion will be presented to identify the pertinent scaling parameters and show how these generate the required model characteristics. Similarly, three-degree-of-freedom calculations of store trajectories will be presented to show the resultant motion of the models, and how this motion relates to that of the full-scale store.

II. EQUATIONS OF MOTION

The significant factors in defining the motion of a store model during a freedrop separation trajectory can be readily seen by considering motion in a single vertical plane. The coordinate axes and notation to be used are shown in Fig. 1. It is convenient to define the forces acting on the body in the body-axis system, and then utilize

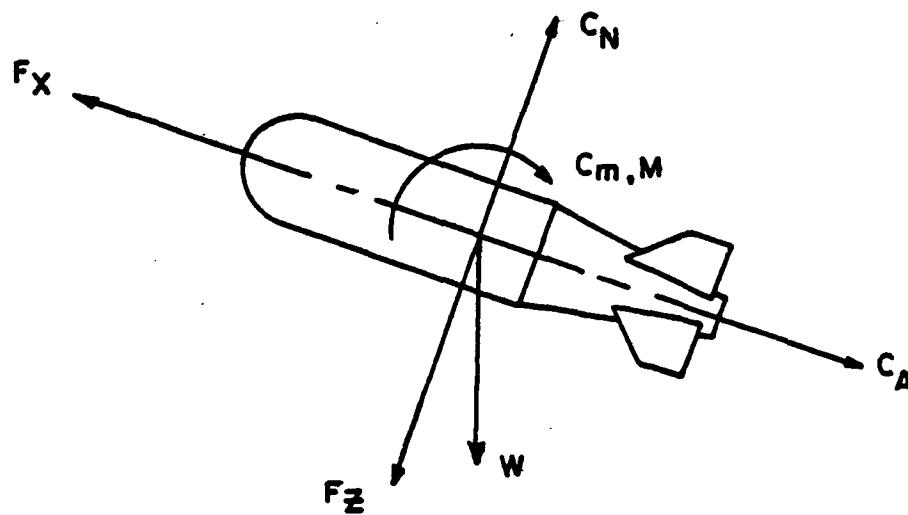
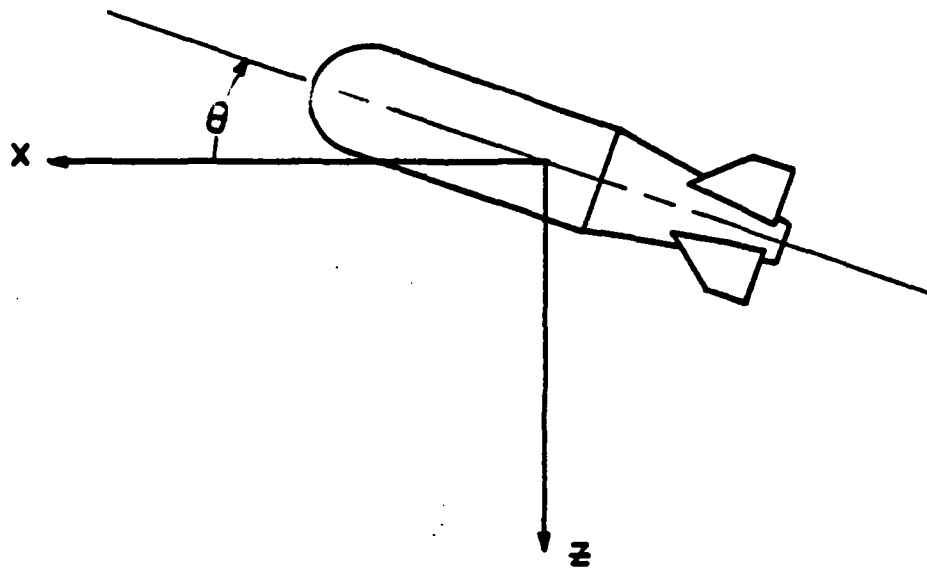


Figure 1 Coordinate Notation

an earth-oriented coordinate system to define the motion so that gravity only affects one of the position coordinates. Summing forces and moments give the relations

$$F_X = -C_A q_\infty S - W \sin \theta \quad (1)$$

$$F_Z = -C_N q_\infty S + W \cos \theta + F_{EJ} \quad (2)$$

$$M = \left[C_m + C_{m_q} \left(\frac{d\dot{\theta}}{2V_\infty} \right) \right] q_\infty S d - F_{EJ} X_{EJ} \quad (3)$$

The motion equations are obtained by taking force and moment components parallel to the earth coordinate axes, dividing by the proper inertial quantity, and setting the result equal to the acceleration. Thus,

$$\ddot{X} = - \left[C_A \cos \theta + C_N \sin \theta \right] \left(\frac{q_\infty S}{m} \right) + \left(\frac{F_{EJ}}{m} \right) \sin \theta \quad (4)$$

$$\ddot{Z} = - \left[C_N \cos \theta - C_A \sin \theta \right] \left(\frac{q_\infty S}{m} \right) + \left(\frac{F_{EJ}}{m} \right) \cos \theta + g \quad (5)$$

$$\ddot{\theta} = \left[C_m + C_{m_q} \left(\frac{d\dot{\theta}}{2V_\infty} \right) \right] \left(\frac{q_\infty S d}{I} \right) - \left(\frac{F_{EJ} X_{EJ}}{I} \right) \quad (6)$$

Generally speaking, the quantities enclosed in square brackets represent the vehicle aerodynamics, while those quantities in parentheses contain the geometric and inertial properties of the store. Because the store is moving through a flow field perturbed by the proximity of the aircraft, the aerodynamic properties become a function of position within the flow field, and the aerodynamics are thereby coupled to the inertial response of the store as it moves away from the aircraft. The nature of this interaction can be seen by making a few simplifying assumptions about the aerodynamics of the store in this flow field. The conclusions reached should be valid for more complex flow models as long as the aerodynamics of the store can be considered to be ordered functions of the position and attitude within the flow field. Specifically, it will be assumed that the angular motion is small enough that the aerodynamic normal-force and pitching-moment coefficients vary linearly with angle of attack, and the axial-force coefficient and pitch-damping derivative are constant. Further, it will be assumed that the flow field spatial variations in streamline inclination and curvature can be represented by incremental values of angle of attack and pitching-moment coefficient, respectively. These assumptions produce the following aerodynamic characteristics;

$$C_N = C_{N_\alpha} \left(\theta + \frac{\dot{z}}{V_\infty} + \Delta\alpha \right) \quad (7)$$

$$C_A = \text{constant} \quad (8)$$

$$C_m = C_{m_\alpha} \left(\theta + \frac{\dot{z}}{V_\infty} + \Delta\alpha \right) + \Delta C_m \quad (9)$$

$$C_{m_q} = \text{constant} \quad (10)$$

Substituting these relationships into Equations 4, 5, and 6 results in a set of linear, coupled differential equations which describe the store motion in such a manner as to make the source and meaning of the dynamic simulation parameters more readily apparent.

$$\begin{aligned} \left(\frac{\ddot{x}}{g} \right) = & - \left[C_A \cos \theta + C_{N_\alpha} \left(\theta + \frac{\dot{z}}{V_\infty} + \Delta\alpha \right) \sin \theta \right] \left(\frac{q_\infty S}{mg} \right) \\ & + \left(\frac{F_{EJ}}{mg} \right) \sin \theta \end{aligned} \quad (11)$$

$$\begin{aligned} \left(\frac{\ddot{z}}{g} \right) = & 1 - \left[C_{N_\alpha} \left(\theta + \frac{\dot{z}}{V_\infty} + \Delta\alpha \right) \cos \theta - C_A \sin \theta \right] \left(\frac{q_\infty S}{mg} \right) \\ & + \left(\frac{F_{EJ}}{mg} \right) \cos \theta \end{aligned} \quad (12)$$

$$\begin{aligned} \ddot{\theta} = & \left[C_{m_\alpha} \left(\theta + \frac{\dot{z}}{V_\infty} + \Delta\alpha \right) + C_{m_q} \left(\frac{d\dot{\theta}}{2V_\infty} \right) + \Delta C_m \right] \left(\frac{q_\infty S d}{I} \right) \\ & - \left(\frac{F_{EJ} x_{EJ}}{I} \right) \end{aligned} \quad (13)$$

In these equations, the aerodynamic parameters C_A , C_{N_α} ,

C_{m_α} , and C_{m_q} are all constants and represent the aerodynamic characteristics of the store in an undisturbed free-stream airflow.

By inspection, it can be noted that there are no parameters in Equation 11 that are not also in Equation 12. We may thus effectively reduce the problem to two dimensions, z and θ , and conduct the similitude analysis by examining only Equations 12 and 13.

III. DYNAMIC SIMULATION RELATIONSHIPS

A. FROUDE SCALING

The relationships among geometric shape, mass properties, and airstream characteristics to reproduce store

motion with small scale models can be deduced from Equations 12 and 13 by examining the quantities in parentheses for both full-scale flight and the model-scale simulation. It is assumed that the basic store aerodynamic characteristics will be reproduced if all model dimensions (store and aircraft) are linearly scaled, and the airstream viscous and compressibility characteristics are reproduced or closely simulated. This is basic in the use of the wind tunnel to predict flight characteristics. If it is further assumed that all parameters in the equations of motion for the model-scale store have a linear relationship with the corresponding parameters for the full-scale store, a group of relationships can be developed which define the necessary model-scale store and airstream properties. These relationships can be simplified even more by requiring geometric similarity; i.e., the linear factor relating model position coordinates (X', Z') to the full-scale store position coordinates (X, Z) is the same as the model scale factor, and the model pitch attitude (θ') is equal to the store pitch attitude (θ) at corresponding points along the trajectory path. With these conditions, the resulting relationships are

$$Z' = Z (\lambda) \quad (14a)$$

$$\theta' = \theta \quad (14b)$$

$$m' = m (\sigma) (v^2) (\lambda^2) (g/g') \quad (14c)$$

$$I' = I (\sigma) (v^2) (\lambda^4) (g/g') \quad (14d)$$

$$F_{EJ}' = F_{EJ} (\sigma) (v^2) (\lambda^2) \quad (14e)$$

$$X_{EJ}' = X_{EJ} (\lambda) \quad (14f)$$

$$V_{\infty}' = V_{\infty} \sqrt{(\lambda) (g'/g)} \quad (14g)$$

$$t' = t (\lambda)/(v) \quad (14h)$$

where λ = model scale factor

$$\sigma = (\rho_{\infty}'/\rho_{\infty})$$

$$v = (V_{\infty}'/V_{\infty})$$

The relationships given above provide all the information necessary to establish a model-scale experiment to generate trajectories in a wind tunnel which should reproduce the motion of a store released from an aircraft in flight. This form of experimental scaling is often referred

to as Froude Scaling because the velocity scaling given by Equation 14g is equivalent to the hydrodynamic Froude Number which relates buoyancy forces to inertial forces. Although the gravitational constant is not generally considered a variable, it has been included as such in these relationships to demonstrate the influence of gravity on the simulation. By rearrangement and substitution of the various parameters, the mass and moment of inertia can be written also as

$$m' = m (\sigma) (\lambda^3) \quad (15a)$$

$$I' = I (\sigma) (\lambda^5) \quad (15b)$$

which state that the ratio of model density to store average density is the same as the ratio of wind tunnel airstream density to flight altitude density, and the mass distribution in the model is the same as in the store.

B. MACH SCALING

The relationships developed above are suitable for many situations involving subsonic flight conditions. However, it requires that the model-scale experiment be conducted at velocities much lower than the equivalent flight velocity unless significant increases in the gravitational constant can be effected. Reduced velocity means generally a change in the basic store aerodynamics and in the aircraft flow field characteristics due to Mach number dependency. These effects begin to appear above Mach number 0.6, where local sonic flow is first experienced around protuberances on the store, and are obviously a major factor for supersonic flight where the shock waves generated by the aircraft will markedly alter the flow field characteristics. To deal with this situation, compromise methods of simulation have been developed which retain the flight Mach number matching at the expense of some other parameter.

Perhaps the most widely used technique for Mach Scaling is that generally called Heavy Scaling. In this technique, the quantities removed from simulation are the factors

$\left(\frac{\dot{z}}{V_\infty}\right)$ and $\left(\frac{d\theta}{2V_\infty}\right)$ in Equations 12 and 13. In their stead, the wind tunnel Mach number is set equal to the flight Mach number, which results in essentially (though not quite) equal velocities. The resulting scaling relationships for Heavy Mach Scaling are then;

$$z' = z (\lambda) \quad (16a)$$

$$\theta' = \theta \quad (16b)$$

$$m' = m (\sigma) (v^2) (\lambda^2) (g/g') \quad (16c)$$

$$I' = I (\sigma) (v^2) (\lambda^4) (g/g') \quad (16d)$$

$$F_{EJ}' = F_{EJ} (\sigma) (v^2) (\lambda^2) \quad (16e)$$

$$X_{EJ}' = X_{EJ} (\lambda) \quad (16f)$$

$$V_{\infty}' = V_{\infty} \sqrt{T_{\infty}'/T_{\infty}} \quad (16g)$$

$$t' = t \sqrt{(\lambda) (g/g')} \quad (16h)$$

These appear the same as for Froude Scaling, except for the last two. The difference comes when accounting for the increased velocity. Thus, for the case of constant gravity ($g' = g$) the mass and moment of inertia relationships are

$$m' = m (q_{\infty}'/q_{\infty}) (\lambda^2) \quad (17a)$$

$$I' = I (q_{\infty}'/q_{\infty}) (\lambda^4) \quad (17b)$$

$$\text{where } (q_{\infty}'/q_{\infty}) = (\sigma) (v^2)$$

Unless the wind tunnel dynamic pressure can be reduced significantly below the flight value, these relationships state that the model density will be much higher than for the store, although the mass distribution remains the same.

The effect of relaxing the velocity ratio simulations is seen primarily in the angular motions. The pitch damping term in the angular acceleration equation is reduced by a factor equal to the square root of the scale factor (λ) so that the amplitude of the pitch oscillations is too large. This will have a secondary effect on the linear motions because of the dependence of the aerodynamic coefficients on angle of attack.

When the angular motion response is of primary concern, another form of Mach Scaling can be used. This form is referred to as Light Scaling because the mass density increase indicated above is alleviated. Light Scaling is achieved by assuming that the gravitational constant may be arbitrarily increased in the model-scale experiment. Retaining the velocity ratio simulation terms as in Froude Scaling, and setting the desired gravitational constant to

$$g' = g (v^2)/(\lambda) \quad (18)$$

the scaling relationships for Light Mach Scaling are then

$$z' = z (\lambda) \quad (19a)$$

$$\theta' = \theta \quad (19b)$$

$$m' = m (\sigma) (\lambda^3) \quad (19c)$$

$$I' = I (\sigma) (\lambda^5) \quad (19d)$$

$$F_{EJ}' = F_{EJ} (\sigma) (v^2) (\lambda^2) \quad (19e)$$

$$X_{EJ}' = X_{EJ} (\lambda) \quad (19f)$$

$$V_{\infty}' = V_{\infty} \sqrt{(T_{\infty}'/T_{\infty})} \quad (19g)$$

$$t' = t (\lambda) / (v) \quad (19h)$$

The mass and moment of inertia ratios are seen to be the same as for Froude Scaling, while the ejector force is increased to account for the increased accelerations resulting from the decrease in the model time scale.

Since, in reality, the model will experience gravitational forces based on the constant "g" instead of "g'," the vertical acceleration will be in error by an amount

$$\Delta g' = g' - g = g \left[(v^2/\lambda) - 1 \right] \quad (20)$$

and the vertical displacement will be too small because of this discrepancy. Corrections can be made to the observed trajectories to compensate for this effect, but some errors will remain due to the spatial variations of the aircraft flow field. Difficulties can also be encountered if the motion is such as to cause collision between the store model and the aircraft model. Further compensation can be made by increases in the ejector force to keep the model near the correct path, but this is achieved only at the expense of the desired velocity ratio simulation. An increase in the ejector force by an amount

$$\Delta F' = m' (\Delta g') \quad (21)$$

is recommended to produce the correct motion at the end of the ejector stroke. The point of action of the ejector must also be shifted to maintain the correct moment. The adjusted ejector location is

$$X_{EJ}' = X_{EJ} (\lambda) \left(\frac{F_{EJ}'}{F_{EJ}' + \Delta F'} \right) \quad (22)$$

The effects of augmenting the ejector force to compensate for gravity deficiency will be shown in subsequent sections of this paper.

IV. AERODYNAMIC MODELS FOR ANALYSIS

To evaluate the characteristics and merits of the various scaling techniques, it is necessary to define aerodynamic models of both the store and the aircraft flow field through which it traverses. These models should have characteristics which exercise the various assumptions made in establishing the scaling laws. To this end, the aerodynamic models selected have the following features: (1) the store free-stream aerodynamics are Mach number dependent, (2) the aircraft flow field is an exponentially decaying function of both the vertical and axial position coordinates of the store with respect to the aircraft, (3) the aircraft flow field is also Mach number dependent, and (4) the aerodynamic characteristics of both the store and the aircraft flow field were selected to be representative of actual measured values. Two sets of data were selected for consideration herein; a large, stable store carried singly on a wing pylon, and a smaller unstable store carried in a multiple-carriage configuration on a rack. In both cases, the aerodynamic characteristics at transonic speeds were based on available experimental data, while the low Mach number characteristics were assumed values so as to demonstrate the need for Mach Scaling as an alternative to the Froude Scaling methods.

A. STABLE STORE

This store is assumed to be a large, slender, finned bomb in the 2000 lb class that is carried and released from individual pylon stations on various aircraft. The free-stream aerodynamics show a significantly stable static margin so that the angular motion is restricted generally to low amplitude oscillation. The free-stream aerodynamic coefficients assumed for this store are shown in Fig. 2. Typical flow-field effects on a store of this type are shown in Fig. 3. Data are shown for angles of attack only up to 20 deg since the motion of this type of store is generally limited to this range.

B. UNSTABLE STORE

This store is assumed to be a medium size, unstable store in the 750 lb class typical of those that may be carried in multiple carriage configurations. At transonic

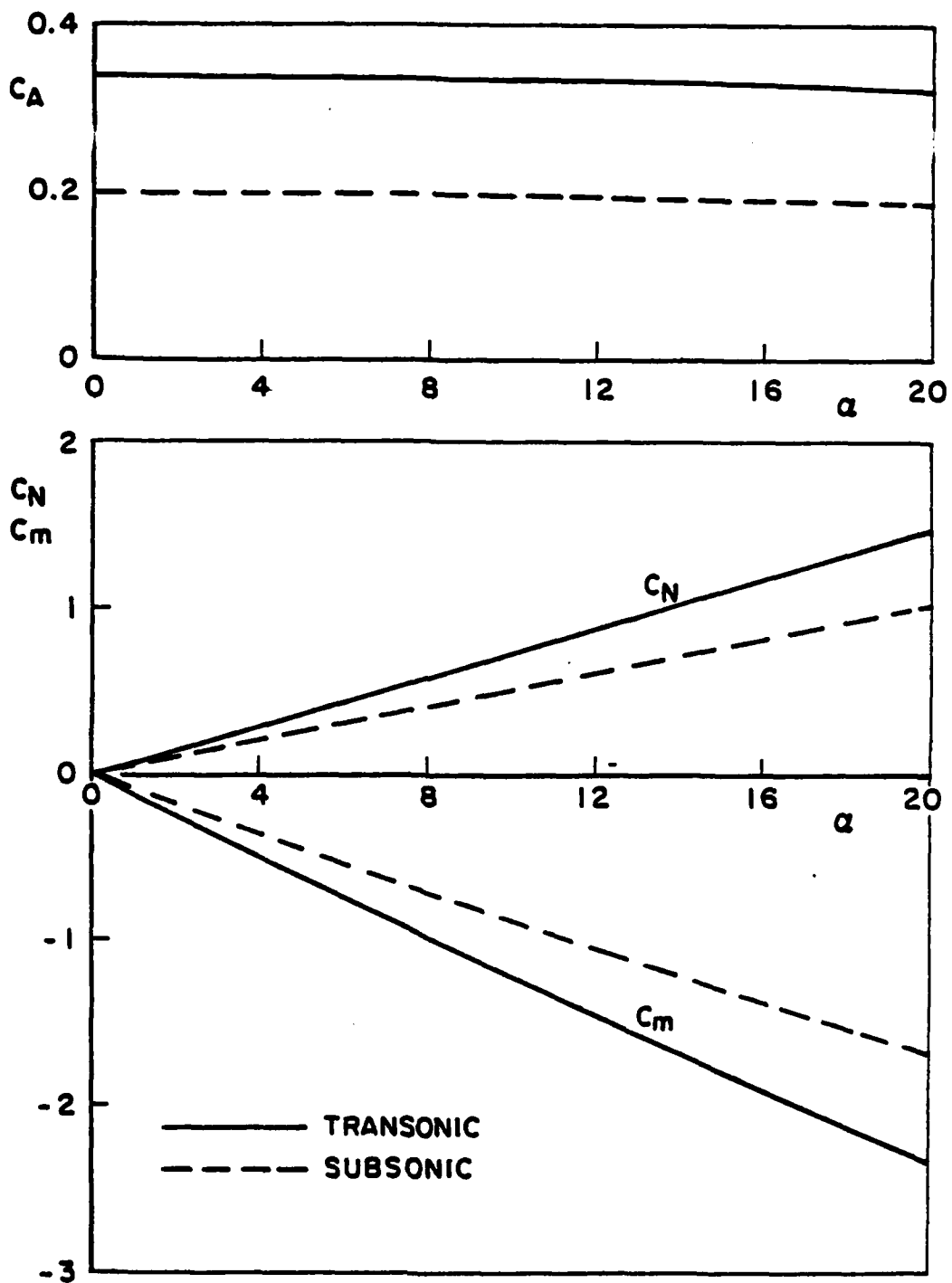
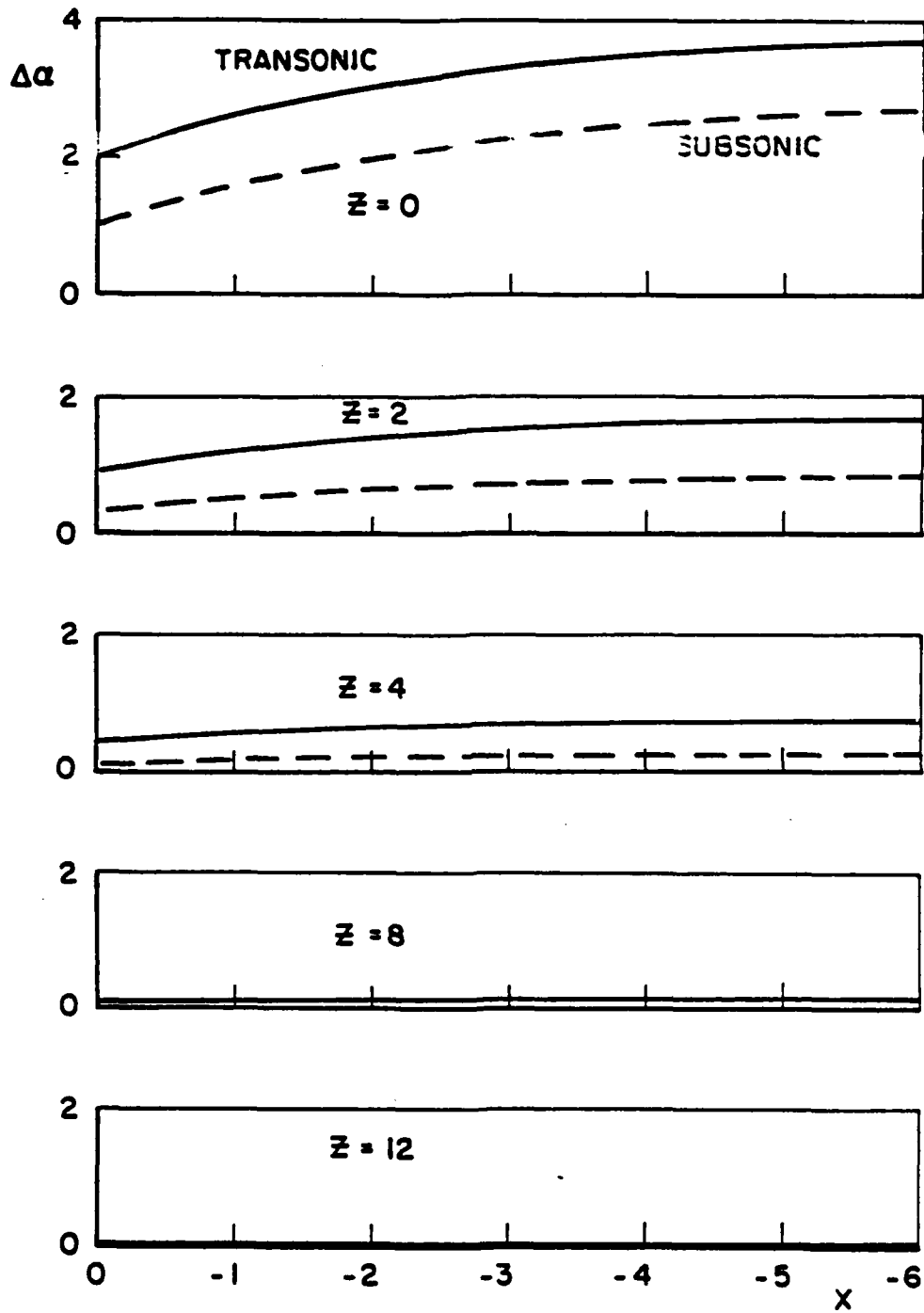
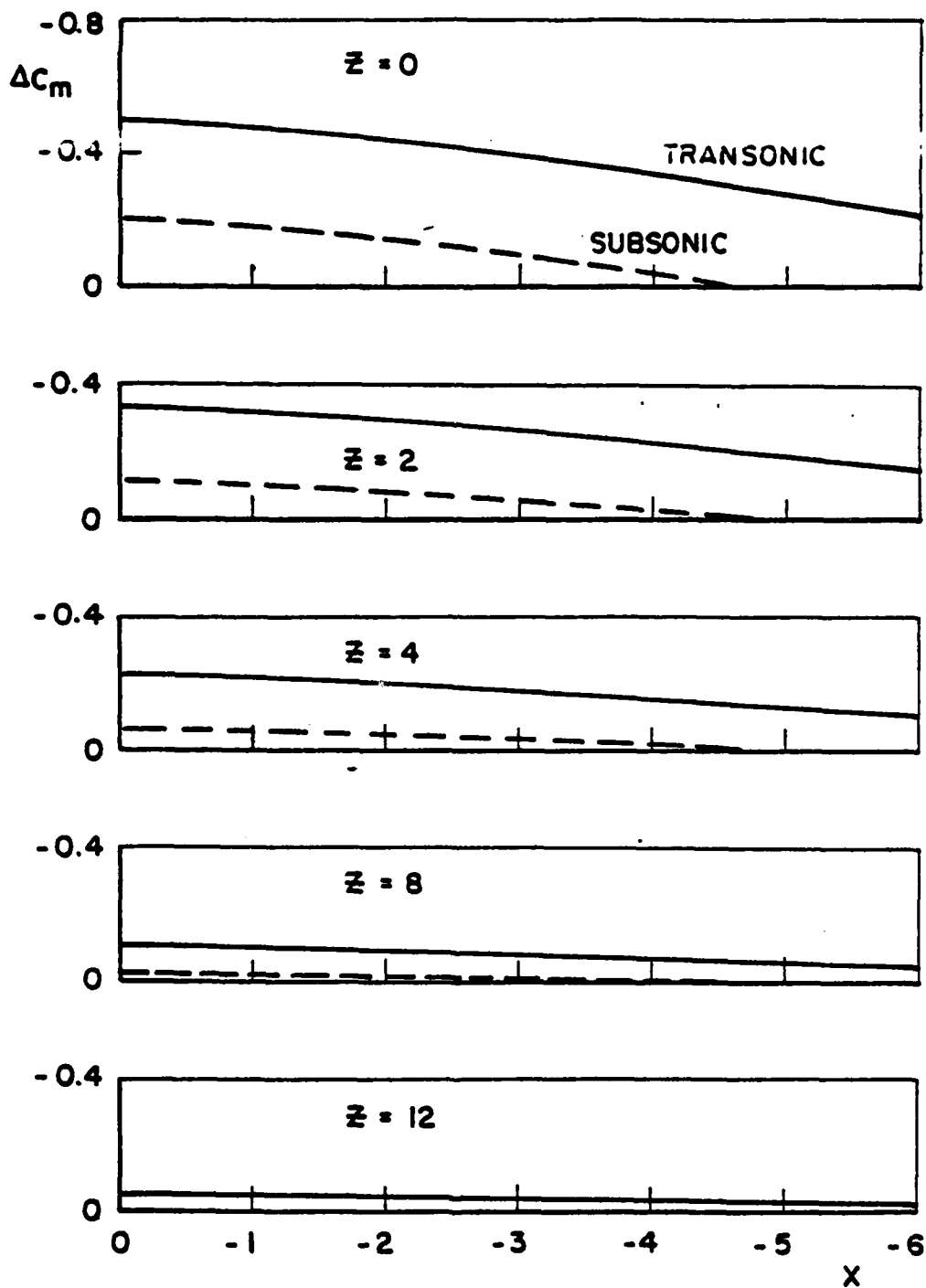


Figure 2 Stable Store Aerodynamics



a. Incremental Flow Angle

Figure 3 Aircraft Flow Field for Stable Store



b. Incremental Pitching-Moment Coefficient
Figure 3 Concluded

speeds, these stores may be subjected to rather large nose-down pitching moments in the carriage position. This characteristic is shown in the aerodynamic data for this store shown in Figs. 4 (free stream) and 5 (flow-field effects). Aerodynamic data for this store are presented for angles of attack up to 180 deg since it may be expected to experience a tumbling motion upon release from the aircraft.

V. TRAJECTORY CALCULATIONS

To calculate the motion of the two selected stores, a three-degree-of-freedom set of equations was programmed on a digital computer based on the relations in Equations 4, 5, and 6. In these equations, the aerodynamic coefficients were calculated as the sum of the attitude (free stream) contribution plus the position (flow-field effect) contribution, according to the relations described in Figs. 2 and 3 or Figs. 4 and 5. The base data were calculated for mass properties and flight conditions of the full-scale store at the indicated Mach number and altitude. The characteristic motion of wind tunnel models designed according to the various scaling laws was calculated using the same equations, but with model mass properties and wind tunnel operating parameters used as input quantities. For these calculations, a model scale factor of 0.05 was used. Wind tunnel parameters were calculated using a total temperature of 110°F and dynamic pressures of 50 psf for Froude Scaling, 200 psf for Heavy Mach Scaling, and 600 psf for Light Mach Scaling. The equivalent full-scale position coordinates and time scale were then determined through the appropriate scaling relationships. The comparisons are based on the thus-determined full-scale motion.

A. STABLE STORE

Trajectory calculations for the large stable store are presented in Figs. 6, 7, and 8. The full-scale flight conditions were assumed to be Mach number 0.95 at an altitude of 6000 feet. Each figure shows both the full-scale trajectory calculation and the coordinates determined from model-scale calculations using one of the three scaling techniques. Froude Scaling data are shown in Fig. 6 for two cases: (1) both store and aircraft flow field aerodynamics are independent of Mach number, and (2) both store and aircraft flow-field aerodynamics vary with Mach number as shown in Figs. 2 and 3. The first case shows that the inertial scaling relationships are correctly stated, since the scaled-up trajectory motion reproduces that of the full-scale store. The second case shows the limitation of the Froude Scaling technique where transonic or supersonic effects influence the aerodynamic scaling.

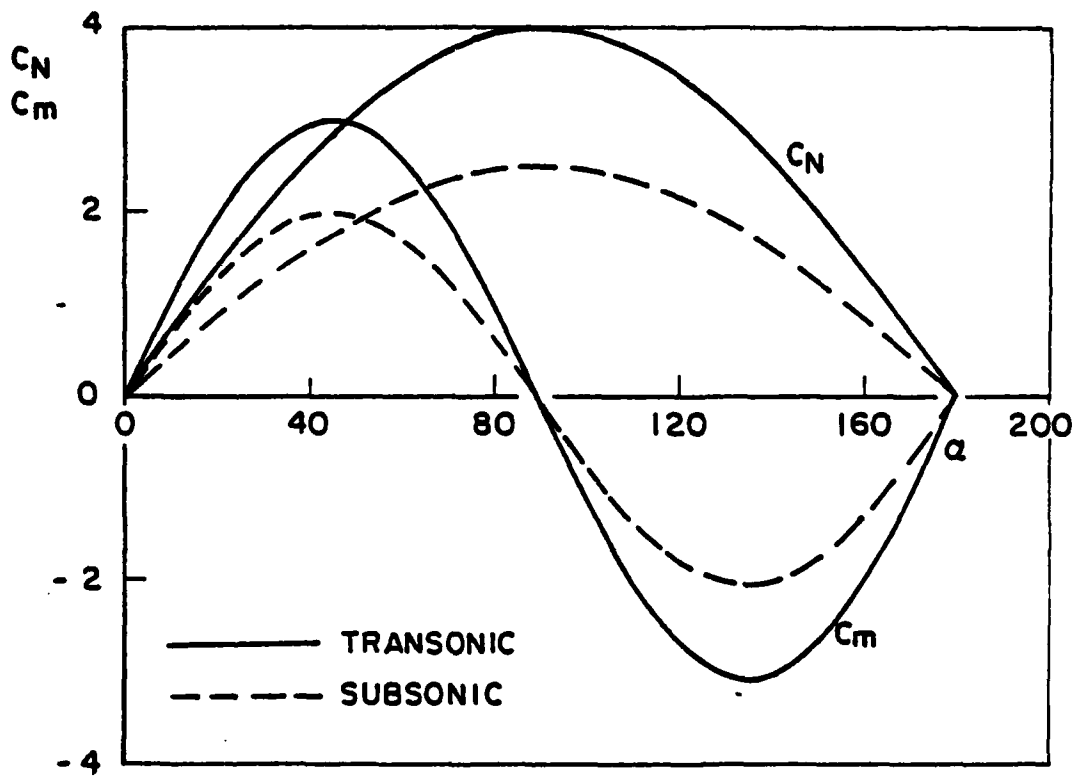
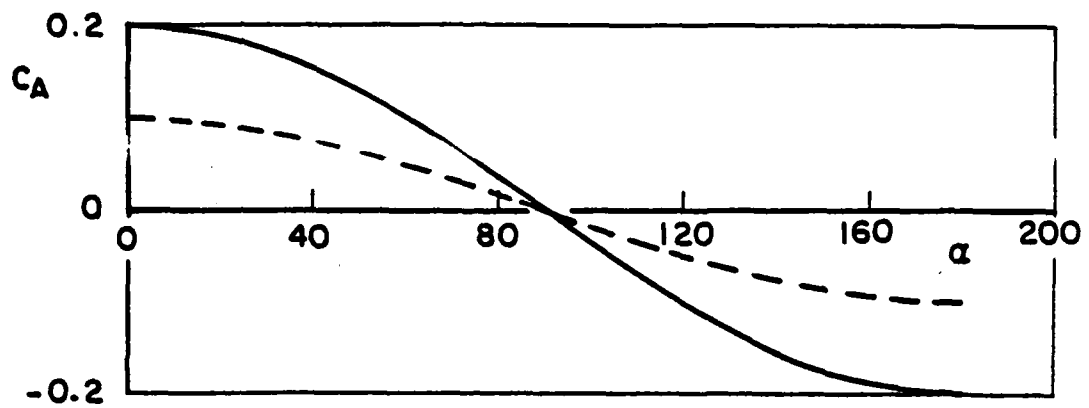
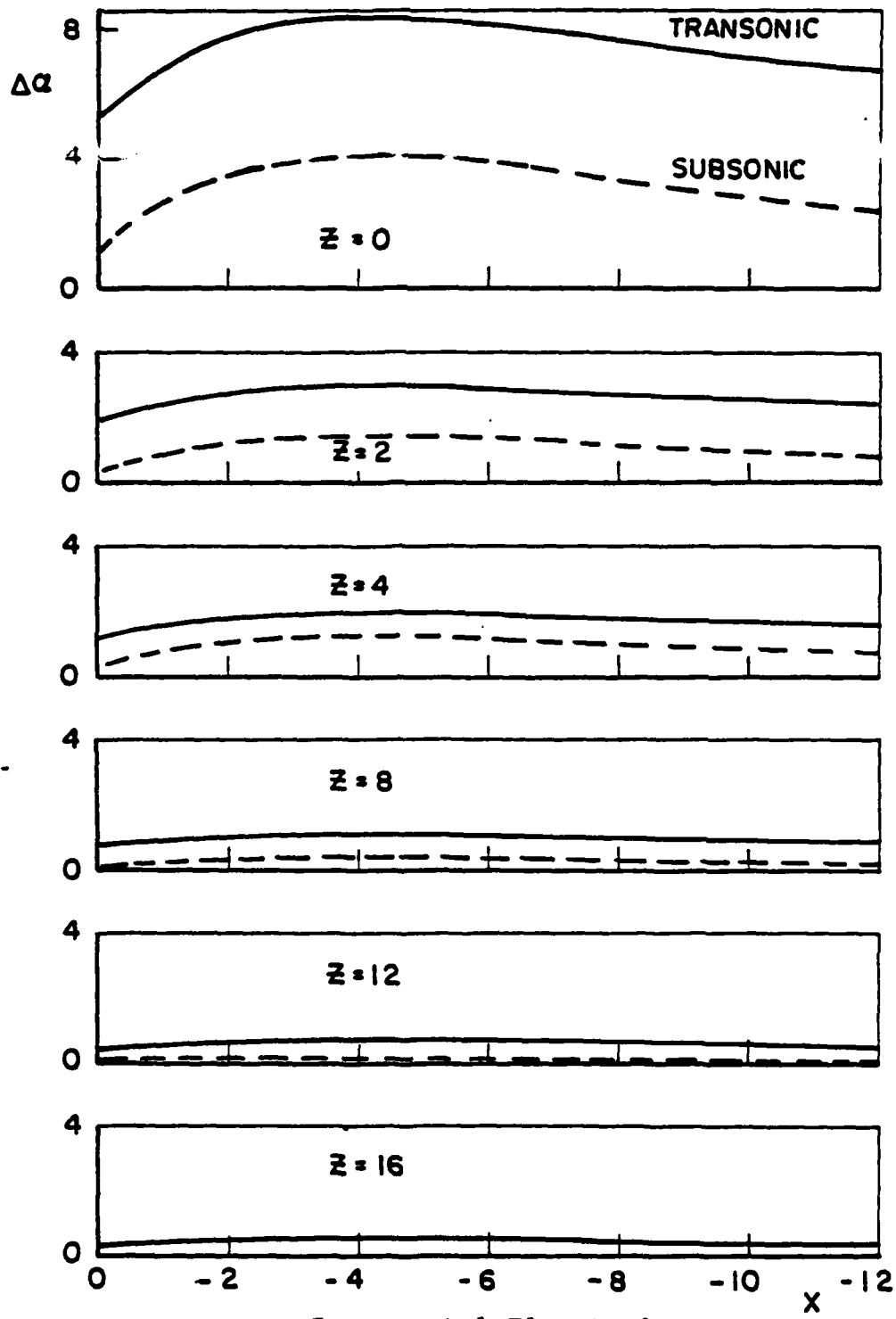
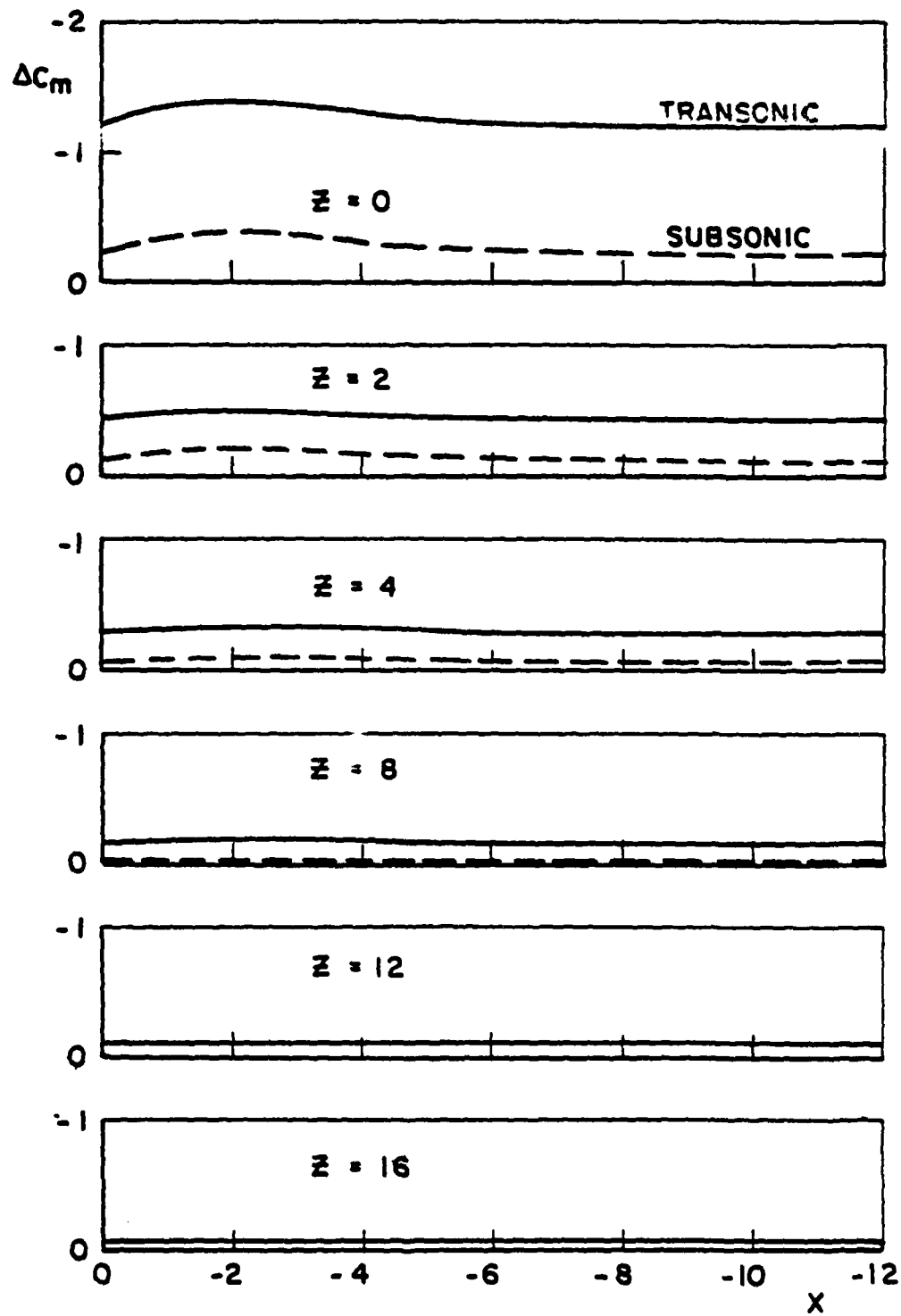


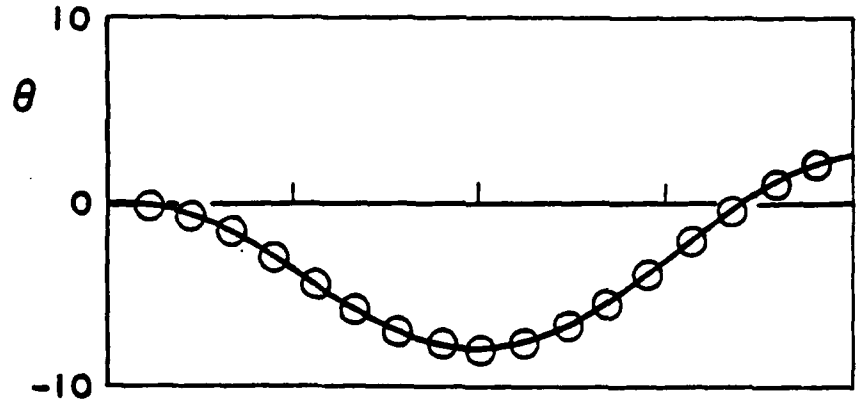
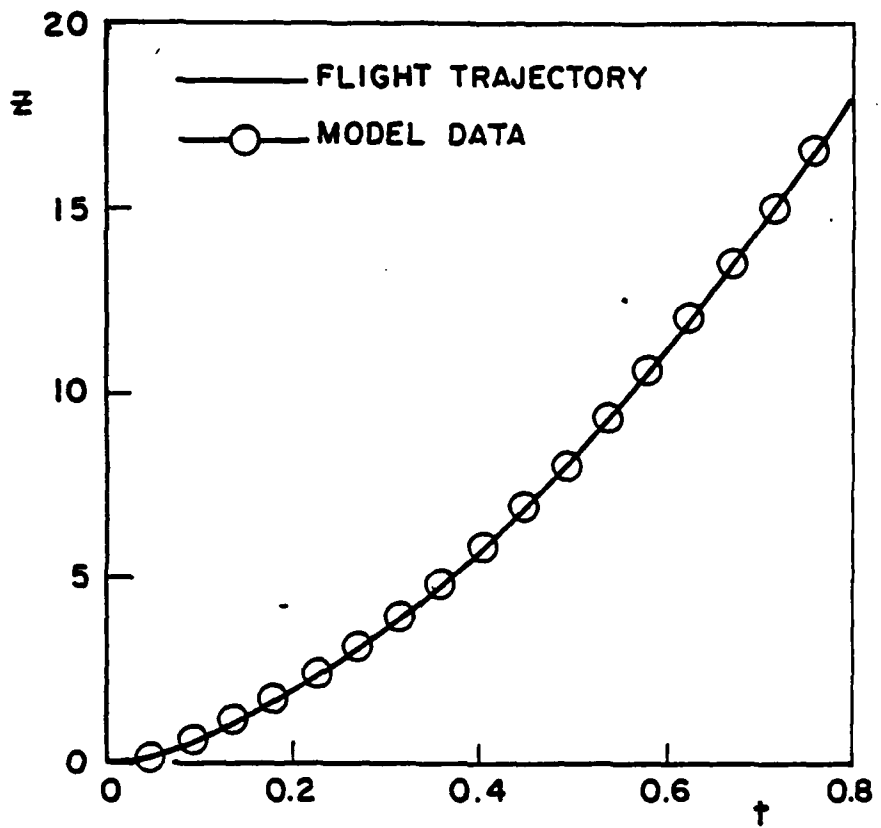
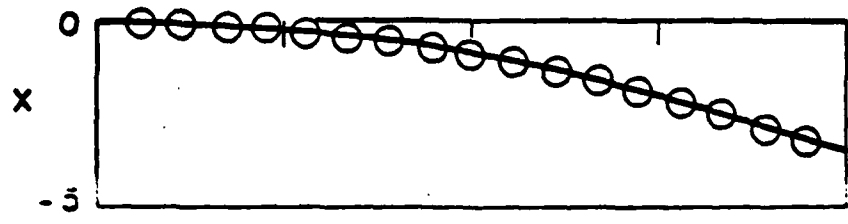
Figure 4 Unstable Store Aerodynamics



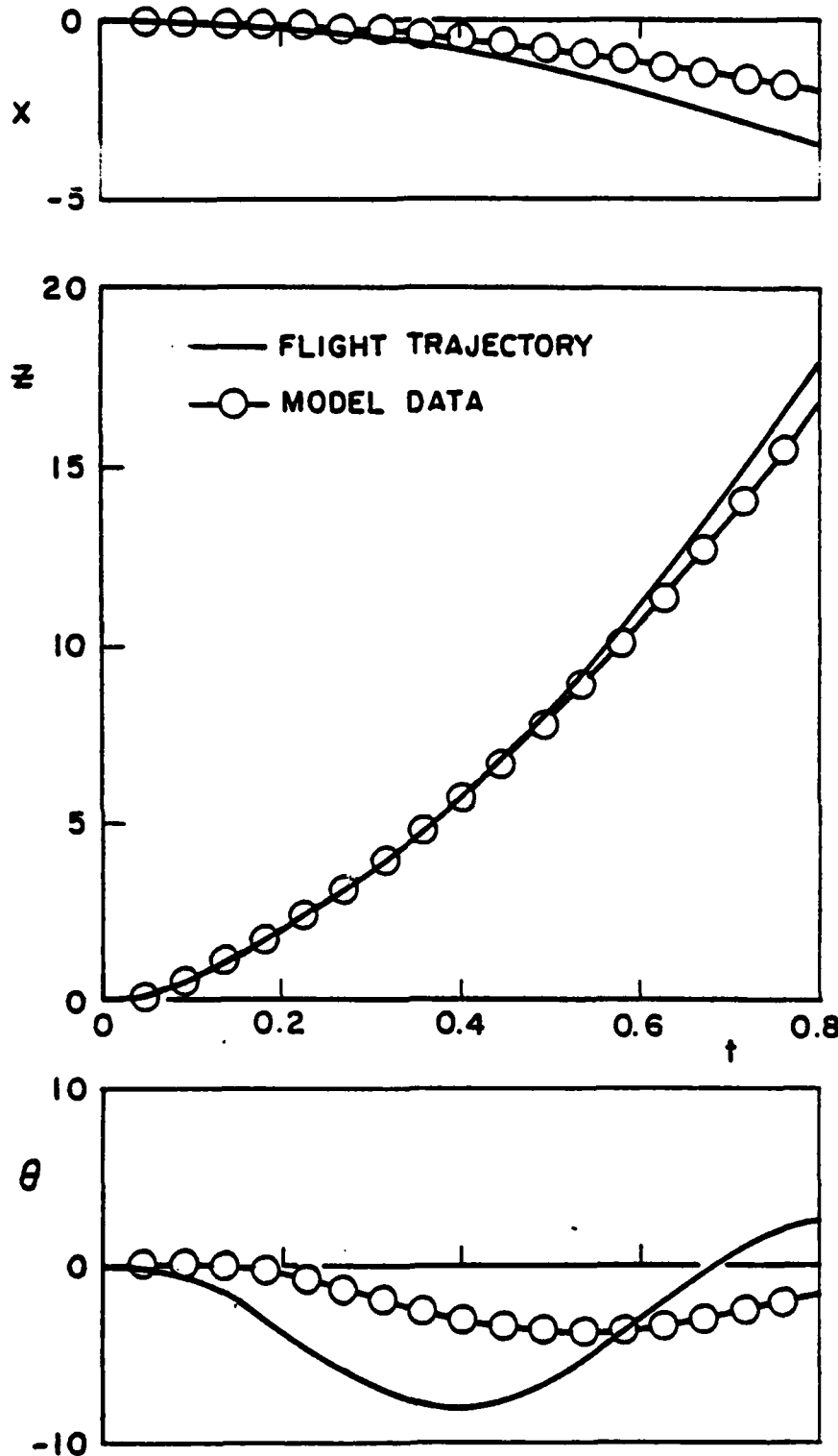
a. Incremental Flow Angle
 Figure 5 Aircraft Flow Field for Unstable Store



b. Incremental Pitching-Moment Coefficient
Figure 5 Concluded



a. Transonic Aerodynamics
 Figure 6 Froude Scaling with Stable Store



b. Subsonic Aerodynamics
Figure 6 Concluded

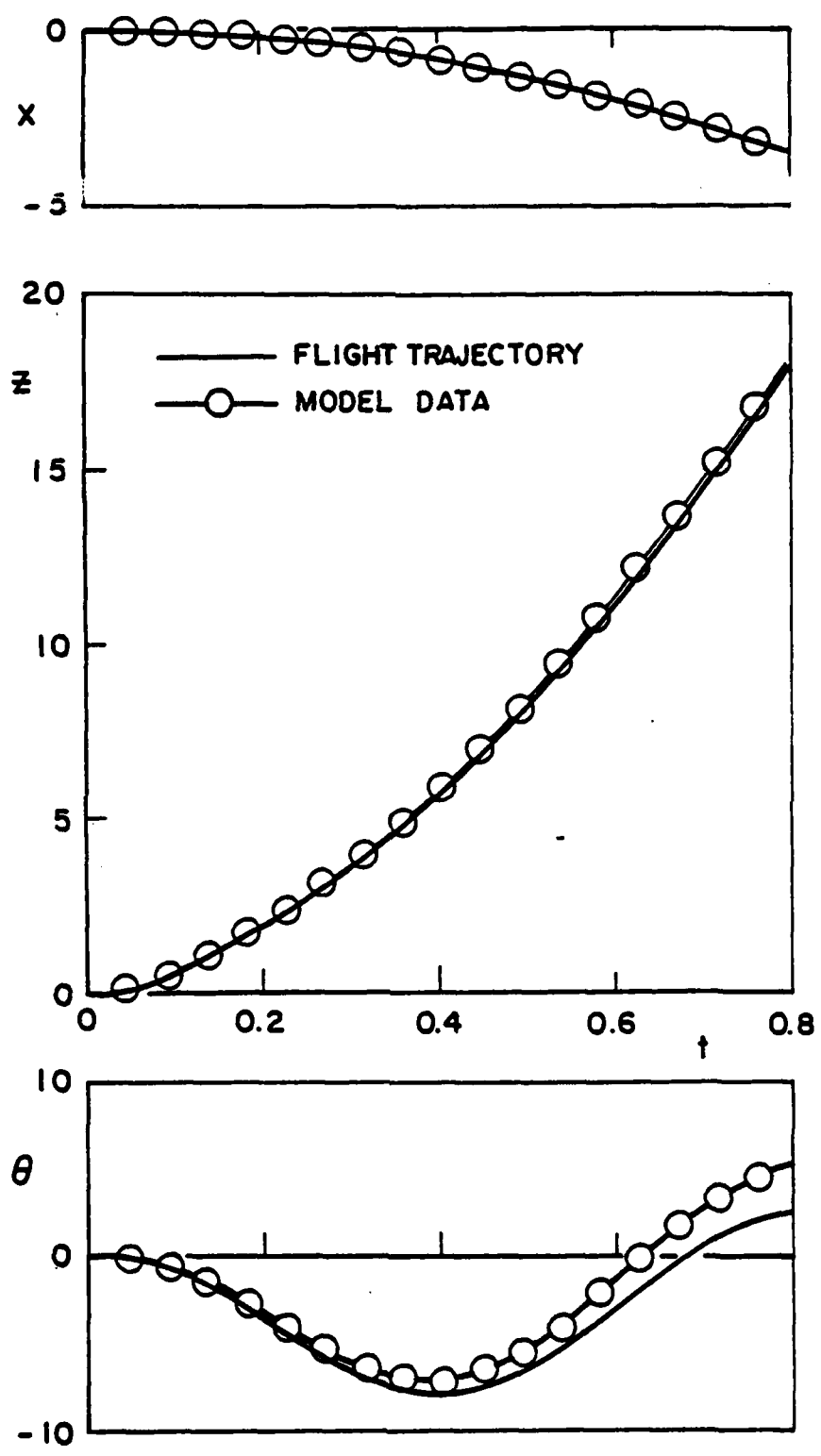
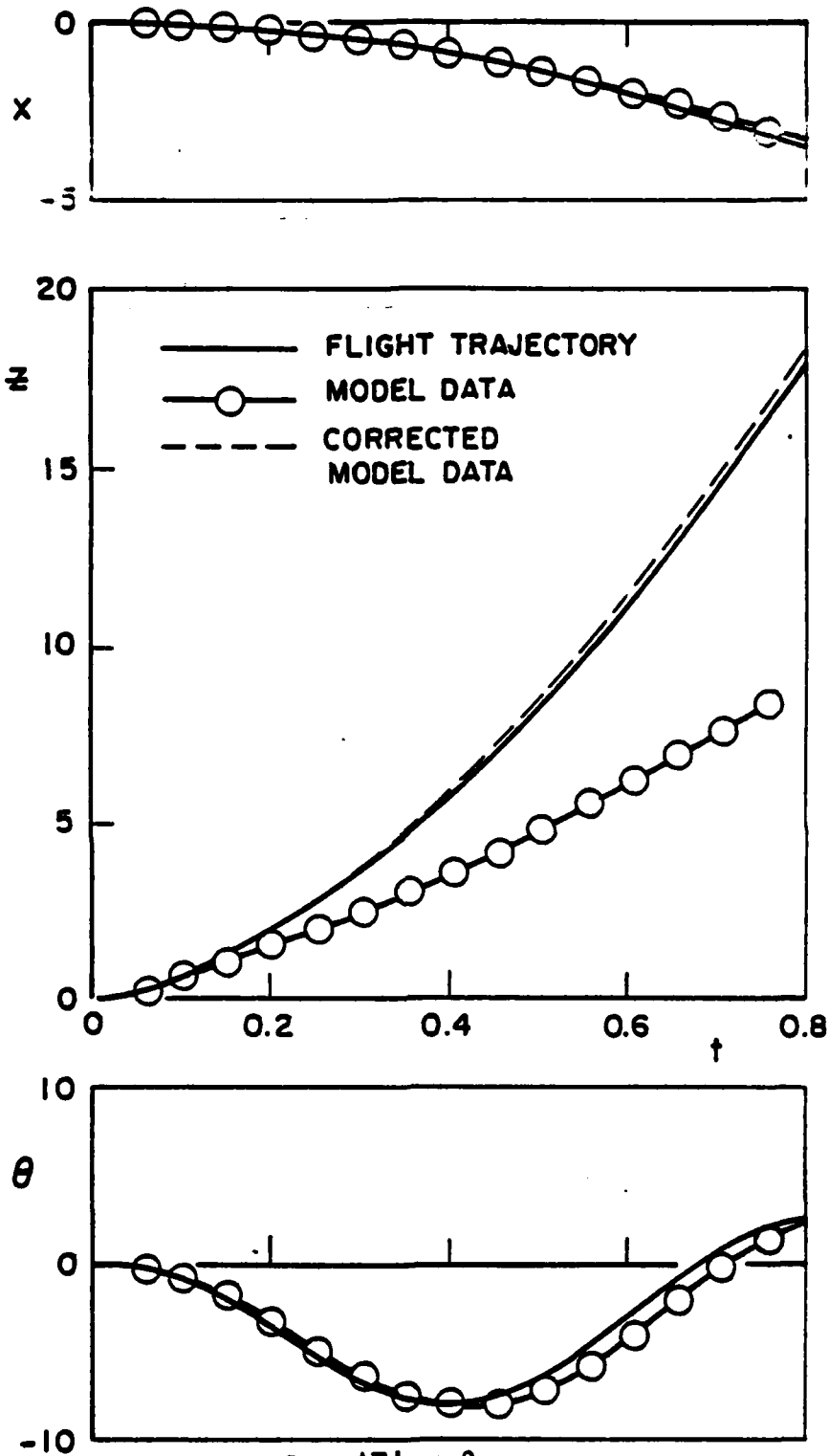
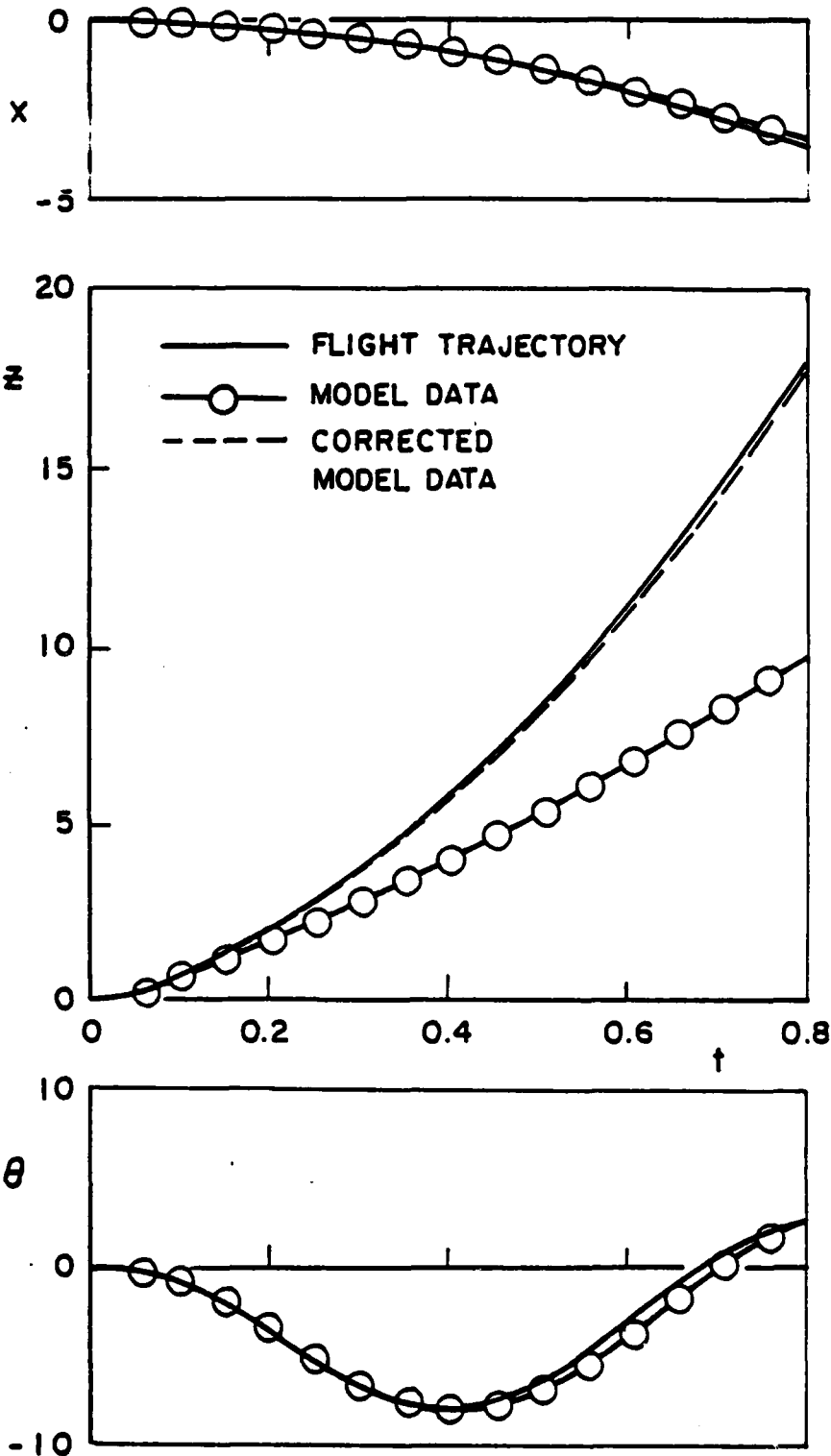


Figure 7 Heavy Mach Scaling with Stable Store

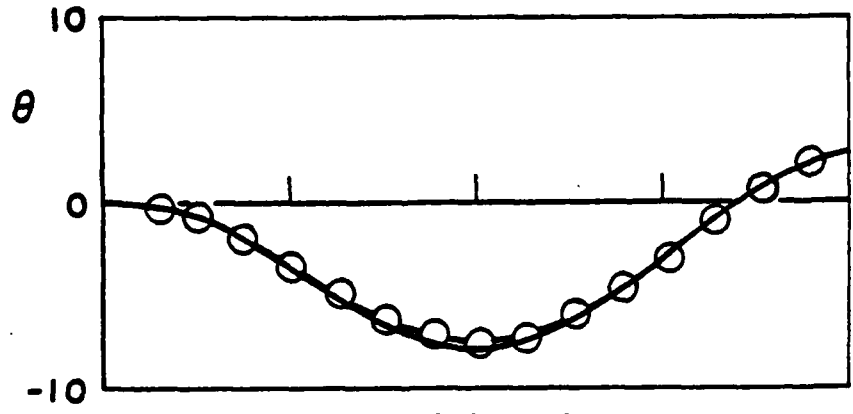
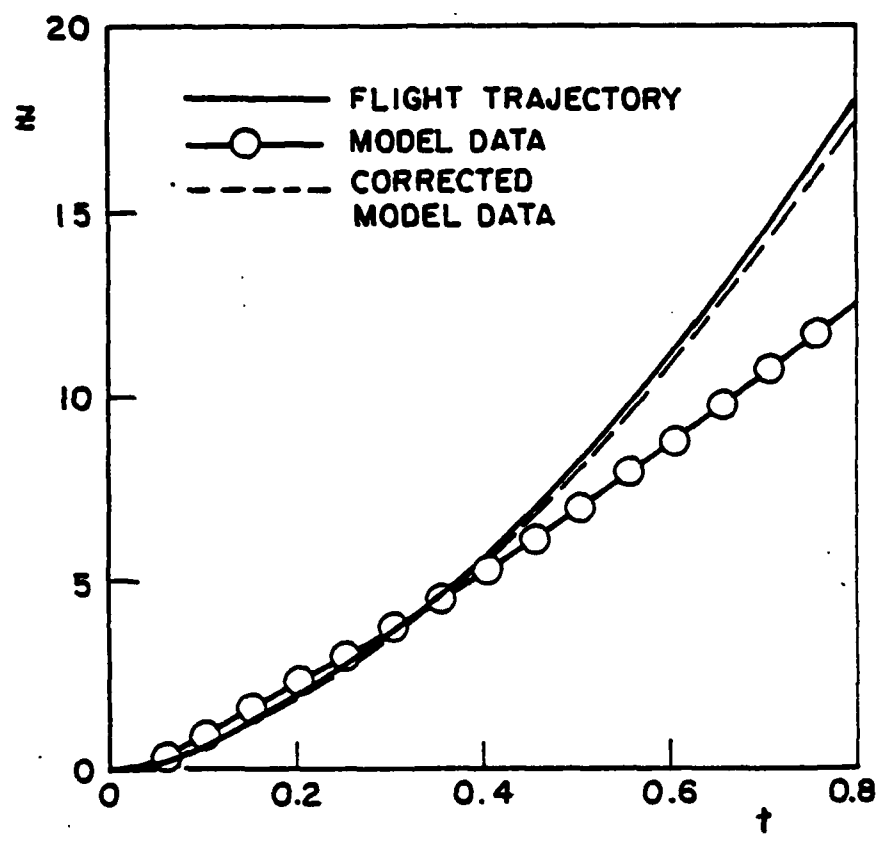
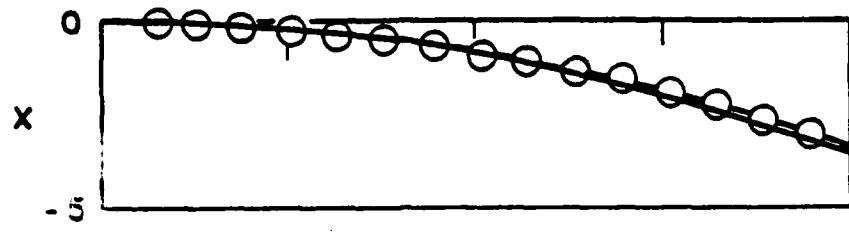


a. $\Delta F' = 0$

Figure 8 Light Mach Scaling with Stable Store



b. $\Delta F' = m' (\Delta g')$
 Figure 8 Continued



c. $\Delta F' = 3m' (\Delta g')$
 Figure 8 Concluded

The results of the Heavy Mach Scaling technique are shown in Fig. 7. For this configuration, the primary discrepancy between model-scale and full-scale calculations is the underdamped pitch oscillation due to lack of correct velocity scaling.

Calculations using the Light Mach Scaling technique are shown in Fig. 8 for three cases: (1) ejector force scaled from the full-scale values according to Equation 19e, (2) the scaled ejector force augmented by the amount indicated in Equation 21 to offset the gravity deficiency during ejector action, and (3) the scaled ejector force augmented by three times the amount in case (2) in order to provide store clearance from the aircraft during the initial critical period following release. These data show better simulation of the pitch motion than for either the Froude Scaling with Mach number effects or the Heavy Mach Scaling, but this is achieved only at the expense of the vertical motion simulation.

Also shown in Fig. 8 is an adjusted vertical displacement curve calculated with an empirical correction based on the known variation from true simulation. The correction is applied to the model-scale calculation, and is given by

$$\text{for } t' < t_e'$$

$$\Delta z' = \frac{1}{2} (\Delta g') (t')^2 - \frac{1}{2} \left(\frac{\Delta F'}{m'} \right) (t')^2 \quad (23)$$

$$\text{for } t' \geq t_e'$$

$$\Delta z' = \frac{1}{2} (\Delta g') (t')^2 - \frac{1}{2} \left(\frac{\Delta F'}{m'} \right) (t_e') (2t' - t_e') \quad (24)$$

where $(\Delta g')$ is defined in Equation 20, $(\Delta F')$ is ejector force augmentation, and t_e' is the time at which the ejector action ceases. The term with $(\Delta g')$ accounts for the deficiency in the gravity force, while the term with $(\Delta F')$ accounts for the additional velocity imparted by the augmented ejector force. Application of this correction requires knowledge of the time of action of the ejector, which generally requires knowledge of the applied aerodynamic forces. However, an estimate of the time of action can be made assuming no aerodynamic forces, and the resulting error in the corrected displacement will be typically on the order of 2 percent. In Fig. 8, it can be seen that the correction is quite good for all three cases.

B. UNSTABLE STORE

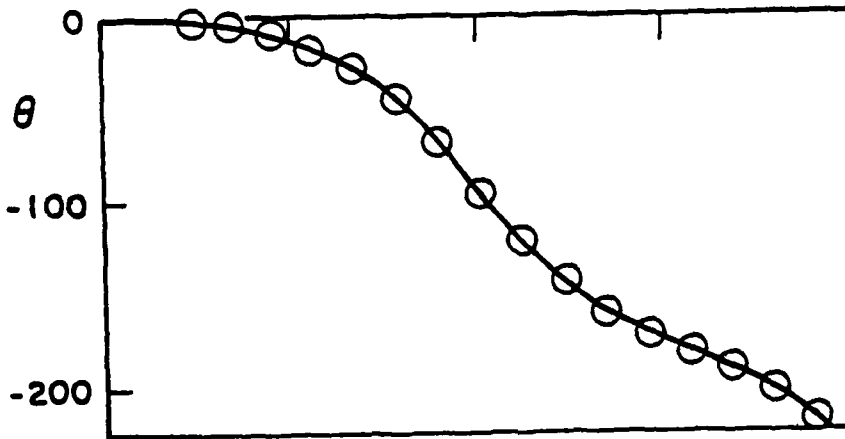
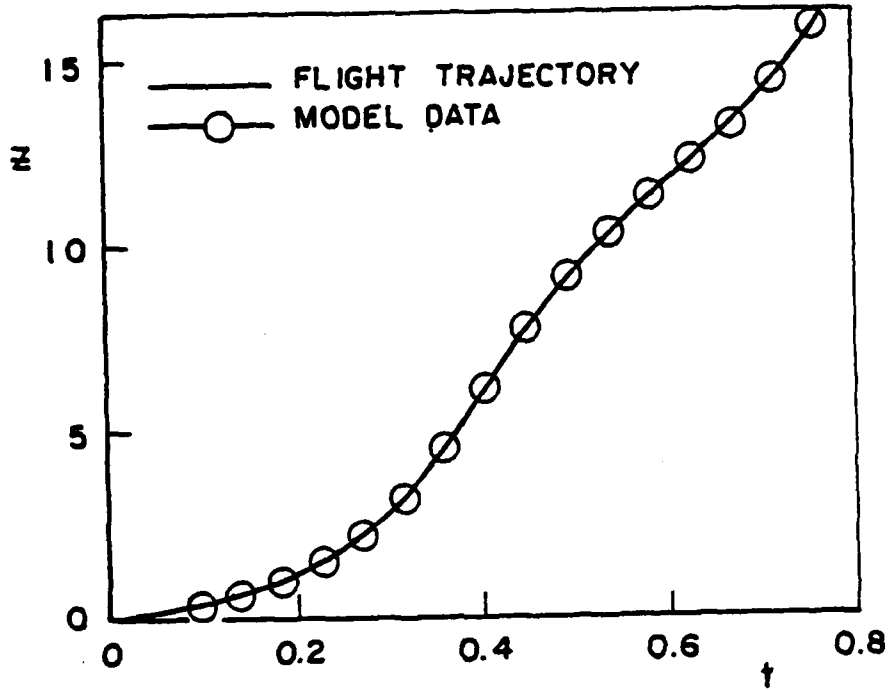
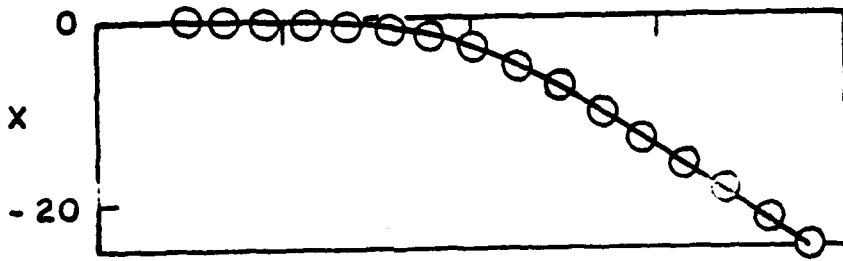
Trajectory calculations for the smaller unstable store are presented in Figs. 9, 10, and 11 for the same combination of scaling techniques as stated above for the stable store. In this case, the full-scale flight conditions were assumed to be Mach number 0.9 at an altitude of 5000 feet. The effect of Mach number dependency of the aerodynamic coefficients has an even more pronounced effect on the Froude Scaling results for this store, changing the motion from tumbling to oscillatory. The aerodynamic characteristics chosen for this example were specifically selected to show this change, and may overstate the case relative to any actual store. However, it is important to realize the changes that may occur so as not to be misled in interpreting test results.

The Heavy Mach Scaling data show reasonably good simulation of the motion, again demonstrating the lack of full damping of the pitch motion.

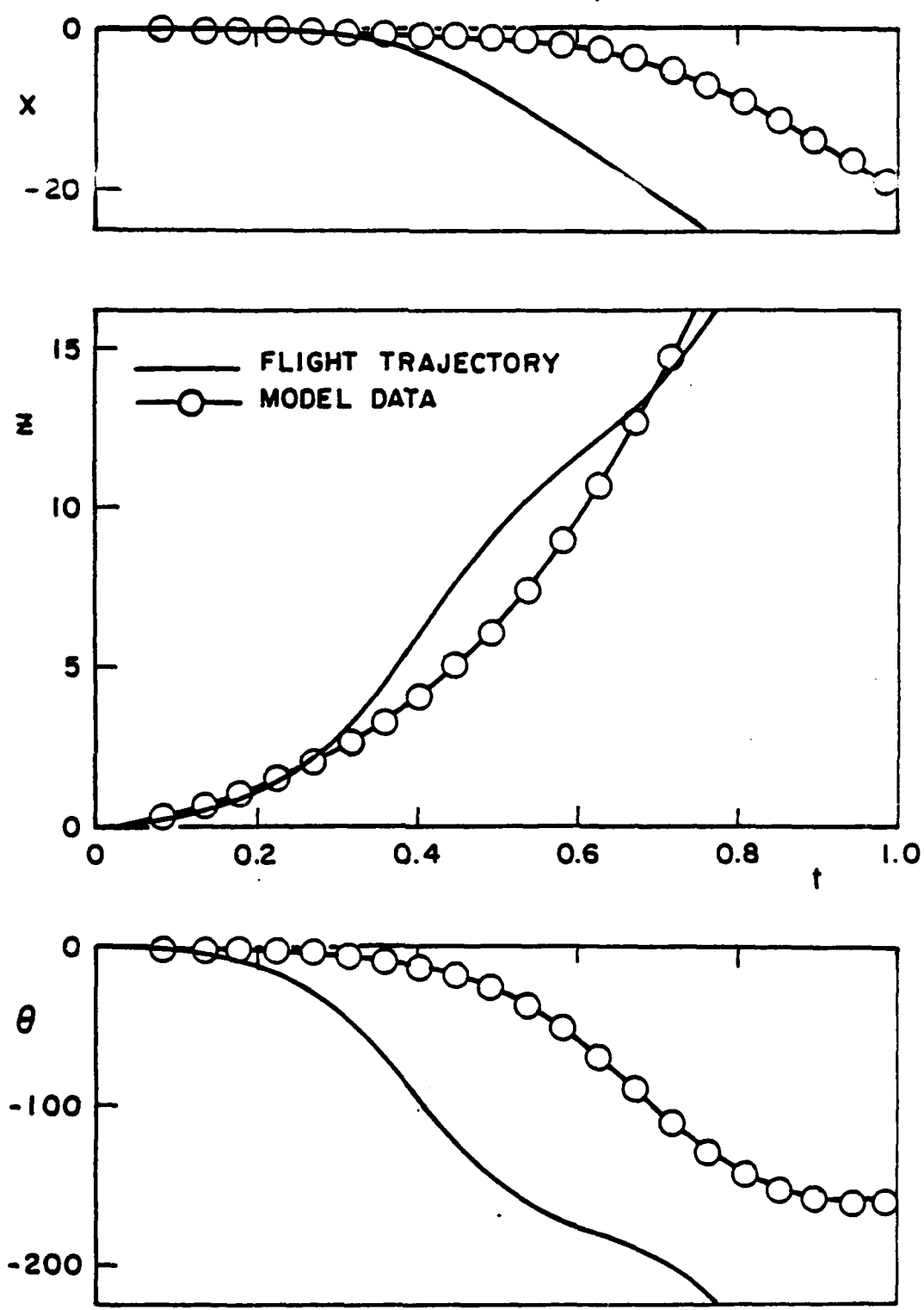
The effects of augmented ejector force on the Light Mach Scaling data for the unstable store are much the same as for the stable store except that in this case the rapid tumbling makes collision more likely. Thus, the need to maintain a model flight path below the true flight path is more critical. The amount of augmentation required will depend on the store size and shape, and the geometry of the installation on the aircraft. However, it appears that an augmentation force ($\Delta F'$) of two to three times the gravity deficiency correction would be suitable, and the corrected data of Fig. 11 indicate that this would provide a reasonable simulation.

VI. DISCUSSION

On the basis of the development of the scaling relationships, it would be desirable to be able to utilize the method referred to herein as the Froude Scaling technique. To do so with confidence requires the knowledge, or assumption, that the aerodynamic forces and moments imposed on the store model will be independent of the wind tunnel operating parameters (i.e., Mach number and Reynolds number), or that the aerodynamic loads are so small that typical variations with Mach number will have little effect on the motion. This latter situation would effectively rule out the need for the wind tunnel since, if the aerodynamics are so unimportant, the motion could be evaluated by simple calculation. However, experience has shown that the character of



a. Transonic Aerodynamics
 Figure 9 Froude Scaling with Unstable Store



b. Subsonic Aerodynamics
Figure 9 Concluded

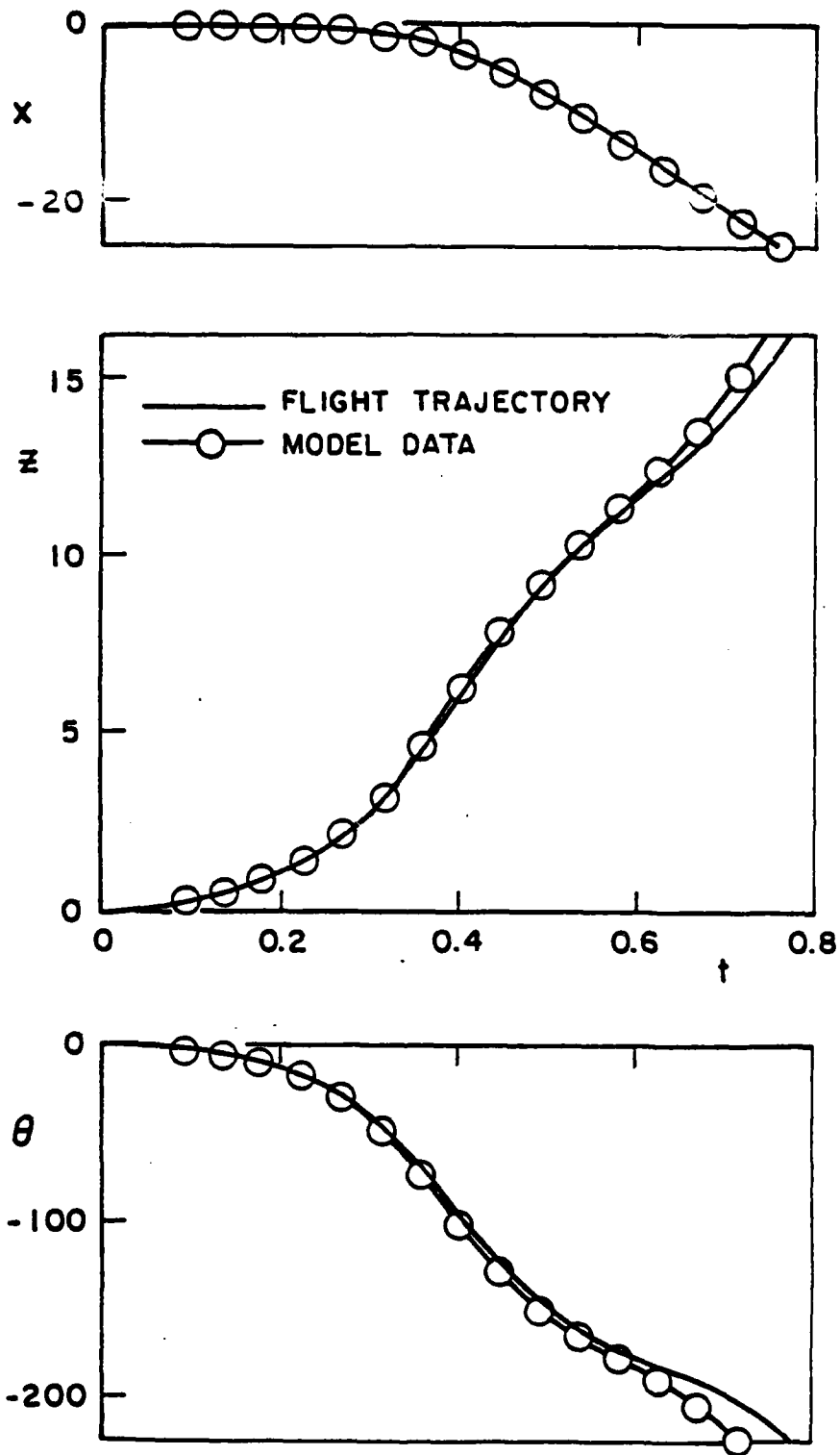
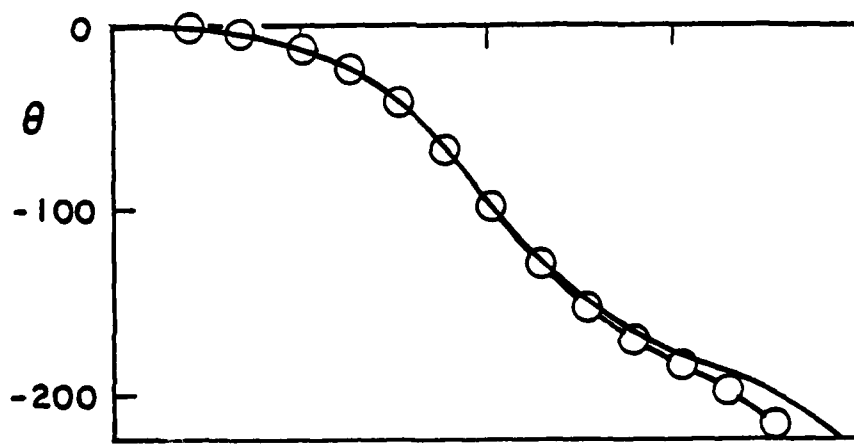
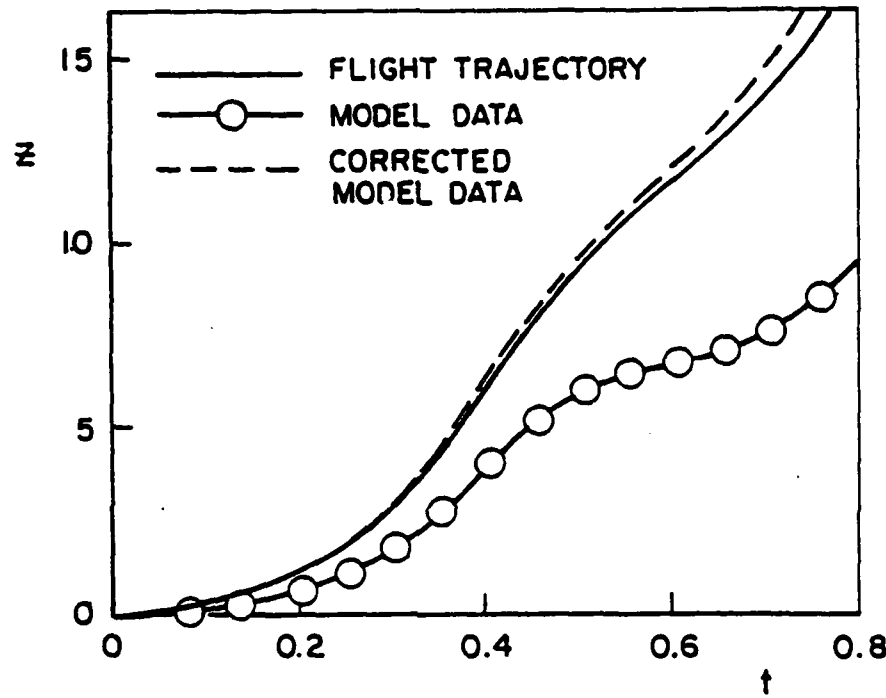
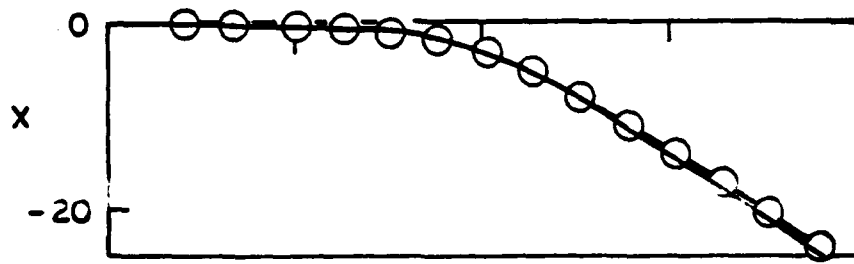
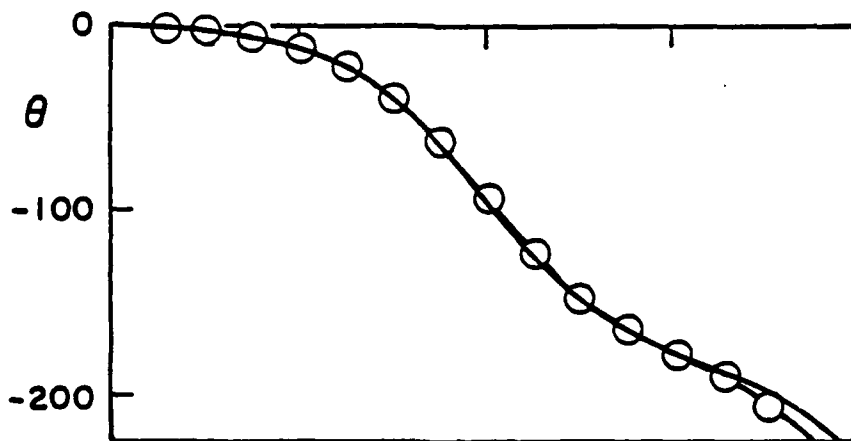
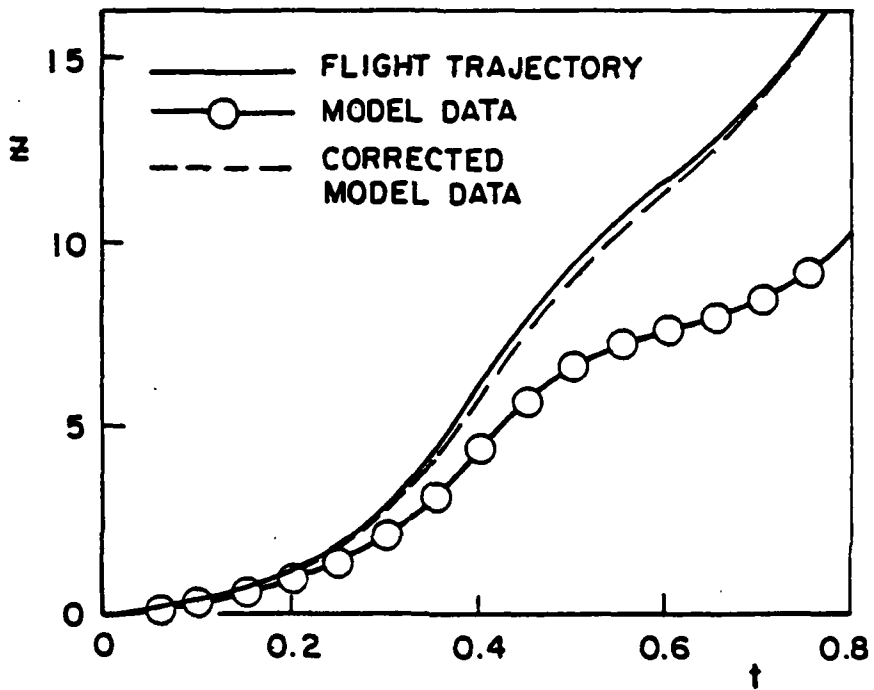
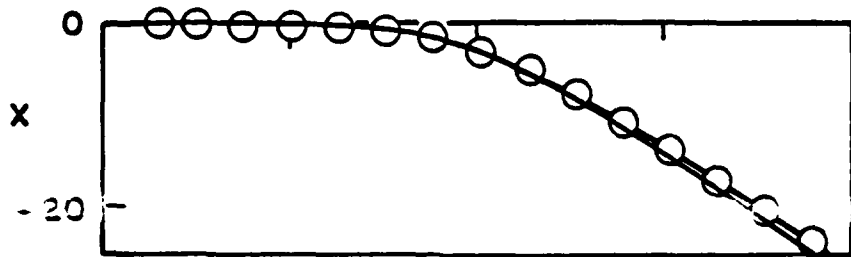


Figure 10 Heavy Mach Scaling with Unstable Store

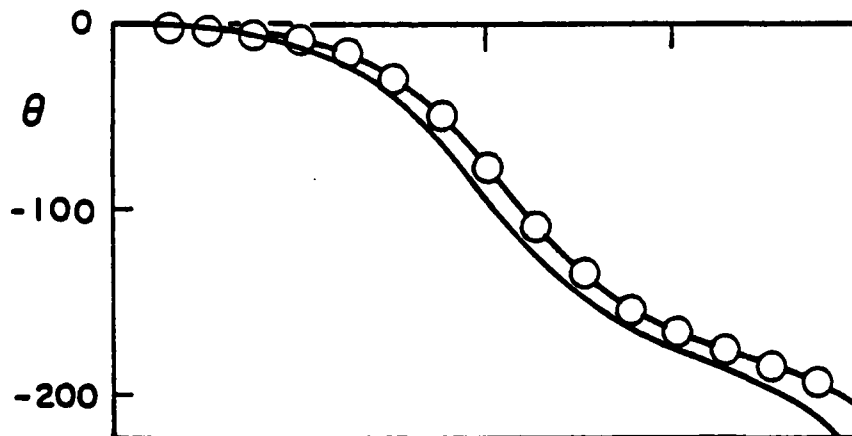
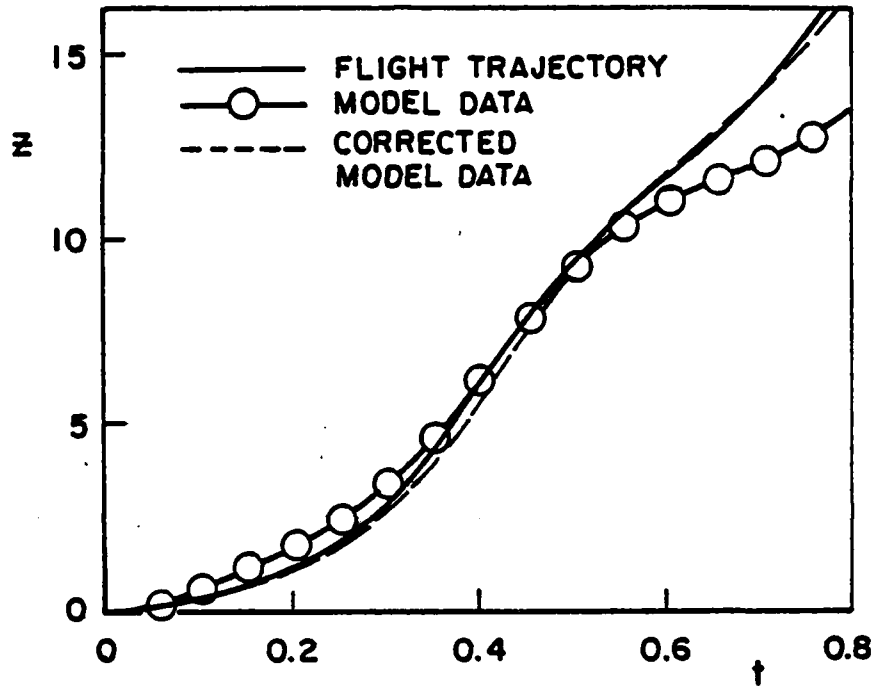
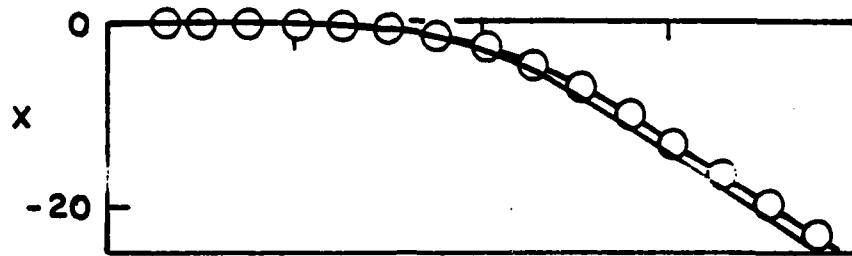


a. $\Delta F' = 0$

Figure 11 Light Mach Scaling with Unstable Store



b. $\Delta F' = m' (\Delta g')$
 Figure 11 Continued



c. $\Delta F' = 3m' (\Delta g')$
 Figure 11 Concluded

the flow around typical aircraft carriage locations has a significant variation with Mach number at transonic and supersonic speeds. Likewise, in this speed range the aerodynamic forces are often the predominant ones, particularly at altitudes typical of tactical aircraft operation. Thus, we must be prepared to deal with the Mach number simulation requirement, which leads to the use of the other scaling techniques.

The calculations presented herein would seem to validate the usual selection of Heavy Mach Scaling as the alternative to Froude Scaling. Certainly, for the examples presented, the comparison of model-scale data with full-scale trajectories would provide an acceptable simulation for all but the most demanding analyses. However, there are some other practical problems that must be considered in selecting the optimum experiment. As pointed out in Section III.2., the Heavy Mach Scaling relationships generally require model densities significantly higher than the density of the full-scale store. For model scale factors in the range of 0.04 to 0.07, typical for many current wind tunnel facilities, this often requires densities available only by use of materials such as platinum, iridium, tungsten, gold, or depleted uranium. Of these, alloys of tungsten are generally selected, although gold has superior qualities of formability, which is especially important for non-axisymmetric shapes. For economic reasons there is understandable, if sometimes irrational, reluctance to use the precious metals for "throw-away" wind tunnel models. Gold at \$200 a Troy ounce would cost \$2670 and \$1060 for the model weights calculated for the trajectories of Figs. 7 and 10, respectively. However, the models are recovered (although often broken or chipped), and the salvage value of the material would reduce the net cost significantly. As an alternative to the use of exotic materials, the wind tunnel operating pressure level may be reduced (assuming a variable density facility) so as to permit the use of more readily available materials. In this case, the Reynolds number simulation is worsened, perhaps to the point of significantly altering the aerodynamic characteristics of the models.

Turning to the use of Light Mach Scaling to alleviate the problems of Heavy Mach Scaling should not be done too hastily, however. Although the data presented herein show that the measured trajectory coordinates can be effectively corrected to infer the true coordinates, some general knowledge of the store behavior is needed in advance to effectively establish the proper experimental parameters. If a

large ejector force augmentation is called for, this can generate model design problems of a different nature than for the Heavy Mach Scaling models. For the data presented in Fig. 11c, the required ejector force was 19 pounds and the model weight was approximately two and one-fourth ounces. This would correspond to a model density about half that of aluminum. Although the required ejector force could be reduced by reducing the wind tunnel pressure level, the model weight would be reduced correspondingly.

The choice among the various available experimental techniques is thus not an easy one. From a purely analytical standpoint, the Froude Scaling and Light Mach Scaling methods appear to offer the best overall simulation of store motion. Model fabrication costs would also appear to favor these methods. However, practical application of these techniques runs afoul of the need to know much about the aerodynamic environment in advance, whereas a primary requirement for freedrop testing results from the highly non-uniform, and largely undescribed, aerodynamic flow field surrounding an aircraft at transonic and supersonic speeds. If we are to continually demand more accurate and detailed answers from the experiments, then we shall have to be more detailed and sophisticated in our preparations for the experiments. Efforts currently underway to establish mathematical models of aircraft flow-field aerodynamics should provide an important new tool to expand motion analyses, such as the one reported herein, to provide greater insight into the requirements for a specific experiment. This would allow calculations to be made using each of the scaling techniques for a given separation situation so that effective trade-offs could be made, and the most suitable experiment could be selected with confidence.

REFERENCES

1. Deitchman, S. J. "Similarity Laws for Dynamic Model Testing, "Cornell Aeronautical Laboratories, Report No. CAL GC-910-C-14, September 1956.
2. Sandahl, C. A. and Faget, M. A. "Similitude Relations for Free-Model Wind-Tunnel Studies of Store-Dropping Problems, "National Advisory Committee for Aeronautics, Technical Note No. TN-3907, January 1957.

John C. Marshall

Mr. Marshall received his engineering education at the California Institute of Technology, being granted a B.S. degree in Mechanical Engineering in 1949 and an M.S. degree in Aeronautics in 1951. He joined ARO, Inc. in 1951 and was associated with the initial development of transonic wind tunnel testing at AEDC. Since 1959, he has been an Engineering Supervisor responsible for conducting wind tunnel test programs and for aerodynamic design of a new test facility. In 1968, he was assigned to develop and conduct experimental test programs related to store separation in the 4-foot transonic wind tunnel using grid survey, captive trajectory, and freedrop test techniques. Mr. Marshall is an Associate Fellow of the AIAA, a registered Professional Engineer in Tennessee, and a special advisor to the SAB Division Advisory Group of the Aeronautical Systems Division (AFSC), Wright-Patterson Air Force Base.

**APPLICATION OF A GENERAL PURPOSE DYNAMIC ANALYSIS
PACKAGE TO THE PROBLEMS OF STORE SEPARATION**

(U)

(Article UNCLASSIFIED)

by

**B. H. Welch and B. J. Richter
Lockheed Missiles & Space Company, Inc.
Sunnyvale, California 94088**

ABSTRACT. (U) A general purpose dynamic analysis package has been developed which accurately simulates complex interactive behavior between structural bodies and surrounding environments. This paper discusses some of the unique capabilities of this analysis package, explains various separation/trajectory problems which have been analyzed with it, and examines the potential application of this new technology to the problems of store separation.

"Approved for public release; distribution unlimited."

LIST OF FIGURES

<u>Figure Number</u>	<u>Title</u>
1	Steps in the Solution of a Separation Mechanics Problem
2	Point/Surface Impact Element
3	Side View and End View of Example System "A" Modelled With No Impacts
4	Side View and End View of Example System "A" Modelled With Impacts
5	Side View and End View of Example System "B"
6	Details of Example System "C"
7	Side View and End View of Example System "C"
8	Isometric View of Example System "D"
9	End View of Example System "D"
10	Side View of Ground Test Simulation
11	End View of Ground Test Simulation

INTRODUCTION

In the past, the analysis of separation mechanics problems has been characterized by a multitude of computer programs, each developed in response to a particular problem or class of problems. By employing this approach, many man-hours are wasted in repeated program development, the probability of errors is increased, and the nonuniformity of the programs makes their general use difficult. To meet the need for a general purpose separation mechanics tool, a dynamic analysis package has been developed which simulates complex interactive behavior between structural bodies and surrounding environments. This analysis package can be utilized in either of two modes: 1) as a finished product in its own right capable of solving many "standard" separation mechanics problems, or 2) as an accurate, efficient framework of computational dynamics to which additional modules can be added to tailor the package to a specific or unique problem. In the field of store separation, for example, complex independently generated aerodynamic theories can be incorporated to form a powerful analytical tool.

DESCRIPTION OF THE ANALYSIS PACKAGE AND ITS CAPABILITIES

The term "analysis package" as used in this paper refers to a collection of computer programs and utility subroutines developed over a period of several years. At the heart of the package, however, are the computer programs DYNAMITE, an acronym for DYNAMIC Analysis of Mechanically Interacting Three-dimensional Elements (Reference 1), and DYNAMOVIE, a computer graphics program.

Because of the intended diversity of application, the package was kept as general as possible. The user is free to select any convenient inertial and body-fixed reference frames for use in the problem. Each body is treated in six degrees of freedom, and the number of bodies which can be accommodated is solely dependent upon the available core storage of the computer. This is accomplished by storing all of the variables in one large "pool" rather than in a number of individual arrays, each with a limiting size. The advantage of this method is that the use of core storage can be optimized merely by changing one dimension statement.

Before proceeding with a discussion of the features of this analysis package, it is appropriate to review the basic steps in the solution of any separation mechanics problem. The block diagram in Figure 1 illustrates these steps and notes with an asterisk those areas where optional modules can be added to account for effects which are unique to a particular problem (e.g., aerodynamics, gasdynamics, or guidance and control).

A library of standard force generating elements is included in the package simulating such things as:

- Linear and nonlinear springs
- Dashpots
- Inertial-fixed forces such as gravity
- Body-fixed forces such as rocket motors
- Mutual impacting/sliding between bodies

This last feature is referred to as the point/surface impact element. It allows the user to model areas of potential impacting/sliding between bodies as a combination of points and surfaces as shown in Figure 2. The location of the impact point in space is monitored at each timestep to determine whether an impact has occurred and, if so, what normal and frictional loads are associated with that impact. Elastic or inelastic collisions can be simulated by specifying a coefficient of restitution or ratio of relative velocity after impact to relative velocity before impact. In addition to simulating collisions between bodies, the point/surface impact element offers the user great flexibility in modelling various constraint guides such as shear lips, guide rails, rollers, etc.

An essential aspect of any computer program is a concise, effective means of presenting the results of the analysis. In the case of a dynamic, multiple-body problem with the possibility of mutual impacting, this can

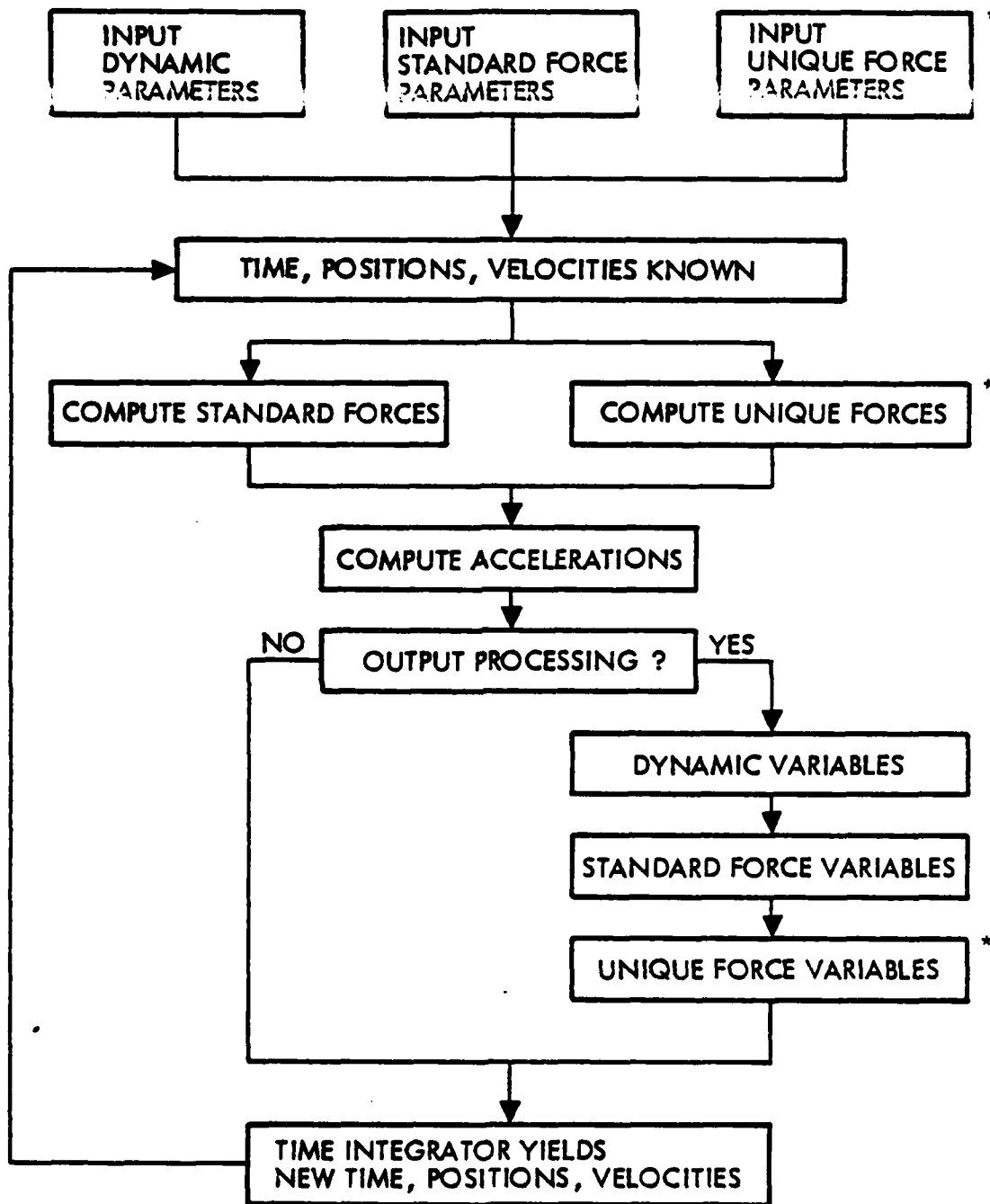


Figure 1
Steps in the Solution of a Separation Mechanics Problem

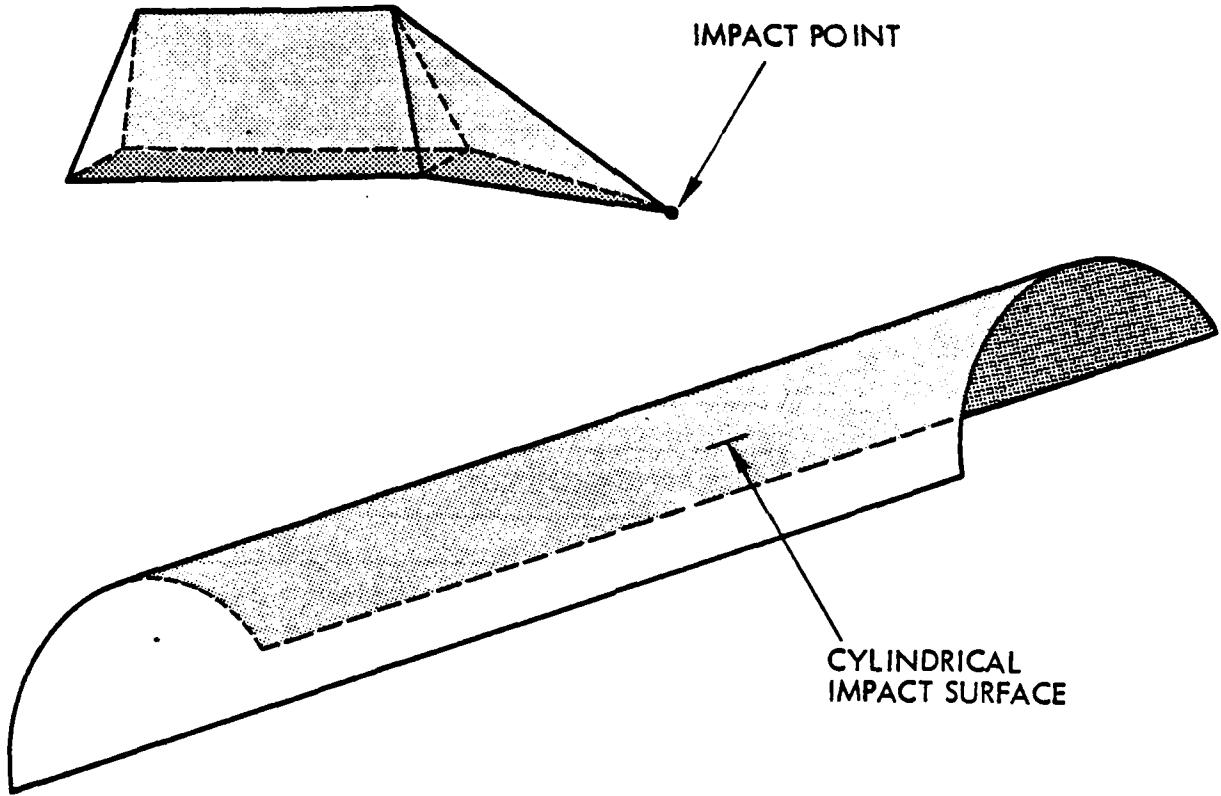


Figure 2
Point/Surface Impact Element

best be accomplished via a computer graphics visualization of the problem. The DYNAMOVIE program mentioned previously can depict complex separation/trajectory events in a variety of forms. The analyst can display some or all of the bodies involved in the problem and can select any viewing angle for the event. This capability can be especially useful when the analytical results are being compared with flight test films. If greater detail is desired, certain areas of the scene can be "blown-up" for closer inspection. The display of the event can be accomplished on scope terminals, hardcopy plots, or in movie form. In addition to providing a dramatic means of presenting the "final results" of a study, a computer graphics visualization can also serve to quickly detect anomalous behavior, suggest design solutions, and assess the effectiveness of these solutions.

APPLICATIONS OF THE ANALYSIS PACKAGE TO SPECIFIC PROBLEMS

Dynamic events to which the package has successfully been applied include missile staging (Reference 2), RPV launch, reentry body separation, deployment of an extendible aerodynamic spike (Reference 3), and submunition dispersal from tactical guided weapons (Reference 4). Each of these examples has exploited different facets of the package's capabilities. The missile staging events have been characterized by various guiding mechanisms such as rollers or guide rails. Reentry body separation requires a precise modelling of the separation mechanism to accurately determine the linear and angular rates imparted to the body and may also require the incorporation of gasdynamic forces due to the body flying through a thruster plume. The separation analysis of tactical guided weapons is a good example of a many-body problem involving aerodynamic forces, the possibility of collisions, and the need to present the results in computer graphics form. The following discussion, taken in part from Reference 5, focuses upon several tactical weapon systems whose basic operation is similar. Following release from the aircraft, the vehicle is cut into a nose section, tail section, payload section, and three panels which surround the payload section. The dispersion of these components may be forced (e. g., resulting from internal pressurization of the vehicle simultaneous to the cutting) or may be due solely to aerodynamic forces.

As a first step in analyzing the separation dynamics of a tactical guided weapon, the computer graphics technique can be used to visually locate specific areas of potential collisions between components. This is accomplished by performing an initial analysis in which no impacts are included in the model, thus allowing bodies to pass through one another. For example, in system "A" depicted in Figure 3, operating with a given set of flight conditions, it is found that: 1) the aft surface of the nose section will impact/slide over the forward part of the payload section, 2) the aft tip of the winged, upper panel will impact/slide along the cylindrical surface of the tail section, and 3) one of the side panels initially moves radially away from the payload section but then returns to impact it. The areas which have been identified can then be modelled to simulate the forces generated by such impacts and the analysis can be rerun as shown in Figure 4. This approach results in a great savings of both man-time and computer time by eliminating the need to model the entire structure to account for all possible impacts.

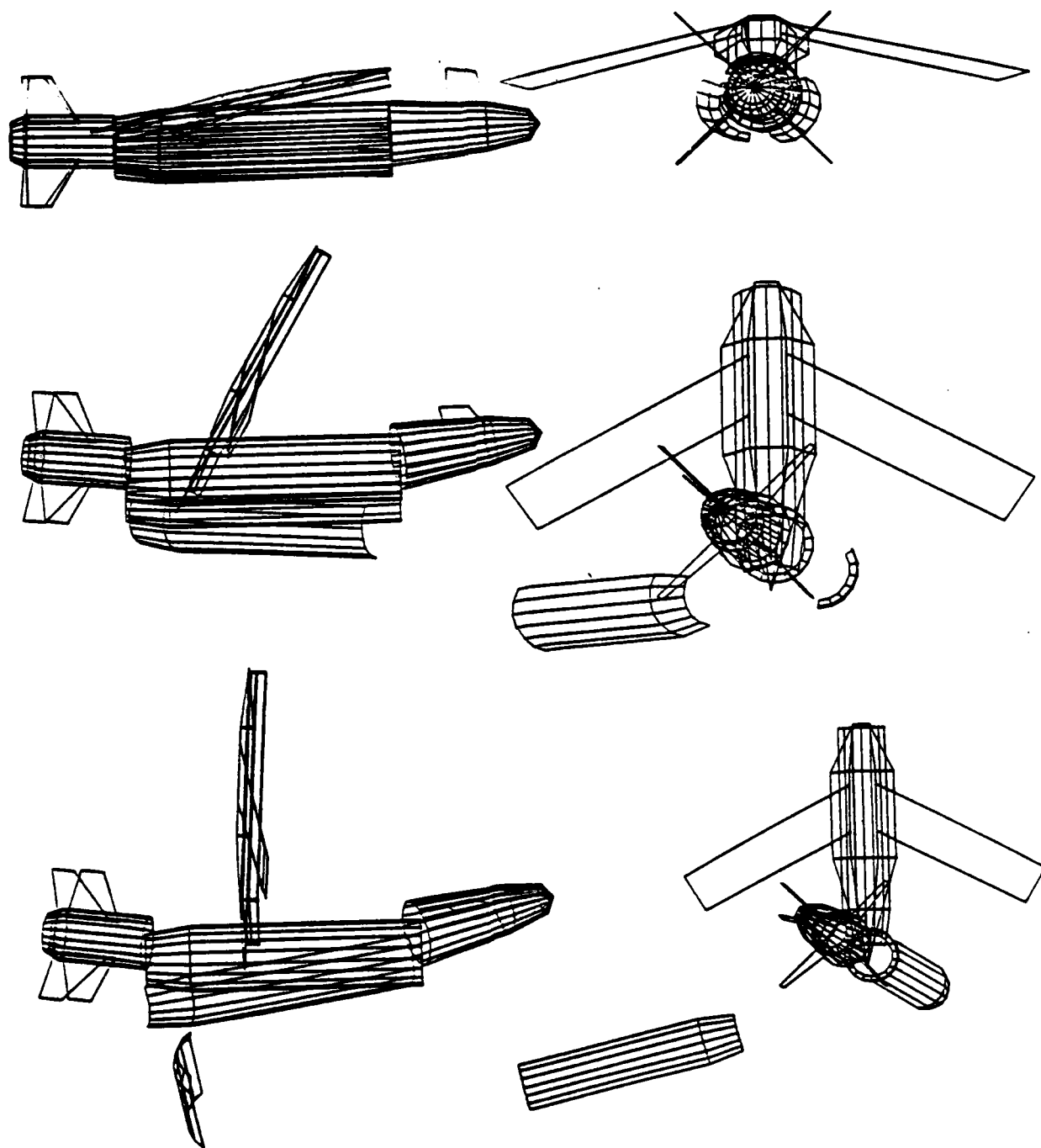


Figure 3
Side View and End View of Example System "A"
Modelled With No Impacts

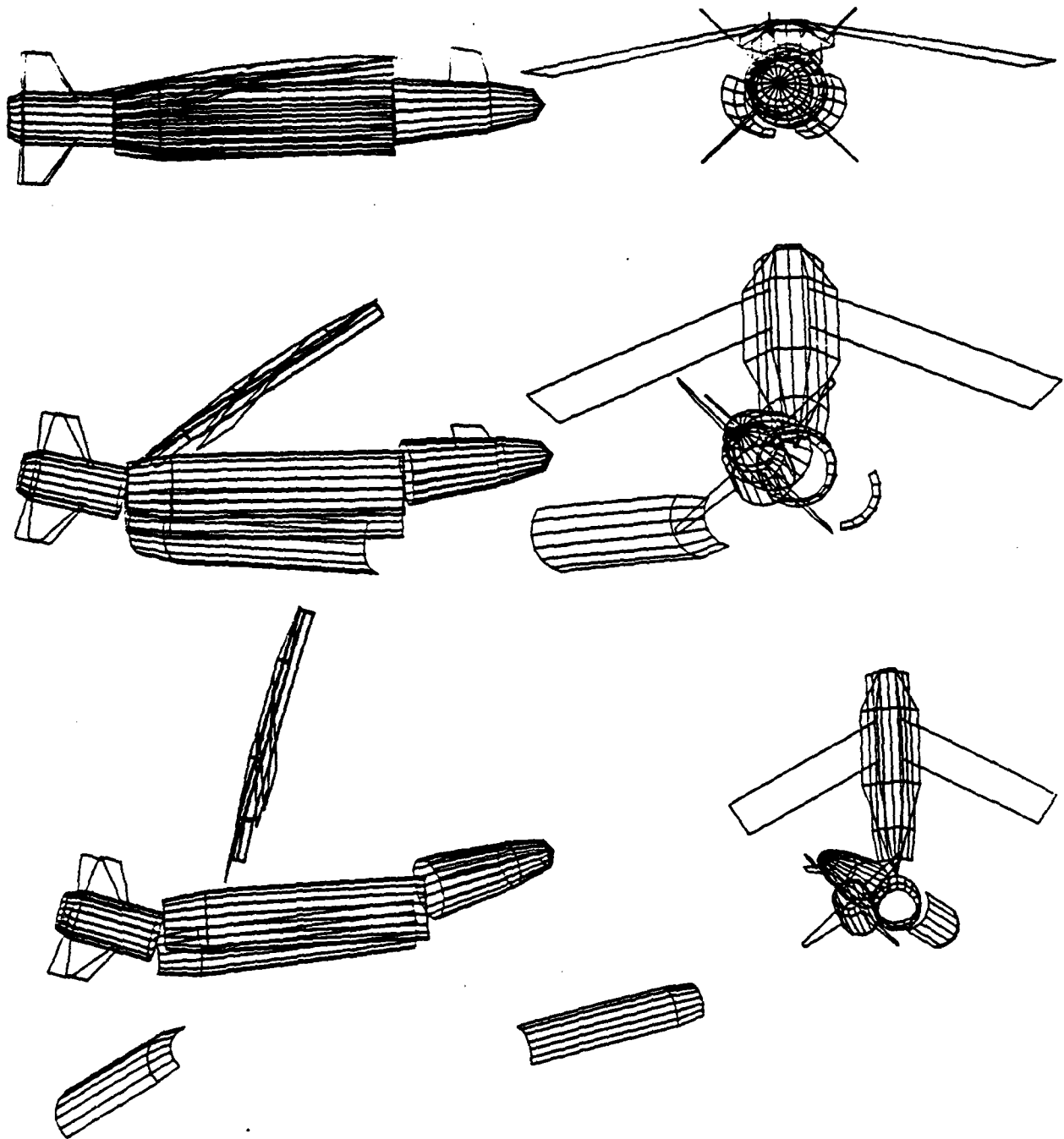


Figure 4
Side View and End View of Example System "A"
Modelled With Impacts

Example system "B" shown in Figure 5 is intended to illustrate two important aspects of using computer graphics to study separation events. Note first that two views of the sequence are necessary to comprehend the relative positions of the components. In this particular case, the nose section happens to pass through the developing pattern of payload bodies untouched. Under slightly different flight conditions it can be expected that the nose section will impact several of these payload bodies. The design modification which was proposed to prevent this anomaly consisted of rigidly connecting the nose and tail sections of the vehicle via a center post. This solution was suggested by viewing the sequential pictures shown in Figure 5. Hence, note second that the computer graphics technique can serve as a visual aid inspiring solutions to operational anomalies.

An example of a more complex separation system is illustrated in Figure 6. A side view of the entire system prior to deployment is shown in Figure 6a, while in Figure 6b the three panels and the payload bodies have been removed to point out that the four tail fins are attached only to the tail cylinder and are cantilevered out over the panels with a small radial clearance or gap. Each of the tail fins is assembled to the tail cylinder by fitting a tab into a mating slot on the tail cylinder as shown in Figure 6c. The tab is then secured in the slot by a single break bolt. This system was originally intended to operate as follows:

- The nose section, tail section, and panels are ordnance severed
- A simultaneous pressurization of the payload section drives the panels and the payload bodies outward
- The panels impact the cantilevered portion of the tail fins, prying them away from the tail cylinder and failing the break bolts (see Figures 6d and 6e)
- The four loose tail fins are then pushed out of the way by the panels allowing the payload pattern to develop

When this system was analyzed as shown in Figure 7, it was found that the forces required to fail the break bolts retarded the deployment of the panels to such an extent that many impacts occurred between the payload bodies and the panels.

The feasibility of "spin-deploying" large numbers of submunitions has also been studied with the analysis package. The vehicle referred to as example system "D" in Figures 8 and 9 was given a large initial angular rate about its longitudinal axis to create a centrifugal deployment force rather than the internal pressurization discussed previously. The separation sequences shown in Figures 8 and 9 reveal that six of the 24 submunitions are impacted by the rotating panels. Often it is necessary to assess the effect of such collisions on the ground impact pattern of the submunitions. This can be accomplished easily via the point/surface impact element described earlier. By modelling the ground as an impact surface and tracking points on the submunitions, the impact location of each submunition will automatically be output.

Another important use which has been made of the analysis package is in conducting pretest and posttest simulations. Figures 10 and 11 are partial representations of a submunition deployment ground test in which an anomaly was discovered. When the deployment charge is released, gasses are created which drive the three submunitions outward but which also act on the left and right bulkheads and result in a net force which drives the support structure to the right in Figure 10. This motion is sufficient to cause a collision between

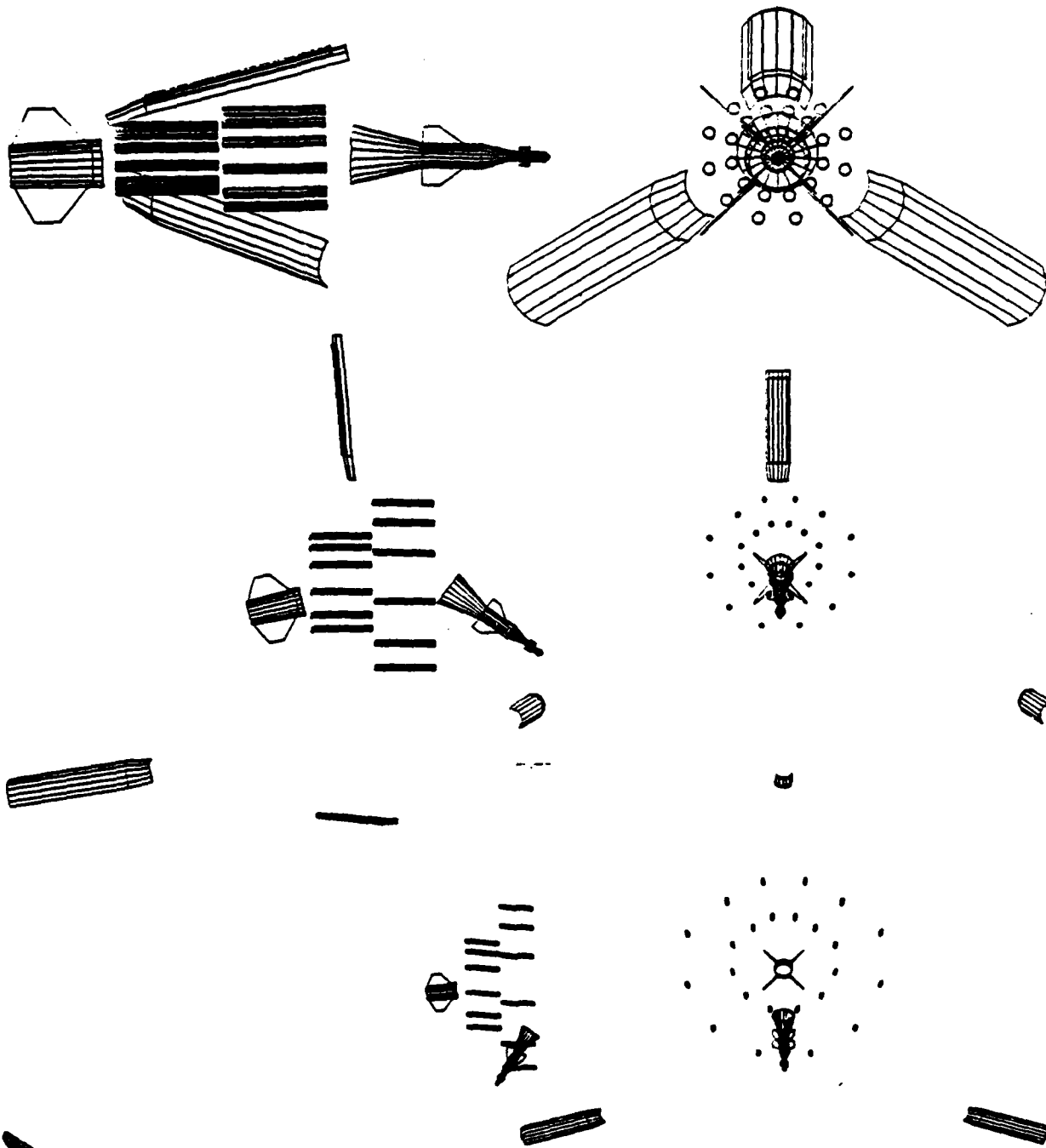


Figure 5
Side View and End View of Example System "B"

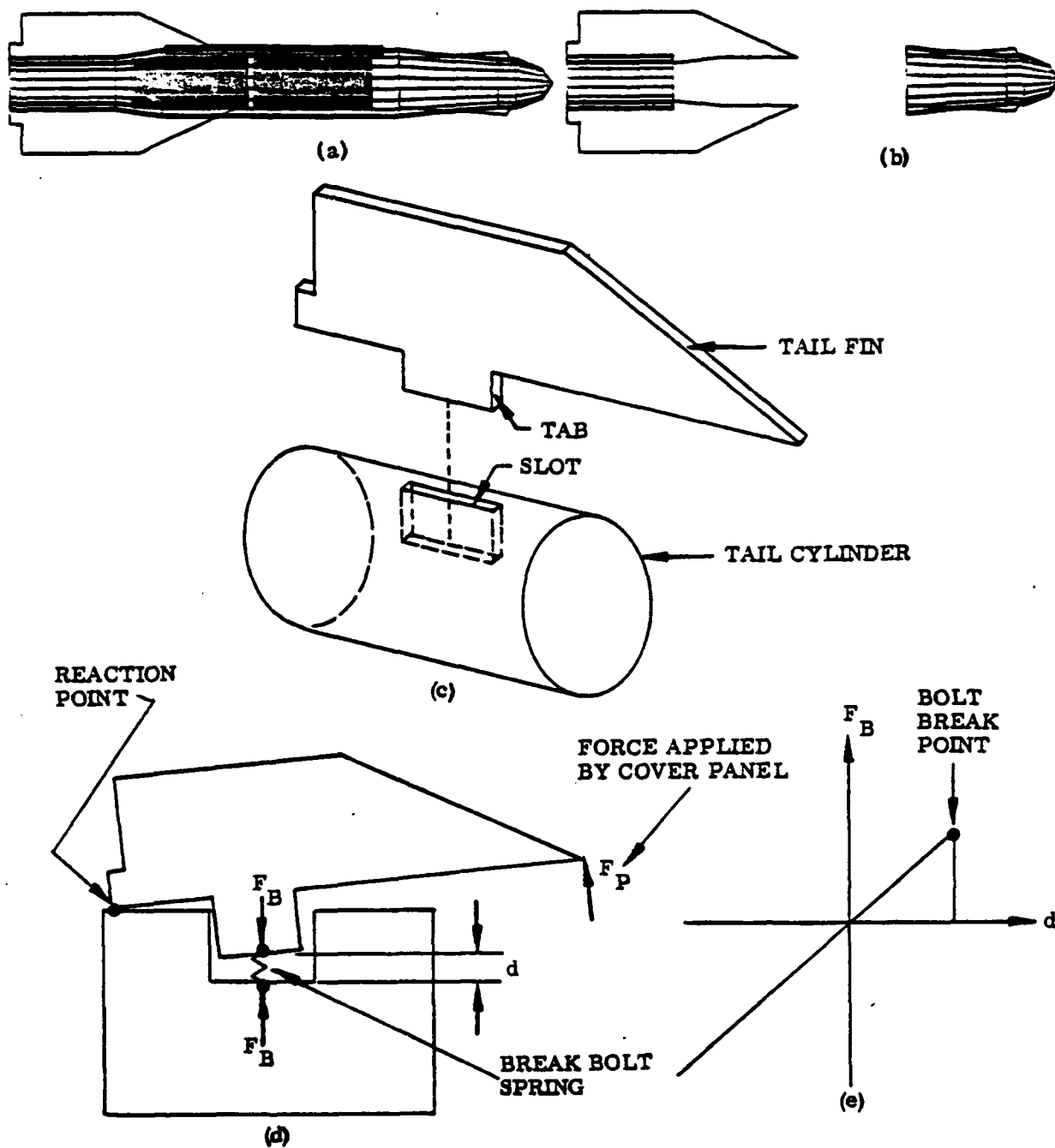


Figure 6
Details of Example System "C"

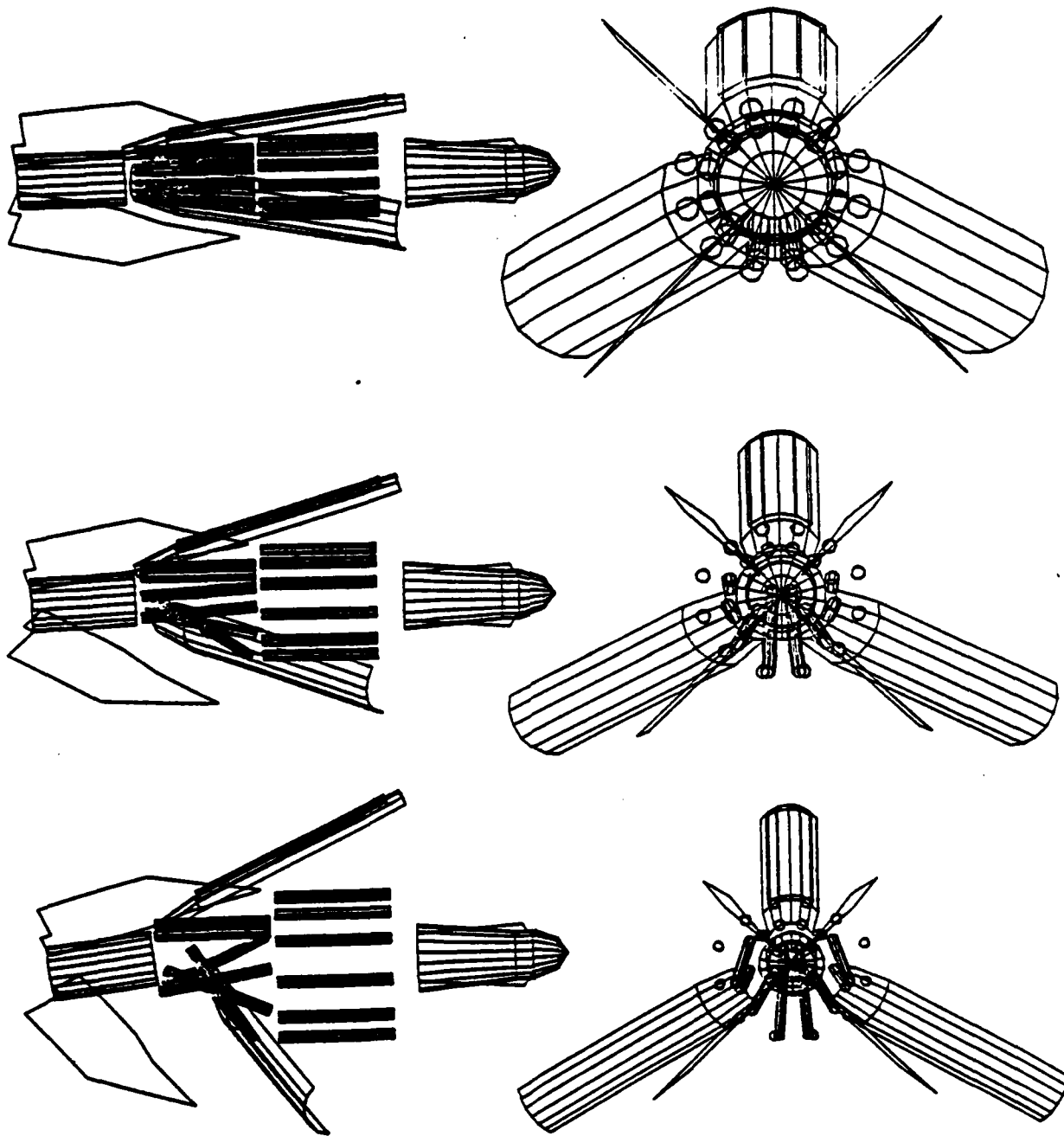


Figure 7
Side View and End View of Example System "C"

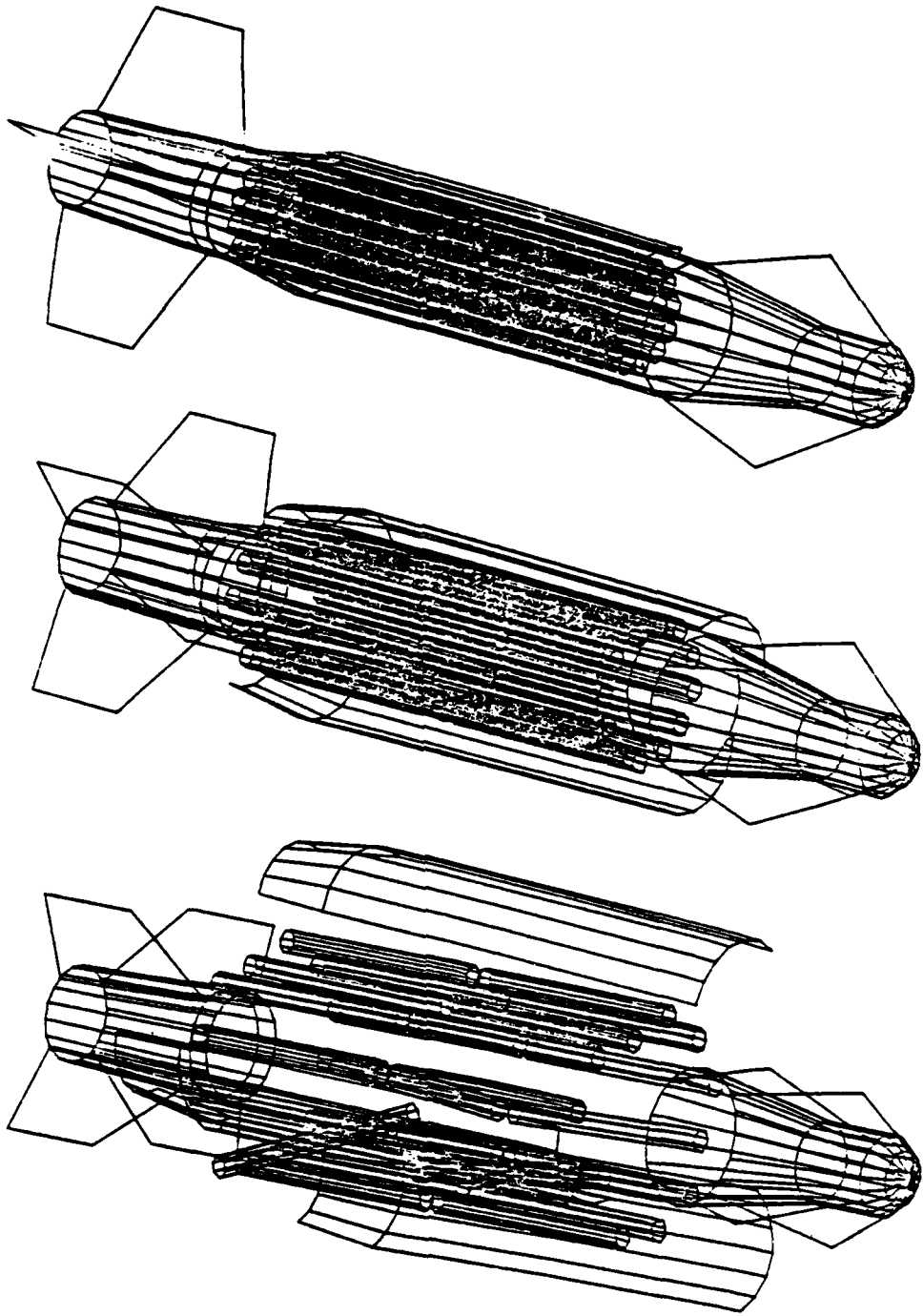


Figure 8
Isometric View of Example System "D"

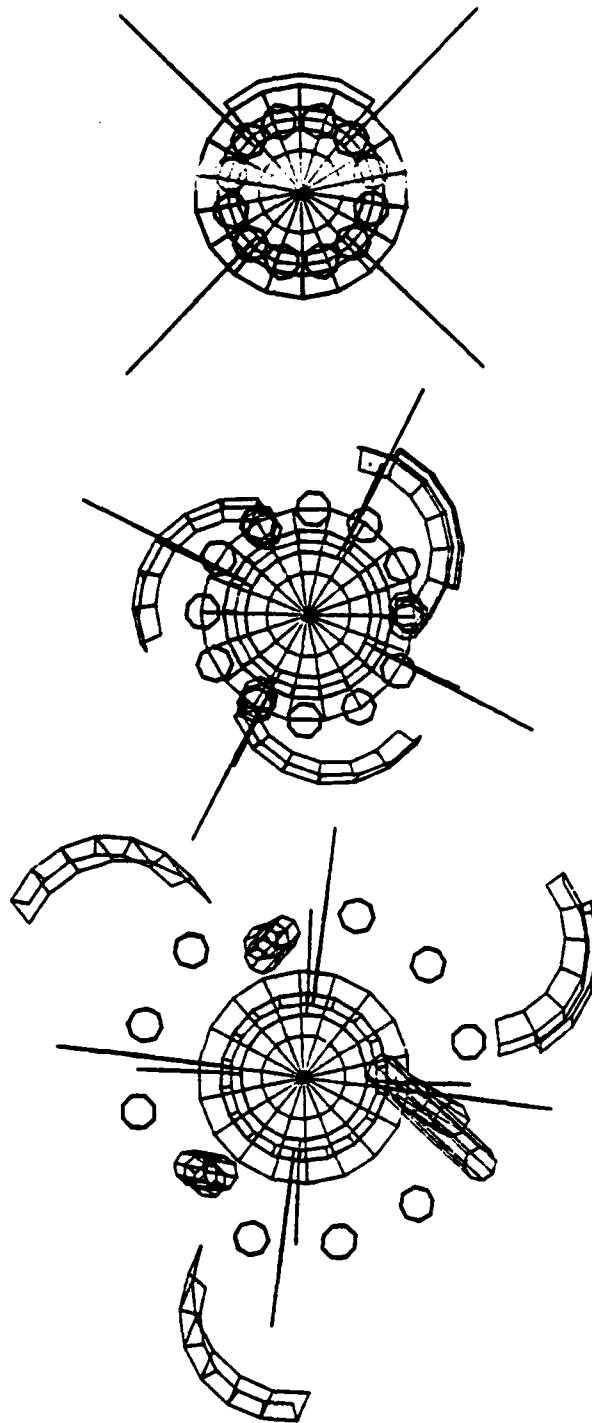


Figure 9
End View of Example System "D"

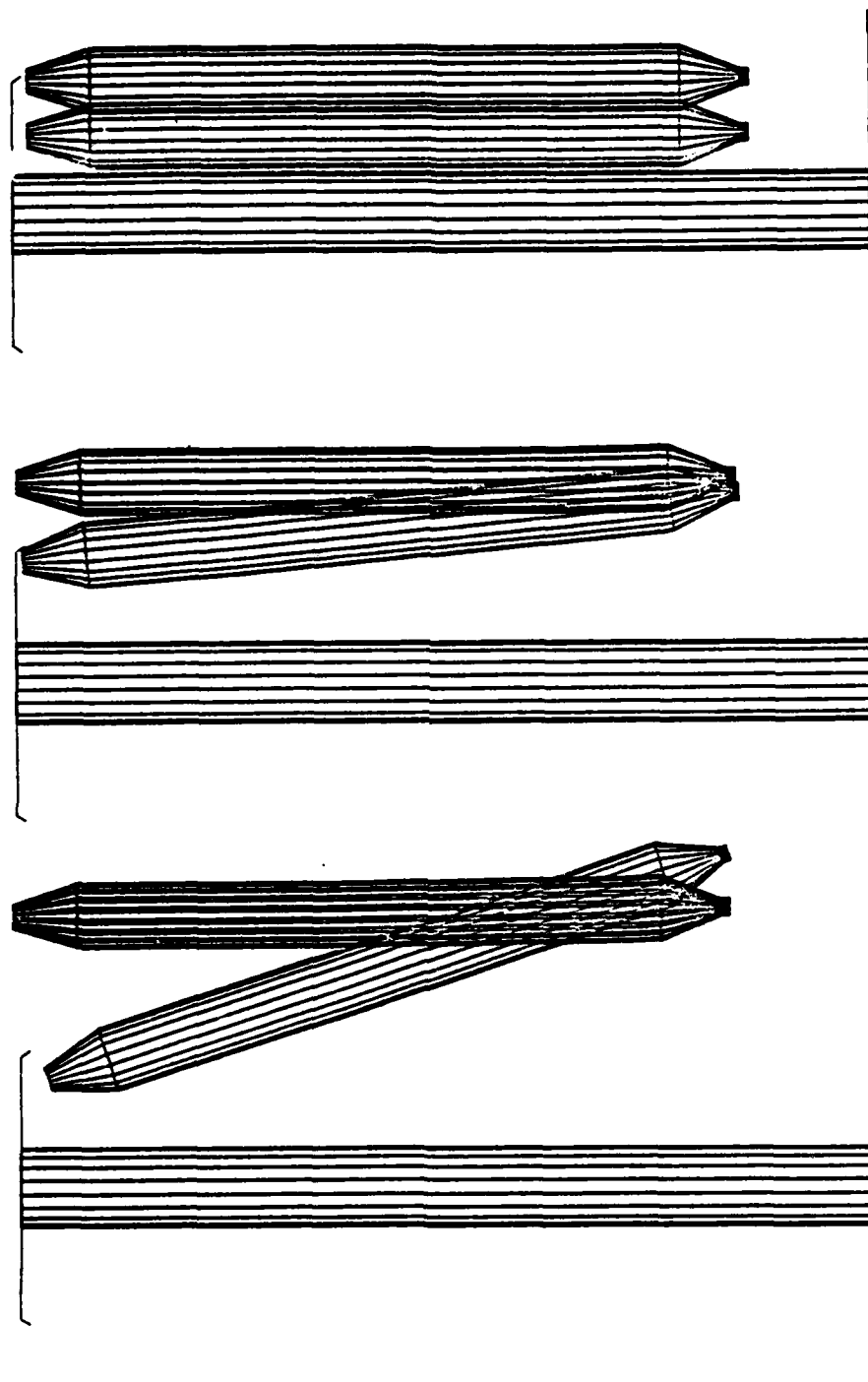


Figure 10
Side View of Ground Test Simulation

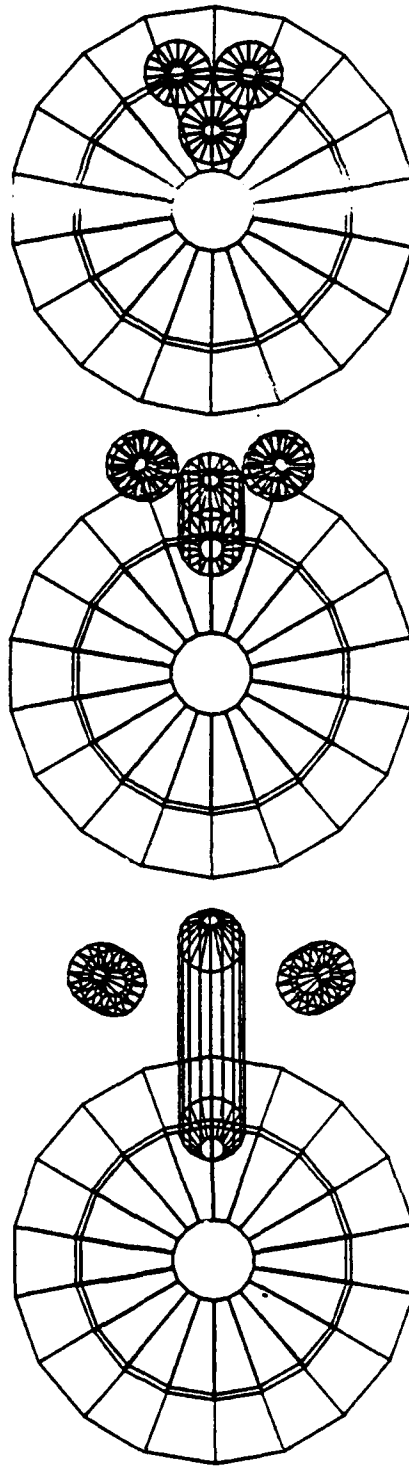


Figure 11
End View of Ground Test Simulation

the inner submunition and a ring which protrudes from the left bulkhead. The accurate reproduction of these test results on the computer allowed the analysis package to be used in assessing and picking a design fix for the problem.

APPLICATION OF THE ANALYSIS PACKAGE TO STORE SEPARATION PROBLEMS

While this dynamic analysis package was not specifically developed for the solution of store-separation problems, it possesses many capabilities which would be useful in that field. The modularity of the package allows it to be tailored to any particular problem. For example, independently generated store-separation aerodynamic routines can be incorporated and evaluated. The package might be used as a base through which various aerodynamic approaches could be compared. Another advantage of this package is that it would allow release mechanisms to be modelled and included in the analysis. By doing so, operational anomalies of the release mechanism may be discovered and the loads imparted to the store and to the aircraft structure by release can be accurately calculated. Parametric studies can be run to determine flight envelopes which ensure collision-free separation of the store. In the case of accidental collisions, impact loads can be calculated and their effect upon the subsequent trajectory accounted for. Perhaps one of the most useful features of the analysis package is the computer graphics capability. The results of a complex dynamic analysis can be presented in a form which promotes a visual understanding of the physical operation of a store separation system.

REFERENCES

1. Richter, B. J., "A Description of the Computer Program DYNAMITE," LMSC-D436926, Lockheed Missiles & Space Company, Inc., Sunnyvale, California, December 1975.
2. Welch, B. H., Richter, B. J., and Sue, P., "TRIDENT I Third Stage Motor Separation System," presented at the 11th Aerospace Mechanisms Symposium, NASA Goddard Space Flight Center, Greenbelt, Maryland, April 1977.
3. Richter, B. J., "Structural Evaluation of Deployable Aerodynamic Spike Booms," presented at the 9th Aerospace Mechanisms Symposium, NASA Kennedy Space Center, Florida, October 1974.
4. Morris, G. W. and Welch, B. H., "SUU-54 Dispersal Interference Study," AFATL-TR-76-69, Air Force Armament Laboratory, Eglin AFB, Florida, June 1976.
5. Richter, B. J. and Welch, B. H., "An Application of Interactive Computer Graphics to the Design of Dispersal Mechanisms," presented at the 11th Aerospace Mechanisms Symposium, NASA Goddard Space Flight Center, Greenbelt, Maryland, April 1977.

AUTOBIOGRAPHY

Byron H. Welch

Mr. Welch graduated from Iowa State University in 1972 with a Bachelor of Science degree in Aerospace Engineering. Since then, he has been in the employ of Lockheed Missiles & Space Company, Inc., Sunnyvale, California. Mr. Welch's efforts have been centered in the fields of structural dynamics and separation mechanics. Recent work includes the analysis of TRIDENT missile staging and separation events, deployment studies of several clustered tactical weapon systems, and the development of computer graphics software.

B. J. Richter

Dr. Richter received his Ph. D. in Applied Mechanics from Stanford University in 1972. Prior to Stanford, he attended the University of Santa Clara where he received a Bachelor of Science degree in Civil Engineering in 1963 and a Master of Science degree in Engineering Mechanics in 1966. Dr. Richter has been employed by Lockheed Missiles & Space Company, Inc., Sunnyvale, California since 1963 and has divided his time among four departments: Structures, Solid Mechanics, Mechanics of Materials, and Dynamics. Currently, he is Technical Leader of the Separation Mechanics Analysis and Development Group within the Dynamics Department. Dr. Richter has performed analyses, developed computer codes, and published papers in the separation mechanics field.

A BROAD BASED TECHNIQUE FOR THE PREDICTION
OF STORE SEPARATION.

(U)

(Article UNCLASSIFIED)

by

D.GARDNER and A.L.GUEST

British Aircraft Corp.Ltd.,
Military Aircraft Div.

A British Aerospace Company
Warton Aerodrome,
Preston. PR4 1AX

ABSTRACT (U). This paper describes the method in use at BAC for the prediction of store separation characteristics.

The basis of the method is a very flexible mathematical model solving for the motion of a store in six degrees of freedom and using input data from a wide range of information gained from the wind tunnel from flight or from theory as available.

The paper discusses, with examples, the shortfalls in some of the various types of wind tunnel information used to support the prediction of store separation. It is suggested that, in view of the restrictions that apply to the interpretation of any single wind tunnel tests, employing even the most sophisticated techniques, there is virtue in a method which basis its predictions on a balanced assessment of a broadly based programme of testing.

Such a broad based technique for the prediction of store separation has been developed by BAC. It is currently in use to predict jettison/release behaviour of a wide range of passive and active stores at speeds from take off to Mach 2+ .

Approved for public release; distribution unlimited.

LIST OF FIGURES

1. The mathematical model (early version)
2. Comparison of flight and computed trajectory at 200 knots
3. Comparison of flight and computed trajectory at 450 knots
4. Aircraft flowfield - description of 'zones'
5. The 'Developed' mathematical model
6. Model installation at low speed for the measurement of store aerodynamics.
7. The effect of Sting Support Systems on Store Stability
8. Aircraft Flowfield 'Wake'
9. Flow Visualisation - Illustration of Sonic Flow between Tanks.
10. Flow Visualisation - Illustration of Shock Development around a Multi Bomb Installation
11. Store 'Trajectory' Load Measurement
12. Ejection Velocity of Bombs from Twin Carrier
13. Missile - Supporting Wind Tunnel Programme
14. Missile - Comparison of Wind Tunnel and Computed Trajectory
15. Missile - Comparison of Store Aerodynamics (low speed)
16. Missile - Interference field at Low Speed
17. Effects of Damping and Stability on Missile Pitch Rate
18. Missile - Further comparisons of Store Aerodynamics and Pitch Damping (low speed)
19. Missile - Comparison of Wind Tunnel and Final Computed Trajectory
20. Missile - Comparison of Wind Tunnel and Final Computed Trajectory
21. Pitching Moment Interference - High Speed
22. Underfuselage Pressures.
23. Tank Pitching Moment Characteristics
24. Effect of Reynolds Number on Tank Pitching Moment
25. Tank - Comparison of Wind Tunnel and Final Computed Trajectory
26. Tank - Comparison of Wind Tunnel and Final Computed Trajectory

1. INTRODUCTION

Military aircraft are generally designed around a set of specific performance and store carriage requirements. These stores are often mounted externally to give the aircraft more flexibility in the numbers and types of stores that can be carried such that it is not unusual to find many hundreds of aircraft configurations are possible by the time the aircraft is in service. The flight clearance, jettison or release of these stores presents a potentially large, costly and hazardous programme of work and a way of minimising such a programme is essential. Many pre-flight analysis methods now exist to fulfil this task, generally based on a mix of analytical and wind tunnel techniques.

This paper discussed with examples, some of the shortfalls in some of the various types of wind tunnel information used to support the prediction of store separation. It is suggested that, in view of the severe restrictions that apply to the interpretation of any single wind tunnel test employing even the most sophisticated techniques, there is virtue in a system which bases its predictions on a balanced assessment of a broadly based programme of testing. Such a system should be capable of employing both wind tunnel results and theoretical estimates in a manner which imposes a compatibility test to the data so as to minimise the potential risks from interpreting the results of any one particular source of data. An additional advantage exists if limited, easily obtained flight data can also be used, such as installed carriage loads.

Such a broadly based method has been developed by the British Aircraft Corporation, Military Aircraft Division, and is currently in use to predict jettison/release behaviour of a wide range of passive and active stores at speeds from take off to Mach 2+ .

The method described is based on a very flexible mathematical model that allows use of a wide range of information inputs from the wind tunnel, from flight or from theory as available.

The examples given are based on experience gained from programmes of testing for several aircraft types.

2. THE BASIS OF THE TECHNIQUE: EARLY VERSION OF THE MODEL

The technique which will be described in this paper is a derivative of earlier mathematical modelling methods which have been under continuous use and development at SAC for many years. It is worth briefly describing the basic principles of the technique and summarising the capabilities of the earlier versions of the model as an introduction to the main discussion.

A computer program calculates store motions with six degrees of freedom and allows for a representation of aircraft manoeuvres. The aerodynamic forces and moments acting on the store are calculated by superposition of store aerodynamic characteristics and aircraft flowfield characteristics. Corrections are applied to allow for flowfield curvature.

Aerodynamic loading in the installed position which often differs drastically from the computed values was allowed for in the earlier versions in the form of local flow increments to the nose and tail of the store. The increments were reduced from the installed position to zero at a depth where it was considered that the interference effects they represented were negligible. The effect of ejector release unit forces and moments were represented where they were applicable. The information which the program used for its calculations was based on both wind tunnel testing and standard estimating methods such as DATCOM. The aircraft flowfield characteristics were calculated after the method of Alford (Reference 1). Figure 1 illustrates the concept very simply and Reference 2 presents the performance of this standard of model.

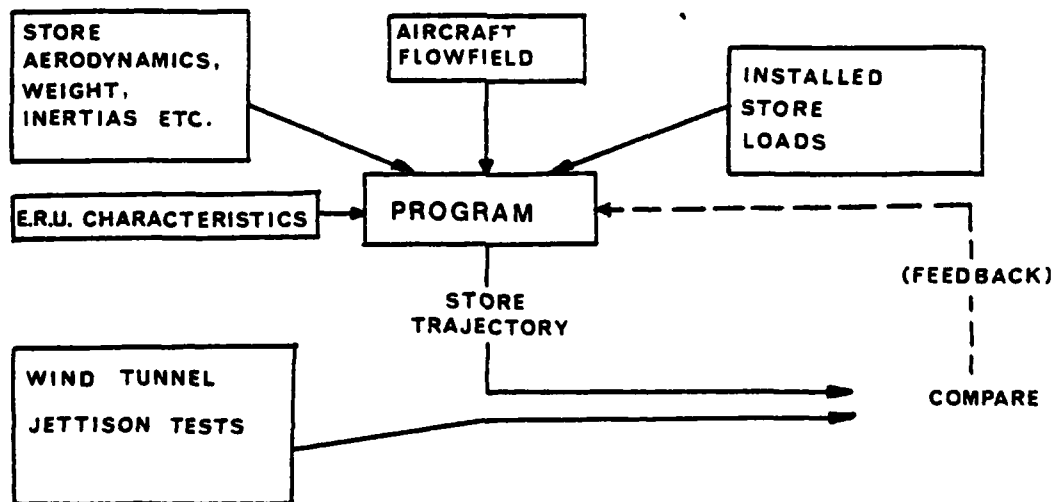


Figure 1. THE MATHEMATICAL MODEL (EARLY VERSION)

Figure 1 also illustrates the technique used to validate the mathematical model, which is referred to as 'matching'. Basically, the mathematical model is used to predict a jettison trajectory under the same conditions as a dynamically scaled wind tunnel jettison test and the two trajectories are compared. The mathematical model is adjusted by varying the inputs shown in the diagram and the trajectory re-calculated. This process of 'matching' the mathematical model to the wind tunnel test is repeated until an acceptable agreement exists. The cycle is repeated for a range of different wind tunnel drop conditions, varying aircraft speed, incidence, and store location, in order to enlarge the validation base as far as possible. When validation is adequate the model can be used to predict jettison trajectories for conditions not covered by wind tunnel jettison test. The model is then used to predict jettison behaviour prior to initial flight trials and as information becomes available from those trials, is re-matched against the full scale results. The updated model can then be used to extrapolate the flight trials results to define the limiting jettison envelope.

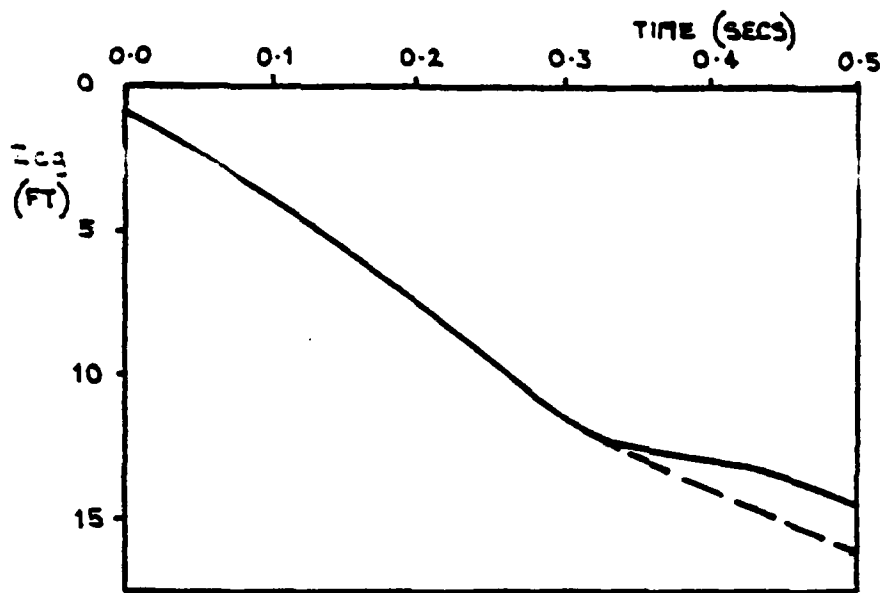
The principle of using a mathematical model to co-ordinate different types of wind tunnel tests and relate them to full scale trials results has proved to be basically very sound. Comparisons with flight trials results, Figures 2 and 3 show that with adequate matching the simulation was excellent. In addition, the method provides a very useful tool for the early stage of an aircraft programme when wind tunnel information is often not available and all predictions are based on estimated aircraft and store parameters. Later in the aircraft programme the model is able to respond far more quickly and flexibility to design changes than is possible with the hardware based wind tunnel techniques.

However, the simulation of sensitive stores was found to require considerable matching effort, and, as a result of the simple treatment of interference effects, was often limited in its ability to extrapolate its predictions accurately very far beyond the range of conditions against which it had been directly matched and particularly into the compressible region.

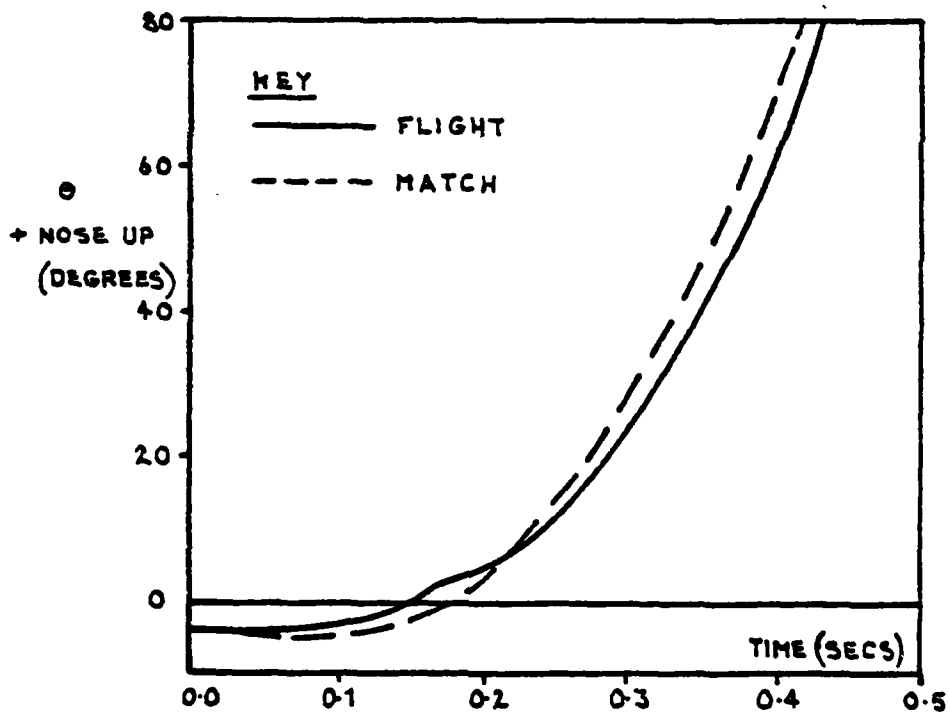
3. DEVELOPMENT OF THE MODEL

Three factors influenced recent development of the model :

1. The requirement to identify and represent aerodynamic interference mechanisms in much more detail.
2. The Tornado aircraft store release and jettison design requirements.
3. The availability of powerful, flexible data storage and access subsystems.

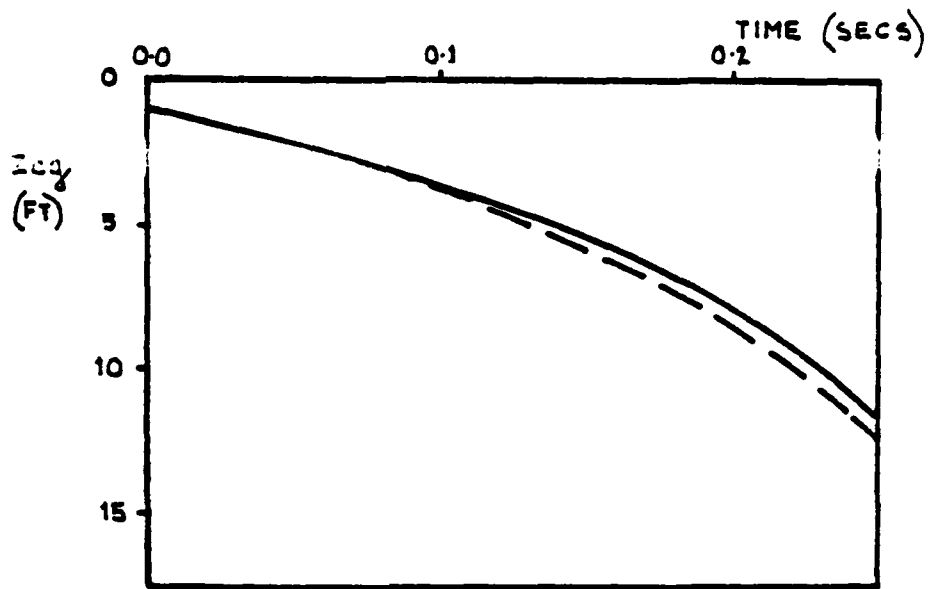


VERTICAL SEPARATION OF STORE ϵ_3 FROM PYLON BASE



STORE INCLINATION RELATIVE TO WING CHORD

FIGURE.2. COMPARISON OF FLIGHT AND COMPUTED TRAJECTORY
OF A FUEL TANK AT 200kts FROM THE WING STATION OF
STRIKE AIRCRAFT.



VERTICAL SEPARATION OF STORE z_{cg} FROM PYLON BASE

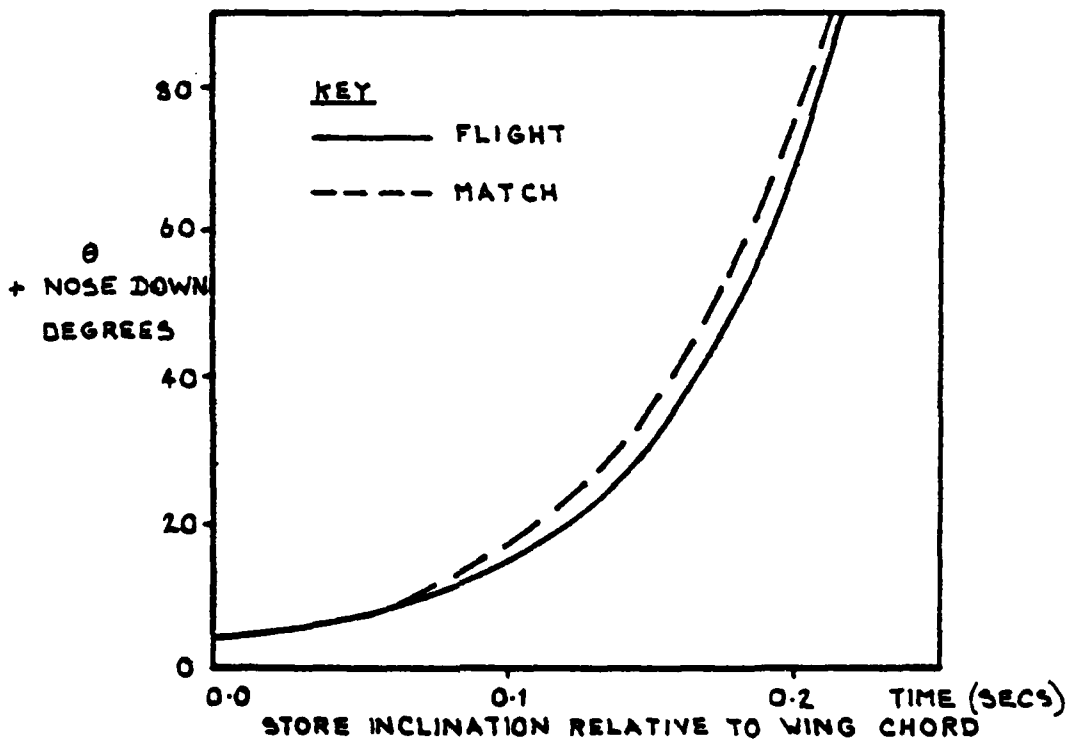


FIGURE.3. COMPARISON OF FLIGHT AND COMPUTED TRAJECTORY OF A FUEL TANK AT 450kts FROM THE WING STATION OF A STRIKE AIRCRAFT.

Early this decade considerable evidence was becoming available, Reference 3, regarding the significance of aircraft/store mutual interference effects, particularly in respect of high speed weapon release problems. The interference mechanisms are too complex to be deduced purely by the matching process already described. From the outset of the development of the program it was expected that wind tunnel testing would be conducted on a broad front to provide sufficient data to permit interpretation of the interference mechanisms when these were known to be important.

The basic drive behind the need to improve the model was supplied by the swing wing multi role Tornado aircraft programme. The philosophy of producing a weapons system with a relatively small airframe carrying a large number and variety of stores which would be released or jettisoned over a wide combination of speeds and wing sweep positions ensured that the demands put upon the stores clearance programme would be very considerable in terms of both quantity and quality. It was evident on purely economic grounds, that in order to minimise flight trials the back-up wind tunnel and jettison simulation facilities should be made as effective as possible.

3.1. DESCRIPTION OF THE DEVELOPED MODEL

The 'matching' process described for the earlier models remains the foundation of the developed model and the treatment of store interference close to the aircraft can be said to be the major area of improvement to the model.

The flow-field through which the store passes as it leaves the aircraft is considered to comprise of three zones (See Figure 4).

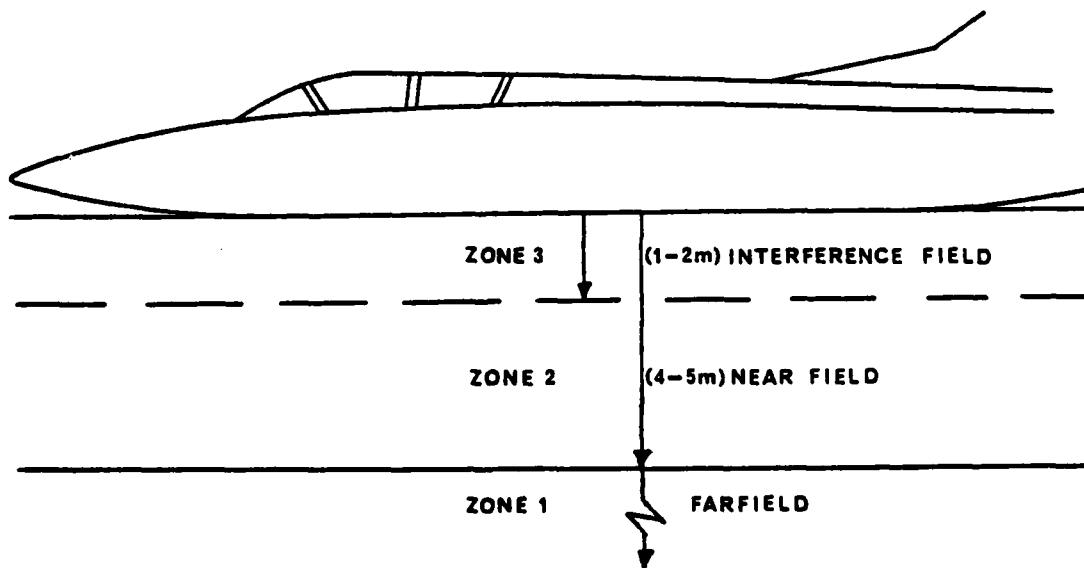


Figure 4 AIRCRAFT FLOWFIELD - DESCRIPTION OF ZONES.

ZONE 1 - Far field :

In this zone, the flow is completely free stream. It is not influenced by the presence of the aircraft.

ZONE 2 - Near field :

In this zone the flowfield is influenced by the presence of the aircraft. Flow direction, local Mach number and local dynamic pressure are all assumed to be influenced by the presence of the aircraft.

ZONE 3 - Interference field :

In this zone, the flowfield is affected by both the presence of the aircraft and the presence of the store due to a mutual interference between them.

The basic calculations in Zones 1 and 2 assume that the aerodynamic forces and moments operating on the store at any position can be calculated by superposition of the store free air aerodynamic characteristics and the local flowfield characteristics that exist, in the absence of the store, at that position.

The forces acting on the store can thus be described by the equation:

$$F = C_{\text{free air characteristics}} \times \text{local flow conditions} \dots\dots\dots 1$$

This assumption has been confirmed as adequate from our earlier modelling experience. The effect of flowfield curvature is allowed for by defining the store as several discrete components having their own local lift slope and moment characteristics. Dynamic terms are defined, normally, as they apply to the total store although they can be applied separately to store components.

In Zone 3 where the presence of the store may drastically distort local flow conditions, it is necessary to define the situation in more detail. In this region additional interference terms must be defined. Conditions in Zone 3 create the initial store disturbance motions that tend to define the character of the subsequent trajectory. An understanding of the nature of this interference is the key to useful extrapolation beyond the available wind tunnel or flight jettison demonstration. Consequently, the majority of available funds and effort is aimed at trying to define conditions in this zone. The forces acting on the store can be described by the equations :

$$F = C_{\text{free air characteristics}} \times \text{local flow conditions} + F_{\text{interference}} \dots\dots\dots 2$$

3.2. THE PROBLEMS OF ZONE 3

Rigorous theoretical treatment of aerodynamic loads on stores in Zone 3, usually dominated by viscous and compressibility effects is not possible at present. The available three dimensional theoretical methods are as yet, of limited value and although progress is being made at BAC and elsewhere, to make some allowance for compressibility and viscosity the allowances tend to be in the nature of empirical corrections rather than an extension of rigorous theory. It is evident that any real attempt to define conditions in this zone must be based on experience and on such wind tunnel and in-flight measurements that can be usefully carried out. To make matters more difficult, the compressibility and viscous effects that cause problems for the theoretician can produce very misleading wind tunnel results as well. It is therefore necessary to be very cautious when interpreting wind tunnel results, and it is unwise to accept unusual loads and moments without understanding their source. Given that wind tunnel testing is prone to a range of modelling and scaling errors it is important to define the interference mechanisms so that a reasoned assessment can be made of the presence and consequence of these errors.

Interference effects cannot generally be measured directly. They must be deduced from the comparison of different types of wind tunnel test. In essence therefore, Equation 2 is re-written in the form :-

$$F_{\text{interference}} = F_{\text{free air}} \left\{ \begin{array}{l} \text{free air} \\ \text{(characteristics)} \end{array} \right\} \times \text{local flow conditions} \dots\dots\dots 3$$

and the engineer's effort is concentrated into understanding $F_{\text{interference}}$.

Loads acting on the store and measured in the installed position; loads measured as the store is traversed through the initial trajectory stages; loads computed from known flowfield and store aerodynamic characteristics; loads inferred from the results of scaled jettison tests; can all be compared directly or indirectly using the mathematical model.

As a result of such comparisons additional testing may then be scheduled to assist definition.

The flowchart in Figure 5 shows the developed model with its variety of data options.

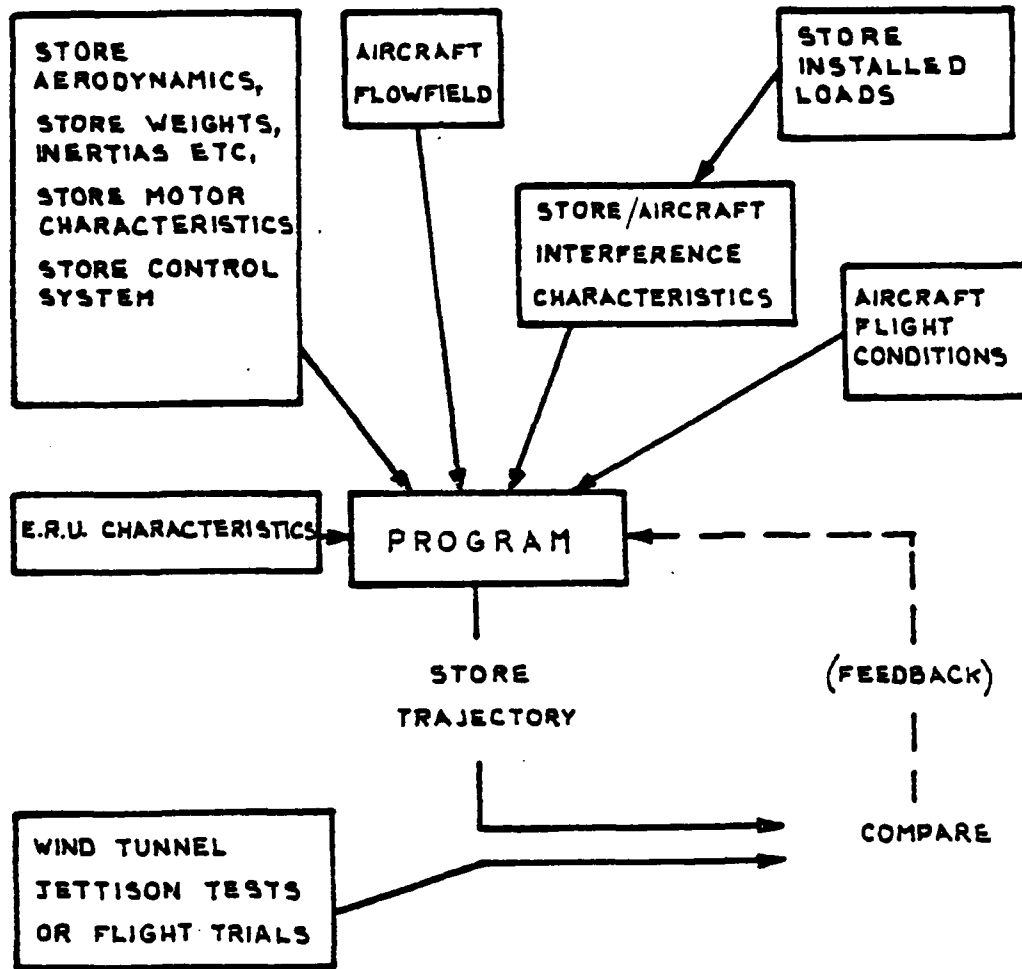


FIGURE.5. DEVELOPED MATHEMATICAL MODEL.

4. USE OF WIND TUNNEL TESTS

There are five principal types of wind tunnel tests which provide data of use in the prediction of store jettison and release. Four of the five are in the nature of static measurements that define the character of the aircraft and the store and their interaction. Without some form of mathematical modelling the information they provide cannot be quantitatively employed.

The five types of test are :-

1. Measurement of aircraft flowfield characteristics
2. Measurement of installed store loads
3. Measurement of store free air aerodynamics
4. Measurement of loads on the store immediately after release (trajectory loads).
5. Dynamically scaled model jettison tests.

4.1. STORE AERODYNAMICS

In general the effect of store stability has a very significant input to the character of a jettison trajectory. Measurement of store stability, in terms of pitching and yawing moments, is made difficult by the susceptibility of both parameters to interference from the model support structure. At low speed, these effects can be minimised by careful use of a rig of the type shown in Figure 6.

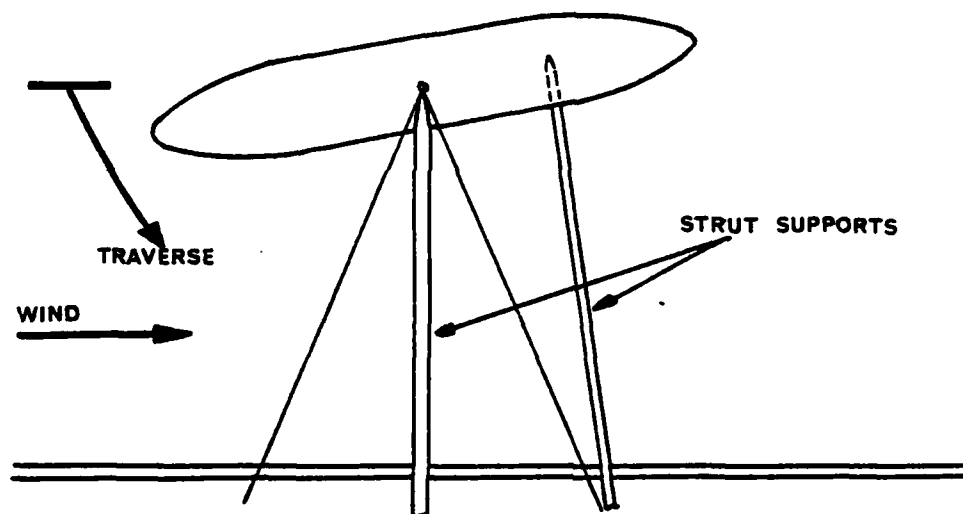


Figure 6 MODEL INSTALLATION AT LOW SPEED FOR THE MEASUREMENT OF STORE AERODYNAMICS .

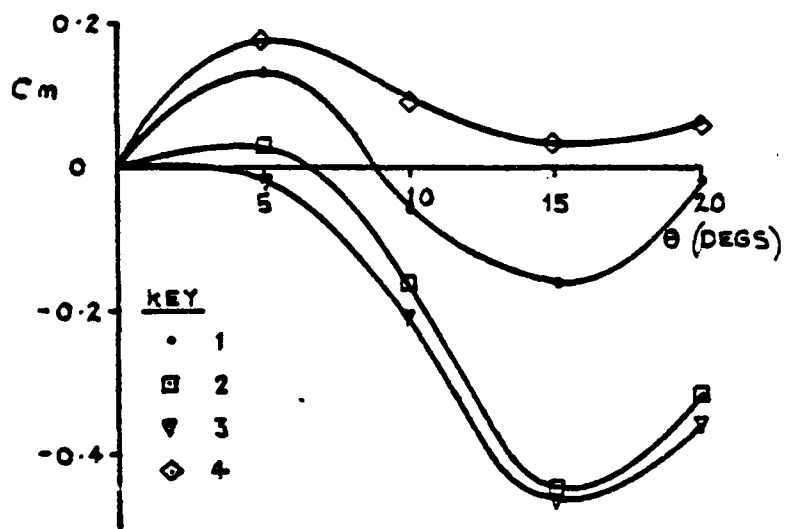
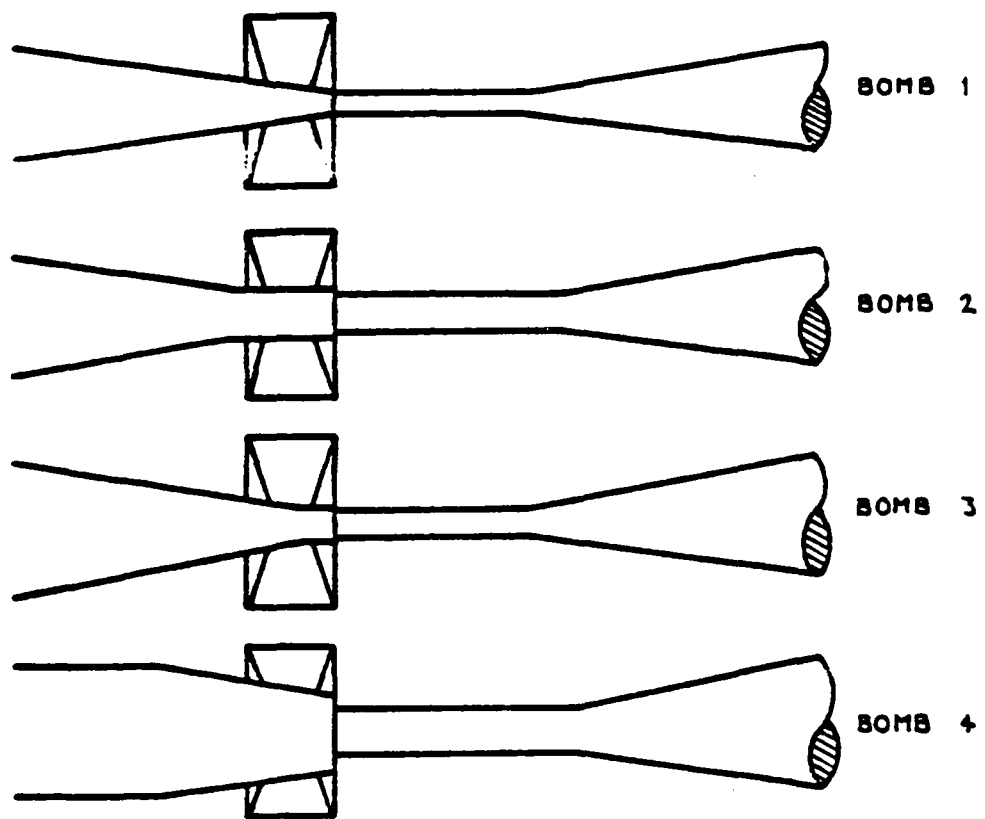


FIGURE.7. EFFECT OF STING SUPPORT SYSTEM ON STORE STABILITY.

However, at high speed where aft sting mounting is almost universal, the interference effects are potentially very serious. In the case of a store with a boattail where the supporting sting inevitably distorts the lines it is pointless to attempt the testing without a subsidiary programme aimed at refining the effect of the distortion. Even in the case of bluff ended stores where distortion may appear to be quite small the effect on store stability can be significant, Fig.7.

Cross flow Reynolds number is known to significantly affect store stability at moderately high incidence which can occur during the trajectory. An understanding of these effects is vital to a sensible interpretation of scaled model jettison tests.

4.2. AIRCRAFT FLOWFIELD

It is not generally cost effective to attempt to measure the aircraft flowfield for a large range of store configurations. In the Tornado programme measurements were taken of four flowfield parameters, at 128 positions beneath the aircraft at 11 incidences, 8 Mach numbers, 3 sideslip angles, and only two aircraft configurations using variations of the rake shown in Figure 8.

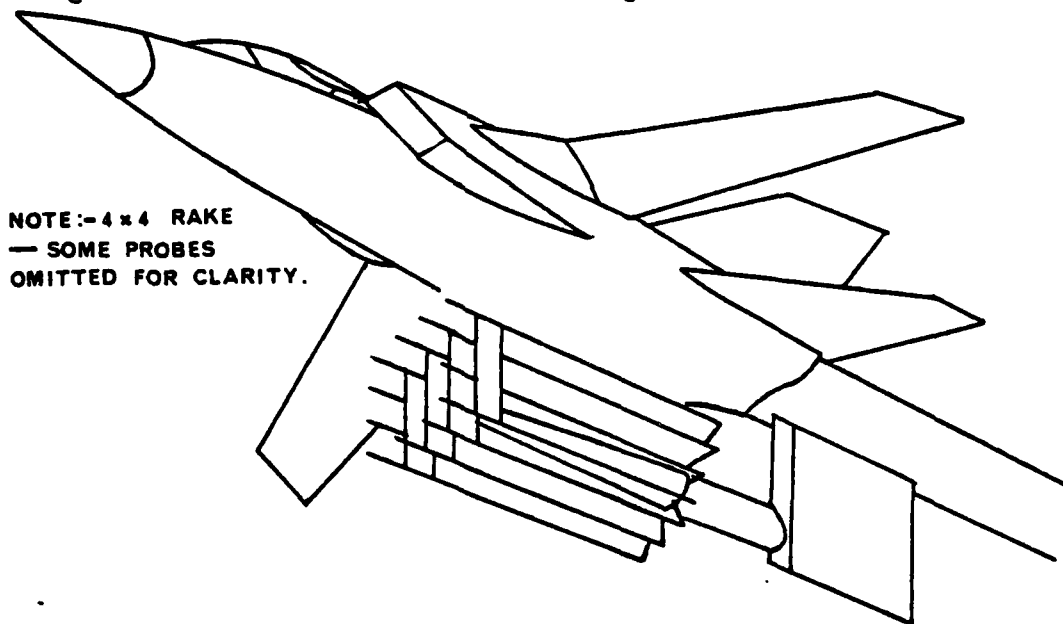


Figure 8. AIRCRAFT FLOWFIELD 'RAKE'.

Although there is no problem arranging for the release program to have access to the required data it is obviously necessary at some stage to scan the data for inconsistencies and errors. It has been necessary to provide considerable programming support to display and cross plot the data in order to minimise the engineer effort required for editing. As anticipated, some difficulties in bringing the rake close to the aircraft have been experienced due to mutual interference between rake and aircraft model.

It has therefore been our aim simply to define in general terms the flowfield of the clean aircraft for use, together with the store aerodynamics, as a base line against which to define interference.

4.3. INSTALLED STORE LOADS

The aerodynamic forces and moments acting at the moment of release can be defined by the measurement of the installed store loads. The advantage of this type of test is that it is relatively straightforward, it can usually give a reliable indication of the onset of compressibility problems and can relatively cheaply scan the full range of aircraft flight conditions. However, in relation to their application to jettison prediction, there are problems of interpretation. Figures 9, and 10 show two types of store installations and by means of flow visualisation illustrate the relevance of installed loads measurements as a means of indicating the sensitivity of jettison conditions to Mach number. In the case of the large stores, fuel tanks, shown with one removed for clarity, there is clear evidence of local sonic flow developing at about 50% length at this aircraft Mach number. In the case of the bombs on a twin store carrier it can be seen that there is effectively no flow between the stores and there is evidence of a shock at 50% of the forward bomb length in response to the general blockage created by the stores. In the first case one can expect the variation of store loads and moments with Mach number to have a predictable effect on jettison behaviour. In the second case flow will not develop between the stores until one of them is jettisoned. The differences between loads installed and loads during the initial movement, which govern jettison behaviour, will be considerable and impossible to predict from a consideration of installed loads alone.

4.4. STORE TRAJECTORY LOADS

These loads are measured using a twin sting rig as used in the captive trajectory concept, Figure 11. The loads and moments on the store are measured as it is positioned below the aircraft approximately within the predicted volume to be swept during a release. The purpose of these measurements is to gain an understanding of the interference mechanism. The store is not generally required to be positioned rigorously along its predicted trajectory history, as in the captive trajectory technique; nor is it positioned using the grid technique which aims to set up a data bank. The purpose of the measurements is to support and investigate data supplied by or deduced from other testing.



FIGURE 9: Flow visualisation - Illustration of sonic flow between tanks.

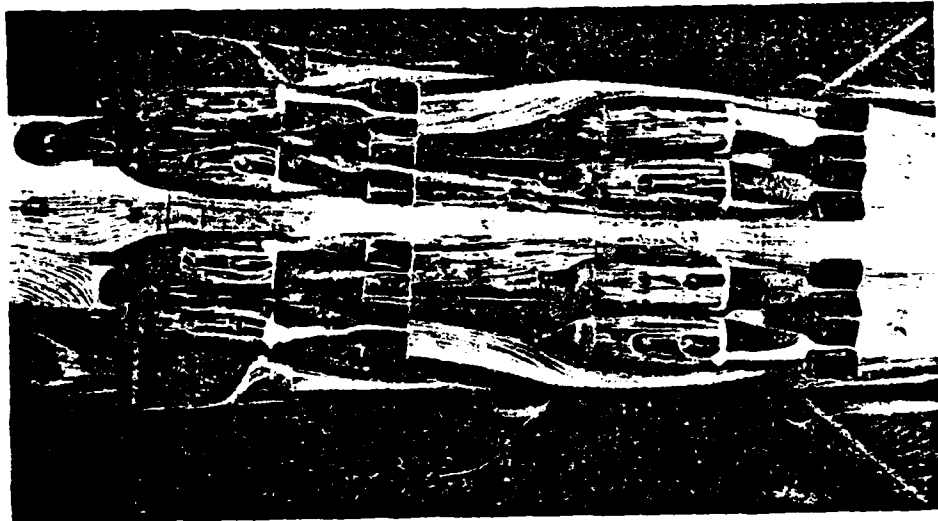


FIGURE 10: Flow visualisation - Illustration of shock development around a multi-bomb installation.

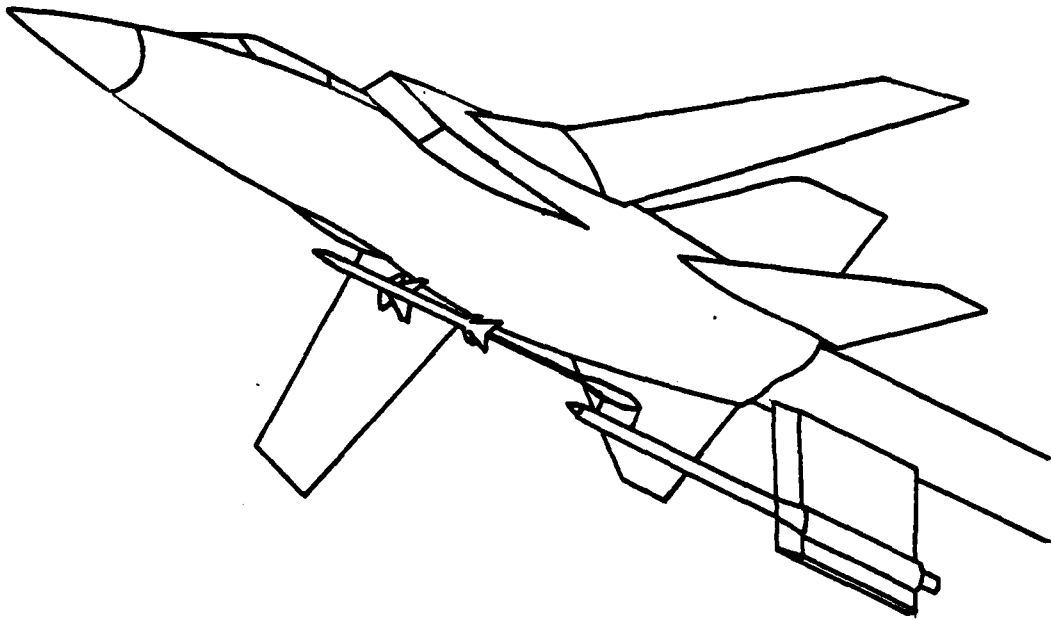


Figure 11. STORE 'TRAJECTORY' LOAD MEASUREMENT.

The difficulties associated with this type of measurement are well known. Apart from the practical difficulties which make it difficult to deal with stores which have very high initial pitch rates and the trade off between rig flexibility and tunnel blockage, the principal problems are associated with rig interference, and results from these measurements again require careful interpretation and understanding.

4.5. DYNAMICALLY SCALED JETTISON TESTS

This test is the corner stone of reliable mathematical modelling. Being the only 'dynamic' test its purpose is to verify the engineers' collecting together and understanding of the other wind tunnel 'static' data and thus by tuning or 'matching' of the model to these tests to provide the final tool for pre-flight analysis of store separation.

It is therefore fundamental that reliable, repeatable information is obtained either from low speed or high speed tests using 'light model' or 'heavy model' techniques; all can be simulated exactly by the

mathematical model and hence all can be used to tune this model. It is likely that the static tests will themselves indicate whether high speed dynamic tests are necessary dependent on the rate of change of interference terms with Mach number.

This simulation is updated by early separation trials in flight and thence continuously as the flight programme develops.

5. E. R. U. PERFORMANCE

ERU performance and the effect of structural flexibility on this performance are necessary inputs to any pre-flight analysis. The former is usually available in general terms from the ERU manufacturers though not always for the mass or throttle setting intended for a particular store. The effect of aerodynamic loads on the ERU performance are not generally known and special tests may be necessary if such effects are anticipated, modelled, and shown to be significant.

A separate mathematical model has been developed at BAC to estimate ERU performance under various loading conditions, using a similar 'matching' technique, with a view to minimising this type of testing.

The effects of structural flexibility on ERU performance must not be ignored and a 'pit drop' is recommended prior to flight where any significant loss in performance is anticipated. An awareness by the engineer of such a situation is necessary, e.g. the second bomb from a twin carrier may exhibit a lower ejection velocity than the first and may prove to be a function of time, see Figure 12.

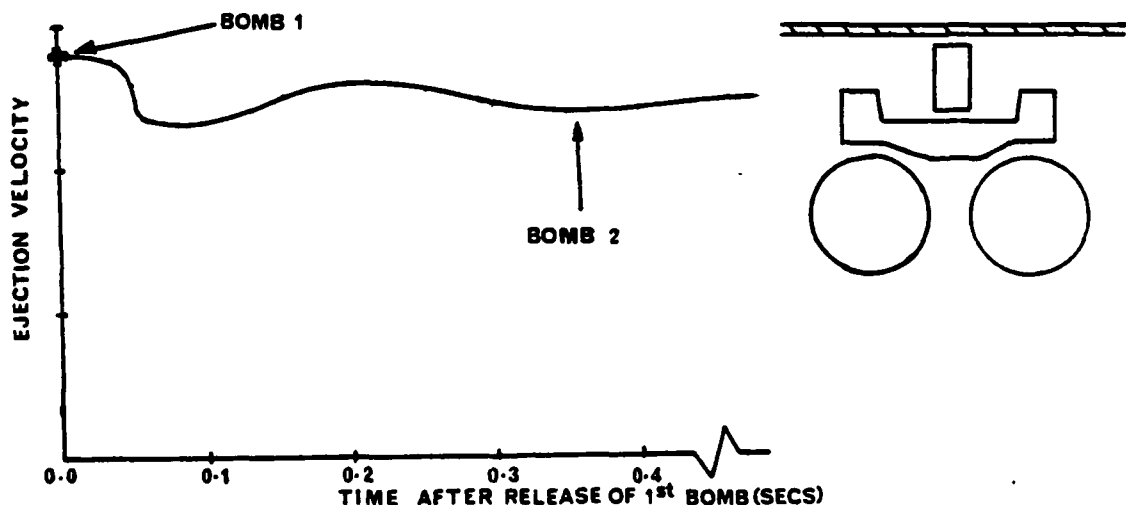


Figure 12 EJECTION VELOCITY OF BOMBS FROM TWIN CARRIER.

6. TYPICAL CASE HISTORIES

The value of using a wide range of information inputs to the model can best be demonstrated by describing typical case histories for a missile and for a large tank.

6.1. CASE HISTORY 1 - MISSILE

In this case the configuration consists of several fuselage mounted missiles. The missiles are ejected from the installation prior to motor fire as opposed to being rail launched. The missile stability was augmented in the release mode but not in the emergency jettison mode. The missile was expected to be vulnerable to release disturbance problems during the ejection phase. The wind tunnel programme as it developed is shown in Figure 13.

6.1.1. Stage 1 - Initial prediction - low speed.

Store aerodynamics data were available from the manufacturers wind tunnel tests, measured at $1/2.8$ scale at speeds down to $M=0.6$. Store installed loads at low and high M , and low speed aircraft flowfield characteristics were the first wind tunnel results available. On the basis of these tests and the manufacturers missile data a series of predictions were made of jettison behaviour at low speed conditions equivalent to those which would be simulated in the low speed scaled jettison tests. On the basis of the installed loads it was expected that in general the missile at Station A would exhibit the worst behaviour through the speed range. A prediction of its behaviour at low speed is shown in Figure 14, compared with an actual tunnel drop. The embarrassing discrepancy gave rise to a period of intensive study of the mathematical model inputs; the flowfield, installed loads, ejector unit, interference assumptions, and missile aerodynamics. Model ejector performance was found to be slightly lower than expected, but did not provide the explanation. From the mathematical modelling of a range of wind tunnel drops, it became apparent that the only two inputs that could influence the jettison in this way were missile stability and damping. This conclusion was reached with some reluctance as the missile data could not be faulted. Estimates of missile aerodynamics using a technique, Reference 4 which included the effects of vortex interference produced results which were compatible with published data.

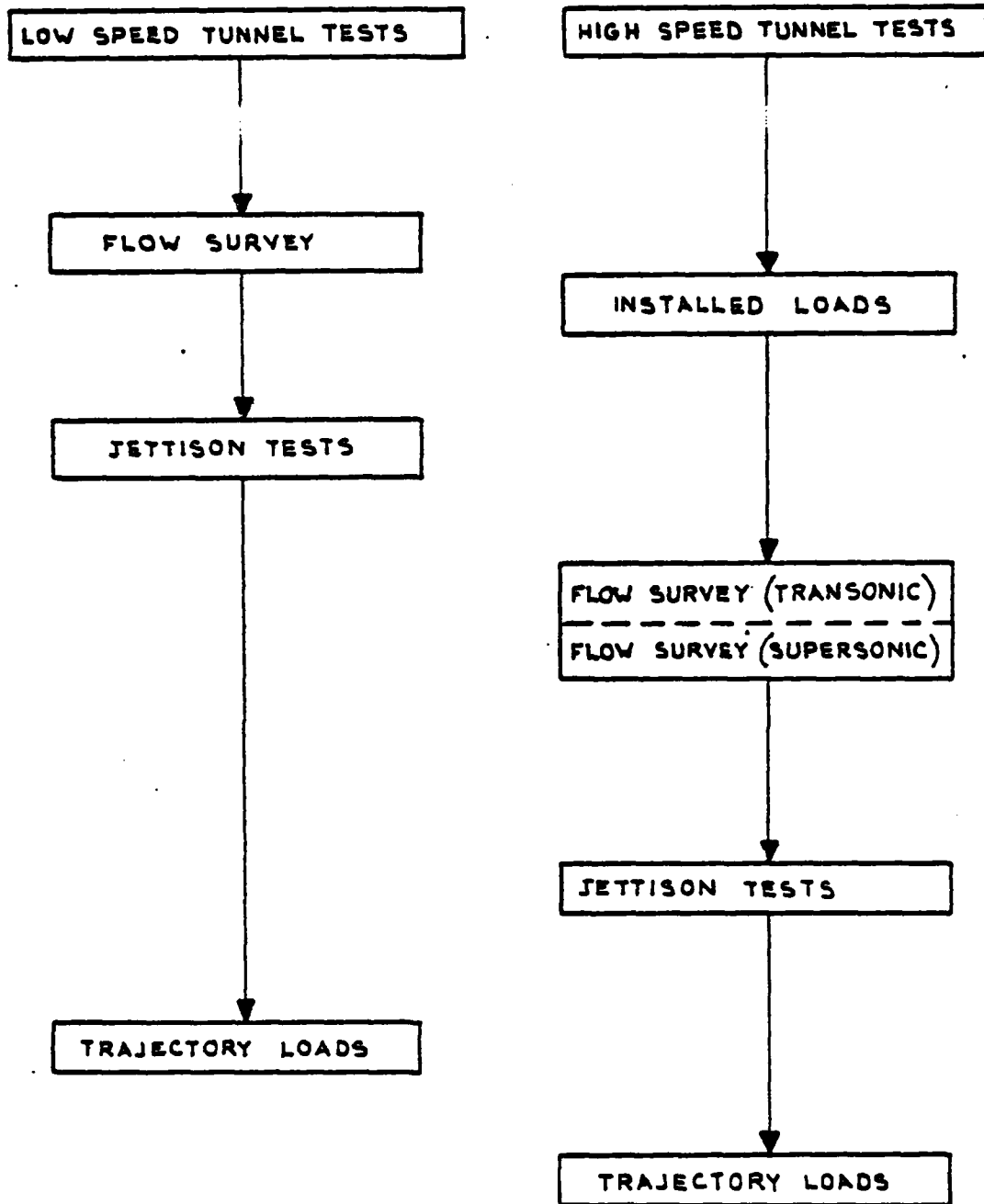


FIGURE.13. MISSILE- SUPPORTING WIND TUNNEL PROGRAMME

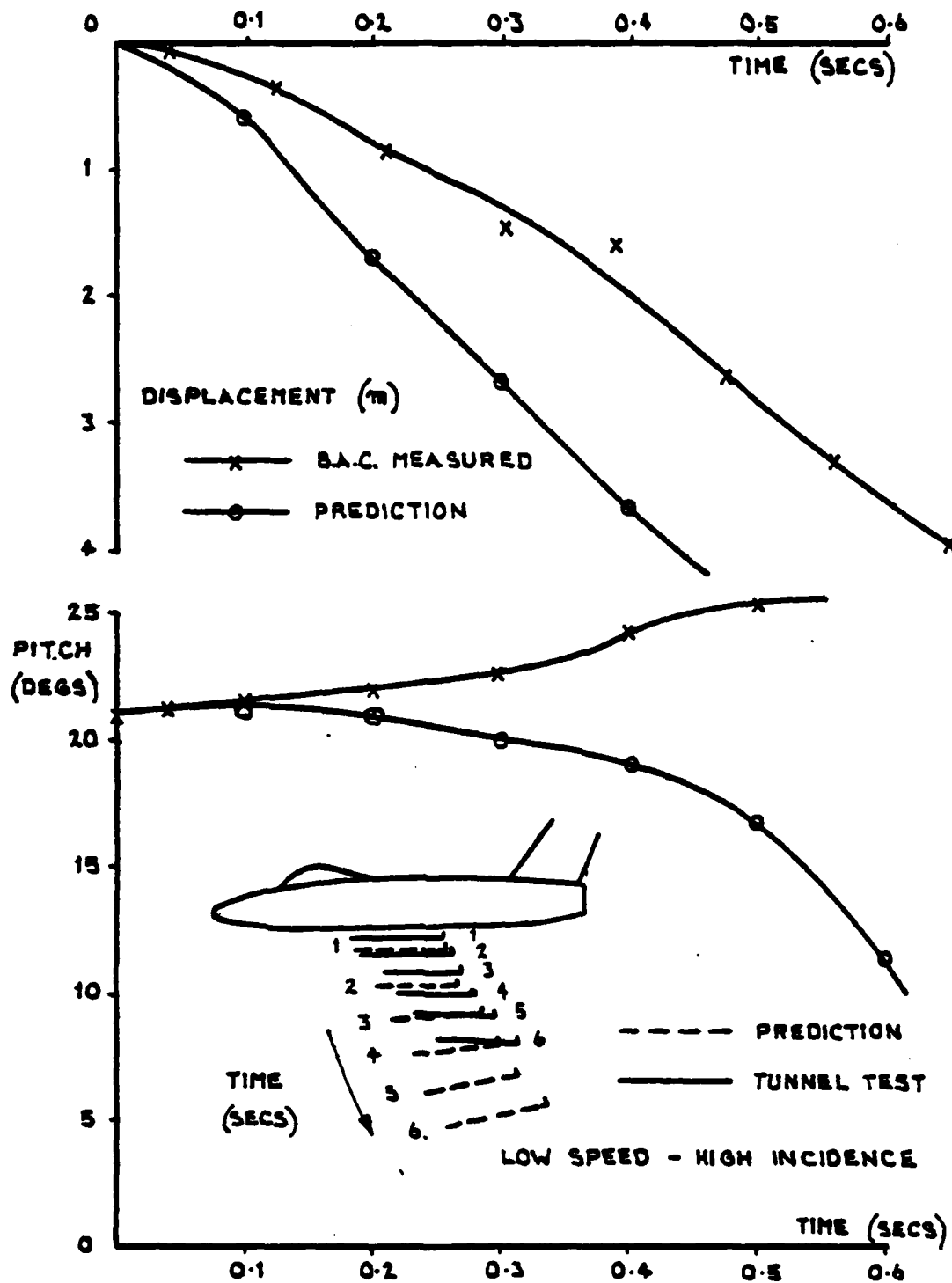


FIGURE.14. MISSILE - COMPARISON OF WIND TUNNEL AND COMPUTED TRAJECTORY.

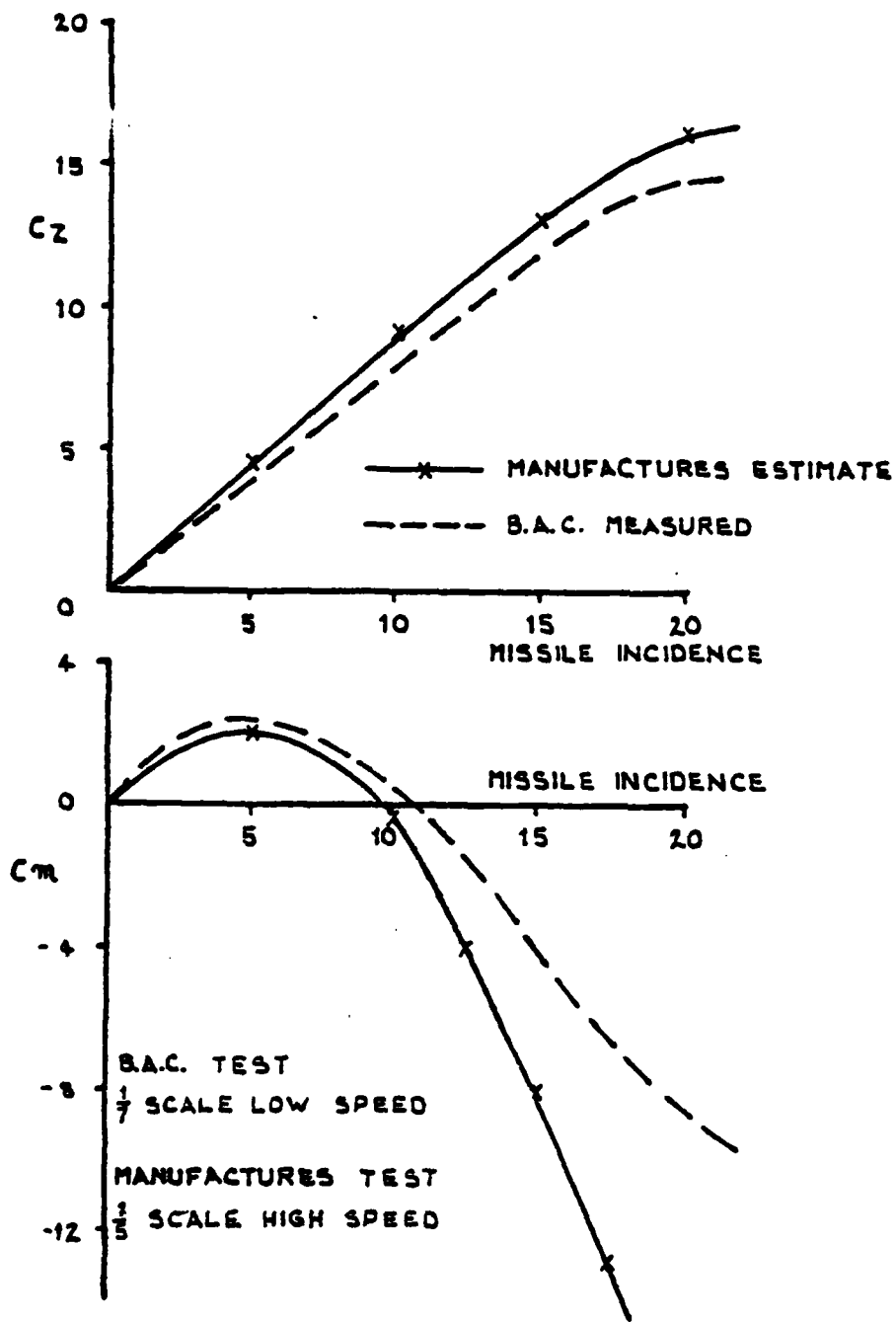


FIGURE.15. MISSILE-COMPARISON OF STORE AERODYNAMICS (LOW SPEED)

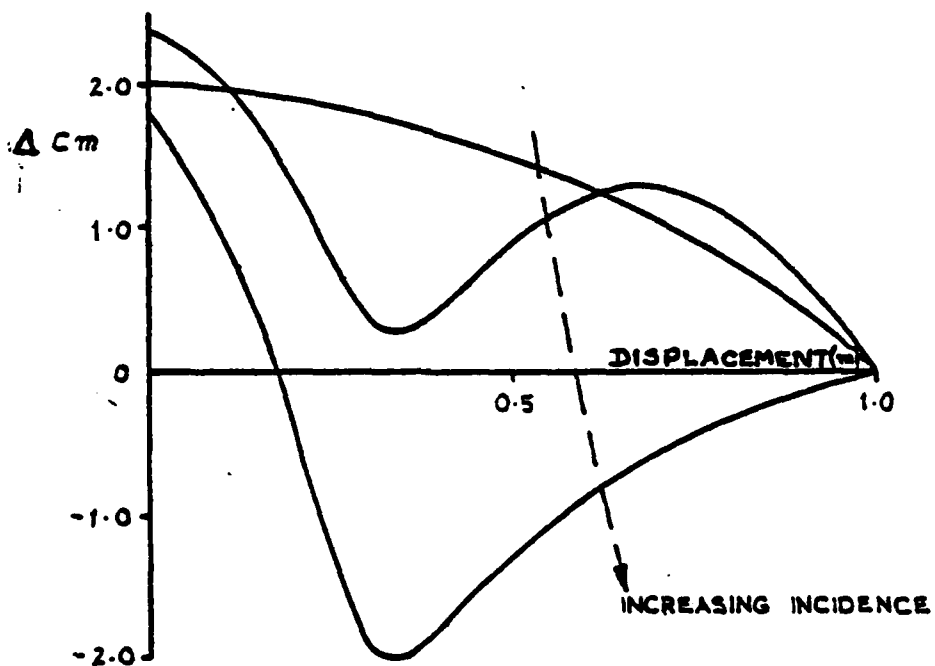
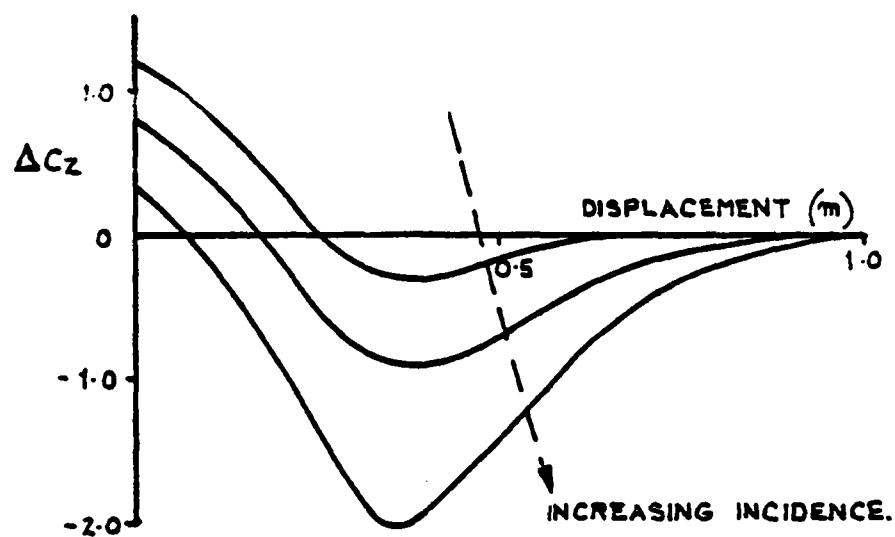


FIGURE.16. MISSILE-INTERFERENCE FIELD AT LOW SPEED.

It was decided to examine the missile aerodynamic characteristics at the speed and scale conditions of the jettison tests. This was undertaken as an extension of the low speed trajectory loads programme which was carried out at the same scale. The sting support system was not expected to influence the missile stability significantly as the design loads, for this low speed testing were small allowing a slender sting and the bluff missile afterbody did not have to be distorted; the sting itself had a parallel section aft of the missile leading gradually to an increase in cross section. The results are shown in Figure 15 compared with the published data, and modelling based on these results was much more successful. The difference is assumed to be due to Reynolds Number but no comprehensive explanation was sought as high speed data became available which indicated that the design case for the system was, overwhelmingly, in the high speed regime.

Following measurement of the aerodynamics of the missile, low speed trajectory loads were measured. These indicated that, at low speed, the interference term was a relatively straightforward function of distance below the aircraft and decayed to zero over a distance of approximately 1m full scale, Figure 16. Using this information together with the measured aerodynamics, 'matching' continued, and a wide range of conditions were matched with variation of aircraft incidence, speed, ejector velocity and pitch rate inputs. It was deduced that missile damping varied considerably with incidence and that a further slight variation of missile stability was required to maintain the match for all conditions. Figure 17 shows the effects of missile stability and damping on missile attitude history.

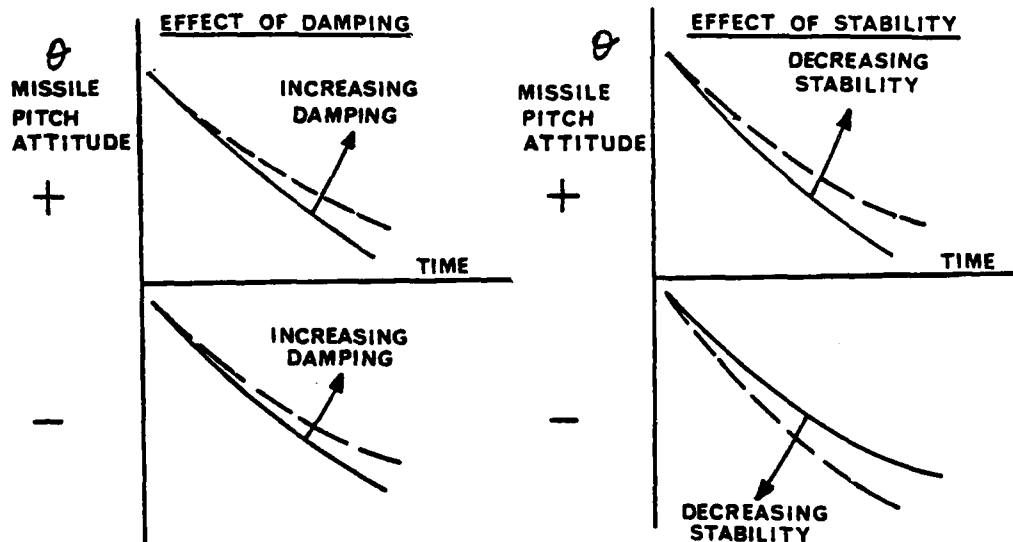


Figure 17. EFFECT OF DAMPING & STABILITY ON MISSILE PITCH RATE.

It can be seen that the two effects can be isolated provided the range of jettison conditions is adequate. The final matched stability is shown in Figure 18 with a comparison of matched damping against the published value. The final standard of match achieved is indicated in Figures 19 and 20 and lies within the tolerances of the film analysis of the wind tunnel drops.

6.1.2. Initial predictions - High speed

High speed measurements of the missile aerodynamic characteristics proved to be very close to the original published information, tending to confirm that the low speed discrepancies were due to the extremely low Re number. These measurements were preceded by high speed flow-field measurements. The flowfield results were un-remarkable except that some probes close to the aircraft produced spurious results due to interference. It is also worth noting that the tests provided no useful indication of the aircraft shock patterns which were subsequently assessed from Schlieren photography which is a standard output of most high speed testing.

As high speed jettison results became available, transonic and supersonic, they proved to be worse than predicted. The predictions had been based on relevant high speed installed loads, but the interference effects had been deduced from low speed results. Examination of the results showed that, as in the low speed tests, the ejector unit was not providing adequate performance. This led to a long study of ejector performance. In order to examine aerodynamic effects ejector performance was by-passed in the model simulation and missile velocity and pitch rate at the end of the ejector stroke were used as the start of the trajectory. Even with this allowance for inferior ejector performance, it was not possible to explain the discrepancy. It was evident that a large nose up pitching was being applied to the missiles with missile 'A' being the worst case. The high speed trajectory loads confirmed that such moments did exist.

6.1.3. Stage 3 - Investigation of high speed interference mechanism

Figure 21 shows pitching moment data measured on two missiles 'A' and 'B' as a function of distance below their installed positions, at a supersonic Mach number. Schlieren photographs showed that the tail of Missile 'A' could be under the influence of a very strong aircraft shock system dominated by the engine intake shock. The system operating on Missile 'A' could conceivably be powerful enough to produce the pitching moment measured on that missile but such a conclusion would not admit a decay in shock strength as it 'carried over' under the fuselage.

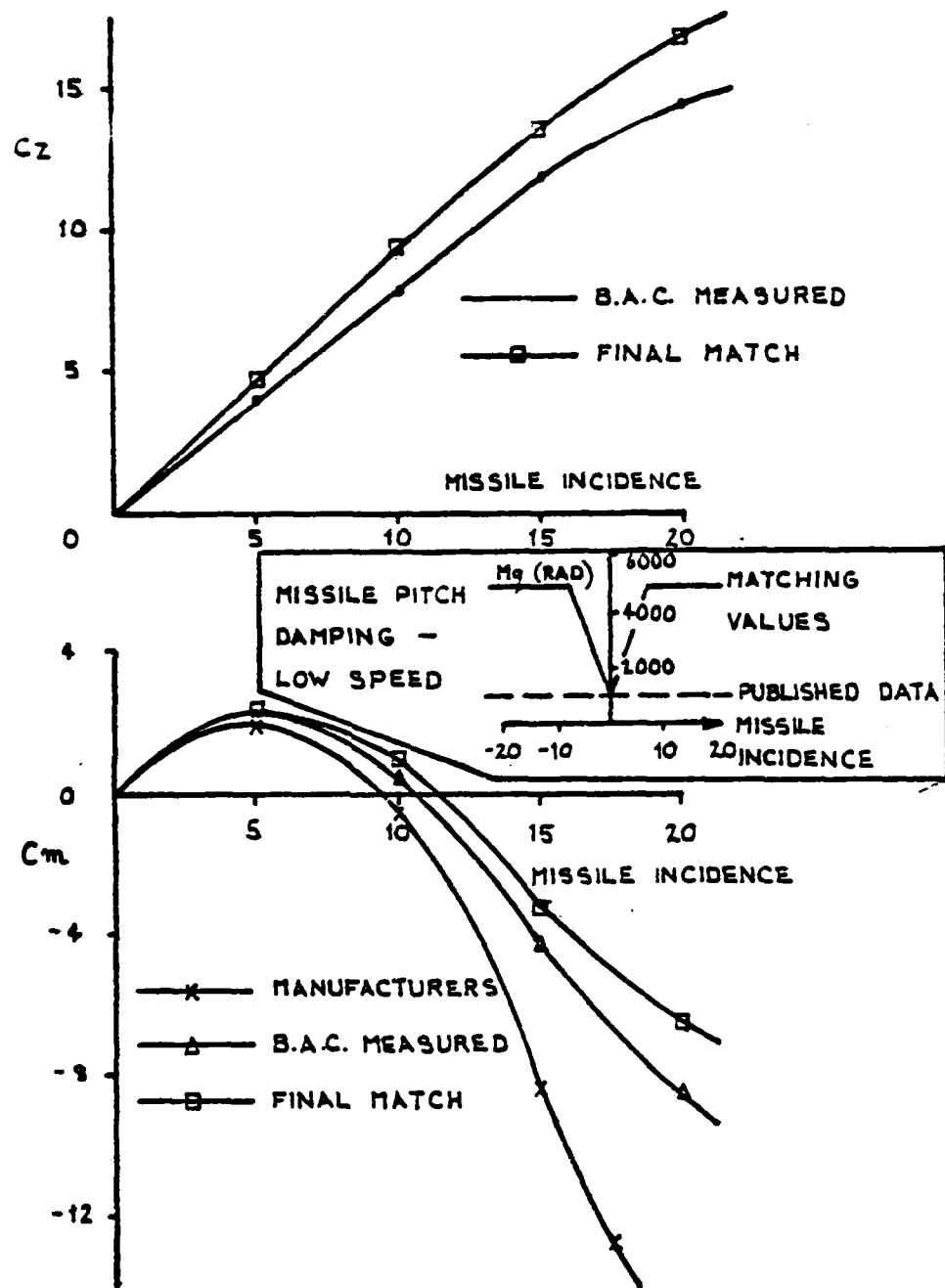


FIGURE 18. MISSILE - FURTHER COMPARISONS OF STORE AERODYNAMICS AND PITCH DAMPING (LOW SPEED).

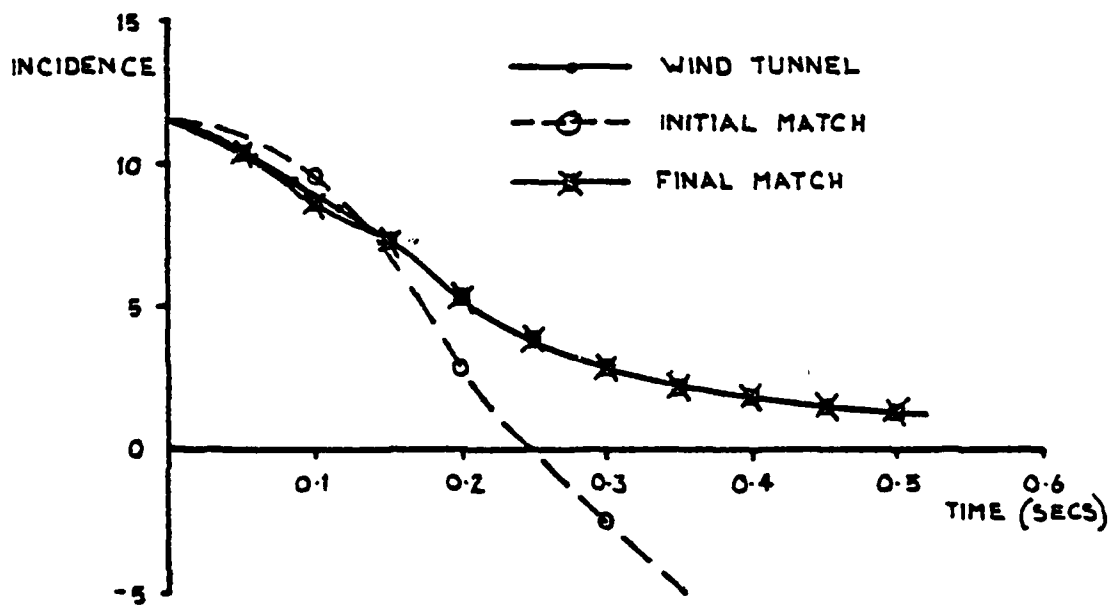
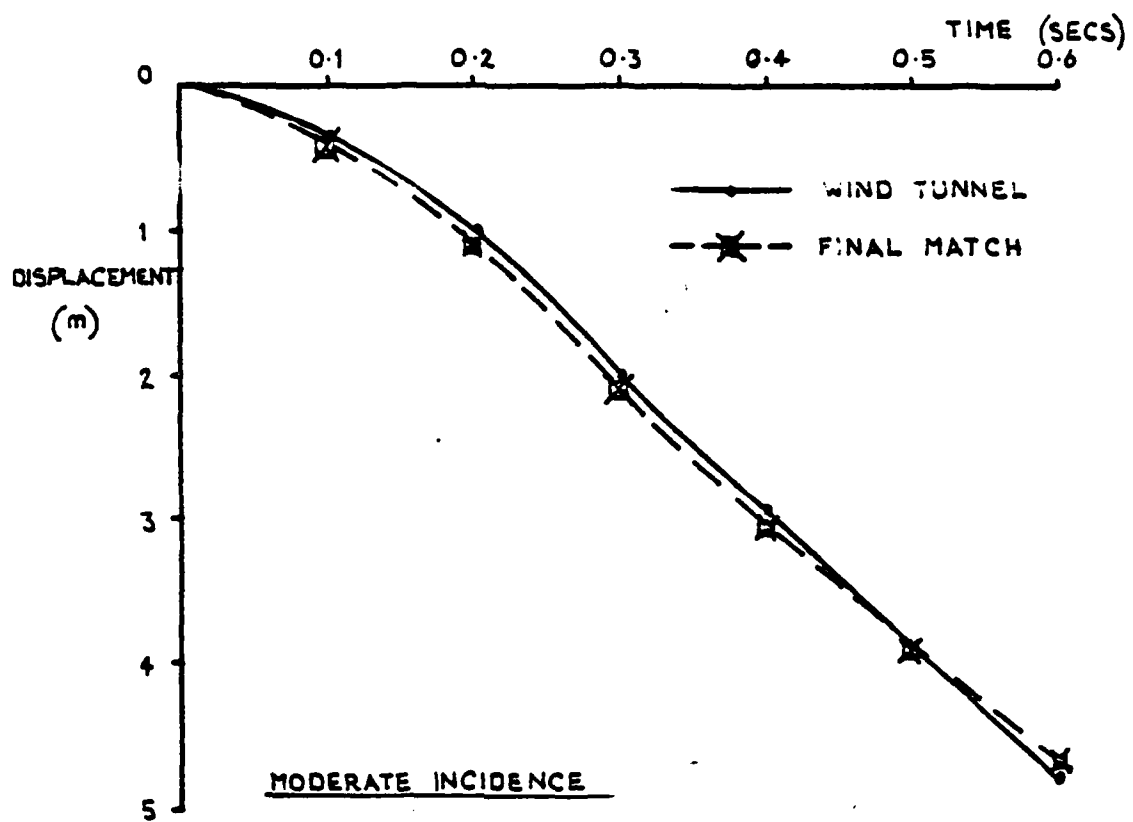


FIGURE.19 MISSILE - COMPARISON OF WIND TUNNEL AND FINAL COMPUTED TRAJECTORY.

LOW SPEED AT MODERATE INCIDENCE

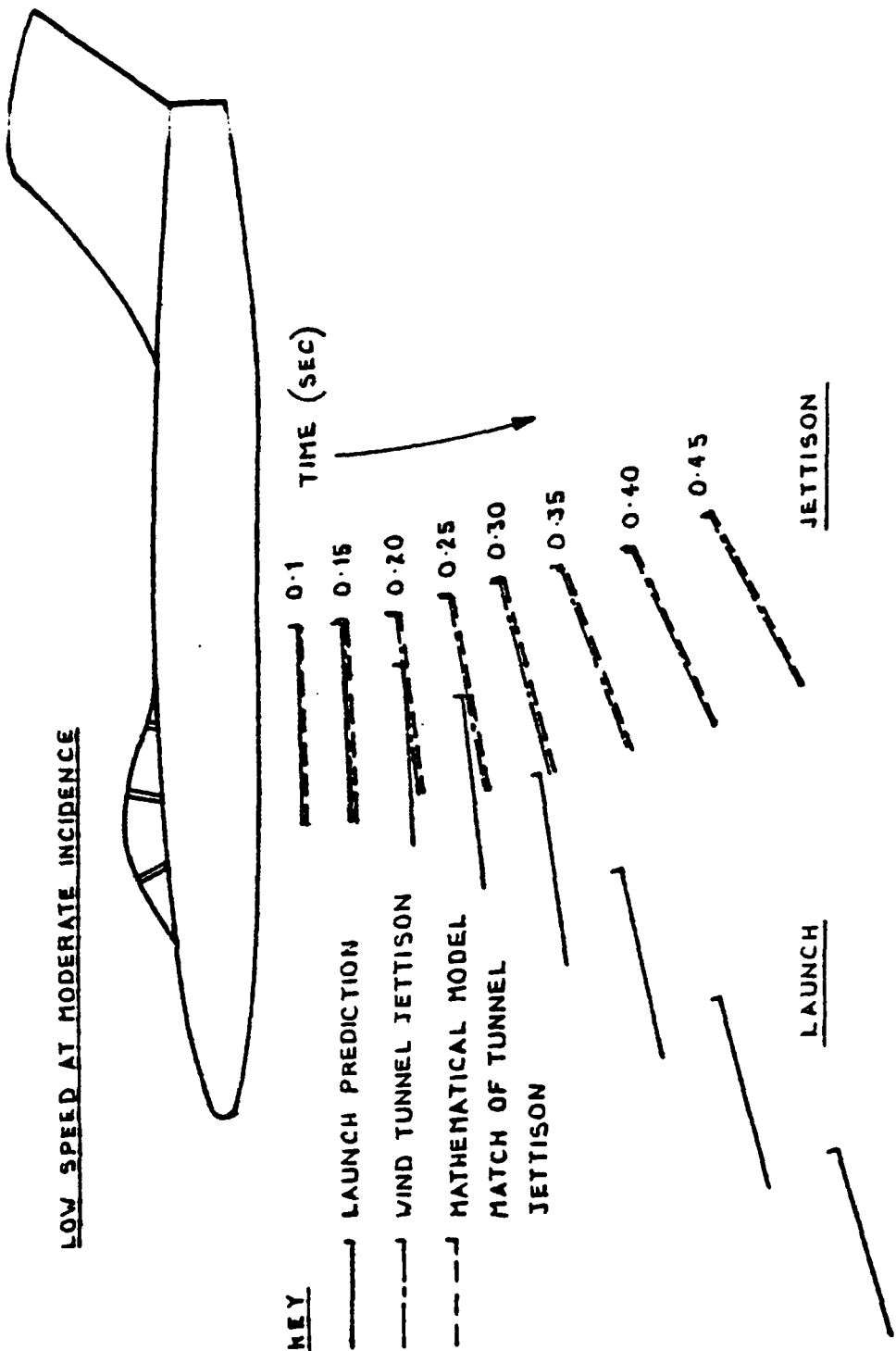


FIGURE 20. MISSILE—COMPARISON OF WIND TUNNEL AND FINAL COMPUTED TRAJECTORY.

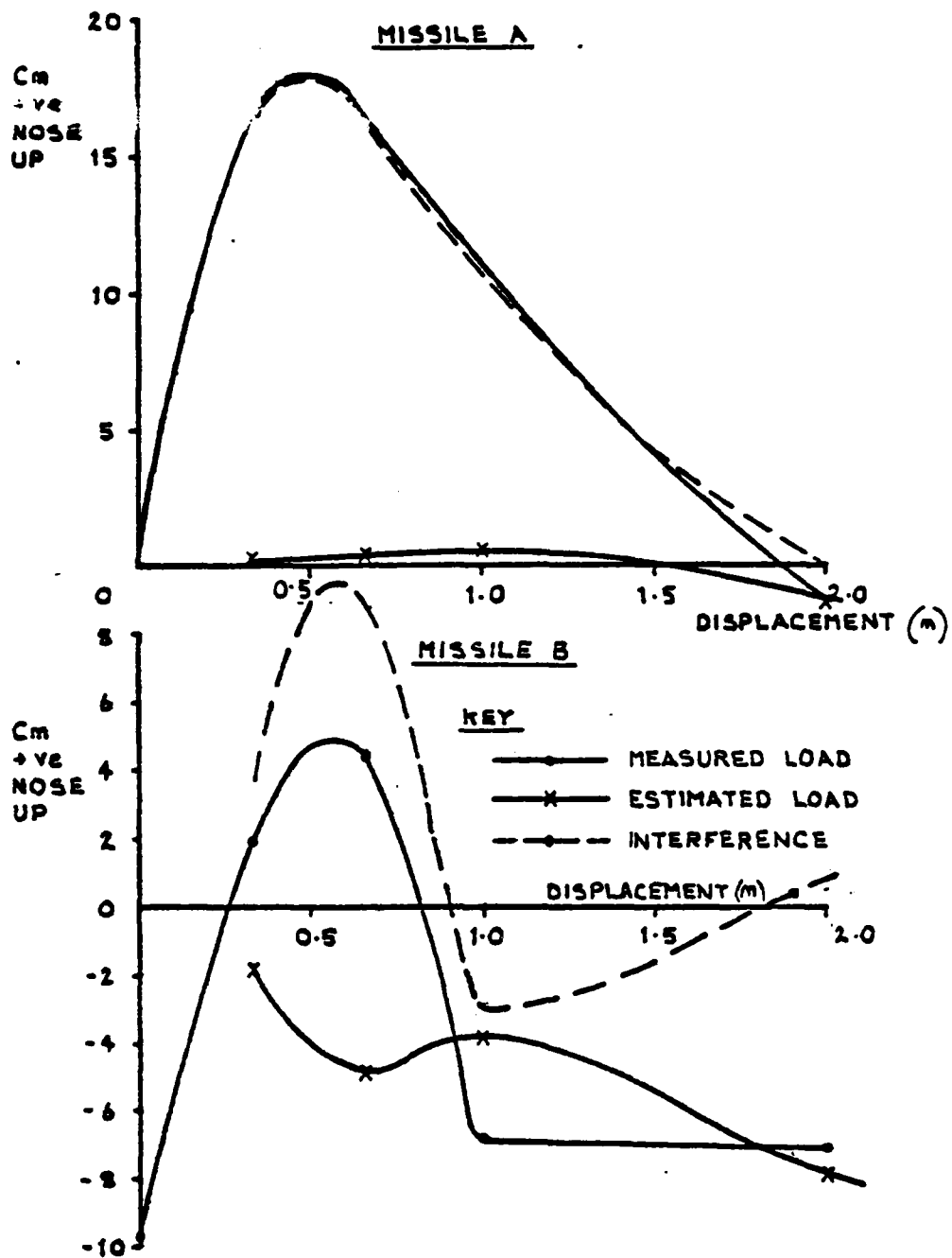


FIGURE.21. PITCHING MOMENT INTERFERENCE -HIGH SPEED.

There was no obvious aircraft shock system operating on Missile 'B' the only interference mechanisms that could cause the pitching moment and normal force combination, as measured, was thought to be the shock from the missile wing reflecting from the aircraft fuselage onto the missile tail during the ejection stroke. Examination of the results at a range of Mach numbers and aircraft and missile attitude combinations supported this conclusion. To confirm this interpretation of the results it was decided to take static pressure measurements along the fuselage to define the point of shock reflection, the results are shown in Figure 22.

Returning to Missile 'A', it was obvious that the same shock reflection mechanism must occur. Subtracting the effect of shock reflection from the measured pitching moment on this missile reduced the effect required from the aircraft intake shock system to a more rational level.

Once the supersonic interference mechanism had been established, and confirmed by matching, it was examined for source of error or misrepresentation. It was obvious that the shock reflection mechanism, affected as it is by boundary layer conditions, will be subject to Reynolds number errors and an estimation of this effect at full scale, with tolerances, can be made.

Another source of error, caused by wind tunnel modelling constraints, was the low model intake mass flow. The model used for both high speed jettison tests and trajectory loads measurements provided subcritical intake flow due to constraints on intake, duct and efflux geometries caused by the need to fit large ejector release units inside the model to cater for the jettison tests. The result was a forward movement of the intake shock system which thus passes the missile at a different position than will be the case at full scale. Recognition of this fact has allowed correction to be applied to the 'interference terms'.

6.1.4. Summary

In the case of this study there is no alternative to mathematical modelling to determine missile launch characteristics, as there is no other way of representing the missile motor, cg variation, and control characteristics. As the wind tunnel data was gathered and analysed predictions of missile launch behaviour were produced and updated to provide evidence for design decisions. The mechanical problems encountered in the jettison tests with the ejector units, could be corrected for in the mathematical model. In the same way the unrepresentative 'light body' scaling of the high speed jettison tests presented no difficulty. Once matched to the high speed tunnel conditions the simulations were exactly represented. In this case the cost effectiveness of a broadly based test programme with sufficient redundancy to allow compatibility checks, is clearly shown. A comparison of the final standard of matching achieved is shown in Figure 20.

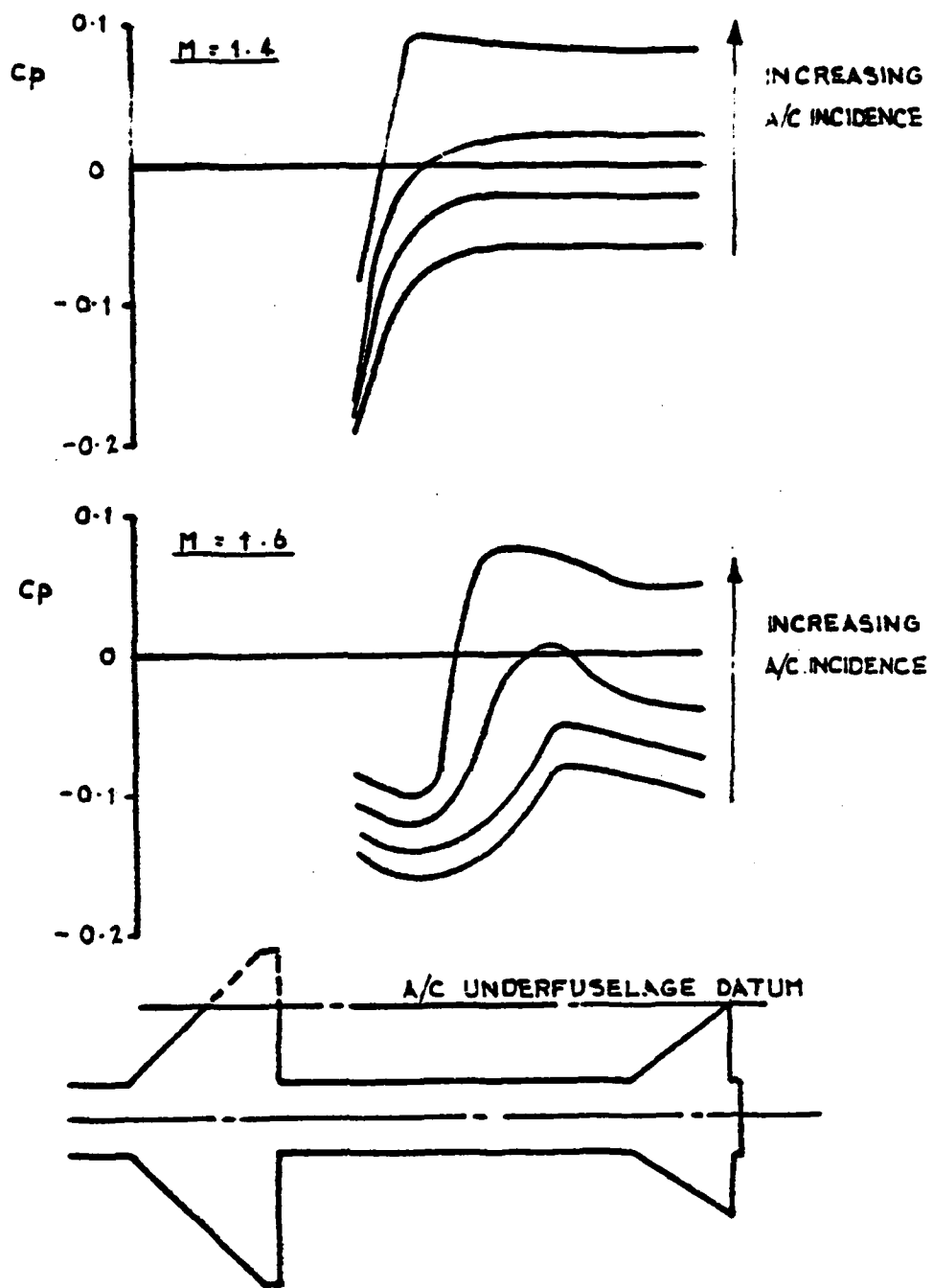


FIGURE.22. UNDERFUSELAGE PRESSURES.

6.2. CASE 2 - EXTERNAL TANK

In this case the store is a large external fuel tank carried on the wing pylon of a strike aircraft. Although the installation itself is relatively straight forward the highly swept wing and high wing loading of the aircraft combine to create strong and unfavourable flowfield effects. The tank tail fins are not symmetric, due to geometrical constraints and hence, tank lateral stability is much lower than tank pitch stability. These aerodynamic problems were rendered more critical by the usual problems associated with this type of store: the large range of store mass and cg position combined with the low density of the empty store.

6.2.1. Stage 1 - Early matching attempts

The aircraft flowfield and store installed loads and moments were defined by wind tunnel testing. The flowfield measurements showed, at the tank installed station, the flowfield sidewash to be of the same order as the aircraft incidence for most of the aircraft incidence range. The significance of this is that the flow vector is effectively rotated 45 degrees out of the pitch plane.

The asymmetry of the tank tails made it difficult to estimate either pitch or yaw stability or stability in a rolled plane. Attempts were made, with partial success, to use the 'matching' process to deduce tank stability. However, there were too many variables involved as the tank, itself pitching and rolling, passed through a rapidly changing flowfield. For limited cases an acceptable match was achieved but the accurate representation of a wide range of cases, which is necessary for validation was not achieved. It was decided that it was essential to measure the store aerodynamics.

6.2.2. Stage 2 - Measurement of the tank free air aerodynamics

The tank aerodynamics were measured in a low speed wind tunnel at 1:3 scale using a rig similar to the one showing in Figure 6. The tank pitching moments are shown in Figure 23. It can be seen that at a roll angle of 90 degrees, equivalent to a zero incidence sideslip condition, there is a large nose up pitching moment. This had not been expected and was found to be due to the local flow effects at the root of the horizontal tails which had significant anhedral.

An important part of the testing was an investigation of Reynolds number effects with particular reference to the conditions at which the low speed jettison tests were conducted. Fig.24 shows the effect of Reynolds number on the pitching moment. It can be seen that at moderate to high incidence the effect of crossflow Reynolds numbers is significant. The results showed that the jettison test results might be misleading in cases where the tank rotated beyond moderate incidence.

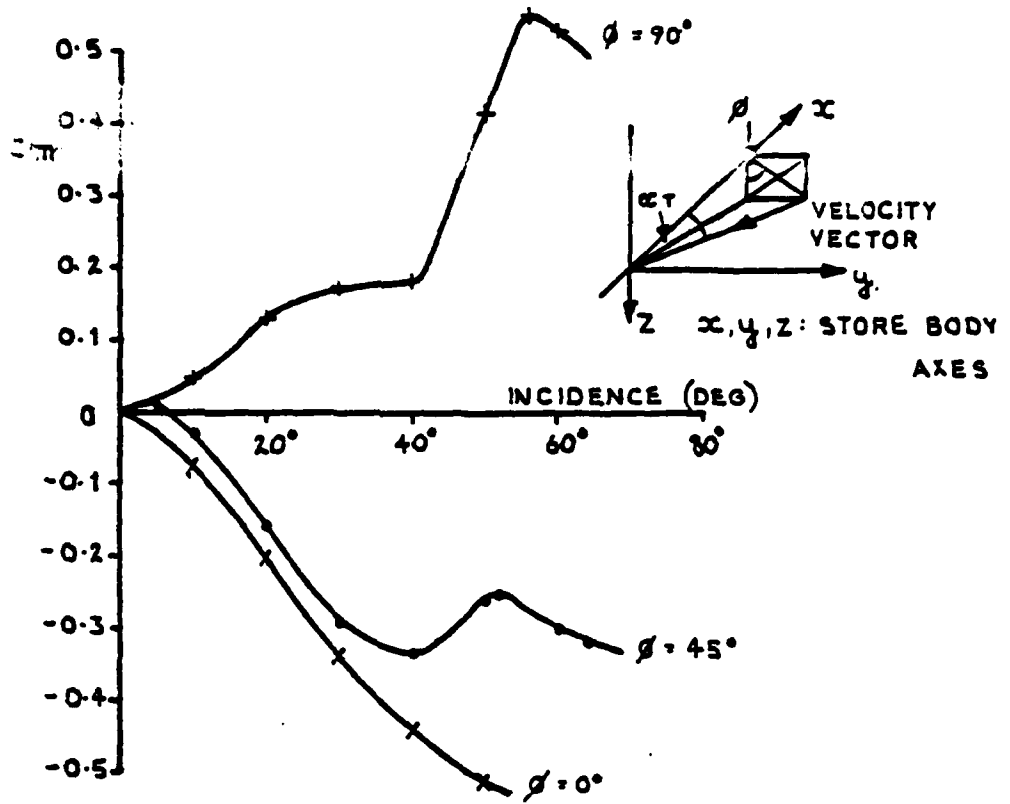


FIGURE.23. TANK PITCHING MOMENT CHARACTERISTICS.

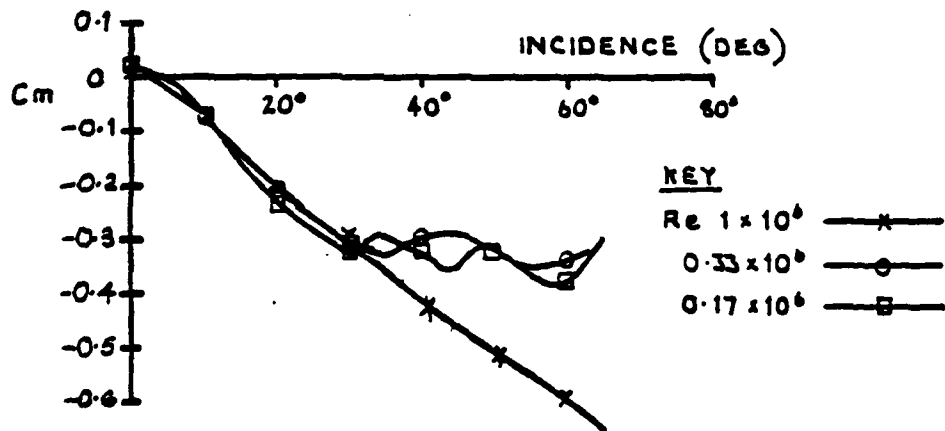


FIGURE.24. EFFECT OF REYNOLDS NUMBER ON TANK PITCHING MOMENT.

6.2.3. Stage 3 - Final matching

Once the complex aerodynamic characteristics of the tank were incorporated in the simulation, matching improved enormously. Figures 25 and 26 indicates the standard of matching that was achieved. The most significant discovery was the extreme sensitivity of the trajectory to tank roll behaviour. This had an important bearing on the interpretation of the jettison tests, where, due to the difficulties of manufacturing very light scaled stores, it had not been possible to maintain the three principal inertias, as well as the correct cg position. A concession had been given on tank roll inertia as it was not considered to be of great significance and this was now shown to be incorrect. Similarly, use of the installed store loads results to extrapolate predictions beyond the speed range covered in the low speed jettison tests required care because balance accuracy was poor in the roll sense.

6.2.4. Summary

Use of the mathematical model in this case established the critical sensitivity of the trajectory to tank roll behaviour. Once this had been established it was possible to correct for errors and examine the effect of realistic tolerances. The mathematical model with its supporting wind tunnel tests permitted a valid interpretation of wind tunnel jettison drops that might otherwise have been misleading.

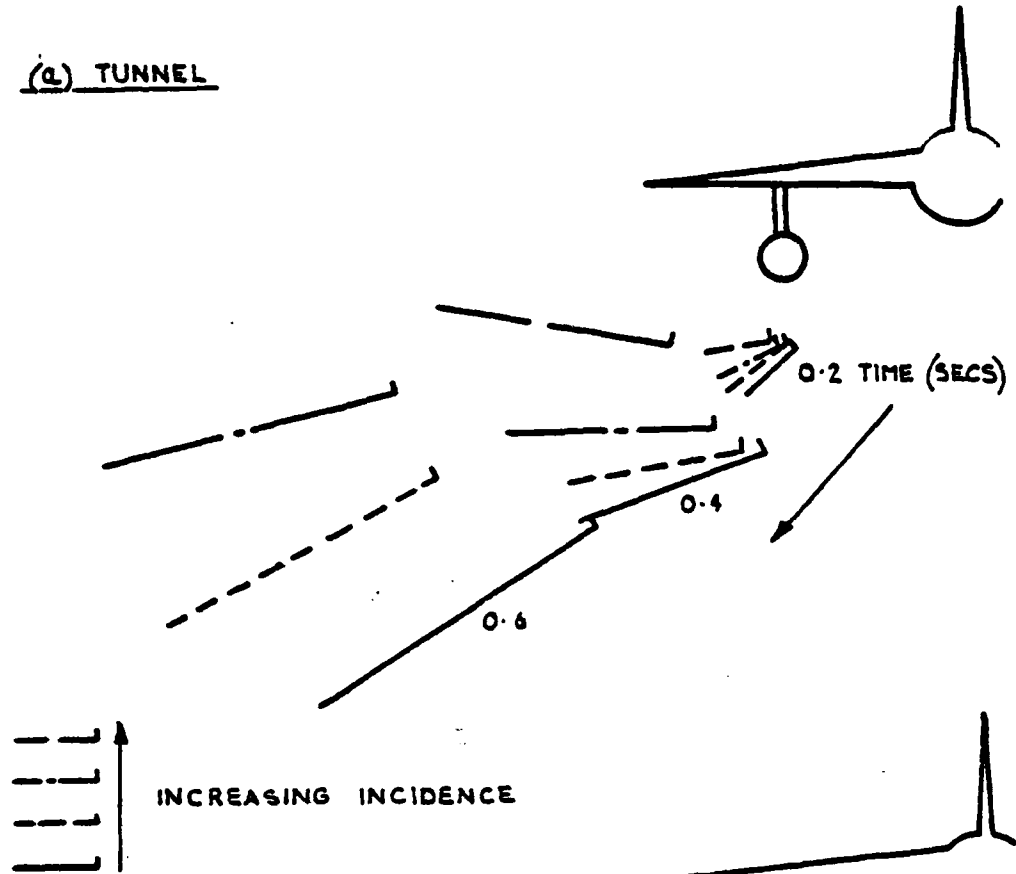
7. CONCLUSIONS

The benefit of the broad based technique described here is its flexibility and adaptability to the input information available. Each part of the input, whether from theory or the wind tunnel requires careful interpretation and this has been demonstrated by the examples described. However, the 'broad base' allows an element of redundancy which we believe gives the technique an advantage over other methods.

8. REFERENCES

1. Alford, W.J. Jr. 'Theoretical and experimental investigation of the subsonic flowfields beneath swept and unswept wings with tables of vortex-induced velocities'. NACA report 1327, 1957.
2. Carr, K. Cox, G.A. 'Comments on mathematical modelling of external store release trajectories, including comparison with flight data.' AGARD Conference proceedings No.187

(a) TUNNEL



(b) MATHEMATICAL MODEL

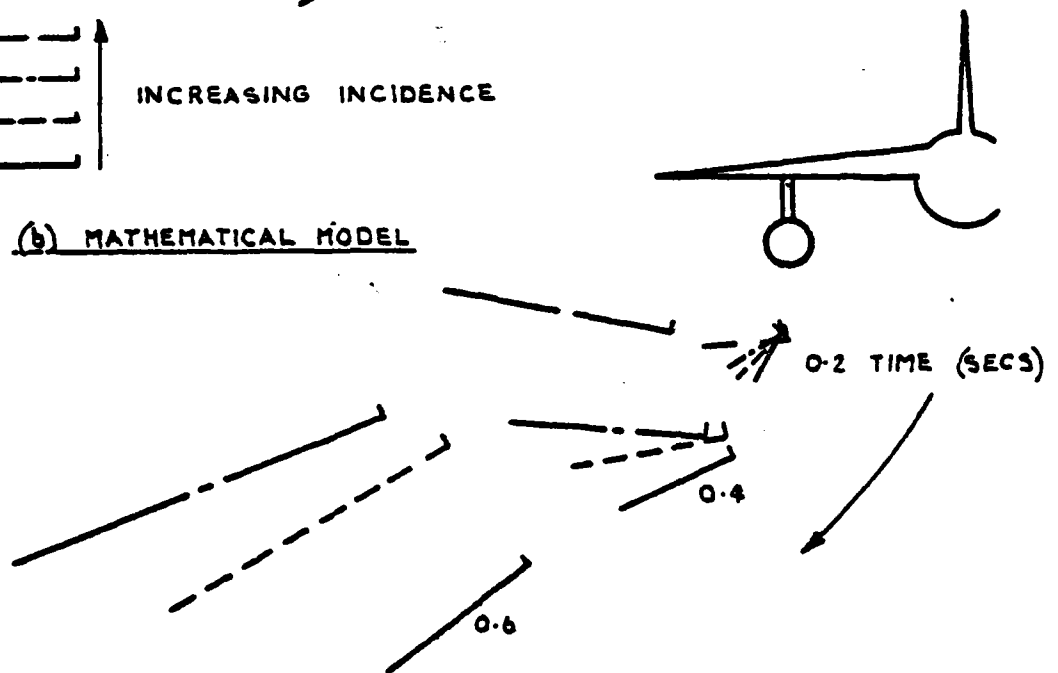


FIGURE.25. TANK-COMPARISON OF WIND TUNNEL AND FINAL
COMPUTED TRAJECTORY.

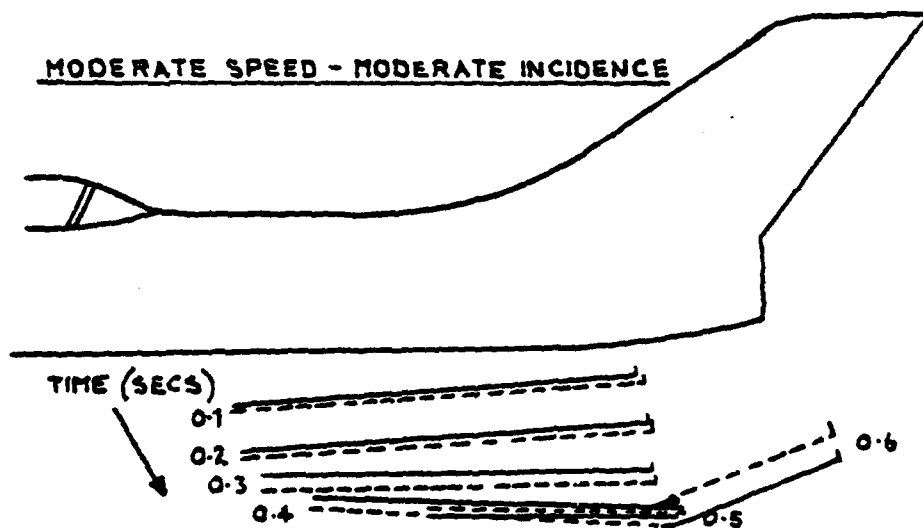
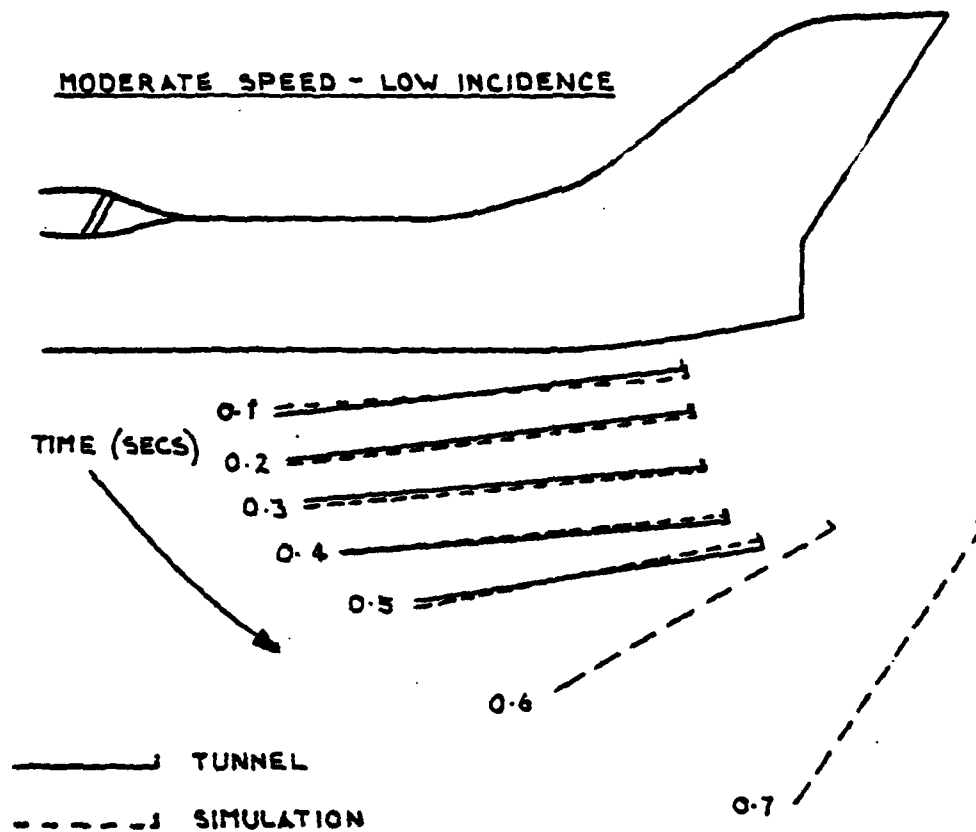


FIGURE 26. TANK-COMPARISON OF WIND TUNNEL AND FINAL COMPUTED TRAJECTORY.

3. Symposium on weapon release characteristics. RAE Farnborough
21 July 1971.

4. Dexter, P.J., Fothergill, E.K. ABACUS - A computer program
which evaluates the longitudinal characteristics of weapon
configurations. BAC Guided Weapons Division, Report ST.14276

AUTOBIOGRAPHY.

Mr D.Gardner received his Bachelor of Technology Aeronautical Engineering Degree from The University of Technology, Loughborough, England in 1963, and immediately joined the Aerodynamics Department of British Aircraft Corporation, Military Aircraft Division. He is a Member of the Royal Aeronautical Society and a Chartered Engineer.

He has been associated with the development of aircraft, such as Strikemaster, Jaguar and Tornado, and is presently Principal Aerodynamicist, Tornado Development. His responsibilities include those of ensuring safe separation during release or jettison of external stores and the aerodynamic design of 'special to type' stores.

Mr. A. L. Guest, Associate Member of the Royal Aeronautical Soc. also received his Bachelor of Technology Aeronautical Degree from the University of Technology, Loughborough, England, in 1969 and he joined British Aircraft Corporation later that year.

He has been associated with store separation work from Strikemaster and Tornado aircraft since 1970 and was appointed Senior Aerodynamicist responsible for a small group of people working on this task in 1974. He is also a member of the Royal Aircraft Establishment Steering Group on aerodynamic interactions of stores and airframes.

SIX DEGREES OF FREEDOM SYSTEM FOR
STORE SEPARATION STUDIES IN ONERA WIND-TUNNELS

(U)
(Article UNCLASSIFIED)

by

Jacques Coste
Office National d'Etudes et de Recherches Aérospatiales (ONERA)
92320 Châtillon (France)

ABSTRACT. (U) The study of airborne store separation can be performed in wind-tunnel by different methods. In particular the "grid" method, where aerodynamic loads are measured on the store placed successively at discrete locations - grid nodes - in the aircraft aerodynamic field, the trajectory being then calculated by flight mechanics formulae, give fairly good results. That kind of testing is currently carried out in ONERA Modane wind-tunnels for any military store. Until now a sting support system with only one remotely controlled degree of freedom, i.e. translation, was used. But several manual operations were needed to modify the other, unmotorized, parameters of location and attitude. Presently a device with six motorized, remotely controlled, degrees of freedom has been built, resulting in a significant time saving for such testing. Associated with a computer controlled servo system, this device can be used not only with the grid method, but also with the captive trajectory method. The mechanical features of the device and the bases for the servo control program are described, along with the first calibration results in the Modane 6ft transonic tunnel.

"Approved for public release ; distribution unlimited."

LIST OF FIGURES

FIGURE NUMBER

- 1 SIX DEGREES-OF-FREEDOM RIG FOR TRAJECTORY STUDIES
(CAPTIVE TRAJECTORY SYSTEM) INSTALLED IN THE TRANSONIC
TEST SECTION OF 52 MODANE WIND TUNNEL (1.75 x 1.75 M²)
- 2 SCHEMATIC MECHANICAL LAYOUT
- 3 ELECTROMECHANICAL JACK-ROLLER SCREW
- 4 GUIDANCE FOR TRANSLATION MOTION
- 5 SIX DEGREES OF FREEDOM RIG-CALIBRATION
- 6 BLOCK DIAGRAM OF CONTROL SYSTEM
- 7 MOTOR CONTROL LOGIC
- 8 FLOW DIAGRAM
- 9 CAPTIVE TRAJECTORIES OBTAINED WITH THE SYSTEM

1 - INTRODUCTION

The study of airborne store separation can be performed in good conditions from wind-tunnel test results, through various methods, the validity of which having been proved. In particular, the "grid" method, where aerodynamic loads are measured on the store placed successively at discrete locations - grid nodes - in the aircraft aerodynamic field, the trajectory being then calculated by the flight mechanics formulae, has been compared to the methods of store model dropping or firing ; this type of testing is currently carried out in the ONERA Modane wind-tunnels for any kind of military store. Until now, a sting supporting system with only one remotely controlled degree of freedom, i.e. translation, was used. It permitted the establishment of the set of aerodynamic forces exerted on the store in the whole aerodynamic field of the parent aircraft, but many manual interventions were necessary for changing the parameters : orientations and displacements.

With a view to alleviate the task of the experimenter, and to increase the testing rate, a rig with six motorized degrees of freedom has been built (figure 1).

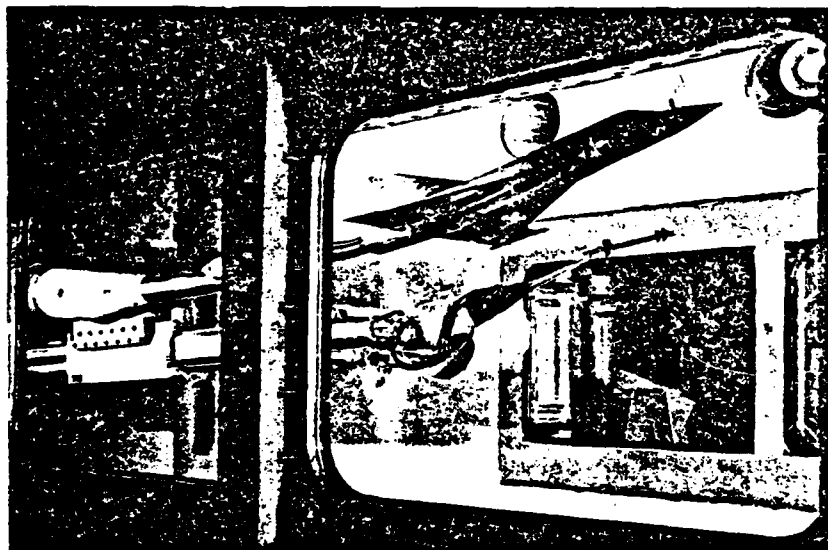


Fig. 1 - Six degrees of freedom rig for trajectory studies (captive trajectory system) installed in the transonic test section of S2 Modane Wind Tunnel (1.76 x 1.75 m²).

This rig is directly controlled by an HP 2100 computer, which calculates and gives to a control logics the set point values for controlling the driving motors. These values are determined from the positions to be obtained for the store. That assembly - mechanical rig plus computer - makes it also possible to use the captive trajectory method. thanks to a computer program which, in that case, determines step by step the anticipated trajectory from the measured aerodynamic forces and other preset data.

2 - DEVICE DESCRIPTION

The test device involves a set of three mobile parts hinged together through gimbal joints. These hinges with two degrees of freedom permit, by combining their rotations, the displacement of the model along the Y and Z axes, and its orientation in pitch and yaw. The upstream element, supporting the model by means of an internal balance, can embody a rotation control system around the roll axis and/or be fitted with a bent sting. The downstream element, mounted on a sliding system, allows the displacement of the model along the X-axis ; figure 2 shows the basic layout of this device.

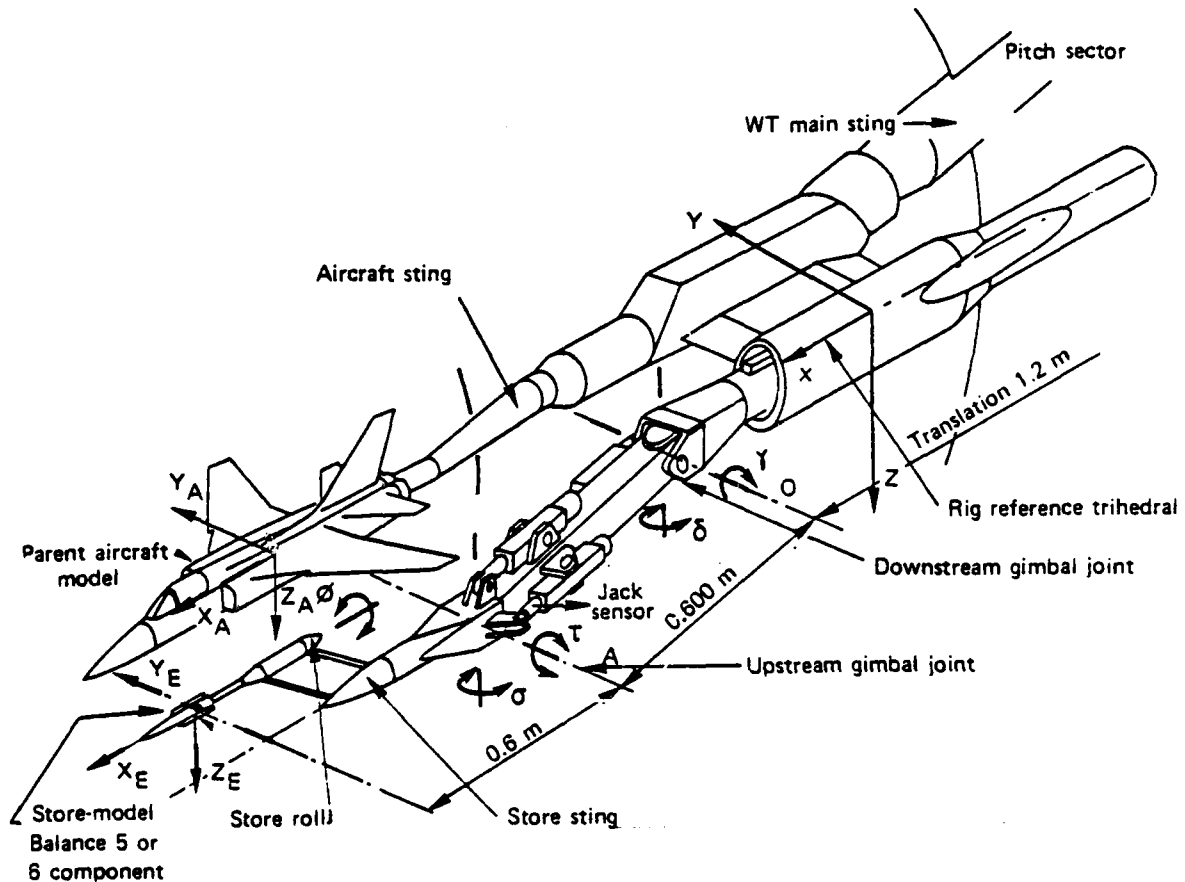


Fig. 2 - Schematic mechanical layout.

Each hinge of the gimbal joints is mounted on smooth looseless axes and the control is ensured by electromechanical jacks fitted with satellite rollers precision screws (figure 3). The driving motoreducers linked to the intermediate leg through finely adjusted ball joint are supplied with 24 V direct current. The translation speed of the screw is about 1 mm/s. The motors involve electromagnetic brakes.

The downstream sliding part is mounted on a guiding system consisting in V-mounted roller pads (figure 4). The motion is driven by a motoreducer actuating a rack gear.

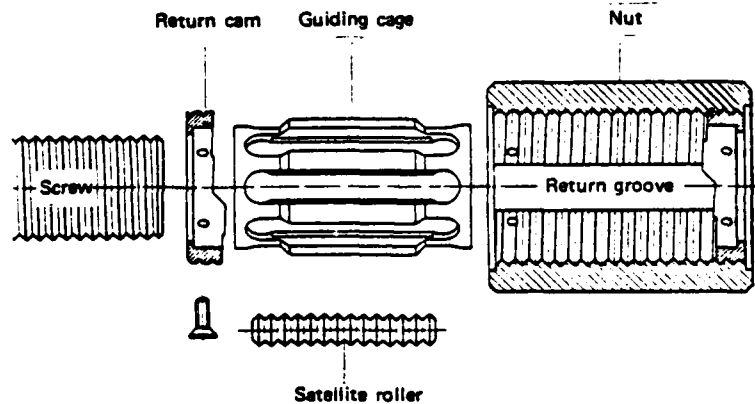


Fig. 3 - Electromechanical jack-roller screw.

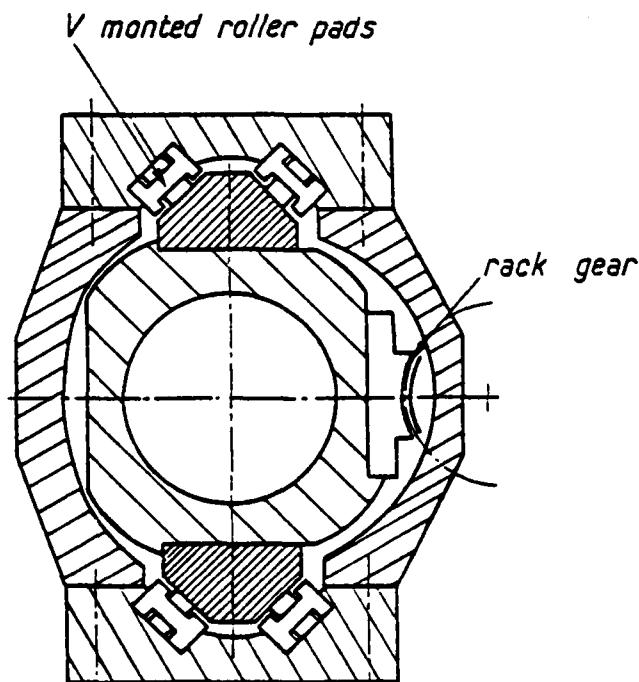


Fig. 4 - Guidance for translation motion.

Each displacement is measured by rotative inductive position sensors of very high precision - say about 30 arc-seconds.

The aircraft model is mounted independently of the store on a sting support which can be either deported or bent, and which is fixed to the rig abreast of the downstream sliding part.

3 - RIG CHARACTERISTICS

The front gimbal joint of the rig has a maximum angular field of $\pm 30^\circ$ on both axes, and the rear one $\pm 20^\circ$, enabling thus tilting the model both in the vertical and horizontal planes up to 15° or 30° , depending on the transverse displacement required. That transverse displacement can reach or even exceed 300 mm in the two directions, along Y as well as along Z.

The overall range along X is 1200 mm, and the roll motion of the model about the rotating sting can reach $\pm 170^\circ$.

The rotational speed about the gimbal axes is about 0.5 degree per second, resulting in a maximum translation speed in Y or Z directions of 10 mm/s, with the rear gimbal joint acting alone. The translation speed in the X direction is at present 6 mm per second, but could be further increased. The rotational speed in roll is 3 degrees per second.

4 - RIG DEFLECTIONS

The setting accuracy of the store position about the parent aircraft being very high, it is necessary to take into account the deflections of the rig due to the weights and aerodynamic forces acting on the various parts. These forces are known, thanks to, on the one hand, the internal balance which measures the aerodynamic forces on the store, on the other hand to dynamometric sensors located at the end of the jacks. These sensors measure the control forces, from which are deduced the aerodynamic loads on each leg.

A calibration on a bench makes it possible to determine, for each leg, the distortion coefficients under the action of forces and moments exerted on their end, and of distributed loads simulating aerodynamic forces (figure 5). These coefficients are put into the control program. For the sliding downstream part, the deflections depend on the displacement in translation, thus the coefficients are given as polynomial functions of the translation, of the third degree for the transverse deflections, and of the second degree for the angular deflections.

The deflections of the aircraft sting are independent of the rig and separately calculated by means of their own distortion coefficients, either by measuring the aerodynamic forces on the model with an internal balance, or by introducing in the computer program the aerodynamic coefficients of the aircraft. A third way can be followed by

measuring directly the angular deflections by means of two goniometers, and introducing in the program a relation between the angular distortion and the corresponding displacement.

These distortions, as they intervene in the calculus at the level of the setting of the store center of gravity location, ought to be transferred for each leg at this point, in the reference trihedral of the control mechanism.

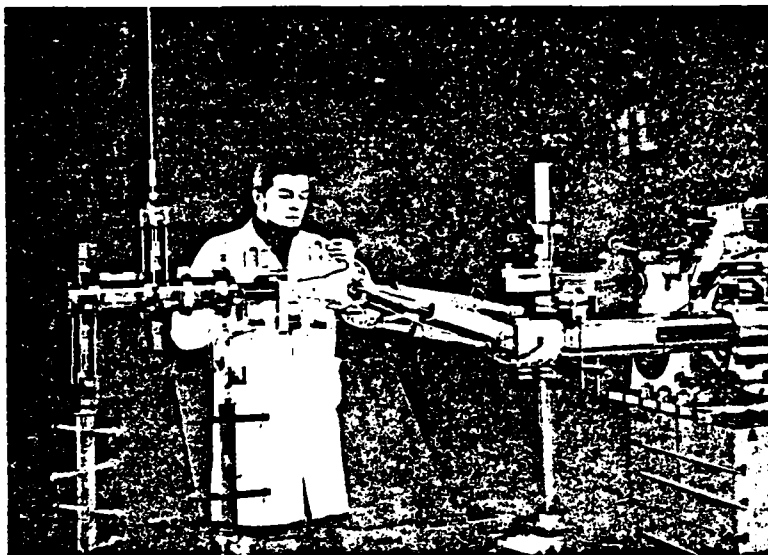


Fig. 5 - Six degrees of freedom rig-calibration.

5 - ACTUATING SYSTEM

Figure 6 gives the principle of the overall actuating system. The computer receives information from the measurement apparatus (wind-tunnel reference parameters, pressure sensors, balances, jacks dynamometers, etc.). It calculates the displacements of the model and sends the resulting information, on the one hand to the control logic, on the other hand to the main computer. The latter displays on its peripheral units the numerical values and the graphs, either on tracing table or on cathoscope screen.

The control logic receives the information formalized as digitized set point values. These values are compared to the indications of the position encoders by means of a numerical comparator which sends a control order to the motors if the discrepancies between the compared values exceed preset tolerance margins (figure 7).

The system can operate either manually, by direct control of the driving motors, or automatically. The automatic control can be in open loop, with presetting of the position to be obtained (grid method), or in closed loop, the successive positions of the store being then calculated by the computer program by means of flight dynamics formulae (captive trajectory method).

During the preparation phase, the governing computer is always linked in a conversational mode with the operator, through a cathoscope and keyboard.

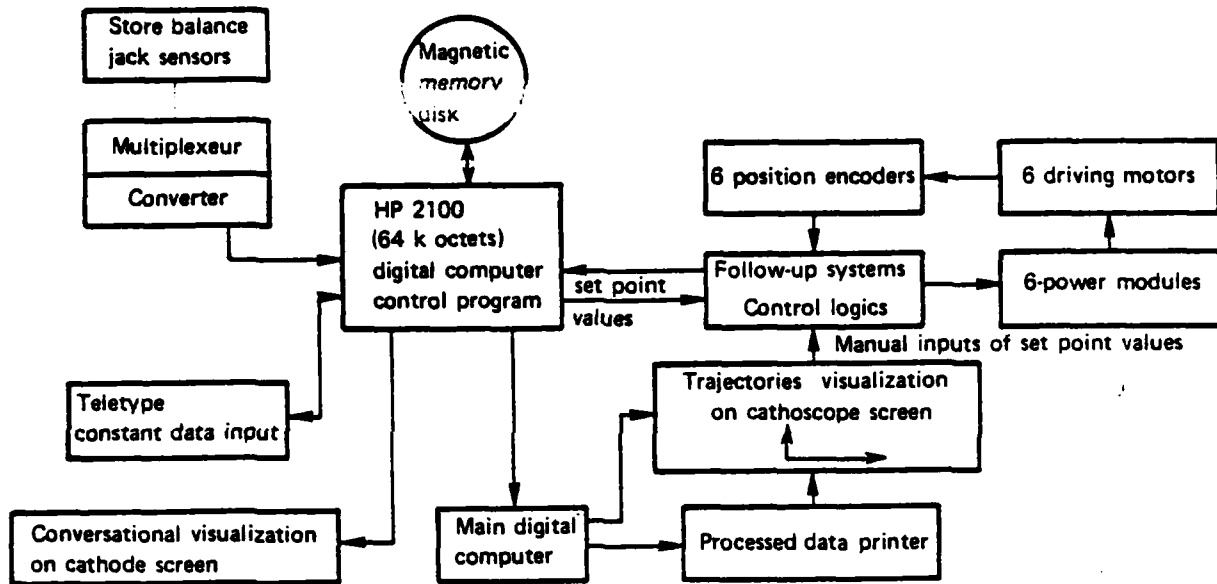


Fig. 6 - Block diagram of control system.

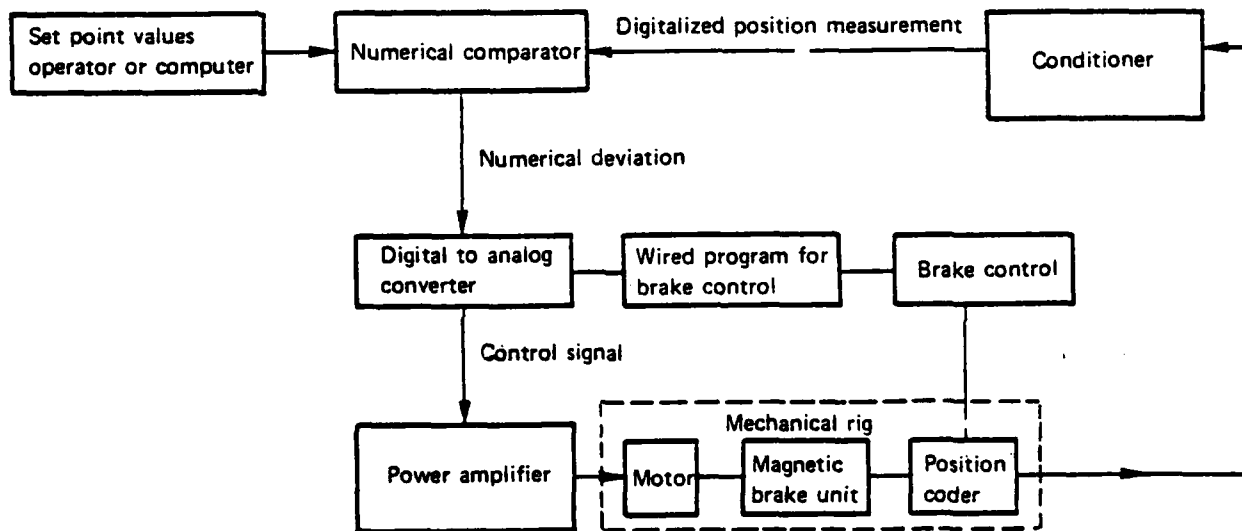


Fig. 7 Motor control logic .

6 - COMPUTER PROGRAM

This program calculates the set point values necessary for the motor control, from the store position about the parent aircraft. In the grid method case, the initial position and attitude are given and the incrementation is made by the program (by constant steps ΔM). In the case of the captive trajectory method, these values are calculated by the program along with the motion derivatives, and the incrementation is made with a constant time interval Δt .

The computing sequence is as follows (figure 8) :

a) Tunnel references calculation, from the pressure and temperature measurements (dynamic pressure, Mach number, wind speed, etc.).

b) Aircraft sting distortion calculation.

These distortions can be determined through three different methods :

- aerodynamic forces measurement by means of an internal balance and distortion calculation with the calibration coefficients ;
- input of the aircraft aerodynamic coefficients into the program data and calculation of the distortions by means of the calibration coefficients ;
- sting angular deflections measurement by means of two goniometers, and transverse linear deflections calculation by means of an experimentally established relation between angular and linear deflections.

c) Store aerodynamic coefficients calculation from the forces measured by means of the store internal balance ; the weight components are subtracted from these forces before the aerodynamic coefficients calculation.

d) Calculation of the store supporting rig distortions ; these distortions are calculated, part after part, from the applied forces and the calibration coefficients in the reference trihedral of each part, and then translated to the point G, store load center, in the reference trihedral of the rig ; the aerodynamic forces on each part are determined from the forces measured on the driving jacks.

e) Calculation of the forces exerted on the real store, from the aerodynamic coefficients previously calculated, altitude conditions, propulsion or ejection forces on the store, weight and load factor.

f) Calculation of the store trajectory about the parent aircraft, from the applied forces in the store reference trihedral and the mass characteristics of the real store (mass and inertia coefficients).

The accelerations and speeds, both angular and linear, are calculated at once. The store orientation about the parent aircraft (Euler's angles) is then determined by calculating previously the Euler's angles of the store about the rig.

Knowing the store speed components, it is then possible to determine the displacement about the aircraft.

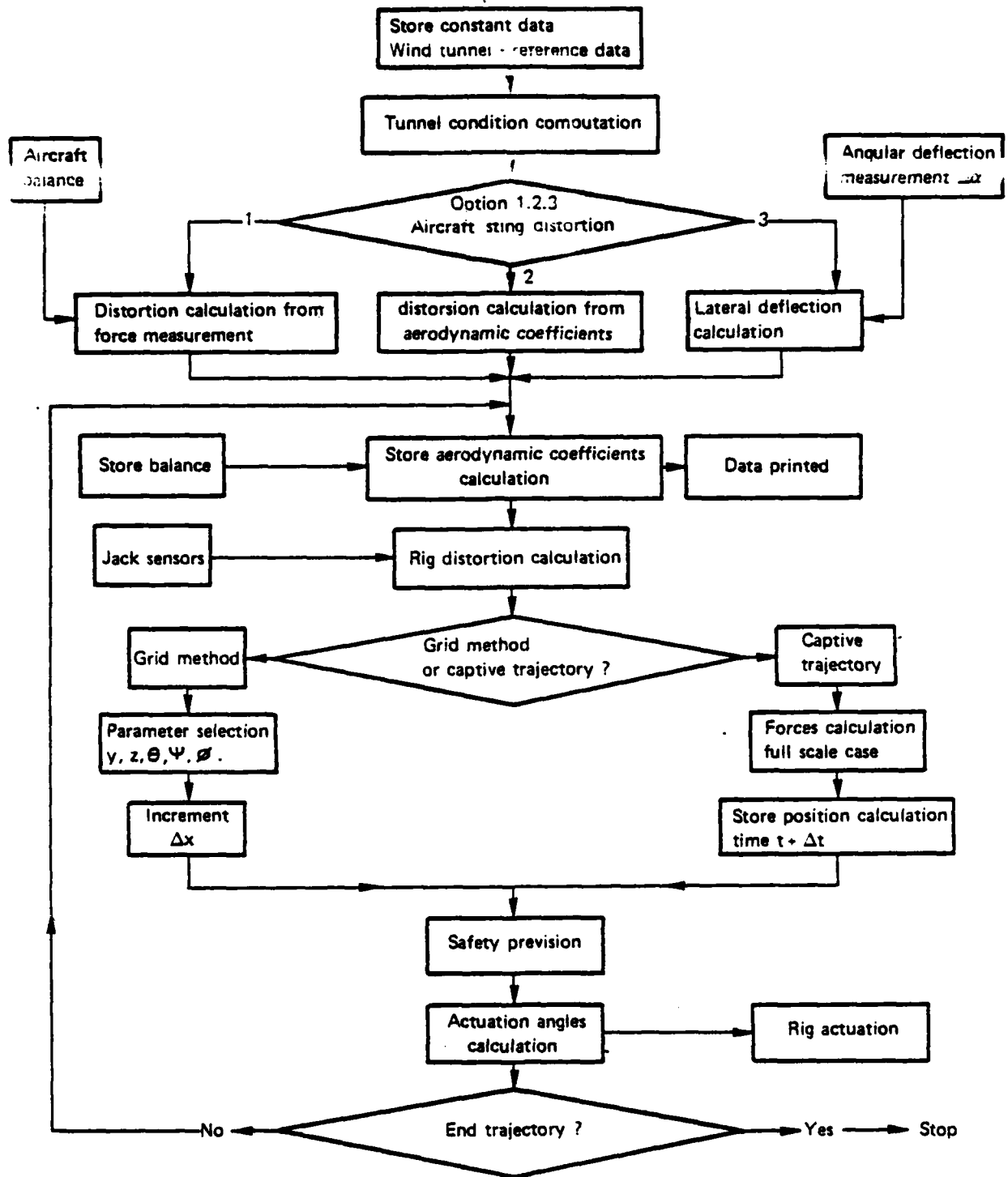


Fig. 8 - Flow diagram.

In the grid option, the relative position of the store about the aircraft is given at once, then incremented along X-axis.

g) Safety calculation. Apart from the mechanical safety devices : electrical contact detectors between store and aircraft, limit switches, initial contact checking etc., precautions are taken with a view to avoid any contact between the aircraft and the mobile parts, by means of the computer program. Before the operation, a security subroutine calculates the position of the critical points of the rig or store about the aircraft envelope, defined by means of a set of drawings. If some collision hazards appear, the operation is interrupted and a diagnosis appears on the operator cathoscope screen.

h) Calculation of the drive angles of the rig. The orientation and displacement of the store being defined in the rig reference trihedral, the rig joints angles are calculated by the computer. This calculus is based on the projection relations of the various parts of the rig in its main reference trihedral, and on some relations determined by identification between two matrices of orientation angles. One of these matrices is established from the Euler's angles of the store, the other from the rig joints angles.

These relations not being independent, the calculation is made by iterations. It will be taken into account, in these calculations, the distortions of the rig and of the aircraft sting support.

7 - ASSESSMENT RESULTS

Bench tests permitted us to assess the accuracy with which it was possible to place the store under the parent aircraft according to the set values. At each cycle of calculus the position obtained was measured and compared with the calculated one. Taking into account only the distortions due to the own weight of the system, the discrepancies appeared to be of the order of 0.15 mm between measured and theoretical values.

The vibratory behaviour of the rig and the automatic control of the motors were then controlled in the wind-tunnel at Mach 0.9. The approach process of the store in the vicinity of the model has been tested, and the first three-dimensional captive trajectories have been successful performed last June.

For example, figure 9 shows two captive trajectories obtained with the system for the same Mach number with two different altitudes and load factors. These tests were carried out in the S2 wind-tunnel.

The second trajectory was stopped by the automatic limit switch, but the missile was already out of aerodynamic field of the aircraft.

The lateral displacement is due to the local wing field.

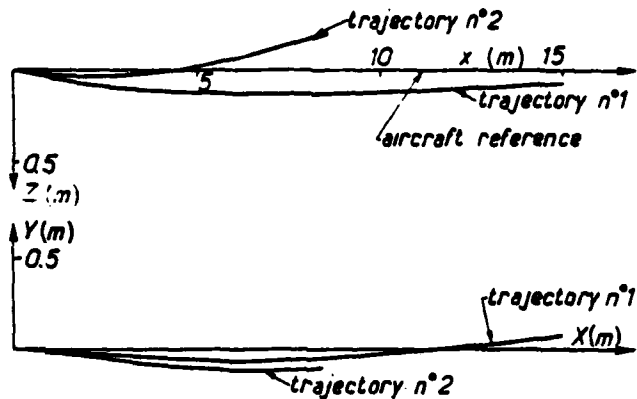


Fig. 9 - Captive trajectories obtained with the system.

8 - CONCLUSION

This 6-degree-of-freedom system has been studied and built by ONERA, on request from aircraft constructors with the support of the Technical Service of Aeronautics.

Thanks to a thorough construction, the precision of the airborne store location and attitude settings about the parent aircraft is quite good. The computer program for the calculation and the control offers the possibility to be adapted to various testing layouts.

Many tests, such as emergency jettisoning, firing of self propelled missiles or store separation by simple dropping or dropping plus firing, can easily be carried out, with the captive trajectory method, or studied with the grid method. The time savings and the setting accuracy given by this system, as compared with previous ones, represents a significant advantage along with a large increase of experimental possibilities.

A-10 AIRCRAFT STORE CERTIFICATION
PROGRAM REVIEW
(U)
(Article UNCLASSIFIED)

by

ROBERT J. ARNOLD
Armament Development and Test Center
Eglin Air Force Base, Florida 32542

and

CAPTAIN STEPHEN C. KORN
Aeronautical Systems Division
Wright-Patterson Air Force Base, Ohio 45433

ABSTRACT. (U) The A-10 stores certification program was uniquely structured to utilize in-house Air Force expertise wherever possible in management, engineering analysis, flight test demonstration, and data reduction. The program was also designed to facilitate the orderly transition from the contractor of all engineering certification efforts once the contracted requirements of the aircraft specifications had been satisfied.

This paper reviews the A-10 stores certification program to include: analysis techniques utilized, test programs conducted, and problems uncovered during the flight test program. Lessons learned during the program are provided, and recommendations are given for the benefit of managers and engineers who may be involved in future store certification programs on other aircraft. The major disciplines which were a part of the A-10 stores certification program are stores separation, loads, flutter, performance, and stability and control. The store separation aspects of the program will be emphasized with a more limited discussion of the other disciplines.

"Approved for public release; distribution unlimited."

LIST OF FIGURES

FIGURE NUMBER

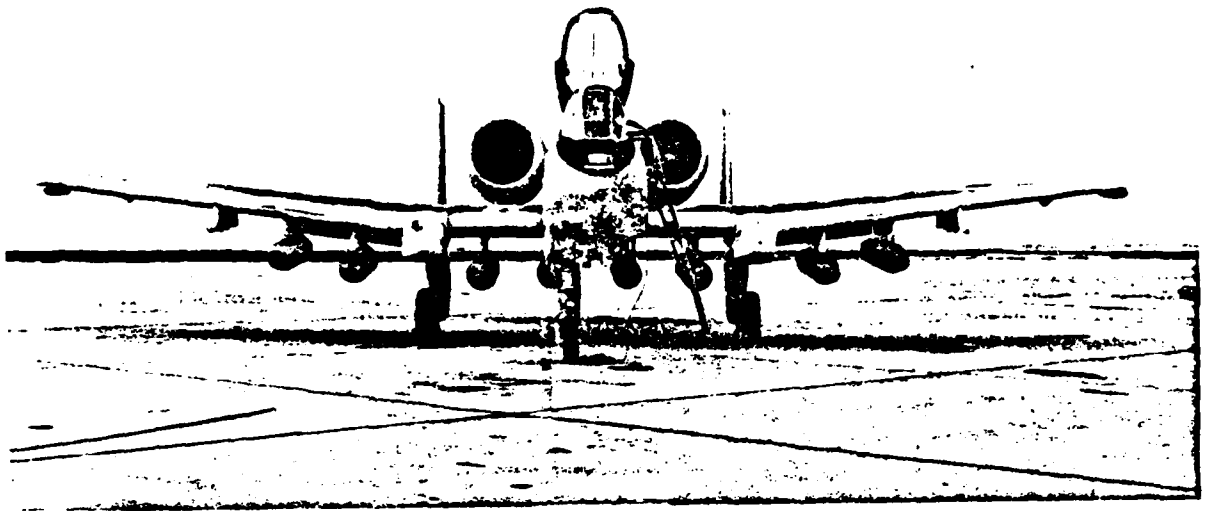
- 1 GENERAL ARRANGEMENT OF A-10A AIRCRAFT
- 2 DUAL PISTON BRU-30 MULTIPLE CARRIAGE RACK

INTRODUCTION

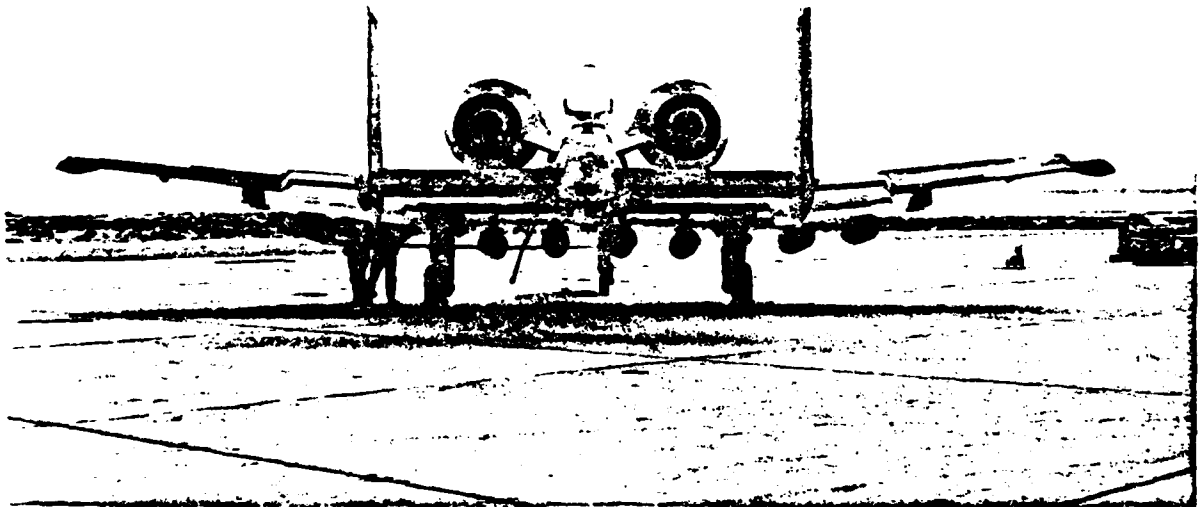
The A-10 stores certification program was uniquely structured to utilize in-house Air Force expertise wherever possible in management, engineering analysis, flight test demonstration, and data reduction. The program was also designed to facilitate the orderly transition from the contractor of all engineering certification efforts once the contracted requirements of the aircraft specifications had been satisfied.

This paper reviews the A-10 stores certification program to include: analysis techniques utilized, test programs conducted, and problems uncovered during the flight test program. The major disciplines which were a part of the A-10 stores certification program are stores separation, loads, flutter, performance, and stability and control. The store separation aspects of the program will be emphasized with a more limited discussion of the other disciplines.

The primary industrial and government organizations involved in the A-10 stores certification program were the following: Fairchild Republic Company (FRC), A-10 System Program Office (SPO), Air Force Armament Laboratory (AFATL), Armament Development and Test Center (ADTC), Air Force Flight Test Center (AFFTC), and Pacific Missile Test Center (PMTC).



FRONT VIEW



TAIL VIEW

FIGURE 1. GENERAL ARRANGEMENT OF A-10A AIRCRAFT
308

A-10 AIRCRAFT DESCRIPTION

The following brief description of the A-10 might be helpful to the reader before discussing the technical aspects of the program.

The A-10 is a single place aircraft designed specifically for the close air-support role by FRC. The aircraft configuration is characterized by a flat bottom fuselage, a straight wing of relatively high aspect ratio and high thickness (all of which serve to enhance aerodynamic performance at low speeds) mounted low on the fuselage, a straight horizontal tail, twin vertical stabilizers mounted on the outboard tips of the horizontal tail, and two high bypass turbo fan engines installed in nacelles mounted on pylons extending from the aft fuselage. Figure 1 shows an overall view of the aircraft.

The aircraft has an internal 30MM gatling gun mounted in the nose of the fuselage. In many respects, the gun system drove the design of the aircraft. This topic is not, however, a subject of concern in this paper.

The aircraft also has eleven non-jettisonable external pylons; three wing mounted pylons outboard of each gear pod, one wing mounted pylon inboard of each gear pod, and three fuselage mounted pylons. Pylons are consecutively numbered from the left outboard (P1) to the right outboard (P11). The designed loading capacity of each pylon station is as follows: 1000 lbs. for P1, P2, P10, and P11, 2500 lbs. for P3 and P9, 3500 lbs. for P4, P5, P7, and P8, and 5000 lbs for P6. P1, P2, P10, and P11 each house a dual-piston MAU-50 bomb ejection rack. The remaining pylons each house a dual-piston MAU-40 bomb ejection rack. The basic difference between the two racks is that the MAU-40 has 14 and 30 inch suspension hooks whereas the MAU-50 only has 14 inch suspension hooks. For the A-10 application, all racks use two ARD-863 ejection cartridges with various orifice combinations selected to enhance store separation characteristics. The reader is referred to reference 1 which contains detailed drawings of aircraft/pylon geometry, locations of suspension lugs, ground clearances, and so forth.

PROGRAM OBJECTIVES

The A-10 stores certification program objectives related to specific performance and functional requirements that the aircraft was required to demonstrate. These performance and functional objectives stemmed from the Development Concept Paper (DCP). The DCP defined what capabilities the A-10 must have to defeat a specific threat. In the DCP, these capabilities were broad in scope but became more specifically defined when the detailed aircraft specifications were subsequently generated and translated into a contractual document between the government and FRC.

The A-10 specifications contained a list of store types, the minimum quantities of each type, and certain specific store loading configurations. The stores list was compiled using inputs from many sources such as the primary using command (Tactical Air Command) and was eventually expanded to approximately 25 store types arrayed in over 200 store loading configurations. This stores list led to the primary objective of the stores certification program; that is, to demonstrate satisfactory compatibility of specific stores in specified loading configurations within the desired flight envelope of the aircraft. Another major objective was to develop an Air Force in-house capability in the store compatibility disciplines (i.e. stability and control) so that all follow-on store certification engineering and testing could be accomplished by the Air Force.

MANAGEMENT PHILOSOPHY

The A-10 SPO was the single-point manager for the A-10 weapon system. As such, the SPO had the responsibility for directing FRC and other government agencies in the accomplishment of tasks that would result in the achievement of program objectives. For the stores certification program, the SPO decided on a joint test concept. Basically, this meant that the program was divided into two phases; a joint FRC/Air Force phase, and a follow-on Air Force phase. The distinction between the two phases was centered on who had prime responsibility for the various areas of testing. During the joint phase, FRC's responsibility was high in all areas in order to allow FRC to demonstrate to the Air Force that performance and design requirements had been met. For example, FRC was contractually required to write test plans, maintain the aircraft, and prepare test reports. The Air Force however, still reviewed all test plans, participated in the flight test engineering decision process, and reviewed all test reports. During the follow-on phase, primary responsibility rested with the Air Force and FRC's responsibility was correspondingly lower.

In order to make the joint test concept successful, the SPO had to orchestrate the efforts of the AFFTC and the AFATL since much of the Air Force engineering expertise resided in these organizations. This was done via a Store Certification Management Plan which defined the duties and responsibilities of all organizations during the two test phases. The plan was developed with inputs from FRC, the AFFTC, and the AFATL.

In soliciting support from the AFFTC, the SPO used Program Introduction Documents (PID's) to define the work load and level of effort the A-10 program would require from AFFTC personnel. As a result of the PID, engineers were assigned to the A-10 Joint Test Force and the AFFTC was funded by the SPO for the test effort. The SPO used less formal documentation in soliciting support from the AFATL. This was because the AFATL had agreed to provide on-site engineering support during the stores compatibility portion of the testing. AFATL engineers acted as technical

advisors and performed much of the engineering data reduction resulting from flight testing. With this arrangement, the SPO was assured that the AFATL was kept in close technical contact with the program and was acquiring the expertise necessary for the follow-on phase.

STORE CERTIFICATION FLIGHT TEST PROGRAM

The joint phase of the program was initiated in August 1974 and extended through March 1976. Testing was conducted with prototype YA-10A and A-10A aircraft and involved the following stores: AGM-65 missile, SUU-20 training dispenser, 600 gallon fuel tank, SUU-23 gun pod, BLU-27 unfinned firebomb, MK-82 LDGP, MK-84 LDGP and MK-82 Snakeye bombs, BDU-33 practice bomb, LAU-68 rocket launcher, GBU-10 and GBU-12 fixed wing laser guided bombs, SUU-25 flare dispenser, and MK-20 cluster bomb. Approximately 120 productive missions were flown during the joint phase. The loading configurations for all missions involved single store types. The results of joint testing are documented in references 2 thru 7. Problems encountered during testing will be discussed in a later section.

The follow-on phase of the program was initiated in April 1976. The bulk of this test phase was completed in January 1977, but continues to date at a low level. Testing was conducted with pre-production A-10A aircraft and involved the following stores: fixed and deployable wing GBU-10 and deployable wing GBU-12 laser guided bombs, LAU-68 rocket launcher, BL-755 dispenser, MK-82 LDGP, MK-84 LDGP and MK-82 Snakeye bombs, BLU-27 finned firebomb, BLU-52 chemical bomb, CBU-58 and MK-20 cluster bombs, and SUU-25 flare dispenser. Approximately 110 productive missions were flown during the follow-on phase. The loading configurations involved both single and mixed store types. The results of follow-on testing are thoroughly documented in reference 8. Problems encountered during testing will also be discussed in a later section. It may be noted that after October 1978, all follow-on testing will be conducted at the ADTC.

CAPTIVE COMPATIBILITY TESTING AND ANALYSIS TECHNIQUES

This section provides a general summary of testing and analyses performed in the disciplines of loads, flutter, stability and control, and performance. The results of analyses in each of these disciplines were used to establish the captive flight envelopes of the aircraft with the various store loadings. References are provided for all disciplines discussed in the event that the reader desires more comprehensive information.

LOADS: FRC designed the A-10 pylons to satisfy Air Force load factor criteria. Criteria were -3.0 to +7.33g for symmetric maneuvers and -1.0

to +5.86g for unsymmetric maneuvers with stores carried singly on parent pylon MAU-40/50 racks. With stores carried on multiple carriage racks, load factor criteria were -2.0 to +5.0g for symmetric maneuvers and -1.0 to +4.0g for unsymmetric maneuvers. FRC provided the Air Force with stress reports for each pylon (reference 9).

Two major test efforts were subsequently conducted to verify the pylon stress analyses and design calculations. The first effort was a static ground test wherein the pylons were subjected to ultimate load limits with forces and moments corresponding to worst case analytical aerodynamic and inertial loadings. The second effort consisted of an in-flight loads survey to verify that analytical forces and moments were accurate enough to validate the design and static testing. The aircraft was allowed to fly to 80% of its design load factor limits prior to this testing with a restriction on roll rate.

The static ground test was accomplished on a complete A-10 aircraft which was identical to the production aircraft except as stated in reference 10. Testing was conducted at the Flight Dynamics Laboratory Static Test Facility located at Wright-Patterson AFB, Ohio. The loading conditions and instrumentation used for these tests are described in references 11 and 12. During testing, the pylons successfully withstood 100% ultimate loads without failure. At one test point, however, the aft hook on a MAU-40 rack deformed and failed at 98% of the ultimate loading. The test condition simulated a +4.0g rolling pullout with a 600 gallon fuel tank mounted on P4. At the present time the A-10 uses F-111 fuel tanks which themselves have a 3.0g acceleration limit so that the failure which occurred during testing did not impact the captive flight envelope. Complete results for the static ground tests are contained in reference 13.

The A-10 flight loads survey was conducted at the AFFTC and was a joint Air Force and contractor flight test. FRC prepared the test plan and instrumented the aircraft in accordance with reference 14. The bomb lugs, swaybrace pad posts, and pylon wing attachment fittings were instrumented. Since no wind tunnel data or flight loads were obtained prior to this testing the 80% flight conditions were surveyed first and quantitatively analysed before proceeding to the 100% limits. The store configurations planned for test and flight conditions can be found in reference 15. The test program started 11 July 1976 and ended 20 October 1976. The final report was not available at the time the paper was written, however, all 100% factors were successfully flown and the 80% load restriction on the A-10 aircraft has been lifted. The precise correlation between predicted and measured loads will be studied by the Air Force to determine how accurate the forces and moments can be predicted.

FLUTTER: FRC was required to design the A-10 to be flutter free to 1.15 times the desired maximum velocity limit of 450 KEAS. Both the Air Force and FRC performed flutter simulations. FRC modeled the A-10 using a NASTRAN simulation while the Air Force used both NASTRAN and the

McDonnell Douglas Corporation FACES simulation. Ultimately, a parametric wind tunnel flutter test, a ground vibration test, and a flight flutter test were conducted.

Due to a tight program schedule, it was necessary to allow the YA-10 prototype aircraft to fly with stores before any of the aforementioned tests could be conducted. Therefore, based on the results of the NASTRAN/FACES simulations, the YA-10 aircraft was allowed to fly at airspeeds up to 300 knots with stores. After wind tunnel testing, where speeds of 730 KEAS were tested with realistic store configurations without achieving flutter, the prototype aircraft were allowed to fly to 420 knots with selected store loading configurations. Reference 16 presents a detailed account of the conduct and results of wind tunnel flutter testing.

Ground vibration testing was conducted at FRC and was a prerequisite for the first flight of the A-10A in January 1975. Testing was satisfactory as described in reference 17. Flight flutter testing was conducted from April through June 1975 at the AFFTC for selected worst case store loading configurations. Testing, which is documented in reference 18, demonstrated a complete absence of flutter throughout the flight envelope of the aircraft.

Although the aircraft is apparently not susceptible to flutter, the Air Force and FRC have not as yet been able to match the frequencies of the wing modes of vibration in the analytical programs to the ground vibration test results. At the present time, the Air Force suspects that possibly the ground vibration test results and the analytical stiffness model for the wing are slightly in error. In an attempt to verify the data base, the Air Force plans on conducting another ground vibration test in early 1978. In the interim, the Air Force and FRC are proceeding cautiously, and carefully evaluating the results of flutter analyses to assure adequate margins of safety exist.

STABILITY AND CONTROL: Static stability and control wind tunnel testing was conducted by FRC early in the program. Data derived from this testing was used to form an analytical stability model for the YA-10 prototype aircraft (data contained in references 19 and 20). Flight testing was subsequently conducted in order to obtain data from which the degree of compliance with applicable specifications could be determined. Based on analysis of wind tunnel data, flight testing was basically conducted with the aircraft in either the ferry configuration (three 600 gallon fuel tanks) or the close air support configuration (18 MK-82 bombs and four TER's).

Flight test results showed the following: (1) The speed stability characteristics of the aircraft were favorable at low speeds with forward center of gravity locations. Also, as the aircraft speed increased towards the limit Mach (0.75), the change in elevator deflection required to trim the aircraft goes to zero. In general, the effects of external stores on the speed stability characteristics of the aircraft were minimal. However, the forward center of gravity location of the aircraft when configured in a

ferry configuration did impact the speed stability characteristics. For this reason, the ferry configuration is limited to a maximum speed of 250 knots. It may be noted that this is the only configuration that has a speed restriction. (2) No appreciable effect due to the stores loading configurations on the maneuver point was detected. (3) The dynamic longitudinal short period disturbances were well damped and in addition, no short period divergence was experienced with any of the store loading configurations tested. (4) The lateral/directional static and dynamic stability characteristics of the aircraft were satisfactory at all speeds although the ferry and close air support configurations did degrade directional stability slightly. (5) The dihedral effect on the aircraft was increased with stores compared to the clean aircraft. (6) The inertial effect of stores on the wings did affect roll performance. However, the aircraft still rolled so fast as to require some roll restriction on a few store configurations because of induced pylon loads. Interestingly, with stores, the roll performance of the aircraft increased with speedbrake deflection. If detailed test results are desired, the reader is referred to references 21 through 29 which presents the results of FRC flight tests while reference 30 presents the results of the Air Force Preliminary Evaluation.

PERFORMANCE: The A-10 performance program was a joint FRC and Air Force effort. The performance flight test work to date with stores has been very limited. However, the SPO has used some very specific MK-82 bomb loading configurations to track actual performance against the aircraft specification requirements. Flight testing to gather sufficient data to validate performance estimates with stores was initiated in July 1977 at the AFFTC. Data from this testing was not available in time to reference in this paper. (See reference 31 for the performance test plan).

CAPTIVE COMPATIBILITY TESTING: Once the flight testing and/or analyses described in the preceding paragraphs had been completed, a flight clearance was authorized by the SPO for the specific configurations to be flown during the stores certification program. Frequently, a flight clearance was issued for a specific configuration by analogy to another configuration which had been extensively tested before. Accordingly, it was necessary to qualitatively evaluate the aircraft handling qualities, performance, and general aircraft/stores compatibility during flight testing prior to initiating separation tests. To make this qualitative assessment, captive compatibility tests were performed for most single store loading configurations using the recommended flight profile contained in reference 32. Due to fuel limitations, two sorties were generally required. The first sortie was devoted to qualitatively assessing aircraft handling qualities and verifying the structural integrity of the aircraft/stores installation by performing, with appropriate build-up, dives to the maximum allowable airspeed and pull-outs to the maximum acceleration limits. During the second sortie, vibration of the aircraft/stores installation and aircraft endurance in low altitude flight at the maximum obtainable airspeed were investigated. Following each sortie, the aircraft was inspected to verify that no discrepancies existed with the stores, suspension racks, pylons and

surrounding aircraft structure, arming wires, and fuzes. It should be noted that stores were not downloaded or adjusted between sorties so that the cumulative effect of both sorties could be ascertained.

SEPARATION TESTING AND ANALYSIS TECHNIQUES

SELECTION OF STORE SEPARATION PREDICTION TECHNIQUE: The captive trajectory technique has been the one most commonly used by Air Force engineers to obtain predicted store separation trajectories. For example, this technique was used during earlier store certification programs involving such aircraft as the F-105, F-111, F-4, A-7, and F-15. Quite naturally then, an estimate was made of the number of wind tunnel occupancy hours which would be required to investigate store separation trajectories for A-10 store loading configurations using this technique. The estimated number of hours proved to be quite high and would have required a significant level of funding. In view of the fiscal constraints of the A-10 program, it was evident that, if feasible, another approach should be adopted. For this reason, in lieu of using the captive trajectory technique, we considered using the grid technique, the drop model technique, theoretical techniques, and a new hybrid method termed the flow angularity technique. We objectively evaluated each of these techniques using primary criteria of accuracy, cost, ease of use, responsiveness, and fault analysis capability. By fault analysis, we are referring to the ability to trace the cause of unexpected or unusual store separation trajectories which occur during actual flight testing.

CAPTIVE TRAJECTORY TECHNIQUE: We should like to point out that had the A-10 store list been composed of fewer store types and loading configurations so as to not require an abnormally large quantity of wind tunnel occupancy hours (and hence cost), the captive trajectory technique would undoubtedly have been used for the A-10 program. We have a preference for this technique because it is so straight forward to use. Specifically, it takes skill and ingenuity to devise the test plan and assemble required input data. But, once these tasks have been completed, our engineers can look forward to obtaining complete six-degree-of-freedom trajectory data without the need of performing any further reduction or other mathematical calculations. However, since each trajectory is calculated for a specific set of flight conditions and input parameters, it is complete by itself. Thus, fault tracing is not possible and where needed, additional wind tunnel testing must be performed.

GRID TECHNIQUE: Relative to the captive trajectory technique, the grid technique was judged to have comparable accuracy, but have the advantage of a fault analysis capability. Unfortunately, grid data would have to be obtained for each type of store loaded on parent pylon and multiple carriage racks with and without the presence of adjacent mounted stores. We estimated that the number of wind tunnel occupancy

hours for this effort would be comparable to captive trajectory testing. Since no net reduction in cost would result by using the grid technique, we rejected its use. The fact that the grid technique is not as responsive as the captive trajectory technique, nor as easy to use, were not considered to be deciding factors. The grid technique is clearly not as responsive as the captive trajectory technique because subsequent to wind tunnel testing, store grid data must be combined with store free stream data in order to obtain interference force and moment coefficients. These coefficients must then be input, along with other pertinent parameters, to a six-degree-of-freedom computer program to calculate store trajectories.

DROP MODEL TECHNIQUE: This technique has several well documented advantages (and disadvantages) compared to the captive trajectory technique. For example, with the drop model technique, extended (rather than abbreviated) trajectories can be obtained using the captive trajectory technique. However, most of the stores designated for carriage on the A-10 are of the stable variety so that this was not an important consideration. With the drop model technique stores may be released in the ripple mode. This is a big plus for an aircraft such as the A-10 which is designed to release large numbers of stores. On the negative side, though, drop model testing can be considerably slower than captive trajectory testing and, therefore, proportionally more costly. The cost of fabricating the drop models themselves can be substantial. Another disadvantage of the drop model technique is that data are only valid for stores released in 1 "g" straight and level flight. This is a particularly severe limitation with regard to the A-10 program since most stores are intended to be released in steep dives up to 60° with corresponding normal accelerations as low as 0.5 "g". Lastly, drop model testing, like captive trajectory testing, produces a complete store trajectory for the specific conditions tested. As a result, fault analysis is not possible.

THEORETICAL TECHNIQUES: Considerable progress has been made in recent years in developing theoretical store prediction techniques. However, while displaying good potential, those with which we are familiar have been infrequently used to date. Consequently, a data base to substantiate the accuracy of a particular technique, when used for specific stores released from a variety of carriage racks and parent aircraft, is not available to our knowledge. Accordingly, confidence as to the accuracy of predicted store separation trajectories calculated by theoretical techniques is, in our opinion, lower than for any of the other techniques discussed. Further, most theoretical techniques are complex, time consuming, and require a certain art in their use. For these reasons, theoretical techniques were rejected for the A-10 program even though their cost is by far the lowest of any technique available.

FLOW ANGULARITY TECHNIQUE: None of the aforementioned techniques adequately met the criteria we considered to be of prime importance for the A-10 program. This is not to say that for another program one of the other techniques might not be the best. We cannot overemphasize this

point. We eventually decided to use the flow angularity technique since this technique appeared to satisfy most of the established criteria at the minimum cost.

The flow angularity technique was developed by Air Force engineers in the early 1970's. It is hybrid by nature in that it utilizes empirically derived data in combination with an analytically derived six-degree-of-freedom computer program. The technique is predicated on the thesis that the predominant factors which affect a store's separation behavior are the forces and moments acting on the store caused by the interference flow field at the nose and tail of the store. To obtain these forces, a novel approach is used. In the wind tunnel, the airplane model is loaded with several stores in desired loading configurations. However, instead of measuring captive store loads with an internally mounted balance, a pressure probe is used to survey the area forward, aft, below, and to the sides of the stores. The output from this test is a set of data which defines the changes in angles of attack and sideslip of the flow caused by the immersion of the stores into the flow field. Another thesis of the technique is that the forces and moments acting on the store in the captive position can be represented by a single force on the nose-body, and a single force on the tail of the store. These forces are obtained by statistically resolving the measured flow angularities into average flow angularities acting over the nose-body of the store and average flow angularities acting over the tail of the store. These flow angularities are then combined, again mathematically, with component free-stream aerodynamic data to obtain store interference coefficients. Store free-stream data are measured during flow angularity testing if not already available. If store free-stream data are available, but not in component form (that is, for the nose-body and the tail), theoretical methods are used to obtain component data. This feature is included in the computer program. Subsequently, store interference coefficients and all other pertinent parameters such as aircraft flight conditions and ejection forces are mathematically input into a six-degree-of-freedom computer program which calculates the store trajectory.

As in the case of the grid technique, the flow angularity technique is readily amenable to fault analysis since input parameters can easily be changed mathematically and a new trajectory obtained by simply making another computer run. However, quite apart from the grid technique, the data from which is only valid for the particular store being tested, a thesis of the flow angularity technique is that the flow angularities resulting from the presence of one type of store in the flow field will not be appreciably altered by the presence of a different type of store so long as their geometric shapes are comparable (i.e. overall length and body diameter). Compared to the grid technique, this thesis immeasurably enhances the versatility of the flow angularity technique. Specifically, by merely combining the free stream aerodynamic data for the store to be investigated with the flow angularities which had been previously measured for comparable stores, predicted store separation trajectories can be obtained by performing low cost computer runs instead of by conducting additional expensive wind tunnel testing. For an in-depth discussion of the flow angularity technique the reader is referred to references 33 and 34.

BRUTE FORCE TECHNIQUE: The brute force technique, for lack of a better term, begins by qualitatively analyzing the actual separation characteristics of the store in question when released from another aircraft. From this analysis, an initial release condition, which will hopefully produce store separation characteristics of a benign nature, is established for first release of the store from the new aircraft to be tested. Film from onboard cameras are reviewed after the store has been released at this first test condition. Depending upon the degree to which actual separation characteristics match expectations, the store is released at progressively expanded flight conditions with films reviewed between missions until the desired employment envelope has been fully explored, or until adverse separation characteristics preclude further expansion. Obviously, the success in using this technique depends on many factors, not the least of which is the level of experience and judgment displayed by cognizant engineering personnel.

The brute force technique was used judiciously during the A-10 program for two reasons. First, the subsonic operating speed of the aircraft was deemed to limit the potential for store-to-store collisions to that of a minor nature. In other words, for the majority of stores, dynamic pressures were not considered to be sufficient to allow them to fly back into the aircraft. Secondly, the prediction of store separation characteristics, under some circumstances, is either too time consuming, too costly, or the results are of dubious accuracy. For example, the very small size of a BDU-33 practice bomb does not readily lend itself to the various prediction techniques. However, this store has been satisfactorily released from practically all existing fighter aircraft at speeds far in excess of the A-10's envelope. Therefore, the risk associated with releasing this store without first conducting empirical or analytical predictions was quite low. Another case of where the brute force technique was effectively used was when stores were released in the ripple mode at low intervals from multiple carriage racks. Other than by conducting drop model testing, the effects of the flow field on stores released in close proximity to one another cannot be easily predicted. Accordingly, stores were initially released in the single mode, the separation characteristics of which having been predicted using the flow angularity technique. Then, following review of onboard film, stores were released in brute force fashion in the ripple mode at progressively lower intervals. It should be noted that during the A-10 program, the brute force technique was never used unless the store had been satisfactorily released from another aircraft with documented test results available or, for aerodynamically unstable stores.

SELECTION OF FLIGHT TEST DATA REDUCTION TECHNIQUE: During the course of flight testing, film from onboard cameras was always reviewed between missions in order to qualitatively assess store separation characteristics. Oftentimes, this qualitative assessment was adequate. However, for any number of reasons, such as when a store displayed sensitivity to variations in release conditions during envelope expansion, it became necessary to compare quantitative store trajectory data with predictions. In this manner, trends could be analyzed and subsequent missions could be modified

as necessary. However, in making such comparisons, the technique used to translate films into digital six-degree-of-freedom trajectory data had to be capable of good accuracy lest erroneous conclusions be reached.

Since the late 60's, the only film reduction technique used by the Air Force at the ADTC has been a photogrammetry technique. Had the A-10 flight test program been conducted at the ADTC, this technique would undoubtedly have been used again. However, since the A-10 program was conducted at the AFFTC the opportunity was taken to use a relatively new film reduction technique available at the Pacific Missile Test Center, Point Mugu, CA, 90 miles from the AFFTC. The technique was originally developed by engineers at the Naval Weapons Center, China Lake, CA. The technique functions in the following manner. One at a time, frames of film are projected through an optical system and a high resolution video camera to a television monitor located on the operator's console. A scale model of the store, having been fabricated previously, is mounted on a nearby six-degree-of-freedom positioning mechanism. A high resolution television camera views this scale model, and with the help of a video mixer, displays its image on the same television monitor as the image from the film. The operator then remotely adjusts the linear position and angular orientation of the scale model until the image of both stores are exactly superimposed. At this point, the operator punches a button which causes the linear position and angular orientation of the scale store model, along with the frame count, to be automatically punched onto an IBM card. Once this process has been performed for all selected frames, usually every fifth frame when the camera operates at a speed of 200 frames/second, the IBM cards are input to a computer program which solves the spatial relationships. The technique produces very accurate trajectory data (± 0.1 inch for linear motions and ± 1.0 degree for angular motions). Those readers desiring a complete technical discussion of this technique are referred to reference 35.

Based on the experience we gained during the A-10 program, the photo-data-analysis technique was proven to be far more versatile and accurate than the photogrammetry technique. For example, unlike the photogrammetry technique, neither the stores nor the pylon/aircraft require the application of a paint scheme (such as a system of dots) and store trajectories can still be calculated even if the store is not visible in the captive carriage position. Not surprisingly, the ADTC is now procuring the equipment necessary to establish its own photo-data-analysis capability in the near future.

USE OF FLOW ANGULARITY AND PHOTO-DATA-ANALYSIS TECHNIQUE: As has been discussed, predicted separation trajectories were calculated for desired stores using the flow angularity technique. Analysis of these data were used to formulate flight test plans. Between each mission, film from onboard cameras were reviewed. When deemed necessary, films were processed using the photo-data-analysis technique and quantitative store trajectories obtained. Actual store trajectories were then compared with predictions. If actual results did not adequately match predictions, a fault analysis was performed. Computer runs were then made in which

pertinent input parameters were varied until the calculated trajectory matched flight test results. Once a match was achieved, the changes required to produce the match were used to conduct additional simulations for stores to be released during the next mission. This "anchoring" of predictions to actual test results from preceding missions insured that predicted store separation characteristics would always be close to actual test results. The truth of this statement is evident by the fact that during the entire A-10 program, there was only one incident in which we incurred a collision of a store with one of the aircraft pylons (which caused minor pylon damage). And, even this one incident, which will be discussed in a later section of this paper, was due to the fact that the wings on a GBU-10C/B store failed to deploy as planned.

RESULTS OF STORE CERTIFICATION FLIGHT TESTING

The purpose of this section is to highlight problems uncovered during the flight test program with specific stores. The reader is referred to the references for an in-depth discussion of each problem area.

AGM-65 MISSILE: Minor paint abrasion, due to the exhaust plume of the missile, was experienced during separation from the inboard launcher position on pylon stations three and nine. The missiles themselves separated satisfactorily throughout the flight envelope without any adverse effect on engine performance. It was determined that periodic painting would be sufficient to arrest abrasion of affected surfaces (horizontal and vertical tail).

COLLISIONS OF MK-82 LDGP STORES RELEASED FROM TANDEM MER STATIONS IN RIPPLE MODE: Flight testing was conducted with multiple carriage racks (MER-10) mounted on pylon stations five and seven. Each rack was fully loaded with MK-82 LDGP stores. Films from onboard cameras showed that stores separated satisfactorily from each rack station when released in the single mode at all test conditions. However, in the ripple mode, using an interval of 50 milliseconds, collisions were incurred between the tail of stores released from the forward rack stations and the nose of stores released from the aft rack stations. The cause of the collisions stemmed from incremental differences in drag and normal acceleration between stores. Stores released from forward rack stations separated with moderate nose-down pitching motions which generated an incremental increase in drag and normal acceleration away from the aircraft. Stores released from aft rack stations separated with neutral to slight nose-up pitching motions which had a minimal effect on store drag, but generated a small incremental decrease in normal acceleration from the aircraft. The net effect of these two factors was to allow stores released from the forward rack stations to "catch up" and collide with stores released from the aft rack stations.

It was determined that store-to-store collisions could be precluded at reduced airspeeds or with increased minimum intervals. However, these

modifications were unacceptable from an operational standpoint. It was also determined that the racks could not be shifted to an area of more favorable flow. That is, to an area in which the flow angularities between stores carried on forward and aft rack stations are better distributed, without incurring a substantial increase in program costs due to engineering analysis which would have to be performed in areas such as structures, flutter and aircraft handling qualities, possible modifications to the airframe itself, and additional flight tests.

Quite by coincidence, at the same time that the aforementioned separation problem was occurring, we were advised that a modification of the standard multiple bomb rack had just been developed by the AFATL and tested on an F-4 aircraft. Basically, the modified rack consisted of a standard MER-10 beam but with each ejector unit modified to incorporate dual pistons instead of the single piston on standard ejector units. This modification did not involve a redesign of the standard ejector unit. A new ejector piston housing was merely bolted onto each end of the ejector unit by using existing bolt holes and appropriate gas tubes were added (see Figure 2). The modified rack is discussed in detail in reference 36. The primary reason for developing the dual piston ejector unit was to obtain a means for imparting ejection moments, in the desired direction, to the store in order to counteract aerodynamic moments.

The modified MER (called the BRU-30) was substituted for the standard MER and flight testing was continued. It was determined that by properly ratioing the forces between the forward and aft pistons, sufficient moment control was obtained such that MK-82 LDGP stores could be released in the ripple mode at maximum desired airspeeds and dive angles and minimum intervals without incurring collisions between stores released from tandem rack stations.

PITCHDOWN OF STORES RELEASED AT AIRSPEEDS ABOVE 350 KNOTS:

BLU-27 Unfinned Firebomb: The release of this store from parent pylon racks showed that the magnitude of pitching motions were quite sensitive to variations in airspeeds above 350 knots. In general, stores separated with divergent nose-down pitching motions at all airspeeds. At airspeeds between 150 and 350 knots, the magnitude of store pitching motions increased only slightly. However, in excess of 350 knots, the magnitude of store pitching motions increased substantially to the point that at the maximum desired release speed of 420 knots, the tail of one store grazed the bottom aft end of the pylon. As a result, the maximum release speed had to be limited to 350 knots to insure safe separation.

CBU-58 Bomb: The magnitude of pitching motions of stores released from the centerline station of triple ejector racks (TER) increased in the same manner as for BLU-27 firebombs at airspeeds above 350 knots. For example, the maximum amplitude of store pitching motions averaged 18° at 300 knots, 26° at 350 knots, 36° at 378 knots, and one store separated with a maximum amplitude of 60° at 426 knots. Above 375 knots, the fins of stores translated vertically above their initial captive

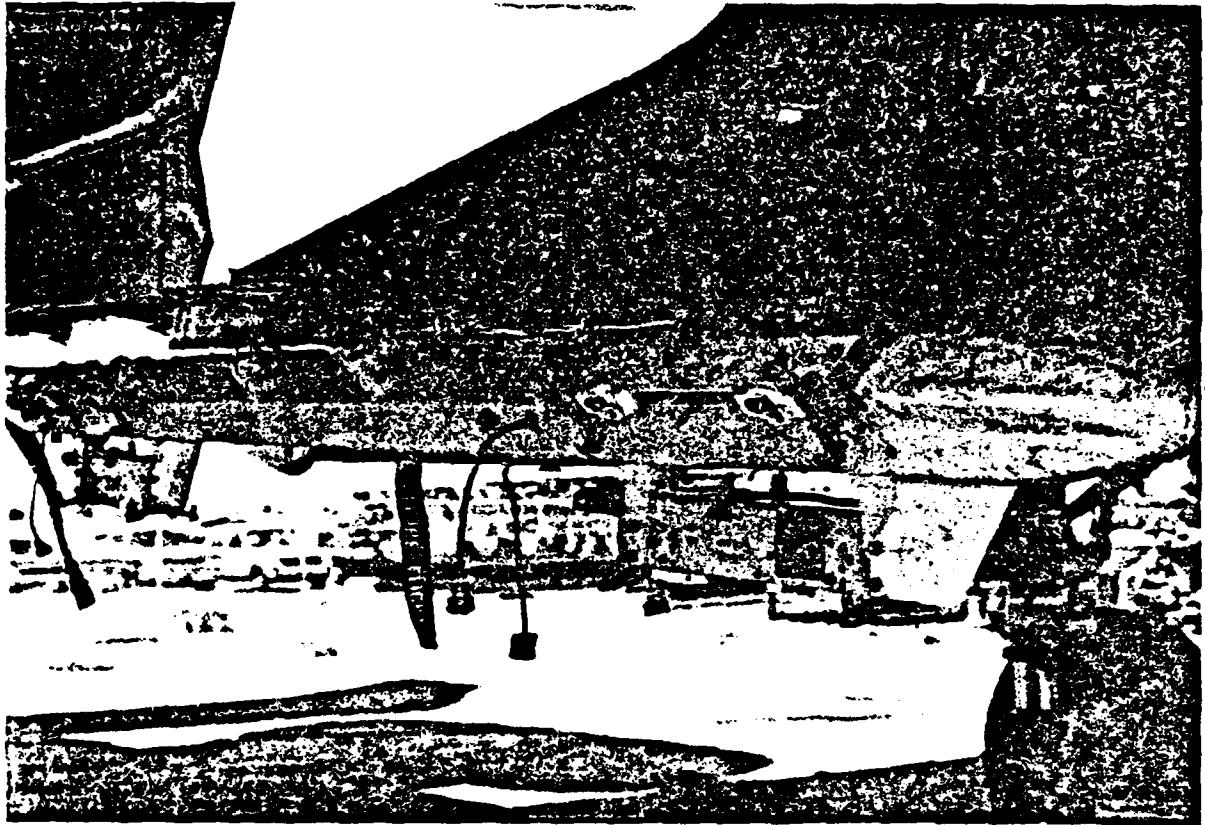


FIGURE 2. DUAL PISTON BRU-30 MULTIPLE CARRIAGE RACK

carriage position and physically contacted the bodies of the captive stores on the TER shoulder stations. However, other than minor scratches, no damage resulted from the contact. Accordingly, this minor interference was considered to be an acceptable tradeoff for the ability to release stores at higher airspeeds.

The pitchdown problem described for the BLU-27 and JSU-58 stores has been attributed to aerodynamic effects stemming from the relatively thick wing of the A-10. This same phenomena incidentally, has been observed (at the same speeds) on the B-57 and A-1E aircraft which also have a thick wing with a relatively blunt leading edge. On aircraft such as the A-7 and F-4 which have fairly thin wings, pitchdown problems do not generally occur until airspeeds on the order of 500 to 550 knots are achieved.

STORE-TO-STORE CLEARANCE IN RIPPLE RELEASE MODE: The relatively close spacing of the ten aircraft pylons precludes the release of stores from more than one pylon in the ripple single or pair modes in an arbitrary manner. We recognized early in the program that some sequence had to be devised if stores were to be safely released from multiple pylon stations without incurring store-to-store collisions below the aircraft. It was determined that the following sequence minimized the probability of store-to-store interference: P8, P4, P11, P1, P10, P2, P9, P3, P7, P6, and P5. If stores are released in the ripple single mode, the preceding sequence applies. In the ripple pair mode the following sequence occurs: P8 and P4, P11 and P1, P10 and P2, P9 and P3, and P6 (or P7 followed by P5). Stores may not be simultaneously carried on P5, P6, and P7. Stores are either carried on P5 and P7 or on P6 only due to close pylon spacing.

Using the aforementioned sequence all required stores, except the MK-82 Snakeye in the high drag mode, were satisfactorily released in the ripple single/pair mode at minimum desired intervals. Because of the span of the open MK-82 Snakeye fins, it was necessary to impose a restriction on the minimum interval in the ripple pair mode.

COLLISION OF MK-20 FINS WITH ADJACENT MOUNTED CAPTIVE STORES DURING SEPARATION: Surprisingly, in spite of the relatively close pylon spacing, only a few store configurations had to be modified so as to preclude physical interference of stores when released in the presence of stores loaded on adjacent pylons. For example, flight testing was conducted with BRU-30 racks mounted on P5 and P7. Each rack was fully loaded with MK-20 cluster bombs. The MK-20 has fins which open almost immediately after release. During testing, numerous instances occurred wherein the open fin of MK-20 stores released from the inboard shoulder station of the BRU on P7 contacted the facing closed fins of the captive MK-20 stores mounted on the inboard shoulder and centerline stations of the BRU on P7. As a result of contact, the fins frequently failed which destroyed the ballistic accuracy of the weapon. Since these collisions occurred at many airspeeds, the solution adopted was to offload stores mounted on the inboard should stations of the BRU on P7.

BLU-52 FIN VIBRATIONS: During captive compatibility flight testing, it was noted that the fins on BLU-52 stores vibrated unsatisfactorily

when carried on TER's at even moderate airspeeds. As a result, it was necessary to delete TER carriage of these stores. The fins on the BLU-52 are identical to the fins on BLU-27. These fins have a history of vibrating, bending, and cracking. Unfortunately, it is most difficult to effect a design change to such a store component after it has been in production for years. Therefore, the only recourse is to use the existing fins and identify discrepancies during compatibility testing and impose restrictions as appropriate. This was done, but the time and cost in performing pre-flight analyses cannot be recovered.

SLOW OPENING OF GBU-10C/B WINGS: The GBU-10C/B store employs wings which are designed to open very quickly after release from the aircraft. Wing opening must in fact occur quickly as the store is statically unstable. To insure that the wings open, the wing release lanyard is hardwired to the rack. Several stores separated satisfactorily and their trajectories matched predictions. However, the wings on one store were slow in opening when released at 420 knots in a 60° dive. This allowed the store to separate with a divergent nose-down pitching motion of over 150°. During the separation from the aircraft one of the closed wings contacted the aft end of the pylon causing minor damage. We conducted post-flight aerodynamic simulations, with the wings closed, and were able to match the actual store trajectory.

This incident highlights the fact that with the ever increasing numbers of guided type stores which have moveable aerodynamic surfaces, deployable wings, and/or autopilot, proper consideration must be given in the event of a store failure. As can be imagined, any incident wherein damage to the aircraft is incurred, no matter how minor, generates probing questions from management. In such instances, the ability to rapidly respond with a fault analysis is essential. The failure analysis for the GBU-10C/B was performed in a matter of days using the flow angularity technique. We do not wish to "push" the flow angularity technique. Rather, we merely want to reiterate that in considering a technique for predicting store trajectories, responsiveness in terms of being able to perform a fault analysis should be emphasized.

CONCLUSIONS

The A-10 stores compatibility program was conducted on schedule and on cost. Clear program objectives and an effective management philosophy were major contributors to the program's success. Many things were learned during the program, some of the more important of which are enumerated below.

- The joint test concept was proven to be a very satisfactory method for structuring the program. Air Force directives stress the desirability of eventual in-house management of stores compatibility programs. By utilizing the joint test

concept, the Air Force is assured of early acquisition of the expertise and data with which to conduct follow-on store compatibility efforts.

- . The aircraft was designed in accordance with pertinent stores compatibility specifications for specific stores loadings within a predefined flight envelope. Accordingly, there are few aircraft restrictions with stores loading configurations.
- . Stores loading configurations are not restricted due to flutter. The known flutter limits are far in excess of the airspeed capability of the aircraft.
- . Stores loading configurations have a minimal effect on aircraft stability and control characteristics. Stores loadings do, of course, have a degrading effect on aircraft performance, particularly heavy loadings.
- . The flow angularity technique proved most effective in accurately predicting store trajectories. The ability to perform fault analyses was a crucial ingredient in the successful use of this technique.
- . Film reduction via the photo-data-analysis technique was rapid, accurate, and cost effective. The computer-graphics capability of the PMTC allowed reduced film data to be plotted in any manner desired and resulted in a net savings of many man-hours.
- . Flight testing demonstrated that there were no measurable effects on the separation trajectory of a store due to the presence of adjacent mounted stores. This significant finding means that any new stores loading configuration can be devised as long as the separation characteristics of each store type has already been determined and trajectory plots in the Y - Z plane show that the store will clear the adjacent stores loading.
- . The thick wing of the aircraft contributed to a marked sensitivity in store pitching motions at airspeeds above 350 knots.
- . Use of a dual piston multiple ejection rack provides sufficient moment control to enable stores to be released from tandem rack stations at maximum desired airspeeds and minimum desired intervals without incurring nose-to-tail collisions between stores.
- . A specially devised pylon sequencing system enables most stores to be released in the ripple mode without incurring store-to-store collisions below the aircraft in spite of the relatively close spacing of the pylons.

- . The tail of a GBU-10C/B store hit and caused minor damage to the bottom aft end of a pylon due to the slow opening of the store wings. The incident highlighted the fact that a failure analysis should be performed for all controllable type stores to determine the ramifications of improper functioning on store separation characteristics.
- . Launching of AGM-65 missiles from certain stations resulted in minor paint abrasion on the horizontal and vertical tails. This abrasion was easily controlled, however, by periodic application of protective coatings.
- . TER carriage of BLU-52 stores was deleted due to unsatisfactory fin vibrations. Since vibrations have also been experienced on other aircraft, the problem was primarily one of faulty fin design.

RECOMMENDATIONS

We learned a few lessons during the A-10 program which we would like to pass on for the benefit of managers and engineers who may be involved in future store certification programs.

First, sufficient consideration must be given to stores compatibility in preliminary design consistent with intended mission requirements. This simply means that if the aircraft is to be designed for the air-to-ground role, stores compatibility should be a driving design factor. If the aircraft is to fill an air superiority role it is possible that only a few store types are intended for carriage. But even in this event, stores compatibility must be considered early in the program to insure that the airframe will not be restricted from a flutter, loads, stability and control, or other standpoint.

We recommend that the general criteria pertaining to stores compatibility as outlined in reference 32 be closely adhered to. This document outlines design and test criteria for insuring satisfactory aircraft/stores compatibility. Included in the document are many pitfalls to be avoided such as close pylon spacing and high wings in combination with low horizontal tails. Conceivably had this document been in existence, and its precepts been followed, the basic design arrangement of the airframe would have been altered. For example, it serves little purpose to have a large number of closely spaced pylons if these pylons cannot be fully loaded without incurring undue restrictions.

Second, proper emphasis must be given to stores compatibility testing early in the flight test program. In the case of the A-10, the emphasis during early testing was on the 30MM gun. Even during the competition phase, testing was limited to demonstrating single carriage/release of

stores at benign speeds. This led to problems such as described in the paper not being discovered soon enough to effect design changes to the airframe or stores installation.

And third, mission requirements must be continuously inputted by the user during design/test phases so as to minimize costly changes later. A good case in point is where considerable funds were expended to certify the BLU-27 store on the A-10 only to learn upon completion of the program that it was no longer desired. Agencies which levy requirements must keep in close touch with all phases of design and testing so as to be in a knowledgeable position to advise system managers accordingly. Requirements change, but every effort should be made to minimize the costs of these changes.

REFERENCES

1. Aircraft Stores Interface Manual, JTCG/ALNNO WP-12-1, Revised 8 August 1977.
2. YA-10 Airplane, External Stores Compatibility Program, Part 1, AGM-65A Missile Flight Tests, Fairchild Republic Company Report No. FT13ORFB01, 11 July 1975.
3. YA-10 Airplane, External Stores Compatibility Program, Part 2, Priority Stores Flight Tests, Fairchild Republic Company Report No. FT13ORFB01, 15 July 1975.
4. A-10A Airplane, A-10A Stores Compatibility Flight Tests, Ripple Release of MK-82 LDGP Bombs from the MER, DEMER and TER, Fairchild Republic Company Report No. FT16ORFB10, 24 October 1975.
5. A-10A DT&E Airplane, External Stores Compatibility Flight Test Program, Part 3, GBU-10A/B and GBU-12A/B Laser Guided Bombs, Fairchild Republic Company Report No. FT16ORFB10, 25 February 1977.
6. A-10A DT&E Airplane, External Stores Compatibility Flight Test Program, Part 2, GBU-8/B Electro-Optical Guided Bomb Separation Characteristics, Fairchild Republic Company Report No. FT16ORFB10, 1 March 1977.
7. A-10A DT&E Airplane, External Stores Compatibility Flight Test Program, Part 4, Separation Characteristics of Miscellaneous Stores, Fairchild Republic Company Report No. FT16ORFB10, 1 March 1977.
8. AFDT&E A-10A Store Certification Tests, AFFTC-TR-77-2, February 1977.
9. Pylon Stress Analysis Reports: SA16OR8101, SA16OR8102, SA16OR8103, SA16OR8104, SA16OR8105, SA16OR8106, Fairchild Republic Company, Farmingdale, L.I. New York.
10. A-10 Full Scale Static Aircraft Test Plan, GT160W0047, Rev B; Fairchild Republic Company, Farmingdale, L.I. New York.
11. A-10 Full Scale Static Aircraft Test Plan, GT160W0047, Addendum 13 (pylon component tests, pylon stations 0, 23, 66, 144, 187, & 230), Fairchild Republic Company, Farmingdale, L.I. New York.
12. Strain Gage Installation - Static Airframe 160K995247, Fairchild Republic Company, L.I. New York.
13. A-10 Full Scale Static Test Data Report - Pylon Component Tests (pylon stations 0, 23, 144, 187, & 230), GT160W0061, Fairchild Republic Company, Farmingdale, L.I. New York.

14. Store Loads Instrumentation and Calibration, FT160SFS01, Addendum 1, Rev A, Amendment 1; Fairchild Republic Company, Farmingdale, L.I. New York.
15. External Store Loads Flight Program, FT160SFS02, Addendum 1, Rev A, A, Amendment 3, Fairchild Republic Company, Farmingdale, L.I. New York.
16. Wind Tunnel Flutter Model Test (A-10A), SF160N0001, Fairchild Republic Company, 26 August 1975, Farming Dale, L.I. New York.
17. A-10A Ground Vibration Test, SF160N0002, 5 December 1975, Fairchild Republic Company, Farmingdale, L.I. New York.
18. Flutter Flight Test (A-10A), SF160N0003, Fairchild Republic Company, 11 July 1975, Farmingdale, L.I. New York.
19. Longitudinal A-10 Data Model Flaps Retracted, Aero Memo 160D-02-013, Rev A, Fairchild Republic Company, 4 March 1975, Farmingdale, L.I. New York.
20. Longitudinal A-10 Data Flaps Extended, Aero Memo 160D-02-020, Fairchild Republic Company, Farmingdale, L.I. New York.
21. DT&E A-10A Aircraft Flying Qualities Introduction and Control System Characteristics Ground Calibrations, FT160RFC03, Part 1, Fairchild Republic Company, 28 February 1977, Farmingdale, L.I. New York.
22. DT&E A-10A Aircraft Flying Qualities Static Longitudinal (Speed) Stability Normal Flight Control System, FT160RFC03 Part 2, Fairchild Republic Company, 13 December 1976, Farmingdale, L.I. New York.
23. DT&E A-10A Aircraft Flying Qualities Maneuvering Longitudinal Stability Normal Flight Control System, FT160RFC03 Part 3, Fairchild Republic Company, 6 December 1976, Farmingdale, L.I. New York.
24. DT&E A-10A Aircraft Flying Qualities Dynamic Longitudinal Stability Control System, FT160RFC03 Part 4, Fairchild Republic Company, Farmingdale, L.I. New York.
25. DT&E Aircraft Flying Qualities Longitudinal Pilot - Enduced - Oscillations Investigation Normal Flight Control System (SAS - OFF), FT160RFC03 Part 5, Fairchild Republic Company, 14 March 1977, Farmingdale, L.I. New York.
26. DT&E A-10A Aircraft Flying Qualities Static and Dynamic Lateral/ Directional Stability - Normal Flight Control System, FT160RFC03 Part 6, Fairchild Republic Company, 4 May 1977, Farmingdale, L.I. New York.
27. DT&E A-10A Aircraft Flying Qualities Volume 1 - Roll Performance Normal Flight Control System, FT160RFC03 Part 7, 8 June 1977, Farmingdale, L.I. New York.

28. DT&E A-10A Aircraft Flying Qualities Trim Changes and Survey Normal Flight Control System, FT16ORFC03 Part 8, Fairchild Republic Company, 3 June 1977, Farmingdale, L.I. New York.
29. A-10A Longitudinal Control Characteristics During Takeoff and Landing, FT16ORFC03 Part 9, February 1977. Farmingdale. L.I. New York.
30. Preliminary Evaluation of A-10A Handling Qualities, AFFTC-TR-76-1, Air Force Flight Test Center, January 1976, Edwards AFB, CA.
31. Air Force A-10A Performance DT&E Test Plan, August 1976, AFFTC, Edwards AFB, CA.
32. Military Standardization Handbook, Guide to Aircraft/Stores Compatibility, MIL-HDBK-244, 1 August 1975.
33. Validation and Expansion of the Flow Angularity Technique for Predicting Store Separation Trajectories, AFATL-TR-72-184, September 1972.
34. Use of the Flow Angularity Technique for Predicting Store Separation Trajectories, Volume 2 of Aircraft/Stores Compatibility Symposium Proceedings, held at Dayton, OH, 7-9 December 1971.
35. Naval Missile Center Photo Data Analysis of Store Separation Films, Volume 2 of Aircraft/Stores Compatibility Symposium Proceedings held at Sacramento, CA, 18-20 September 1973.
36. Performance Demonstration of Modified MAU-46 Bomb Ejector Rack Configured with Dual Ejector Pistons, ADTC-TR-76-21, May 1976.

AUTOBIOGRAPHY

(Robert J. Arnold)

Mr Arnold received a B.S. Degree in Aerospace Engineering from the University of Florida in 1962 at which time he joined the LTV Aerospace Corporation. From 1962-1969, he held aerodynamic assignments in numerous project areas associated with airframe structural design, weapon system integration, and wind tunnel testing. From 1969-1974, he was assigned as a technical advisor to Eglin Air Force Base, Florida, on the A-7D Seek Eagle Weapons Certification Program. In April 1974, Mr Arnold joined the Air Force Armament Laboratory at Eglin Air Force Base as a Compatibility Project Engineer. In July 1974, he was temporarily detached to Edwards Air Force Base, CA, where he was assigned the supervisory responsibility for the F-15 and A-10 store certification programs. Mr Arnold returned to the Armament Laboratory in March 1977 where he continues to serve as the compatibility project engineer for the F-15 and A-10 programs. Mr Arnold has authored and co-authored several papers for previous aircraft/stores compatibility symposiums.

AUTOBIOGRAPHY

(Stephen C. Korn)

Captain Stephen C. Korn received Bachelor and Master of Science Degrees in Aeronautical Engineering from Auburn University in August 1968 and August 1969, respectively. Upon being commissioned, he was assigned to the Air Force Armament Laboratory at Eglin Air Force Base, Florida in September 1969, where he worked in the Aircraft Compatibility and Weapons Flight Dynamics Branch. During a four-year tour, he developed a weapon separation simulation program called the "Flow Angularity Technique" which was presented at the 1972 Stores Compatibility Symposium. Captain Korn was subsequently assigned to the A-10 System Program Office, Wright-Patterson Air Force Base, Ohio, in November 1973. He presently directs the store compatibility program for the A-10 aircraft and manages the engineering design requirements for the A-10 armament control subsystem.

EVALUATION OF PREDICTION METHODS FOR
AIRCRAFT/EXTERNAL STORE FLUTTER CLEARANCE
(U)
(Article UNCLASSIFIED)

by

Samuel J. Pollock and Dale E. Cooley
Analysis and Optimization Branch
Structural Mechanics Division
Air Force Flight Dynamics Laboratory
Wright-Patterson AFB, Ohio 45433

ABSTRACT. (U) A rapid analytical method for flutter prediction of aircraft/external store combinations has been applied and evaluated. This method, called FACES (Flutter of Aircraft Carrying External Stores), was developed by McDonnell Aircraft Company, and is based on a finite section vibration model which includes the wing, fuselage and wing control surfaces. Any mix of single or multiple external stores with up to five pylons per side can be analyzed. Analyses were conducted using FACES for a wing with tip tank and fin to show the effects on flutter of store aerodynamics and store mass center-of-gravity location. Aerodynamics on the tank and fin were found to have a significant effect on the flutter characteristics. Also, movement of the tank center-of-gravity location aft had a drastic, detrimental effect on flutter stability for the configurations analyzed. The flutter results from FACES calculations using both modified strip theory and doublet-lattice unsteady aerodynamics correlated well with actual flutter results available from a flight test incident.

The same configurations were also analyzed using the flutter analysis module within the automated computer program for flutter and strength optimization called FASTOP. FASTOP and FACES gave essentially the same results, with less computer time required by FACES. Areas for further increasing the capability of the FACES program are discussed.

"Approved for public release; distribution unlimited."

LIST OF FIGURES

<u>Figure No.</u>	<u>Title</u>
1	FACES Fast Flutter Routine
2	Wing and Tip Tank Model Used in Analyses
3	Bending and Torsional Stiffness for a Wing with Tip Tank
4	Doublet-Lattice Unsteady Aerodynamic Representations
5	Coupled Wing Bending and Torsion Modes, FACES Calculations
6	Damping Versus Velocity, Wing with Tip Tank and Fin
7	Frequency Versus Velocity, Wing with Tip Tank and Fin
8	Predicted Span Loading on the Wing, Tip Tank and Fin
9	Predicted Center of Pressure on the Wing, Tip Tank and Fin
10	Effect of Tip Tank and Fin Aerodynamics on Damping Versus Velocity, FACES/Doublet-Lattice (Cylindrical Tank)
11	Variation of Flutter Velocity with Center of Pressure on the Tip Tank/Fin, FACES/Modified Strip Theory
12	Variation of Flutter Velocity with Lift Curve Slope on the Tip Tank/Fin, FACES/Modified Strip Theory
13	Variation of Flutter Velocity with Tip Tank Center of Gravity, FACES/Modified Strip Theory

LIST OF TABLES

<u>Table No.</u>	<u>Title</u>
I	Wing and Tank Properties Used in Vibration and Flutter Analyses
II	FACES Vibration Calculations, Wing with Tip Tank
III	Flutter Characteristics, Wing with Tip Tank
IV	Computer Costs per Run for Various Methods

INTRODUCTION

A very large number of external store configurations are possible for attack and fighter aircraft performing a wide variety of military missions. Each configuration of external stores must be evaluated for flutter and cleared to safe flight speeds. Therefore, the flutter safety evaluation program may entail many costly and time consuming computations, flutter model tests, and flight flutter tests. In response to the need for a rapid, economical method to predict flutter of wings with external stores, an evaluation of several approaches was performed under Air Force Flight Dynamics Laboratory sponsorship and is described in Reference 1. Based on this evaluation, the Air Force Flight Dynamics Laboratory has been sponsoring research to develop rapid computational procedures. Two of these methods are described briefly in Reference 2. A perturbation approach which was developed by Northrop (Reference 3) shows promise for significant reduction in computation times (up to 90 percent) where the method is applicable. The second method, called FACES (Flutter of Aircraft Carrying External Stores), is a rapid aircraft/store flutter analysis program (References 4, 5 and 6). The FACES method was developed by McDonnell Aircraft Company and has been applied successfully by several organizations to various aircraft/external store combinations. It is described in more detail in the next section.

The objective of this study was to apply and evaluate the accuracy and efficiency of FACES by comparison with both flight flutter test results for a wing with a nonstandard, aft-ballasted tip tank, and with results from an available, conventional flutter analyses module in the FASTOP flutter-strength optimization program (Reference 7). A secondary objective was to perform parameter variations including tip tank and fin aerodynamics, and tip tank center of gravity for determination of their influence on wing/store flutter. Also, recommendations for further work are discussed.

APPROACH

METHODS

1. FACES

The FACES computer program was developed especially for simplified and efficient aircraft/external store flutter analyses. As shown in Figure 1, the FACES computer program.

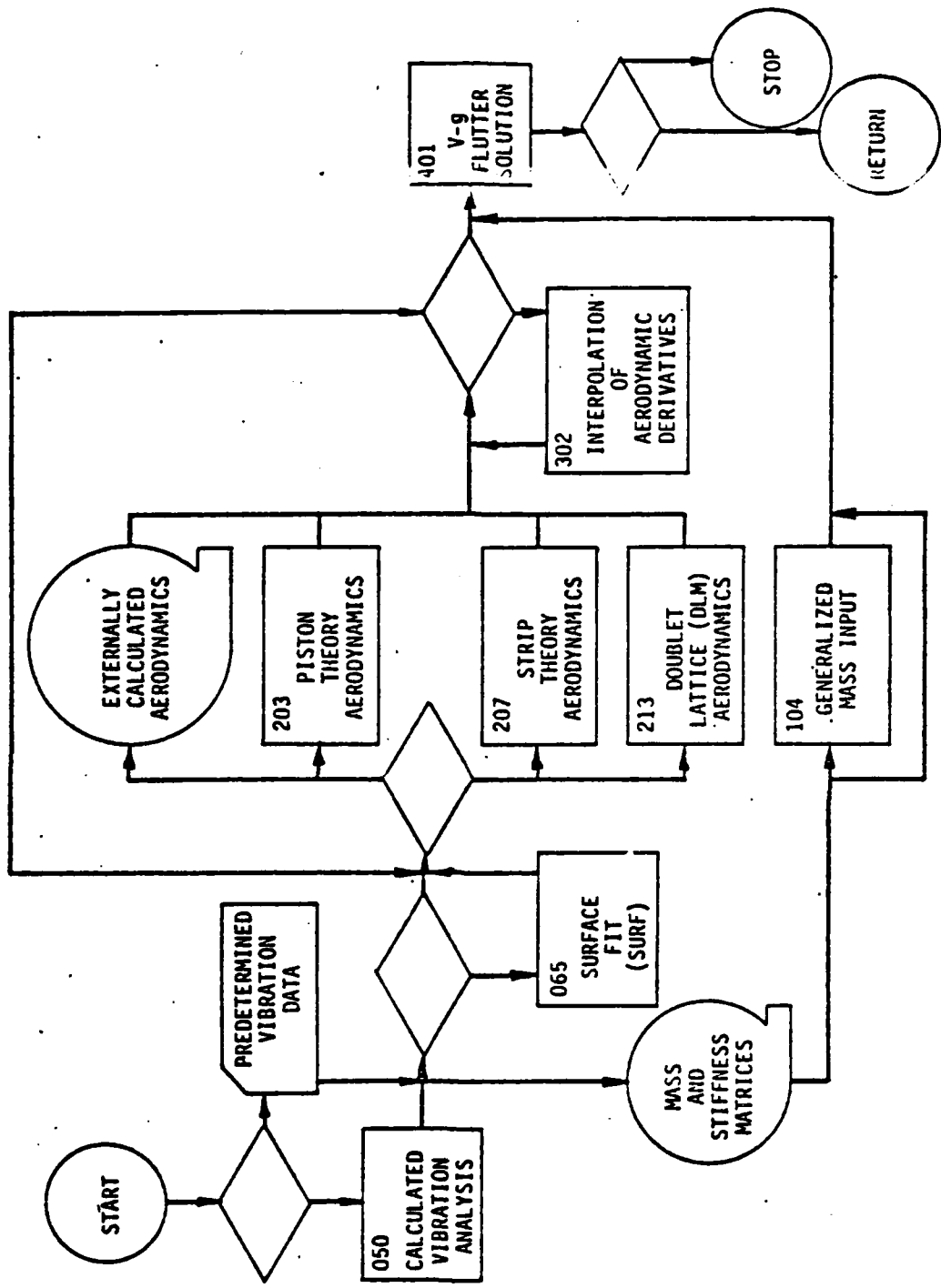


Figure 1. FACES Fast Flutter Routine

is in modular form and requires very simple, straightforward input data. Both batch and graphics versions of the program are available for both CDC and IBM computer equipment. Only 145K octal central memory is required on the Wright-Patterson Air Force Base Cyber 74 computer. Measured vibration data or vibration properties from other analytical methods can be input to the FACES program if desired.

The vibration model for calculation within FACES allows up to 14 wing sections, each with bending and torsion degrees of freedom. The wing mass can be based on stream-wise or elastic axis cuts, while wing elastic properties can be based on simple bending and torsional rigidities, EI and GJ, respectively. Vibration and flutter cases can include cantilever (with and without wing root springs), symmetric and antisymmetric options for a rigid fuselage. For a flexible fuselage, up to 24 sections can be allowed which have vertical bending degrees of freedom in the symmetric case and have lateral bending and torsion degrees of freedom in the antisymmetric case. One to five pylons per side with single, TER or MER carriage of multiple weapons are allowed. Up to two control surfaces per side can be included with a total of 14 sections.

The unsteady aerodynamic theory options available in FACES include doublet-lattice, strip theory, modified strip theory and supersonic piston theory. For subsonic, compressible flow, the doublet-lattice method (Reference 8) is generally considered to be the best available unsteady aerodynamic theory. The unsteady airloads on external stores can be represented in doublet lattice by either lifting surface panels or by a constant cross-section cylinder based on the method of images. Both of these representations were used in this study. The method of images would be expected to provide the best representation of a body, and thus provide the most accurate lifting surface/body interference effects.

The strip theory option assumes that the sectional lift-curve slope, $C_{L\alpha}$, is 2π with the aerodynamic center, a.c., at the quarter chord, in accordance with two-dimensional, incompressible flow theory. Although strip theory analyses are very fast, the two-dimensional theory usually overestimates the aerodynamic forces on three-dimensional surfaces and thus generally provides conservative flutter speed predictions.

To retain the rapid, efficient capability of the strip theory approach and also improve the accuracy, available measured or analytical values for steady state $C_{L\alpha}$ and a.c.

can be used in an option called modified strip theory. In the present study the $C_{L\alpha}$ and a.c. used in modified strip theory were based on steady-state doublet-lattice calculations (cylindrical tank). Piston theory, while available in FACES, is applicable only at high supersonic Mach numbers and was not used in this study.

Flutter calculation in this study using the doublet-lattice method involved the following FACES modules from Figure 1.

- 050 - Calculated Vibration
- 065 - Surface Fit (used to calculate polynomials for the doublet-lattice method)
- 104 - Generalized Mass Input
- 213 - Doublet-Lattice Aerodynamic Method
- 302 - Interpolation of Aerodynamic Derivatives (used for interpolation to reduce expensive computations with the doublet-lattice method)
- 401 - V-g Flutter Solution

For strip or modified strip theory calculations, modules 065, 213 and 302 are replaced by module 207 (Figure 1).

2. FASTOP

FASTOP (Flutter and Strength Optimization Program) is a computer program developed by Grumman for the AFFDL (Reference 7). It performs integrated analysis for sizing (near-minimum weight) of cantilever and free-free lifting surface structures with both strength and flutter-speed constraints. Only the conventional flutter analysis module of FASTOP is used in this study for comparison of results with some of the FACES calculations. The FASTOP flutter module requires 222K octal memory on the WPAFB Cyber 74 computer.

The vibration modes and frequencies which were calculated by the FACES program were used directly as input to the FASTOP flutter analyses. In the FASTOP program, the doublet-lattice method used is an earlier version (Reference 9) which permits only flat plate or panel representation for lifting surfaces and bodies. Therefore, the tip tank was represented by panels as will be discussed in the next section on configurations analyzed.

CONFIGURATIONS ANALYZED

Vibration and flutter calculations were performed for an aircraft wing with a 230 gallon tip tank as shown in Figure 2. This configuration was selected because flutter results were available from flight tests on an F-80 with a nonstandard, aft-ballasted tip tank. These results were obtained during flight flutter tests in July 1950. Flutter was encountered on the F-80 with 85 pounds of lead located in the tank 59 inches aft of the wing elastic axis. This corresponded to 13 gallons of fuel, entirely in the aft end of the tank. The flutter occurred at an altitude of 10,000 feet and an indicated airspeed of 458 mph ($M = 0.63$, $V = 382$ KEAS). Instrumentation aboard the aircraft provided data on damping versus velocity which showed a very rapidly divergent flight instability at a frequency of 5.0 Hz. Considerable damage was done to the wing of the F-80 although the tanks were jettisoned within approximately three seconds after the oscillations began. The aircraft was subsequently landed.

The wing/tank configuration was represented in the FACES vibration calculations by 10 sections as shown in Figure 2. Wing geometry and mass data from Reference 10 were used and are presented in Table I. Spanwise bending and torsional stiffnesses from Reference 11 were used and are shown in Figure 3. Table I and Figure 3 present the required data in the appropriate format for input to the FACES program for vibration calculations.

Using the vibration results calculated with the FACES program, flutter analyses were then performed for $M = 0.63$ with both FACES and FASTOP methods. Unsteady aerodynamic methods used were strip theory, modified strip theory and the various doublet-lattice representations. The strip theory and modified strip theory flutter calculations used the same ten wing sections for the aerodynamic strips as were used for vibration calculations (Figure 2).

Figure 4 is a sketch of the doublet-lattice unsteady aerodynamic representations used in the flutter analyses. In all of the models, 40 boxes were used to represent the wing; four evenly spaced chordwise by 10 spanwise, with the same spanwise divisions as used for the vibration model. For the fin, nine boxes were used; three evenly spaced chordwise by three evenly spaced spanwise. In all of the aerodynamic models the tank was 139 inches in length with a diameter of 25 inches (equal to tank diameter at largest cross-section). The FASTOP doublet-lattice representation for the tank was a hexagon with six equal face panels, each

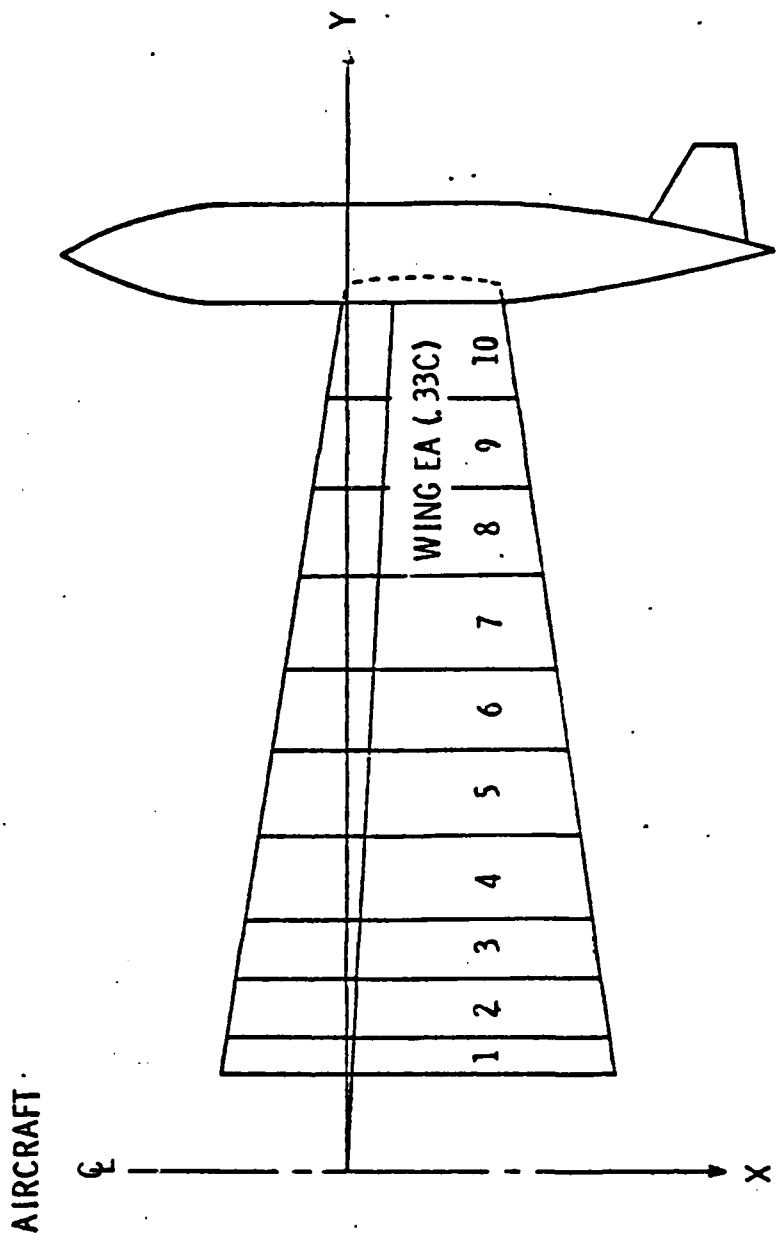


Figure 2. Wing and Tip Tank Model Used in Analyses

Table I. Wing and Tank Properties Used in Vibration and Flutter Analyses

SECTION	X_{cg} , in	Y_{cg} , in	W, lbs	I_p , lb in ²	Δy , in
1	14.5	23.3	59.1	36,985	9.6
2	11.9	41.0	283.8	88,983	14.7
3	12.6	55.7	279.8	75,936	14.7
4	13.3	73.6	280.4	96,367	21.1
5	13.8	94.7	271.6	78,017	21.1
6	14.3	115.8	262.7	62,956	21.1
7	9.8	137.5	156.3	35,527	22.4
8	10.4	159.9	146.5	25,710	22.4
9	11.1	182.3	136.6	16,820	22.4
10	11.8	204.7	126.7	9,230	22.4
Ballasted Tank*	42.8	231.0	263.0	406,801	25.0

* 85 lbs of lead 59 inches aft of wing elastic axis

X_{cg} Chordwise distance of center of gravity from reference axis, positive aft

Y_{cg} Spanwise distance of center of gravity from aircraft center line

W Weight

I_p Pitch Inertia

Δy Section width

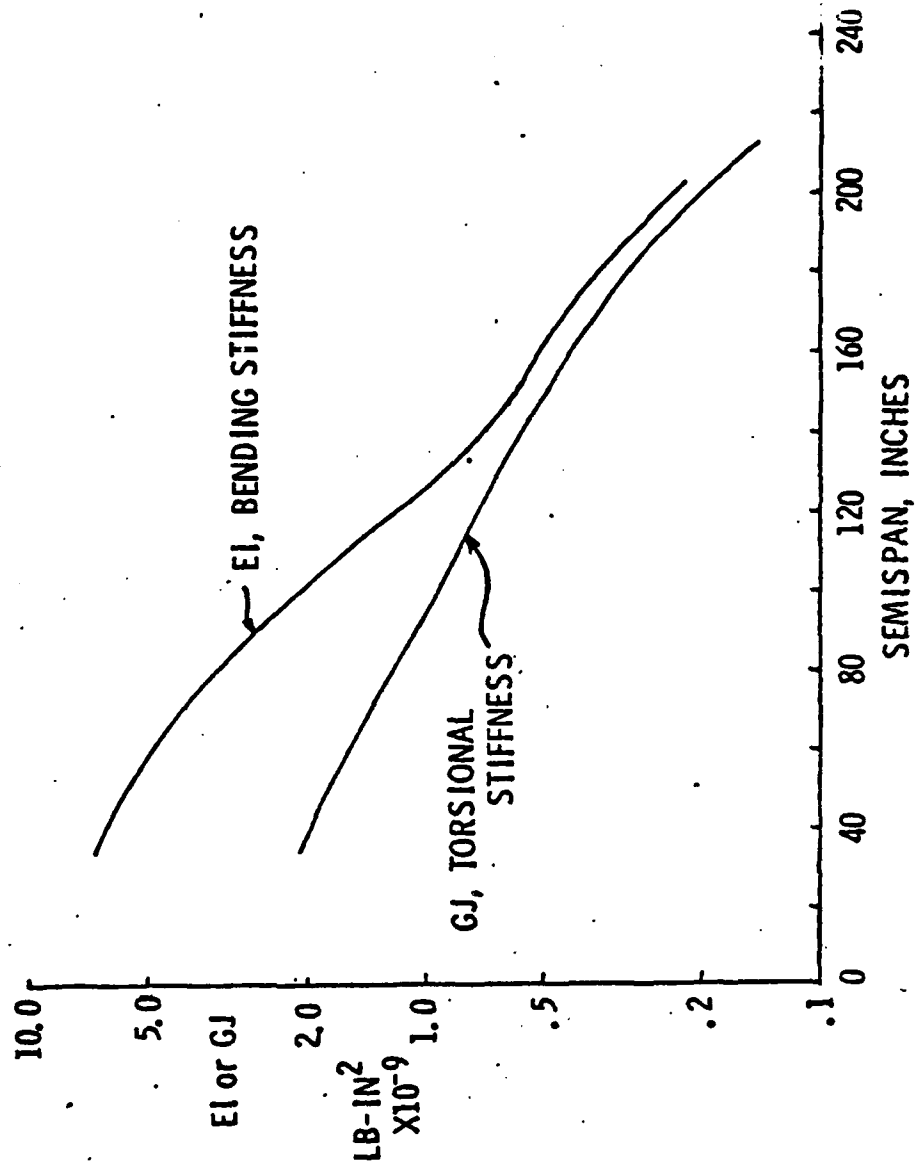


Figure 3. Bending and Torsional Stiffness for a Wing with Tip Tank

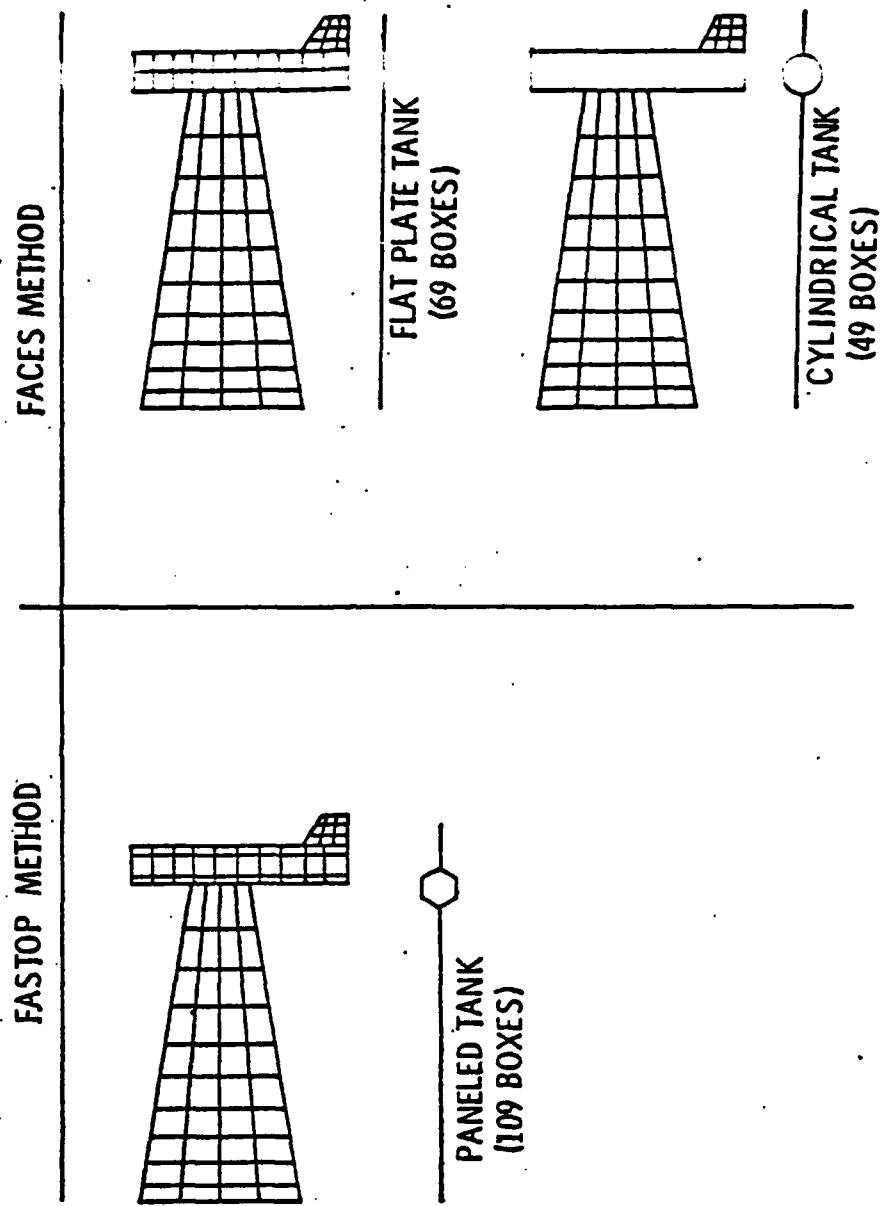


Figure 4. Doublet-Lattice Unsteady Aerodynamic Representations

having ten evenly spaced chordwise boxes as shown in Figure 4. The flat plate tank representation in the FACES doublet-lattice model consisted of ten evenly spaced chordwise boxes by two evenly spaced spanwise boxes. The other FACES tank model used the method of images with the tank represented as a circular cylinder as shown in Figure 4.

RESULTS

VIBRATION CALCULATIONS

Table II gives the vibration frequencies predicted by the FACES program for the first four modes of the F-80 with the tip tank. Figure 5 shows the calculated bending and torsion node lines which are shown in subsequent sections to be the principal modes involved in the flutter mechanism.

FLUTTER CALCULATIONS

The calculated flutter results for correlation with flight test data on the F-80 are presented in Table III and Figures 6 and 7. In Figure 6, both the predicted and measured data on damping versus velocity is plotted for vibration mode 2 (primarily wing torsion) which is the mode that goes unstable. The measured flutter crossing is at a velocity of 382 KEAS, with the slope of the damping versus velocity curve being very steep. This rapidly divergent type of behavior is typical of coupled bending-torsion flutter.

The FACES method using two doublet-lattice unsteady aerodynamic options for the tip tank gave very good agreement with the experimental flutter speed as shown in Figure 6. The FACES cylindrical tank representation gave a flutter speed of 380 KEAS which is within one half percent of the flight value, and the flat plate tank representation gave 375 KEAS, which is within two percent of the flight value. The FASTOP program using the doublet-lattice unsteady aerodynamic representation predicted a flutter velocity of 407 KEAS which is 6.5 percent above the measured value. Thus, both FACES and FASTOP, using doublet-lattice aerodynamics, give reasonably good prediction of the flight flutter speed. The slight differences between FACES and FASTOP can probably be attributed to the different unsteady aerodynamic representations for the tank and also the use of different procedures for interpolating the vibration modes in calculating unsteady aerodynamic loads.

Table II. FACES Vibration Calculations,
Wing with Tip Tank

MODE NR.	FREQUENCY (Hz)	MODE DESCRIPTION
1	3.31	Primarily 1st Wing Bending
2	7.10	Primarily 1st Wing Torsion
3	16.61	Primarily 2nd Wing Bending
4	26.32	Primarily 2nd Wing Torsion

Table III. Flutter Characteristics,
Wing with Tip Tank

ANALYSIS METHOD/AERODYNAMIC REPR	FLUTTER SPEED (KEAS)	FLUTTER FREQ (Hz)
FACES/Doublet-Lattice (Cyl Tank)	380	5.5
FACES/Doublet-Lattice (Plate Tank)	375	5.5
FACES/Strip Theory	283	5.0
FACES/Modified Strip Theory	380	4.8
FASTOP/Doublet-Lattice (P-k)	407	5.3
Flight Test, July 1950	382	5.0

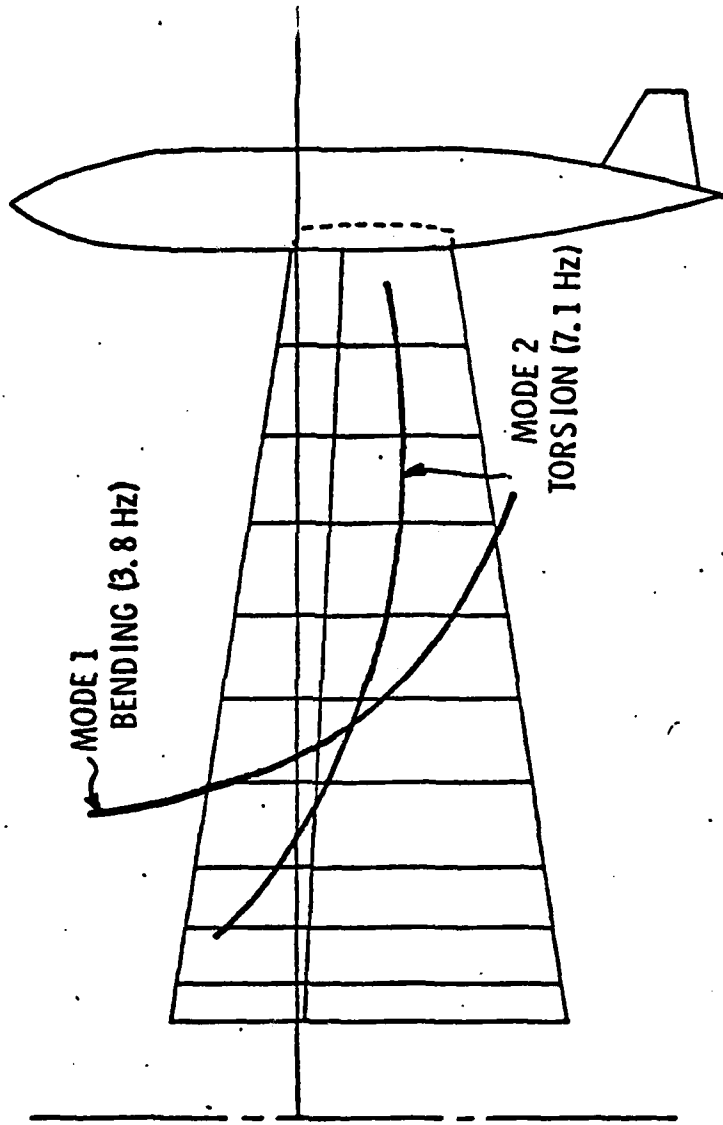


Figure 5. Coupled Wing Bending and Torsion Modes,
FACES Calculations

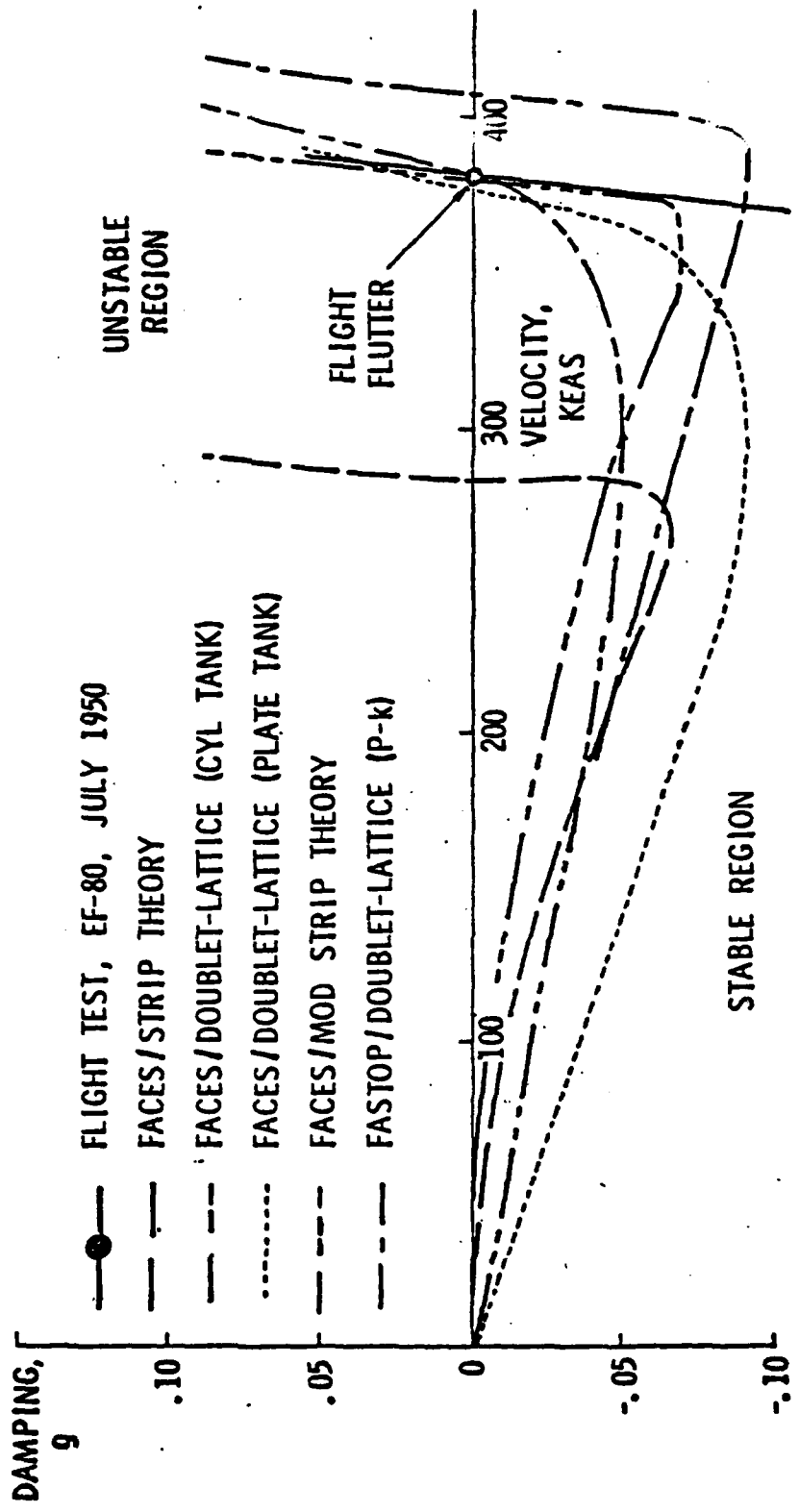


Figure 6. Damping Versus Velocity, Wing with Tip Tank and Fin

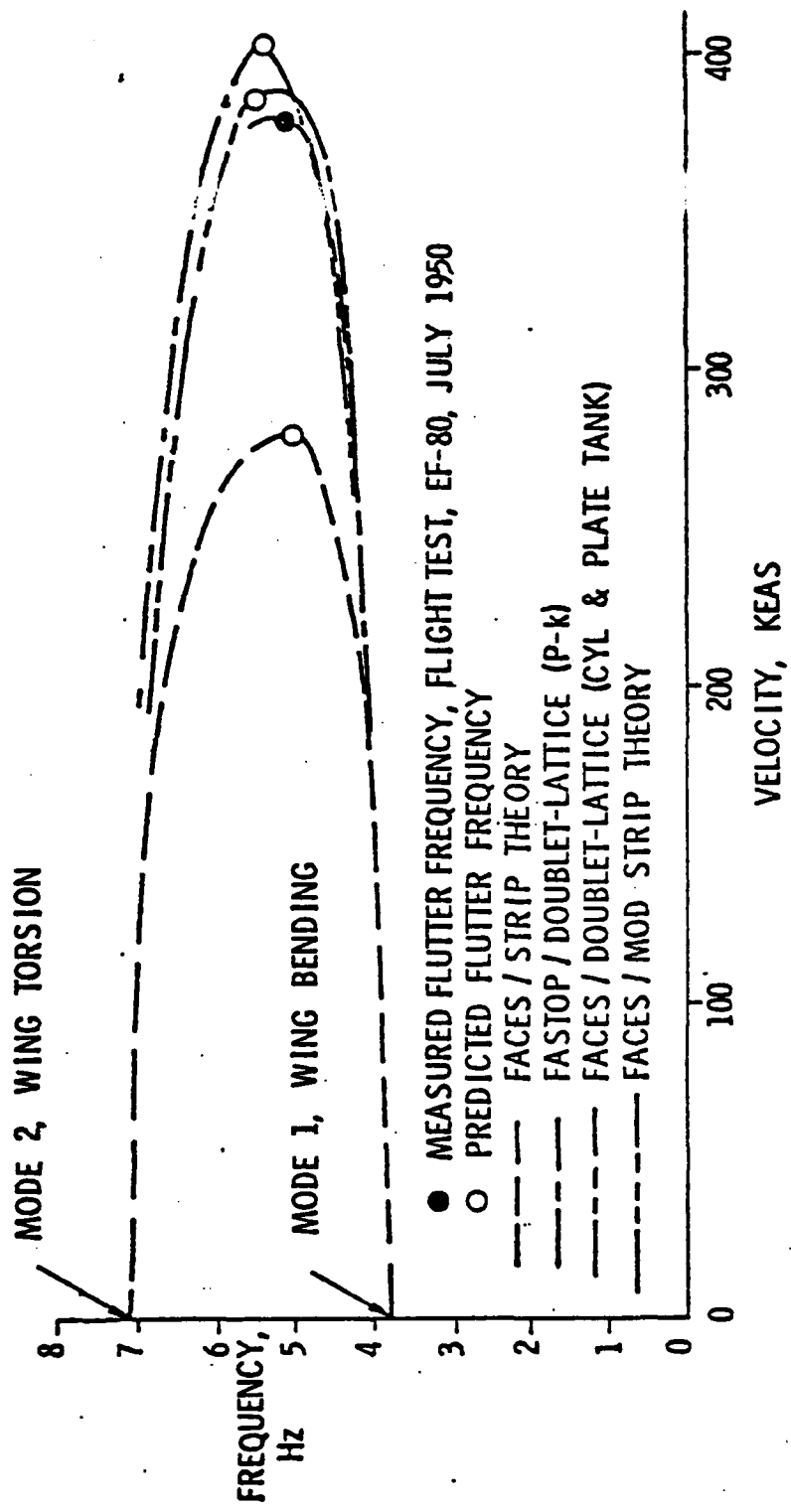


Figure 7. Frequency Versus Velocity, Wing with Tip Tank and In

The FACES method using strip theory unsteady aerodynamics was very conservative, predicting a flutter speed of 283 KEAS which was 26 percent lower than measured. The lower flutter speed predicted by strip theory was expected due to use of the two-dimensional, incompressible lift-curve slope. The modified strip theory calculations gave excellent results using the lift-curve slope and center of pressure based on steady state doublet-lattice calculations (cylindrical tank). The flutter speed predicted with this modified strip theory was 380 KEAS which is the same speed predicted by the FACES doublet-lattice method with the corresponding cylindrical tank representation.

Figure 7 presents the predicted frequency versus velocity for modes 1 and 2. The calculated and measured flutter frequencies are also indicated at the corresponding flutter velocity. The plot shows the coalescence of the two modes with increasing airspeed. Strip theory predicts a flutter frequency of 5.0 Hz which is the same as the measured flutter frequency. FACES with modified strip theory predicts a flutter frequency of 4.8 Hz. Both FASTOP and FACES with doublet-lattice unsteady aerodynamics predict flutter frequencies slightly higher than measured, 5.3 Hz for FASTOP and 5.5 Hz for FACES (both cylindrical and plate tank).

UNSTEADY AERODYNAMICS

The tip tank unsteady aerodynamic loading and interference effect on the wing would be expected to have a significant effect on flutter. Figure 8 is a plot of this aerodynamic loading along the span of the wing/tip tank/fin as predicted by the various unsteady aerodynamic theories. The strip theory loading based on the two-dimensional incompressible value of 2π for the lift-curve slope, CL_{α} , is seen to be much higher than predicted by doublet-lattice on the tank, and also somewhat higher over most of the wing except for a small outboard region. This outboard region is where tank interference effects, as accounted for by doublet lattice, would have the maximum effect of increasing wing loading. The generally higher loading with strip theory accounts for the low flutter speed predicted by this theory.

Figure 8 also indicates that the overall span loadings for the various doublet-lattice unsteady aerodynamic tank models are in fairly good agreement with each other. However, there are some differences in distribution of span loading due to the various tank representations. For instance, the loading on the tank was lowest with the FACES cylindrical representation, higher by 11 percent with the

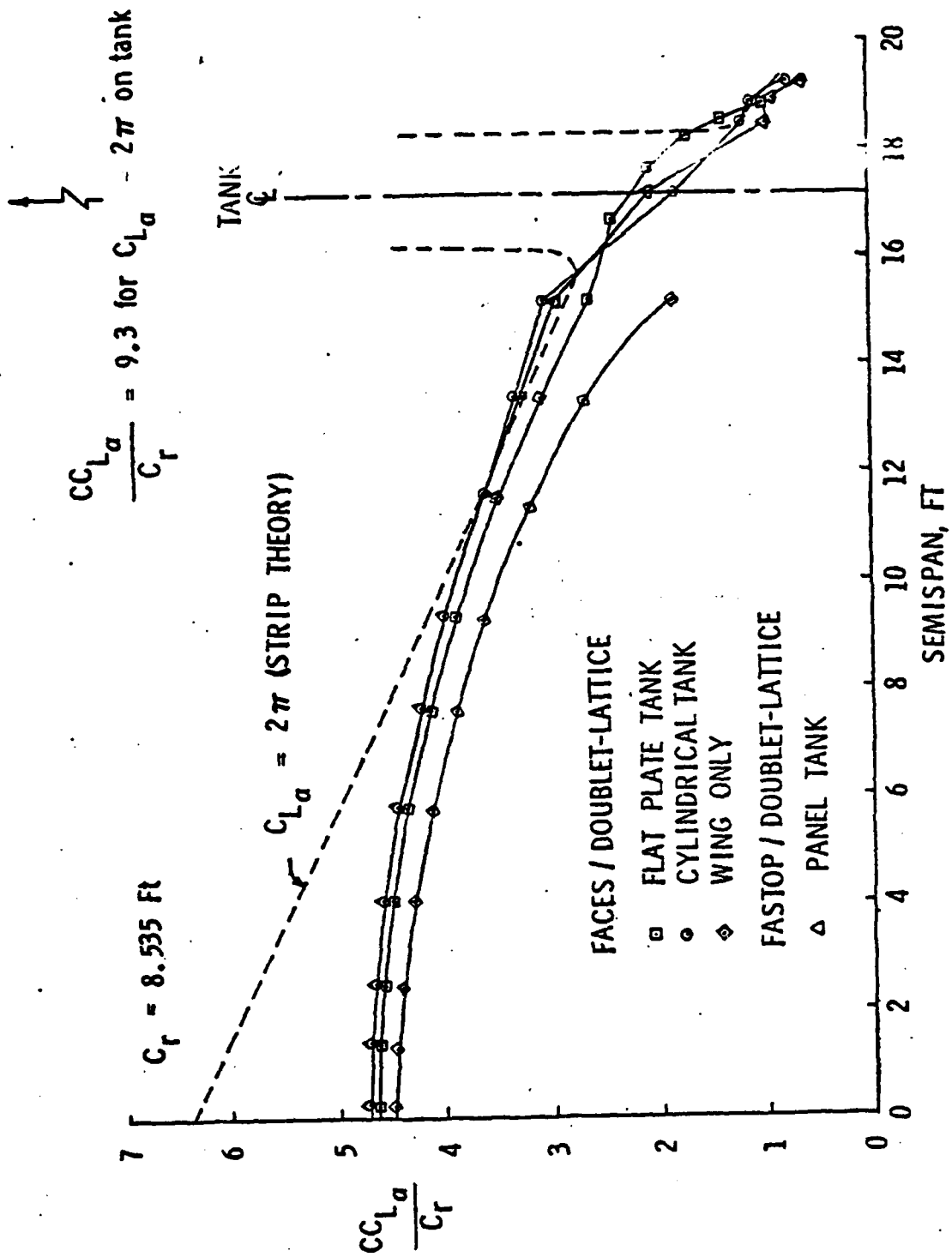


Figure 8. Predicted Span Loading on the Wing, Tip Tank and In

FASTOP paneled (hexagonal) tank and higher by 19 percent with the FACES flat plate tank. The loading on the outboard portion of the wing surface due to the presence of the tank can also be seen in Figure 8. The outboard wing loading was highest with the FACES cylindrical tank representation, lower by four percent with the FASTOP hexagonal tank and lower by 15 percent with the FACES flat plate tank. However, the various span loadings for the different doublet-lattice tank representations resulted in predicted flutter speeds which were in reasonably good agreement (within 6.5 percent of test).

The lift-curve slope for the wing alone (no tank aerodynamics) as predicted by doublet-lattice theory is also shown in Figure 8 for comparison purposes. The span loading on the wing is considerably lower, particularly near the outboard portion, without the tip tank interference effects. For instance, the loading near the wing tip is about 39 percent less when neglecting the tank aerodynamic effects. This indicates a very significant effect on the wing loading due to the presence of the tip tank.

Figure 9 shows the center of pressure, c.p., predicted using the various theories. As expected at this Mach number ($M = 0.63$) the c.p. predicted by the doublet-lattice lifting surface theory is close to 25 percent of the local wing chord except on the tip tank and fin. Both the hexagonal and circular cylindrical tank models predicted a c.p. at 46 percent of the local tank chord while the flat plate model c.p. was about 35 percent. On the fin all of the doublet-lattice models predicted a c.p. of about 19 percent of the local fin chord.

Figure 10 shows the effects of the tip tank and fin aerodynamics being either included or deleted in flutter analyses. The results are based on analyses using the FACES/doublet-lattice (cylindrical tank) method and are presented in the form of damping versus velocity for three different cases: (1) wing with tank and fin aerodynamics included, (2) wing with tank but without fin aerodynamics and (3) wing without tank or fin aerodynamics (wing alone). The vibration modes and mass characteristics were the same for all cases. Including tank and fin aerodynamics (case 1) gives a flutter speed of 380 KEAS which correlates well with the flight flutter speed of 382 KEAS as discussed previously. With wing and tank aerodynamics but no fin aerodynamics (case 2), the predicted flutter speed was 342 KEAS which is a decrease in flutter velocity of 10 percent. This illustrates the stabilizing effect on the flutter speed of including the fin aerodynamics.

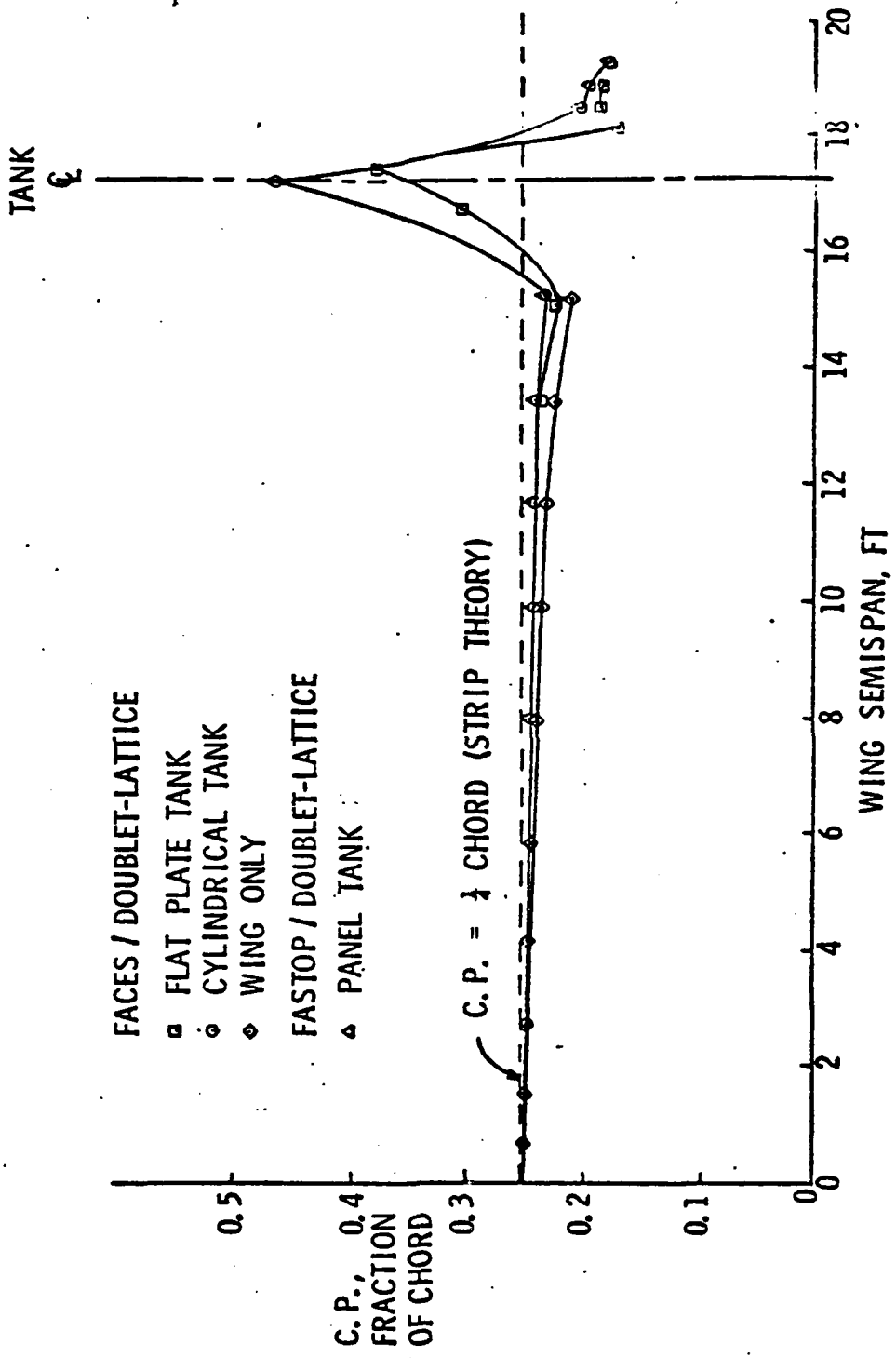


Figure 9. Predicted Center of Pressure on the Wing, Tip Tank and Fin

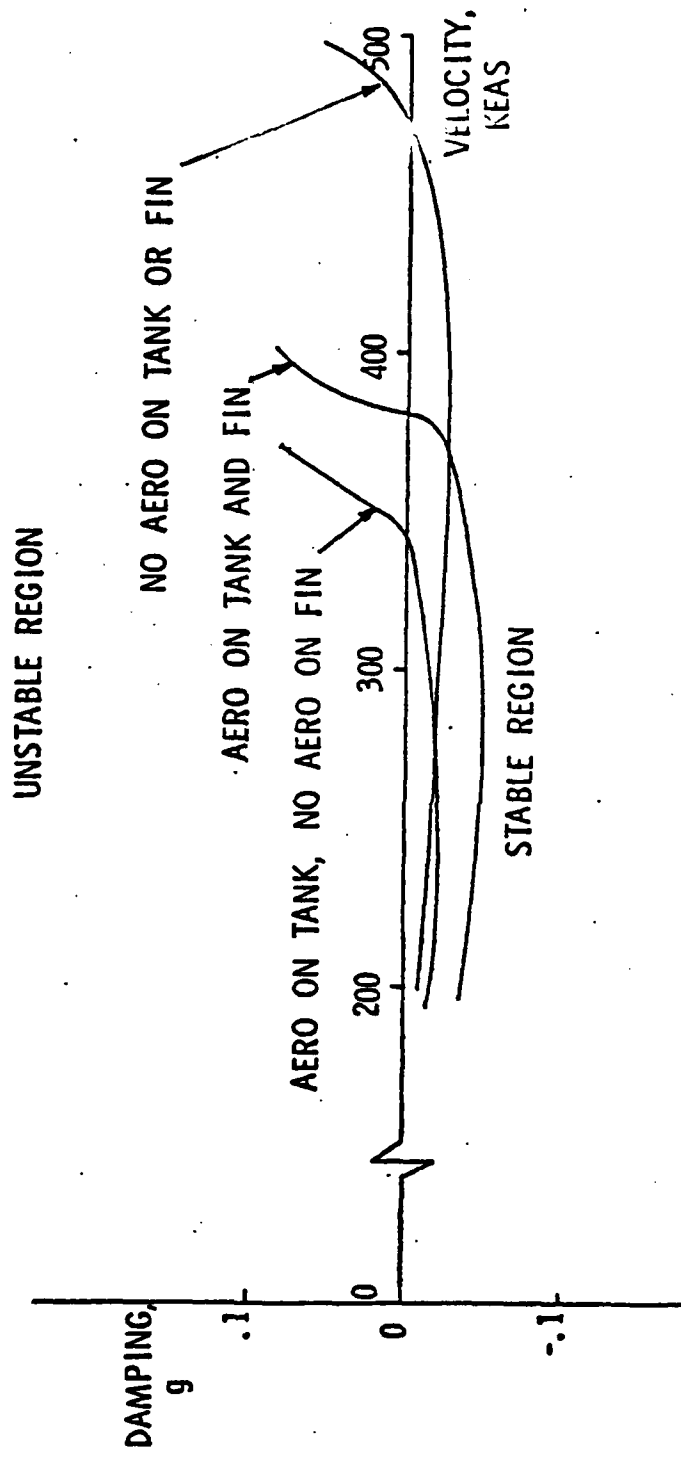


Figure 10. Effect of Tip Tank and Fin Aerodynamics on Damping Versus Velocity, **FACES/Doublet-Lattice (Cylindrical Tank)**

In case 3 on Figure 10, neither tip tank nor fin aerodynamics are included (wing alone). The predicted flutter speed is 476 KEAS, which is 25 percent higher than case 1 where wing/tank/fin aerodynamics were included.

The very destabilizing effect on flutter of including the tip store aerodynamics can be seen by comparing case 2 with 3 from Figure 10. The flutter speed with the tank aerodynamics included (case 2) when compared with the wing alone aerodynamics (case 3) shows a decrease of 28 percent. This illustrates the importance of properly accounting for the store aerodynamic effect in flutter analyses.

PARAMETER VARIATION EFFECTS ON FLUTTER

To illustrate the application of the FACES program in identifying important flutter parameters the following variations were studied. The modified strip theory aerodynamic approach was used because of its efficiency and the ease of making such parametric trend variations.

1. Center of Pressure Location on the Tip Tank and Fin

The effect on flutter velocity of center of pressure variation on the tip tank/fin (10th section) was determined while holding lift-curve slope constant at the value predicted by doublet-lattice theory. The area of the 10th section includes the tip tank, fin and tip of the wing. Figure 11 is a plot of flutter velocity versus center of pressure and shows that as the c.p. moves forward the flutter velocity decreases. This decrease is 14 percent for the c.p. range investigated (.59 chord to .20 chord). The primary effect of the fin is to move the c.p. aft which is shown to be beneficial from a flutter standpoint.

2. Lift-Curve Slope of the Tip Tank and Fin

Figure 12 gives the variation of flutter speed and flutter frequency with lift-curve slope of the tip tank and fin (Section 10), holding center of pressure constant at the doublet-lattice value. The flutter velocity decreases 16 percent as lift-curve slope on the tip tank/fin goes from 25 percent less than the doublet-lattice value to 25 percent greater than the doublet-lattice value.

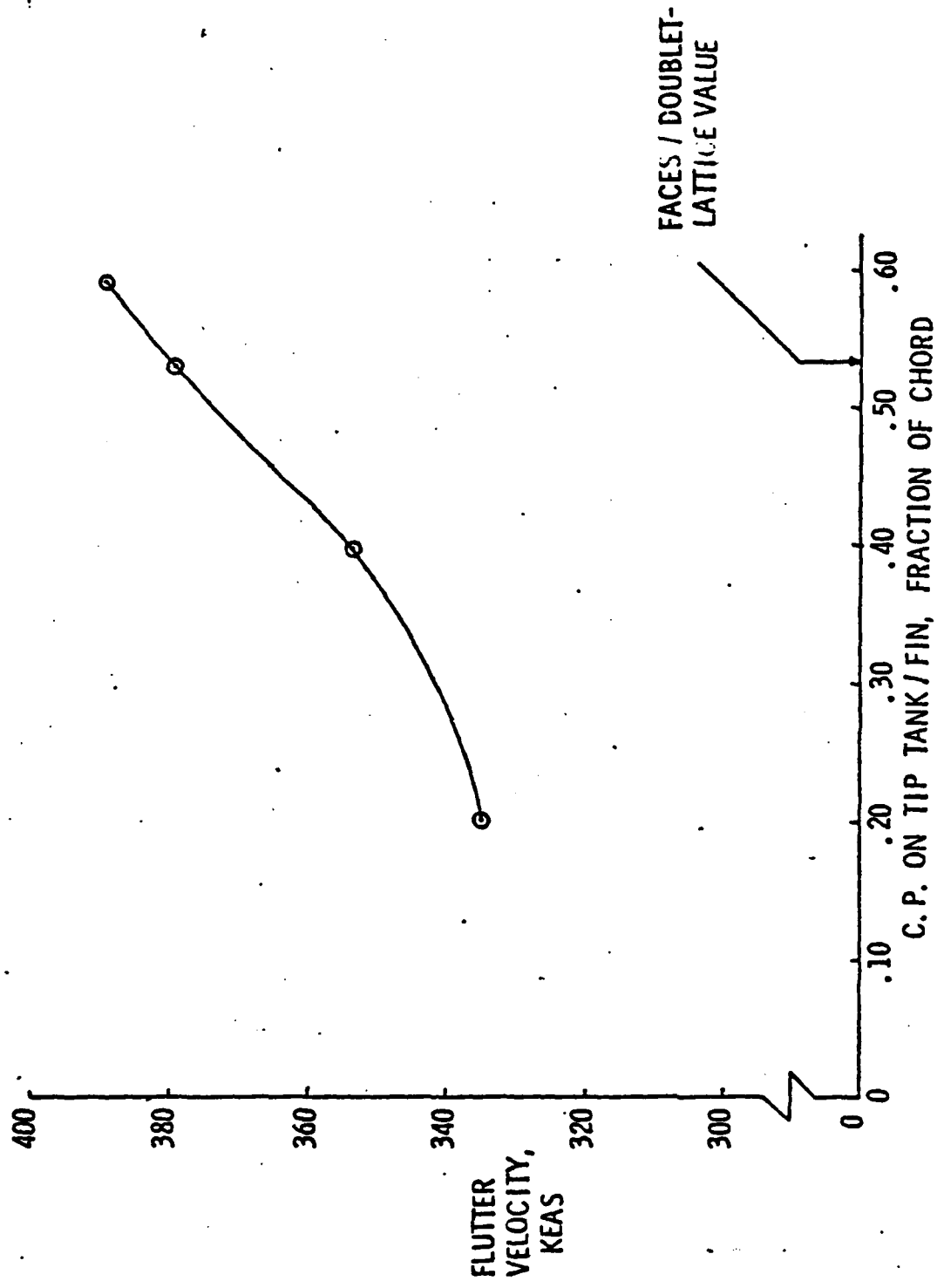


Figure 11. Variation of Flutter Velocity with Center of Pressure on the Tip Tank/Fin, FACES/Modified Strip Theory

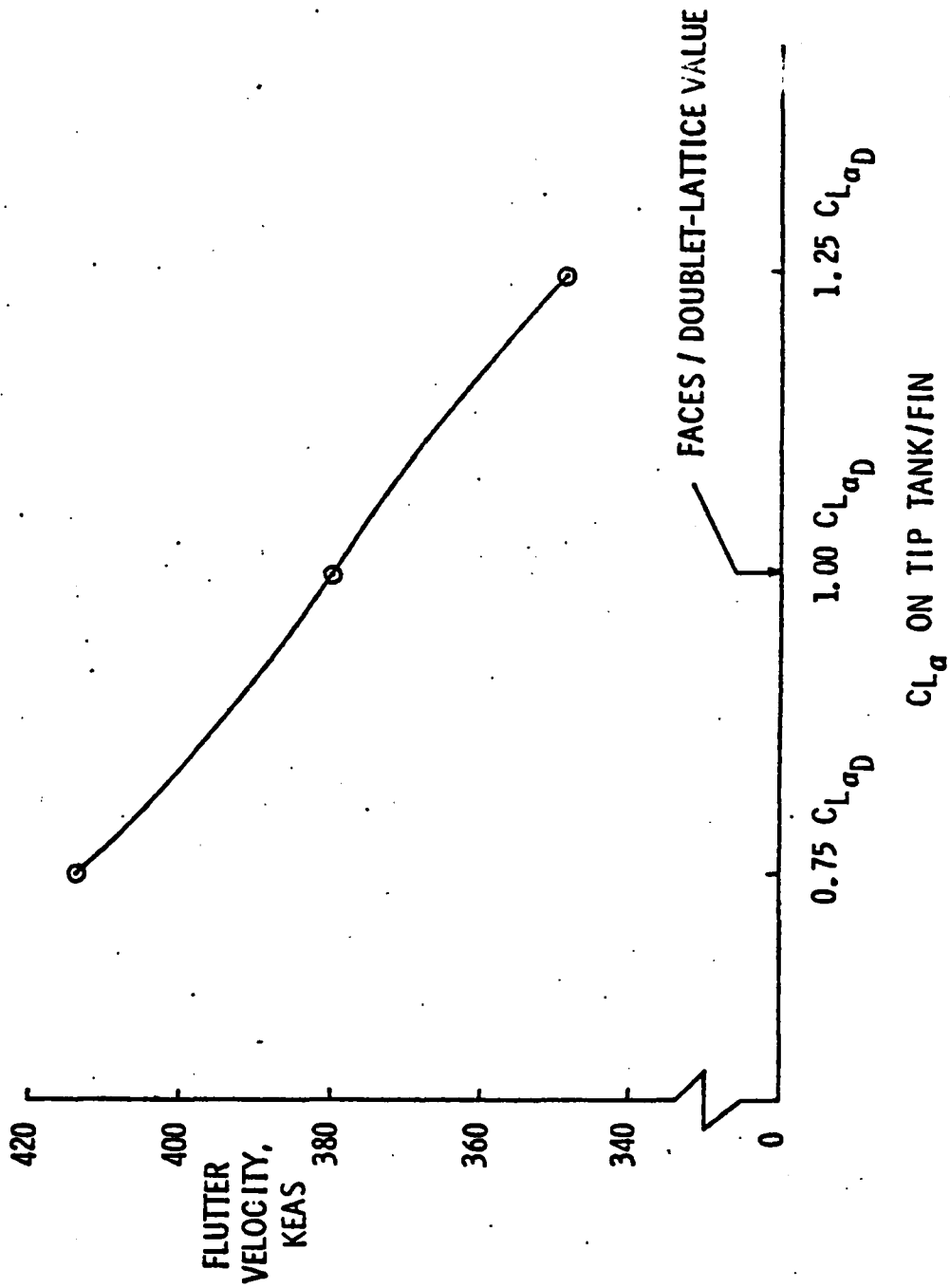


Figure 12. Variation of Flutter Velocity with Lift Curve Slope on the Tip Tank/Fin, FACES/Modified Strip Theory

3. Center of Gravity, c.g., Location of the Tip Tank

Figure 13 shows the effect of tip tank c.g. location on flutter speed and frequency. The c.g. is varied from 12 inches forward to 6 inches aft of the tank c.g. for this study. The flutter speed decreased 28 percent and the flutter frequency decreased 13 percent due to the movement of the c.g. 18 inches aft. This illustrates the drastic effect of c.g. on flutter which means caution should be exercised whenever tip tank modifications are made.

COMPUTER TIME AND COST

A very significant and practical aspect in flutter analyses is the computer time and cost. For the configuration analyzed the computer costs per run on the Cyber 74 varied from \$2.90 for FACES with strip theory and modified strip theory aerodynamics to \$33.09 per run for FASTOP/doublet lattice (see Table IV). The cost per run for FACES with the flat plate doublet-lattice model was \$12.12 while the cylindrical tank doublet-lattice model with FACES cost \$20.60. The most economical approach for the cases considered is FACES with strip theory aerodynamics although unfortunately, as discussed previously, this is the least accurate approach. However, the FACES modified strip theory offers the advantages of equally low cost and very accurate results provided either measured wing aerodynamics or calculations using a good lifting surface theory such as doublet-lattice are available. Thus, the modified strip theory is an especially attractive approach for parametric studies which are useful for store flutter investigations. The doublet-lattice unsteady aerodynamic method, although more expensive than strip theory, provides a valuable tool when reasonably accurate three-dimensional effects of the flow need to be included in the analyses to obtain reliable flutter prediction for flutter safety confirmation.

CONCLUSIONS AND RECOMMENDATIONS

The results of this investigation lead to the following conclusions and recommendations:

1. Applications of the FACES computer program to a wing with tip store/fin indicates the procedure is functioning properly and capable of providing very good flutter speed predictions based on comparison with available flight test

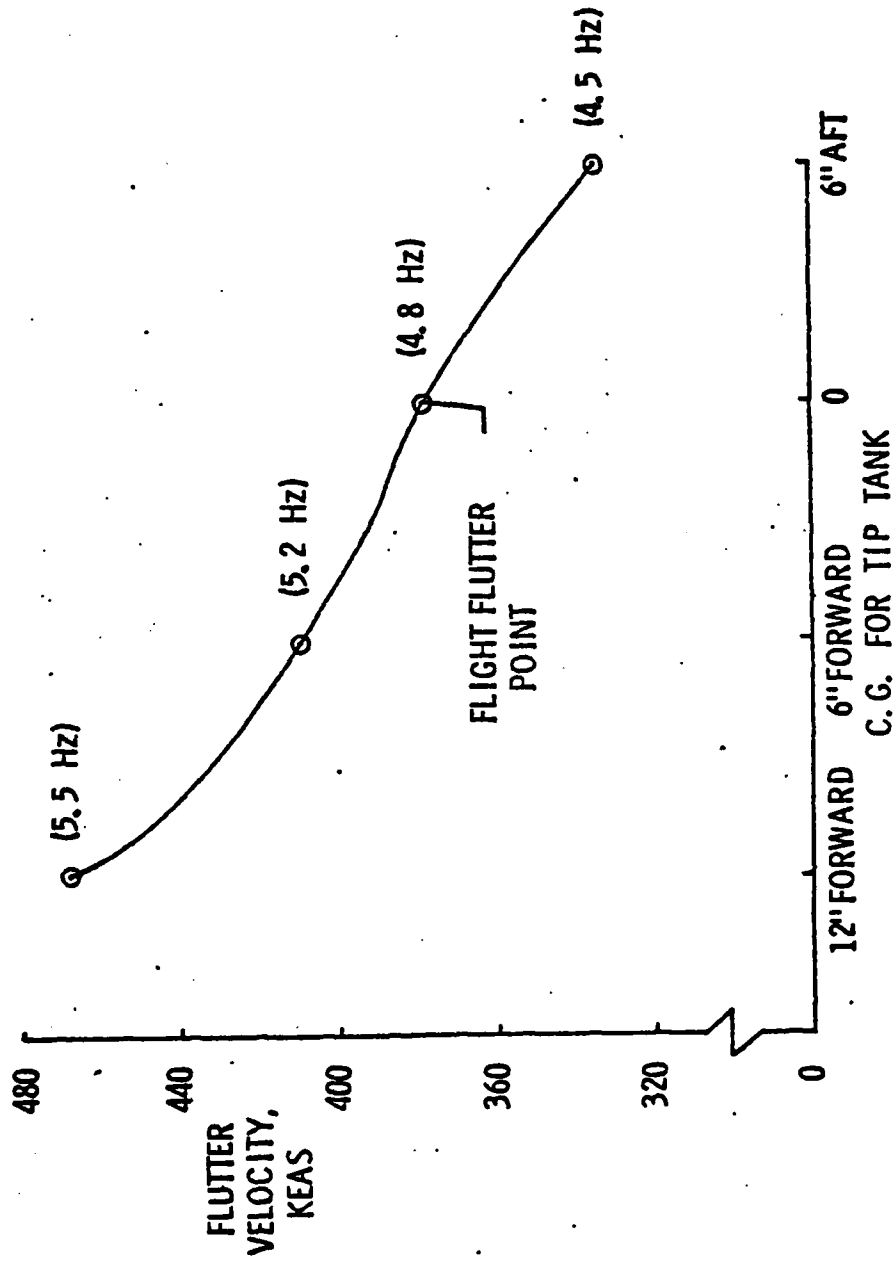


Figure 13. Variation of Flutter Velocity with Tip Tank Center of Gravity, FACES/Modified Strip Theory

Table IV. Computer Costs per Run
for Various Methods

METHOD/AERO REPRESENTATION	COMPUTER COST/RUN (CDC 6600)
<u>FACES</u>	
DOUBLET-LATTICE/CYLINDRICAL TANK	\$20.60
DOUBLET-LATTICE/FLAT PLATE TANK	\$12.12
STRIP THEORY	\$2.90
MODIFIED STRIP THEORY	\$2.90
<u>FASTOP</u>	
DOUBLET-LATTICE/PANELS ON TANK	\$33.09

data and with results of a conventional, general purpose analysis method.

2. The FACES/doublet-lattice unsteady aerodynamic representations used for the store body (method of images and lifting surface panels) both provided comparable and very good flutter speed prediction for the cases evaluated and would be considered the most accurate theory for the subsonic compressible flow region. The two-dimensional incompressible strip theory option gave very low, conservative flutter speed predictions. The modified strip theory method using spanwise $C_{L\alpha}$ and c.p. corrections based on steady-state doublet-lattice calculations gave very good flutter speed predictions with significant time and cost savings and is particularly suitable for many parametric variation calculations such as for wing/store flutter clearance.

3. The effect on flutter of unsteady aerodynamic loadings on the tank and fin were shown to be extremely significant. If the aerodynamics on the tip store and fin were neglected, the predicted flutter speed would be 25 percent higher (unconservative) than if they are included. The aerodynamic effect of the fin is stabilizing, increasing the flutter speed about 10 percent for this case.

4. Parameter variations for this wing/tip tank/fin configuration showed:

a. Effect of Lift-Curve Slope. Increasing the lift-curve slope on the tip tank/fin decreased the flutter speed.

b. Effect of Center of Pressure. Aft movement of the center of pressure on the tip tank/fin increased the flutter speed.

c. Effect of Tip Tank Center of Gravity. Aft movement of the center of gravity on the tip tank decreased both flutter speed and flutter frequency.

5. While the FACES program has been shown to be a very useful analytical tool for wing/store flutter predictions, some suggestions are offered on further refinements, capability extensions, and applications as follows:

a. Flexible Empennage Capability - McDonnell Aircraft Company has recently been awarded an AFFDL contract to add a flexible empennage capability to FACES in response to Air Force system requirements. This is expected to be

completed by September 1978. With this additional capability, the FACES program will be able to analyze complete aircraft/external store configurations.

b. Aerodynamic Influence Coefficients (AIC's) - The FACES program could be improved by computing and storing within the program the AIC's for the doublet-lattice procedure. This would provide the capability to more rapidly perform multiple flutter calculations for various external store configurations at the same flight condition without repeating the lengthy doublet-lattice calculations. The capability to incorporate AIC's in FACES would greatly reduce the computation time and cost for analyses involving parametric trend investigations for multiple store loadings.

c. Supersonic Unsteady Aerodynamic Method - For flutter analyses involving external store carriage in the low supersonic speed range (up to about Mach 2.5), a three-dimensional supersonic unsteady aerodynamic method should be incorporated into the FACES program. The well-known Mach box procedure is a numerical three-dimensional method which represents the wing with a box grid having diagonals parallel to Mach lines. Also, other theoretical developments being pursued for this flow regime may prove to be worthy of consideration.

d. Finite Element Vibration Model - A finite element capability would be desirable within the FACES program for predicting vibration characteristics of low aspect ratio wings. Since the FACES program has the capability to use predetermined vibration data this could also be accomplished by interfacing FACES with an available finite element method.

e. Additional Verification of Flutter Prediction Method - Further applications of the FACES program would be desirable for correlation with available or future wind tunnel and flight unsteady aerodynamic and flutter data on aircraft/store combinations. Particular emphasis should be placed on the transonic speed regime which is often flutter critical and difficult to predict, and on those configurations where aerodynamic interference effects for the wing/pylon/store combinations would be significant.

REFERENCES

1. Siegel, S., and Andrew, L.V., "Evaluations of Methods to Predict Flutter of Wings with External Stores", AFFDL-TR-69-101, May 1970.
2. Mykytow, W.J., "Recent Analysis Methods for Wing-Store Flutter" in AGARD Conference Proceedings No. 162, Wing-With-Stores Flutter, Munich, Germany, 6-12 October 1974, Published April 1975.
3. Cross, A.K., and Albano, E.A., "Computer Techniques for the Rapid Flutter Clearance of Aircraft Carrying External Stores, Part I. Perturbation Theory and Applications", AFFDL-TR-72-114, Part I, February 1973.
4. Ferman, M.A. and Unger, W.H., "A New Approach for Rapid Flutter Clearance of Aircraft with External Stores", Aircraft/Stores Compatibility Symposium Proceedings, Sacramento, California, 18-20 September 1973.
5. Ferman, M.A. and Unger, W.H., "An Extension of the FACES Technique for Rapid Wing Store Flutter Clearance", Aircraft/Stores Compatibility Symposium, Arlington, Virginia, 2-4 September 1975.
6. Ferman, M.A., "An Extension of the Rapid Method for Flutter Clearance of Aircraft with External Stores", Volume I, "Theory and Application", AFFDL-TR-75-101, Volume I, November 1975.
7. Wilkinson, K. et al., "An Automated Procedure for Flutter and Strength Analysis and Optimization of Aerospace Vehicles", AFFDL-TR-75-137, December 1975.
8. Giesing, J.P., Kalman, T.P., and Rodden, W.P., "Subsonic Unsteady Aerodynamics for General Configurations", Part II, "Application of the Doublet-Lattice Method and the Method of Images to Lifting-Surface/Body Interference", AFFDL-TR-71-5, Part II, April 1972.
9. Giesing, J.P., Kalman, T.P., and Rodden, W.P., "Subsonic Unsteady Aerodynamics for General Configurations", Part I, Direct Application of the Nonplanar Doublet-Lattice Method", AFFDL-TR-71-5, Part I, November 1971.
10. Sewall, J.L., Herr, R.W., and Igoe, W.B., "Flutter Investigation of a True-Speed Dynamic Model with Various Tip-Tank Configurations", NASA-TN-D-187, March 1960.

11. Bleakney, W.M., "Vibration and Flutter Analysis, XP-80",
Lockheed Aircraft Corporation Report No. LR-4455, December
1940.

AUTOBIOGRAPHIES

Samuel J. Pollock

Mr. Pollock is an aerospace engineer in the Air Force Flight Dynamics Laboratory. He received a Bachelor of Aeronautical and Astronautical Engineering Degree from Ohio State University in 1961 and has completed the course requirements for a Master's in Engineering. In addition he has attended several short courses such as heat transfer, shell dynamics, computer graphics and nonstationery aerodynamics. For the past 16 years he has been project engineer on several efforts in the aeroelastic area. Mr. Pollock is the author of technical reports on the investigation of dynamic characteristics of inflatable structures and applications of unsteady aerodynamic methods. Recently, he has been project engineer on the development of methods for decreasing the time and cost of flutter prediction for clearance of aircraft carrying external stores. One of these methods, the FACES computer program, has been used extensively by Mr. Pollock at the AFFDL. In addition, Mr. Pollock has provided consultation to engineers using the FACES program to predict vibration and flutter for aircraft such as the A-10 and F-15 carrying external stores. Mr. Pollock is a member of the Scientific Research Society of North America.

Dale E. Cooley

Mr. Cooley is Technical Manager, Aeroelastic Group, Structural Mechanics Division, Air Force Flight Dynamics Laboratory, Wright-Patterson AFB, Ohio. His duties include planning, establishing and directing research and development programs in the field of prediction and prevention of aeroelastic instabilities in flight vehicles. He received a Bachelor's Degree in Aeronautical Engineering from Wichita State University, and a Master's Degree in Aeronautical and Astronautical Engineering from Ohio State University. Mr. Cooley has worked at The Boeing Company, Wichita, Kansas, and has been with the Air Force research and development laboratories at Wright-Patterson AFB, Ohio since 1955. Mr. Cooley is a member of the American Institute of Aeronautics and Astronautics and the Scientific Research Society of North America.

INVESTIGATION OF THE UNSTEADY AIRLOADS
ON WING-STORE CONFIGURATIONS IN
SUBSONIC FLOW

(U)

(Article UNCLASSIFIED)

by

J.W.G. van Nunen
R. Roos
J.J. Meijer
National Aerospace Laboratory NLR
Anthony Fokkerweg 2
1059 CM Amsterdam
The Netherlands

ABSTRACT.(U) A description and results are given of an extensive research program set up to determine the unsteady aerodynamic loading on oscillating wing-store configurations. It is shown that the tools developed in the course of the program allow for a more accurate prediction of the unsteady airforces introduced by wing mounted stores.

"Approved for public release; distribution unlimited."

This investigation was carried out under contract for the Scientific Research Branch, Air Materiel Directorate, Royal Netherlands Air Force, (RNLAFF).

This paper was presented also at the AGARD Fluid Dynamics Panel Symposium on "Unsteady Aerodynamics", Ottawa, Canada, 26-28 September 1977.

LIST OF FIGURES

- Figure 1 : Schematic outline of the NLRI-method
- Figure 2 : Model of the wing with tip tank and store mounted in the testsection of the wind tunnel
- Figure 3 : Sketch of the wing/tip tank/store configuration
- Figure 4 : Chordwise distribution of the unsteady pressure jump across the wing near the tip tank
- Figure 5 : Unsteady pressure distribution along the tip tank
- Figure 6 : Unsteady normal load distribution along the tip tank
- Figure 7 : Unsteady normal load distribution on the wing for the different configurations
- Figure 8 : Unsteady pressure distribution along the store
- Figure 9 : Unsteady normal load distribution along the store
- Figure 10: Unsteady side load distribution along the store
- Figure 11: Sketch of the flutter model
- Figure 12: Experimental flutter results for the model
- Figure 13: Comparison between theoretical and experimental flutter results for the wing only
- Figure 14: Comparison between theoretical and experimental flutter results for the wing with tip tank
- Figure 15: Comparison between theoretical and experimental flutter results for the wing with tip tank and under-wing store
- Figure 16: Comparison of theoretical and experimental flutter results for an aircraft equipped with stores

LIST OF SYMBOLS

- [A] submatrix of aerodynamic influence coefficients
- a velocity of sound
- C_p unsteady pressure coefficient ; $C_p = p_i s / q_\infty d$
- C_y local side load coefficient ; $C_y = \text{side load} / q_\infty \ell$
- C_z local normal load coefficient ; $C_z = \text{normal load} / q_\infty \ell$
- c local chord
- \bar{c} mean chord
- c_r root chord
- d displacement of reference point ($x/c=0.871$, $y/s=0.143$)
- f frequency ; $f = \omega / 2\pi$
- k reduced frequency ; $k = \omega s / U_\infty$
- ℓ reference length ; wing : $\ell = c$, body : $\ell = \text{max.diam.}$
- M Mach number
- p_i unsteady pressure
- p_o stagnation pressure
- \vec{q} velocity vector
- q_∞ dynamic pressure
- S surface of wing or body
- s semi span
- t time
- U_∞ free stream velocity
- x, y, z right-hand cartesian coordinate system
- ΔC_p unsteady pressure jump between the lower and upper wing surface
- ξ angular coordinate on the body
- σ source strength
- ϕ velocity potential
- ϕ perturbation velocity potential
- ω oscillation frequency

Superscripts

- B referring to the body
- D referring to the lifting surface
- ' referring to the component in phase with the motion
- " referring to the component in quadrature with the motion

Subscripts

- o referring to the steady flow field
- 1 referring to the unsteady flow field
- ∞ referring to the freestream conditions

1. INTRODUCTION

In the last decade the development of military aircraft has shown a clear tendency towards larger stores, being carried in close proximity to the wing and the fuselage. To investigate the implications of this on the aeroelastic characteristics of an aircraft (flutter, gust response and manoeuvring loads), the NLR has carried out an extensive research program. This program was focussed on an accurate determination of the unsteady aerodynamic loading on complex wing-store configurations. It consisted of three distinct parts:

1. the development of a calculation method to compute the unsteady loading on such oscillating configurations
2. unsteady pressure measurements on an oscillating wing-tip tank-store wind tunnel model
3. the verification of the calculation method in a series of flutter tests, both with the (adapted) wind tunnel model and with the real aircraft.

In this paper the different facets of this research program are touched upon. First a short outline of the calculation method is given, followed by a description of the experimental investigation on the unsteady pressure distributions. Results of these tests are shown in a comparison with theoretically obtained unsteady pressure and load distributions. Finally, both flutter experiments are described and their results are compared with flutter data obtained by using theoretically determined aerodynamic loads.

2. THE "NLRI" CALCULATION METHOD

2.1 General observations

Until recently the unsteady loading on oscillating airplane configurations was approximated by "thin wing theory", such as lifting surface or lifting lattice techniques. The effects introduced by the fuselage and/or the stores were neglected or taken into account by using slender body theory. Kalman, Rodden and Giesing (Ref. 1) were the first to attempt a more thorough computation of wing/body interference effects. Lately, their original ring-wing concept as applied in the doublet lattice method has evolved into a more complete method (Ref.2), which can be expected to produce satisfactory results as far as unsteady aerodynamic coefficients are concerned. Recently, Morino et al (Ref. 3 and 4) have developed a computer program, which can treat complex configurations in steady and unsteady, subsonic and supersonic flow. As far as unsteady flow is concerned, an evaluation of both methods still awaits a comparison with experimental data for a complex wing/body configuration.

The method developed at NLR (NLRI-method) is set up to meet two requirements. It should provide:

1. the unsteady aerodynamic forces on wing/body configurations for aeroelastic analysis
2. detailed pressure distributions to support unsteady wind tunnel measurements and to obtain more information about the distribution of the loading over the configuration.

This means that the method has to compute both local and overall aerodynamic coefficients and generalized aerodynamic coefficients as well as detailed pressure distributions on both the body and the wing. These requirements have been met by combining the already existing doublet-lattice method with an unsteady source panel method.

The next chapter gives a short outline of the NLRI-method. For a more detailed description of the method and its formulations, the reader should consult references 5 and 6.

2.2 Outline of the method

The flow field about a configuration is described with a velocity potential $\phi = U_\infty x + \varphi$. The perturbation potential φ satisfies the linearized equation:

$$(1-M_\infty^2)\varphi_{xx} + \varphi_{yy} + \varphi_{zz} - \frac{1}{a_\infty^2}\varphi_{tt} - \frac{2M_\infty}{a_\infty}\varphi_{xt} = 0. \quad (1)$$

The flow is assumed to remain tangential to the surface of the configuration as is expressed by the boundary condition

$$\frac{DS}{Dt} = \frac{\partial S}{\partial t} + \vec{q} \cdot \nabla S = 0 \quad (S=0) \quad (2)$$

in which $S(x,y,z,t) = 0$ describes this surface. The configuration is taken to perform harmonic oscillations about a steady mid-position. Therefore the perturbation potential φ is split into a steady part φ_0 and an unsteady part $\varphi_1 e^{i\omega t}$. This results in a decoupling of the steady and the unsteady flowfields, for which the governing equations can be reduced to the Laplace equation and the Helmholtz equation respectively. The solution for both flow fields can be found in terms of an integral over a source distribution on the surface of the configuration and a dipole distribution on the camber surface and the wake. The strength of these distributions is found by applying boundary condition (2) in which now S represents the surface of the harmonically oscillating surface. The result is a set of integral equations for both the steady and the unsteady flow field, of which for practical applications a solution can be found only with a panel method approach.

The approach used here is a combination of a lifting lattice method for the lifting surfaces and a constant source panel method for the bodies. In particular for the unsteady flow field the choice fell on the well-known doublet-lattice method and an unsteady source panel method of the type described by Hess (Ref. 7). The doublet-lattice method is chosen because of its established success and flexibility in applications on interfering lifting surfaces. The constant source panel method is preferred in view of the experience available at the NLR with this method for steady flow fields.

With the discretization in panels the integral equations are reduced to sets of algebraic equations which in matrix form read:

$$\begin{bmatrix} A^{BB} & A^{BD} \\ A^{DB} & A^{DD} \end{bmatrix} * \begin{bmatrix} \sigma \\ \Delta C_p \end{bmatrix} = \begin{bmatrix} F^B \\ F^D \end{bmatrix} \quad (3)$$

with σ being the yet unknown source strengths on the body panels (B) and ΔC_p the group of lifting line strengths (equivalent to the pressure jump across the surface) for the 1/4-chord lines of each lifting surface panel (D). F^B and F^D stand for the prescribed normal velocity (boundary condition) in all collocation points of respectively the body and lifting surface panels. The matrix of aerodynamic influence coefficients is partitioned into four submatrices. The coefficients in the submatrices $[A^{BB}]$ and $[A^{DB}]$, which represent the normal velocity induced by a body panel with a unit source strength, are computed with the formulations of the constant source panel method for respectively steady and oscillatory flow. The coefficients in the submatrices $[A^{BD}]$ and $[A^{DD}]$ represent the normal velocity induced by a lifting surface panel with a lifting line of unit strength. These are computed following the lines of the vortex and doublet lattice methods.

For the solution of the matrix equation a method is used based on the expected properties of the submatrices. First the subset of equations containing $[A^{BB}]$ is solved with an iterative Gauss-Seidel process. Then, the residue is determined and used to solve the set containing $[A^{DD}]$ with a direct Crout process. The residue is determined again and the process is started from the beginning. This iteration process is repeated several times until the increment, which during each run is added to the solution of σ and ΔC_p , has become smaller than a certain value. A relaxation factor takes care of large oscillations during the first few iteration steps.

From the computed source strength σ the velocity and pressure distribution on the bodies can be determined while the pressure jump ΔC_p across the lifting surfaces is known already. Integration leads to both local and overall aerodynamic coefficients.

A schematic diagram, indicating the important steps in the calculation method is given in figure 1. As was mentioned before dividing the perturbation potential in a steady and an oscillatory part results in a decoupling of the steady and unsteady flow fields. As indicated in figure 1, the coupling is restored if in the unsteady boundary condition and the expression for the unsteady pressure at the body surface the effects of the local changes in the steady flow field due to the presence of the bodies are taken into account. The realization of this coupling requires the computation of second order derivatives of the steady perturbation potential, which on certain parts of the configuration turn out to violate the small perturbation assumption (the first derivative remains small). Clearly a constant source panel method is not suited to compute higher order derivatives. Therefore in the computations which yielded the results mentioned in this paper, the coupling was ignored, which means that first order boundary conditions and pressure formula were used.

3. UNSTEADY WIND TUNNEL MEASUREMENTS

3.1 The experiment

To obtain an insight into the aerodynamic consequences of the addition of stores on a wing oscillating in subsonic flow and further to have a first check on results computed with the NLRI-method, a wind tunnel experiment was performed. The model concerned was a swept tapered wing equipped with a tip tank and a detachable under-wing store (see figure 2). A sketch of the model, showing the planform and its overall dimensions is given in figure 3.

The model could be driven into sinusoidal pitching oscillations with adjustable frequencies and two locations of the pitch axis (15% and 50% of the root chord). To determine the vibration mode of the model during the tests, the wing and stores were equipped with miniature accelerometers. Using the NLR unsteady pressure measuring system, which employs pressure tubes connected to scanning valves, a detailed mapping of the unsteady pressure distribution was obtained on the wing as well as on the tip tank and the store. The number of pressure orifices totalled 160 on the wing, 78 on the tip tank and 86 on the under-wing store. Dynamic calibration of the measuring system was provided by some miniature pressure transducers built in the wing.

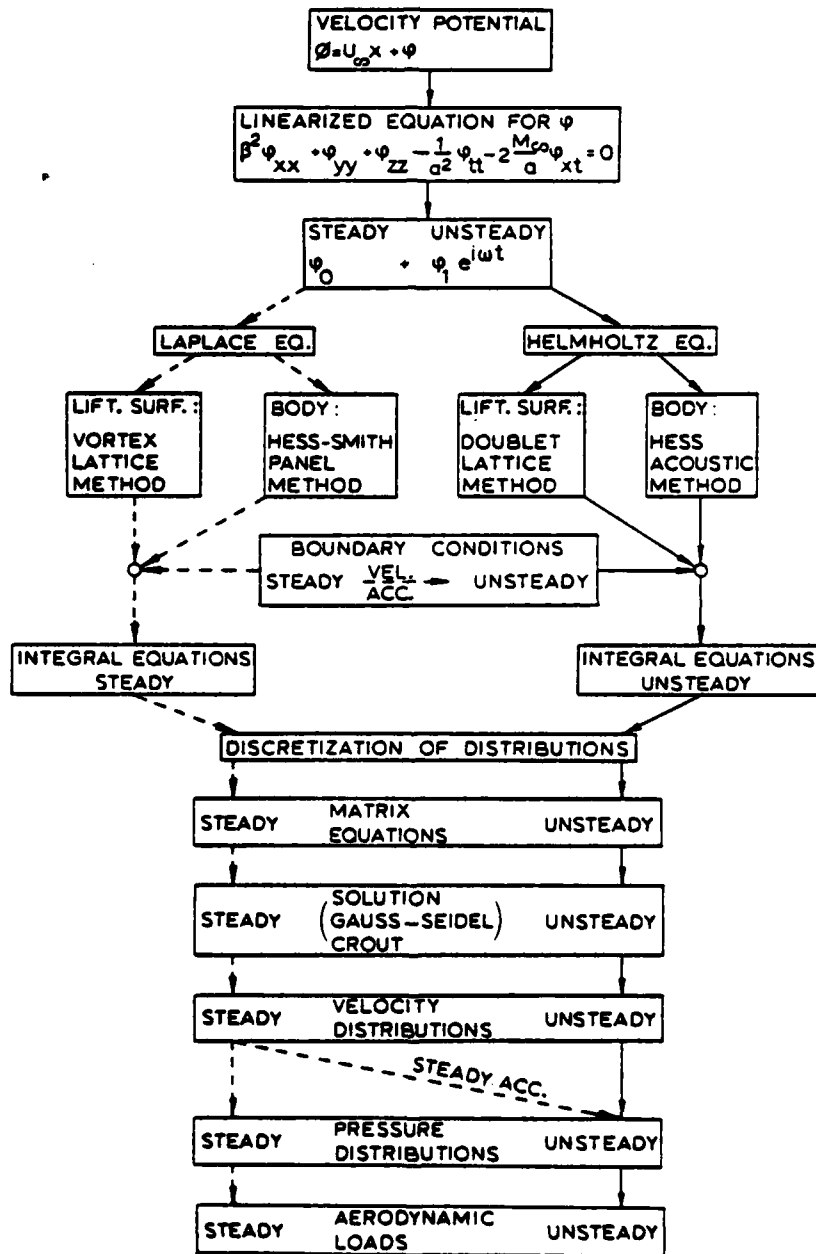


Figure 1 : Schematic outline of the NLRI-method

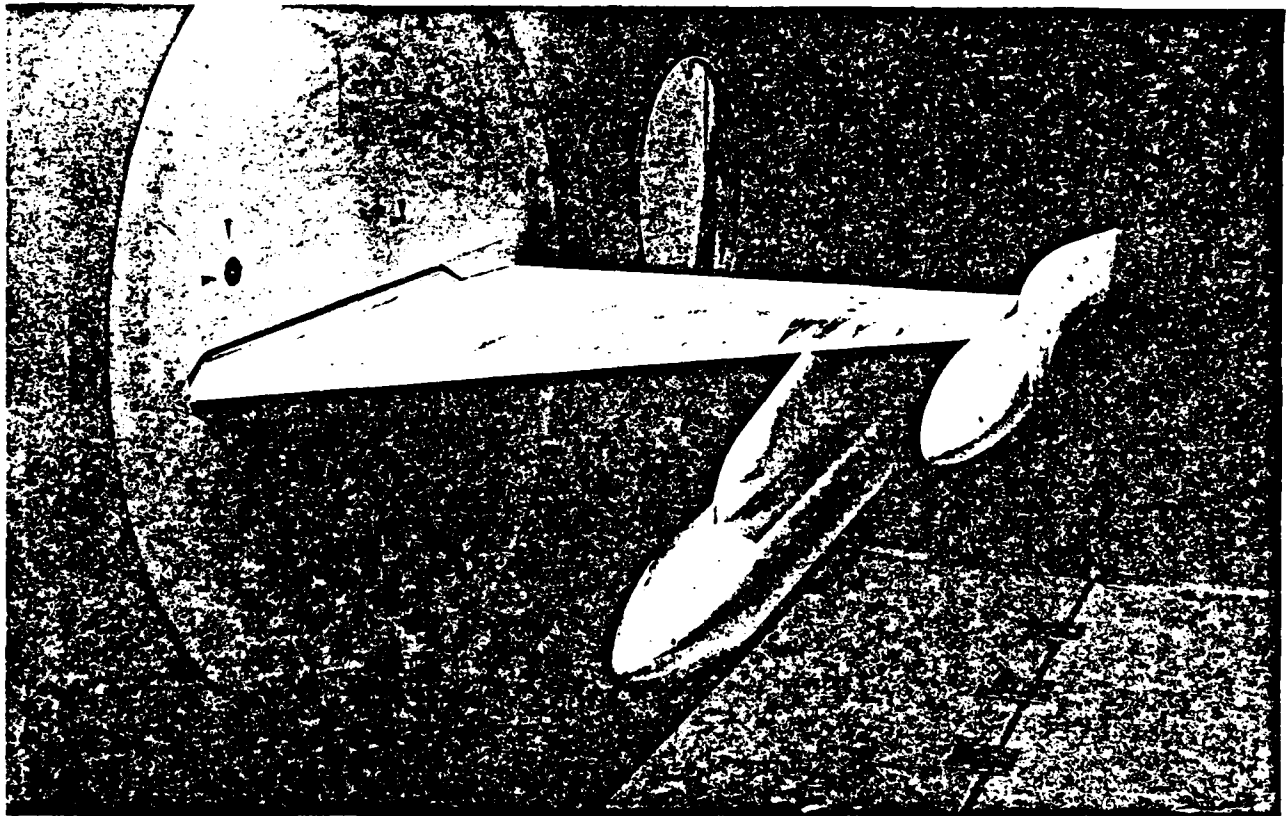


Figure 2: Model of the wing with tip tank and store mounted in the testsection of the wind tunnel

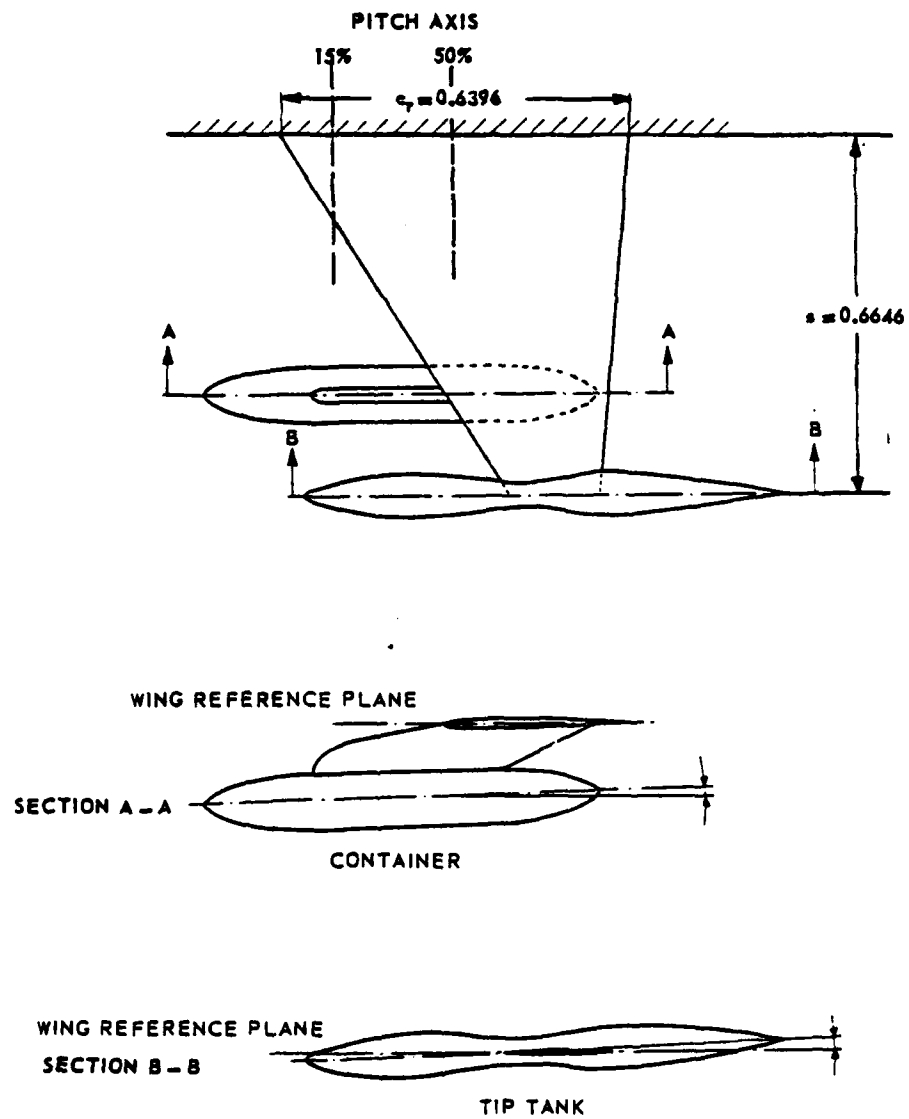


Figure 3 : Sketch of the wing/tip tank/store configuration

The measurements were carried out for several combinations of Machnumber, frequency and pitch axis location. Further all tests were run for two model configurations: wing with tip tank and wing with tip tank and under-wing store.

A more detailed description of the experiment was given by Renirie (Ref.8), who also presented some preliminary data. In this paper a few additional results, taken from reference 6, are shown. Here the data are used as a check on the results obtained with the aforementioned NLRI-method.

3.2 Comparison of experimental and theoretical results

The results presented next concern both configurations, with and without store, pitching about the 15% chord axis with a frequency of 11 Hz at a Machnumber 0.45.

For the wing with tip tank figure 4 contains the chordwise distribution of the unsteady pressure jump ΔC_p across the wing in a section close to the tip tank. The experimental data are seen to be in satisfactory agreement with the theory. Since the model tip tank was not detachable its influence could not be determined separately, but the computed results for the wing with and without tip tank show this influence clearly. Apparently addition of the tip tank results in an increase of the pressure jump near the wing tip.

The measured and calculated pressure distribution in axial direction on the tip tank (fig. 5) shows a rather good agreement except at the rear where in reality separation is present. Both theory and experiment show the influence of the wing in terms of the relatively large pressures near the attachment position. Integration of the pressure distribution in angular direction leads to the unsteady normal force distribution presented in figure 6.

Figure 7 shows the spanwise unsteady normal load distribution for the two different configurations. The theoretical curves show that the tip tank acts as an endplate, preventing the loading to go to zero at the tip. Addition of the pylon and store under the wing is seen to introduce a jump in the spanwise load distributions. This jump indicates that circulation is carried off by the pylon towards the store. As a result of this, the pylon and store will experience an outward pointing side load. Although the magnitude of the jump and the trend of the theoretical and experimental curves are about the same, the overall level of the measurements is somewhat lower, at least for the in phase loading. This feature is common for "flat plate" theories, which exhibit an infinite pressure peak at the leading edge.

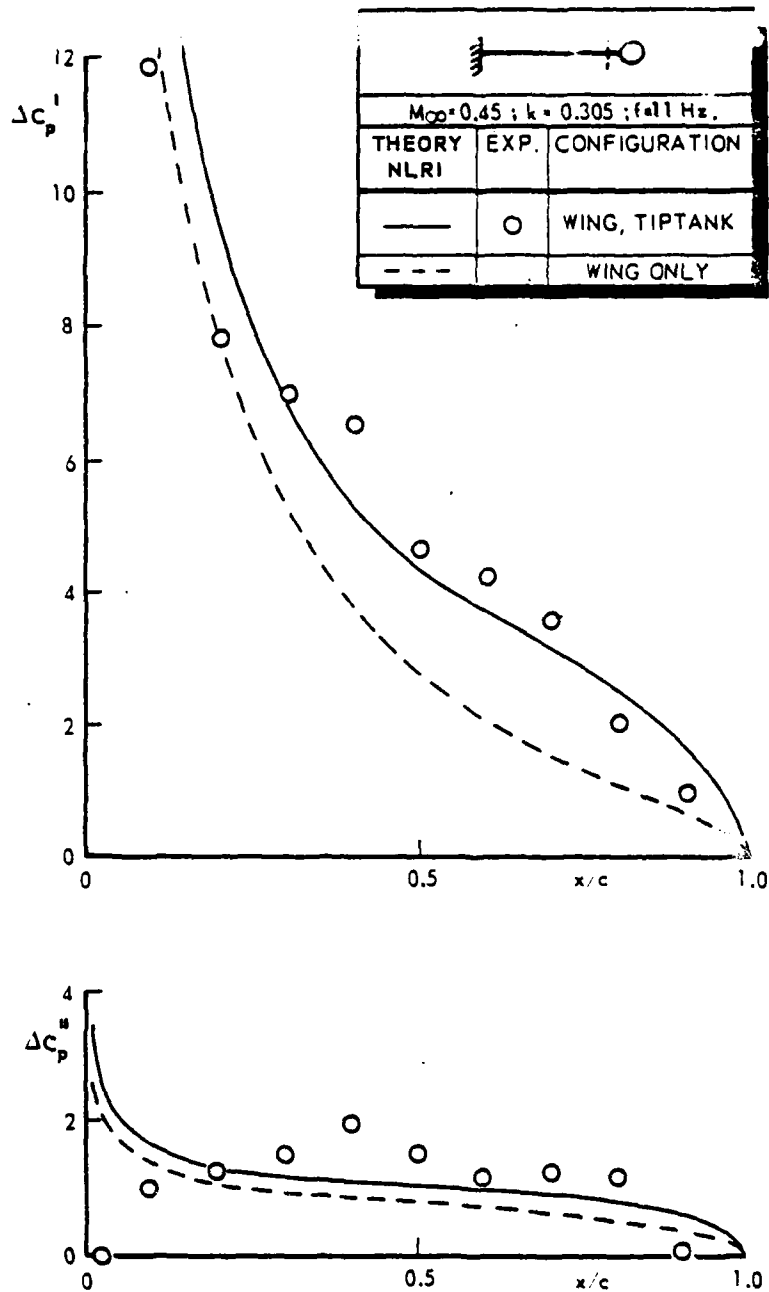
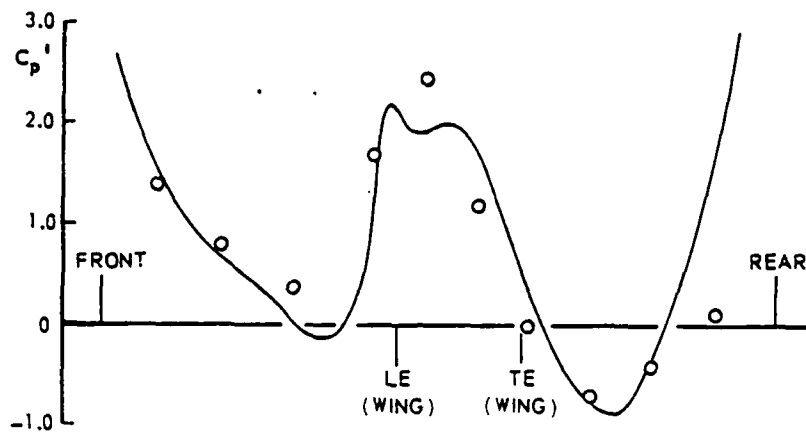


Figure 4 : Chordwise distribution of the unsteady pressure jump across the wing near the tip tank



$M_\infty = 0.45$
 $k = 0.305 ; f = 11 \text{ Hz}$
 ○ EXPERIMENT
 — THEORY NLRI

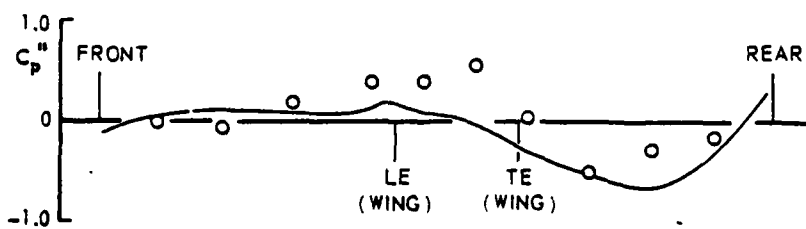
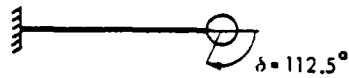
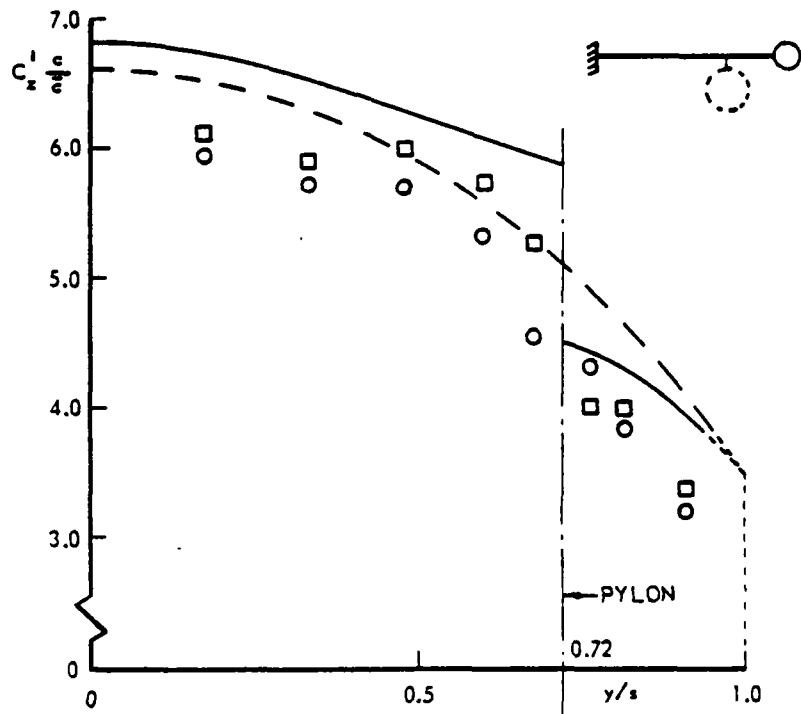


Figure 5 : Unsteady pressure distribution along the tip tank



$M_{\infty} = 0.45 ; k = 0.305 ; f = 11 \text{ Hz.}$

THEORY	EXP.	CONFIGURATION
—	□	WING, TIPTANK
- - -	○	WING, TIPTANK PYLON, STORE

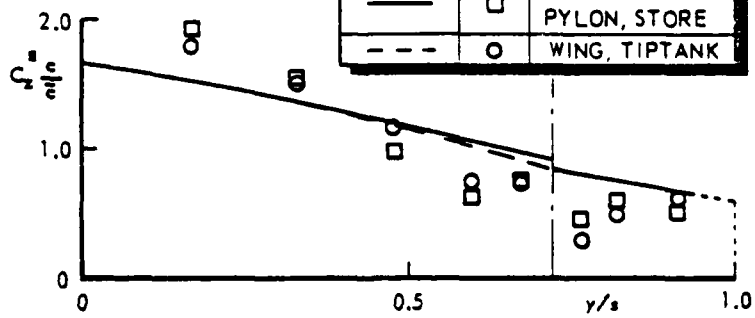


Figure 7 : Unsteady normal load distribution on the wing for the different configurations

An example of an unsteady pressure distribution along the under-wing store is given in figure 8. The agreement between experiment and theory is rather satisfactory except near the rear of the store where separation is present. The calculations made for the isolated store and the wing with the store only show that the presence of the wing and pylon introduces a marked interference, which is largest near the attachment of the pylon with a maximum near the wing leading edge. Adding the tip tank has only a marginal effect.

In figure 9 and 10 the normal and side load distributions along the store are presented for the same three configurations. On the isolated store the normal load distribution is antisymmetrical, reflecting the fact that the front and rear end are identical. In figure 10 the isolated store is missing since for a rotational symmetric body the side load is zero. Interference effects introduced by wing and pylon are clearly visible in both figures. The side load on the store is in agreement with the observations made on the jump in the normal load distribution on the wing.

When comparing the load distributions on the wing, the tip tank and the store it is essential to notice that they are nondimensionalized in a different way. The scaling factors are given in the figures. For the case considered here (15% pitch axis) it is found that the loading on the tip tank and store is of the order of 7% to 10% of the wing loading. However, as will become evident in the last part of this paper, this does not necessarily mean that these loadings can be neglected in aeroelastic calculations.

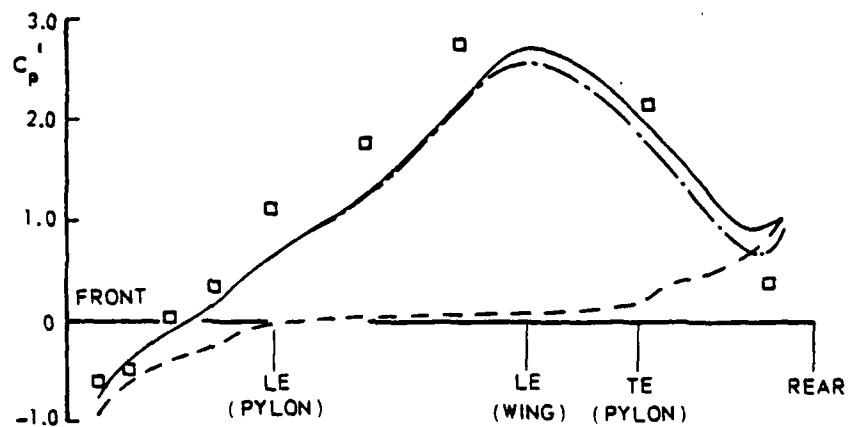
4. FLUTTER TESTS

4.1 General

Considering the reasons for developing the NLRI-method, a further check on the quality of the results of this method was obtained by applying them in a flutter investigation. To acquire data for comparison, flutter experiments were carried out on complex configurations to which it was sensible to apply the NLRI-method. These experiments consisted of flutter test in the wind tunnel on the model previously used for the unsteady pressure measurements, as well as a series of flight tests with the aircraft on which the model was based (except for a difference in under-wing store). In the following these tests are discussed shortly and the data are compared with results of flutter calculations with aerodynamic input from the NLRI-method.

4.2 Model experiments

To convert the model, used for the pressure measurements, into a simple flutter model its suspension mechanism was modified



$M_{\infty}=0.45 ; k=0.305 ; f=11 \text{ Hz.}$

THEORY NLRI	EXP.	CONFIGURATION
—	□	WING, TIPTANK PYLON, STORE
- - -		WING, PYLON, STORE
- - -		STORE ONLY

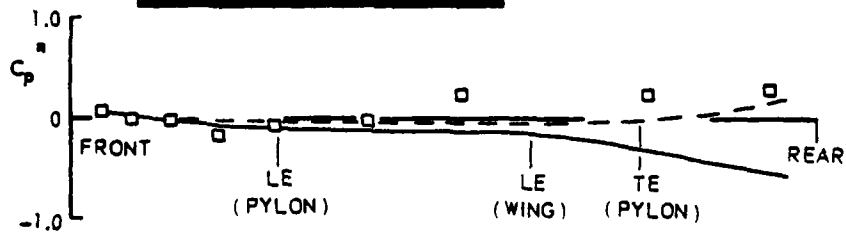


Figure 8 : Unsteady pressure distribution along the store

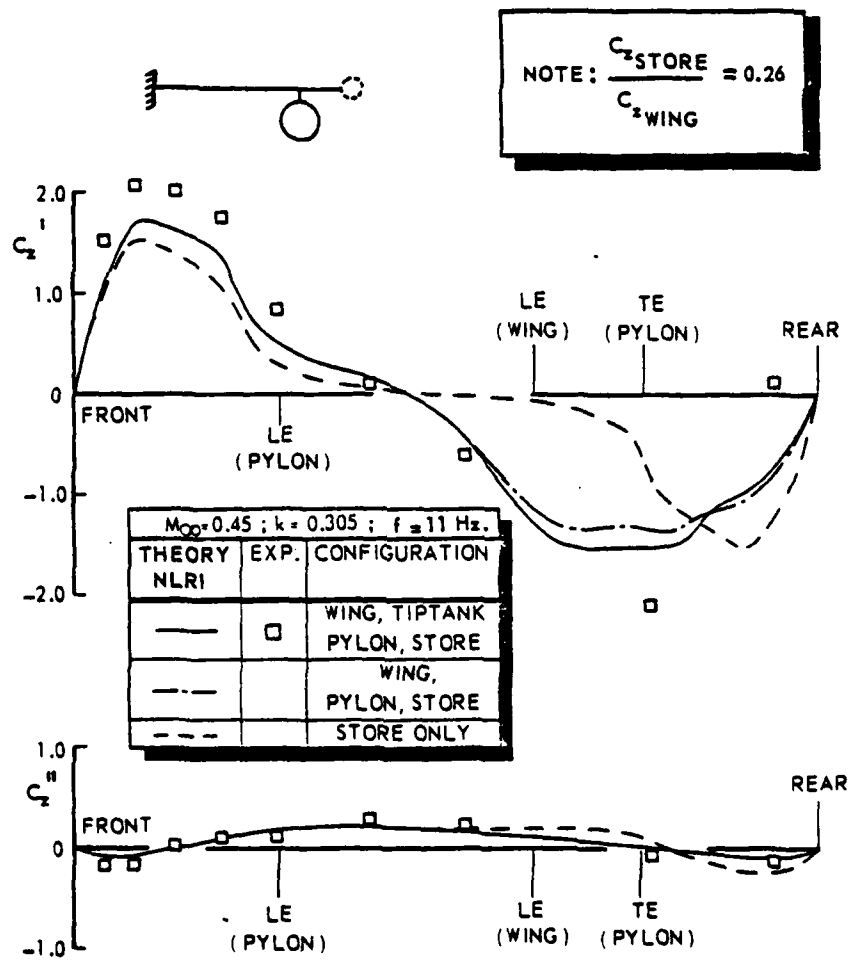
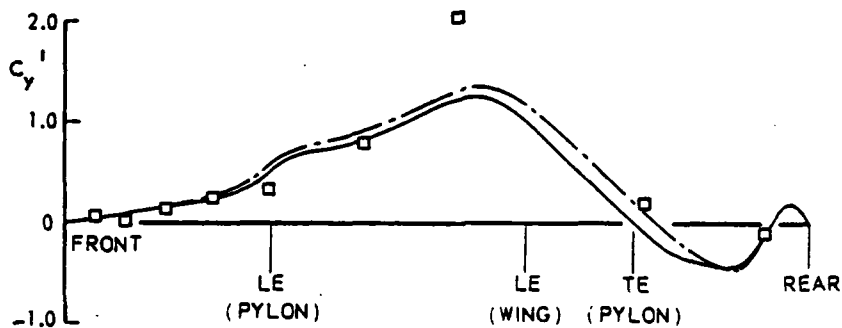


Figure 9 : Unsteady normal load distribution along the store



NOTE: $\frac{C_{y\text{STORE}}}{C_{z\text{WING}}} = 0.26$



$M_{\text{op}} = 0.45 ; k = 0.305 ; f = 11 \text{ Hz.}$

THEORY	EXP.	CONFIGURATION
—	□	WING, TIPTANK PYLON, STORE
- - -		WING, PYLON, STORE

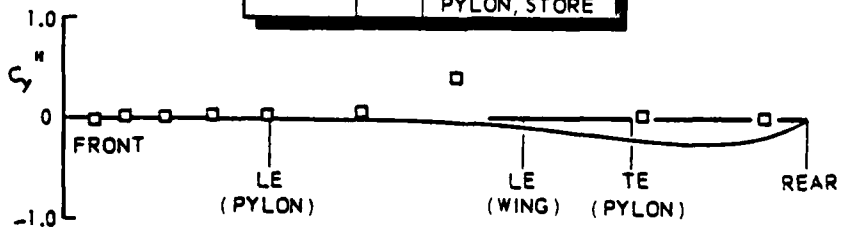


Figure 10 : Unsteady side load distribution along the store

(see fig. 11). The root of the model was suspended in a set of elastic springs resulting in a two degree of freedom system: pitch and roll. The stiffness of the springs was designed such, that a flutter condition could be reached within the test limits of the variable density wind tunnel HST of the NLR. A further requirement, set to the stiffness of the springs, was that the resonance frequencies of the model remained within the range of frequencies covered in the earlier unsteady pressure measurements. Moreover, at these frequencies the model itself could be regarded as almost stiff thus leading to rather simple vibration modes.

In order to get as complete a check on the NLRI-procedure as possible the model was tested in three different configurations: the plain wing, the wing with tip tank and finally the wing with tip tank and under-wing store. All three configurations were tested at about the same resonance frequencies and vibration modes. This was achieved by replacing the tip tank and the pylon-store combination, when not present, by additional masses outside the airstream, thus keeping the inertia characteristics the same. In this manner all differences in the flutter behaviour of the three configurations should in principle be attributed to the variations in the unsteady aerodynamics as caused by the presence of the bodies and not to the combined variation of unsteady aerodynamics and inertial characteristics.

Finally the flutter experiments were carried out at a constant Mach number but varying stagnation pressure. The Mach number was fixed at $M_{\infty} = 0.7$ in order to avoid transonic effects, which are not included in the unsteady aerodynamic theory.

The results of the flutter experiments performed on the three configurations are gathered in figure 12. This flutter diagram gives the behaviour of the hysteresis damping and frequency of the various modes as a function of the stagnation pressure at a constant Mach number. It should be mentioned that the results shown are obtained by averaging the data of several repeated tests. Further, all wind tunnel tests were carried out for conditions below the actual flutter points. The latter were determined by applying the method of Zimmerman and Weissenburger (Ref. 9).

From figure 12 it can be observed that the flutter behaviour of the three configurations is very different indeed. While the two frequencies and the damping for the bending mode remain relatively unaffected by the change in configuration, the damping for the torsion mode and the predicted flutter point vary considerably. The more complex this configuration becomes, the lower the damping in torsion and the lower the stagnation pressure required for flutter will be.

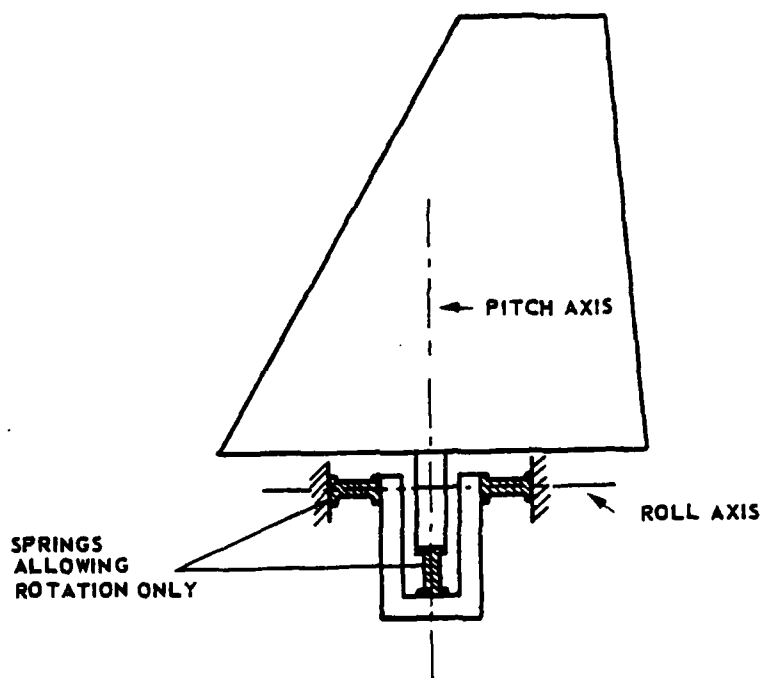


Figure 11 : Sketch of the flutter model

Evidently this effect is caused by the unsteady aerodynamic loads generated by the external bodies, for the differences in inertial characteristics between the various configurations are made negligibly small.

A comparison between the theoretical and experimental flutter characteristics is presented in fig. 13 through 15. In the first plot (fig. 13) the flutter diagram is shown for the bare wing. As can be expected the agreement between computed and measured flutter behaviour is rather good. Both resonance frequencies and the development of the corresponding dampings are predicted very well. Only at higher stagnation pressures a small difference between theoretical and experimental results can be observed. Then the two vibration modes appear to couple less in theory than in the experiment and as a consequence the theoretical flutter point occurs at a higher stagnation pressure than when predicted on the basis of the subcritical experimental data points. Thus the unsteady aerodynamic forces appear to be a little more effective than predicted by theory. In this respect it should be noted that when the results are transformed to actual flight speed, these differences amount to not more than about 3 per cent. This means that for the purpose of flutter speed prediction an excellent agreement is obtained.

The theoretical and experimental flutter results for the configuration of the wing with tip tank are compared in figure 14. Although the trend is predicted correctly, the agreement is not as good as in the case above. The theory predicts flutter to occur at a lower stagnation pressure than indicated by the experimental data. Apparently, the unsteady aerodynamic forces are slightly overestimated by the theory.

To find out to what extent the unsteady aerodynamic forces generated by the tip tank itself contribute to the flutter behaviour of the present configuration, additional calculations were performed in which the unsteady aerodynamic loads on the tip tank were omitted. The unsteady interference loads from the tip tank onto the wing were not excluded. Although the flutter characteristics develop in the same manner as before (fig. 14), the difference in the damping curves of the two vibration modes is remarkable. The stagnation pressure at which flutter is predicted has shifted considerably: from about $p_0 = 1.53$ bar for the case the unsteady loads on the tip tank are taken into account to about $p_0 = 1.76$ bar for the case these loads are omitted from the calculations. Apparently the unsteady aerodynamic loads on the tip tank decrease the dynamic pressure at which flutter is encountered by about 12%.

$M_{CO} = 0.7$	
EXP.	AERO. THEORY: DL
X +	COMPL. CONFIG.

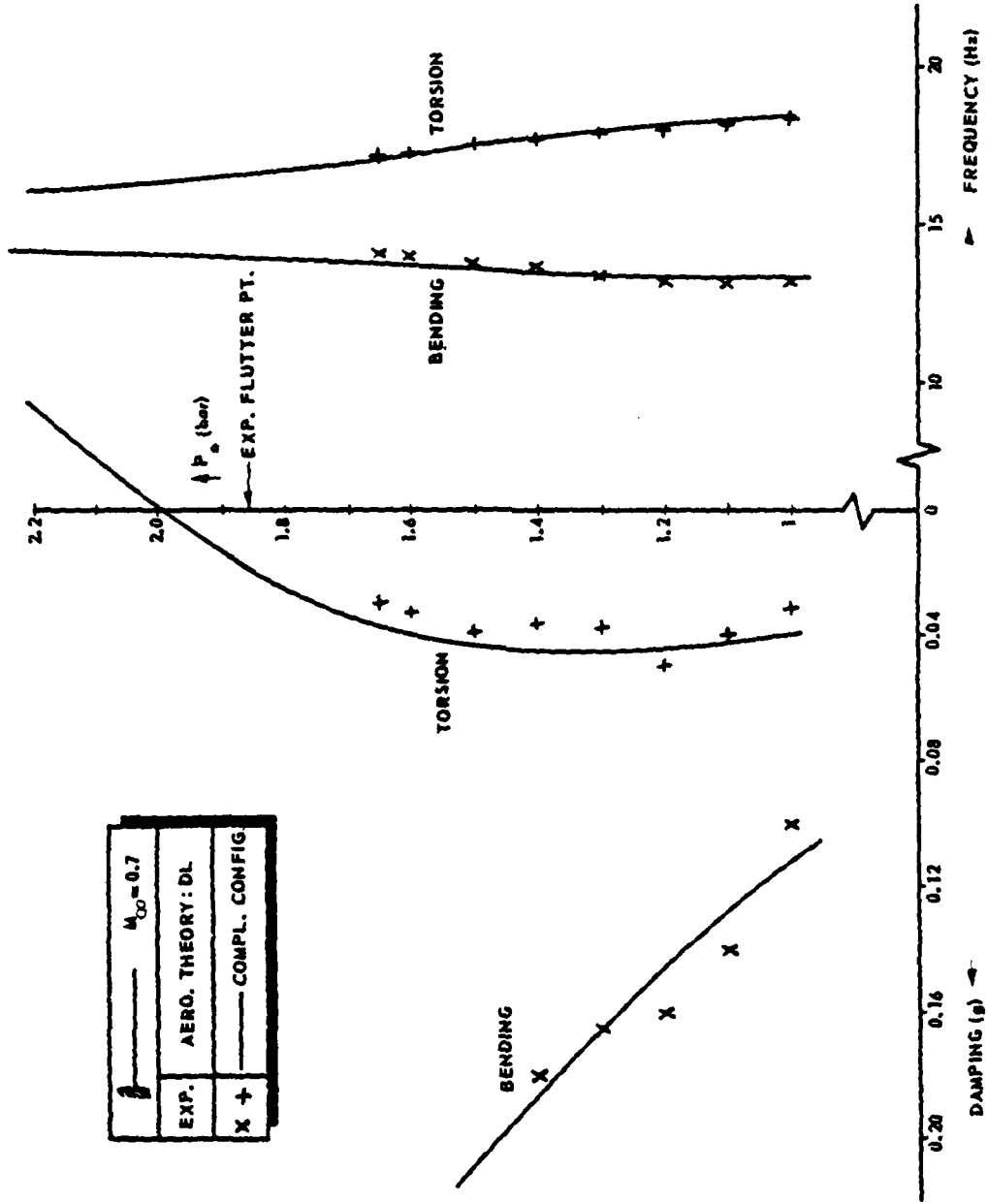


Figure 13 : Comparison between theoretical and experimental flutter results for the wing only

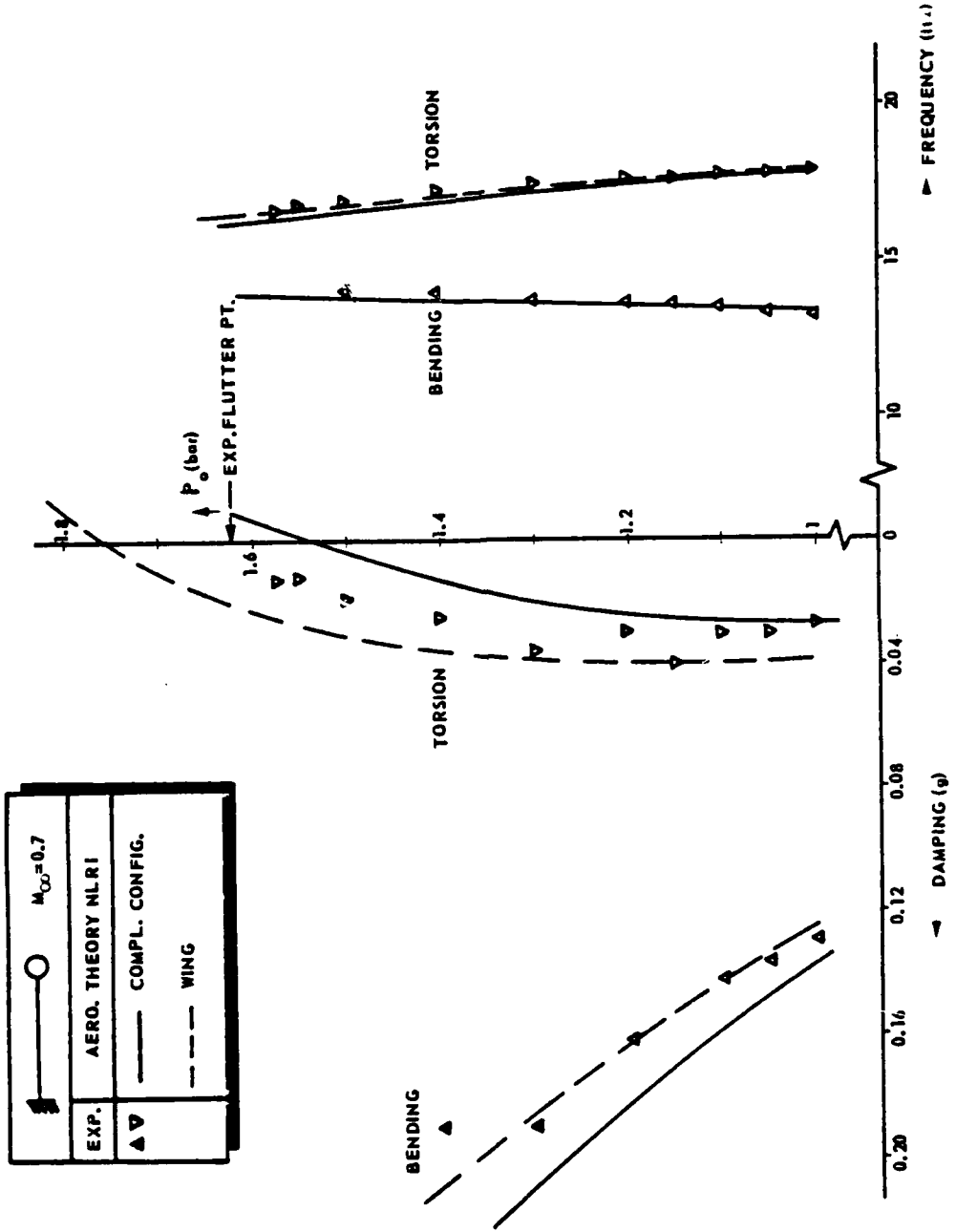


Figure 14 : Comparison between theoretical and experimental flutter results for the wing with tip tank

The flutter results for the wing with tip tank and pylon-store combination are presented in fig. 15. When comparing the experimental data with the results predicted by theory, again a rather good agreement is found, so that the experiments lead to a lower flutter stagnation pressure than predicted by theory. For this configuration the unsteady aerodynamic loads are slightly underestimated by the theory.

For this configuration also it was analysed to what extent the flutter characteristics are governed by the unsteady aerodynamic loads on the externally mounted bodies. To that end two sets of additional calculations were performed: firstly, flutter calculations in which the unsteady aerodynamic loads on both the tip tank and the store were omitted and secondly calculations with only the unsteady loads on the tip tank omitted. In both cases the interference loads from tip tank and store onto the wing were taken into account. The results of these calculations are incorporated in fig. 15. As can be expected from comparison with the previous configuration, the omission of the unsteady loads on the external bodies leads to more stable configurations. When the aerodynamic forces on the tip tank are omitted, the stagnation pressure at which flutter is predicted goes up from about $p_0 = 1.3$ bar to about 1.5 bar. Neglecting the aerodynamic loading on the under-wing store also causes the pressure to rise to about $p_0 = 1.65$ bar, which compared to the complete configuration means an increase of 25 per cent. Comparing these figures it may be observed that some 40% of the difference between the configuration with and without external bodies can be attributed to the unsteady aerodynamic loads on the store under the wing. Evidently the remaining 60% of the difference is due to the unsteady loads on the tip tank. The cause for this is very much related to the location of the two bodies as compared to the two vibration modes of the model.

4.3 Flight tests

The flight flutter tests were performed on a fighter airplane of which the wings were equipped with a tip tank and two external stores mounted at two separate wing stations: an outboard and an inboard station. The test data were gathered at a constant altitude and varying Mach number.

The two basic vibration modes that are important here, are: first wing bending and first wing torsion. In both cases the tip tank exhibits a considerable amount of pitch roughly about its midpoint.

An illustrative result of these flight flutter tests is presented in fig. 16. It concerns the flutter characteristics for a flight Mach number of $M_\infty = 0.8$. The theoretical results in figure 16 have become available from flutter calculations in

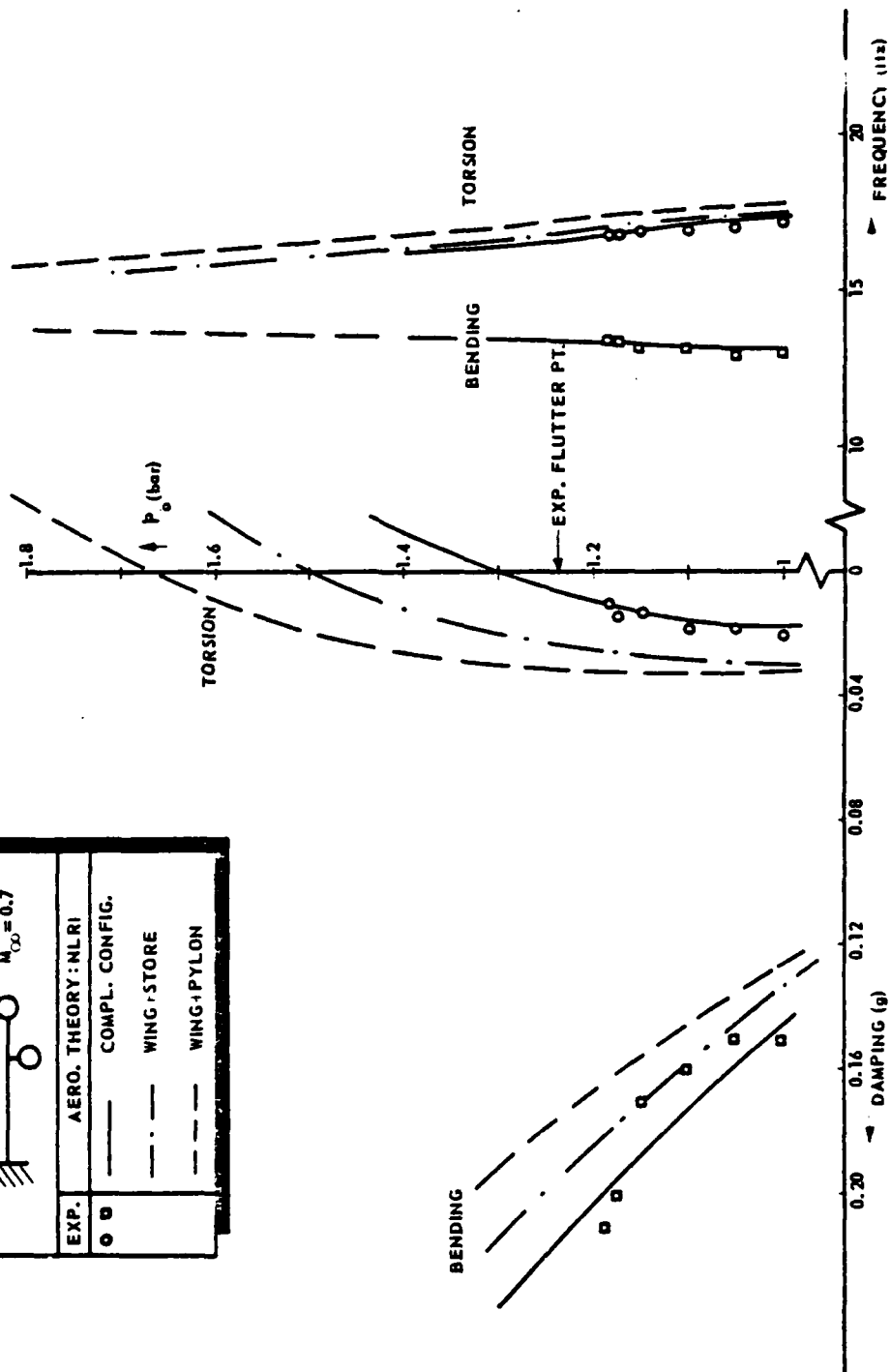
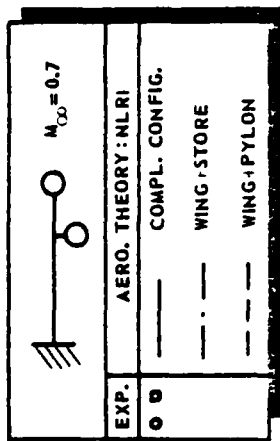
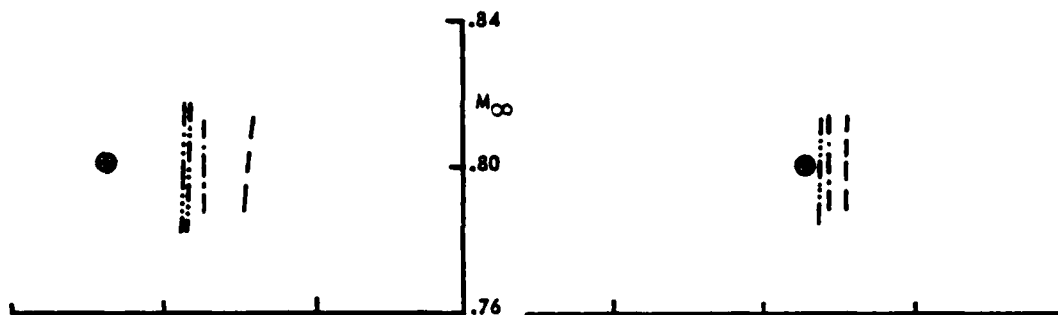
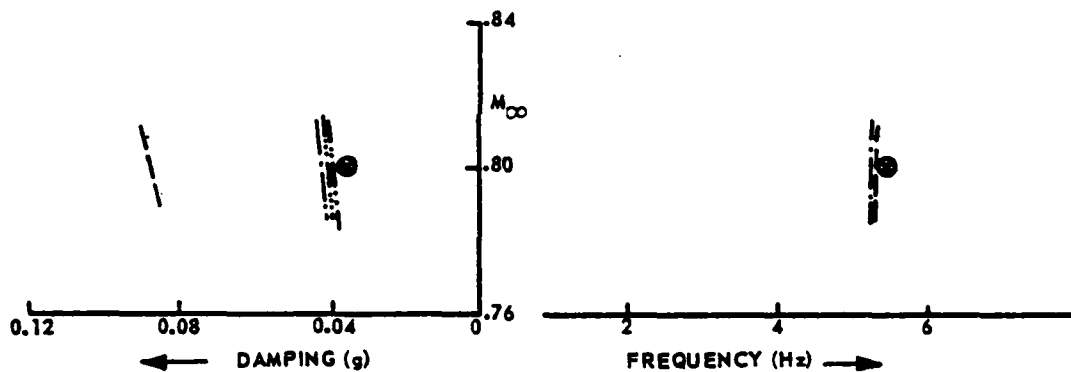


Figure 15: Comparison between theoretical and experimental flutter results for the wing with tip tank and under-wing store

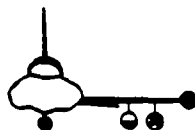
FIRST WING TORSION



FIRST WING BENDING



CONFIGURATION



ALT. : 5000 ft

FLIGHT TESTS ● ●

THEORY: $M_{\infty} = .8$

AEROD. LOADS METHOD :

----- DL : WING ONLY

- - - - - NLRI : WING+TIPTANK

..... NLRI : WING+TIPTANK+INBOARD STORE

———— NLRI : WING+TIPTANK+INBOARD AND OUTBOARD STORE

Figure 16 : Comparison of theoretical and experimental flutter results for an aircraft equipped with stores

which various assumptions were made with respect to the unsteady aerodynamic forces taken into account. First of all calculations were made in which the unsteady loads on the external bodies were neglected. A comparison of these theoretical results with the experimental data reveals, that especially for the damping values the theoretical prediction is rather poor. However, adding the unsteady aerodynamic forces on the tip tank brings the theoretical values of the damping for both the bending and the torsion mode much more in agreement with the experimental values. A further expansion of the unsteady aerodynamic forces with those on the inboard and outboard store on the other hand hardly modifies the result obtained already. It may be concluded that in this case unsteady forces generated by the underwing stores hardly contribute to the flutter behaviour of the airplane. Apparently this is due to the fact that the vibration modes under concern both have a considerable and effective displacement in the region of the tip tank, whereas at the location of the inboard and outboard store the amplitude of vibration is rather small.

5. CONCLUSION

In the present paper a description is given of an extensive investigation of the unsteady airloads on wing-store configurations oscillating in subsonic flow and of their effect on the flutter characteristics. This has resulted in a theoretical method to predict these unsteady airloads, which is verified by two different types of experiments: unsteady pressure measurements and flutter tests in both the wind tunnel and free flight. It is found that reliable predictions can be obtained and that the unsteady aerodynamic loads on the external bodies, although being small in comparison with the unsteady loads on the wing, may influence the flutter characteristics greatly.

REFERENCES

1. Kalman, T.P., Rodden, W.P., and Giesing, J.P., "Application of the doublet-lattice method to nonplanar configurations in subsonic flow", J.Aircraft, Vol. 8, No. 6, 1971, pp 406-413.
2. Giesing, J.P., Kalman, T.P., and Rodden, W.P., "Subsonic steady and oscillatory aerodynamics for multiple interfering wings and bodies", J. Aircraft, Vol. 9, No. 10, 1972, pp 693-702.
3. Morino, L., "A general theory of unsteady compressible potential aerodynamics". NASA CR-2464, Dec. 1974.
4. Tseng, K., and Morino, L., "Fully unsteady subsonic and supersonic potential aerodynamics of complex aircraft configurations for flutter applications". Proc. AIAA/ASME/SAE 17th Struc.Dyn. and Materials Conf., King of Prussia, Pa, May 1976, pp 626-638.
5. Bennekens, B., Roos, R., and Zwaan, R.J., "Calculation of aerodynamic loads on oscillating wing/store combinations in subsonic flow", AGARD Specialists Meeting on Wing-with-Stores Flutter, CP-162, Paper No. 4, Munich, 1974.
6. Roos, R., Bennekens, B., and Zwaan, R.J., "Calculation of unsteady subsonic flow about harmonically oscillating wing/body configurations", J. Aircraft, Vol. 14, No. 5, 1977, pp 447-454.
7. Hess, J.L., "Calculation of acoustic fields about arbitrary three-dimensional bodies by a method of surface source distributions based on certain wave number expansions", Douglas Aircraft Comp., Long Beach, Calif., DAC 66901, March 1968.
8. Renirie, L., "Analysis of measured aerodynamic loads on an oscillating wing-store combination in subsonic flow", AGARD Specialists Meeting on Wing-with-Stores Flutter, CP-162, Paper No. 5, Munich, 1974.
9. Zimmerman, N.H., and Weissenburger, J.T., "Prediction of flutter onset speed based on flight testing at subcritical speeds", J.Aircraft, Vol. 1, No. 4, 1964, pp 190-202.

AUTOBIOGRAPHY

T.W.G. van Nunen

Senior Research Engineer

National Aerospace Laboratory NLR

Mr. van Nunen received an "Ingenieur"- degree, which is equivalent to a Master of Science, in Aeronautical Engineering from Delft Technological University in 1960.

After having fulfilled his military duties he joined the National Aerospace Laboratory in 1962 and was assigned to the Department of Aeroelasticity. In this specific field he specialized in experimental investigations. Throughout the years he has conducted and actually managed a large variety of experimental projects ranging from studies in the unsteady aerodynamics, like ground wind loads and buffet on the ELDO launching vehicle, to the unsteady aerodynamics on oscillating airfoils in transonic flow. Aside from this he has conducted flutter experiments on wind tunnel models as well as full scale aircraft. The experience obtained in the field of aeronautics have been applied more generally also. He has been responsible for projects in the field of building aerodynamics and the vibrational behaviour of civil constructions.

After first having been involved directly with the execution and interpretation of the experiments he is now active as a group leader.

AUTOBIOGRAPHY

R. Roos

Senior Research Engineer

National Aerospace Laboratory NLR

Mr. Roos received an "Ingenieur" degree in Aeronautical Engineering from Delft Technological University in 1966, an M.S. degree in Aeronautics and Astronautics from Purdue University in 1967 and a Ph.D. degree in Engineering Sciences from Purdue University in 1970.

Upon returning from the U.S., he joined the Department of Aeroelasticity at the National Aerospace Laboratory in 1970. He specialized in unsteady aerodynamics with special emphasis on theoretical methods. From 1972 to 1976 he acted as project leader in the development of an unsteady panel method for wing-store configurations. Since 1976 he is active in running projects that involve the prediction of unsteady airloads for flutter investigations as well as dynamic stability derivatives.

AUTOBIOGRAPHY

J.J. Meijer

Senior Research Engineer

National Aerospace Laboratory NLR

Mr. Meijer received an "Ingenieur" degree (equivalent to an M.S. degree) in Aeronautical Engineering from Delft Technological University in 1968.

After two years of postgraduate studies on aeroelastic subjects he joined the National Aerospace Laboratory in 1970. Being stationed at the Department of Aeroelasticity he has specialized in flutter and riding qualities investigations. From 1970 until 1977 he has been responsible for the development of chains of computer programs for theoretical flutter and response calculations. As a project leader he has been involved in aeroelastic investigations on both wind tunnel models and real aircraft.

PARAMETRIC APPROACH TO FLUTTER
CLEARANCE OF AIRCRAFT CONFIGURED
WITH EXTERNAL STORES
(U)

(Article UNCLASSIFIED)

By

Alexander E. Clelland
ASD/ENFSL
Wright-Patterson AFB, Ohio 45433

ABSTRACT. (U) Flutter certification of an aircraft configured with external stores is, in general, a highly complex and cumbersome task. The most difficult aircraft to deal with are transonic fighter aircraft configured with large underwing and wing tip stores. On past aircraft weapon system programs, a limited number of specific stores (baseline stores) have been certified during aircraft development and additional store loadings (follow-on stores) have been certified on an individual basis as required by the users through ECP's. Thus, the aircraft is only minimally engineered with respect to external stores carriage at the end of program development phase and considerable and often redundant flutter effort continues throughout the life of the weapon system.

The parametric approach to flutter clearance of aircraft with external stores advocated herein focuses on the understanding of the fundamental flutter mechanisms involved and the identification of flutter boundaries for all potential store loadings up to the design limit of the aircraft. Thus, during design phase, the aircraft is completely engineered with regard to external store carriage capability. The residual follow-on store certification can be accomplished by analogy or minimal flutter analysis.

"Approved for public release; distribution unlimited."

LIST OF FIGURES

<u>FIGURE NO.</u>	<u>CAPTION</u>
1	Typical Transonic Fighter Stores Configuration
2	Flow of Conventional Flutter Clearance Program
3	Range of Store Station Loadings
4	Aircraft Flutter Speeds vs Store Weight & Inertia
5	Realistic Store Loadings
6	Flutter Stability Boundaries
7	Test & Analysis Sequence
8	Final Flutter Stability Boundaries
9	Flow of Parametric Program
10	Flutter Velocity Contours for a 10-160 ECM Pod Suspended Directly from the B.L. 132.50 MAU-12A/B Pylon; F-4C Aircraft
11	F-5E/F Store Configurations
12	Weight vs Pitch Inertia for AIM-9 Clearance Program
13	Weight - vs Static Unbalance for AIM-9 Clearance Program

INTRODUCTION

The enormity of the task facing the aeroelastician when required to certify many types of external stores for carriage on an aircraft arises not so much from the technical procedure required to certify a particular loading (for using state-of-the-art analyses, flutter model tests, airframe rigidity tests, and flight flutter tests a safe clearance speed can be confidently established) but from certifying many external store loadings within imposed time constraints and using only limited engineering resources. Obviously, if more than a few stores are to be certified, all take-off loadings and associated down loadings cannot be individually analyzed and tested. Therefore, judgement must be used to identify the critical loading configurations to be examined.

The term flutter as used in this paper refers to classical flutter of the aircraft wing. The structural modes which couple to produce divergent motion may be aircraft modes modified by the presence of external stores or may be aircraft modes coupling with store/pylon modes. Other aeroelastic phenomena such as divergence and store flutter occurs for relatively uncommon, but easily recognizable store loadings which are most efficiently investigated on an individual basis as required. Aeroservoelastic phenomena can be treated as additional degrees of freedom in the flutter analysis. Those store loadings which modify the dynamics of the aircraft so as to cause interaction between the flight control system and the aircraft structural modes can be identified and the appropriate flight control system changes made.

Flutter clearance of any aircraft which is required to carry many types of external stores presents a formidable problem. However, the transonic fighter aircraft is generally considered the most difficult to deal with. This is the case which will be used as a basis for discussion; all comments apply to other aircraft to some degree or other. For the transonic fighter aircraft, the heavier stores tend to be comparable in weight to the weight of the wing; thus, significantly altering the clean wing flutter mechanism and/or introducing new aircraft/store flutter mechanisms. Several underwing store stations are usually provided per half span along with a wing tip station, resulting in millions of potential aircraft loading configurations. In addition, the problem is aggravated by the carriage of "variable mass stores" such as fuel tanks, rocket pods, and MER & TER configurations. To further compound the problem, much of the operation of the aircraft while configured with external stores is in the transonic flight regime, where normally flutter speeds are the lowest and flutter margins at a minimum. Since aircraft store

flutter usually occurs well within the performance flight envelope, flutter boundaries must be identified as well as clearance speeds.

In the past, in order to reduce the scope of the problem to manageable proportions, some simplifying restrictions have been suggested. While some of the restrictions have been acceptable for some particular aircraft, most of them compromise the potential of modern day aircraft as a weapon system, and thus, are not acceptable to the user or corporate management, as the following reassessment shows.

a. Keep all store stations as close to the fuselage as possible: If the aeroelastician succeeds in having the external store stations moved inboard, no sooner is this accomplished than it is realized that the outboard wing is an ideal place to mount additional weapon pylons, thereby enhancing aircraft capability. With the versatility demanded in modern transonic fighters, the maximum number of store stations which physically fit are apt to be installed. The F-16 aircraft and F-5 series aircraft are prime examples.

b. Tune the pylons: This action is only effective if the pylon is to be configured with a permanently installed non-varying store, such as an engine. If stores encompassing a broad range of weights and inertia are to be carried, then tuning for one weight range results in de-tuning for another. Thus, high flutter speeds can be established for some weight ranges, but low flutter speeds must still be dealt with for other weight ranges.

c. Restricting types of stores to be carried on a particular pylon: This is not within realm of authority of the aeroelastician. However, acceptable alternate configurations can be suggested. If a particular loading is required, flutter clearance speeds must be identified.

d. Conformal Carriage: In practice, conformal carriage has limited application. Fuel tanks and ordnance such as rocket pallets lend themselves to this type of carriage. However, for conventional ordnance, underwing installation is preferred since it allows much greater freedom from geometric constraints.

Some things which the aeroelastician can do to promote high flutter speeds are to specify wing stiffnesses which results in as high bare wing flutter speeds as possible and identify optimum pylon stiffness and fore and aft location. Aside from these, there is little that aeroelastician can do with regard to dictating aircraft design which will result in high flutter speeds for the store carrying mode and will reduce the number of possible flutter critical store configurations. The parametric approach to be discussed herein

will illustrate how an orderly, logical, and efficient approach to this seemingly overwhelming problem, can be accomplished.

For the purposes of further discussions, consider a transonic fighter aircraft with the general store loading capability of a wing tip missile, two underwing store stations per wing, and a centerline store station as shown in Figure 1. This example is representative of current inventory aircraft.

CONVENTIONAL EXTERNAL STORES CLEARANCE PROGRAM

General Review of Past Procedures.

On past weapon system programs involving aircraft configured with external stores, the approach taken has been to identify the basic aircraft missions and the specific stores required to support these missions and then require that only these specific stores, termed baseline stores, be certified for carriage during the development phase of the aircraft. Occasionally other stores termed follow-on stores, will be identified as being potential candidates for carriage at some future date. However, in many cases it has been asserted that the need for carriage of other stores will never exist and therefore, certification of the baseline stores will satisfy, for all time, the external store carriage requirements. Of course, experience has shown that throughout the life of a store carrying aircraft that, because of aircraft mission changes, introduction of new stores into the inventory, and modifications to existing stores, the certification of additional stores is inevitable. Whether or not the certification of follow-on stores has been initially recognized, the immediate concern has been to address, almost exclusively, the baseline stores, and postpone dealing with follow-on stores. As the aircraft weapon system progresses into the operational phase, separate groups of follow-on stores are certified in response to user requests. External store certification continues in this fashion throughout the life of the system. As shown in Figure 2, groups of stores are still being certified many years after completion of basic aircraft development effort.

Flutter Certification for Conventional Program.

As external stores flutter clearance programs have proceeded in the past, the aeroelastician is initially tasked with analyzing, testing, and establishing safe flutter clearance speeds for the aircraft configured with only the baseline stores; an effort which, in itself, is formidable even if the stores list is very restricted. Since consideration of all possible loadings which can be constructed from the baseline stores list is prohibitive, the flutter analyst must

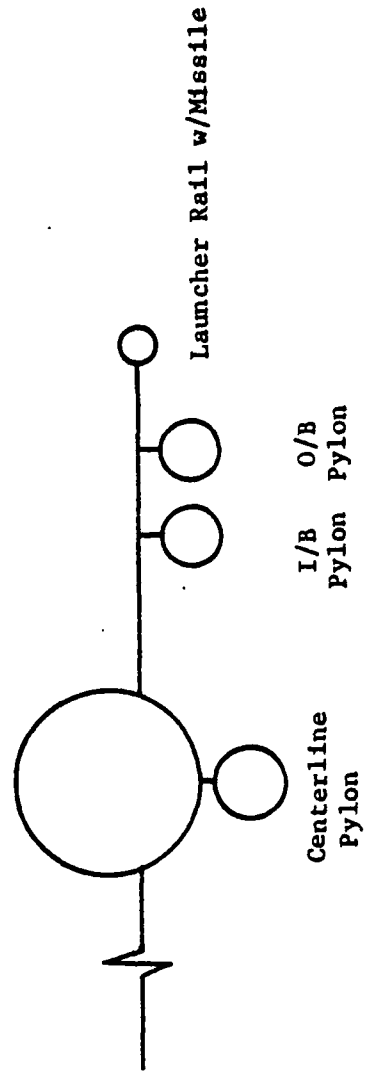


FIGURE 1 TYPICAL TRANSONIC FIGHTER STORES CONFIGURATION

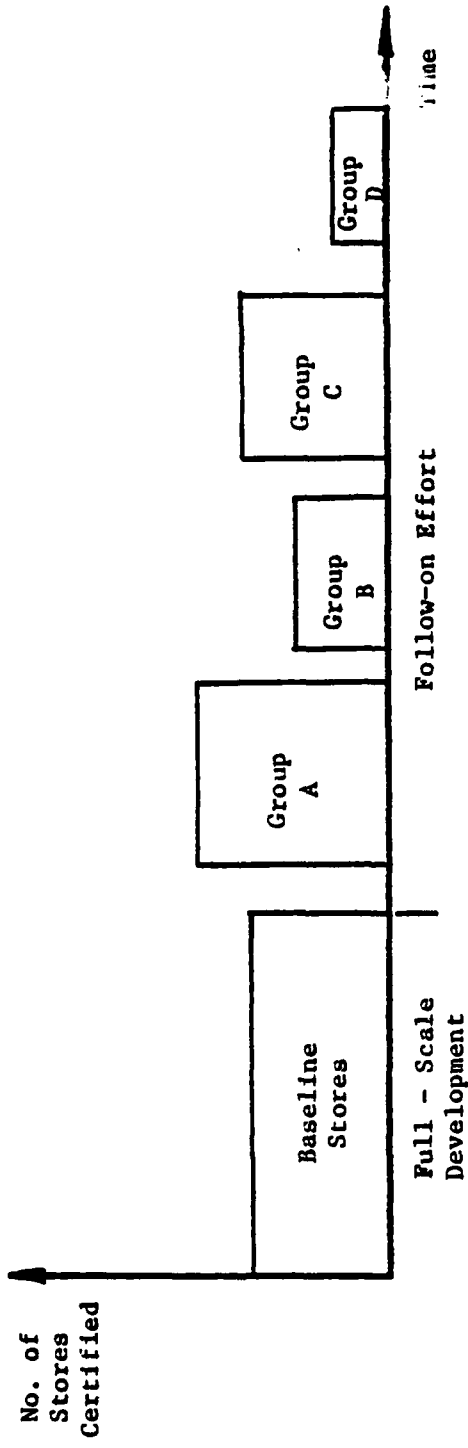


FIGURE 2 FLOW OF CONVENTIONAL FLUTTER CLEARANCE PROGRAM

identify the store loadings to be analyzed and tested and those to be cleared by analogy.

Once the basic aircraft design has been established, the aircraft parameters which influence flutter speeds are fixed at nominal values: thus, the variation in flutter speed of the aircraft/store combination is dependent upon variation in store parameters. External store aerodynamics have little effect upon aircraft flutter speeds, with the possible exception of unusual stores configured with large lifting surfaces. Thus, it is the mass properties of the external stores which are responsible for altering the flutter stability characteristics of the aircraft. Store weight, pitch inertia, and center-of-gravity location are the critical parameters for aircraft stability. For most external stores, the center-of-gravity is located within a narrow range mid-way between the attach lugs, and thus, once the pylon fore and aft locations are established, can be considered essentially constant for all stores. Exceptions are easily identified and can be assessed individually. Thus, store weight and pitch inertia become the controlling parameters. Figure 3 shows the store weight versus pitch inertia diagram which is conventionally used to characterize external store loadings. The external stores flutter clearance program essentially reduces to determining the aircraft flutter speed for various weight and inertia loadings for the pylons individually and in combination with all others. As can be seen in Figure 3, the baseline stores constitute a very small portion of the achievable store weight versus pitch inertia region.

By examining only those points associated with baseline stores the flutter mechanisms and sensitivity to critical parameters can only be investigated in an rudimentary manner, since flutter speeds associated with important flutter mechanisms are not tracked as a function of critical store parameters and flutter speed contours not analytically established and verified. Figure 4 shows the flutter speed of various baseline stores for a selected aircraft loading configuration. The speeds are established for baseline stores in the normal manner, by using flutter analyses, ground tests, and flight flutter tests. When additional stores are required for certification which vary more than about 5% in mass properties from previously cleared stores, few, if any, can be cleared by similarity with any degree of confidence. What is generally done, is that a flutter clearance program consisting of analysis, ground test, and flight flutter test and similar in scope to the baseline program is conducted for each additional group of follow-on stores. Referring again to Figure 2, many times stores in later follow-on groups, such as group C are more critical than stores in earlier groups such as A. If group C stores had been certified first, the clearance of group A could have been made by analogy. Thus, the amount of flutter effort

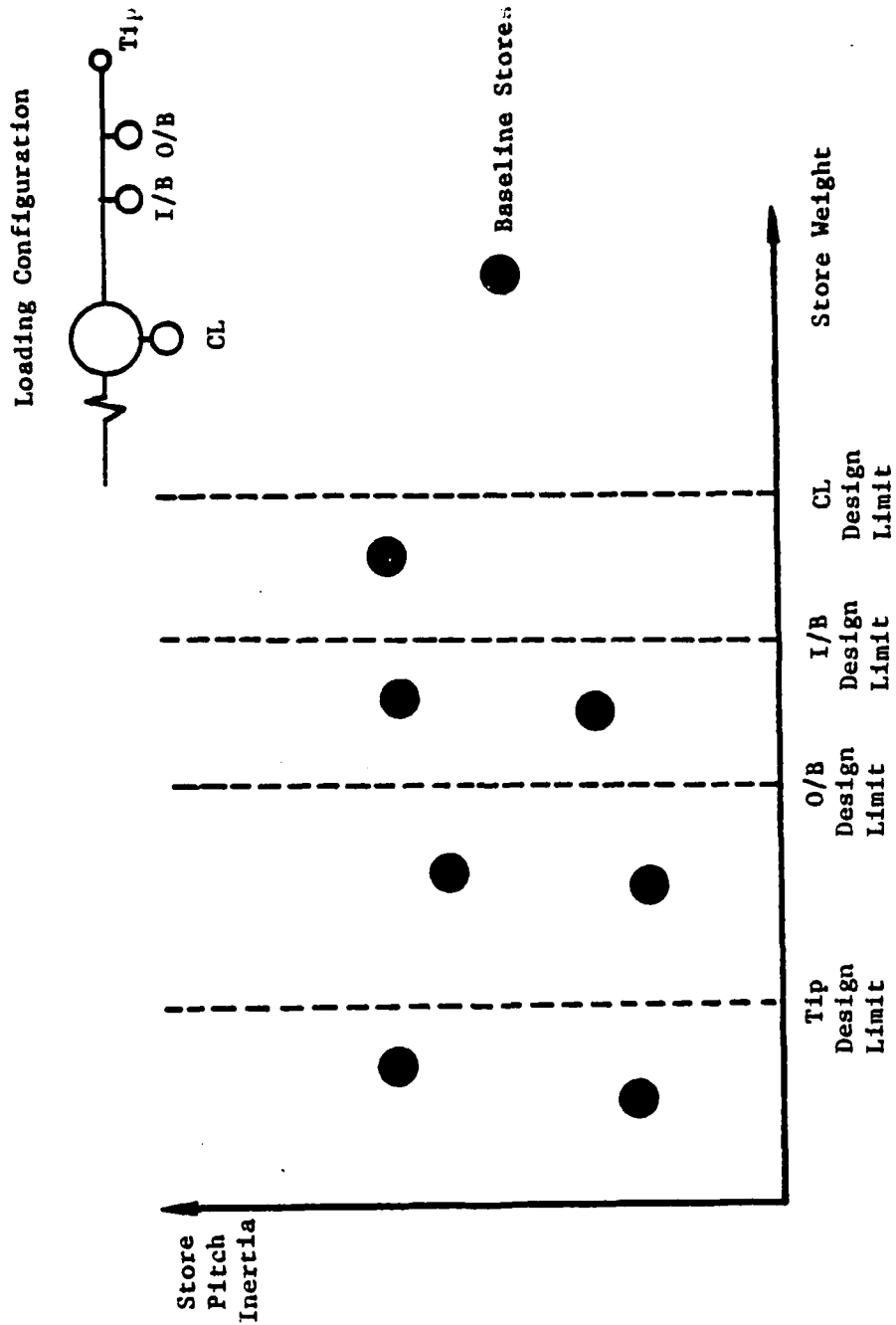


FIGURE 3 RANGE OF STORE STATION LOADINGS

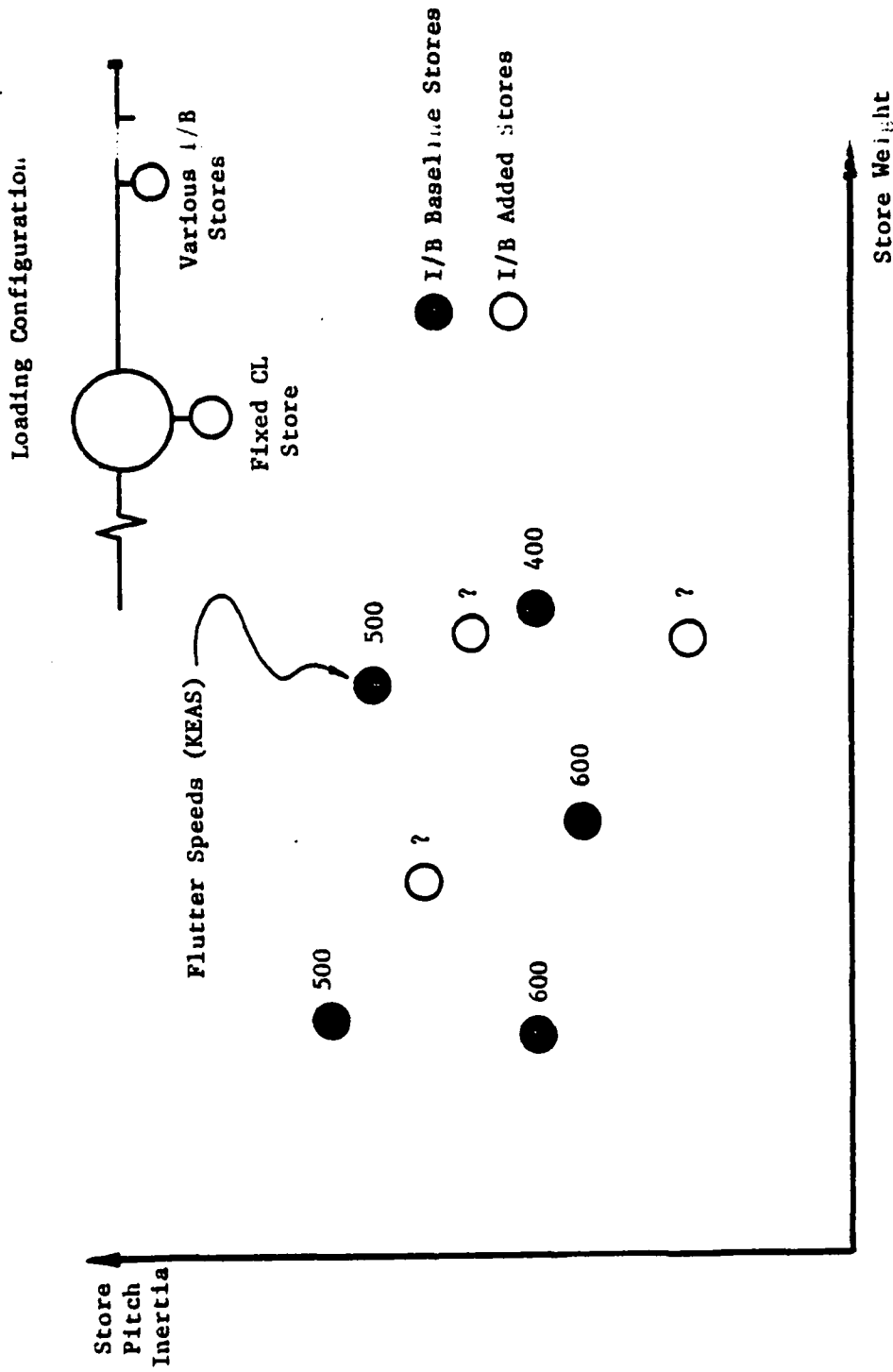


FIGURE 4 AIRCRAFT FLUTTER SPEEDS V.S. STORE WEIGHT & INERTIA

required to certify each group of stores independently as a separate entity is greater than that which would be required if all stores were identified for certification initially.

Problems Associated With Conventional Approach.

When the aircraft enters the inventory, the external stores carriage capability has only been minimally developed. Long lead times are required to respond to user requests for certification of additional stores. This has especially been a problem in the past during wartime situations, when store carriage requirements are immediate. Aircraft systems are ready for retirement before full stores carriage capability has been developed. The conventional approach also leads to redundant flutter effort; thus, is not cost effective.

PARAMETRIC APPROACH TO FLUTTER CLEARANCE

Goal of Parametric.

The intended goal of the parametric approach to flutter certification of aircraft configured with external stores is to identify and investigate the flutter characteristics of the aircraft configured with any combination of pylon or launcher rail loadings which are consistent with the structural design limits of the aircraft.

Scoping Level of Effort.

Initially, when the goal of the parametric flutter program is considered with regard to the aircraft of the type shown in Figure 1, it appears to be an all encompassing, forbidding task requiring an infinite amount of time and resources. This indeed would be the case if a strict methodical approach were adopted which considered the independent variations of all store and aircraft parameters which could affect the aircraft flutter characteristics, since literally millions of unique dynamic cases can be constructed. Fortunately, the situation is actually not that grim. The task can initially be reduced to comprehensible, although still monumental proportions by consideration of the operational aspects of the aircraft and the practical, realistic limits of external store parameters.

Figure 5 shows the aircraft pylon design weight limits for the example aircraft in relation to the bounded region which limits weight and pitch inertia to realistic values representing physically viable stores.

For operational simplicity, a limited number of safe speed clearance values are established for the aircraft while configured

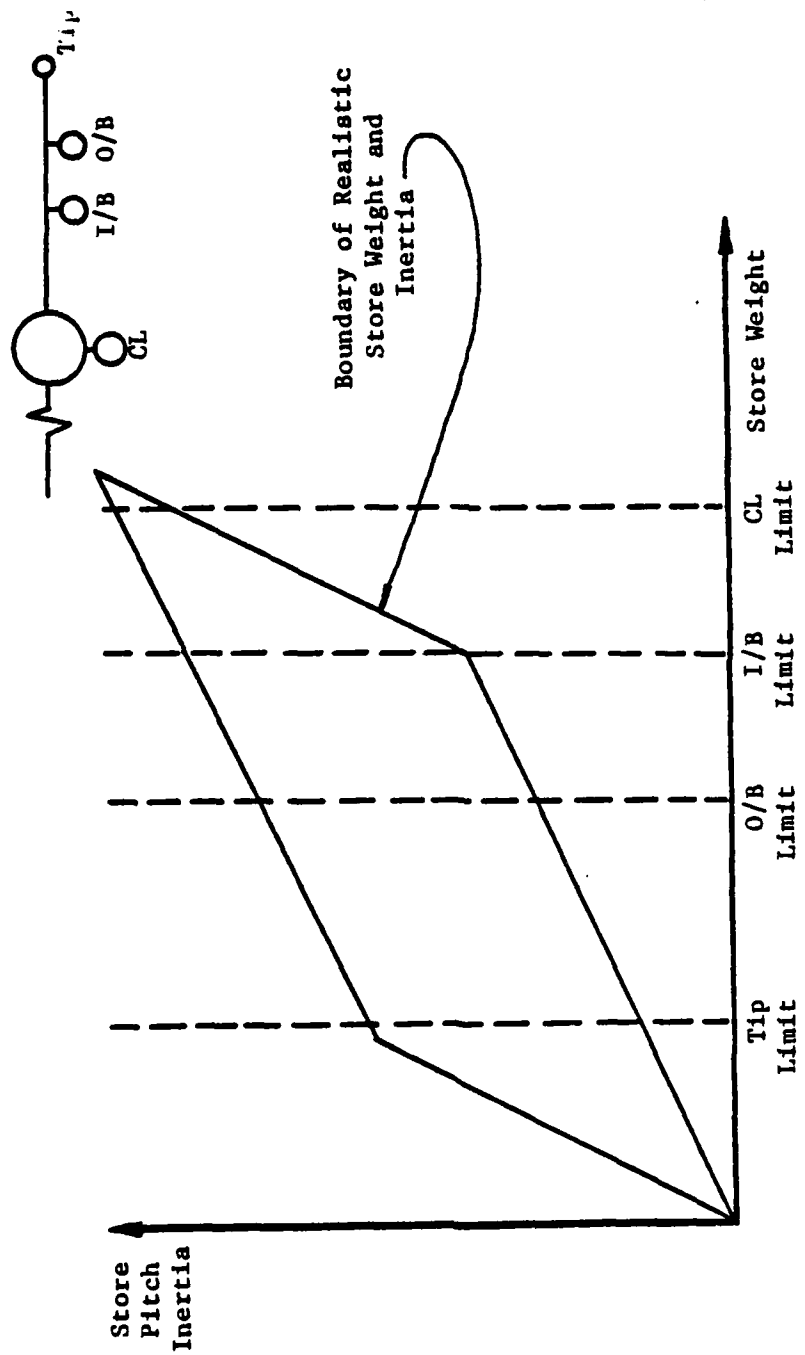


FIGURE 5 REALISTIC STORE LOADINGS

with external stores. An example may be 650 KEAS, 600 KEAS, 520 KEAS, and 450 KEAS. All external store configurations are assigned one of these clearance speeds, which is the highest speed possible without exceeding the flutter speed for that configuration. As will be discussed, this simplifies store clearance by analogy.

Basic Approach.

The parametric approach to flutter clearance of an aircraft configured with external stores requires a departure from traditional thinking. Flutter speeds are not calculated for specific store configurations per se. Instead, the dynamic characteristics, flutter mechanisms and flutter speeds of the aircraft are examined with respect to the range of weight and pitch inertia possible for each store station singly and in combination with all others. Thus, the effects of these important parameters, such as static unbalance of the wing tip store must be included as additional variables. Flutter clearance boundaries are established as shown in Figure 6. The store configurations to be ground and flight tested to verify analysis may be actual stores available in the inventory or may be store ballast to represent a critical loading.

Role of Analyses and Tests.

The feasibility of performing a parameteric flutter investigation depends upon the following:

a. The ability to rapidly identify types of potentially critical store loadings and compute corresponding aircraft flutter speeds for various combination of weight and pitch inertia for each pylon singly and in combination with all others.

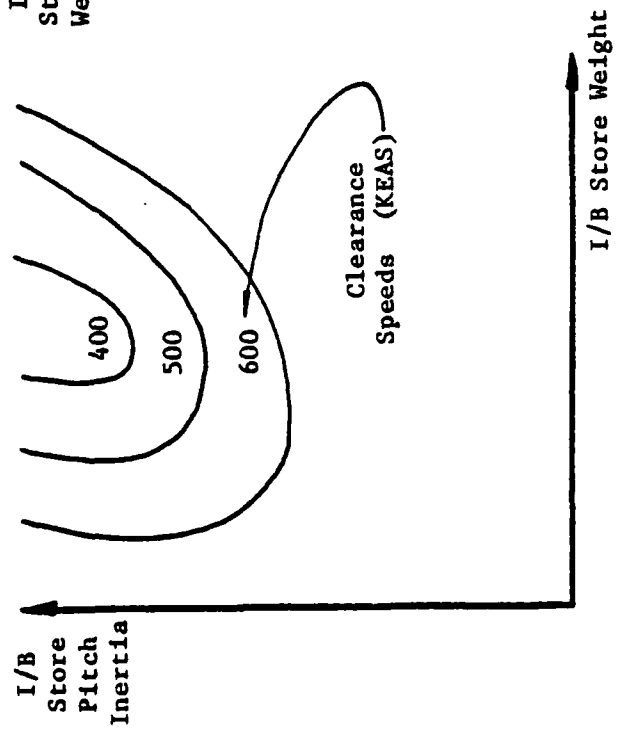
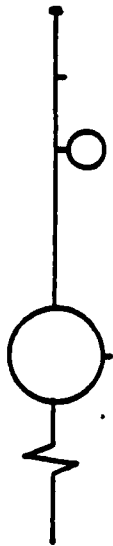
b. The ability to construct and verify an analytical model of the aircraft store combination which accurately represents the actual structure and can be used for detailed investigation of previously identified critical loading cases.

Some recently developed digital methods useful for performing rapid flutter calculations are presented in references 1 and 2. A successful analog approach is reviewed in reference 3.

During the preliminary analysis, a rapid search of aircraft stability versus weight and pitch inertia for loadings at the various store stations is made. Figure 6 shows the type of flutter stability plots which would be generated for various loadings.

It is important that the flutter analysis be refined during the flutter investigated and verified as aircraft experimental data

Single Store Case



Multiple Store Case

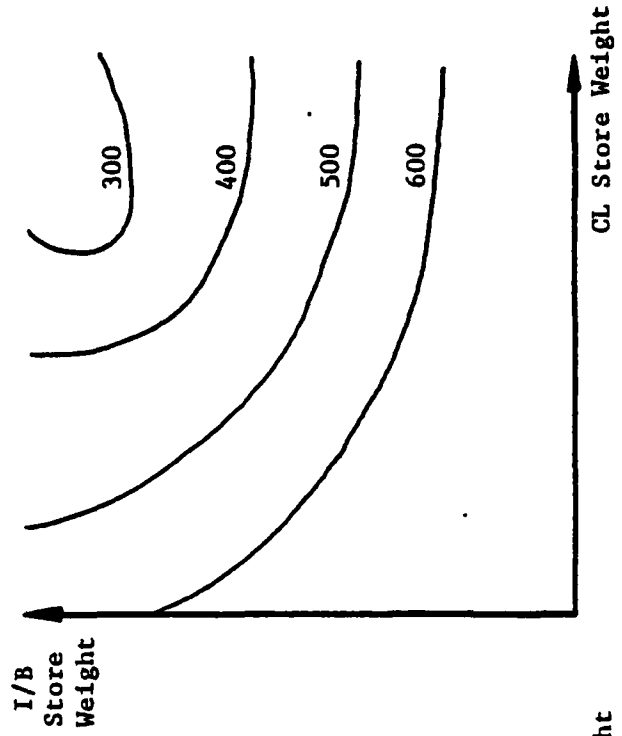
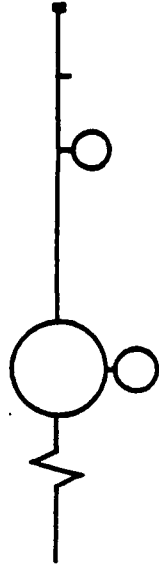


FIGURE 6 FLUTTER STABILITY BOUNDARIES

becomes available. A general suggested sequencing of test and analysis is shown in Figure 7. The division of the wind tunnel test, ground vibration test, and flight flutter test into several segments allows for optimum updating of analysis and reverification so that an analysis described in (b) above evolves and all critical loadings cases are identified and tested. Some important points to note are:

- a. Pylon (and if so equipped launcher rail) stiffness and cantilevered ground vibration tests should be performed as early as possible to eliminate uncertainties in analysis.
- b. Careful attention should be paid to measurement of modes and frequencies during ground vibration test to insure that the "pure" important normal modes are measured and none are omitted.
- c. Low speed flutter model tests provide excellent opportunity to acquire flutter data for correlation with analysis. For many external store cases, the onset of flutter is mild and the low speed flutter model can be taken to the flutter boundary with little probability of destruction.

Flutter Stability Contour Plots.

Once the flutter analysis has been suitably verified, flutter stability boundary plots can be generated for all pylon weight and pitch inertia loadings. Not all types of stores configurations will be critical. For the example aircraft, configurations involving inboard stores only could be highly critical and require careful attention whereas configurations involving both inboard and outboard stores may be stable and require only minimal analysis. The identification of the critical configurations is dependent upon the judgement of the flutter analyst.

Figure 8 shows an example of the final flutter stability boundary curves, with the specific stores to be certified during development and some follow-on stores. The speeds associated with the stability boundaries correspond to the speeds of the safe aircraft carriage speed categories. The clearance speeds of follow-on stores can be readily established, although the actual flutter speeds are only approximately determined. For instance, follow-on store number 2 falls well within this range above 520 KEAS, and can thus, be cleared for carriage at this speed. For stores which fall at or on the flutter boundaries, either the next lower speed category can be selected or, if maximum clearance speed is absolutely required, the refined flutter analysis can be employed. External stores with unusual properties may also require refined analysis.

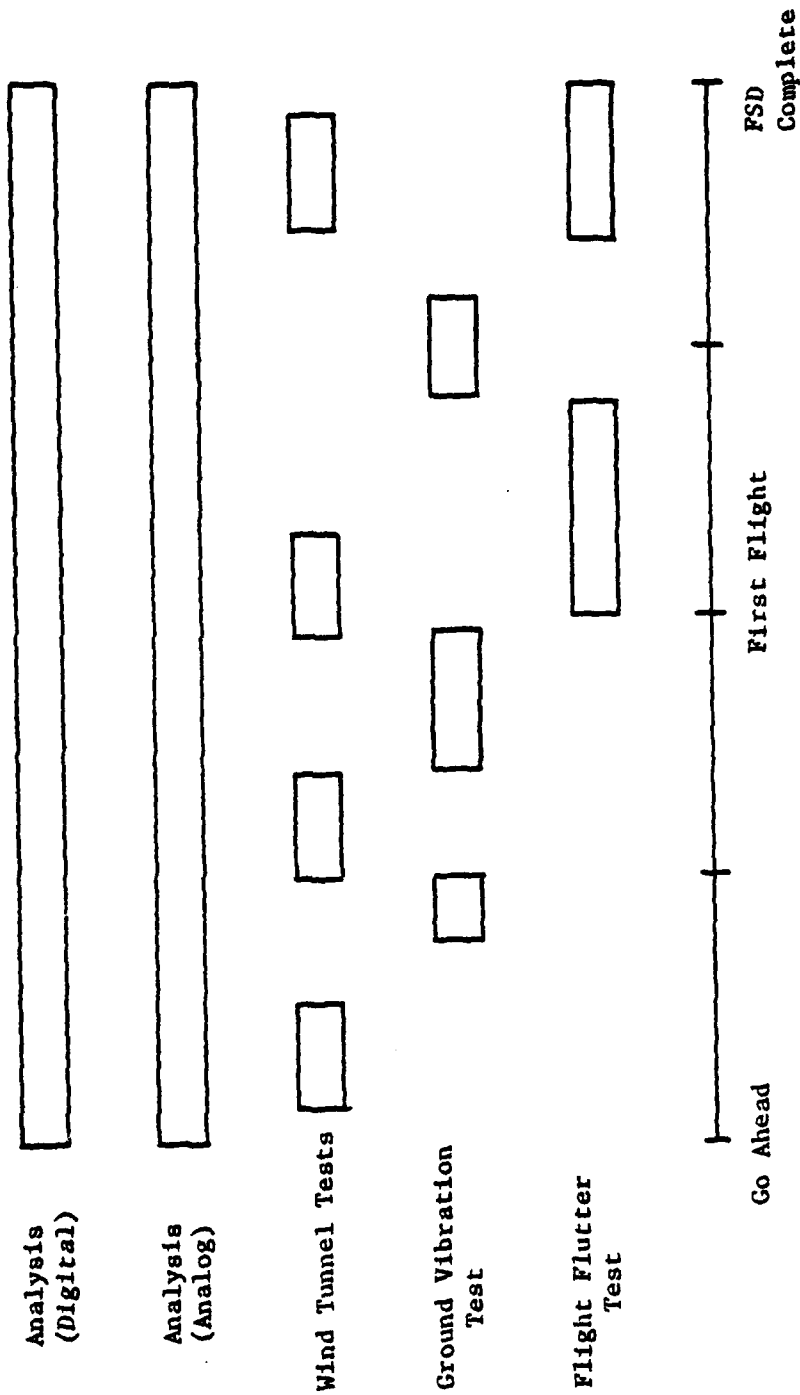


FIGURE 7 TEST & ANALYSIS SEQUENCE

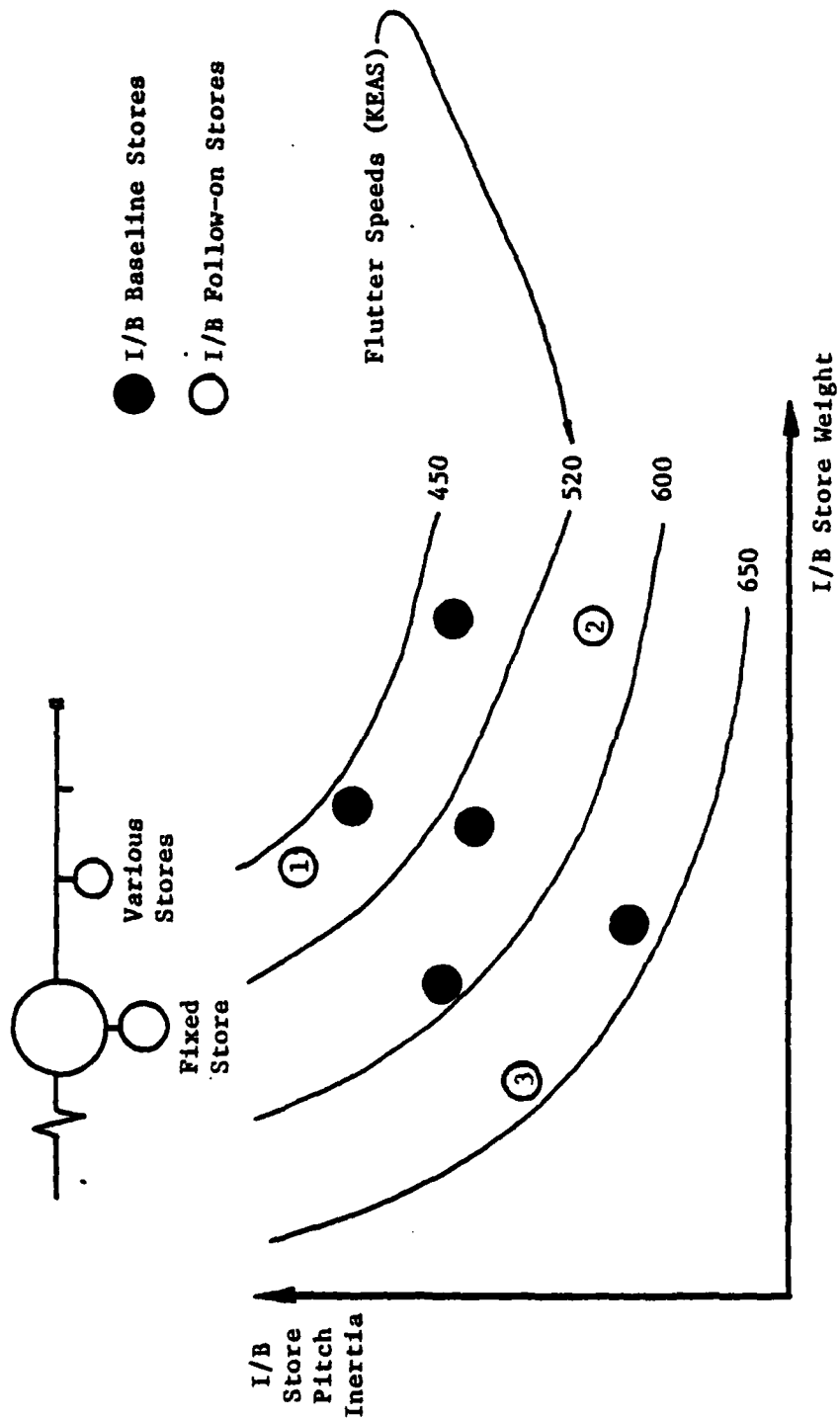


FIGURE 8 FINAL FLUTTER STABILITY BOUNDARIES

Flutter stability boundary plots of the type shown in Figure 8, which are intended for practical use, associate the flutter clearance contours with the established safe aircraft/store carriage speed categories. Plots of this nature are sufficiently accurate to allow determination of safe carriage speeds for most follow-on stores. If the velocity increment between the flutter clearance boundaries were reduced to 1 knot, and correspondingly the definition of safe carriage speeds required to the nearest knot, then this type of plot would have highly questionable validity. However, this latter case is only of passing academic interest.

Summary of Parametric Approach.

In summary, the parametric approach to flutter clearance of aircraft/stores combination require that all possible pylon weight and pitch inertia loadings be examined in conjunction with all others, and that the effect of all other important parameters be assessed. Critical store loadings, which may not be constructed of inventory stores, are chosen for ground and flight testing. The flutter analysis is constantly refined and verified and finally, at the conclusion of the flutter investigation, a data base has been assembled which identifies all critical store configurations and which allows most follow-on stores to be cleared by analogy. In addition, a highly refined and verified analytical flutter program evolves which can be used to clear all unusual store configurations which cannot be cleared by analogy. Figure 9 shows the general flow of the parametric flutter program as Figure 2 does for the conventional program.

PAST PARAMETRIC FLUTTER INVESTIGATIONS

The concept of utilizing the parametric approach for performing flutter investigation is, of course, not new. However, the parametric approach has not been widely accepted throughout the industry, although it has been used and validated in a limited sense on recent aircraft systems. The external stores certification programs for the U.K. Jaguar (reference 4) utilized the parametric approach. This aircraft is configured with two store stations per wing and a center-line station. Not only were pylon loadings with singly store considered, but fuel tanks and multiple carriage racks were also included. Flight testing of 4 configurations resulted in full flight envelope clearance for 85 possible combinations. Another U.K. aircraft, the Harrier MK. 50 (reference 5) also utilized the parametric approach to flutter clearance.

Reference 6 presents the results of a parametric investigation for carriage of ECM pods on the F-4C aircraft. This study is limited in terms of the weight and pitch inertia values considered for only two pylons, but is much broader in terms of the technical disciplines

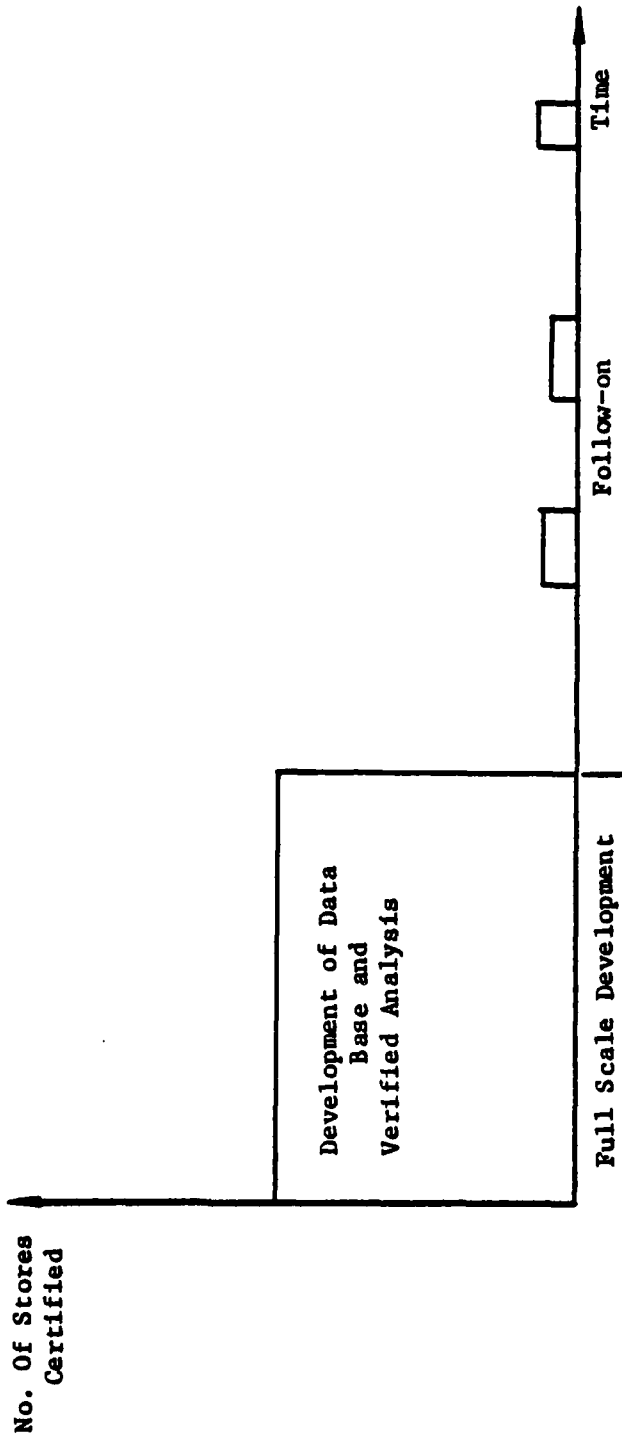


FIGURE 9 FLOW OF PARAMETRIC PROGRAM

considered. This parametric study was conducted to provide flight clearance information on separation of speeds, allowable maneuvers, aircraft stability with stores, and landing loads in addition to flutter speeds. Figure 10 is an example flutter contour plot taken from reference 6. These plots have been used by ASD/ENFSL to clear follow-on ECM pods on the F-4C aircraft.

CURRENT F-5 PARAMETRIC

Currently, a parametric flutter program is being conducted on the F-5 series aircraft (F-5A/B/E/F models) to certify modified versions of the AIM-9 series missiles on the wing tip in conjunction with all other currently authorized store loadings (Figure 11 shows F-5 general store configurations). The flutter characteristics of the F-5 series aircraft configured with underwing stores are highly sensitive to the weight, static unbalance, and pitch inertia of the wing tip missile. The modifications being made to the AIM-9 missiles significantly alter the missile mass properties with respect to the flutter sensitivity of the aircraft.

It was determined that a parametric flutter program to clear the specifically modified missiles and all future AIM-9 variants would be the most cost effective approach. Figures 12 and 13 show the relationship between the currently cleared weight versus pitch inertia and weight versus static balance ranges and the corresponding envelope to be cleared by the parametric program.

Flutter analyses using newly developed perturbation techniques are to be conducted to determine critical missile loadings. Flight flutter testing will be conducted for these configurations. The specific missiles to be flight tested may not be currently existing missiles, but may be ballasted to achieve the most critical case. Dynamic loads and stress will also be evaluated and composite clearance contours encompassing all these technical disciplines will be developed.

CONCLUDING REMARKS

This paper has reviewed the conventional external stores clearance program, the parametric approach to external stores flutter clearance and provided some examples of use on actual aircraft systems. Some of the advantages of the parametric approach were discussed and are listed below in summary.

- a. Early discovery of flutter problems which could impact design.
- b. Full development of aircraft potential for stores carriage at end of full scale development.

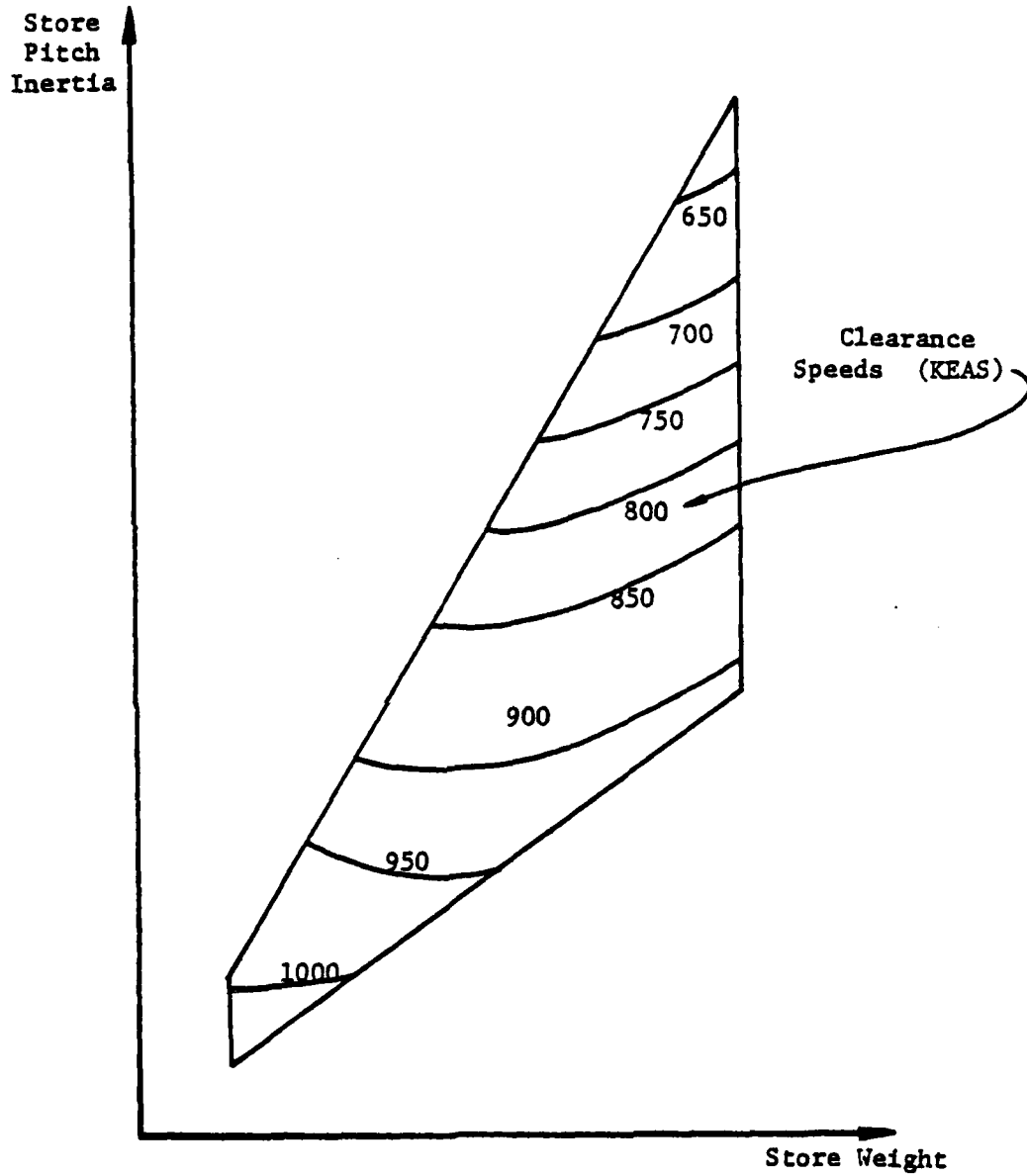


FIGURE 10 FLUTTER VELOCITY CONTOURS FOR A 10-160 ECM POD
 SUSPENDED DIRECTLY FROM THE B.L. 132.50 MAU-12A/B
 PYLON; F-4C AIRCRAFT

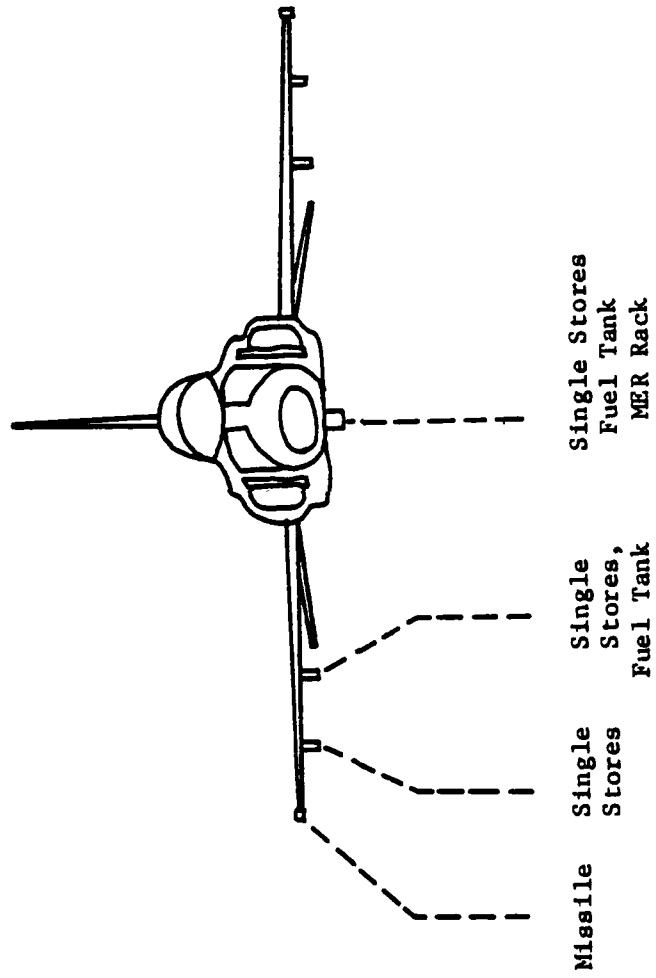


FIGURE 11 F-5E/F STORE CONFIGURATIONS

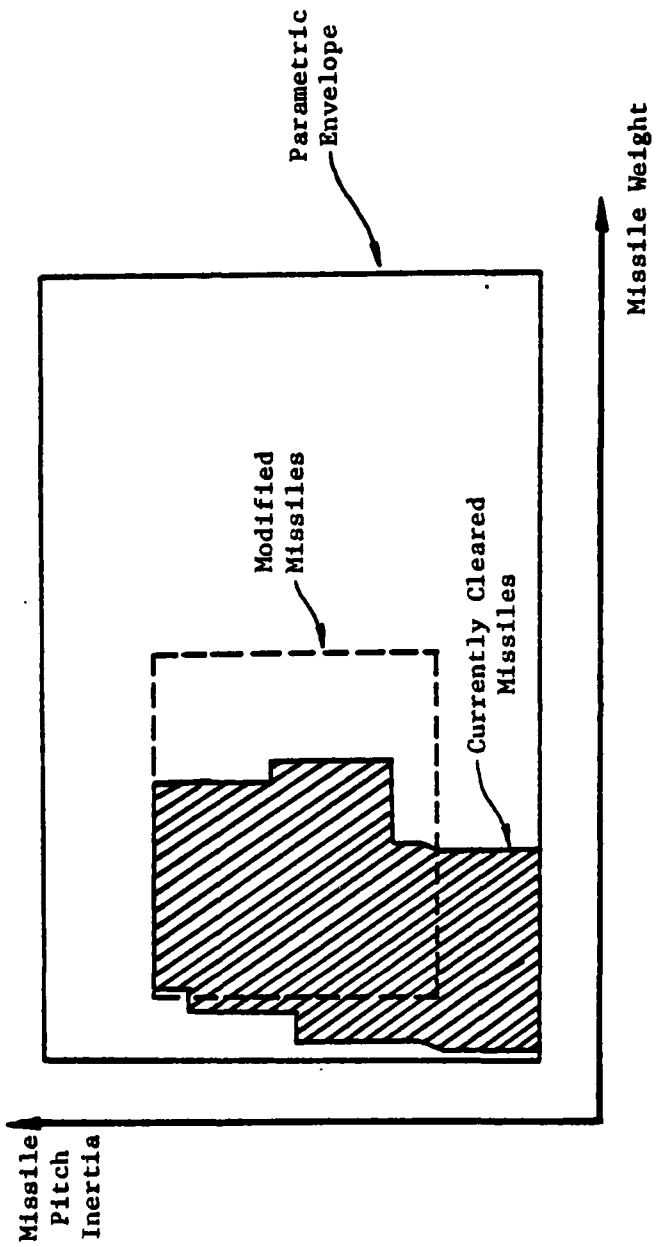


FIGURE 12 WEIGHT V.S. PITCH INERTIA FOR AIM-9 CLEARANCE PROGRAM

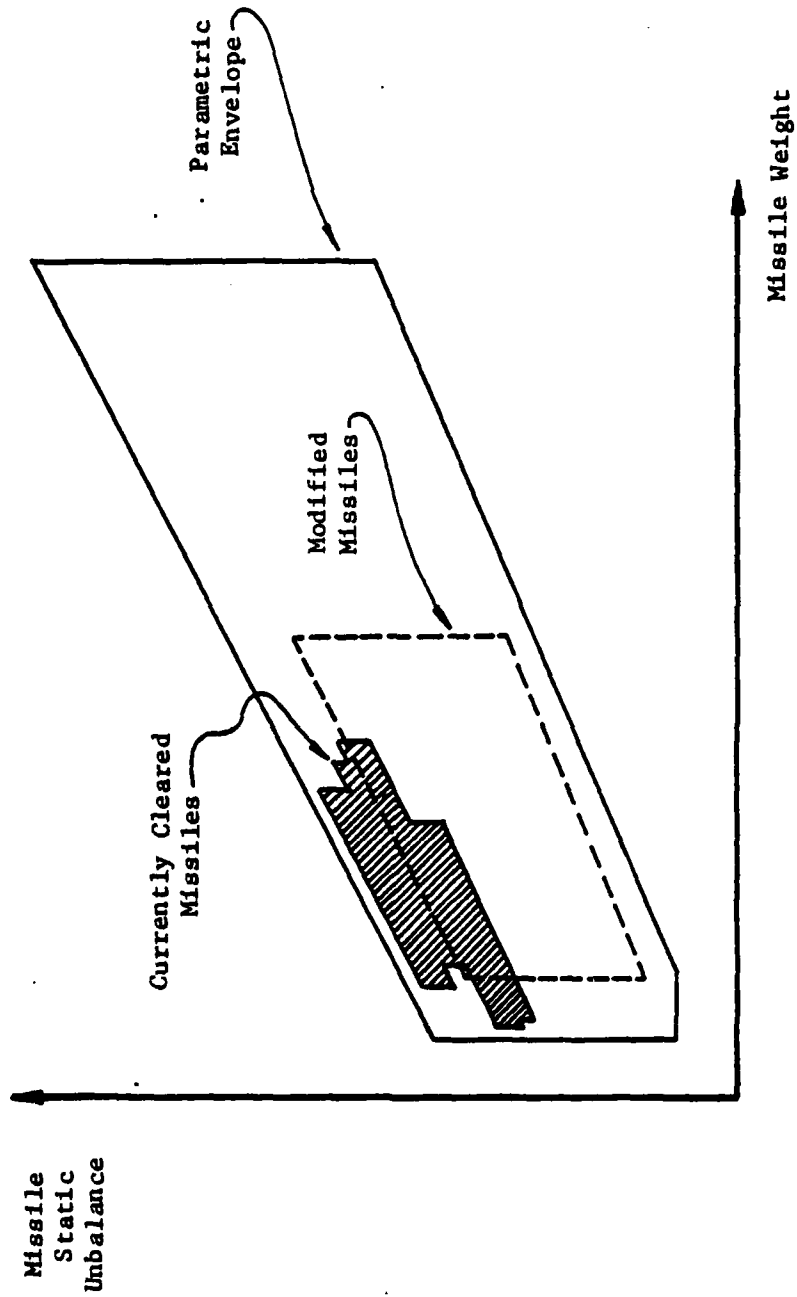


FIGURE 13 WEIGHT - V.S. STATIC UNBALANCE FOR AIM-9 CLEARANCE PROGRAM

c. Ability to certify additional stores without significant time delay through clearance by analogy or minimal analysis.

d. Full and efficient utilization of contractor capability during aircraft full scale development to establish data base and verified refined analytical flutter computer program for follow-on store certification.

There has been a shift in attitude in USAF which is detailed in reference 10 toward baseline and follow-on aircraft/stores certification programs. In the future, along with certification of initial stores, a mature technical data base will be established by the contractor which will be used by government agencies for in-house certification of follow-on stores. A parametric approach is ideally suited for accomplishment of this goal with respect to flutter clearance.

REFERENCES

1. Ferman, M. A., Unger, W. H., Wells, J. R., "An Extension of the Rapid Method for Flutter Clearance of Aircraft with External Stores," AFFDL-TR-75-101, Vols. I, II, and III, November 1975.
2. Cross, A. K. and Albano, E. A., "Computer Techniques for the Rapid Clearance of Aircraft Carrying External Stores," AFFDL-TR-72-114, February 1973.
3. Epperson, T. B., "A Different Approach to the Problem of Flutter of Aircraft with External Stores," Ft. Worth Division of General Dynamics, November 1969.
4. Lodge, C. G. and Omerod, M., "U. K. Jaguar External Store Flutter Clearance," AGARD-CP-162, October 1974.
5. Hawker Siddeley Aviation Ltd. Report No. AEN/S/324, "A Parametric Flutter Study of Wing-Store Configuration for the Harrier MK 50, January 1971.
6. Katz, H., Carlton, L. A., Clark, H. T., Pittman, R., and Schoch, D., "Investigation of an ECM Pod Installation for the Model F-4C Aircraft," March 1967.
7. Katz, H., "Flutter of Aircraft with External Stores," McDonnell Douglas Report MDC-69-030, November 1969.
8. Baird, E. F. and Clark, W. B., "Recent Observations on External Store Flutter," October 1974.
9. Chipman, R. R. and Malone, J. B., "Application of Optimization Technology to Wing/Store Flutter Prediction," AIAA Paper No. 77-453, March 1977.
10. Aeronautical Systems Division Regulation 80-1, 9 March 1977.

AUTOBIOGRAPHY

A. Clelland
Aeronautical Systems Division
WPAFB, Ohio

Mr. Clelland received a B.S. degree in Physics from the University of Minnesota in 1968. Since that time, he has been employed in the Directorate of Flight Systems Engineering, Aeronautical Systems Division, at WPAFB. His experience in the area of flutter ranges from large transport aircraft to flutter critical transonic fighter aircraft equipped with external stores.

PREDICTION OF THE UNSTEADY AIRLOADS ON HARMONICALLY
OSCILLATING SPHEROIDS BASED ON AN ANALYTICAL SOLUTION
OF THE GOVERNING WAVE EQUATION

(U)

(Article UNCLASSIFIED)

by

K. -L. Chao and H. Försching
Deutsche Forschungs- und Versuchsanstalt
für Luft- und Raumfahrt e. V.
- Aerodynamische Versuchsanstalt Göttingen -
Göttingen, Fed. Rep. Germany

ABSTRACT. (U) Analytical solutions are presented for the unsteady aerodynamic pressure distributions on slender ellipsoids of revolution, oscillating harmonically in subsonic compressible flow. The governing potential equation is first transformed into the classical Helmholtz wave equation by applying a gauge transformation and a coordinate scale transformation. Then, with introduction of non-orthogonal prolate spheroidal coordinates, the wave equation is solved for the prescribed body surface and flow field boundary conditions through application of the method of separation of variables. For a variety of slender spheroids, performing harmonic rigid body plunging and pitching oscillations, the unsteady aerodynamic pressure on the body surface is calculated. These analytical results are compared to corresponding experimental results and to numerical results obtained from a panel approach and from Slender-Body-Theory.

"Approved for public release; distribution unlimited."

LIST OF FIGURES

- Fig. 1 Non-orthogonal spheroidal coordinate system
- Fig. 2 Unsteady aerodynamic pressure distributions on a prolate spheroid at harmonic plunging oscillations
- Fig. 3 Unsteady aerodynamic pressure distributions on a prolate spheroid at harmonic pitching oscillations
- Fig. 4 Unsteady aerodynamic pressure distributions on three spheroids at harmonic plunging oscillations
- Fig. 5 Unsteady aerodynamic pressure distributions on three spheroids at pitching oscillations
- Fig. 6 Comparison of computed and measured unsteady aerodynamic pressure distributions on a spheroid performing harmonic plunging oscillations in incompressible flow
- Fig. 7 Comparison of computed and measured unsteady aerodynamic pressure distributions on a spheroid performing harmonic pitching oscillations in incompressible flow

NOTATION

Coordinates

x, y, z	cartesian coordinates
x_0, y_0, z_0	transformed cartesian coordinates, see eq. (14)
ξ, η, θ	prolate spheroidal coordinates, see eq. (15)

Other notations

a_∞	velocity of sound of the undisturbed flow
a	semi-major axis of the spheroid
b	semi-minor axis of the spheroid
c	characteristic length of the spheroid, see eq. (21)
$c_p = p/q_\infty$	pressure coefficient
c'_p, c''_p	real and imaginary part of c_p
$f(x, y, z)$	body surface function
$\bar{f}(x, y, z)$	amplitude of the body surface disturbance
h	parameter of the spheroidal functions, see eq. (23)
$i = \sqrt{-1}$	unit imaginary number
p	amplitude of the unsteady pressure
$q_\infty = \rho_\infty U_\infty^2 / 2$	dynamic pressure of the undisturbed flow
t	time
\bar{z}	amplitude of the plunging oscillation

A_{mn}, \bar{A}_{mn}	coefficients of the spheroidal wave function
$D_k^{mn}(h), E_k^{mn}(h)$	coefficients of the spheroidal functions
$F(x, y, z, t)$	surface function of the oscillating body
$I_i(l, n), J_i(l, n)$	integrals over the spheroidal functions $S_1(h, \eta)$
Ma_∞	Mach number of the undisturbed flow
$P_n^m(\xi)$	associated Legendre function of the first kind for $\xi > 1$
$P_n^m(\eta)$	associated Legendre function of the first kind for $\eta \leq 1$
$Q_n^m(\xi)$	associated Legendre function of the second kind
$R_{mn}(h, \xi)$	spheroidal radial function of fourth kind
$R'_{mn}(h, \xi)$	spheroidal radial function of first kind
$R''_{mn}(h, \xi)$	spheroidal radial function of second kind
$S_{mn}(h, \eta)$	spheroidal angle function of the first kind
U_∞	velocity of the undisturbed flow
α	reciprocal numerical eccentricity of the spheroid
β	Prandtl factor, see eq. (12)
γ	characteristic parameter, see eq. (24)
$\delta = \bar{z}/a$	dimensionless plunging amplitude
ξ_0	radial coordinate of the spheroid surface, see eq. (21)
χ	wave number, see eq. (4)

ρ_{∞}	fluid density of undisturbed flow
σ	angular amplitude of the pitching oscillation
ϕ	gauged wave function
ψ	wave function, see eq. (11)
Ψ	perturbation velocity potential
ω	circular frequency of oscillation
ω^*	reduced frequency, see eq. (27)

INTRODUCTION

In designing aircraft carrying external stores, aeroelastic aspects are of considerable importance. The carriage of stores on wings may significantly change their dynamic characteristics, and often adversely affect their aeroelastic properties as a result of reduced wing frequencies and the introduction of critical frequency ratios together with inertia, elastic and aerodynamic coupling between loads. Adverse flutter stability characteristics and considerably lowered flutter speeds may occur, and these restrictions severely constrain the flight envelope and the manoeuvrability of the aircraft.

As a prerequisite for performing aeroelastic analyses of aircraft carrying external stores, one needs knowledge of the unsteady airloads generated by the structural oscillations of the wing/store configurations. Whereas for general lifting surface configurations, sufficiently substantiated theoretical methods and computer routines are available, the prediction of the motion-induced unsteady airloads on oscillating non-lifting bodies still requires further development.

For the numerical prediction of the unsteady airloads on oscillating bodies, the Slender-Body-Theory, as originally established by G.N. Ward (1) and further developed by many investigators (2), was for a long time the most important approach. However, with the advent of high-speed computers and the development of panel techniques for the numerical solution of lifting surface integral equations, new possibilities became available. Thus, in recent time, several panel integration techniques for the prediction of the steady and unsteady airloads on bodies and wing/body configurations have been developed, as shown in references 3 to 5.

It is well-known, however, that a reliable prediction of the typical pressure peaks at the front and rear part of a non-lifting body exposed to an airstream is a difficult problem, and that the magnitude of these pressure peaks is extremely sensitive to the local box arrangement used with the panel techniques. For checking the quality of such numerical approaches and for obtaining a better insight with regard to an optimum panel arrangement, the knowledge of the related exact solutions would be of great benefit. The elaboration of such exact solutions for slender ellipsoids of revolution oscillating harmonically in subsonic compressible flow is the subject of this paper.

GOVERNING WAVE EQUATIONS AND BOUNDARY CONDITIONS

The governing equation for a body oscillating with small amplitudes about a steady mean position in compressible flow is the well-known linearized potential equation (ref. 7)

$$\frac{\partial^2 \Psi}{\partial x^2} + \frac{\partial^2 \Psi}{\partial y^2} + \frac{\partial^2 \Psi}{\partial z^2} - \frac{1}{a_\infty^2} \left(U_\infty \frac{\partial}{\partial x} + \frac{\partial}{\partial t} \right)^2 \Psi = 0 \quad (1)$$

where $\Psi(x, y, z, t)$ is the perturbation velocity potential and a_∞ the velocity of sound of the undisturbed flow. If we specialize our considerations to simple harmonic motions, for which $\Psi(x, y, z, t)$ becomes

$$\Psi(x, y, z, t) = \psi(x, y, z) e^{i\omega t} \quad (2)$$

with ω as the circular frequency of oscillation, eq. (1) reads:

$$\left(1 - \text{Ma}_\infty^2\right) \frac{\partial^2 \psi}{\partial x^2} + \frac{\partial^2 \psi}{\partial y^2} + \frac{\partial^2 \psi}{\partial z^2} - 2i\kappa \text{Ma}_\infty \frac{\partial \psi}{\partial x} + \kappa^2 \psi = 0 \quad (3)$$

This equation is a modified (generalized) wave equation, where $\psi(x, y, z)$ is the so-called wave function, and

$$\kappa = \frac{\omega}{a_\infty} \quad (4)$$

the wave number. For $\text{Ma}_\infty = 0$ eq. (3) takes the form of the classical Helmholtz wave equation for the medium at rest. If a solution of eq. (3) has been found, then a solution for any oscillation can be derived for a given initial condition by application of the principle of superposition.

The condition at the boundary of a body states that, over its surface, the normal component of fluid velocity $\partial\psi/\partial n$ is fixed by the body's motion. The geometry of the oscillating body at time t is given through the equation of motion of its surface:

$$F(x, y, z, t) = 0 \quad (5)$$

In steady state the body surface is given through

$$f(x, y, z) = 0 \quad (6)$$

so that the equation of the surface of a body oscillating harmonically with small amplitudes about a steady mean position can be expressed as follows:

$$F(x, y, z, t) = f(x, y, z) + \bar{f}(x, y, z) e^{i\omega t} \quad (7)$$

where $\bar{f}(x, y, z)$ is a given disturbance function (mode shape) of the body surface. Then, the linearized kinematic boundary condition over the body surface reads (ref. 7)

$$\frac{\partial f}{\partial x} \frac{\partial \psi}{\partial x} + \frac{\partial f}{\partial y} \frac{\partial \psi}{\partial y} + \frac{\partial f}{\partial z} \frac{\partial \psi}{\partial z} = - \left(U_{\infty} \frac{\partial \bar{f}}{\partial x} + i\omega \bar{f} \right) . \quad (8)$$

In addition to eq. (8), the condition must be fulfilled that the wavelike disturbances are propagating outward away from the body surface to infinity without reflexion.

Finally, when the wave function ψ is found, the unsteady pressure $p(x, y, z)e^{i\omega t}$ can be calculated from the following relation:

$$\frac{p}{q_{\infty}} = - \frac{2}{U_{\infty}} \left(\frac{\partial \psi}{\partial x} + \frac{i\omega}{U_{\infty}} \psi \right) , \quad (9)$$

where $q_{\infty} = \rho_{\infty} U_{\infty}^2 / 2$ denotes the dynamic pressure of the undisturbed flow.

SOLUTION OF THE BOUNDARY VALUE PROBLEM FOR AN OSCILLATING SPHEROID

BASIC CONCEPT OF SOLUTION

Equation (3) together with the afore-mentioned boundary conditions describes a boundary value problem of the Neumann type. In order to find solutions of the modified wave equation (3) we try to make use of the well-known solutions of the classical Helmholtz wave equation

$$\frac{\partial^2 \varphi}{\partial x_0^2} + \frac{\partial^2 \varphi}{\partial y_0^2} + \frac{\partial^2 \varphi}{\partial z_0^2} + k^2 \varphi = 0 , \quad (10)$$

which describes the radiation of waves in a x_0, y_0, z_0 coordinate system at rest relative to the flow, where $\varphi(x_0, y_0, z_0)$ is the wave function for an observer who moves with the undisturbed free flow. Solutions of eq. (10) can be found by application of the method of separation of variables. Consequently it must be possible to find solutions of eq. (3) in the same manner, provided it is possible to transform eq. (3) in such a way that it takes the form of eq. (10) in an appropriate new coordinate system. Then the known solutions of eq. (10) can be taken and retransformed into the original coordinate system, thus yielding a solution of the modified wave equation (3).

However, before we can follow this way, we have to remove yet an obstacle. Since eq. (3) is non self-adjoint, i. e. non-invariant with respect to a reflexion $x \rightarrow -x$, we first must transform eq. (3) into an adjoint differential equation. This is possible by applying a gauge transformation (see ref. 6)

$$\psi(x, y, z) = \varphi(x, y, z) \exp\left(ix \frac{\sqrt{1-\beta^2}}{\beta^2} x\right) \quad (11)$$

where

$$\beta = \sqrt{1 - \text{Ma}_\infty^2} \quad (12)$$

is the well-known Prandtl factor. With this transformation, eq. (3) reads

$$\beta^4 \frac{\partial^2 \varphi}{\partial x^2} + \beta^2 \frac{\partial^2 \varphi}{\partial y^2} + \beta^2 \frac{\partial^2 \varphi}{\partial z^2} + \kappa^2 \varphi = 0 \quad (13)$$

Then, by application of a coordinate scale transformation

$$\left. \begin{aligned} x &= \beta^2 x_0 \\ y &= \beta y_0 \\ z &= \beta z_0 \end{aligned} \right\} \quad (14)$$

eq. (13) finally takes exactly the form of the classical Helmholtz wave equation (10).

INTRODUCTION OF NON-ORTHOGONAL SPHEROIDAL COORDINATES

In order to apply the concept of separation of variables for the solution of eq. (10) for a harmonically oscillating spheroidal body we introduce the following prolate spheroidal coordinates:

$$\left. \begin{aligned} x_0 &= c \xi \eta \\ y_0 &= c \sqrt{\xi^2 - 1} \sqrt{1 - \eta^2} \cos \theta \\ z_0 &= c \sqrt{\xi^2 - 1} \sqrt{1 - \eta^2} \sin \theta \end{aligned} \right\} \quad (15)$$

with

$$1 \leq \xi \leq \infty ; \quad -1 \leq \eta \leq 1 ; \quad 0 \leq \theta \leq 2\pi . \quad (16)$$

Here the x-axis is chosen as the axis of rotation. The coordinate surfaces $\xi = \text{const}$ consist of confocal ellipsoids with the linear eccentricity c , whereas $\eta = \text{const}$ describes confocal hyperboloids, see Fig. 1. $\theta = \text{const}$ represents planes going through the x-axis. All these coordinate surfaces are normal to each other. Hence the coordinate system ξ, η, θ is orthogonal with respect to the initial coordinate system x_0, y_0, z_0 .

In the coordinate system ξ, η, θ the Helmholtz wave equation (10) takes the form

$$\begin{aligned} & \frac{1}{c^2(\xi^2 - \eta^2)} \left\{ \frac{\partial}{\partial \xi} \left[(\xi^2 - 1) \frac{\partial \varphi}{\partial \xi} \right] + \frac{\partial}{\partial \eta} \left[(1 - \eta^2) \frac{\partial \varphi}{\partial \eta} \right] + \right. \\ & \left. + \frac{\xi^2 - \eta^2}{(\xi^2 - 1)(1 - \eta^2)} \frac{\partial^2 \varphi}{\partial \theta^2} \right\} + \kappa^2 \varphi = 0 . \end{aligned} \quad (17)$$

Introduction of eqs. (15) into eqs. (14) yields the following coordinate relations:

$$\left. \begin{aligned} x &= \beta^2 c \xi \eta , \\ y &= \beta c \sqrt{\xi^2 - 1} \sqrt{1 - \eta^2} \cos \theta , \\ z &= \beta c \sqrt{\xi^2 - 1} \sqrt{1 - \eta^2} \sin \theta , \end{aligned} \right\} \quad (18)$$

That is, with these coordinate transformations, eq. (13) can be transformed into eq. (17) and can then be solved by applying the concept of separation of variables.

It is mentioned in passing that the coordinate surfaces $\theta = \text{const}$ are perpendicular to the surfaces $\xi = \text{const}$ and $\eta = \text{const}$, respectively. But this is not the case for the normals to the coordinate surfaces $\xi = \text{const}$ and $\eta = \text{const}$ as illustrated in Fig. 1. Moreover, upon introduction of eqs. (18) into the surface equation of the spheroid under consideration

$$\frac{x^2}{a^2} + \frac{y^2 + z^2}{b^2} = 1 , \quad (19)$$

one gets

$$a = \beta^2 c \xi_0 , \quad b = \beta c \sqrt{\xi_0^2 - 1} , \quad (20)$$

and therefrom

$$c = \frac{\sqrt{a^2 - \beta^2 b^2}}{\beta^2}, \quad \xi_0 = \frac{a}{\sqrt{a^2 - \beta^2 b^2}}. \quad (21)$$

In the ξ, η, θ coordinate system, c describes a characteristic length of the spheroid, which changes into the linear eccentricity $c = \sqrt{a^2 - b^2}$ for $\beta = 0$. The surface of the spheroid is given by $\xi = \xi_0$.

Finally, we have yet to apply the transformations expressed in eq. (11) and eq. (18) to eq. (8) and eq. (9). In the spheroidal coordinate system, the boundary condition, eq. (8), reads

$$\begin{aligned} & \frac{2\xi_0^2}{ac\alpha^2(\xi_0^2 - \eta^2)} \left[(\alpha^2 - \eta^2) \frac{\partial \varphi}{\partial \xi} + \frac{\alpha^2(1 - \beta^2)}{\beta^2 \xi} \eta(1 - \eta^2) \frac{\partial \varphi}{\partial \eta} + \right. \\ & \left. + \frac{i\gamma\alpha^2}{\beta^2\xi^3} \eta(\xi^2 - \eta^2) \varphi \right]_{\xi = \xi_0} e^{i\gamma\eta} = - \left[U_{\infty} \frac{\partial \bar{f}}{\partial x} + i\omega \bar{f} \right]_{\xi = \xi_0}, \end{aligned} \quad (22)$$

with

$$h = cx, \quad (23)$$

$$\gamma = h \sqrt{1 - \beta^2} \xi_0, \quad (24)$$

$$\alpha = \frac{a}{\sqrt{a^2 - b^2}}, \quad (25)$$

where h is a characteristic parameter of the spheroidal functions and α the reciprocal numerical eccentricity.

The pressure distribution, eq. (9), in spheroidal coordinates reads

$$\frac{p}{q_{\infty}} = - \frac{2}{\beta^2 c U_{\infty}} \left[\frac{\eta(\xi^2 - 1)}{\xi^2 - \eta^2} \frac{\partial \varphi}{\partial \xi} + \frac{\xi(1 - \eta^2)}{\xi^2 - \eta^2} \frac{\partial \varphi}{\partial \eta} + \frac{i c \omega^*}{2a} \varphi \right]_{\xi = \xi_0} e^{i\gamma\eta}, \quad (26)$$

where

$$\omega^* = \frac{2a\omega}{U_{\infty}} \quad (27)$$

denotes the reduced frequency which is based on the body length $2a$ as characteristic length.

SOLUTION OF THE WAVE EQUATION FOR A PROLATE SPHEROID

The possibilities of solving eq. (17), by applying the method of separation of variables, have extensively been discussed by several investigators in refs. 8 to 11. In particular, for a prolate spheroid, the solution has been given by C. Flammer (9). This solution to eq. (17) consists in a superposition of all partial waves expressed by the Lamé-product

$$\varphi = a U_{\infty} \sum_{m=1}^{\infty} \sum_{n=m}^{\infty} A_{mn} R_{mn}(h, \xi) S_{mn}(h, \eta) \sin m\theta \quad (28)$$

The spheroidal angle function of the first kind $S_{mn}(h, \eta)$ of the degree m and order n is given through the associated Legendre functions of the first kind $P_n^m(\eta)$:

$$S_{mn}(h, \eta) = \sum_{k=1}^{\infty} D_k^{mn}(h) P_{m+2k-\bar{n}}^m(\eta) \quad (29)$$

with

$$\bar{n} = \begin{cases} 2, & \text{if } n-m \text{ is even} \\ 1, & \text{if } n-m \text{ is odd} \end{cases} \quad (30)$$

The spheroidal radial function of fourth kind $R_{mn}(h, \xi)$ is given by

$$R_{mn}(h, \xi) = R'_{mn}(h, \xi) - i R''_{mn}(h, \xi) \quad (31)$$

with

$$R'_{mn}(h, \xi) = \frac{1}{K'_{mn}} \sum_{k=1}^{\infty} D_k^{mn}(h) P_{m+2k-\bar{n}}^m(\xi) \quad (32)$$

and

$$R''_{mn}(h, \xi) = \frac{1}{K''_{mn}} \left[\sum_{k=1}^{\infty} D_k^{mn}(h) Q_{m+2k-\bar{n}}^m(\xi) + \sum_{k=1}^m E_k^{mn}(h) Q_{m-2k+2-\bar{n}}^m(\xi) + \sum_{k=m+1}^{\infty} E_k^{mn}(h) P_{2k-m-3+\bar{n}}^m(\xi) \right] \quad (33)$$

where $Q_n^m(\xi)$ denotes the associated Legendre function of the second kind. The coefficients D_k^{mn} , E_k^{mn} , K_{mn}^I and K_{mn}^{II} are given in ref. 12, whereas the unknown coefficients A_{mn} are to be determined from the boundary condition, eq. (22), as shown later. Then, with the coefficients A_{mn} , the unsteady aerodynamic pressure can be calculated from eq. (26) as follows:

$$\begin{aligned} \frac{p}{q_\infty} = & -2\xi_0 \sum_{m=1}^{\infty} \sum_{n=m}^{\infty} A_{mn} \left\{ \frac{\eta(\xi^2-1)}{\xi^2-\eta^2} \frac{dR_{mn}(h,\xi)}{d\xi} S_{mn}(h,\eta) + \right. \\ & + \frac{\xi(1-\eta^2)}{\xi^2-\eta^2} R_{mn}(h,\xi) \frac{dS_{mn}(h,\eta)}{d\eta} + \\ & \left. + \frac{i\omega^*}{2\beta^2\xi} R_{mn}(h,\xi) S_{mn}(h,\eta) \right\}_{\xi=\xi_0} \sin m\theta e^{i\gamma\eta} \end{aligned} \quad (34)$$

SOLUTIONS FOR RIGID BODY PLUNGING AND PITCHING OSCILLATIONS

Since external stores of aircraft are relatively rigid bodies compared to the flexible wing, their oscillatory motions in a wing/store vibration mode consist primarily of rigid body motions. Thus, the rigid body motions are of main concern in unsteady aerodynamics of external stores, so that we may focus our further considerations on rigid body plunging and pitching oscillations of the spheroid.

When the spheroid with the surface function

$$f(x,y,z) = \frac{x^2}{a^2} + \frac{y^2+z^2}{b^2} - 1 \quad (35)$$

is undergoing harmonic rigid body plunging oscillations with amplitude $\bar{z} = a\delta$, the surface function has the form

$$F(x,y,z,t) = \frac{x^2}{a^2} + \frac{y^2}{b^2} + \frac{(z - a\delta e^{i\omega t})^2}{b^2} - 1 \quad (36)$$

For small amplitudes it follows from eq. (7)

$$\bar{f} = -\frac{2a\delta}{b^2} z \quad , \quad (37)$$

and the right hand side of eq. (22), taking into account eq. (18) and eq. (20), reads:

$$-U_{\infty} \left(\frac{\partial \bar{f}}{\partial x} + i\omega \bar{f} \right)_{\xi = \xi_0} = \frac{i\omega^* U_{\infty} \delta}{b} \sqrt{1 - \eta^2} \sin \theta \quad . \quad (38)$$

In the case of rigid body pitching oscillations with small angular deflections σ about an axis $x = \bar{x}$ parallel to the y -axis, the surface function is

$$F(x, y, z, t) = \frac{(x + z\delta e^{i\omega t})^2}{a^2} + \frac{y^2}{b^2} + \frac{[z - (x - \bar{x})\sigma e^{i\omega t}]^2}{b^2} - 1 \quad . \quad (39)$$

For small amplitudes, one gets

$$\bar{f} = -\frac{2\sigma}{\alpha^2 b^2} (x - \alpha^2 \bar{x}) z \quad , \quad (40)$$

and the right hand side of eq. (22) formulates as follows:

$$- \left[U_{\infty} \frac{\partial \bar{f}}{\partial x} + i\omega \bar{f} \right]_{\xi = \xi_0} = \frac{2\sigma U_{\infty}}{\alpha^2 b} \left[1 + \frac{i\omega^*}{2} (\eta - \alpha^2 \bar{\eta}) \right] \sqrt{1 - \eta^2} \sin \theta \quad , \quad (41)$$

with

$$\bar{\eta} = \frac{\bar{x}}{a} \quad . \quad (42)$$

From eqs. (38), (41) and (22) it becomes obvious that for rigid body motions only the wave function φ of degree $m = 1$ is needed. Thus, the solution given in eq. (28) takes the form

$$\varphi = a U_{\infty} \sum_{n=1}^{\infty} A_{1n} R_{1n}(h, \xi) S_{1n}(h, \eta) \sin \theta \quad . \quad (43)$$

After introduction of eqs. (38), (41) and (43) into eq. (22), one gets the following equation for the determination of the unknown coefficients A_{1n} :

$$\sum_{n=1}^{\infty} \bar{A}_{1n} \left[(\alpha^2 - \eta^2) \frac{dR_{1n}(h, \xi)}{d\xi} S_{1n}(h, \eta) + \frac{\alpha^2 (1 - \beta^2)}{\beta^2 \xi} \eta (1 - \eta^2) \right] \times \quad (44)$$

$$\times R_{1n}(h, \xi) \frac{dS_{1n}(h, \eta)}{d\eta} + \frac{i\gamma\alpha^2}{\beta^2\xi^3} \eta(\xi^2 - \eta^2) R_{1n}(h, \xi) S_{1n}(h, \eta) \Big]_{\xi = \xi_0} =$$

$$= \begin{cases} \frac{\alpha^2}{\beta\xi_0^2\sqrt{\xi_0^2-1}} \frac{i\omega^*}{2} (\xi_0^2 - \eta^2) \sqrt{1-\eta^2} e^{-i\gamma\eta}, & \text{for plunging oscillations} \\ \frac{1 + \frac{i\omega^*}{2}(\eta - \alpha^2\bar{\eta})}{\beta\xi_0^2\sqrt{\xi_0^2-1}} (\xi_0^2 - \eta^2) \sqrt{1-\eta^2} e^{-i\gamma\eta}, & \text{for pitching oscillations} \end{cases}$$

with

$$\bar{A}_{1n} = \begin{cases} \frac{A_{1n}}{\delta}, & \text{for plunging oscillations,} \\ \frac{A_{1n}}{\sigma}, & \text{for pitching oscillations.} \end{cases} \quad (45)$$

In order to determine the unknown coefficients A_{1n} from eq. (44) we multiply both sides of eq. (44) with the function $S_{1l}(h, \eta)$ of degree $m=1$ and order l , and integrate the resulting equation over η from -1 to 1 . Then we obtain the following set of linear algebraic equations with constant complex coefficients for the determination of the complex unknowns A_{1n} , ($n = 1, 2, 3, \dots, \infty$):

$$\sum_{n=1}^{\infty} \bar{A}_{1n} \left[\frac{dR_{1n}(h, \xi)}{d\xi} \Big|_{\xi_0} I_0(l, n) + \frac{\alpha^2(1-\beta^2)}{\beta^2\xi_0} R_{1n}(h, \xi_0) I_1(l, n) + \right. \quad (46)$$

$$\left. + \frac{i\gamma\alpha^2}{\beta^2\xi_0^3} R_{1n}(h, \xi_0) I_2(l, n) \right] =$$

$$= \begin{cases} \frac{\alpha^2}{\beta\xi_0^2\sqrt{\xi_0^2-1}} \frac{i\omega^*}{2} \left[\xi_0^2 J_0(l) - J_2(l) \right], & \text{for plunging oscillations} \\ \frac{1}{\beta\xi_0^2\sqrt{\xi_0^2-1}} \left\{ \left(1 - \frac{i\omega^*}{2} \alpha^2 \bar{\eta} \right) \left[\xi_0^2 J_0(l) - J_2(l) \right] + \frac{i\omega^*}{2} \left[\xi_0^2 J_1(l) - J_3(l) \right] \right\}, & \text{for pitching oscillations} \end{cases}$$

with $l = 1, 2, 3, \dots, \infty$.

Therein $I_i(l, n)$, ($i = 0, 1, 2$) and $J_i(l, n)$, ($i = 0, 1, 2, 3$) are integrals over the spheroidal functions $S_1(h, \eta)$, the solutions of which are given in ref. 12.

In practical calculations, we have always to limit ourselves to a finite number, N , of equations. It has been found that for $N = 100$, full convergence within the range of computer accuracy can be attained. The solution of the resulting system of N complex or $2N$ real algebraic equations for the determination of the N unknown coefficients A_{1n} can then be performed, applying standard matrix routine procedures. Upon introduction of these coefficients into eq. (34), the unsteady pressure distributions for the spheroid oscillating in plunge and pitch can be calculated.

NUMERICAL RESULTS

In order to compare these analytical results with those obtained from panel and slender body approaches and from measurements, a computer program has been developed. Some typical results for the pressure distributions on a spheroid with $a/b = 4$ oscillating harmonically in rigid body plunging and pitching mode at various reduced frequencies ω^* and Mach numbers Ma_∞ are illustrated in Fig. 2 and Fig. 3. For the same mode shapes, Fig. 4 and Fig. 5, show the pressure distributions on various spheroids at $Ma_\infty = 0.5$ and $\omega^* = 2$. It is seen that strong pressure peaks appear near the front and the rear body part. These contribute considerably to the overall generalized airloads in aeroelastic modal analyses.

Finally, in Fig. 6 and Fig. 7, for a slender spheroid oscillating again in plunge and pitch, the results of the present theory are compared to those obtained from Geißler's panel procedure (3), from Slender-Body-Theory (2) and from experiment (13). With the exception of the front and the rear part of the body there is generally good agreement between the theoretical results. Around the rear and front body parts, Slender-Body-Theory yields necessarily a singular pressure behavior, whereas Geißler's panel results are somewhat superelevated. From that it becomes clear that a reliable prediction of the pressure peaks in these regions is difficult, and that the magnitude of these peaks is very sensitive to the local arrangement of the integration boxes adopted in a panel procedure.

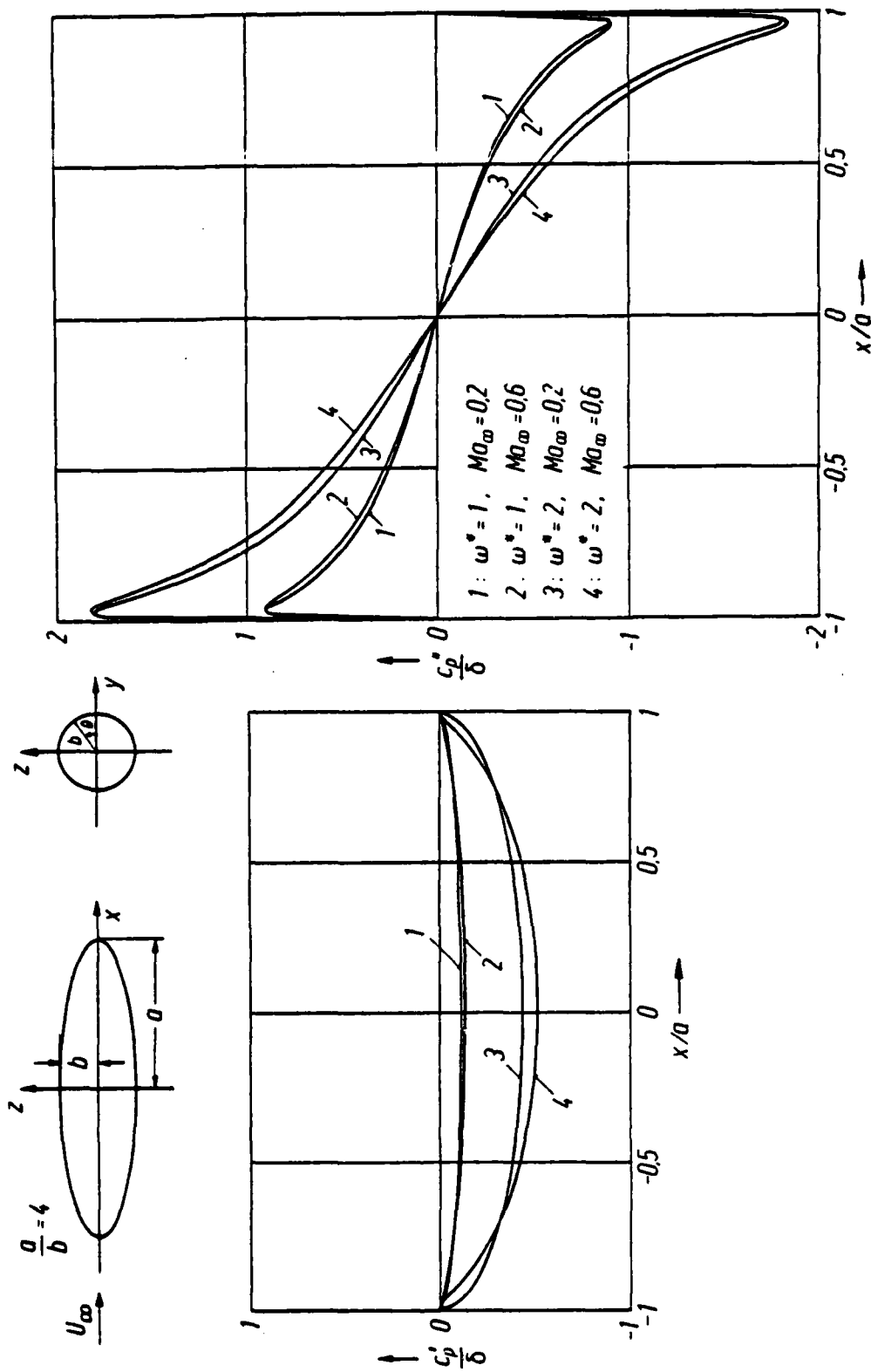


Fig. 2 Unsteady aerodynamic pressure distributions on a prolate spheroid at harmonic plunging oscillations

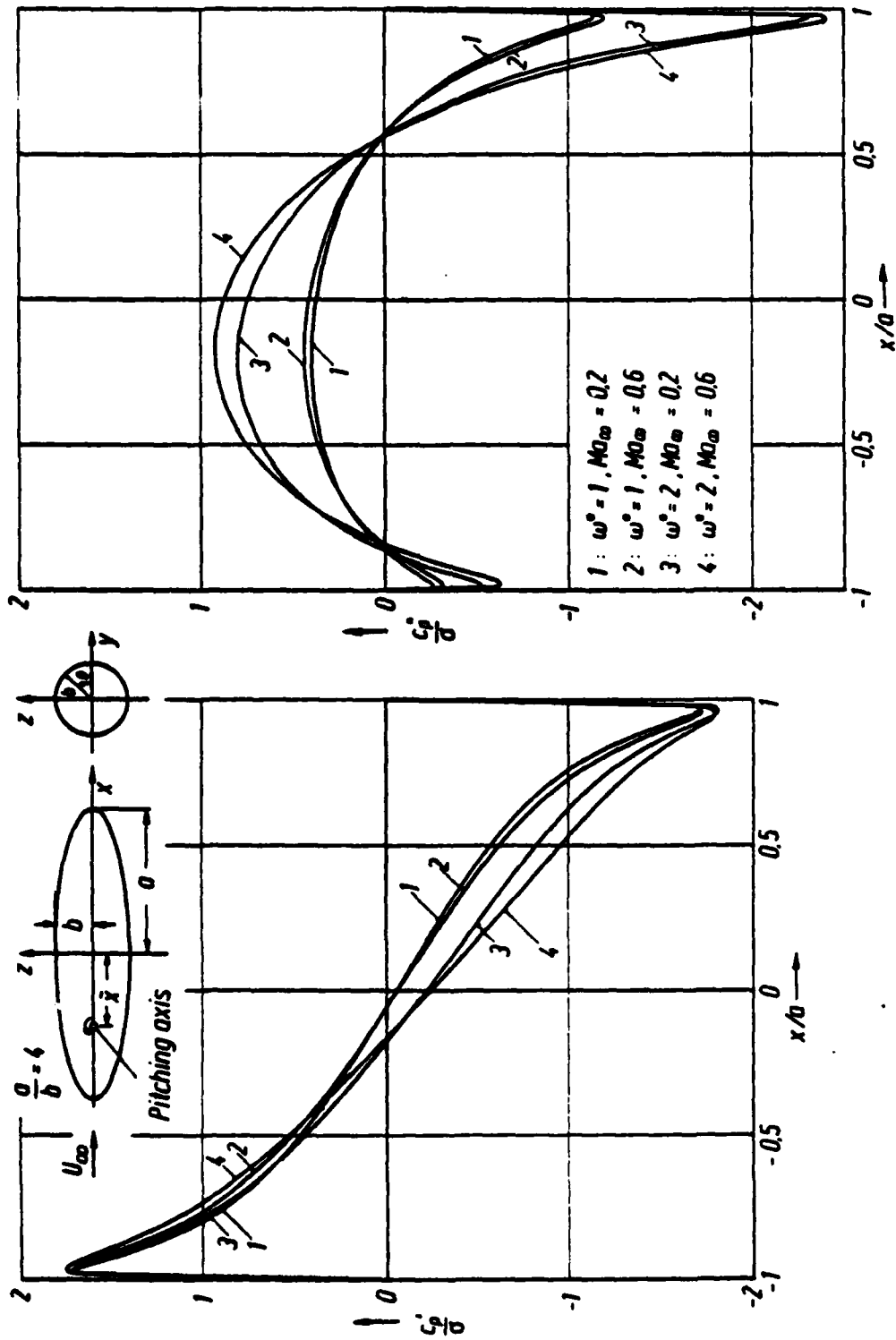


Fig. 3 Unsteady aerodynamic pressure distributions on a prolate spheroid at harmonic pitching oscillations

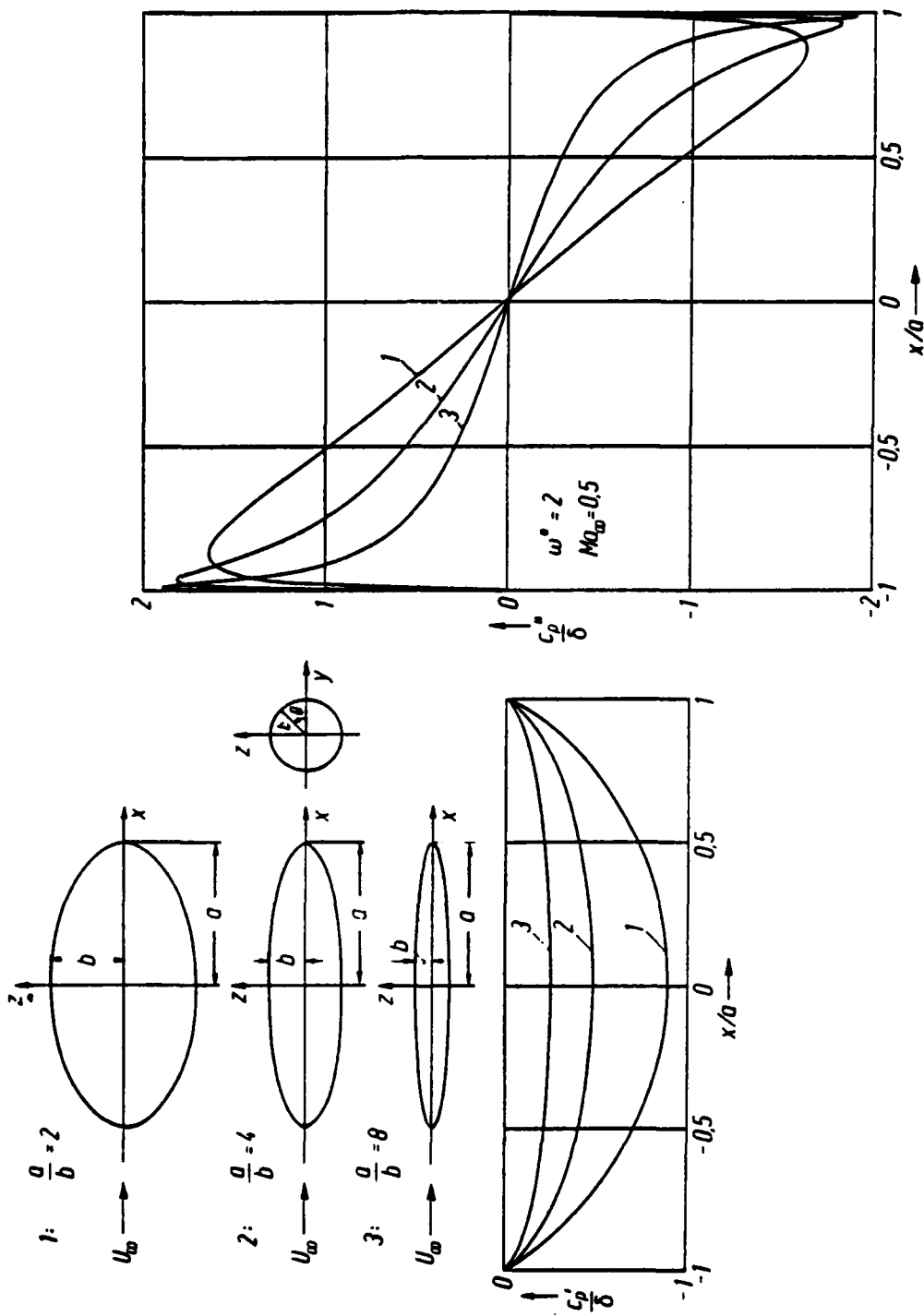


Fig. 4 Unsteady aerodynamic pressure distributions on three spheroids at harmonic plunging oscillations

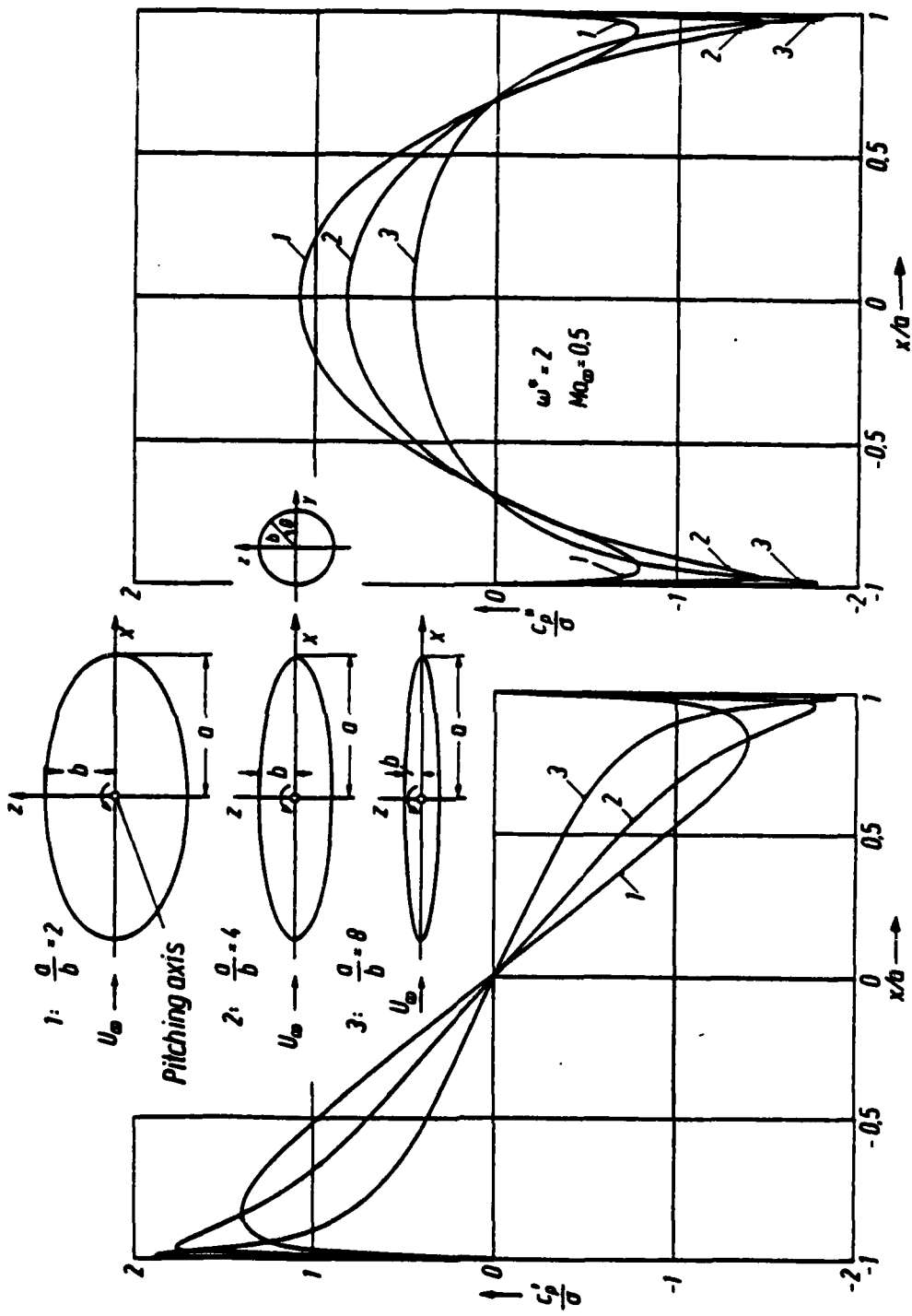


Fig. 5 Unsteady aerodynamic pressure distributions on three spheroids at pitching oscillations

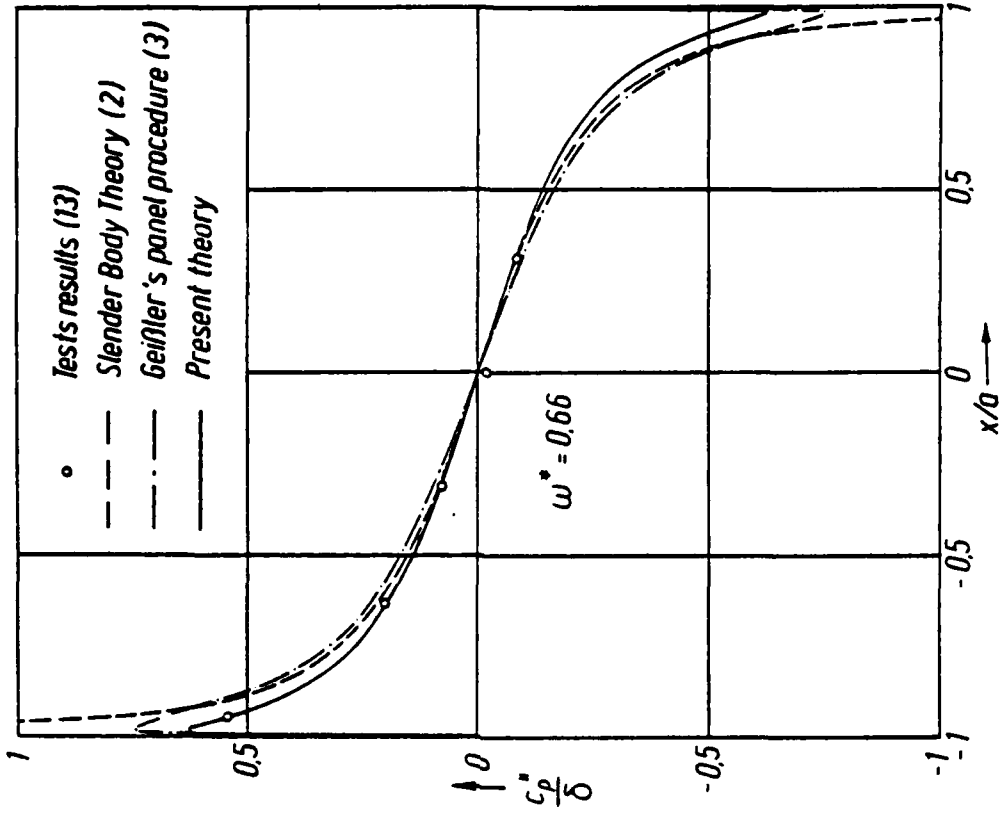
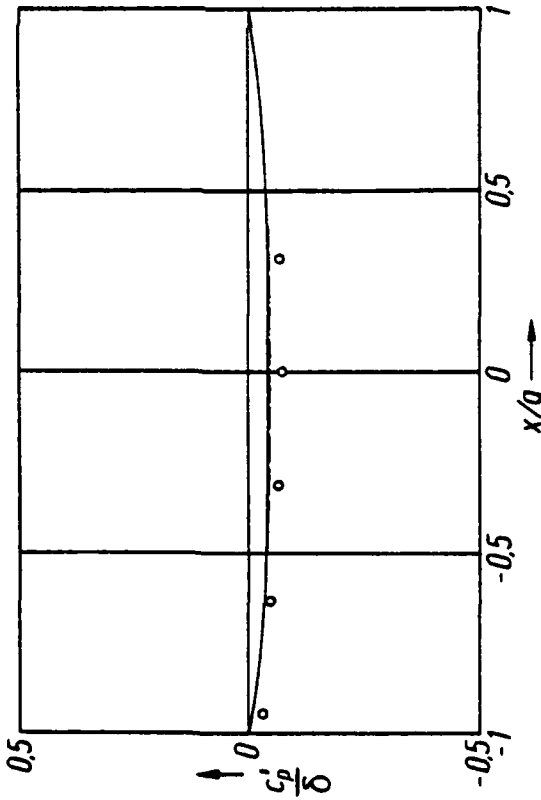
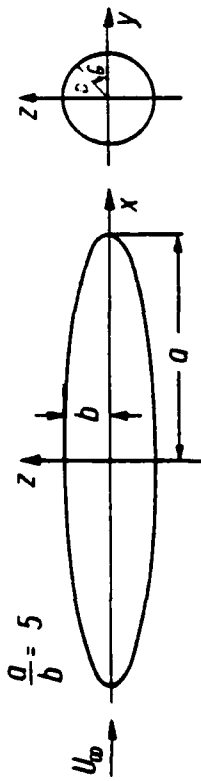


Fig. 6 • Comparison of computed and measured unsteady aerodynamic pressure distributions on a spheroid performing harmonic plunging oscillations in incompressible flow

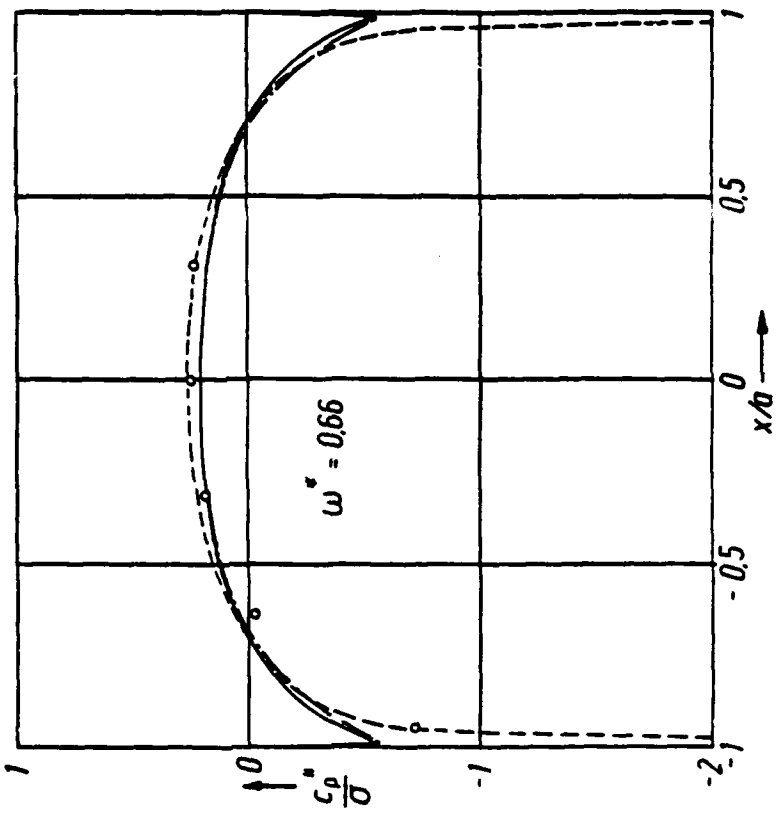
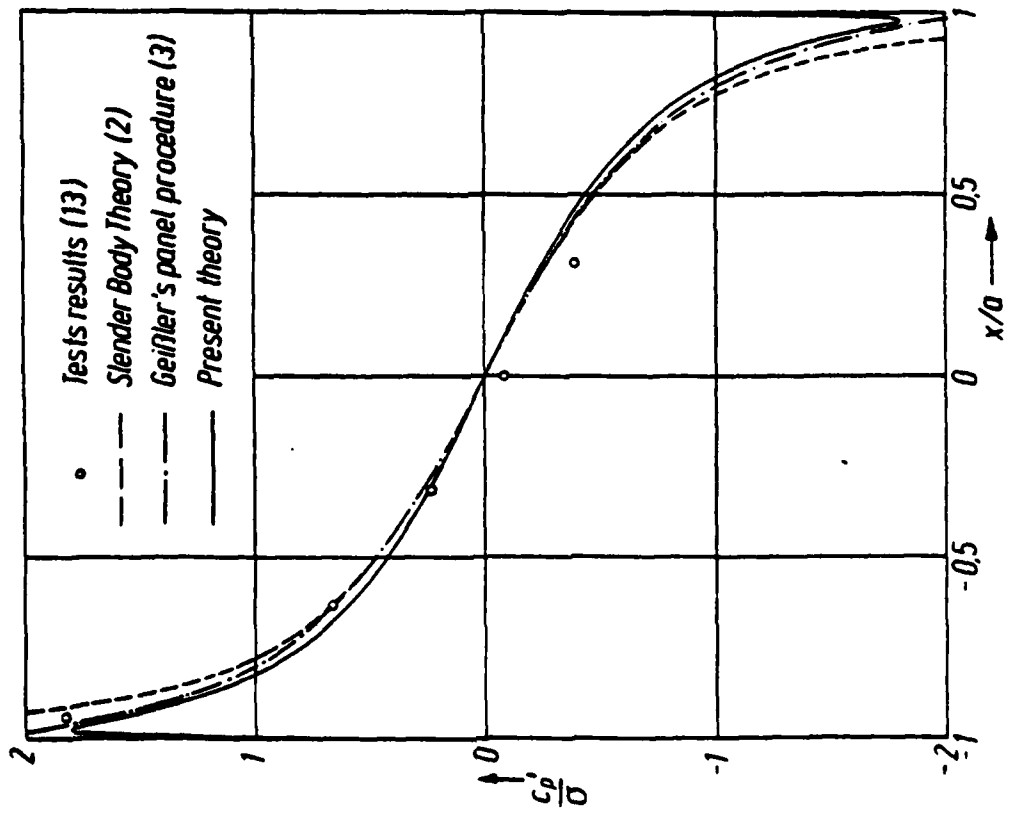
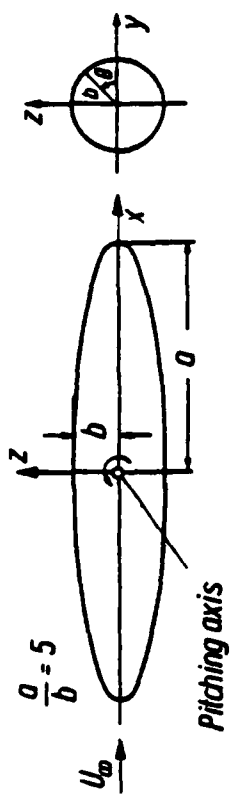


Fig. 7 Comparison of computed and measured unsteady aerodynamic pressure distributions on a spheroid performing harmonic pitching oscillations in incompressible flow

REFERENCES

- 1 Ward, G. N. Supersonic Flow Past Slender Pointed Bodies.
Quart. J. Mech. Appl. Math. , Vol. 2 (1949)
p. 75-120.
- 2 Woodcock, D. L. Slender-Body-Theory.
Manual on Aeroelasticity Vol. 2, Chap. 7 (1968).
- 3 Geißler, W. Berechnung der Druckverteilung an harmonisch oszillierenden dicken Rumpfen in inkompressibler Strömung.
DFVLR-AVA-Bericht 253 - 76 J 05 (1976).
- 4 Roos, R.
Bennekens, S.
Zwaan, R. J. A Calculation Method for Unsteady Subsonic Flow about Harmonically Oscillating Wing-Body Configurations.
AIAA-Paper 75-864 (1975).
- 5 Giesing, J. P.
Kalman, I. P.
Rodden, W. P. Subsonic Unsteady Aerodynamics for General Configurations.
Part I: Direct Application of the Non-planar Doublet-Lattice-Method.
AFFD-TR-71-5, U. S. Airforce Flight Dynamics Lab. , Dayton/Ohio (1972).
- 6 Courant, R.
Hilbert, H. Methoden der mathematischen Physik I.
Berlin, Heidelberg, New York: Springer-Verlag (1958).
- 7 Försching, H. Grundlagen der Aeroelastik.
Berlin, Heidelberg, New York: Springer-Verlag (1974).
- 8 Morse, P. M.
Feshbach, H. Methods of Theoretical Physics, Part II.
New York: Mc Graw-Hill Book Company, Inc. (1953)
- 9 Flammer, C. Spheroidal Wave Functions.
Stanford (California): Stanford Univ. Press. (1957).

- 10 Van Buren, A. L. Acoustic Radiation Impedance of Caps and Rings on Prolate Spheroids.
J. of the Acoustical Society of America Vol. 50 (1971) p. 1344.
- 11 Chertock, G. Sound Radiation from Prolate Spheroids.
J. of the Acoustical Society of America Vol. 33 (1961) p. 871.
- 12 Chao, K. -L. Analytische Lösung der verallgemeinerten Helmholtz-Wellengleichung für kompressible Unterschallströmung und Berechnung der instationären Druckverteilungen an harmonisch schwingenden rotationselliptischen Körpern.
DLR-FB 77-11 (1977).
- 13 Triebstein, H. Instationäre Druckverteilungsmessungen an Flügel-Außenlastkombinationen in inkompressibler Strömung.
DFVLR-AVA-Bericht 253 - 76 J 10 (1976).

F-16 FLUTTER MODEL STUDIES WITH EXTERNAL WING STORES
(U)
(Article UNCLASSIFIED)

by

Jerome T. Foughner, Jr.
NASA Langley Research Center
Hampton, VA 23665

and

Charles T. Bensinger
General Dynamics Corporation
Fort Worth, TX 76101

ABSTRACT. (U) The flutter prevention and clearance task for the F-16 airplane is being accomplished in a combined analysis, wind tunnel dynamic model test, and flight flutter test program. This paper presents highlight results from transonic flutter model studies. The flutter model was constructed to support the flutter prevention and clearance program from preliminary design through flight flutter tests. The model tests were conducted in the National Aeronautics and Space Administration's Langley Transonic Dynamics Tunnel. The large full-span free-flying model is shown to be an effective tool in defining airplane flutter characteristics by demonstrating freedom from flutter for most configurations and by defining optimum solutions for a few troublesome configurations.

"Approved for public release; distribution unlimited."

LIST OF FIGURES

1. F-16 Carries a Variety of External Stores
2. F-16 Full Scale Development Take-Off Store Loadings
3. Quarter-Scale Flutter Model Installation
4. Wing Pylon Store Locations
5. Asymmetry Increases Flutter Speed
6. Launcher Ballast Improves Missile Flutter Speed
7. Low Damping Precedes GBU-8/B Flutter
8. External Tank Fuel Usage Sequence Change Increases Flutter Speed

INTRODUCTION

The prediction and the prevention of flutter on fighter aircraft carrying stores is a subject which is currently receiving widespread attention (for example, see ref. 1). Because tactical airplanes such as the F-16, shown in figure 1, carry a variety of external stores, numerous potentially flutter critical store combinations must be evaluated during flutter clearance studies. The addition of external stores to the wing changes the structural dynamics of the airplane usually resulting in a reduction of flutter speed.

The flutter prevention and clearance task for the F-16 airplane is being accomplished in a combined analysis, wind-tunnel dynamic-model test, and flight flutter test program. The purpose of this paper is to present some results obtained from transonic flutter model studies of the F-16 airplane with external wing stores. The flutter model was constructed to support the flutter prevention and clearance program from preliminary design through flight flutter tests. The wind-tunnel results were used to demonstrate the required flutter speed margin and to verify analytical methods. Approximately 270 wing-store configurations have been identified for the F-16 airplane from the 21 take-off store loadings shown in figure 2. The vast majority were found by analysis to present no problem. A few loadings were found to be marginal from a flutter standpoint with respect to the required flutter margin of safety. The flutter model test configurations were chosen to include the marginal loadings along with a representative cross-section of store weights and shapes and those configurations to be flight flutter tested.

The model tests were conducted in the National Aeronautics and Space Administration's Langley transonic dynamics tunnel. This facility was specifically designed (refs. 2 and 3) for experimental studies on flutter and other aeroelastic phenomena. The quarter-scale, full-span, free-flying transonic flutter model was designed and constructed by the Fort Worth Division of General Dynamics Corporation. The model was dynamically and aeroelastically scaled to simulate the F-16 airplane during sea level flight at Mach number of 1.2. The quarter-scale F-16 model wind-tunnel test program was initiated in June 1975 and continued into March 1977. One hundred and forty-nine model configurations were tested during four tunnel entries made during this period, 86 days of testing. The first two entries were preliminary tests where the model design was based on calculated values of airplane mass, stiffness, and vibration modes. For entries three and four the model was updated to incorporate measured airplane mass and stiffness.

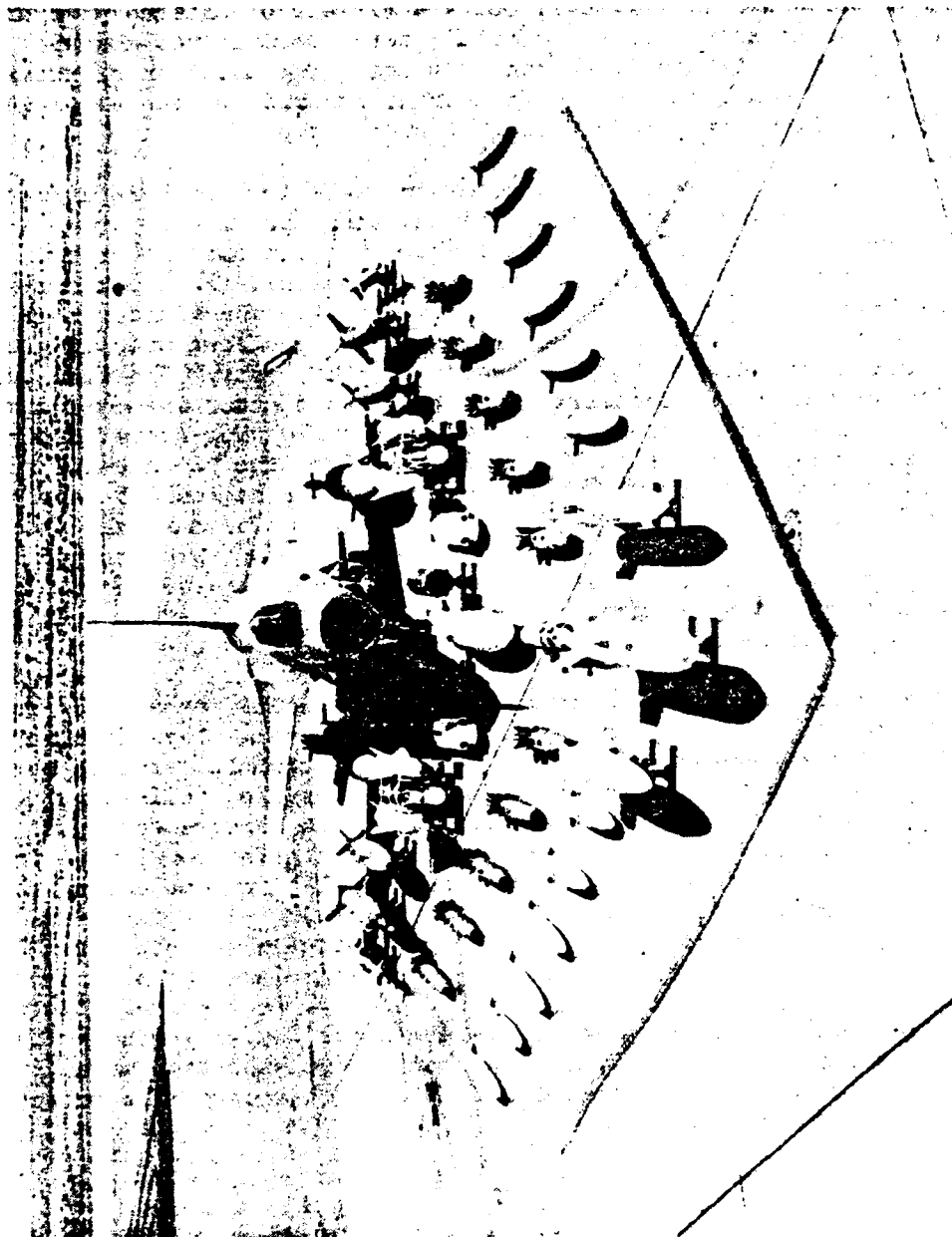


Figure 1.- F-16 Carries a Variety of External Stores.

LOADING	TIP	0.83	0.63	0.37	CENTERLINE	0.37	0.63	0.83	TIP
AIR-TO-AIR									
1	AIM-9J	-	-	370 TK	-	370 TK	-	-	AIM-9J
2	AIM-9J	AIM-9J	-	370 TK	ALQ-119-12	370 TK	-	-	AIM-9J
3	AIM-9J	-	ALQ-119-14	370 TK	-	370 TK	ALQ-119-14	-	AIM-9J
23	AIM-9J	-	ALQ-119-14	370 TK	300 TK	370 TK	ALQ-119-14	-	AIM-9J
AIR-TO-GROUND									
4	AIM-9J	-	ALQ-119-12	(6) MK-82	300 TK	(6) MK-82	-	-	AIM-9J
5	AIM-9J	-	(3) MK-82	370 TK	ALQ-119-12	370 TK	(3) MK-82	-	AIM-9J
6	AIM-9J	-	(3) MK-82R	370 TK	ALQ-119-12	370 TK	(3) MK-82R	-	AIM-9J
7	AIM-9J	-	(1) MK-82R	(4) MK-82R	300 TK	(4) MK-82R	(1) MK-82R	-	AIM-9J
8	AIM-9J	-	(1) MK-84	370 TK	ALQ-119-12	370 TK	(1) MK-84	-	AIM-9J
9	AIM-9J	-	-	DELETED	-	-	-	-	AIM-9J
10	AIM-9J	-	(3) AGM-65	370 TK	ALQ-119-12	370 TK	(3) AGM-65	-	AIM-9J
11	AIM-9J	-	(1) GBUI0A/B	370 TK	ALQ-119-12	370 TK	(1) GBUI0A/B	-	AIM-9J
12	AIM-9J	-	(1) GBUB/B	370 TK	ALQ-119-12	370 TK	(1) GBUB/B	-	AIM-9J
13	AIM-9J	-	-	DELETED	-	-	-	-	AIM-9J
14	AIM-9J	-	ALQ-119-12	(4) CBU-58/B	300 TK	(4) CBU-58/B	(2) CBU-58/B	-	AIM-9J
15	AIM-9J	-	(1) SUU-25C/A	370 TK	ALQ-119-12	370 TK	(1) SUU-25C/A	-	AIM-9J
16	AIM-9J	-	(3) MK-20 MOD 4	370 TK	ALQ-119-12	370 TK	(3) MK-20 MOD 4	-	AIM-9J
17	AIM-9J	-	ALQ-119-12	370 TK	B-43	370 TK	-	-	AIM-9J
18	AIM-9J	-	ALQ-119-12	370 TK	B-57	370 TK	-	-	AIM-9J
19	AIM-9J	-	ALQ-119-12	370 TK	B-61	370 TK	-	-	AIM-9J
20	LAUNCHER	-	(1) SUU-20B/A	370 TK	-	370 TK	(1) SUU-20B/A	-	LAUNCHER
	LAUNCHER	-	w/BDU-33B/B	370 TK	-	370 TK	w/BDU-33B/B	-	LAUNCHER
21	LAUNCHER	-	(1) SUU-20B/A	370 TK	-	370 TK	(1) SUU-20B/A	-	LAUNCHER
	LAUNCHER	-	w/MK-106	370 TK	-	370 TK	w/MK-106	-	LAUNCHER
22	LAUNCHER	-	-	370 TK	FERRY	370 TK	-	-	LAUNCHER
	LAUNCHER	-	-	370 TK	300 TK	370 TK	-	-	LAUNCHER

Figure 2.- F-16 Full Scale Development Take-Off Store Loadings.

MODEL

The quarter-scale flutter model is shown installed in the Langley transonic dynamics tunnel in figure 3. The model is suspended in the wind-tunnel test section by a two-cable mount system. The use of the two-cable mount system (ref. 4) allows close simulation of the free-flight rigid-body modes of complete aircraft in the wind tunnel. The system consists of a pair of cables which pass through pulleys in the model; one cable extends upstream in a horizontal plane and the other extends downstream in a vertical plane. The cable mounted model was "flown" in the wind tunnel by means of remotely controlled horizontal tails which provided roll and pitch trim control.

MODEL FABRICATION

The wing, horizontal tail, and vertical tail were all constructed in a similar manner. Precured fiberglass skins were bonded to a contoured Nomex honeycomb core. A machined aluminum fitting was bonded to the root of each surface to provide a means of attachment to the fuselage. Proper mass distributions for each surface were obtained during assembly by use of ballast weights which were a mixture of tungsten chips and epoxy resin. The wing included leading-edge and trailing-edge devices. The leading-edge actuator stiffness was simulated by four tuned steel springs. The flaperon actuator restraint stiffness was simulated by a steel spring at the root. The wing assembly was bolted to steel support beams which are rigidly attached to the fuselage spar. The fuselage consists of a thin wall steel spar box with fiberglass shell sections attached. The nine shell sections are of sandwich construction with fiberglass skins bonded to Nomex core. A flow through inlet duct was installed on the model to insure correct flow around the fuselage. This inlet duct is a fiberglass shell with a cross-sectional area sized to establish the proper flow conditions at a simulated sea level altitude and a Mach number of 0.90.

WING PYLON STORE STATIONS

As shown in figure 4, external stores can be mounted at nine stations-- one on the fuselage centerline, six under the wing, and two at the wing tips. Electronic countermeasure pods, bombs, and fuel tanks are examples of stores carried on the fuselage centerline. Three types of flexible pylons (fuel, weapons, adapter) attach to wing hardpoints. Flexible pylon locations are shown in figure 4 as a fraction of wing semi-span. The fuel tank store stations are located inboard (0.37) near the fuselage. The air-to-ground stores are carried at the weapons station located outboard of the wing mid-span (0.63) and at the inboard station. (0.37). Air-to-air missiles are carried on an adapter pylon (0.83) and on a launcher located at the wing tip.

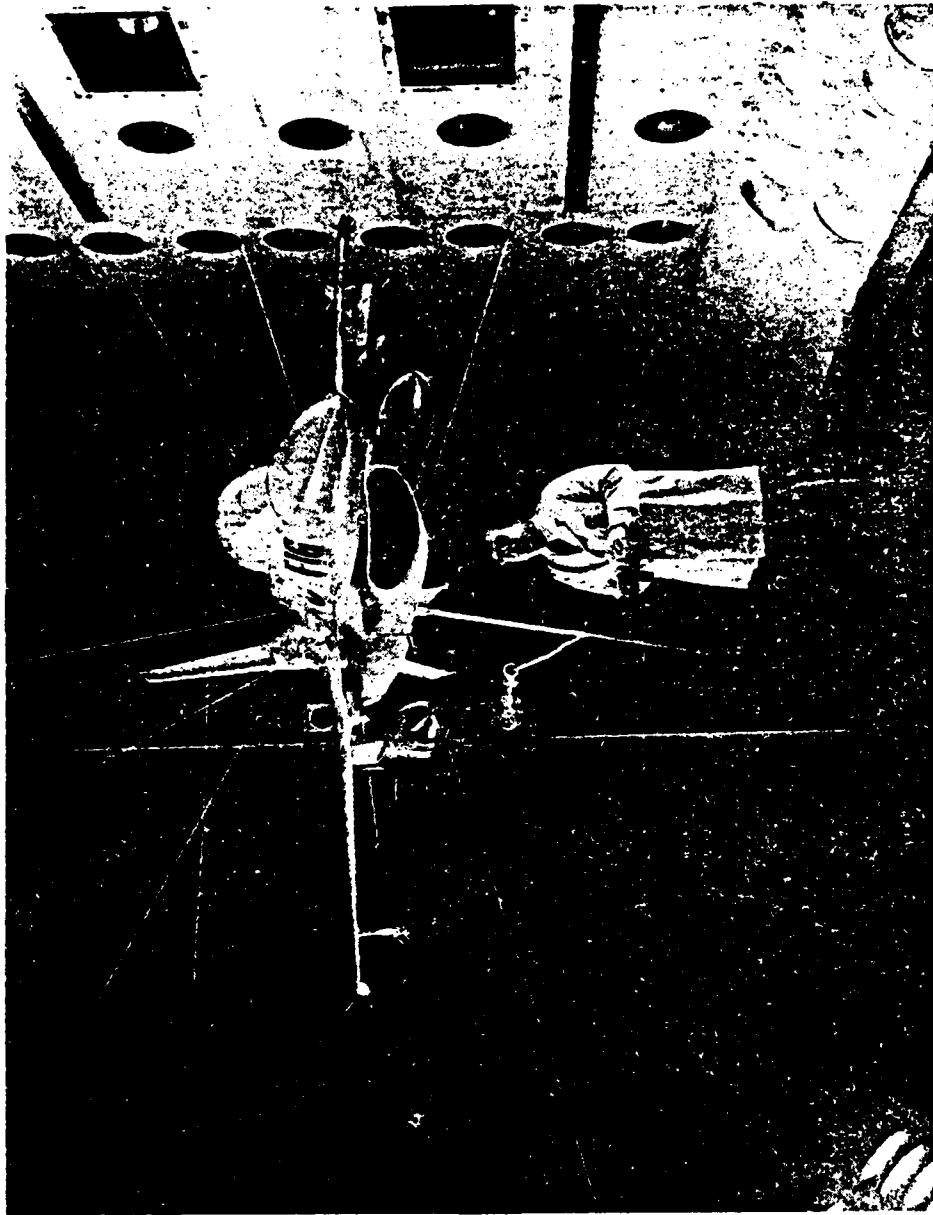


Figure 3.- Quarter-Scale Flutter Model Installation.

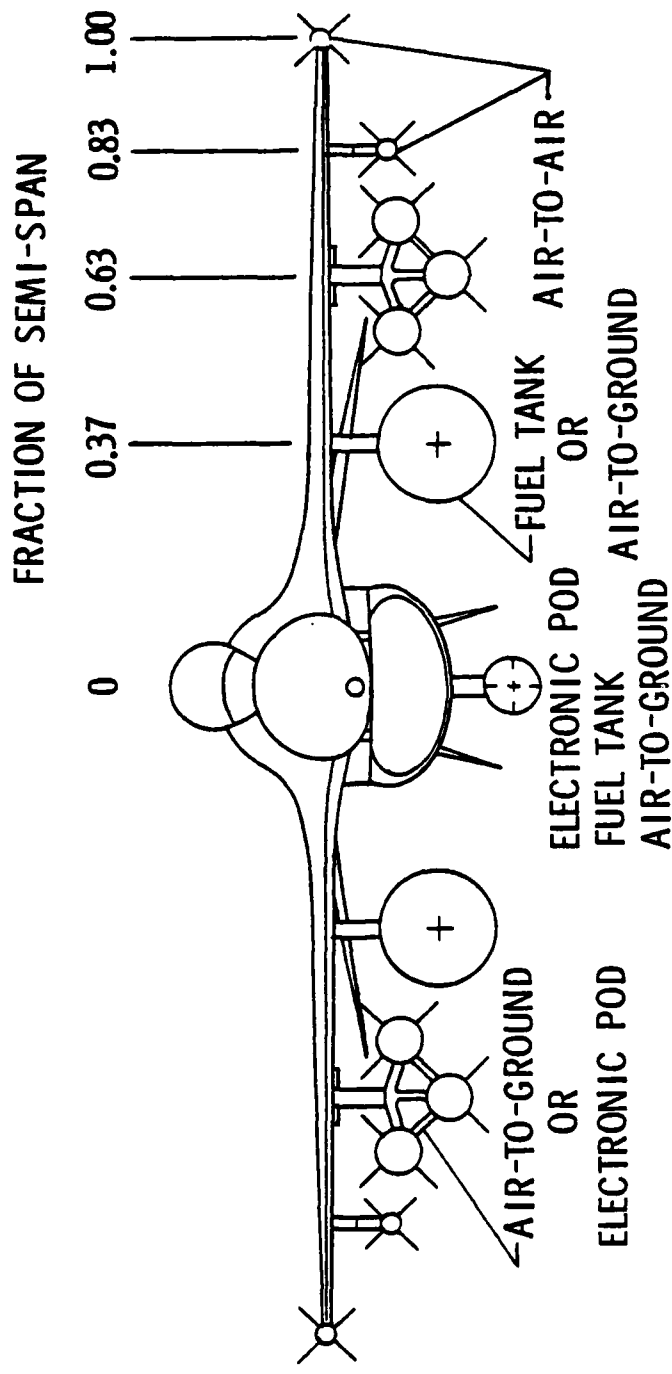


Figure 4.- Wing Pylon Store Locations.

ANALYSIS

In support of the wind-tunnel tests, flutter analyses were made at Mach numbers of 0.9 and 1.2 for each configuration to be tested. These calculations were made by Dave Shelton, Darlene Watts, and Paul Waner of the General Dynamics Corporation. The aerodynamic representation used in the wing-store analyses was based on the technique developed by Cunningham in reference 5.

It was found that the analysis gave a conservative prediction of the wind tunnel test results. Differences between the analyses and test results are attributed to the difficulties in accurately predicting the flutter speed of lowly damped roots. In cases where the analytical and model experimental results differ, the model results are considered to be more reliable in predicting full scale airplane flutter characteristics.

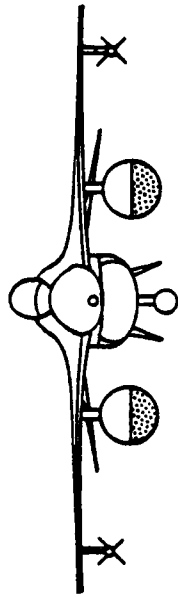
RESULTS AND DISCUSSIONS

Highlight results from the wind-tunnel model studies are presented in this section. The wind-tunnel model results are presented in the form of a reference equivalent airspeed ratio V/V_{REF} as a function of Mach number. The following topics are covered herein:

1. Asymmetrical Store Configurations Have Higher Flutter Speeds
2. Flutter With Air-To-Air Missiles Increased By Use of Ballast
3. Low Damping Precedes Flutter of a GBU-8/B Heavy Bomb
4. External Fuel Tank Usage Sequence

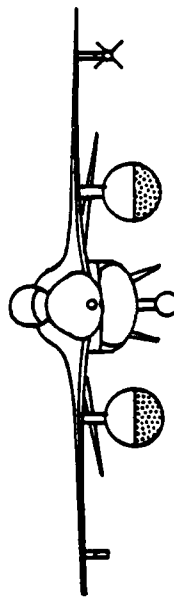
ASYMMETRICAL STORE CONFIGURATIONS HAVE HIGHER FLUTTER SPEEDS

Asymmetrical external store configurations are possible for an airplane such as the F-16; that is, the store loading on one wing differs from that on the other. The use of a complete flutter model flown on the two-cable mount system allows for experimental flutter clearance of asymmetrical external store configurations. A procedure often used (refs. 6 and 7) to reduce the size of the flutter prevention task is to analyze all configurations as being carried symmetrically. The assumption is that asymmetric configurations are inherently more stable than symmetric configurations. Experimental evidence to support this assumption for the F-16 is presented in figure 5. For the symmetrical fuel tank and underwing missile configuration shown at the top of figure 5, antisymmetric



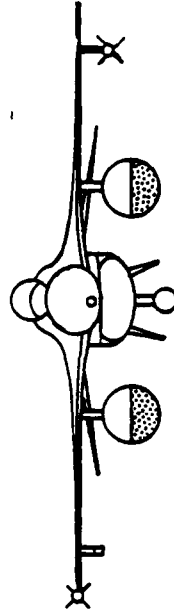
SYMMETRIC CONFIGURATION

ANTISYMMETRIC FLUTTER $V/V_{REF} = 0.875$



ASYMMETRIC CONFIGURATION

ANTISYMMETRIC FLUTTER $V/V_{REF} = 0.958$



ASYMMETRIC CONFIGURATION

NO FLUTTER $V/V_{REF} = 1.05$

Figure 5.- Asymmetry Increases Flutter Speed.

flutter occurred at a reference equivalent airspeed ratio of 0.875. The asymmetric configuration shown at the bottom left of figure 5 was obtained by removing an under-wing missile. Flutter then occurred at a reference equivalent airspeed ratio of 0.958. For the asymmetric configuration of a wing-tip missile on one wing and under-wing missile on the other wing, as shown at the bottom right of figure 5, no flutter occurred out to an equivalent airspeed ratio of 1.05. The symmetrical configuration fluttered at a lower speed than either asymmetrical configuration shown in figure 5. The effect of asymmetrical store configurations in this case is to increase the flutter speed.

FLUTTER SPEED WITH AIR-TO-AIR MISSILES INCREASED BY USE OF BALLAST

A large portion of the flutter model tests was devoted to configurations with four air-to-air AIM-9J missiles. Preliminary model test results are given in figure 6a. For the basic four missile configuration symmetric flutter occurred at Mach numbers 1.12 and 1.09, near the required flutter margin of safety boundary. As seen in figure 6a, removal of the tip missiles resulted in antisymmetric flutter occurring at reduced airspeeds at Mach number of 1.0 and 1.07. This flutter mode was the result of coupling between two closely spaced antisymmetric modes, under-wing missile pitch at 9.55 Hz, and wing first bending at 9.62 Hz. In view of the above results, an analytical and model parametric study was undertaken to evaluate methods of increasing the flutter speed by increasing the frequency separation of these two modes. Methods examined included moving the under-wing missiles forward, stiffening the missile launchers, and adding ballast weight to the missile launchers.

When the first method (moving missile forward) was tested, the model and analysis showed different trends. However, by refining the analysis to include aerodynamic interaction between the wing and the missile, better correlation with the model results was obtained. The flutter model results showed that a 0.254 meter forward movement of the under-wing missile was beneficial for the loading with the two under-wing missiles, but decreased the flutter speed ten percent for the four missile loading.

The second method, stiffening the missile launchers, was successful in increasing the flutter speed, but required too large a weight penalty and was not considered an acceptable solution.

The third method, adding a small ballast weight to the missile launchers, was selected to improve the flutter characteristics of the four missile case. Ballasted-launcher test results are presented in figure 6b. The changes in the model from the initial test are slightly lengthened missile launchers (required to accommodate potential change over to AIM-9L missiles) which have a small ballast added in the nose. With launcher ballast, the four-missile loading (figure 6b) fluttered at a Mach number of 1.10, at an airspeed slightly higher than the initial case (figure 6a). The loading with the tip missile removed showed no flutter (figure

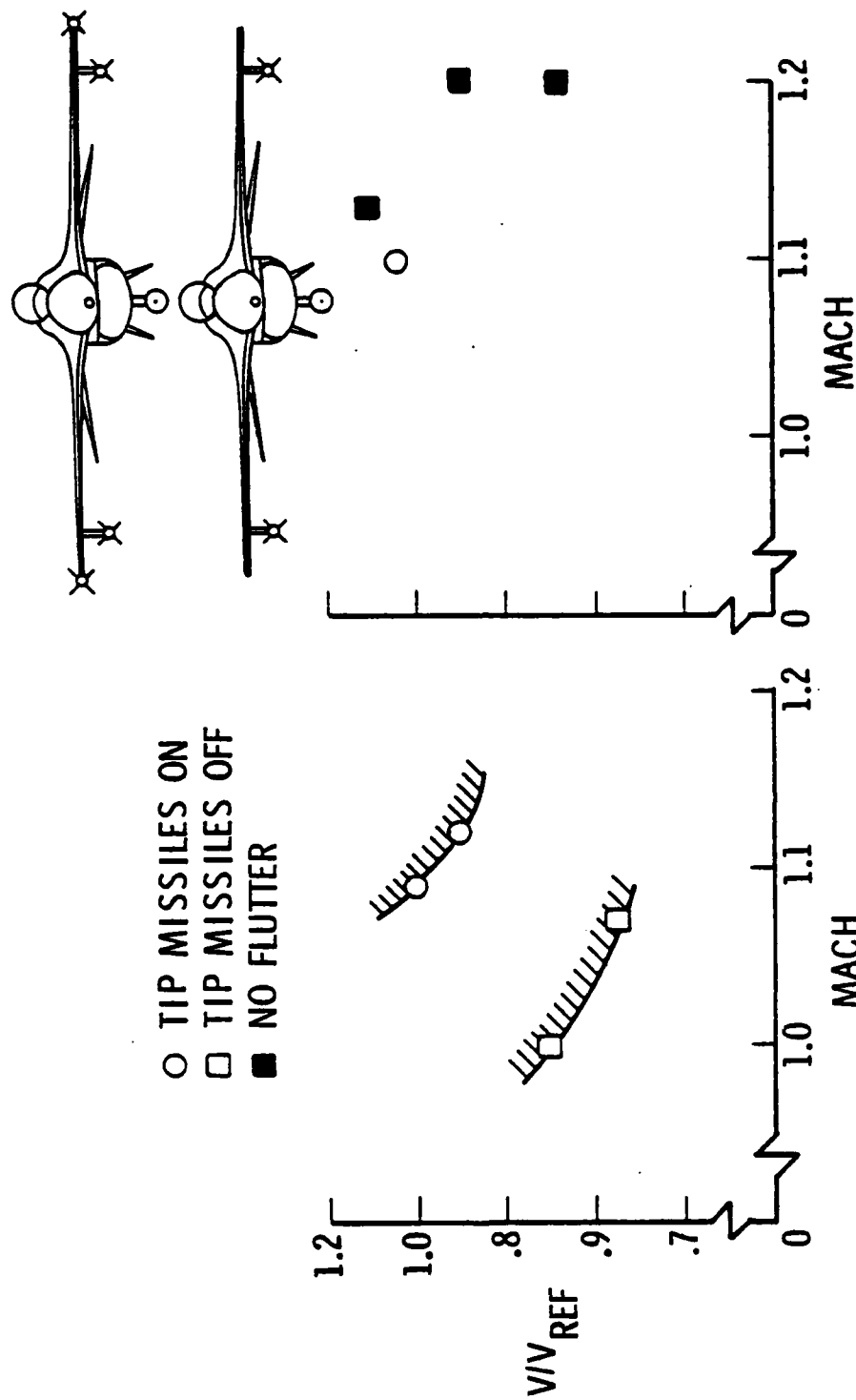


Figure 6.- Launcher Ballast Improves Missile Flutter Speed.

6b) out to a Mach number of 1.13. The model test was terminated at this point (near maximum tunnel dynamic pressure) due to the development of a lateral instability of the model on the cables. With the addition of ballast to each airplane launcher, substantial improvement in flutter characteristics for the loading with the tip missile removed is seen. This result impacted the airplane design in that the airplane missile launchers have been modified for flutter speed improvement.

LOW DAMPING PRECEDES FLUTTER OF A GBU-8/B (HEAVY BOMB)

Flutter model test results for a GBU-8/B heavy air-to-ground weapon (1027 Kg, 2265 LBM) are presented in figure 7. This particular bomb is the only one out of the list of air-to-ground weapons which may be marginal from a flutter standpoint. All other weapons carried at the 63 percent span have more than the required flutter margin of safety based on model test results.

Mild symmetric flutter was observed just beyond the required carriage envelope (0.9 Mach). This flutter was preceded by a wide band of lowly damped oscillations as shown on the right of figure 7. Similar results were obtained with a half full 1400 liter (370 gallon) tank added to the wing at the inboard station as shown on the left of figure 7. The flutter occurred at approximately the same airspeed, but at a lower Mach number. Again the flutter points were outside the flight boundary. Variations in weapon pylon stiffness did not significantly change the test results.

The tunnel results indicate the possibility of encountering some lowly damped oscillations in flight although limited past experience (ref. 6) has shown this phenomena to be more prevalent in the wind tunnel than in flight. Possible alternate carriage configurations for this heavy weapon were investigated in the wind tunnel. Configurations without the AIM-9J missiles or with the wing tip missile moved inboard to the under-wing missile station were shown to substantially increase the flutter speed.

EXTERNAL TANK FUEL USAGE SEQUENCE CHANGE INCREASES FLUTTER SPEED

External tank fuel usage sequence was found to be important for a downloading of the four missile air-to-air configuration with a partially full 1400 liter (370 gallon) fuel tank at the inboard station. The effect of tank fuel usage sequence on flutter speed with the tanks half full is presented in figure 8. The configuration shown at the top of figure 8 consists of the fuel tanks and under-wing AIM-9J missiles. The half full tank shown in the lower tank sketch simulates the initial fuel usage sequence: forward bay first, then aft bay, then center bay. Antisymmetric flutter occurred for this configuration.

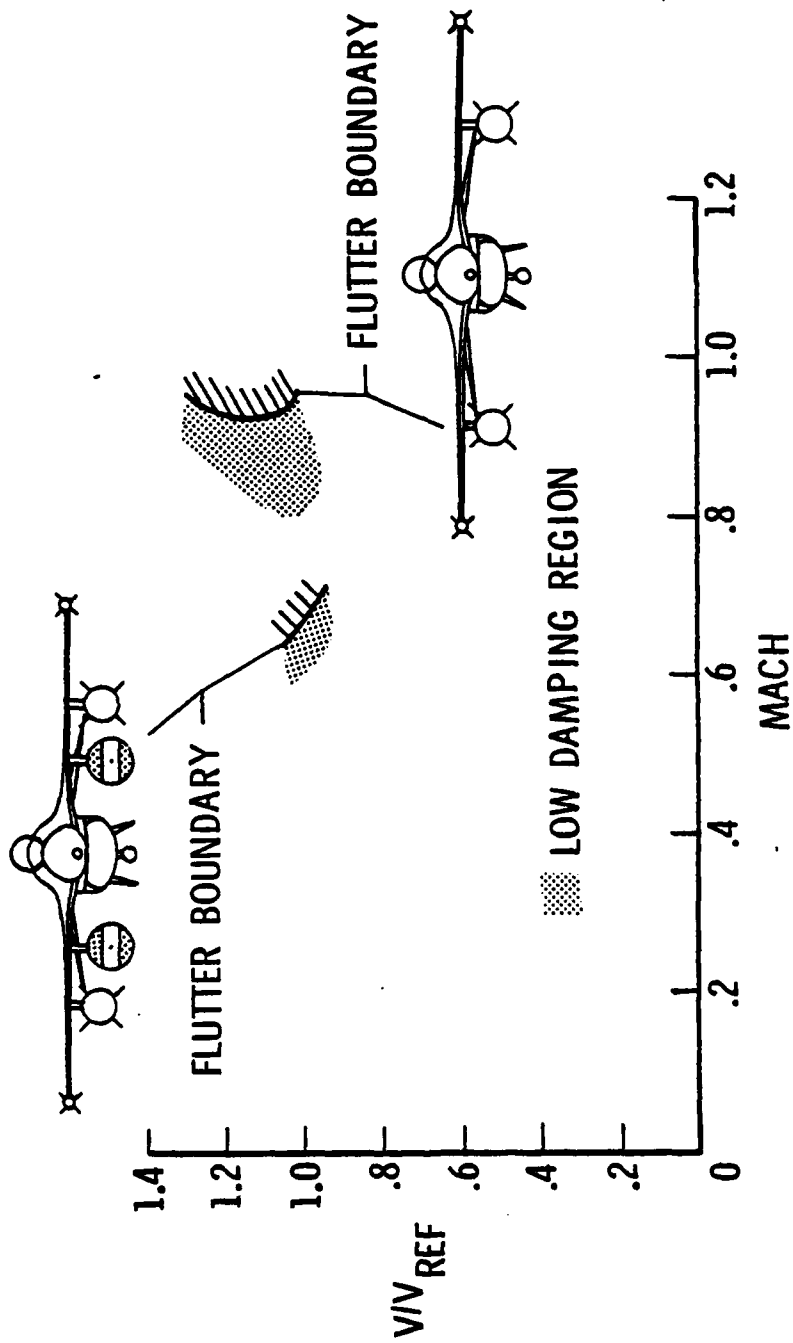


Figure 7.- Low Damping Precedes CBU-8/B Flutter.

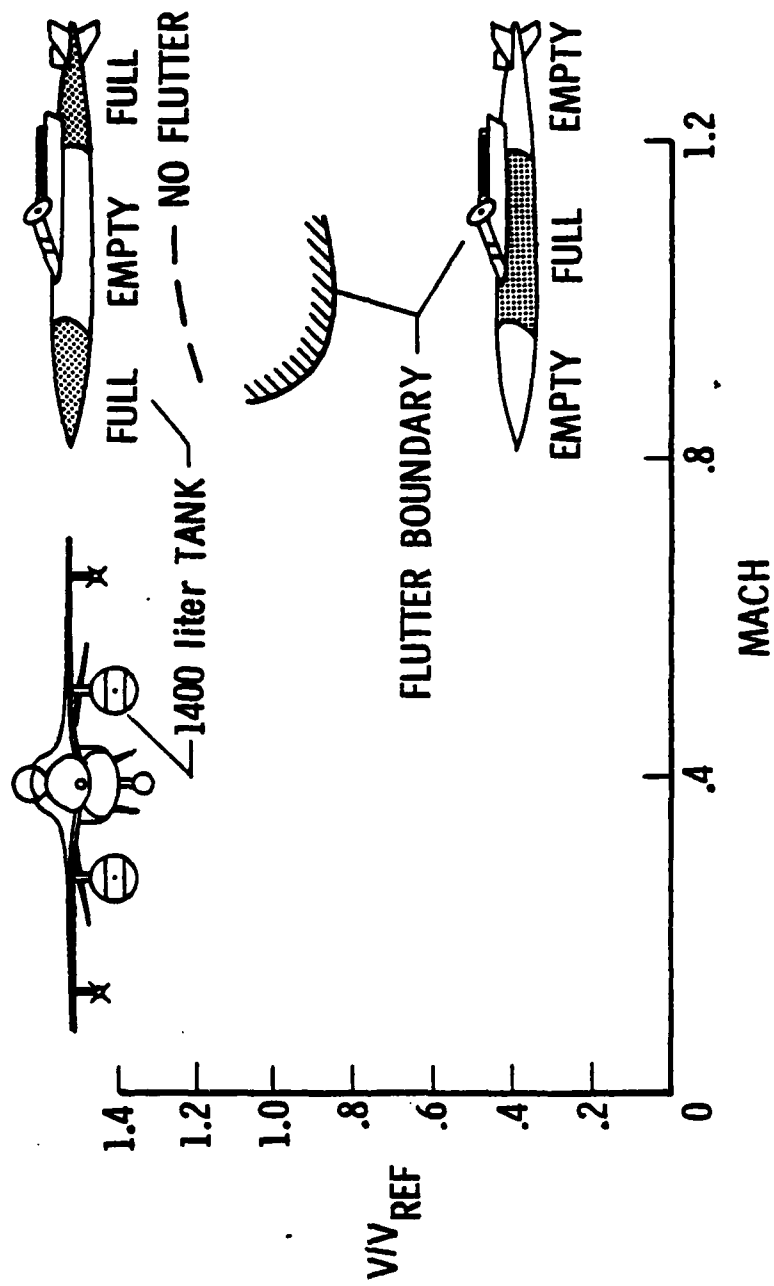


Figure 8.- External Tank Fuel Usage Sequence Change Increases Flutter Speed.

The flutter onset was preceded by a period of lowly damped response. Substantial improvement in flutter speed is shown for the half full tank (upper tank sketch) with the fuel usage sequenced so that fuel was used out of the center bay first. This modified fuel sequencing increases by a factor of four the pitch moment of inertia about the tank center-of-gravity for the half-full tank and eliminates flutter. This result impacted the airplane in that the external fuel tank usage sequence has been modified for flutter improvement.

CONCLUDING REMARKS

A large full span free flying model has proved to be an effective tool in defining flutter characteristics prior to flight tests of a high performance airplane with external wing stores. Satisfactory carriage has been demonstrated for a wide variety of external store loadings. The model test results were used to verify analytical methods and resulted in improved carriage capability of certain store loadings by changes to the missile launcher and external tank fuel usage sequence.

REFERENCES

1. Many Authors: Specialists Meeting On Wing-With-Stores Flutter. AGARD-CP-162, April 1975.
2. Yates, E. Carson, Jr.; Land, Norman S.; and Foughner, Jerome T.: Measured and Calculated Subsonic and Transonic Flutter Characteristics of A 45° Sweptback Wing Planform In Air and In Freon-12 In The Langley Transonic Dynamics Tunnel. NASA TN D-1616, 1963.
3. Reed, Wilmer H, III: Correlation With Flight Of Some Aeroelastic Model Studies In The NASA Langley Transonic Dynamics Tunnel. Paper number 10, NASA Symposium on Flutter Testing Techniques, Oct. 1975, NASA SP-415.
4. Reed, W. H., III; and Abbott, F. T., Jr.: A New "Free-Flight" Mount System For High Speed Wind-Tunnel Flutter Models. Proceedings of the Symposium on Aeroelastic Dynamic Modeling Technology, U.S. Air Force Systems Command, RTD-TDR-63-4197, Part I, 1964.
5. Cunningham, Atlee, M., Jr.: A Steady and Oscillatory Kernel Function Method for Interfering Surfaces in Subsonic, Transonic, and Supersonic Flow. NASA CR-144895, 1976.
6. Ness, H. B.; Murphy, A. C.; and Wilson, L. E.: The Experimental Program for Flutter Prevention on the F-111 With Wing Mounted Stores. Ft. Worth Division of General Dynamics Corp., presented at Aircraft/Stores Compatibility Symposium, November 1969.
7. Katz, H.: Flutter Of Aircraft With External Stores. McDonnell Aircraft Co., presented at Aircraft/Stores Compatibility Symposium, November 1969.

AUTOBIOGRAPHY - Jerome T. Foughner, Jr.

Mr. Foughner received his B.S. degree in Physics from the University of Georgia in 1958. He is an aerospace engineer with the Aeroelasticity Branch, Structures and Dynamics Division at NASA Langley Research Center. He has nineteen years of aeroelastic research experience concerned with a variety of problems of aircraft, spacecraft, and space launch vehicles. Mr. Foughner is the NASA project engineer for the F-16 flutter model studies.

AUTOBIOGRAPHY - Charles T. Bensinger

Mr. Bensinger received his B.S. degree in Mechanical Engineering from Oklahoma State University in 1959. He was employed at Tinker Air Force Base from 1959 to 1963 where he was a member of a team which developed theoretical and experimental jet engine vibration analysis techniques. He graduated from Oklahoma University in 1963 with a Masters degree in Aerospace Engineering. Since 1963, he has been employed by General Dynamics/Fort Worth as a structural dynamicist. He has developed new dynamic modeling techniques for both the F-111 and F-16, including the application of advanced composites to aeroelastic models. Mr. Bensinger is responsible for F-16 structural dynamics ground tests including flutter model tests and airplane ground vibration tests.

THE USE OF FEEDBACK CONTROL AGAINST FLUTTER
DUE TO EXTERNAL WING MOUNTED STORES

(U)

(Article UNCLASSIFIED)

by

Rolland Dat, Roger Destuynder and Jean-Jacques Angélini
Office National d'Etudes et de Recherches Aérospatiales (ONERA)
92320 Châtillon (France)

SUMMARY. (U) This paper shows the reasons why the store induced flutter of military aircraft is a privileged field of application of active flutter control. Then the mathematical formulation of flutter control is presented and the significance of the methods used to derive a control law on a rational basis is shown. The activity of ONERA in the field of flutter control is briefly presented.

"Approved for public release ; distribution unlimited."

LIST OF FIGURES

FIGURE NUMBER

- 1 WING BENDING-TORSION FLUTTER
- 2 CONTROL SECTION
- 3 SELECTIVE CONTROL ON THE FLUTTERMODE (FROM REF.[1])
- 4 ACTIVE FLUTTER CONTROL WITH THE DISSIPATIVITY CONDITION
- 5 MEASUREMENT OF PRESSURE DISTRIBUTION IN THE CONTROL SECTION FOR A CONTROL SURFACE OSCILLATION
- 6 RECTANGULAR MODEL WITH ITS STORE IN THE LOW SPEED WIND TUNNEL
- 7 FLUTTER CONTROL ON A RECTANGULAR HALF WING WITH EXTERNAL STORE
- 8 MEASURED NORMAL MODES OF THE RECTANGULAR WING WITH STORES
- 9 FREQUENCIES AND DAMPING RATIOS MEASURED IN THE WIND TUNNEL, WITH CONTROL OFF AND ON
- 10 RECORDING OF A FLUTTER ONSET AND RESTABILIZATION SEQUENCE OBTAINED BY CUTTING THE CONTROL AND SWITCHING IT ON AGAIN

1 - INTRODUCTION

The classical solution used so far to improve the flutter characteristics of an existing aircraft consisted in structural modifications : mass balancing, modification of the stiffness distribution, or overall stiffness augmentation.

With the improvement of electronic and electrohydraulic actuator technology, the active flutter control has been made possible for present and future aircraft. In this solution, an aerodynamic control surface driven by an actuator is used to generate stabilizing aerodynamic forces. The rotation of the control surface is related to the signals of sensors located inside the wing, through a "control-law" which characterizes the whole feedback system, including the actuator.

The flexibility of this solution is particularly interesting when the wing is prone to meeting several marginal flutter instabilities due to changes of configuration.

In most cases, the active control also provides a lighter solution than that of a structural modification.

The major difficulties of active control are met in the determination of the control law. The first difficulty lies in the choice of a mathematical criterion, allowing its derivation on a rational basis ; the second difficulty is due to an insufficient knowledge of the unsteady aerodynamic forces, and the third one, which is met in the actual realization of the control law, is of technological nature.

In this paper, the mathematical formulations proposed for the derivation of a control law are presented and it is shown that they may be classified according to the degree of knowledge of the structural characteristics and aerodynamic forces which they need for their application.

In the last paragraph, the investigations performed at ONERA are presented and wind tunnel experiments are shown in a movie.

2 - STORE-INDUCED FLUTTER

The flutter instability of a wing is due to the coupled aerodynamic forces, i.e. to the forces which are produced by the bending and torsional deflections of the wing and modify its natural vibration modes. As a first approximation, it may be assumed that the aerodynamic forces depend *linearly* upon the motion of the structure, in the same way as the structural, inertial and elastic forces ; this assumption is also extended to the structural dissipative forces, which are assimilated to viscous forces. But instead of being only conservative and dissipative, as the

structural forces, the aerodynamic forces may be *active* and perform a positive work when the structure is performing a periodic vibration ; that means that the generalized aerodynamic forces have a component in phase with the velocity of vibration of the structure.

In the classical bending-torsion flutter, the structure motion is a combination of at least two degrees of freedom of the structure, and it is the phase lag between these two component motions which makes possible the transfer of energy from the flow to the structure. This motion is produced naturally only when the frequencies of the two natural vibration modes are close enough. In figure 1, the full lines show, in a qualitative manner, the variation of frequencies and damping ratios with velocity, at a constant altitude, for a typical wing bending-torsion flutter. The flutter instability occurs only when the two frequencies are close to each other.

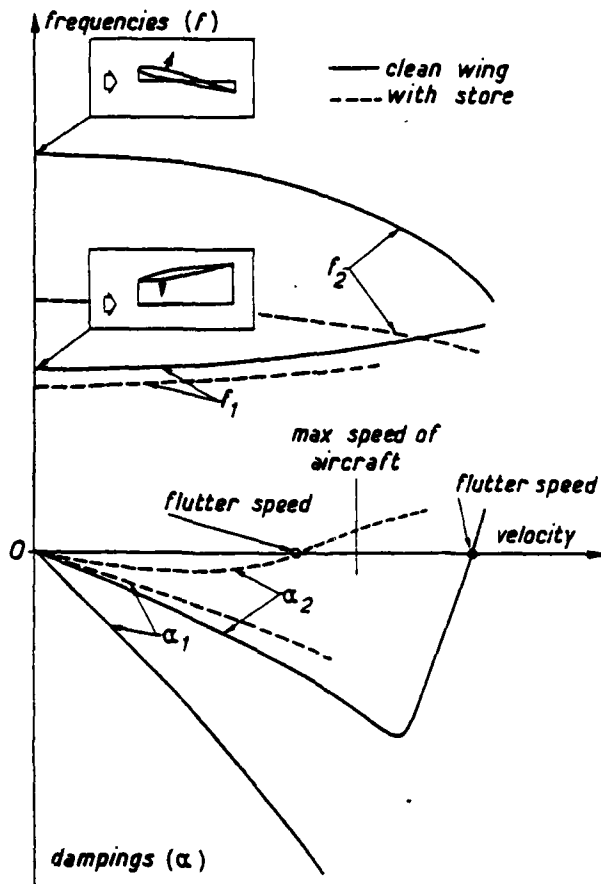


Fig. 1 - Wing bending-torsion flutter.

The rapidity of evolution of the frequencies toward their crossing point is strongly dependent on the structural stiffness and on the mass and stiffness distribution. The military aircraft wings are generally stiff and they are designed with a view to make their flutter speed much higher than the maximum speed of the aircraft in the clean wing configuration, as shown in figure 1. But this design does not guarantee that the aircraft will remain clear from flutter when external stores are fixed on the wing.

The addition of a store with large mass and inertia makes the vibration modes "heavier", with lower frequencies and modified mode shapes. It may have a stabilizing or a destabilizing effect according to the store's relative values of mass and inertia and to the location of its centre of gravity and elastic axis. Usually the store is destabilizing when its centre of gravity is in a rearward position and its pitching inertia is high compared to its mass. This effect may be large enough to make flutter appear inside the flight envelope. The instability obtained in this manner is generally much milder than the initial flutter of the clean wing, because the flutter velocity and frequency are smaller and the amount of energy which the flow can provide at each cycle of vibration is smaller, compared to the elastic energy, than it was in the initial flutter.

But actually, the effect of a store is complicated by the flexibility of its pylon : instead of considering the store as an additional mass and inertia, the designer must consider it and its pylon as an additional conservative system with two or more degrees of freedom, which modifies the initial vibration modes of the structure. Among the modifications observed, one of the most remarkable concerns the torsion mode which is generally split into two modes : a false torsion mode at low frequency, in which the predominant motion is the pitching oscillation of the store, and the actual torsion mode, at a frequency a little higher than the clean wing torsion frequency. The flutter instability is mainly due to the coupling between the false torsion and the bending mode.

The difficulty of flutter prevention of a military aircraft lies in the number of combinations of stores which the aircraft is required to carry. This number is so high that the structure cannot be expected to be flutter free for all the store configurations. The classical means of preventing flutter by a structural modification is not satisfactory in that case, because it would necessitate several structural configurations in order to clear all the stores combinations. Obviously, that solution is not flexible enough and, further more, the additional mass or stiffness necessary to prevent flutter in the most critical store combination may be relatively heavy.

On the other hand, the active flutter control is much attractive for its flexibility : instead of changing a structural configuration when the store combination is changed, one has only to change the control

law. Furthermore, since the store-induced flutter is mild, its active control can be performed safely with a relatively small amount of energy storage.

3 - MATHEMATICAL FORMULATION

3-1 - FLUTTER EQUATIONS

The equations which govern the response of a wing in a flow to a harmonic excitation may be written :

$$\mathbf{Z}(i\omega) \mathbf{q} = \mathbf{Q} \quad (1)$$

where \mathbf{Z} is the impedance matrix given by :

$$\mathbf{Z}(i\omega) = -\omega^2 \boldsymbol{\mu} + \boldsymbol{\gamma} + \rho V^2 \mathbf{A}(i\omega) + i\omega \rho V \mathbf{B}(i\omega) \quad (2)$$

$\boldsymbol{\mu}$ and $\boldsymbol{\gamma}$ are the symmetric positive structural matrices of, respectively, the generalized mass and the generalized stiffness (the structural damping has been omitted for the sake of simplicity) ;

\mathbf{A} and \mathbf{B} are aerodynamic matrices ;

\mathbf{q} is the column vector of generalized coordinates : when the modal representation is used, q_i defines the contribution of the i^{th} normal mode to the motion ;

\mathbf{Q} is a column of hypothetical generalized harmonic external forces, which is written here only to justify the harmonic response.

The natural frequencies and dampings of the structure coupled with the flow are determined by the poles s of the impedance matrix $\mathbf{Z}(s)$. Flutter occurs when the real part of one of the poles is positive.

3-2 - ACTIVE CONTROL

If a rotation β is given to the control surface (see figure 2), the equations giving \mathbf{q} must be written :

$$\mathbf{Z}(i\omega) \mathbf{q} + \bar{\mathbf{U}} \mathbf{C} \beta = \mathbf{Q} \quad (3)$$

where $\mathbf{C}(i\omega)$ is the column matrix giving the force and moment at the reference axis of the control section due to the control surface rotation :

$$\begin{pmatrix} F_b \\ M \end{pmatrix} = - \begin{pmatrix} \mathbf{C} \end{pmatrix} \beta \quad (4)$$

F and M result from the inertial and aerodynamic effects of the control surface and C may be written :

$$C = -\omega^2 \begin{pmatrix} S \\ I + \alpha_c S \end{pmatrix} + \rho v^2 b^2 l \begin{pmatrix} k_\beta \\ m_\beta \end{pmatrix} \quad (5)$$

where $k_\beta(i\omega)$ and $m_\beta(i\omega)$ are the complex coefficients of aerodynamic lift and moment due to control surface rotation; S , I , b , l and α_c are inertial and geometric characteristics of the control surface and control section (figure 2).

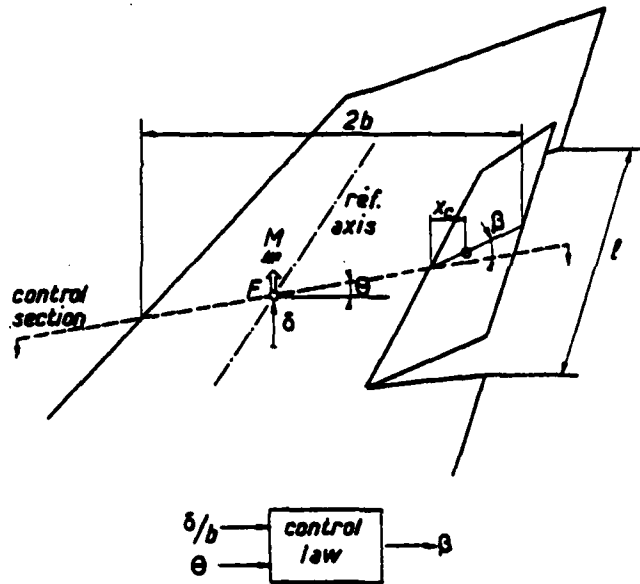


Fig. 2 - Control section.

U is the matrix of modal deflexions and torsions at the reference axis of the control section :

$$U = \begin{bmatrix} \dots & d_{r/b} & \dots \\ \dots & \theta_r & \dots \end{bmatrix}$$

and the resulting deflection and torsion are given by :

$$\begin{pmatrix} \delta/b \\ \theta \end{pmatrix} = U q$$

\bar{U} is the conjugate transpose of U .

With two sensors in the control section, δ and θ can be measured and used as input signals to the servo-control which determines β . The control law relating the output β to the inputs δ and θ can be defined by a column matrix of order two, $X(i\omega)$. We have :

$$\beta = \bar{X}(i\omega) \begin{pmatrix} \delta/b \\ \theta \end{pmatrix}$$

where \bar{X} is the conjugate transpose of the column X .

Then equation (3) may be written as :

$$[Z + \bar{U}C\bar{X}U]q = Q \quad (6)$$

This equation shows that the impedance matrix has been modified by the active control and is now $Z + \Delta Z$ with :

$$\Delta Z = \bar{U}C\bar{X}U \quad (7)$$

ΔZ is a singular matrix since its columns are proportional to the same column $\bar{U}C$.

If several control surfaces are used for the active control, ΔZ may be written as :

$$\Delta Z = \sum_k [\bar{U}]_k (C)_k (\bar{X})_k [U]_k$$

The uncontrolled wing is unstable if one of the poles of $Z(s)$ is on the right hand side of the complex plane. In that case we must find a control law $X(i\omega)$ such that the poles of $Z + \Delta Z$ are all on the left hand side. Since there is an infinity of solutions to this problem, we must use a mathematical criterion to select a satisfactory one. Several criteria are analysed in this paragraph.

3-3 - SELECTIVE CONTROL OF THE FLUTTER MODE

The selective control of the flutter mode has been investigated at ONERA by J.J. Angélini (1). In this method, the problem which is solved is :

- to determine a control law which modifies only the damping of the unstable mode, and makes it positive, without modifying the other modes.

This problem can be solved if the impedance matrix is perfectly known ; figure 3 from ref. (1), shows an example of computed frequencies and dampings with and without the control.

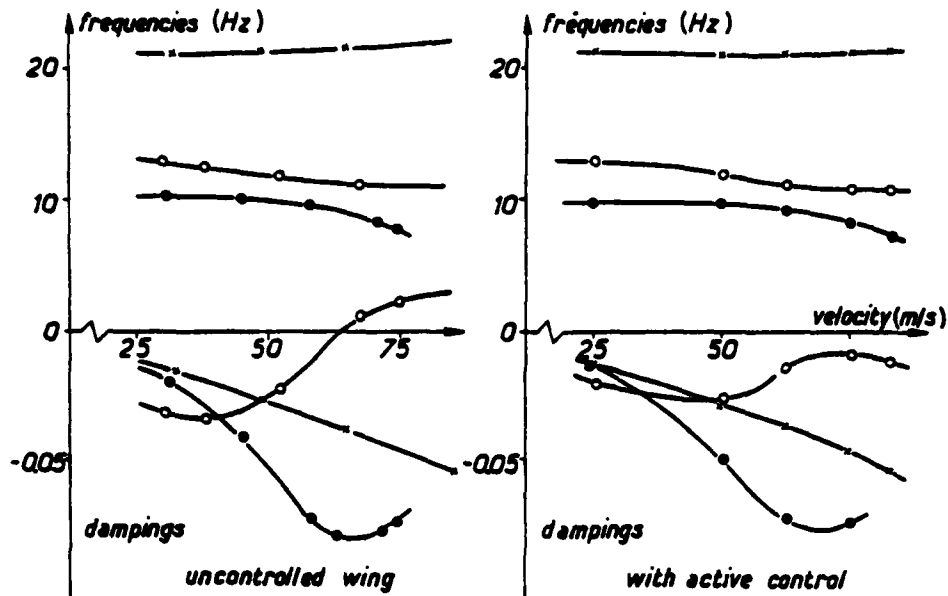


Fig. 3 - Selective control on the fluttermode (from ref. [1]).

In this method, the resulting control law provides damped natural vibrations with the minimum of control surface deflections, for given initial conditions. Unfortunately it cannot be applied in many practical cases, and particularly in transonic flow, for the lack of accurate information on the actual values of the coefficients of the aerodynamic matrices **A** and **B**.

3-4 - ENERGY CONSIDERATIONS

By premultiplying equation (1), by $-i\omega\bar{q}$ we obtain the complex power delivered by the generalized forces **Q** :

$$w = -i\omega\bar{q}Zq = w' + iw''$$

The real and imaginary parts of w can be separated :

$$w' = -\frac{1}{2}\omega\bar{q}i[Z-\bar{Z}]q ; w'' = -\frac{1}{2}\omega\bar{q}[Z+\bar{Z}]q$$

The real part w' is the active power delivered by **Q**, or the power dissipated by the structure and the surrounding flow. If $w' > 0$, power is actually dissipated, and if $w' < 0$ the dissipated power is negative, i.e. the flow provides active power to the structure.

The imaginary part w'' is an imaginary or "reactive" power corresponding to the out-of-phase components of velocity and force. It characterizes the effect of the conservative forces such as elastic or inertia forces.

Let us define :

$$\mathbf{D} = -\frac{i}{2} [\mathbf{Z} - \bar{\mathbf{Z}}] , \text{ as the matrix of dissipative power} \quad (8)$$

$$\mathbf{R} = -\frac{1}{2} [\mathbf{Z} + \bar{\mathbf{Z}}] , \text{ as the matrix of reactive power} \quad (9)$$

With \mathbf{Z} given by (2), we have :

$$\mathbf{D} = -\frac{i}{2} \rho V^2 [\mathbf{A} - \bar{\mathbf{A}}] + \frac{\omega}{2} \rho V [\mathbf{B} + \bar{\mathbf{B}}] \quad (10)$$

$$\mathbf{R} = -\left[\gamma - \omega^2 \mu + \frac{1}{2} \rho V^2 (\mathbf{A} + \bar{\mathbf{A}}) - \frac{i\omega}{2} \rho V (\mathbf{B} - \bar{\mathbf{B}}) \right] \quad (11)$$

The flutter is possible only if the dissipated power can be made negative, i.e. if there exists \mathbf{q} such that $\bar{\mathbf{q}} \mathbf{D} \mathbf{q} < 0$. Therefore, the necessary condition for flutter to occur is that at least one eigen value of the matrix \mathbf{D} be negative.

The matrix \mathbf{R} characterizes a reactive procedure which cannot provide the transfer of power from the flow to the structure in a cyclic vibration. Nevertheless its influence is predominant on the natural frequencies, and it plays an important part in the determination of the flutter velocity and frequency.

When the active control is provided to the wing, the matrices \mathbf{D} and \mathbf{R} are modified and become respectively : $\mathbf{D} + \Delta \mathbf{D}$ and $\mathbf{R} + \Delta \mathbf{R}$ with :

$$\Delta \mathbf{D} = -\frac{i}{2} [\Delta \mathbf{Z} - \Delta \bar{\mathbf{Z}}] \quad (12)$$

$$\Delta \mathbf{R} = -\frac{1}{2} [\Delta \mathbf{Z} + \Delta \bar{\mathbf{Z}}] \quad (13)$$

$\Delta \mathbf{D}$ may be called the control dissipative matrix and $\Delta \mathbf{R}$ the control reactive matrix.

3-5 - NISSIM'S METHOD

In the Nissim's method (2), the problem which is solved is :

- to provide a control dissipative matrix $\Delta \mathbf{D}$ such that the resulting matrix $\mathbf{D} + \Delta \mathbf{D}$ is made positive or at least semi-positive, i.e. it has no more negative eigen values.

In order to apply this method it is necessary to know the aerodynamic matrices **A** and **B** which determine the matrix **D** according to eq. (10). But since the property of positivity is not modified by a variable change, it is sufficient to know the aerodynamic influence coefficients which are independent of the structural dynamic characteristics. On the other hand, since what we are seeking in this method is to make the eigen values of **D** + Δ **D** positive or null, it is not necessary to know the matrix **D** as accurately as in the preceding method of selective control.

But generally, the condition of semi positivity of **D** + Δ **D** can be fulfilled only with several independent control surfaces. For example, this method has been investigated at the NASA on a model with two control surfaces : one leading edge control and one at the trailing edge [3].

3-6 - DISSIPATIVITY CONDITION

In this method, which is investigated at ONERA, the problem which is solved is to find a control law **X** preventing the control matrix Δ **Z** from providing active power.

This condition is fulfilled if the matrix Δ **D** is positive or semi-positive.

With Δ **Z** given by (7) we have :

$$\Delta \mathbf{D} = - \frac{i}{2} \bar{\mathbf{U}} (\mathbf{C}\bar{\mathbf{X}} - \mathbf{X}\bar{\mathbf{C}}) \mathbf{U}$$

Since the transformation by the matrix **U** does not change the property of positivity, the same condition can be applied to the matrix $\Delta \mathbf{D}'$ given by :

$$\Delta \mathbf{D}' = \frac{1}{2} [\mathbf{C}\bar{\mathbf{Y}} + \mathbf{Y}\bar{\mathbf{C}}]$$

with $\mathbf{Y} = i\mathbf{X}$

The eigen values of $\Delta \mathbf{D}'$ are solutions of the problem :

$$[\mathbf{C}\bar{\mathbf{Y}} + \mathbf{Y}\bar{\mathbf{C}} - 2\lambda] \mathbf{V} = 0 \quad (14)$$

Since the matrix $\Delta \mathbf{D}'$ is built with the two vectors **C** and **Y**, it has only two eigen values and the corresponding eigen vectors are linear combinations of **C** and **Y** :

$$\mathbf{V} = a \mathbf{C} + b \mathbf{Y} \quad (15)$$

After substitution of (15) into (14) it is found that the eigen values λ_1 and λ_2 are solutions of the second degree equation :

$$4\lambda^2 - 2\lambda (\bar{\mathbf{Y}}\mathbf{C} + \bar{\mathbf{C}}\mathbf{Y}) - (\bar{\mathbf{C}}\mathbf{C}\bar{\mathbf{Y}}\mathbf{Y} - \bar{\mathbf{Y}}\mathbf{C}\bar{\mathbf{C}}\mathbf{Y}) = 0$$

λ_1, λ_2 is negative, and consequently one of the eigen values is negative, except if Y is proportional to C .

Then it can easily be found that $X = -iY$ must be given by $X = kC$ where $k(i\omega) = k' + ik''$ is a complex function in the lower part of the complex plane. Then according to (7), $\Delta Z = k U C C U$

If $k' = 0$, the matrix ΔZ is anti-Hermitian and the feedback control is purely dissipative: it modifies the dampings and has only a small effect on the natural frequencies;

If $k'' = 0$, ΔZ is Hermitian and the feedback control is equivalent to a reactive system which may have a significant effect on the frequencies and modify the flutter velocity, by its effect on the frequency separation of the two coupled modes.

The control surface rotation is given by: $\beta = \bar{k} \bar{C} \begin{pmatrix} \delta/b \\ \theta \end{pmatrix}$

or $\beta = \bar{k} u$

with $u = \bar{C}_1 \delta/b + \bar{C}_2 \theta$

where $C_1(i\omega)$ and $C_2(i\omega)$ are the coefficients of the column C .

Therefore C determines the relative contribution of δ and θ to the control surface rotation. The function $u = \bar{C}_1 \delta/b + \bar{C}_2 \theta$ can be built directly with the signals provided by the two sensors, as shown in figure 4.

The column C is determined by the inertial characteristics of the control surface and by the aerodynamic coefficients of lift and moment due to control surface rotation. The experimental values of these coefficients can be determined in flight or in a wind tunnel with pressure transducers distributed in the control section. In these measurements, the control surface can be oscillated with the actuator (figure 5).

When the column C has been determined it remains to determine the complex function $k(i\omega)$. But k is the transfer function relating β to u , and the techniques used for the determination of feedback controls with only one input and one output functions can be used. For instance, k may be derived from open loop transfer function measurements or from a systematic analysis of the variation of eigen values with the modulus and argument of k , as shown, for instance, in reference [6] and [7].

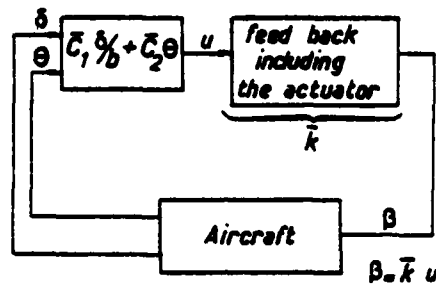
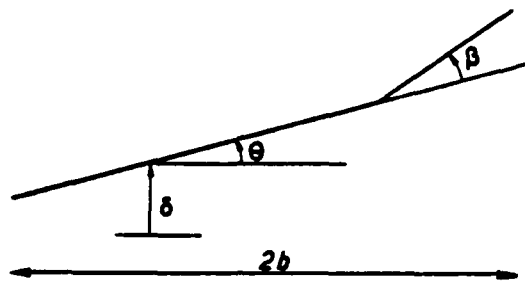


Fig. 4 - Active flutter control with the dissipativity condition.

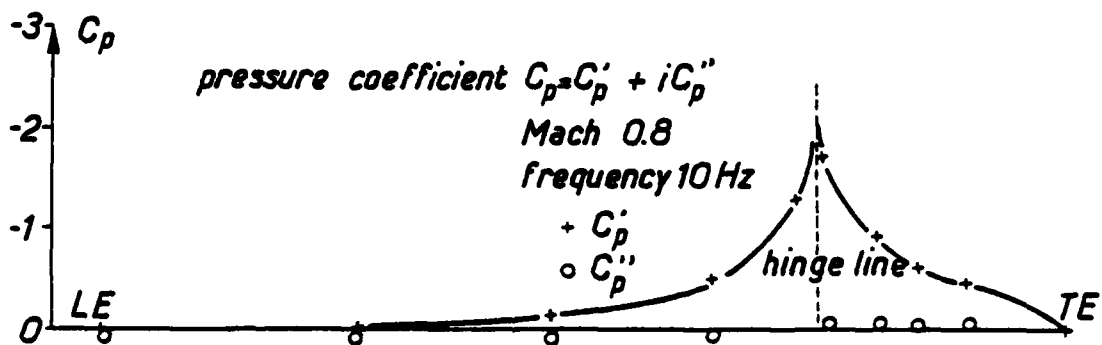


Fig. 5 - Measurement of pressure distribution in the control section for a control surface oscillation.

Notice that C_p'' is small, so that k_β and m_β are almost real.

4 - THE ACTIVITY OF ONERA ON ACTIVE FLUTTER CONTROL

The ONERA has been investigating active flutter control for several years.

A theoretical investigation of the method of selective control of the flutter mode was performed by J.J. Angélini [1] in 1973.

The experimental researches will be presented only briefly since they will be illustrated by the movie.

Tests were performed in a low speed wind tunnel and in the transonic S2 wind tunnel of Modane.

The model tested at low speed was a rectangular wing, and flutter was obtained in the wind tunnel domain with a store mounted on a flexible pylon [4]. In the first series of tests, a small winglet was mounted at the wing tip, as shown in figure 6, to provide an "Identical Location of Accelerometer and Force" (ILAF) type of control. This control worked satisfactorily and a substantial gain in flutter speed was obtained, but the addition of a control surface specialized in flutter control could not be considered as a realistic solution.

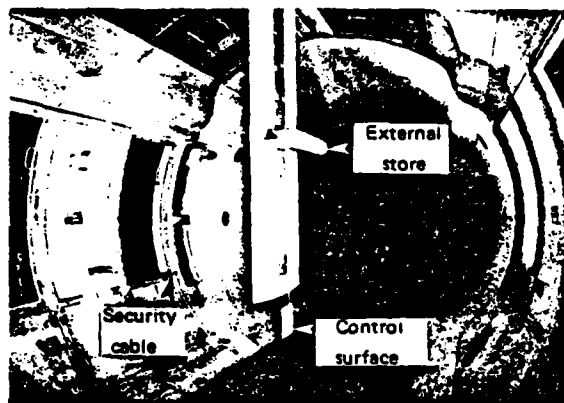


Fig. 6 - Rectangular model with its store in the low speed wind tunnel.

The active flutter control is provided by the winglet at the wing-tip.

More recently, experiments have been performed in the transonic S2 wind tunnel of Modane on a dynamic model of a military aircraft which was modified in order to have a flutter instability with a store, inside the wind tunnel domain. In that case also, the model was stabilized with a trailing edge control.

The feedback control used in these experiments had only one input (i.e. one sensor only was used) and one output (or one control surface). The control law was derived from the Nyquist diagram made with open loop transfer function measurements performed with the wind on. The influence of the phase of the control law was also investigated in order to evaluate the phase margin.

We now intend to use two input sensors and to combine them with the dissipative condition. The experimental determination of the lift and moment due to control rotation, which is necessary in this case, will be based on unsteady pressure measurements in the control section as shown in figure 5.

In another series of tests, the active control was performed with a classical trailing edge control surface [5].

Figure 7 to 10 show respectively :

- the model plan form,
- the model mode shapes measured in the laboratory,
- the variation of frequencies and damping ratios with velocity, with and without control,
- the recording of a flutter onset and restabilization obtained by cutting the control and switching it on again.

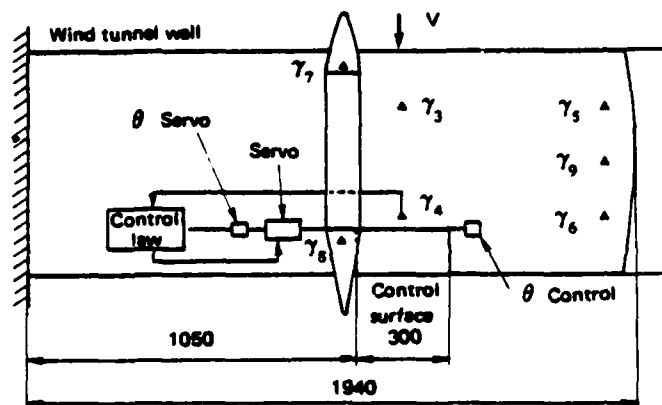


Fig. 7 - Flutter control on a rectangular half wing with external store.

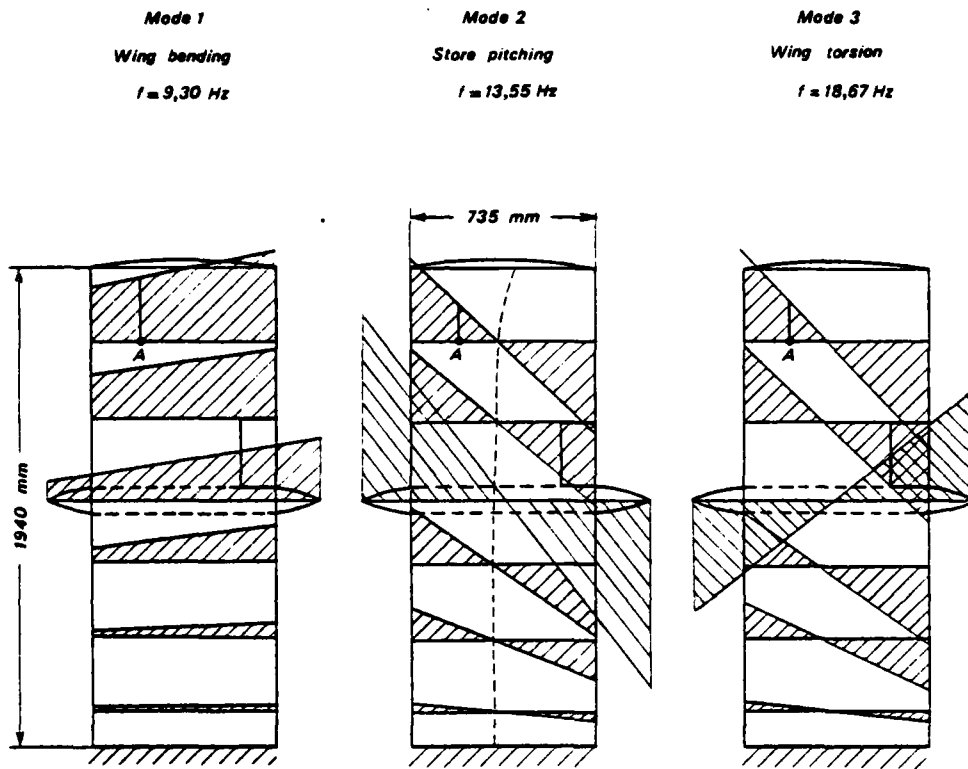


Fig. 8 – Measured normal modes of the rectangular wing with stores.

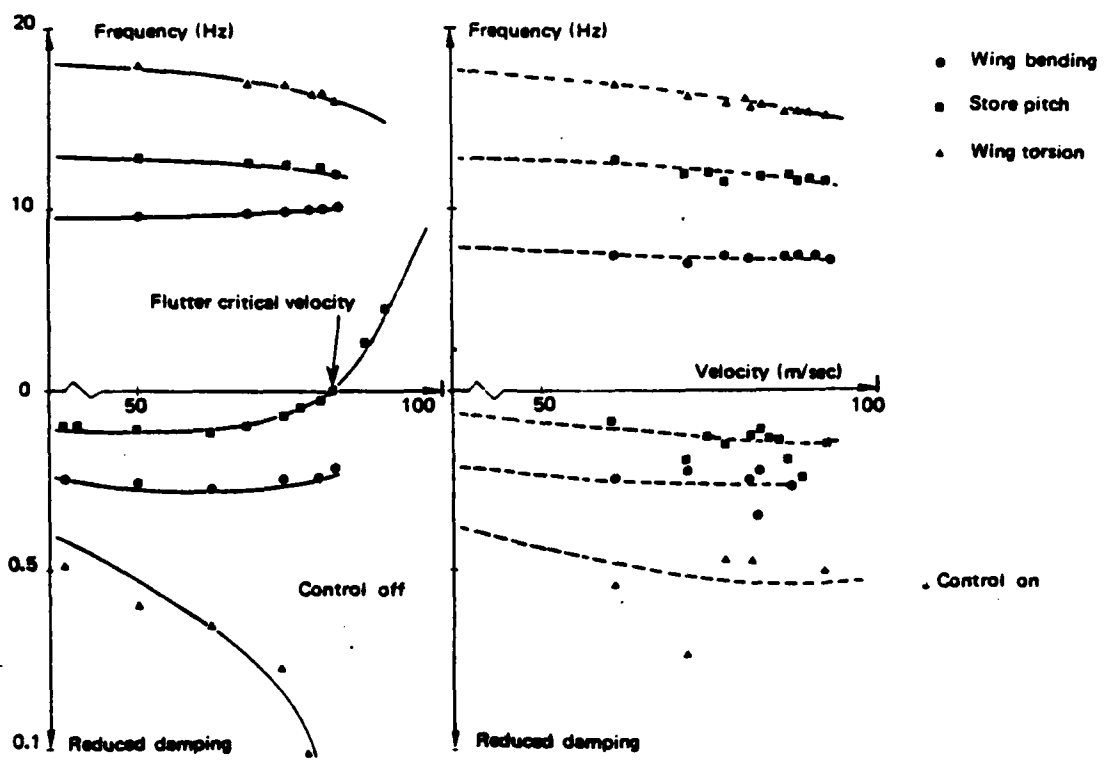


Fig. 9 - Frequencies and damping ratios measured in the wind tunnel, with control off and on.

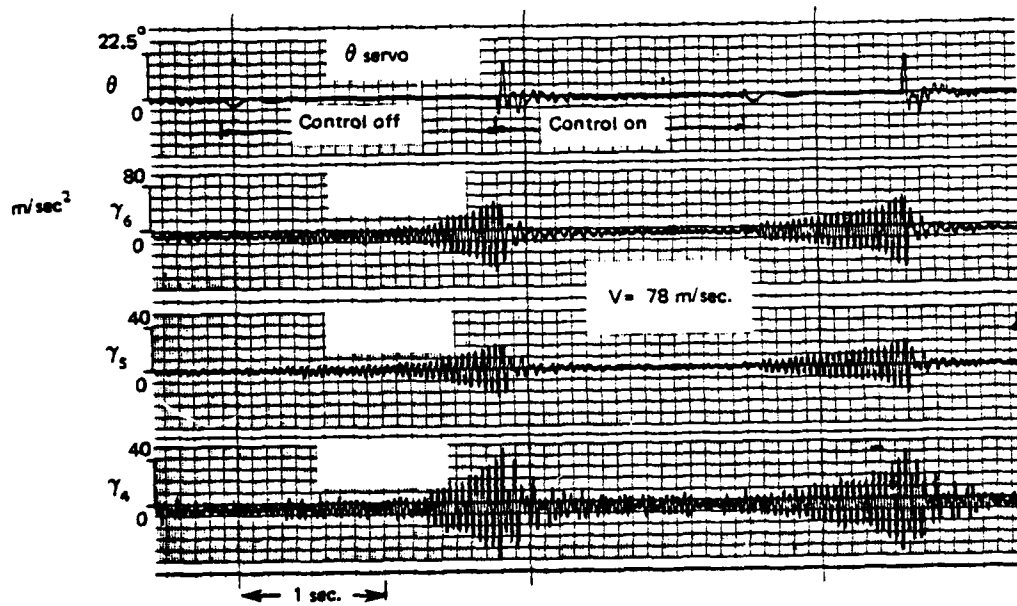


Fig. 10 — Recording of a flutter onset and restabilization sequence obtained by cutting the control and switching it on again.

A small electro-hydraulic actuator developed by ONERA was used in all these experiments.

The implementation of methods for measuring frequency and damping in a turbulent flow was also necessary.

5 - CONCLUDING REMARKS

The problem of active flutter control has been formulated and discussed. The determination of a stabilizing control law with one input and one output (or with one sensor and one control surface, in this particular case) is a classical problem. But as soon as several inputs or outputs are used, new mathematical criteria are necessary in order to determine the relative contribution of the different inputs and/or outputs. An important characteristic of these methods is the possibility of their application with an imperfect knowledge of the unsteady aerodynamic forces.

In this paper the effects of non linearities and the technological difficulties met in the realization of the control laws have not been considered.

The first attempts to damp out store-induced flutter on wind tunnel models have been successful even if the control law were not optimized, and many experiments show that the stabilization with the active control is generally relatively easy. But this does not mean that the problem of active flutter control has already been solved : it remains to investigate the response of the active control surface to turbulence or gusts, and the power delivered by the electro-hydraulic actuator in the presence of turbulence.

REFERENCES

- [1] - J. Angélini - Contrôle du flottement par déplacement d'une valeur propre, in "Active Control Systems for Load Alleviation, Flutter Suppression and Ride Control", AGARD ograpb AG 175 (1973).
- [2] - Nissim E. - Flutter Suppression Using Active Control Based on the Concept of Aerodynamic Energy - NASA TN D 6199 (1971).
- [3] - Abel I. and Standford M.C. - Status of two studies on Active Flutter Control on Aeroelastic Response at NASA Langley Research Centre, AGARD ograpb AG 175 (1973).
- [4] - Destuynder R. - Essai en soufflerie d'un supprimeur de flottement sur une aile droite, in "Flutter Suppression and Structural Load Alleviation", AGARD Confer. Roc. CP 175 (1975).
- [5] - Destuynder R. - Etude en soufflerie d'un supprimeur de flottement Rech. Aérosp. N. (1976) 4, p. 233-241.
- [6] - Triplett W.E., Kappus HPF and Landy R.J. - Active flutter suppression systems for Military Aircrafts - A Feasibility Study - AFFDL TR 72-116 - Feb. 1973.
- [7] - Haidl G., Lötze A. and Sensburg O. - Active Flutter Suppressor on wings with external stores, in AGARD AG 175 (1975).

AUTOBIOGRAPHY

MR. ROLLAND DAT

Mr. Rolland Dat [REDACTED] He joined ONERA in 1946 in the Structures Department where he is now Deputy Director. Since 1953, h3 has been engaged in research in the field of aeroelasticity. He has performed wind tunnel flutter tests, developed methods of calculating unsteady aerodynamic forces based on the linear lifting surface theory and developed vibration testing methods. In recent years, he has worked mainly in the field of helicopter dynamics and he is engaged in a cooperative effort with the US Army R&D Laboratory at Ames.